

International Journal on

Advances in Telecommunications



2012 vol. 5 nr. 3&4

The *International Journal on Advances in Telecommunications* is published by IARIA.

ISSN: 1942-2601

journals site: <http://www.ariajournals.org>

contact: petre@aria.org

Responsibility for the contents rests upon the authors and not upon IARIA, nor on IARIA volunteers, staff, or contractors.

IARIA is the owner of the publication and of editorial aspects. IARIA reserves the right to update the content for quality improvements.

Abstracting is permitted with credit to the source. Libraries are permitted to photocopy or print, providing the reference is mentioned and that the resulting material is made available at no cost.

Reference should mention:

International Journal on Advances in Telecommunications, issn 1942-2601
vol. 5, no. 3 & 4, year 2012, <http://www.ariajournals.org/telecommunications/>

The copyright for each included paper belongs to the authors. Republishing of same material, by authors or persons or organizations, is not allowed. Reprint rights can be granted by IARIA or by the authors, and must include proper reference.

Reference to an article in the journal is as follows:

<Author list>, "<Article title>"
International Journal on Advances in Telecommunications, issn 1942-2601
vol. 5, no. 3 & 4, year 2012, <start page>:<end page>, <http://www.ariajournals.org/telecommunications/>

IARIA journals are made available for free, proving the appropriate references are made when their content is used.

Sponsored by IARIA

www.aria.org

Copyright © 2012 IARIA

Editor-in-Chief

Tulin Atmaca, IT/Telecom&Management SudParis, France

Editorial Advisory Board

Michael D. Logothetis, University of Patras, Greece
Jose Neuman De Souza, Federal University of Ceara, Brazil
Eugen Borcoci, University "Politehnica" of Bucharest (UPB), Romania
Reijo Savola, VTT, Finland
Haibin Liu, Aerospace Engineering Consultation Center-Beijing, China

Editorial Board

Fatma Abdelkefi, High School of Communications of Tunis - SUPCOM, Tunisia
Seyed Reza Abdollahi, Brunel University - London, UK
Habtamu Abie, Norwegian Computing Center/Norsk Regnesentral-Blindern, Norway
Taufik Abrao, Universidade Estadual de Londrina, Brazil
Joao Afonso, FCCN - National Foundation for Scientific Computing, Portugal
Rui L. Aguiar, Universidade de Aveiro, Portugal
Javier M. Aguiar Pérez, Universidad de Valladolid, Spain
Mahdi Aiash, Middlesex University, UK
Akbar Sheikh Akbari, Staffordshire University, UK
Ahmed Akl, Arab Academy for Science and Technology (AAST), Egypt
Hakiri Akram, LAAS-CNRS, Toulouse University, France
Bilal Al Momani, Cisco Systems, Ireland
Anwer Al-Dulaimi, Brunel University, UK
Muhammad Ali Imran, University of Surrey, UK
Muayad Al-Janabi, University of Technology, Baghdad, Iraq
Jose M. Alcaraz Calero, Hewlett-Packard Research Laboratories, UK / University of Murcia, Spain
Erick Amador, Intel Mobile Communications, France
Ermeson Andrade, Universidade Federal de Pernambuco (UFPE), Brazil
Abdullahi Arabo, Liverpool John Moores University, UK
Regina B. Araujo, Federal University of Sao Carlos - SP, Brazil
Pasquale Ardimento, University of Bari, Italy
Ezendu Ariwa, London Metropolitan University, UK
Miguel Arjona Ramirez, São Paulo University, Brasil
Radu Arsinte, Technical University of Cluj-Napoca, Romania
Tulin Atmaca, Institut Mines-Telecom/ Telecom SudParis, France
Marco Aurelio Spohn, Federal University of Fronteira Sul (UFFS), Brazil
Philip L. Balcaen, University of British Columbia Okanagan - Kelowna, Canada
Marco Baldi, Università Politecnica delle Marche, Italy

Javier Barria, Imperial College London, UK
Ilija Basicovic, University of Novi Sad, Serbia
Carlos Becker Westphall, Federal University of Santa Catarina, Brazil
Mark Bentum, University of Twente, The Netherlands
David Bernstein, Huawei Technologies, Ltd., USA
Eugen Borgoci, University "Politehnica" of Bucharest (UPB), Romania
Christos Bouras, University of Patras, Greece
David Boyle, Tyndall National Institute, University College Cork, Ireland
Martin Brandl, Danube University Krems, Austria
Julien Broisin, IRIT, France
Dumitru Burdescu, University of Craiova, Romania
Andi Buzo, University "Politehnica" of Bucharest (UPB), Romania
Shkelzen Cakaj, Telecom of Kosovo / Prishtina University, Kosovo
Enzo Alberto Candreva, DEIS-University of Bologna, Italy
Rodrigo Capobianco Guido, University of Sao Paulo, Brazil
Hakima Chaouchi, Telecom SudParis, France
Emmanuel Chaput, IRIT-CNRS, France
Silviu Ciochina, Universitatea Politehnica din Bucuresti, Romania
José Coimbra, Universidade do Algarve, Portugal
Hugo Coll Ferri, Polytechnic University of Valencia, Spain
Denis Collange, Orange Labs, France
Noel Crespi, Institut TELECOM SudParis-Evry, France
Leonardo Dagui de Oliveira, Escola Politécnica da Universidade de São Paulo, Brazil
Gerard Damm, Alcatel-Lucent, USA
Danco Davcev, University for Information Science & Technology "St. Paul the Apostle", Ohrid, Macedonia
Francescantonio Della Rosa, Tampere University of Technology, Finland
Chérif Diallo, Consultant Sécurité des Systèmes d'Information, France
Klaus Drechsler, Fraunhofer Institute for Computer Graphics Research IGD, Germany
Jawad Drissi, Cameron University, USA
António Manuel Duarte Nogueira, University of Aveiro / Institute of Telecommunications, Portugal
Alban Duverdier, CNES (French Space Agency) Paris, France
Nicholas Evans, EURECOM, France
Fabrizio Falchi, ISTI - CNR, Italy
Mário F. S. Ferreira, University of Aveiro, Portugal
Bruno Filipe Marques, Polytechnic Institute of Viseu, Portugal
Robert Forster, Edgemount Solutions, USA
John-Austen Francisco, Rutgers, the State University of New Jersey, USA
Kaori Fujinami, Tokyo University of Agriculture and Technology, Japan
Shauneen Furlong, University of Ottawa, Canada / Liverpool John Moores University, UK
Ana-Belén García-Hernando, Universidad Politécnica de Madrid, Spain
Bezalel Gavish, Southern Methodist University, USA
Christos K. Georgiadis, University of Macedonia, Greece
Mariusz Glabowski, Poznan University of Technology, Poland
Katie Goeman, Hogeschool-Universiteit Brussel, Belgium
Hock Guan Goh, Universiti Tunku Abdul Rahman, Malaysia
Pedro Gonçalves, ESTGA - Universidade de Aveiro, Portugal

Valerie Gouet-Brunet, Conservatoire National des Arts et Métiers (CNAM), Paris
Christos Grecos, University of West of Scotland, UK
Stefanos Gritzalis, University of the Aegean, Greece
William I. Grosky, University of Michigan-Dearborn, USA
Vic Grout, Glyndwr University, UK
Xiang Gui, Massey University, New Zealand
Huaqun Guo, Institute for Infocomm Research, A*STAR, Singapore
Song Guo, University of Aizu, Japan
Ching-Hsien (Robert) Hsu, Chung Hua University, Taiwan
Javier Ibanez-Guzman, Renault S.A., France
Lamiaa Fattouh Ibrahim, King Abdul Aziz University, Saudi Arabia
Theodoros Iliou, University of the Aegean, Greece
Mohsen Jahanshahi, Islamic Azad University, Iran
Antonio Jara, University of Murcia, Spain
Carlos Juiz, Universitat de les Illes Balears, Spain
Adrian Kacso, Universität Siegen, Germany
György Kálmán, ABB AS, Norway
Eleni Kaplani, Technological Educational Institute of Patras, Greece
Behrouz Khoshnevis, University of Toronto, Canada
Ki Hong Kim, ETRI: Electronics and Telecommunications Research Institute, Korea
Atsushi Koike, Seikei University, Japan
Ousmane Kone, UPPA - University of Bordeaux, France
Dragana Krstic, University of Nis, Serbia
Archana Kumar, Delhi Institute of Technology & Management, Haryana, India
Romain Laborde, University Paul Sabatier (Toulouse III), France
Massimiliano Laddomada, Texas A&M University-Texarkana, USA
Thomas D. Lagkas, University of Western Macedonia, Greece
Wen-Hsing Lai, National Kaohsiung First University of Science and Technology, Taiwan
Zhihua Lai, Ranplan Wireless Network Design Ltd., UK
Jong-Hyouk Lee, INRIA, France
Wolfgang Leister, Norsk Regnesentral, Norway
Elizabeth I. Leonard, Naval Research Laboratory - Washington DC, USA
Jia-Chin Lin, National Central University, Taiwan
Chi (Harold) Liu, IBM Research - China, China
Haibin Liu, China Aerospace Science and Technology Corporation, China
Diogo Lobato Acatauassu Nunes, Federal University of Pará, Brazil
Andreas Loeffler, Friedrich-Alexander-University of Erlangen-Nuremberg, Germany
Michael D. Logothetis, University of Patras, Greece
Renata Lopes Rosa, University of São Paulo, Brazil
Hongli Luo, Indiana University Purdue University Fort Wayne, USA
Christian Maciocco, Intel Corporation, USA
Dario Maggiorini, University of Milano, Italy
Maryam Tayefeh Mahmoudi, Research Institute for ICT, Iran
Krešimir Malarić, University of Zagreb, Croatia
Zoubir Mammeri, IRIT - Paul Sabatier University - Toulouse, France
Herwig Mannaert, University of Antwerp, Belgium

Adrian Matei, Orange Romania S.A, part of France Telecom Group, Romania
Natarajan Meghanathan, Jackson State University, USA
Emmanouel T. Michailidis, University of Piraeus, Greece
Ioannis D. Moscholios, University of Peloponnese, Greece
Djafar Mynbaev, City University of New York, USA
Pubudu N. Pathirana, Deakin University, Australia
Christopher Nguyen, Intel Corp., USA
Lim Nguyen, University of Nebraska-Lincoln, USA
Brian Niehöfer, TU Dortmund University, Germany
Serban Georgica Obreja, University Politehnica Bucharest, Romania
Peter Orosz, University of Debrecen, Hungary
Patrik Österberg, Mid Sweden University, Sweden
Harald Øverby, ITEM/NTNU, Norway
Tudor Palade, Technical University of Cluj-Napoca, Romania
Constantin Paleologu, University Politehnica of Bucharest, Romania
Stelios Papaharalabos, National Observatory of Athens, Greece
Gerard Parr, University of Ulster Coleraine, UK
Ling Pei, Finnish Geodetic Institute, Finland
Jun Peng, University of Texas - Pan American, USA
Cathryn Peoples, University of Ulster, UK
Dionysia Petraki, National Technical University of Athens, Greece
Dennis Pfisterer, University of Luebeck, Germany
Timothy Pham, Jet Propulsion Laboratory, California Institute of Technology, USA
Roger Pierre Fabris Hoefel, Federal University of Rio Grande do Sul (UFRGS), Brazil
Przemyslaw Pochec, University of New Brunswick, Canada
Anastasios Politis, Technological & Educational Institute of Serres, Greece
Adrian Popescu, Blekinge Institute of Technology, Sweden
Neeli R. Prasad, Aalborg University, Denmark
Dušan Radović, TES Electronic Solutions, Stuttgart, Germany
Victor Ramos, UAM Iztapalapa, Mexico
Gianluca Reali, Università degli Studi di Perugia, Italy
Eric Renault, Telecom SudParis, France
Leon Reznik, Rochester Institute of Technology, USA
Joel Rodrigues, Instituto de Telecomunicações / University of Beira Interior, Portugal
David Sánchez Rodríguez, University of Las Palmas de Gran Canaria (ULPGC), Spain
Panagiotis Sarigiannidis, University of Western Macedonia, Greece
Michael Sauer, Corning Incorporated, USA
Reijo Savola, VTT Technical Research Centre of Finland, Finland
Marialisa Scatà, University of Catania, Italy
Zary Segall, Chair Professor, Royal Institute of Technology, Sweden
Sergei Semenov, Renesas Mobile Europe, Finland
Sandra Sendra Compte, Polytechnic University of Valencia, Spain
Dimitrios Serpanos, University of Patras and ISI/RC Athena, Greece
Adão Silva, University of Aveiro / Institute of Telecommunications, Portugal
Pushpendra Bahadur Singh, MindTree Ltd, India
Danai Skournetou, Tampere University of Technology, Finland

Mariusz Skrocki, Orange Labs Poland / Telekomunikacja Polska S.A., Poland
Leonel Sousa, INESC-ID/IST, TU-Lisbon, Portugal
Liana Stanescu, University of Craiova, Romania
Cosmin Stoica Spahiu, University of Craiova, Romania
Radu Stoleru, Texas A&M University, USA
Young-Joo Suh, POSTECH (Pohang University of Science and Technology), Korea
Hailong Sun, Beihang University, China
Jani Suomalainen, VTT Technical Research Centre of Finland, Finland
Fatma Tansu, Eastern Mediterranean University, Cyprus
Ioan Toma, STI Innsbruck/University Innsbruck, Austria
Božo Tomas, HT Mostar, Bosnia and Herzegovina
Piotr Tycza, Poznan University of Technology, Poland
John Vardakas, University of Patras, Greece
Andreas Veglis, Aristotle University of Thessaloniki, Greece
Luís Veiga, Instituto Superior Técnico / INESC-ID Lisboa, Portugal
Calin Vladeanu, "Politehnica" University of Bucharest, Romania
Natalija Vlajic, York University - Toronto, Canada
Benno Volk, ETH Zurich, Switzerland
Krzysztof Walczak, Poznan University of Economics, Poland
Krzysztof Walkowiak, Wroclaw University of Technology, Poland
Yang Wang, Georgia State University, USA
Yean-Fu Wen, National Taipei University, Taiwan, R.O.C.
Bernd E. Wolfinger, University of Hamburg, Germany
Riaan Wolhuter, Universiteit Stellenbosch University, South Africa
Yulei Wu, Chinese Academy of Sciences, China
Mudasser F. Wyne, National University, USA
Gaoxi Xiao, Nanyang Technological University, Singapore
Bashir Yahya, University of Versailles, France
Abdulrahman Yarali, Murray State University, USA
Mehmet Erkan Yüksel, Istanbul University, Turkey
Pooneh Bagheri Zadeh, Staffordshire University, UK
Giannis Zaoudis, University of Patras, Greece
Liaoyuan Zeng, University of Electronic Science and Technology of China, China
Rong Zhao, Detecon International GmbH, Germany
Zhiwen Zhu, Communications Research Centre, Canada
Martin Zimmermann, University of Applied Sciences Offenburg, Germany
Piotr Zwierzykowski, Poznan University of Technology, Poland

CONTENTS

pages: 111 - 119

Bare PC SIP User Agent Implementation and Performance for Secure VoIP

Roman Yasinovskyy, Towson University, USA
Andre Alexander, Towson University, USA
Alexander Wijesinha, Towson University, USA
Ramesh Karne, Towson University, USA

pages: 120 - 130

Blocking Performance of Multi-rate OCDMA PONs with QoS Guarantee

John S. Vardakas, University of Patras, Greece
Ioannis D. Moscholios, University of Peloponnese, Greece
Michael D. Logothetis, University of Patras, Greece
Vassilios G. Stylianakis, University of Patras, Greece

pages: 131 - 140

Analysis of a MAC Layer Covert Channel in 802.11 Networks

Ricardo Goncalves, CINA, Portugal
Murali Tummala, Naval Postgraduate School, USA
John McEachen, Naval Postgraduate School, USA

pages: 141 - 152

A framework for the design, development and evaluation of Cognitive Wireless Sensor Networks

Alvaro Araujo, Universidad Politecnica de Madrid, Spain
Elena Romero, Universidad Politecnica de Madrid, Spain
Javier Blesa, Universidad Politecnica de Madrid, Spain
Octavio Nieto-Taladriz, Universidad Politecnica de Madrid, Spain

pages: 153 - 162

Understanding Internet User Behavior: Towards a Unified Methodology

Christina Lagerstedt, Acreo AB, Sweden
Andreas Aurelius, Acreo AB, Sweden
Olle Findahl, World Internet Institute, Sweden
Hemamali Pathirana, Acreo AB, Sweden
Claus Popp Larsen, Acreo AB, Sweden

pages: 163 - 172

Using Network Proximity for Context-aware Browsing

Dmitry Namiot, Lomonosov Moscow State University, Russia
Manfred Sneps-Sneppe, Ventspils University College, Latvia

pages: 173 - 187

Inter-domain Peering and Overlay Topologies Support for Content-Aware Networks Dedicated to Multimedia Applications

Eugen Borcoci, University POLITEHNICA of Bucharest, Romania

Radu Dinel Miruta, University POLITEHNICA of Bucharest, Romania
Serban Georgica Obreja, University POLITEHNICA of Bucharest, Romania

pages: 188 - 203

PAPR Reduction of OFDM Signals using Gradual Projection Active Constellation Extension and Sequential Block Grouping Tone Reservation Hybrid Scheme

Eugen Victor Cuteanu, Politehnica University, Faculty of Electronics and Telecommunications, Romania
Alexandru Isar, Politehnica University, Faculty of Electronics and Telecommunications, Romania

pages: 204 - 215

Application of Control theory to a Commercial Mobile Service Support System

Payam Amani, Dept. of Electrical and Information Technology, Lund University, Sweden
Bertil Aspernäs, Ericsson AB, Sweden
Karl Johan Aström, Dept. of Automatic Control, Lund University, Sweden
Manfred Dellkrantz, Dept. of Automatic Control, Lund University, Sweden
Maria Kihl, Dept. of Electrical and Information Technology, Lund University, Sweden
Gabriela Radu, Lund University, Sweden
Anders Robertsson, Dept. of Automatic Control, Lund University, Sweden
Andreas Torstensson, Ericsson AB, Sweden

pages: 216 - 228

The MoSaKa QoS System: Architecture and Evaluation

Philipp Drieß, Ilmenau Technical University, Germany
Florian Evers, Ilmenau Technical University, Germany
Markus Brückner, Ilmenau Technical University, Germany

pages: 229 - 238

Throughput, Stability and Fairness of RFID Anti-Collision Algorithms with Tag Cooperation

Ramiro Sámano-Robles, Instituto de Telecomunicações, Portugal
Atilio Gameiro, Instituto de Telecomunicações, Portugal

pages: 239 - 251

Information Content of Very High Resolution SAR Images: Study of Dependency of SAR Image Structure Descriptors with Incidence Angle

Corneliu Octavian Dumitru, German Aerospace Center (DLR), Germany
Mihai Datcu, German Aerospace Center (DLR), Germany

pages: 252 - 263

Efficient Forwarding Approach on Boundaries of Voids in Wireless Sensor Networks

Mohamed Aissani, Ecole Militaire Polytechnique (EMP), Algeria
Sofiane Bouznad, Ecole Militaire Polytechnique (EMP), Algeria
Salah-Eddine Allia, Ecole Militaire Polytechnique (EMP), Algeria
Abdelmalek Hariza, Ecole Militaire Polytechnique (EMP), Algeria

pages: 264 - 273

Carrier Phase Discrimination for a Common Correlation Interval GNSS Receiver Architecture

Pedro A. Roncagliolo, Universidad Nacional de La Plata, Argentina
Javier G. Garcia, Universidad Nacional de La Plata, Argentina
Carlos H. Muravchik, Universidad Nacional de La Plata, Argentina

pages: 274 - 283

Maximal Rate of Mobile Wireless Optical Link in Indoor Environment

Nicolas Barbot, Xlim C2S2 UMR CNRS 7252 University of Limoges, France

Seyed Sina Torkestani, Xlim C2S2 UMR CNRS 7252 University of Limoges, France

Stephanie Sahuguede, Xlim C2S2 UMR CNRS 7252 University of Limoges, France

Anne Julien-Vergonjanne, Xlim C2S2 UMR CNRS 7252 University of Limoges, France

Jean-Pierre Cances, Xlim C2S2 UMR CNRS 7252 University of Limoges, France

pages: 284 - 296

Reliable JPEG Image Transmission Using Unequal Error Protection with Modified Non-Binary Turbo Codes

Tulsi Pawan Fowdur, Universtiy of Mauritius, Mauritius

Yashvin Beni, University of Mauritius, Mauritius

Bare PC SIP User Agent Implementation and Performance for Secure VoIP

Roman Yasinovskyy, Andre L. Alexander, Alexander L. Wijesinha, and Ramesh K. Karne

Department of Computer & Information Sciences

Towson University

Towson, MD 21252

USA

e-mail: {ryasinovskyy, aalexander, awijesinha, rkarne}@towson.edu

Abstract—Bare PC systems, which run applications without using any operating system (OS) or kernel, are immune to attacks targeting a specific OS. They also perform better than conventional systems due to their reduced overhead. We describe the design, implementation and performance of a SIP user agent (UA) for secure VoIP on a bare PC system. In particular, we discuss SIP functions and message handling, and CPU tasking. We also give details of the UA design and code that enable a lean implementation of SIP to be intertwined with the network protocols needed for secure VoIP on a bare PC softphone. The interoperability of the bare PC SIP UA is verified by conducting tests using OS-based as well as bare PC SIP servers and UAs. We also study bare PC SIP UA performance by comparing timings for key SIP UA operations for the bare PC softphone with timings for a compatible Linux softphone. The results show that processing times for the SIP register and invite operations for the bare PC SIP softphone are significantly less than the corresponding times for the Linux softphone regardless of whether a bare PC or a Linux-based SIP server is used. Finally, we propose a simple security extension to SIP authentication that enables the session key exchange for media protection to be encrypted without incurring the overhead of TLS or IPsec. Bare PC SIP softphones can be used for building secure and efficient VoIP systems that do not require any OS support.

Keywords—bare PC; SIP implementation; SIP performance; SIP user agent; VoIP; VoIP security.

I. INTRODUCTION

The session initiation protocol (SIP) is a general-purpose protocol that can be used for video conferencing, instant messaging and gaming. However, its primary use today is in VoIP systems, where it serves as a support protocol for registering and locating users, and for call set up and management. Conventional SIP implementations in servers and softphones require the support of an operating system (OS) such as Windows or Linux, or some form of an OS kernel. SIP phones are also frequently implemented in hardware/firmware typically with an embedded OS. The SIP implementations in OS-based systems take advantage of their rich supporting environment and capabilities, and are convenient to use.

Bare PC systems (also known as bare machine computing systems) enable self-supporting applications to run directly on the hardware of an ordinary PC (desktop or laptop) without using an OS or kernel. A bare PC provides immunity against OS-based attacks, and bare PC applications perform better than applications running on conventional systems due to the elimination of OS overhead.

We describe the design, implementation and performance of a SIP user agent (UA) for secure VoIP on bare PC systems. The SIP UA is integrated with the bare PC softphone application. In [1], the design and implementation of a SIP server and UA for VoIP on a bare PC were described. However, that study did not consider UA performance or the elimination of additional protocols such as TLS or IPsec to secure the key exchange over SIP to protect the VoIP call. Other studies [2], [3] dealt extensively with bare PC SIP server (but not SIP UA) implementation and performance. This paper extends [1] by 1) providing software design and code details for the UA to illustrate protocol intertwining; 2) presenting performance data in the form of timings for key SIP operations on the UA that are compared with timings on a compatible Linux-based SIP softphone; and 3) proposing a simple security extension to SIP/SDES authentication that enables the key exchange for media protection (via SRTP) to be encrypted using AES without incurring the overhead of any additional protocols.

The design details and code snippets for the bare PC SIP UA provided here help in understanding how the lean implementation of SIP is intertwined with the other necessary network protocols in the self-supporting bare PC environment with no OS or kernel resulting in improved performance of the UA compared to OS-based SIP UAs. This paper only focuses on the implementation, performance, and security aspects of the bare PC SIP UA since bare PC SIP server implementation and performance are discussed in detail in [3].

In secure environments, an OS-based full SIP implementation may not be needed and a lean implementation of SIP on a bare PC is useful due to the low overhead and inherent immunity of the application against attacks targeting vulnerabilities in a typical OS such as Linux or Windows. Compared to their OS-based counterparts, bare PC systems also have reduced code complexity and code size, making it easier to analyze the code and fix security

flaws. Moreover, bare PC systems have fewer avenues open for attackers to exploit since they only provide essential functionality and services. The low overhead and performance improvements of bare PC applications compared to applications on conventional systems are due to using direct interfaces to the hardware, fewer context switches, application-specific optimizations, efficient inter-layer communication, and streamlined versions of the necessary protocols and drivers.

As with other bare PC applications, the SIP UA implementation and interfaces to the hardware constitute a single self-supporting executable, implements only the essential elements of SIP and is UDP-based. The bare PC SIP UA and softphone application currently runs on an IA32 (Intel Architecture 32-bit) or Intel 64-bit architecture in 32-bit mode.

The rest of this paper is organized as follows. In Section II, we briefly survey related work. In Section III, we give an overview of bare machine computing. In Section IV, we describe the bare PC SIP UA software design and operations. In Section V, we give details of the UA implementation and provide some code snippets. In Section V, we describe testing scenarios, and in Section VI, we give UA performance data for bare PC and Linux-based SIP UAs. In Section VIII, we propose a modification to SIP authentication for protecting session key exchange for media protection, and in Section IX, we present the conclusion.

II. RELATED WORK

There are numerous implementations of conventional SIP servers and SIP softphones on various OS platforms. These SIP servers and UAs run on conventional OSs. In [4], a SIP server is implemented on top of an existing SIP stack. In [5], SIP servers and SIP UAs are implemented on the Solaris 8 OS. A client-side SIP service offered to all applications based on a low-level SIP API is described in [6]. In [7], the features of a new language StratoSIP for programming UAs that can act respectively as a UA server to one endpoint and as a UA client to another are presented. In [8], the UA is a SIP-based collaborative tool implemented by using existing SIP and SDP stacks. In [9], a Java-based SIP UA is proposed for monitoring manufacturing systems over the Internet. The focus of [10] is a SIP adaptor for both traditional SIP telephony and user lookup on a P2P network that does not have a SIP server. The goal of such SIP servers and SIP UAs is to offer enhanced services to clients by using existing low-level SIP stacks that rely on an OS. In contrast, bare PC SIP servers and UAs that are implemented directly on the hardware will have less overhead and are more suited for secure low-cost environments.

Intertwining bare PC Web server or email server application and application protocols (i.e., HTTP or SMTP) with the TCP protocol contributes to its improved performance over OS-based servers [11], [12]. In [2] and [3], the performance of a bare PC SIP server is compared with that of OS-based servers, and it is shown that the bare PC SIP server performs better except in a few cases. The SIP server performance studies did not discuss the SIP UA design details or its implementation. The design,

implementation, and performance of a bare PC softphone for peer-to-peer communication are discussed in [13] and [14]. However, the softphone does not support SIP and does not incorporate a UA of any kind; hence it lacks the ability to communicate with SIP servers and other SIP softphones. Details of the SIP protocol itself are given in [15].

III. BARE MACHINE COMPUTING

Bare PC application development is based on the bare machine computing paradigm, also referred to as the dispersed operating system (DOS) paradigm [16]. In this paradigm, a single self-supporting application object (AO) encapsulating all of the necessary functionality for a few (typically one or two) applications executes on the hardware without an OS. Bare machine applications only use real memory; a hard disk is not used. The AO, which is loaded from a USB flash drive or other portable storage medium, includes the application and boot code.

The application code is intertwined with lean implementations of the necessary network and security protocols. If required by the application, the AO also includes cryptographic algorithms, as well as network interface and other device drivers, such as an audio driver in case of the bare PC softphone. The interfaces enabling the application to communicate with the hardware [17] are also included in the AO. The AO code is written in C++ with the exception of some low-level assembler code. The AO itself manages the resources in a bare machine including the CPU and memory. For example, every bare PC AO has a main task that runs whenever no other task is running, and network applications require a Receive (Rcv) task that handles incoming packets. Additional tasks may be used depending on the applications included in the AO, such as an audio task for the bare PC softphone.

IV. BARE PC SIP UA SOFTWARE DESIGN

The software design of the bare PC SIP UA is simple and modular. It manages data associated with log in, dialing, incoming and connected calls, media IP address and port, and STUN state [18]. The main data structures in the SIPUA object are `phone_book`, `media`, `call_session`, `configuration`, `call_log`, and `via_headers`. The `call_log` struct with some of its fields is shown in Figure 1. For each char array, an int variable is used to store its actual size. For example, `int call_id_size` stores the size of the char array `call_id`.

In addition, the SIPUA object defines numerous constants, variables, and arrays. These are used to store UA timers, counters, tags, authentication data, menu controls, and user account information. As in all bare PC applications, a TCB table [3], [11] is used to store information such as addresses and ports needed to process incoming packets.

The SIP UA code and methods are designed based on the various states the UA can be in. Since there is no OS or conventional protocol stack, the self-supporting SIP UA application itself sends and responds to messages using the necessary protocols. This requires that the UA manage memory, CPU and task scheduling without any OS support. All memory is real and mapped statically, i.e., there is no provision to load any modules dynamically at run-time,

which significantly increases security of the SIP UA and prevents attackers from gaining access to other parts of memory or execute code other than the legitimate SIP application itself.

```

struct call_log
{
    int phone_state;
    int app_state;
    char call_id[70];
    char cseq[5];
    char password[20];
    char account_name[20];
    char account_domain[20];
    char account_ip[16];
    char account_port[6];
    char media_ip[16];
    char media_port[6];
    char call_tag[100];
    char callee[40];
    char callee_sip_ip_text[16];
    unsigned int callee_sip_port_hex;
    unsigned int callee_media_port_hex;
    int srtp; int srtp_match;
    int originator; struct configuration config;
    ...
};

```

Figure 1. Example of a UA Data Structure

Excluding methods for booting and loading the UA code from a USB flash drive (or other portable media), other “low-level” methods that are common to all bare PC applications, and the method that runs the Main task, the remaining methods of the SIP UA consist of those that initialize the UA, display menus and call state, and interact with the user via keyboard, and methods that implement key SIP functionality. The primary user data and SIP state are contained in char arrays and pointers, and the method parameters enable the data to be accessed and manipulated based on SIP messages that are received including REGISTER, INVITE, and BYE. Authentication is enabled by default, but can be turned off by the user prior to making a call.

In Figure 2, SIP UA method declarations appearing in the SIPUA.h file and their parameters are shown. It can be seen that method parameters reference user account, and IP address and port number information, as well as SIP/SDP headers and tags in incoming and outgoing messages. In addition, the local data structures referred to earlier are directly manipulated by these methods. The methods instantiate other objects such as DHCP, STUN, and SRTP [19] together with the usual RTP, UDP, IP, and Ethernet objects used for network communication. Keyboard input and screen output is done via special bare PC interfaces that are used by all bare PC applications. Although the bare PC SIP implementation is lean, it requires strict adherence to the SIP protocol specifications given in [15] in order to communicate with both OS-based and bare PC SIP servers and UAs. From a security viewpoint, the code is simpler and there are no hidden dependencies on external libraries or code other than that of the SIP UA application itself. The elimination of OS or kernel code and external dependencies enables only functionality that is essential to the SIP

application to be implemented, which simplifies code analysis and detection of vulnerabilities.

Figure 3 shows the call flow relationships among the key methods in the UA. The method parameters and return types are omitted since they were specified in Figure 2. It can be seen that several methods in the UA are also used by the SIP server [3]. These include siphandler, sipsenddata, format_sip_response, parse_headers, copy_tag_line, create_packet, copy_sip_request, create_response_packet, and generate_sip_response, and several methods that are used to parse tags. The main difference between the SIP server code and the UA code is that the server also contains code to manage the database storing registration and authentication information for users. In contrast, the UA contains code to process SIP authentication (i.e., handle the SDP challenge/response messages), secure the VoIP media stream via SRTP, and provide the user interface via menus and keyboard input.

When the UA is booted, sipuainit and sipuser_init are used to initialize the UA and store user information respectively; generate_sip_response sets up memory for the packet to be sent and calls sipsenddata; sipsenddata in turn calls format_sip_response to construct the SIP message, and then calls the relevant methods in the UDP, IP, and Ethernet objects to construct the necessary protocol headers and send the packet; format_sip_response constructs the SIP message in the following cases: received INVITE, TRYING, RINGING, ACK, BYE, OK, UNAUTHORIZED, or PROXY_AUTH; or sent INVITE, RINGING, REGISTER, ACK, BYE, DECLINE, BUSY, or REGISTER_LOGOUT.

As shown in Figure 3, when a packet is received, siphandler calls parse_headers to determine the type of the received SIP message, and then calls handle_session to retrieve or store state information, followed by generate_sip_response to construct the response; parse_headers in turn calls several methods to parse tags including copy_tag_line, parse_from_to_tag, and parse_call_id_tag; copy_sip_request, create_packet, and create_response_packet are used to create SIP packets; parse_authenticate is used to parse an authentication challenge and compute an authentication response; route_packet method is used to determine whether the packet can be delivered directly or whether it needs to be sent to the default gateway; and shout_or_route is called directly from the main task for start-up, displaying menus, registering the user, and initiating calls. SIPUA also includes methods for displaying menus and submenus, switching screens, and quick dialing.

After shout_or_route is called as above and the user is registered, the user can initiate a new call. Incoming calls are handled as follows. When the Rcv task receives a UDP message containing a SIP Invite, the main task activates a SIP task. Then siphandler is invoked and the SIP responses (TRYING and RINGING) are sent by using the relevant methods in the SIPUA application as described above. When a SIP response message such as an ACK or 200 OK is received, the TCB entry is used to retrieve the information needed to process the message.

Figure 4 shows the relationship between protocols and the Main, Rcv and SIP tasks in the SIP UA. Tasks handling audio processing [14] are not shown here. All upper layer protocols use UDP/IP/Ethernet and SRTP uses RTP. Incoming UDP packets are handled by the Rcv task regardless of the upper layer protocol. The SIP task handles SIP processing that is initiated by siphandler, and passes control back to the main task after sipseendata terminates.

```

unsigned short get_destsipport (char *data_array, int size);
void sipuinit();
int route_packet(char *source_ip, char *dest_ip, char *subnet_mask,
char *dest_mac);
void shout_or_route();
void siphandler(char *packet_array, int packet_size);
int create_packet (char *cat_array, char *data_array, int datasize);
int parse_headers (char *data_array, int size_array);
int parse_call_id_tag (char *data_array, char *tag_line, int start);
int parse_from_to_tag (char *data_array, int start, int end,
char *account_name, int account_name_size, char *account_domain,
int account_domain_size);
void generate_sip_response(char *data_array, int response);
void sipseendata(char *cptrl, long lnPtr, char *data_array, int response);
int format_sip_response(char *send_buffer, char *data_array, int
response);
int create_response_packet (char *cat_array, char *data_array, int
datasize);
int copy_sip_request (char *cat_array, char *data_array, int
new_data_size, int datasize, int enddatasize);
int copy_tag_line (char *data_array, char *tag_line, int start, int end);
int get_ip(char *data_array, int start, int end);
char parse_sdp_ip(char *ip_address_string, int size, int octet);
void parse_sdp_media(char *data_array, int start, int end);
void parse_sdp_attribute(char *data_array, int start, int end);
int parse_crypto_tag (char *data_array, int start);
int parse_encrypt_tag (char *data_array, int start);
int text_ip(char *data_array, int end, char *hex_ip);
int handle_session(char *address_name, int address_name_size, char
*address_domain, int account_domain_size, int type);
int int_text(int i, char *port_string);
int check_media();
void init_sdp_media();
void reset_values();
void sipuser_init();
void sipserver_init(int flag);
void parse_authenticate(char *data_array, int start, int end);
int parse_cseq_tag (char *data_array, int start, int end);
int parse_expires_tag (char *data_array, int start, int end);
int parse_contact_tag (char *data_array, int start, int end);
void clear_all_menus(int type);
void header_label();
void footer_label(int type);
void middle_label();
void call_connected_menu();
void incoming_call_menu();
void selected_item(int type);
void button_press();
int wait_timer(int type);
void switch_screen();
void main_start_menu();
void sub_main_menu();
void sub_quick_dial_menu(int type);
void sub_phone_config_menu();
void sub_stun_menu();
void sub_ip_config_menu();
    
```

Figure 2. SIP UA methods and parameters

V. BARE PC SIP UA IMPLEMENTATION

The bare PC SIP user agent (UA) is integrated with the bare PC softphone enabling calls to be set up. Its operational characteristics are similar to those of a SIP UA in a conventional OS-based SIP softphone. However, the UA implementation is different due to the absence of an OS and a built-in protocol stack, and results in a UA with less overhead and better security. The UA can also directly communicate with a peer on a local network (without using a SIP server).

A. UA Operation/User Interface

As in the case of the bare PC SIP server, only two tasks Main and Rcv are needed for the UA, and arriving SIP messages and responses are processed in a single thread of execution as described earlier. When the UA is booted, if an IP address for the UA has not been preconfigured, the UA sends out a request for an IP address and obtains one using DHCP. If this is a private address, the UA is behind a NAT and uses STUN [18] to learn its public IP address and port. In this case, the UA first sends a DNS request and obtains the IP address of a public STUN server. The bare PC STUN implementation is described in more detail below.

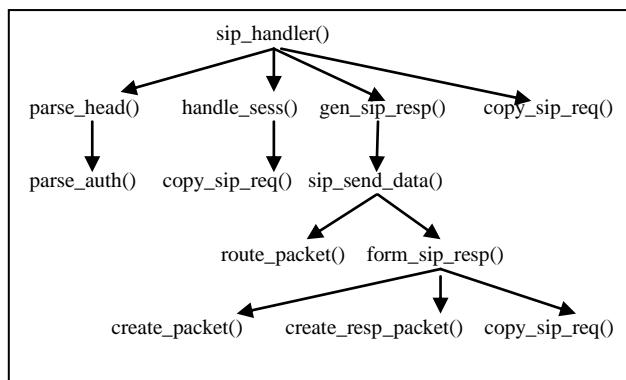


Figure 3. UA call flow relationships

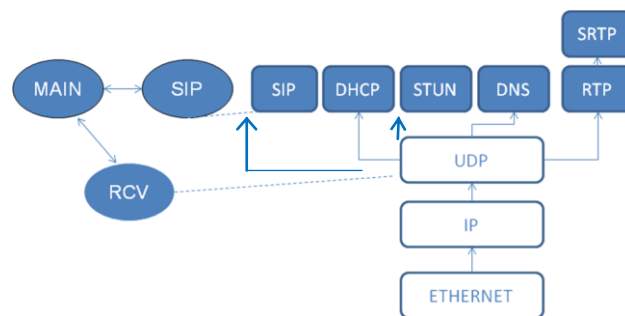


Figure 4. UA protocol/task relationships

After UA completes the initialization process it displays the main login menu, which enables the user to login-in to a particular SIP server or to communicate directly with a peer as noted earlier. In case SIP server login is selected, the UA sends a SIP Register request to the server after performing a DNS resolution if needed. Once the 200 OK messages are

received from the SIP server, the UA displays a “main menu” screen as in Figure 5. The menu has several options, which enables the user to see the IP configuration information from DHCP, and NAT mappings from STUN that show the external IP address and internal/external SIP and RTP ports for the softphone. Such information is useful to troubleshoot connectivity problems. In addition, a separate option shows call status and connectivity information, and indicates whether security is on. A “quick dial” option for selecting specific users is also available.



Figure 5. UA Main Menu Screen.

The essential UA functionality contained in the SIPUA object consists of about 3000 lines of C++ code. This object is supplemented by 1) objects for cryptographic and other algorithms needed for key establishment (HMAC, SHA-1, MD5, AES, and Base64); 2) objects implementing the essential elements of the necessary auxiliary protocols (STUN, DHCP, and DNS); and 3) objects needed by the bare PC softphone including the Ethernet, IP, and UDP objects, the RTP, audio, and G.711 objects that handle voice data processing, recording, and playback on the bare PC softphone, and the SRTP object [19] that provides VoIP media security. The SRTP protection is optional and can be turned off. However, the additional overhead due to using SRTP is low [20].

B. User Agent Client and User Agent Server

The bare UA consists of two independent components: the SIP user agent server (UAS) and SIP user agent client (UAC). The UAS is operationally similar to the bare PC SIP server with respect to its handling of SIP packets. For example, it listens for call requests and its actions are activated by the Rcv task when a packet arrives as discussed earlier for the case of the SIP server. The UAC can be activated by keyboard input. The UA functionality is contained in a SIPUA object that is responsible for processing SIP messages and SDP tags, displaying the SIP UA interface, and interacting with the user. The SIPUA object is integrated in a single AO with several other objects needed to implement the UA.

C. STUN/DHCP/DNS/SRTP

The public IP address and port learned from the public STUN server is used in SIP Invite requests to enable the peer to communicate with the UA behind the NAT. The bare PC SIP UA sends out multiple STUN messages to find the external port for its voice channel over RTP. Since the

signaling channel is proxied through the SIP server, STUN is not needed to discover the external SIP signaling port. After the bare PC client is booted, STUN messages for the media channel are sent every 30 seconds until the SIP UA establishes the call. The Invite message contains the last known media channel external port number. Since the NAT binding may change, the UA sends voice packets to the destination host using a sequence of consecutive ports. The UA stops sending on the other ports once voice packets are received on a particular port.

The bare PC SIP UA also needs to send DHCP messages to automatically obtain an IP address and other essential configuration information at start-up. Since there is no OS and no built-in protocol stack on the bare PC softphone, a lean implementation of DHCP is used. The DHCP messages follow the typical DHCP call flow (Discover, Offer, Request, and Ack). The softphone can also send DNS requests to resolve the domain name of the SIP or STUN server. As noted earlier, the implementation of the DHCP and DNS protocols have only the minimal features needed by the bare PC SIP softphone.

The bare PC SIP UA is also integrated with SRTP. The implementation and performance of SRTP on a bare PC softphone are presented in [20]. SRTP allows the UA to communicate securely with conventional SIP UAs that are SRTP capable. The bare PC softphone AO includes implementations of SHA-1, MD5, HMAC, and AES in counter mode, which are used by SRTP. The bare PC SRTP implementation also supports addition of a recommended authentication tag to the end of the RTP packet. The UA currently implements the SDP Offer/Answer model via SDES for key exchange. This method is used by several conventional SRTP clients. The keys used to generate the session keys are Base64 encoded by the bare PC softphone prior to transmission. Since this approach for transmitting keys is not secure, a more secure alternative is described in Section VIII.

D. Protocol Intertwining

An essential component of the bare PC SIP UA application is code that intertwines the necessary network protocols with the SIP UA application code. Since there is no protocol stack and a distinction between user space and kernel space as in a conventional OS-based system, it is necessary to provide methods that can directly instantiate objects of other protocols and invoke their methods. To illustrate this idea, we consider two methods in the SIPUA object: `generate_sip_response` and `sipsenddata` in Figs. 6 and 7. Comments and code lines unessential to the present discussion are not shown.

In Figure 6, the SIPUA object instantiates the bare PC Ethernet object `EtherObj`. This enables the UA to access the Ethernet buffer directly, which significantly reduces overhead. It can be seen that addresses and memory in the bare PC are directly manipulated by the SIPUA. Such “hardcoding” makes the SIP UA code more secure: it is more difficult for an attacker to perform standard buffer manipulations since different bare PC SIPUAs can use a

different memory layout. The last action of the generate_sip_response method is to invoke sipseendata.

In Figure 7, the code for the sipseendata method is shown. This code illustrates how the SIP UA directly instantiates the necessary protocol and “lower layer” objects: DHCP, UDP, IP, and Ethernet. The method calls route_packet, which calls ARP to find the MAC address, then calls format_sip_response to create the correct SIP response (depending on the current state determined by a received SIP message such as an INVITE), and finally sends the data via a call to UDP. Again, it can be seen that header sizes are “hardcoded”, which improves security, and that direct invocation of the necessary protocols eliminates the overhead of interlayer communication and context switching that would be present in a conventional OS-based system.

VI. TESTING

Operational tests of the bare PC SIP server and SIP softphone implementations with and without authentication and SRTP security were conducted using Dell GX-260 desktops with Intel Pentium 4 2.4 GHz processors, 1.0 GB RAM, and a 3COM Ethernet 10/100 PCI network card. The test network consists of a dedicated LAN within the Towson University network, and an external network connected through an ISP as shown in Figure 8. The bare PC SIP server and user agents were first tested within the dedicated LAN. Testing was performed to verify 1) correct operation between the bare PC SIP server and bare PC SIP softphones; 2) interoperability of bare PC SIP softphones with the OpenSer v3.0.0 server [21]; 3) interoperability of the bare PC SIP server with Linphone 2.1.1 [22] and Snom360-5.3 softphones [23]; and 4) interoperability of bare PC SIP softphones with the Linphone and Snom softphones.

```
void SIPUAObj::generate_sip_response(char *data_array, int response)
{
    EtherObj EO;
    char *sip_send_buffer;
    long *p1;
    long cb;
    char ca;
    long InPtr = 0;
    long x = 0;

    p1 = &cb;
    sip_send_buffer = &ca;

    x = EODownListPointer + EO.SendInPtr * 32 + 8 - ADDR_OFFSET;

    p1 = (long*)x;
    sip_send_buffer = (char*) *p1;

    InPtr = EO.SendInPtr;
    EO.SendInPtr++;
    if (EO.SendInPtr == EO.SndLstSize)
    {
        EO.SendInPtr = 0;
    }
    sip_send_buffer = sip_send_buffer + 14 + 20 + 8 - ADDR_OFFSET;

    sipseendata(sip_send_buffer, InPtr, data_array, response);
}
```

Figure 6. Code to generate a SIP response

```
void SIPUAObj::sipseendata(char *cptr1, long InPtr, char *data_array,
int response)
{
    static int jj = 0;
    EtherObj EO;
    UDPObj udp;
    DHCPObj dhcp;
    IPObj ip;
    char *send_buffer;
    char c1;
    send_buffer = &c1;
    int retcode = 0;
    int SIPPack_size=0;

    //call route packet to get proper mac
    route_packet(dhcp.ip_data.ip_address, SIPDestIP, dhcp.ip_data.subnet,
SIPDestMac);

    send_buffer = cptr1;

    //format_sip_response creates the SIP response packet
    SIPPack_size = format_sip_response(send_buffer, data_array,
response);

    send_buffer = send_buffer - 8; //8 byte UDP header
    retcode = udp.FormatDHCPUDPpacket(send_buffer, SIPPack_size,
udp.SIPSourcePort, udp.SIPDestPort, 0);
    SIPPack_size = SIPPack_size + 8;
    send_buffer = send_buffer - 20; //20 byte IP header
    retcode = ip.FormatIPpacket(send_buffer, SIPPack_size, SIPDestIP,
SIPDestMac, UDP_Protocol, 0);
    SIPPack_size = SIPPack_size+20;
    send_buffer = send_buffer - 14; //14 byte ethernet header
    retcode = EO.FormatEthPacket(send_buffer, SIPPack_size, IP_TYPE ,
SIPDestMac, InPtr, 0x04, 0);
    SIPPack_size = SIPPack_size+14;
}
```

Figure 7. Code to send a SIP message

Similar tests were conducted over the Internet by establishing calls between a softphone on the external network and another on the dedicated LAN when the SIP servers are connected to the LAN. These tests also served to verify that the UA and the lean DHCP, STUN, and DNS implementations on the bare PC SIP softphone work correctly when it is connected to the Internet. In particular, the bare PC STUN implementation was found to be adequate for connecting between clients behind NATs on the dedicated test LAN and on an ISP network.

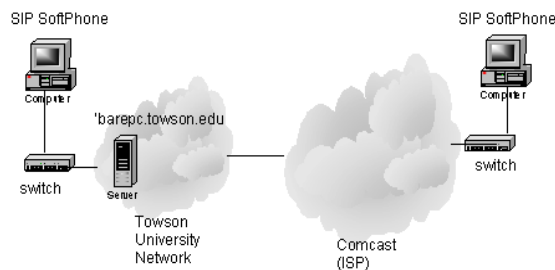


Figure 8. Test Network.

VII. SIP UA PERFORMANCE

To evaluate performance of the SIP UA, experiments were conducted using a 100 Mbps Ethernet test LAN consisting of two SIP UA client machines and a SIP server. All machines were Dell GX260 with Intel Pentium 4 (2.4 GHz), 1.0 GB RAM, and 3COM Ethernet 10/100 PCI network cards. The OS-based (non-bare) machines ran Linux CentOS 5.6 (2.6.18). The non-bare SIP server and SIP UA used were OpenSER 1.3.4 [21] and Linphone 2.1.1 [22] respectively.

Times to complete each of the four SIP message exchanges corresponding to REGISTER, INVITE, SESSION OK and BYE as shown in Figure 9 were measured by capturing the relevant packets using Wireshark 1.5.0 [24]. Each exchange was repeated several times to ensure that the measurements were stable.

The results are shown in Figs. 10-12. In Figs. 10 and 11, Linux SIP UAs are connected to a bare PC or Linux SIP server. The times for completing REGISTER in each case are seen to be highest compared to the other SIP exchanges. In Figs. 12 and 13, bare PC SIP UAs are connected to a bare PC or Linux SIP server. The times to complete all exchanges except for SESSION OK are much smaller for the bare PC SIP UA than for the Linux SIP UA. For both UAs, it does not make much difference whether a Linux or bare PC SIP server is used. For the REGISTER and INVITE exchanges in particular, it can be seen that the time for the bare PC SIP UA is less than 1 ms, whereas the Linux SIP UA averages 67 ms and 15 ms respectively. As expected, the BYE exchange takes negligible time for both SIP UAs. The excessive time taken by the bare PC SIP UA for the SESSION OK exchange (compared to the Linux SIP UA) is due to processing the media stream prior to sending the ACK. This time could be reduced by only processing SIP messages in this case as done by the Linux SIP UA.

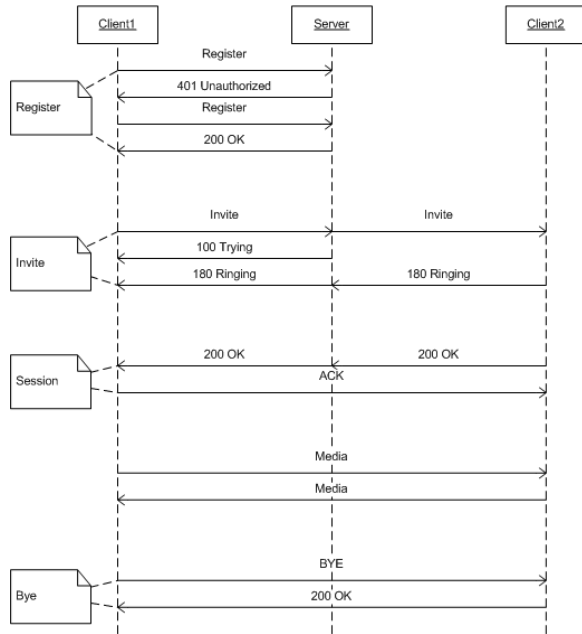


Figure 9. SIP message exchanges

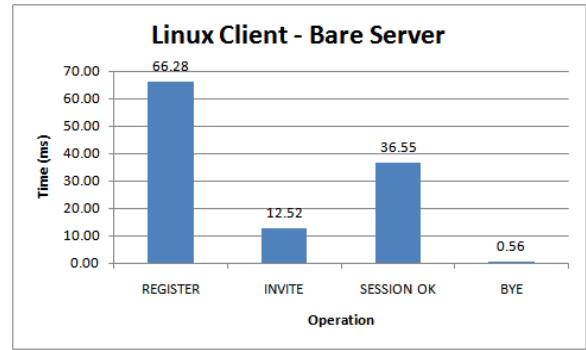


Figure 10. SIP message processing time (Linux client/bare server)

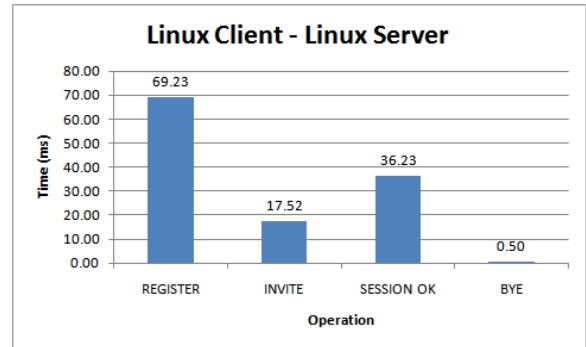


Figure 11. SIP message processing time (Linux client/Linux server)

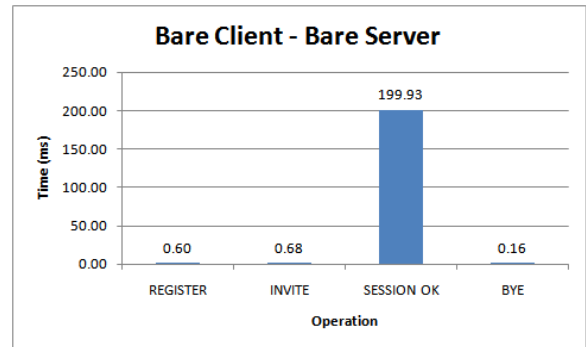


Figure 12. SIP message processing time (bare client/bare server)

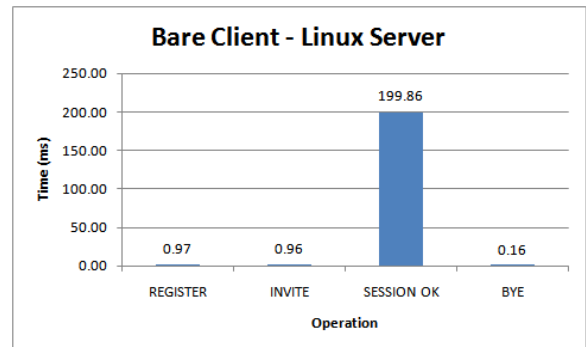


Figure 13. SIP message processing time (bare client/Linux server)

VIII. SECURE KEY EXCHANGE

Security is an important aspect of VoIP. First, the caller and callee must be authenticated; and second, the voice packets must be encrypted and their integrity needs to be ensured. SRTP provides a standardized convenient method to achieve these requirements. Since SRTP does not mandate a specific key exchange method, a variety of methods are used in practice. A common approach used by many softphones is to use TLS to protect the SRTP key exchange. However, TLS key establishment is expensive and the handshake requires TCP. This means significant overhead and delay may be incurred prior to the beginning of a call before voice packets secured by SRTP can be exchanged. A low overhead alternative is to send Base64-encoded SIP/SDES messages to exchange the SRTP keys [20]. Unfortunately, this method is not useful from a security viewpoint. We describe below a simple modification using SIP/SDES that significantly enhances security without incurring the penalty of TLS.

The proposed key exchange technique is an adaptation of a technique that is frequently used for establishing a shared encryption key between clients when a trusted key server is available. We assume that the local SIP servers S1 and S2 associated with the caller and callee are trusted, and that S1 and S2 pre-share secrets s1 and s2 respectively with the caller and callee. For convenience, we also assume that these secrets are the respective passwords used for SIP registration and authentication by the caller and callee (or derived from the passwords), and that the caller and callee share the same SIP server S i.e., $S1=S2=S$. The technique is easily extended when the caller and callee have different SIP servers S1 and S2 (provided that S1 and S2 have a secure pre-established channel or an IPsec tunnel between them to encrypt the payload of any messages exchanged between them).

At most one new message is required when using this technique to secure the SRTP key exchange. It works as follows. Whenever a SIPUA initiates a call with authentication, the usual challenge/response technique requires that a nonce be generated by the SIP server and sent to the SIPUA in order to verify that the SIPUA has the correct password/secret (see Section IV). If two nonces instead of one are sent by the SIP server, the second nonce can be used as a seed for the TLS PRF (pseudorandom function) [25] in order for the SIP server and SIPUA to generate a common AES encryption key of length 128, 192 or 256 bits for encrypting SIP/SDES messages. The TLS PRF uses the following data expansion function:

$$P_hash(secret, seed) = HMAC(secret, A(1)||seed) || HMAC(secret, A(2)||seed) || \dots$$

Here $||$ denotes concatenation. HMAC can use any one-way hash function such as MD5, SHA-2 or SHA-3, and $A(i)=HMAC(secret, A(i-1))$ for $i \geq 1$ with $A(0)=seed$. For a 128-bit AES key, the TLS PRF needs to be iterated only once with either an MD5 or SHA-2 hash; for a 256-bit key, at most two iterations are needed depending on the hash size. This technique enables the SIP server and the SIPUA at the caller and callee respectively to compute common AES keys k1 and k2 of desired lengths. The SIP server can now

exchange messages with the caller and callee that are encrypted with the keys k1 and k2 respectively. In particular, the server can send a message encrypted with the key k2 that transfers the key k1 to the callee. The key k1 can then be used by the caller and callee to encrypt the SIP/SDES SRTP key exchange over UDP/IP without incurring the overhead of a TCP connection or an expensive TLS handshake. Since implicit authentication based on knowledge of a pre-shared key is used instead of verifying a certificate as in TLS, the proposed technique trades off reduced security for less overhead.

In effect, the single message used to authenticate a SIPUA also serves to transfer the extra nonce for generating an AES key. The only additional cost is the cost to transfer an extra nonce within this message, which should be insignificant, and the cost of the extra message to the callee to transfer the key k1. For each call, a different AES key is generated since the nonce will be different. If the caller and callee have different SIP servers S1 and S2, it will be necessary for S1 to securely transfer the key k1 to S2 so that it can be relayed to S2. This can be done via IPsec or TLS as usual, or by use of preshared keys. In a local network, two bare PC SIP UAs can directly establish a secure VoIP call after authentication without using a SIP server. In this case, authentication is based on a preshared secret, and the preceding technique can be used for the caller and callee to generate a common AES key to encrypt the SRTP key exchange between them.

IX. CONCLUSION

We described the design, implementation, and performance of a bare PC SIP UA, which provides essential SIP functionality with less overhead and better security than a conventional OS-based SIP UA due to the absence of an OS. The underlying bare PC system enables the bare PC SIP UA to benefit from simple tasking, lean protocols, and efficient data handling.

To illustrate SIP implementation for VoIP on a bare PC, we discussed the software design and provided code snippets for sample data structures and methods of the bare PC SIP UA. In particular, we provided details about the data structures used to store information associated with the user and for setting up and managing calls. We then examined the key methods in the SIPUA and the call flow relationships among these methods.

The tests conducted show that the bare PC SIP UA can interoperate with both bare PC and OS-based SIP UAs and SIP servers. In addition, we conducted experiments to compare the performance of the bare PC SIP UA and a compatible Linux SIP softphone with respect to key SIP operations. The experimental performance results show that regardless of whether a bare PC SIP server or OS-based SIP server is used, the time for the Register and Invite operations using a bare PC SIP UA are significantly less than the time for these operations using a Linux SIP softphone.

To enhance VoIP security, we proposed a simple modification to the technique used for SIP authentication to generate an AES key for encrypting the SIP/SDES SRTP key exchange. The modification does not require any new

messages and does not incur the overhead of a TCP/TLS exchange.

The bare PC UA provides essential SIP functionality with better performance than OS-based SIP UA, and immunity from OS-based attacks due to the absence of an OS. Bare PC SIP softphones can thus be used for improving performance in VoIP networks with OS-based SIP servers and softphones, or for building secure communication systems consisting of only bare PC SIP servers and UAs.

REFERENCES

- [1] A. Alexander, A. L. Wijesinha, and R. Karne, "Implementing a VoIP SIP Server and User Agent on a Bare PC," 2nd International Conference on Future Computational Technologies and Applications (Future Computing), pp. 8-13, 2010.
- [2] A. Alexander, A. L. Wijesinha, and R. Karne, "A Study of Bare PC SIP Server Performance," 5th International Conference on Systems and Network Communications (ICSNC) pp. 392-397, 2010.
- [3] A. Alexander, R. Yasinovskyy, A. L. Wijesinha, and R. Karne, "SIP Server Implementation and Performance on a Bare PC," 5th International Journal on Advances in Telecommunications, vol. 4, no. 1 & 2, 2011.
- [4] L. Chen, and C. Li, "Design and Implementation of the Network Server Based on SIP Communication Protocol," World Academy of Science, Engineering and Technology, pp. 138-141, 2007.
- [5] S. Zeadally and F. Siddiqui, "Design and Implementation of a SIP-based VoIP Architecture," AINA, 2004.
- [6] A. Singh, A. Acharya, P. Mahadeva, and Z-Y, Shae, "SPLAT: a unified SIP services platform for VoIP applications," International Journal of Communication Systems, vol. 19, no. 4, pp. 425-444, 2006.
- [7] P. Zave, E. Cheung, G. W. Bond, and T. M. Smith, "Abstractions for Programming SIP Back-to-Back User Agents," IPTComm, 2009.
- [8] S Siddique, RK Ege, SM Sadjadi, "X-Communicator: Implementing an advanced adaptive SIP-based User Agent for Multimedia Communication," SoutheastCon, pp. 271-276, 2005.
- [9] K. J. Kim, Y. Jang, J. W. Chung, and J. H. Seo, "Design and implementation of SIP UA for a manufacturing network," International Journal of Advanced Manufacturing Techniques, vol. 28, no. 7-8, pp. 822-826, 2006.
- [10] K. Singh and H. Schulzrinne, "Peer-to-Peer Internet Telephony using SIP," International Workshop on Network and Operating System Support for Digital Audio and Video, pp. 63-68, 2005.
- [11] L. He, R. Karne, and A. Wijesinha, "The Design and Performance of a Bare PC Web Server," International Journal of Computers and Their Applications, vol. 15, pp. 100 - 112, June 2008.
- [12] G. Ford, R. Karne, A. Wijesinha, and P. Appiah-Kubi, "The Performance of a bare machine email server," 21st International Symposium on Computer Architecture and High Performance Computing, SBAC-PAD, pp.143-150, 2009.
- [13] G. H. Khaksari, A. L. Wijesinha, R. K. Karne, L. He, and S. Girumala, "A Peer-to-Peer bare PC VoIP Application," IEEE Consumer and Communications and Networking Conference (CCNC), pp. 803-807, 2007.
- [14] G. H. Khaksari, A. L. Wijesinha, R. Karne, Q. Yao, and K. Parikh, "A VoIP Softphone on a Bare PC," Embedded Systems and Applications Conference (ESA), 2007.
- [15] J. Rosenberg, H. Schulzrinne, G. Camarillo, A. Johnston, J. Peterson, R. Sparks, M. Handley, and E. Schooler, "SIP: Session Initiation Protocol," RFC 3261, 2002.
- [16] R. K. Karne, K. V. Jaganathan, T. Ahmed, and N. Rosa, "DOSC: Dispersed Operating System Computing," 20th Annual ACM Conference on Object Oriented Programming, Systems, Languages, and Applications (OOPSLA), Onward Track, pp. 55-61, 2005.
- [17] R. K. Karne, K. V. Jaganathan, and T. Ahmed, "How to Run C++ Applications on a Bare PC?" 6th International Conference on Software Engineering, Artificial Intelligence, Networking and Parallel/Distributed Computing (SNPD), pp. 50-55, 2005.
- [18] J. Rosenberg, R. Mahy, P. Matthews, and D. Wing, "Session Traversal Utilities for NAT (STUN)," RFC 5389, 2008.
- [19] M. Baugher, D. McGrew, M. Naslund, E. Carrara and K. Norrman, "The Secure Real-time Transport Protocol (SRTP)," RFC 3711, 2004.
- [20] A. Alexander, A. L. Wijesinha, and R. Karne, "An Evaluation of Secure Real-Time Protocol (SRTP) Performance for VoIP," 3rd International Conference on Network and System Security (NSS), pp. 95-101, 2009.
- [21] Kamailio (OpenSER) SIP server, [Online]. Available: <http://sourceforge.net/projects/openser> Accessed: November 12, 2012.
- [22] Linphone, [Online]. Available: <http://www.linphone.org> Accessed: November 12, 2012.
- [23] Snom VoIP phones, [Online]. Available: <http://www.snom.com> Accessed: November 12, 2012.
- [24] Wireshark, [Online]. Available: <http://www.wireshark.org> Accessed: November 12, 2012.
- [25] T. Dierks and E. Rescorla, "The Transport Layer Security (TLS) Protocol Version 1.2," RFC 5246, 2008.

Blocking Performance of Multi-rate OCDMA PONs with QoS Guarantee

John S. Vardakas*, Ioannis D. Moscholios[†], Michael D. Logothetis*, and Vassilios G. Stylianakis*

*WCL, Dept. of Electrical and Computer Engineering

University of Patras, Patras, 265 04, Greece,

Emails: {jvardakas, m-logo, stylian}@wcl.ee.upatras.gr

[†]Dept. of Telecommunications Science and Technology

University of Peloponnese, 221 00, Tripolis, Greece,

Email: idm@uop.gr

Abstract—In this paper, we propose a new teletraffic model for the calculation of blocking probabilities in an Optical Code Division Multiple Access (OCDMA) Passive Optical Network (PON) supporting multiple service-classes of Poisson traffic. OCDMA is a promising candidate of PON configuration for the provision of moderate security communications with large dedicated bandwidth to each end user. The PON accommodates multiple service-classes that are differentiated by either different data-rates or different Quality of Service levels. Parameters related to the additive noise, multiple access interference and user activity are incorporated into our analysis. Based on a two-dimensional Markov chain, we propose a recursive formula for the calculation of the number of in-service codewords, when the OCDMA PON guarantees Quality of Service (QoS), or not. To evaluate the proposed model, the analytical results are compared with simulation results to reveal that the model's accuracy is quite satisfactory.

Keywords—Passive Optical Network; Optical Code Division Multiple Access; Multiple Access Interference; Blocking Probability; Quality of Service; Parallel Mapping.

I. INTRODUCTION

The exponential growth of the Internet traffic volume and popularity of broadband applications have accelerated the demand for higher data rates. In backbone networks the capacities have been significantly increased, mainly due to the utilization of the Wavelength Division Multiplexing (WDM) with hundreds of channels in each optical fiber. On the other hand, current solutions in the access domain, such as the Digital Subscriber Line (DSL), are inadequate to deal with the growing bandwidth-hungry applications. To break the bottleneck between the access networks and the ultrahigh-speed backbone networks, high capacity and cost effective access solutions are required. The Passive Optical Network (PON) has received a tremendous attention from both academic [1] and industrial [2] communities, mainly due to the low operational cost, the enormous bandwidth offering and the absence of active components between the central office and the customer's premises.

Over the years, several standards for PONs have been evolved, in the form of the G.983 ITU-T recommendations, which include Asynchronous Transfer Mode PONs (ATM-PONs) and Broadband PONs (BPONs) [3], or in the form of

IEEE 802.3ah for the Ethernet PON (EPON) [4], etc. These PONs are based on a Time Division Multiple Access (TDMA) scheme and they typically use a 1550 nm wavelength for downstream and a 1310 nm for upstream [5]. While these TDMA-PONs employ two wavelengths for the upstream and downstream direction, respectively, the WDM-PON utilizes multiple wavelengths, so that two wavelengths are allocated to each user for down/upstream transmissions. A different approach for the provision of multiple access in PONs is the Optical Code Division Multiple Access (OCDMA). In contrast to the other multiple access schemes, OCDMA can multiplex a number of channels on the same wavelength and on the same time-slot [6]. In addition, OCDMA offers full asynchronous transmission, soft capacity on demand, low latency access, simple network control and better security against unauthorized access [7].

In OCDMA, each communication channel is distinguished by a specific optical code. At the receiver each data is multiplied by a unique code sequence either in the time domain [8], or in the wavelength domain [9], or in a combination of both (simultaneously) [10]. The decoder receives the sum of all encoded signals from different transmitters and recovers the data from a specific encoder, by using the same optical code. All the remaining signals appear as noise to the specific receiver; this noise is known as multiple access interference (MAI) and is the key degrading factor of the network's performance. Apart from MAI, other forms of additive noise deteriorate the network performance, such as beat noise, shot noise, thermal noise and fiber-link noise, and worth considering them in performance analysis [11].

Service differentiation in OCDMA networks can be performed by considering either different data-rates or different QoS levels for the supported service-classes. For the provision of data-rate differentiation several solutions have been investigated. A simple approach is based on the utilization of multi-length codes [12]; however, under multi-length coding, short-length codes introduce significant interference over long-length codes, while high error probability emerges for high rate users. Optical fast-frequency hopping has been also proposed for multi-rate OCDMA networks [13]. This technique is based on multiple wavelengths, which requires multi-wavelength

transmitters with high sensitivity on power control. Another way to provide data-rate differentiation is the assignment of several codes to each service-class. This procedure is known as the parallel mapping technique [14]. In this case the number of codes is proportional to the data rate of the assigned service-class. For the provision of differential QoS, one-dimensional and two-dimensional variable-weight optical codes have been introduced in order to control the Bit Error Rate (BER) at the receiver [15], [16].

A call-level performance analysis of an OCDMA PON supporting multiple service-classes of infinite traffic source population, appears in [17]. The shared medium (link between Optical Line Terminal (OLT) and Passive Optical Splitter/Combiner (PO-SC), see Fig. 1) is modelled by a two dimensional Markov chain. Based on this chain, an approximate recursive formula for the calculation of blocking probabilities in the PON is presented. However, in [17], no mathematical proof is provided for the recursive formula; its proof appears in [1]. To prove it, we rely on the distribution of the occupied bandwidth in the PON, which is calculated recursively. The analysis takes into account the user activity, by incorporating different service times for active and passive (silent) periods. The capacity of the PON is defined by the total number of codewords assigned to active users. An arriving call is blocked, if the resulting number of codewords assigned to all in-service calls exceeds a predefined threshold which represents the PON capacity. This case defines the Hard Blocking Probability (HBP). A call may also be blocked in any other system state due to the existence of different forms of additive noise (thermal noise, shot noise, beat noise). The latter case is expressed by the Local Blocking Probability (LBP).

In this paper, (a) we include the analysis presented in [1] and [17], (b) we provide further evaluation of the proposed loss model, and (c) we extend our analysis (and the evaluation) to cover the case of a multi-rate OCDMA PON that provides QoS support. The QoS differentiation is performed by considering variable-weight code lengths, in order to achieve different BER levels at the receiver. Furthermore, we calculate the link utilization in the PON either without, or with QoS support. Finally, in both cases, we provide the analysis for the determination of the Burst Blocking Probability (BBP), which is the probability that a call cannot return to the active state from the passive state, due to the unavailability of codewords, or due to the presence of additive noise. The accuracy of the proposed methodology is evaluated through simulation and is found to be quite satisfactory.

The rest of the paper is organized as follows. In Section II, we discuss about related works. In Section III, we present the system model. In Section IV, we present the recursive formula for the calculation of blocking probabilities in a multi-rate OCDMA PON. This analysis is extended in Section V, in order to cover the case of multiple service-classes with different QoS levels. Section VI is the evaluation section. We conclude in Section VII.

II. RELATED WORKS

There is a significant research activity on OCDMA networks, but it is mainly focused on the performance of several OCDMA components, and not on the teletraffic performance of the overall network, like a PON. Only a few analytical models have been presented in the literature involving the computation of blocking probabilities in OCDMA networks.

Goldberg and Prucnal [18] provide analytical models for the determination of blocking probabilities and for the teletraffic capacity in OCDMA networks. The results of paper [18] are applicable to OCDMA PONs, too. The capacity of the OCDMA PON can be defined by the traditional way, as the number of continuously transmitting users, which depend on the number of codewords that the PON supports, given that each user needs a codeword. Obviously, when the number of users exceeds the number of codewords in the PON, call blocking occurs. The PON capacity is limited not only due to the limited number of codewords, but also due to the presence of MAI, as well as due to additive noise in OCDMA PONs. In [18], only the MAI is taken into account. Due to MAI, when the number of transmitting users in the PON becomes excessive, the BER at the receiver degrades, causing an outage; that is, blocking occurs. The number of users is assumed constant (instead of considering Poisson arrivals). In addition, the authors take into account in the analysis the stochastic nature of the offered traffic by a user. As it is clearly stated in [18], the proposed analysis is independent of the spreading code used by the OCDMA network. However, it has the important limitation of considering just one service-class.

A similar study is performed in [19]. It is concentrated on the performance analysis of the teletraffic capacity of a hybrid WDM/DS(Direct Sequence)-PON. In such a PON, for each wavelength, each user data bit is temporarily encoded with a given sequence of pulses. By this temporal encoding, the same codewords are shared among different users; thus many users can simultaneously communicate with each other by using the same restricted number of codewords. In other words, the user capacity performance is increased in a cost effective way per wavelength for a hybrid WSM/DS-OCDMA PON configuration. In determining the teletraffic capacity of this PON, two considerations are taken into account: (a) The so called nominal resource capacity, which is defined as the maximum number of resources both in WDM and OCDMA system, that is: (number of wavelengths) x (number of codewords). (b) The so called simultaneous user capacity in OCDMA system, defined as the maximum simultaneous transmitting users at acceptable BER performance. As in [18], it is also assumed in [19] that only the MAI affects the BER. Blocking occurs when the system reaches either its nominal resource capacity or the simultaneous user capacity. It is shown that the blocking (and teletraffic capacity) performance depends on the code family used in the OCDMA system. Again, this paper considers a single service-class, which is a serious limitation in the study of broadband networks, like PONs.

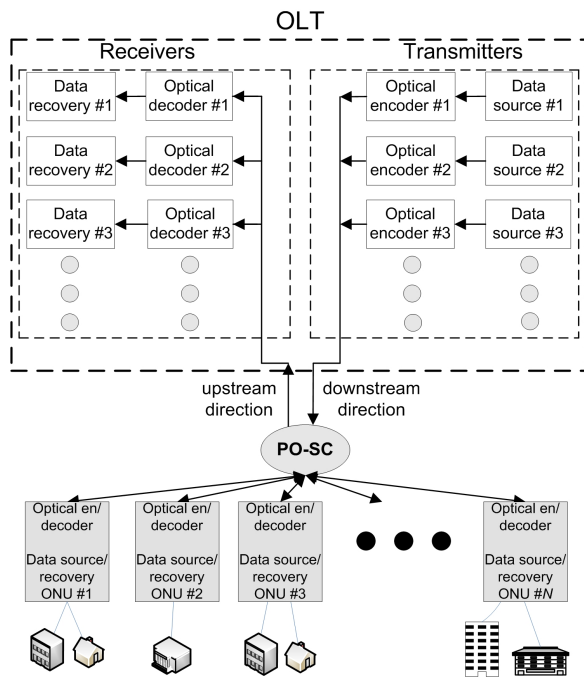


Fig. 1. A basic configuration of an OCDMA PON.

We also provide a call-level analysis of hybrid WDM-OCDMA PONs [20], to determine connection failure probabilities due to unavailability of a wavelength in the considered WDM system with dynamic wavelength assignments, and call blocking probabilities due to the MAI of the OCDMA system. The springboard of the analysis presented in [20] is well-established teletraffic models, developed for Wireless CDMA systems [21].

III. SYSTEM MODEL OF A MULTI-RATE OCDMA PON

We consider the OCDMA PON of Fig. 1. A number of Optical Network Units (ONUs) located at the users' premises are connected to an OLT (located to Central Office) through a PO-SC (quite close to the ONUs). The PO-SC is responsible for the broadcasting of traffic from the OLT to the ONUs (downstream direction) and for the grouping of data from the ONUs and the transmission of the collected data to the OLT through one fiber (upstream direction). We study the upstream direction; however, the following analysis can be applied to the downstream direction. Users which are connected to an ONU, switch between active and passive (silent) periods. The PON utilizes $(L, W, \lambda_a, \lambda_c)$ codewords, which have the same length L , the same W , while the auto-correlation λ_a and the cross-correlation λ_c parameters are defined according to the desired value of the BER at the receiver. The PON supports K service-classes. The service-differentiation in this OCDMA system is realized using the parallel mapping technique. Under this technique, the OLT assigns b_k codewords to a service-class k call that is accepted for service and these codewords are used by the call for its entire duration. In particular, during a service-class k call, b_k data bits are transmitted in parallel in

each bit period. One codeword is used in order to encode data bit "1", while data bit "0" is not encoded. Therefore, in each bit period at most b_k data bits are encoded and this number is equal to the number of "1" data bits that are transmitted during this bit period. In this way, we avoid the complex procedure of assigning codewords to calls in each bit period. Also, the data rate of service-class k is equal to $b_k \cdot D$, where D is the data rate of a single codeword call, since b_k data bits are transmitted in parallel during a bit period.

When a single codeword is applied to an active call, the received power of this call at the receiver is denoted by I_{unit} , where I_{unit} corresponds to the received power per bit, for a specific value of BER. Since different service-classes require different data-rates, the maximum interference I_k that an active service-class k call causes to the receiver is proportional to I_{unit} , because b_k data bits of service-class k are transmitted in parallel, during a bit period, therefore:

$$I_k = b_k \cdot I_{unit} \quad (1)$$

This maximum value of the received power of a service-class k call refers to the power of the call when all b_k parallel bits are "1".

Calls that are accepted for service, start an active period and may constantly remain in the active state for the entire duration of the call, or alternate between active and passive states. Throughout an active state, the traffic source sends bursts, while during a passive state no transmission of data occurs. When a call is transferred from the active state to the passive state, the number of codewords that this call was utilizing in its active state are released, and these codewords become available to new arriving calls. When a call attempts to become active again, it re-requests the same number of codewords (as in the previous active state); if the total number of codewords of all in-service calls does not exceed a maximum value, a new active period begins; if not, burst blocking occurs and the call remains in the passive state. At the end of the active period the total number of codewords held by all in-service calls is reduced by b_k and the call either jumps to the passive state with probability v_k , or departs from the system with probability $1 - v_k$. Furthermore, calls that belong to service-class k arrive to an ONU according to a Poisson process; the total arrival rate from all ONUs is denoted λ_k . The service time of service-class k calls in state i , ($i=1$ indicates the active state, $i=2$ the passive state) is exponentially distributed with mean μ_{ik}^{-1} .

A. Local Blocking Probabilities

According to the principle of the CDMA technology, a call should be blocked if it increases the noise of all in-service calls above a predefined level, given that a call is noise for all other calls. This noise is known as MAI. We distinguish the MAI from other forms of noise, the shot noise, the beat noise, the thermal noise and the fiber-link noise. The thermal noise is generally modelled as Gauss distribution $(0, \sigma_{th})$, the fiber-link noise is modelled as Gauss distribution $(0, \sigma_{fb})$ [22], while the beat noise is also modelled as a Gauss distribution

$(0, \sigma_b)$ [11]. The shot noise is modelled as a Poisson process where its expectation and variance are both denoted by p [22]. According to the central limit theorem, we can assume that the additive shot noise is modelled as Gauss distribution (μ_N, σ_N) , considering that the number of users in the PON is relatively large. Therefore, the interference I_N caused by the four types of noise is modelled as a Gaussian distribution with mean $\mu_N = p$ and variance $\sigma_N = \sqrt{\sigma_{th}^2 + \sigma_{fb}^2 + \sigma_b^2 + p^2}$.

The Call Admission Control (CAC) in the OCDMA PON under consideration is performed by measuring the total received power at the receiver. When a new call arrives (which automatically enters an active state), the CAC checks the total received power and if it exceeds a maximum value I_{\max} , the call is blocked and lost. This condition is expressed by the following relation:

$$\sum_{k=1}^K (n_k^1 I_k \cdot P_{\text{interf}}) + I_k + I_N > I_{\max} \Leftrightarrow \frac{I_N}{I_{\max}} > 1 - \sum_{k=1}^K (n_k^1 \frac{I_k}{I_{\max}} \cdot P_{\text{interf}}) - \frac{I_k}{I_{\max}} \quad (2)$$

where n_k^1 represent the number of the service-class k calls in the active system and P_{interf} is the probability of interference. This probability is a function of the maximum cross-correlation parameter λ_c , the weight W and the length L of the codewords and the hit probabilities between two codewords that are used to encode data bits of different users. The hit probabilities $p_{\lambda_c, i}$ of getting i hits during a bit period out of the maximum cross-correlation value λ_c are given through [23]:

$$\sum_{i=0}^{\lambda_c} i \cdot p_{\lambda_c, i} = \frac{W^2}{2L}, \quad \text{while} \quad \sum_{i=0}^{\lambda_c} p_{\lambda_c, i} = 1 \quad (3)$$

where the factor $1/2$ is due to the fact that data-bit “0” is not encoded. For $\lambda_c = 1$, the percentage of the total power of another’s user bit that interferes with a bit of the new call is $1/W$, since 1 out of W “1” of the codewords may interfere. In this case $P_{\text{interf}} = (1/W) p_{\lambda_c, 1} = W/2L$. In the general case where the maximum value of the cross-correlation is $\lambda_c \geq 1$ the probability of interference is given by:

$$P_{\text{interf}} = \sum_{i=0}^{\lambda_c} \frac{i}{W} p_{\lambda_c, i} = \frac{W}{2L} \quad (4)$$

The same condition is used at the receiver, when a passive call jumps to an active state. Based on (2), we define the LBP $lb_k(n_k^1)$ that a service-class k call is blocked due to the presence of the additive noise, when the number of active calls is n_k^1 :

$$lb_k(n_k^1) = P \left(\frac{I_N}{I_{\max}} > 1 - \sum_{k=1}^K \left(n_k^1 \frac{I_k}{I_{\max}} \cdot P_{\text{interf}} \right) - \frac{I_k}{I_{\max}} \right) \quad (5)$$

or

$$1 - lb_k(n_k^1) = P \left(\frac{I_N}{I_{\max}} \leq 1 - \sum_{k=1}^K \left(n_k^1 \frac{I_k}{I_{\max}} \cdot P_{\text{interf}} \right) - \frac{I_k}{I_{\max}} \right) \quad (6)$$

Since the total additive noise I_N follows a Gaussian distribution (μ_N, σ_N) , the variable I_N/I_{\max} , which is used for the LBP calculation also follows a Gaussian distribution $(\mu_N/I_{\max}, \sigma_N/I_{\max})$. Therefore the right-hand side of (6), which is the Cumulative Distribution Function (CDF) of I_N/I_{\max} , is denoted by $F_n(x) = P(I_N/I_{\max} \leq x)$ and is given by:

$$F_n(x) = \frac{1}{2} \left(1 + \text{erf} \left(\frac{x - (\mu_N/I_{\max})}{(\sigma_N/I_{\max})\sqrt{2}} \right) \right) \quad (7)$$

where $\text{erf}(\bullet)$ is the well-known error function. Using (6) and (7) we can calculate the LBP, $lb_k(n_k^1)$ by means of the substitution $x = 1 - \sum_{k=1}^K (n_k^1 \frac{I_k}{I_{\max}} \cdot P_{\text{interf}}) - \frac{I_k}{I_{\max}}$:

$$lb_k(x) = \begin{cases} 1 - F_n(x), & x \geq 0 \\ 1, & x < 0 \end{cases} \quad (8)$$

B. The Distribution of the Number of Active and Passive Calls

The following analysis is inspired by the multi-rate ON-OFF model for the call-level performance of a single link, presented in [24], [25], which considers discrete state space. We consider that the PON capacity is C_1 . This is a discrete parameter, since it represents the total number of codewords that can be assigned to the end-users. When a call is at the passive state, it is assumed that it produces a fictitious interference of a fictitious system, with a discrete capacity C_2 . This *passive system* is used to prevent new calls to enter the system when a large number of calls are at the passive state. In order to employ the analysis presented in [24], we use the following notations:

- the total number of codewords assigned to all in-service active calls is denoted by j_1 .
- the total (fictitious) number of codewords assigned to all in-service passive calls is denoted by j_2 .

Based on the analysis presented in the previous section, a new call will be accepted for service if the total number of codewords assigned to all in-service active calls together with the requirements in codewords of the new call, will not exceed C_1 , which is the PON capacity. Moreover, in order to avert the acceptance of new calls when a large number of calls are in the passive state, the requirements in codewords of the new call together with the total number of codewords assigned to all in-service active calls and the number of codewords assigned to all in-service passive calls should not exceed the fictitious PON capacity (which is expressed by the discrete value C_2). Based on this analysis, a new service-class k call will be accepted for service in the system, if it satisfies both the following constraints:

$$j_1 + b_k \leq C_1 \quad \text{and} \quad j_1 + j_2 + b_k \leq C_2 \quad (9)$$

If we denote by Ω the set of the permissible states, then the distribution $\vec{j} = (j_1, j_2)$, denoted as $q(\vec{j})$ can be calculated by the proposed two-dimensional approximate recursive formula:

$$\sum_{i=1}^2 \sum_{k=1}^K b_{i,k,s} p_{i,k}(\vec{j}) q(\vec{j} - B_{i,k}) = j_s q(\vec{j}) \quad (10)$$

where

$$\vec{j} \in \Omega \Leftrightarrow \left\{ \left(j_1 \leq C_1 \cap \left(\sum_{s=1}^2 j_s \leq C_2 \right) \right) \right\} \quad (11)$$

The parameter s refers to the systems ($s = 1$ indicates the active system, $s = 2$ the passive system), while i refers to the states ($i = 1$ specifies the active state, $i = 2$ specifies the passive state). Also,

$$b_{i,k,s} = \begin{cases} b_k, & \text{if } s = i \\ 0, & \text{if } s \neq i \end{cases} \quad (12)$$

and $B_{i,k} = (b_{i,k,1}, b_{i,k,2})$ is the i,k row of the $(2K \times 2)$ matrix B , with elements $b_{i,k,s}$. Also, $p_{i,k}(\vec{j})$ is the utilization of the i -th system by service-class k :

$$p_{i,k}(\vec{j}) = \begin{cases} \frac{\lambda_k [1 - lb_k(j_1 - b_k)]}{(1 - v_k) \mu_{1k}} & \text{for } i = 1 \\ \frac{\lambda_k v_k}{(1 - v_k) \mu_{2k}} & \text{for } i = 2 \end{cases} \quad (13)$$

Moreover, j_s is the occupied capacity of the system:

$$j_s = \sum_{i=1}^2 \sum_{k=1}^K n_k^i b_{i,k,s} \quad (14)$$

Proof: In order to derive the recursive formula of (10) we introduce the following notation:

$$\begin{aligned} \vec{n} &= (n^1, n^2), \quad n^i = (n_1^i, n_2^i, \dots, n_K^i), \\ n_{k+}^i &= (n_1^i, \dots, n_k^i + 1, \dots, n_K^i), \\ n_{k-}^i &= (n_1^i, \dots, n_k^i - 1, \dots, n_K^i), \\ \vec{n}_{k+}^1 &= (n_{k+}^1, n^2), \quad \vec{n}_{k+}^2 = (n^1, n_{k+}^2), \\ \vec{n}_{k-}^1 &= (n_{k-}^1, n^2), \quad \vec{n}_{k-}^2 = (n^1, n_{k-}^2) \end{aligned} \quad (15)$$

Having determined the steady state of the system $\vec{n} = (n^1, n^2)$, we proceed to the depiction of the transitions from and to state \vec{n} , as it is shown in Fig. 2. The horizontal axis of the state transition diagram of Fig. 2 reflects the arrivals on new calls and the termination of calls. More specifically, when the system is at state (A) it will jump to state (B) with a rate λ_k , when a new service-class k call arrives at the system. This rate is multiplied by the probability $1 - lb_k(n_k^1 - 1)$ that this call will not be blocked due to the presence of the additive noise. Similarly, we define the rate from state (C) to state (A). From state (B) the system will jump to state (A) $\mu_{1,k}(n_k^1 + 1)(1 - v_k)$ times per unit time, since one of the $n_k^1 + 1$ active calls of service-class k (in state (B)) will depart from the system with probability $(1 - v_k)$. The transition from state (A) to state (C) is defined in a similar way.

The vertical axis of the state transition diagram of Fig. 2 defines the transition from the active state to the passive state and vice versa. In particular, when the system is at state (A) it will jump to state (D) $\mu_{2,k} n_k^2 [1 - lb_k(n_k^1)]$ times per unit time. In this case a transition from the passive state to the active state occurs; this transition will be blocked only due to

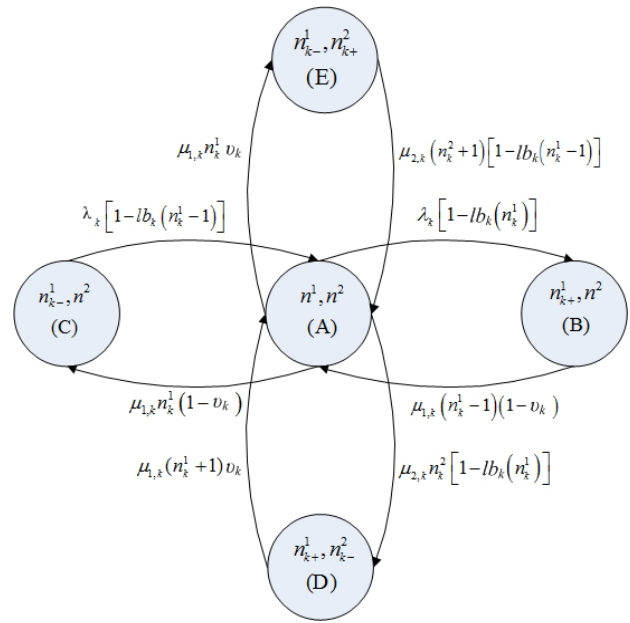


Fig. 2. State transition diagram of the OCDMA system with active and passive users.

the presence of the additive noise, which is expressed by the LBP. The reverse transition (from state (D) to state (A)) occurs when one of $n_k^1 + 1$ active calls jumps to the passive state with probability v_k . Similarly, we can define the transitions between states (E) and (A).

Let $P(\vec{n})$ be the probability of the steady state of the state transition diagram. Assuming that local balance exists between two subsequent states, we derive the local balance equations:

$$\begin{aligned} P(\vec{n}) \mu_{1k} n_k^1 v_k &= P(\vec{n}_{k-+}) \mu_{2k} (n_k^2 + 1) [1 - lb_k(n_k^1 - 1)] \\ P(\vec{n}) \lambda_k [1 - lb_k(n_k^1)] &= P(\vec{n}_{k+}^1) \mu_{1k} (n_k^1 + 1) (1 - v_k) \\ P(\vec{n}) \mu_{2k} n_k^2 [1 - lb_k(n_k^1)] &= P(\vec{n}_{k+}^2) \mu_{1k} (n_k^1 + 1) v_k \\ P(\vec{n}) \mu_{1k} n_k^1 (1 - v_k) &= P(\vec{n}_{k-}^1) \lambda_k [1 - lb_k(n_k^1 - 1)] \end{aligned} \quad (16)$$

We assume that the system of (16) has a Product Form Solution (PFS):

$$P(\vec{n}) = \frac{1}{G} \prod_{i=1}^2 \prod_{k=1}^K \frac{p_{i,k}^{n_k^i}(n_k)}{n_k!} \quad (17)$$

where G is a normalization constant and $p_{i,k}(n_k)$ is given by:

$$p_{i,k}(n_k) = \begin{cases} \frac{\lambda_k [1 - lb_k(n_k^1 - 1)]}{(1 - v_k) \mu_{1k}} & \text{for } i = 1 \\ \frac{\lambda_k v_k}{(1 - v_k) \mu_{2k}} & \text{for } i = 2 \end{cases} \quad (18)$$

In order for (17) to satisfy all equations of the system of (16) using (18), we assume that $1 - lb_k(n_k^1) \approx 1 - lb_k(n_k^1 - 1)$, i.e. the acceptance of one additional call in active state does not affect the LBP. This is the first assumption that we take into account in order to derive (10). By using (18) and this assumption, the last equation of (16) can be re-written as:

$$n_k^i P(\vec{n}) = p_{i,k}(n_{k-}) P(\vec{n}_{k-}^i) \quad (19)$$

The probability $q(\vec{j})$ is given by:

$$q(\vec{j}) = P(\vec{j} = \vec{n} \cdot B) = \sum_{\vec{n} \in \Omega_{\vec{j}}} P(\vec{n}) \quad (20)$$

where $\Omega_{\vec{j}} = \left\{ \vec{n} \in \Omega_{\vec{j}} : \vec{n}B = \vec{j}, n_k^i \geq 0, i=1, 2, k=1, \dots, K \right\}$. By multiplying both sides of (19) with $b_{i,k,s}$, and summing over $k = 1, \dots, K$ and $i = 1, 2$, we have:

$$P(\vec{n}) \sum_{i=1}^2 \sum_{k=1}^K b_{i,k,s} n_k^i = \sum_{i=1}^2 \sum_{k=1}^K b_{i,k,s} p_{i,k}(n_{k-}) P(\vec{n}_{k-}) \quad (21)$$

By using (14) and summing both sides of (21) over the set of all states of $\Omega_{\vec{j}}$, we have:

$$j_s \sum_{\vec{n} \in \Omega_{\vec{j}}} P(\vec{n}) = \sum_{i=1}^2 \sum_{k=1}^K b_{i,k,s} p_{i,k} \sum_{\vec{n} \in \Omega_{\vec{j}}} p_{i,k}(n_{k-}^i) P(\vec{n}_{k-}^i) \quad (22)$$

The second assumption that we consider is that:

$$\sum_{\vec{n} \in \Omega_{\vec{j}}} p_{i,k}(n_{k-}^i) P(\vec{n}_{k-}^i) \approx p_{i,k}(n_{k-}^i) \sum_{\vec{n} \in \Omega_{\vec{j}}} P(\vec{n}_{k-}^i) \quad (23)$$

Based on the fact that $(\vec{n}B = \vec{j}) \Rightarrow (n_{k-}^i B = j - B_{i,k})$, (18) is equal to (13), and (20) can be rewritten as:

$$q(\vec{j} - B_{i,k}) = \sum_{\vec{n} \in \Omega_{\vec{j}}} P(n_{k-}^i) \quad (24)$$

Finally, we derive the recursive formula of (10), by using the assumption of (23) and substituting (20) and (24) to (23). The LBP is a function of the total interference of the in-service active calls j_1 , i.e. $lb_k(n_k^1) = lb_k(j_1)$, since

$$\begin{aligned} x &= 1 - \sum_{k=1}^K (n_k^1 \frac{I_k}{I_{\max}} \cdot P_{\text{interf}}) - \frac{I_k}{I_{\max}} \Leftrightarrow \\ x &= 1 - \sum_{k=1}^K (n_k^1 \frac{b_k \cdot I_{\text{unit}}}{I_{\max}} \cdot P_{\text{interf}}) - \frac{b_k \cdot I_{\text{unit}}}{I_{\max}} \Leftrightarrow \\ x &= 1 - (j_1 \cdot \frac{I_{\text{unit}}}{I_{\max}} \cdot P_{\text{interf}}) - \frac{b_k \cdot I_{\text{unit}}}{I_{\max}} \end{aligned} \quad (25)$$

C. Performance Metrics

The CBP is calculated by combining LBP and HBP as follows:

$$Pb_k = \sum_{\vec{j} \in \Omega - \Omega_h} lb_k(j_1) q(\vec{j}) + \sum_{\vec{j} \in \Omega_h} G^{-1} q(\vec{j}) \quad (26)$$

where $\Omega_h = \left\{ \vec{j} \mid [(b_{i,k,1} + j_1) > C_1] \cup [(b_{i,k,2} + j_1 + j_2) > C_2] \right\}$. The first summation of the right part of (26) refers to the probability that a new call could be blocked at any system state due to the presence of the additive noise. The second summation signifies the HBP, which is derived by summing the probabilities of all the blocking states that are defined by (9). Note that the bounds of the first summation in (26) are

accidentally different than those of the corresponding equation in [17] due to a misprint in (10) of [17].

The calculation of the BBP is based on the fact that burst blocking occurs when a passive call cannot return to the active state. This situation occurs when at least one of the two reasons are valid: the first reason refers to the case where the number of codewords assigned to the call (so that this call could be transferred from passive to active state) together with the number of codewords assigned to all in-service active calls exceeds the capacity of the PON. The effect of this reason can be determined by the number n_k^2 of service-class k calls in passive state, when the system is at any burst blocking state:

$$\vec{j} \in \Omega^* \Leftrightarrow \left\{ \left(C_1 - b_k + 1 \leq j_1 \leq C_1 \cap \left(\sum_{s=1}^2 j_s \leq C_2 \right) \right) \right\} \quad (27)$$

By multiplying n_k^2 by the corresponding probability $q(\vec{j})$ and the service rate in the passive state μ_k^2 we calculate the rate that service-class k calls depart from a burst blocking state, if it was possible. Then, we sum the rates that a service-class k call would depart from any burst blocking state:

$$\sum_{\vec{j} \in \Omega^*} n_k^2 q(\vec{j}) \mu_{2k} \quad (28)$$

The second reason refers to the case where a passive call cannot return the active state due to the presence of the additive noise. Following the same procedure resulted in (28), we calculate the sum of the rates that a service-class k call would depart from any state, except from the burst blocking states. Due to local blocking, however, each rate is multiplied by the corresponding value of $lb_k(\vec{j})$:

$$\sum_{\vec{j} \in \{\Omega - \Omega^*\}} n_k^2 lb_k(\vec{j}) q(\vec{j}) \mu_{2k} \quad (29)$$

By normalizing the sum of (28) and (29) (i.e. by taking into account the state-space Ω), we obtain the BBP of service-class k , B_{b_k} :

$$B_{b_k} = \frac{\sum_{\vec{j} \in \Omega^*} n_k^2 q(\vec{j}) \mu_{2k} + \sum_{\vec{j} \in \{\Omega - \Omega^*\}} n_k^2 lb_k(\vec{j}) q(\vec{j}) \mu_{2k}}{\sum_{\vec{j} \in \Omega} n_k^2 q(\vec{j}) \mu_{2k}} \quad (30)$$

The utilization \bar{R}_s of the shared link s ($s=1$ corresponds to the active link and $s=2$ corresponds to the passive link) is given by:

$$\bar{R}_s = \sum_{i=1}^{C_s} i R_s(i) \quad (31)$$

where $R_s(i)$ is the marginal link occupancy distribution of the link s and is given by:

$$R_s(i) = \sum_{\{\vec{j} \mid j_s = i\}} q(\vec{j}) \quad (32)$$

IV. SYSTEM MODEL OF A MULTI-RATE OCDMA PON WITH QoS GUARANTEES

In OCDMA networks, QoS differentiation can be realised by the utilization of codewords with different weights. To this end, we assume that the PON supports $K = T \cdot F$ service-classes: F service-classes are differentiated by the data rate, while each one of these F service-classes supports T different QoS levels that express different values of the BER at the receiver. We also consider that the PON assigns $(L, W_t, \lambda_a, 1)$ codewords to service-class t , $t = 1, \dots, T$. Calls of these T service-classes require the same number $b_{f,t}$ ($f = 1, \dots, F$) of codewords, while they are differentiated by the weight W_t . The received power per bit "1" of service-class f, t is denoted as $I_{\text{unit}}^{f,t}$, while the received power that corresponds to a call of service-class f, t is at most $I_{f,t}^{\text{act}} = b_{f,t} \cdot I_{\text{unit}}^{f,t}$. The traffic parameters of service-class f, t are denoted as $(\lambda_{f,t}, \mu_{1,f,t}^{-1}, \mu_{2,f,t}^{-1}, v_{f,t})$. To simplify the presentation of these parameters we use one notation for the service-classes; we denote that the parameters of service-class k ($k = 1, \dots, T \cdot F$) are $I_{\text{unit}}^k = I_{\text{unit}}^{f,t}$, $I_{\text{act}}^k = I_{f,t}^{\text{act}}$, $b_k = b_{f,t}$, $\lambda_k = \lambda_{f,t}$, $\mu_{ik}^{-1} = \mu_{i,f,t}^{-1}$ and $v_k = v_{f,t}$.

In order to determine the LBP of service-class k , we use the following relation, which is based on (6):

$$lb_k(n_k^1) = P \left(\frac{I_N}{I_{\text{max}}} > 1 - \sum_{x=1}^{T \cdot F} \left(n_k^1 \frac{b_x \cdot I_{\text{unit}}^x}{I_{\text{max}}} P_{\text{interf}}^{x,k} \right) - \frac{I_{\text{act}}^k}{I_{\text{max}}} \right) \Leftrightarrow$$

$$1 - lb_k(n_k^1) = P \left(\frac{I_N}{I_{\text{max}}} \leq 1 - \sum_{x=1}^{T \cdot F} \left(n_k^1 \frac{b_x \cdot I_{\text{unit}}^x}{I_{\text{max}}} P_{\text{interf}}^{x,k} \right) - \frac{I_{\text{act}}^k}{I_{\text{max}}} \right) \quad (33)$$

where the probability of interference $P_{\text{interf}}^{x,k}$ between two codewords with weights W_x and W_k is a function of the hit probability [26]:

$$p_{x,k} = \frac{W_x W_k}{2L} \quad (34)$$

The probability of interference of a codeword of a service-class k assigned to a new arriving call and a codeword of service-class x can be calculated by following the same procedure that was used in order to derive (3):

$$P_{\text{interf}}^{k,x} = \frac{1}{W_x} \frac{W_x \cdot W_k}{2L} = \frac{W_k}{2L} \quad (35)$$

The LBP $lb_k(j)$ can be calculated by using (8), where the variable x can be calculated through (33) as follows:

$$x = 1 - \sum_{k=1}^{T \cdot F} \left(n_k^1 \frac{b_k \cdot I_{\text{unit}}^k}{I_{\text{max}}} \cdot P_{\text{interf}}^k \right) - \frac{I_k}{I_{\text{max}}} \Leftrightarrow$$

$$x = 1 - \sum_{k=1}^{T \cdot F} \left(n_k^1 \frac{b_k \cdot I_{\text{unit}}^k}{I_{\text{max}}} \cdot P_{\text{interf}}^k \right) - \frac{b_k \cdot I_{\text{unit}}^k}{I_{\text{max}}} \Leftrightarrow \quad (36)$$

$$x = 1 - \left(\frac{j-1}{I_{\text{max}}} \cdot \sum_{k=1}^{T \cdot F} (P_{\text{interf}}^k \cdot I_{\text{unit}}^k) - \frac{b_k \cdot I_{\text{unit}}^k}{I_{\text{max}}} \right)$$

For the case of the multi-rate OCDMA PON with QoS differentiation the distribution of active and passive calls is given by (10), where the upper bound of the summations that refers to the total number of service-classes has to be changed (from K) to $T \cdot F$. The same change has to be applied in (26), (30) and (31) in order to calculate the CBP, the BBP and the link utilization, respectively.

V. EVALUATION

We evaluate the proposed analytical models through simulation. To this end we simulate the OCDMA PON of Fig.1 by using the Simscript II.5 simulation tool [27]. The simulation results are mean values from 6 runs with confidence interval of 95%. The resulting reliability ranges of the simulation measurements are small and, therefore, we present them only in tables; in figures we provide only mean values. We consider two application examples. In the first example, which is simpler for clarification, we assume that the OCDMA PON supports $K=2$ service-classes that are only differentiated by the data rate, without QoS differentiation. The PON utilizes the (211,4,1,2) codewords, which result in a maximum number of 105 codewords. Based on the analysis presented in [28] and considering a typical value of $\text{BER}=10^{-6}$, the total number of codewords is reduced to C_1 for $I_{\text{unit}} = 0.4\mu\text{W}$. The traffic description parameters of the two service classes are $(b_1, b_2) = (7, 2)$, $(\mu_{11}^{-1}, \mu_{12}^{-1}) = (0.8, 1.0)$, $(\mu_{21}^{-1}, \mu_{22}^{-1}) = (1.1, 1.4)$, $(v_1, v_2) = (0.9, 0.95)$. We assume that the maximum received power is equal to $4 \mu\text{W}$, while the total number of

TABLE I
ANALYTICAL VS SIMULATION CBP RESULTS FOR THE 1ST APPLICATION EXAMPLE.

Arrival Rate (calls/sec)	CBP 1 st service-class		CBP 2 nd service-class	
	Analysis (%)	Simulation (%)	Analysis (%)	Simulation (%)
0.10	0.187	0.183±6.80E-03	0.023	0.023±3.66E-03
0.11	0.309	0.316±1.44E-02	0.041	0.043±3.40E-03
0.12	0.487	0.490±1.65E-02	0.070	0.066±5.93E-03
0.13	0.731	0.715±2.12E-02	0.112	0.110±5.76E-03
0.14	1.056	1.061±2.44E-02	0.172	0.175±8.67E-03
0.15	1.473	1.488±2.91E-02	0.252	0.249±5.15E-03
0.16	1.993	1.995±2.55E-02	0.356	0.3625±4.76E-03
0.17	2.624	2.637±3.89E-02	0.488	0.4789±8.11E-03
0.18	3.371	3.355±5.55E-02	0.648	0.6548±1.17E-02
0.19	4.237	4.118±2.79E-01	0.839	0.8239±5.46E-02
0.20	5.220	5.213±6.16E-02	1.061	1.0773±1.94E-02

TABLE II
ANALYTICAL VS SIMULATION BBP RESULTS FOR THE 1ST APPLICATION EXAMPLE.

Arrival Rate (calls/sec)	BBP 1 st service-class		BBP 2 nd service-class	
	Analysis (%)	Simulation (%)	Analysis (%)	Simulation (%)
0.1	6.65E-03	6.5E-03 ± 5.53E-04	8.25E-04	8.69E-04±1.7E-04
0.11	9.91E-03	1.1E-02 ± 1.22E-03	1.27E-03	1.41E-03±1.8E-04
0.12	1.40E-02	1.4E-02 ± 1.27E-03	1.85E-03	1.81E-03±2.4E-04
0.13	1.88E-02	1.9E-02 ± 1.21E-03	2.56E-03	2.43E-03±2.8E-04
0.14	2.43E-02	2.4E-02 ± 1.09E-03	3.42E-03	3.48E-03±3.5E-04
0.15	3.04E-02	2.9E-02 ± 1.10E-03	4.40E-03	4.36E-03±3.3E-04
0.16	3.69E-02	3.7E-02 ± 1.01E-03	5.52E-03	5.78E-03±5.3E-04
0.17	4.37E-02	4.4E-02 ± 1.86E-03	6.74E-03	6.62E-03±3.4E-04
0.18	5.05E-02	5.1E-02 ± 2.55E-03	8.06E-03	8.24E-03±6.9E-04
0.19	5.73E-02	5.7E-02 ± 1.33E-03	9.47E-03	9.60E-03±5.6E-04
0.2	6.38E-02	6.3E-02 ± 1.49E-03	1.10E-02	1.11E-02±5.7E-04

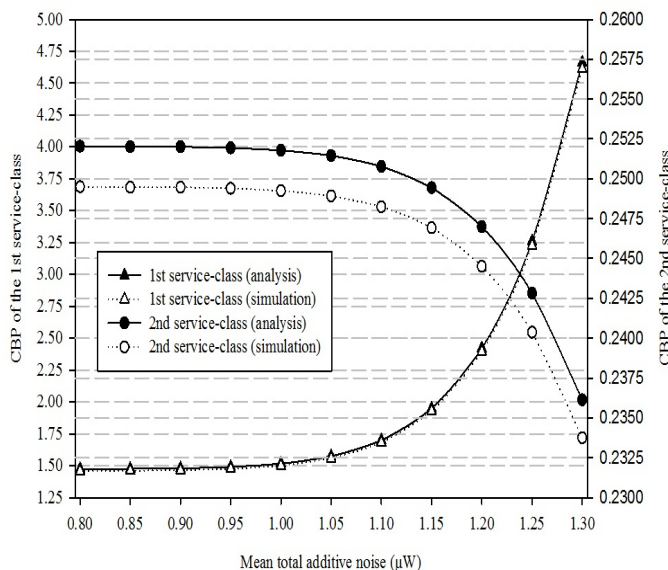


Fig. 3. Analytical and simulation CBP results of the two service-classes versus the mean total additive noise.

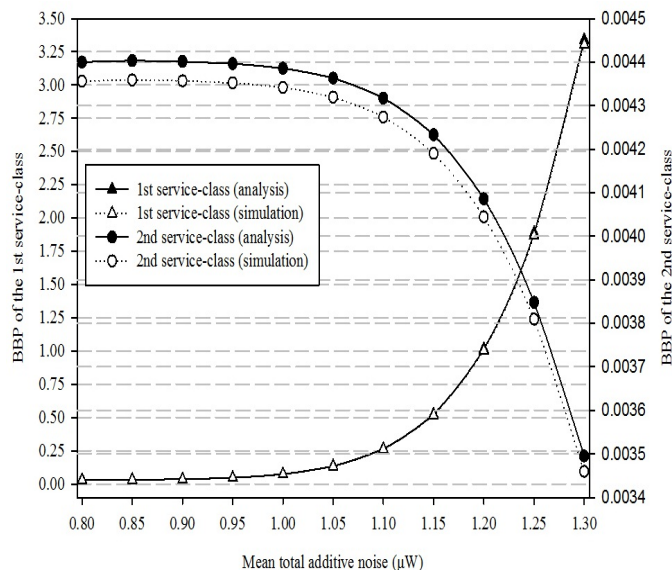


Fig. 4. Analytical and simulation BBP results of the two service-classes versus the mean total additive noise.

fictional codewords is $C_2 = 45$. The total additive noise follows a Gauss distribution $(1, 0.1) \mu W$.

In Tables I and II, we present analytical and simulation results of the two service-classes for the CBP and BBP, respectively, versus the arrival rate. We assume that the arrival rate is the same for the two service-classes. In Table III we present analytical and simulation results for the utilization of the active and the passive link, versus the arrival rate of the two service-classes. As the results of the three tables reveal, the accuracy of the proposed analysis is absolutely satisfactory.

We also investigate the impact of various network parameters on the CBP and the BBP. To this end, Fig. 3 and 4 present analytical and simulation results of the CBP and the BBP, respectively, for the two service-classes, versus different mean values μ_N of the total additive noise, while σ_N is kept constant. In both Fig. 3 and 4 the arrival rate of the two service-classes is $(0.15, 0.15)$ calls/sec, while the values of all other parameters are the same with those used in Tables I,

II and III. The comparison of analytical and simulation results of Fig. 3 and 4 shows that the accuracy of the proposed model is completely satisfactory for call-level performance. As it is expected from (5) and (6), higher values of the mean total additive noise results in higher values of the LBP and therefore higher values of CBP and BBP. The increase of the mean total additive noise results in the increment of both CBP and BBP of the first service-class, while the values of the CBP and BBP of the second service-class are slightly decreased. This is due to the fact that higher values of the total additive noise increases the LBP; therefore the CBP and the BBP of the first service-class, which has the highest demands in codewords, increases. But in this case more codewords are available for the second service-class, which has lower demands in codewords. Further increase of the mean total additive noise will result in the increase of the CBP and BBP of the second service-class.

Another parameter that we examine is the total interference I_{max} at the receiver. In Fig. 5 and 6, we present analytical and simulation results for the CBP and BBP, respectively, of the

TABLE III

ANALYTICAL VS SIMULATION RESULTS FOR THE UTILIZATION OF THE ACTIVE AND THE PASSIVE LINK FOR THE 1ST APPLICATION EXAMPLE.

Arrival Rate (calls/sec)	Active link utilization		Passive link utilization	
	Analysis (%)	Simulation (%)	Analysis (%)	Simulation (%)
0.1	5.594	5.588±8.88E-03	5.827	5.865±1.12E-02
0.11	6.149	6.144±7.35E-03	6.405	6.448±8.56E-03
0.12	6.701	6.699±7.86E-03	6.980	7.029±1.00E-02
0.13	7.249	7.245±1.15E-02	7.550	7.6021±1.46E-02
0.14	7.792	7.783±9.91E-03	8.115	8.1633±1.18E-02
0.15	8.328	8.318±1.14E-02	8.671	8.7234±1.38E-02
0.16	8.855	8.848±9.63E-03	9.219	9.2751±1.18E-02
0.17	9.372	9.363±9.11E-03	9.756	9.8106±1.07E-02
0.18	9.877	9.863±1.07E-02	10.280	10.3317±1.24E-02
0.19	10.370	10.358±1.35E-01	10.789	10.7811±1.55E-01
0.2	10.848	10.837±1.38E-02	11.283	11.3404±1.69E-02

TABLE IV

ANALYTICAL VS SIMULATION CBP RESULTS OF THE 1ST AND 2ND SERVICE-CLASSES FOR THE 2ND APPLICATION EXAMPLE.

Arrival Rate (calls/sec)	CBP 1 st service-class		CBP 2 nd service-class	
	Analysis (%)	Simulation (%)	Analysis (%)	Simulation (%)
0.01	0.005	0.005±8.39E-03	0.001	0.001±6.99E-03
0.015	0.056	0.055±2.04E-02	0.009	0.009±1.70E-02
0.02	0.284	0.278±2.62E-02	0.047	0.046±2.18E-02
0.025	0.884	0.867±3.01E-02	0.147	0.144±2.51E-02
0.03	2.037	1.997±3.15E-02	0.348	0.342±2.62E-02
0.035	3.835	3.760±4.80E-02	0.685	0.672±4.00E-02
0.04	6.259	6.138±6.85E-02	1.184	1.161±5.71E-02
0.045	9.208	9.029±3.44E-01	1.856	1.820±2.87E-02
0.05	12.537	12.293±7.60E-02	2.699	2.647±6.34E-02

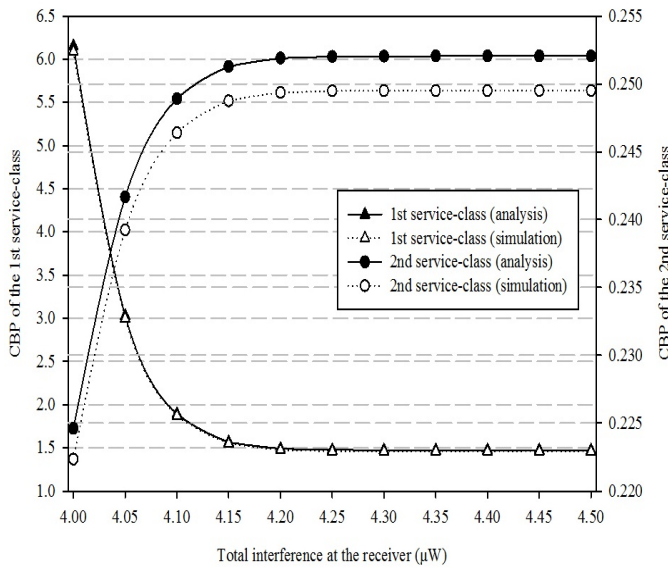


Fig. 5. Analytical and simulation CBP results of the two service-classes versus the total interference.

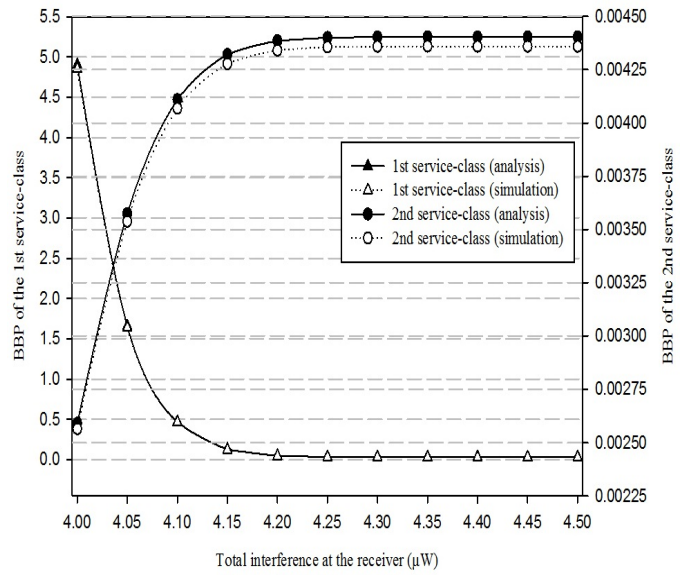


Fig. 6. Analytical and simulation BBP results of the two service-classes versus the total interference.

two service-classes, versus different values of the parameter I_{max} . In both figures the arrival rate of the two service-classes is (0.15, 0.15) calls/sec, while the values of all other parameters are the same with those used in Tables I, II and III. As the results of Fig. 5 and 6 reveal, the accuracy of the proposed model is absolutely satisfactory, even for small values of the total interference I_{max} . The decrease of the total interference at the receiver results in higher values of both CBP and BBP of the first service-class, since less interference can be received; therefore less calls of the first service-class can be accommodated at the PON. As in the case of Fig. 3 and 4, this situation results in lower CBP and BBP values of the second service-class, which requires smaller number of codewords. Nevertheless, high values of I_{max} can be achieved by receivers with higher sensitivity, which are more complicated and therefore more costly.

In order to demonstrate the effect of the fictitious capacity to the CBP and BBP, in Fig. 7 and 8 we present analytical CBP and BBP results, respectively, versus different values of

the total number of fictitious codewords. In both Fig. 7 and 8 the arrival rate of the two service-classes is (0.15, 0.15) calls/sec, while the values of all other parameters are the same as the ones were used previously. The increment of the total number of fictitious codewords results in lower CBP values for both service-classes, since more calls can be accommodated to the passive system. However, this increment results in higher values of the BBP, because the contention for the transition from the passive to the active state. Note that when $C_1 = C_2$ no burst blocking occurs, but at the expense of higher CBP.

We now proceed to the second application example, which refers to the case of a multi-rate OCDMA PON with QoS differentiation. The PON supports 4 service-classes. Service-classes s_1 and s_3 require the same number of codewords (same data-rate), as well as service-classes s_2 and s_4 require the same number of codewords, but different than that of s_1 and s_3 . Service-classes s_1 and s_2 utilize the (211,4,1,1)-codewords, while service-classes

TABLE V
ANALYTICAL VS SIMULATION CBP RESULTS OF THE 3RD AND 4TH SERVICE-CLASSES FOR THE 2ND APPLICATION EXAMPLE.

Arrival Rate (calls/sec)	CBP 3 rd service-class		CBP 4 th service-class	
	Analysis (%)	Simulation (%)	Analysis (%)	Simulation (%)
0.01	0.013	0.012 ± 8.24E-03	0.001	0.001 ± 0.006941
0.015	0.082	0.080 ± 2.00E-02	0.009	0.009 ± 0.01685
0.02	0.342	0.334 ± 2.57E-02	0.047	0.046 ± 0.02165
0.025	0.989	0.967 ± 2.96E-02	0.147	0.144 ± 0.024918
0.03	2.201	2.153 ± 3.09E-02	0.348	0.341 ± 0.026041
0.035	4.063	3.974 ± 4.72E-02	0.685	0.670 ± 0.039726
0.04	6.552	6.408 ± 6.73E-02	1.184	1.158 ± 0.056678
0.045	9.560	9.350 ± 3.38E-01	1.856	1.816 ± 0.28472
0.05	12.537	12.262 ± 7.47E-02	2.699	2.640 ± 0.062908

TABLE VI
ANALYTICAL VS SIMULATION BBP RESULTS OF THE 1ST AND 2ND SERVICE-CLASSES FOR THE 2ND APPLICATION EXAMPLE.

Arrival Rate (calls/sec)	BBP 1 st service-class		BBP 2 nd service-class	
	Analysis (%)	Simulation (%)	Analysis (%)	Simulation (%)
0.01	6.36E-05	6.22E-05 ± 1.44E-06	7.79E-06	7.62E-06 ± 1.44E-07
0.015	5.33E-04	5.22E-04 ± 3.50E-06	7.57E-05	7.40E-05 ± 3.50E-07
0.02	2.11E-03	2.06E-03 ± 4.50E-06	3.23E-04	3.16E-04 ± 4.50E-07
0.025	5.52E-03	5.39E-03 ± 5.18E-06	8.78E-04	8.59E-04 ± 5.18E-07
0.03	1.11E-02	1.09E-02 ± 5.41E-06	1.81E-03	1.77E-03 ± 5.41E-07
0.035	1.88E-02	1.84E-02 ± 8.26E-06	3.08E-03	3.01E-03 ± 8.26E-07
0.04	2.81E-02	2.75E-02 ± 1.18E-05	4.60E-03	4.50E-03 ± 1.18E-06
0.045	3.83E-02	3.74E-02 ± 5.92E-05	6.24E-03	6.11E-03 ± 5.92E-06
0.05	4.88E-02	4.77E-02 ± 1.31E-05	7.91E-03	7.74E-03 ± 1.31E-06

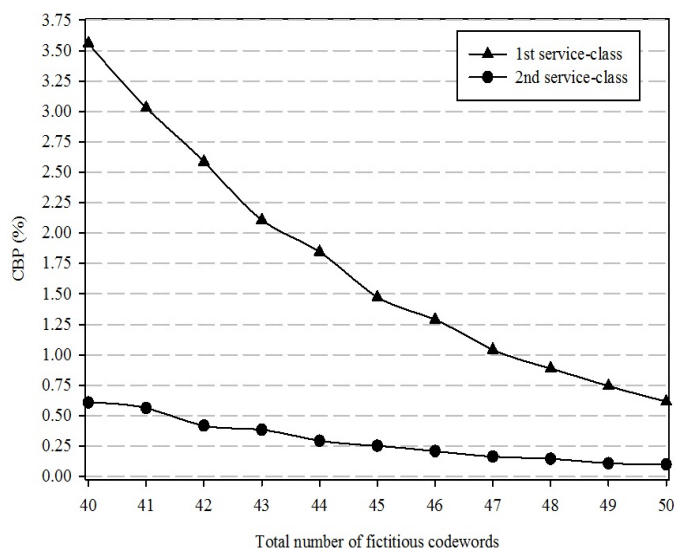


Fig. 7. Analytical CBP results of the two service-classes versus the total number of fictitious codewords.

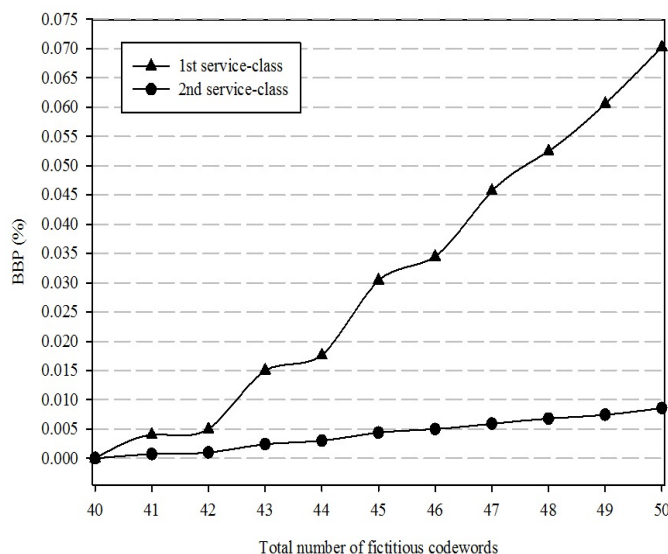


Fig. 8. Analytical BBP results of the two service-classes versus the total number of fictitious codewords.

s_3 and s_4 utilize the (211,5,1,1)-codewords. The total number of codewords is assumed to be equal to $C_1=45$ for $I_{unit}^1 = I_{unit}^2 = 0.3 \mu W$ and $I_{unit}^3 = I_{unit}^4 = 0.4 \mu W$. The traffic description parameters of the 4 service-classes are $(b_1, b_2, b_3, b_4)=(7,2,7,2), (\mu_{11}^{-1}, \mu_{12}^{-1}, \mu_{13}^{-1}, \mu_{14}^{-1})=(1.0, 1.0, 1.0, 1.1), (\mu_{21}^{-1}, \mu_{22}^{-1}, \mu_{23}^{-1}, \mu_{24}^{-1}) = (1.5, 1.9, 1.5, 1.1), (v_1, v_2, v_3, v_4) = (0.9, 0.9, 0.95, 0.95)$. The maximum received power at each receiver is assumed to be equal to $4.0 \mu W$, while the total number of fictitious codewords is 52. The total additive noise follows a Gauss distribution (1, 0.1) μW .

In Tables IV and V, we present analytical and simulation CBP results of the four service-classes, versus the call arrival rate. Tables VI and VII present analytical and simulation BBP results of the four service-classes, versus the call arrival rate. Also, in Table VIII we present analytical and simulation results for the utilization of the active and the passive link, versus the arrival rate. Comparison between analytical and simulation results shows that the accuracy of the proposed model with QoS differentiation is quite satisfactory. Note that although

the traffic characteristics of service-classes s_1 and s_3 as well as of s_2 and s_4 , justify almost the same CBP and BBP results (the small declinations are due to the effect of the LBP), the obtained results are further differentiated because of the different BER which is expressed by the different codewords.

VI. CONCLUSION

In conclusion, we present analytical models for the blocking performance of multirate OCDMA PONs with or without QoS guarantees. Our analysis takes into account parameters related to the additive noise, MAI and user activity. We provide and prove an approximate recurrent formula for the efficient calculation of the CBP, which is a function of the LBP, and of the HBP. The accuracy of the proposed analysis is quite satisfactory, as it was verified by simulations. Of course, the efficient applicability of OCDMA technique to PON need further study. As a future work we will incorporate a finite population of traffic sources in the CBP calculation, while we will study the case where the receiver has an interference cancellation capability.

TABLE VII

ANALYTICAL VS SIMULATION BBP RESULTS OF THE 3RD AND 4TH SERVICE-CLASSES FOR THE 2ND APPLICATION EXAMPLE.

Arrival Rate (calls/sec)	BBP 3 rd service-class		BBP 4 th service-class	
	Analysis (%)	Simulation (%)	Analysis (%)	Simulation (%)
0.01	8.14E-03	7.96E-03 ± 1.98E-04	7.80E-06	7.63E-06 ± 2.92E-04
0.015	2.60E-02	2.55E-02 ± 4.81E-04	7.57E-05	7.40E-05 ± 7.08E-04
0.02	6.00E-02	5.87E-02 ± 6.17E-04	3.23E-04	3.16E-04 ± 9.10E-04
0.025	1.12E-01	1.09E-01 ± 7.11E-04	8.78E-04	8.59E-04 ± 1.05E-03
0.03	1.79E-01	1.75E-01 ± 7.43E-04	1.81E-03	1.77E-03 ± 1.09E-03
0.035	2.56E-01	2.51E-01 ± 1.13E-03	3.08E-03	3.01E-03 ± 1.67E-03
0.04	3.40E-01	3.33E-01 ± 1.62E-03	4.60E-03	4.50E-03 ± 2.38E-03
0.045	4.26E-01	4.17E-01 ± 8.12E-03	6.24E-03	6.11E-03 ± 1.20E-02
0.05	5.10E-01	4.98E-01 ± 1.79E-03	7.90E-03	7.73E-03 ± 2.64E-03

TABLE VIII

ANALYTICAL VS SIMULATION RESULTS FOR THE UTILIZATION OF THE ACTIVE AND THE PASSIVE LINK FOR THE 2ND APPLICATION EXAMPLE.

Arrival Rate (calls/sec)	Active link utilization		Passive link utilization	
	Analysis (%)	Simulation (%)	Analysis (%)	Simulation (%)
0.01	2.7398	2.67968 ± 4.67E+00	4.3648	4.269022 ± 0.013886
0.015	4.1076	4.017466 ± 7.00E+00	6.544	6.400404 ± 0.033708
0.02	5.4658	5.345863 ± 9.32E+00	8.70897	8.517867 ± 0.04331
0.025	6.79756	6.6484 ± 1.16E+01	10.83055	10.59289 ± 0.049847
0.03	8.0781	7.90084 ± 1.38E+01	12.86798	12.58561 ± 0.052094
0.035	9.281585	9.077917 ± 1.58E+01	14.7777	14.45343 ± 0.079469
0.04	10.3875	10.15956 ± 1.77E+01	16.5254	16.16278 ± 0.113382
0.045	11.3842	11.13439 ± 1.94E+01	18.0911	17.69412 ± 0.569564
0.05	12.2689	11.99968 ± 2.09E+01	19.47	19.04277 ± 0.125843

ACKNOWLEDGMENT

This work was supported by the research program Caratheodory, of the Research Committee of the University of Patras, Greece.

REFERENCES

- [1] J.S. Vardakas, I.D. Moscholios, M.D. Logothetis, and V.G. Stylianakis, "Blocking performance of Multi-rate OCDMA PONs", in *proc. of the Third International Conference on Emerging Network Intelligence, EMERGING 2011*, November 20-25, 2011, Lisbon, Portugal.
- [2] F. Effenberger, D. Cleary, O. Haran, G. Kramer, R. Li, M. Oron, T. Pfeiffer, "An Introduction to PON Technologies", *IEEE Communications Magazine*, Vol. 45, No. 3, March 2007, pp. S17-S25.
- [3] H. Ueda, K. Okada, B. Ford, G. Mahony, S. Hornung, D. Faulkner, J. Abiven, S. Durel, R. Ballart and J. Erickson, "Deployment status and common technical specifications for a B-PON system", *IEEE Communications Magazine*, Vol.39, No.12, December 2001, pp. 134-141.
- [4] Ethernet in the First Mile Study Group, IEEE std. 802.3ah-2004, 2004 [Online]. Available: <http://www.ieee802.org/3/efm/public/index.html>.
- [5] T. Koonen, "Fiber to the Home/Fiber to the Premises: What, Where, and When?", *Proceedings of the IEEE*, Vol. 94, No. 5, May 2006, pp. 911-934.
- [6] K. Fouli and M. Maier, "OCDMA and Optical Coding- Principles, Applications, and Challenges", *IEEE Communications Magazine*, August 2007, pp. 27-34.
- [7] P. R. Prucnal, *Optical Code Division Multiple Access: Fundamentals and Applications*, New York: Taylor & Francis, 2006.
- [8] M. Azizoglu, J.A. Salehi, and Y. Li, "Optical CDMA via temporal codes", *IEEE Transactions on Communications*, Vol.40, No. 7, July 1992, pp. 1162-1170.
- [9] D. Zaccarin and M. Kavehrad, "An optical CDMA system based on spectral encoding of LED", *IEEE Photonics Technology Letters*, Vol. 5, No. 4, 1993, pp. 479-482.
- [10] M. Morelle, C. Goursaud, A. J.-Vergonjanne, C. A.-Berthelebot, J.-P. Cances, J.-M. Dumas, and P. Guignard, "2-Dimensional optical CDMA system performance with parallel interference cancellation", *Microprocessors and Microsystems*, Vol. 31, No. 4, June 2007, pp. 215-221.
- [11] X. Wang and K. Kitayama, "Analysis of Beat Noise in Coherent and Incoherent Time-Spreading OCDMA", *IEEE/OSA Journal of Lightwave Technology*, Vol. 22, No. 19, October 2004, pp. 2226-2235.
- [12] W.C. Kwong and G.C. Yang, "Multiple-Length extended Carrier-Hopping Prime Codes for Optical CDMA systems supporting Multirate Multimedia services", *IEEE/OSA Journal of Lightwave Technology*, Vol. 23, No. 11, November 2005, pp. 3653-3662.
- [13] E. Intay, H. M. H. Shalaby, P. Fortier, and L. A. Rusch, "Multirate optical fast frequency-hopping CDMA system using power control", *IEEE/OSA Journal of Lightwave Technology*, Vol. 20, No. 2, February 2002, pp. 166-177.
- [14] A.R. Forouzan, N-K. Masoumeh, and N. Rezaee, "Frame Time-Hopping patterns in Multirate Optical CDMA Networks using Conventional and Multicode schemes", *IEEE Transactions on Communications*, Vol. 53, No. 5, May, 2005, pp. 863-875.
- [15] V. Baby, W. C. Kwong, C.-Y. Chang, G.-C. Yang, and P. R. Prucnal, "Performance analysis of variable-weight multilength optical codes for wavelength-time O-CDMA multimedia systems", *IEEE Transactions on Communications*, Vol. 55, No. 6, July 2007, pp. 1325-1333.
- [16] G.-C. Yang, "Variable-weight optical orthogonal codes for CDMA network with multiple performance requirements", *IEEE Transactions on Communications*, Vol. 44, No. 1, January 1996, pp. 47-55.
- [17] J.S. Vardakas, I.L. Anagnostopoulos, I.D. Moscholios, M.D. Logothetis and V.G. Stylianakis, "A Multi-Rate Loss Model for OCDMA PONs", in *Proc. of the 13th ICTON 2011*, Stockholm, Sweden, 26-30 June 2011.
- [18] S. Goldberg and P. R. Prucnal, "On the Teletraffic Capacity of Optical CDMA", *IEEE Transactions on Communications*, Vol. 55, No. 7, July 2007, pp. 1334-1343.
- [19] M. Gharraei, C. Lepers, O. Affes, and P. Gallion, "Teletraffic Capacity Performance of WDM/DS-OCDMA Passive Optical Network", *NEW2AN/ruSMART 2009*, LNCS 5764, Springer-Verlag Berlin Heidelberg, 2009, pp. 132-142.
- [20] J.S. Vardakas, V.G. Vassilakis and M.D. Logothetis, "Call-Level Analysis of Hybrid OCDMA-WDM Passive Optical Networks", in *Proc. of the 10th ICTON 2008*, Athens, Greece, 22-26 July 2008.
- [21] V.G. Vassilakis, G.A. Kallos, I.D. Moscholios, and M.D. Logothetis, "The Wireless Engset Multi-Rate Loss Model for the Call-level Analysis of W-CDMA Networks", in *Proc. of the 8th IEEE PIMRC 2007*, Athens 2007.
- [22] W. Ma, C. Zuo, and J. Lin, "Performance Analysis on Phase-Encoded OCDMA Communication System", *IEEE/OSA Journal of Lightwave Technology*, Vol. 20, No. 5, May 2002, pp. 798-803.
- [23] H.-W. Chen, G.-C. Yang, C.-Y. Chang, T.-C. Lin and W. C. Kwong, "Spectral Efficiency Study of Two Multirate Schemes for Asynchronous Optical CDMA", *IEEE/OSA Journal of Lightwave Technology*, Vol. 27, No.14, July 2009, pp. 2771-2778.
- [24] M. Mehmet Ali, "Call-burst blocking and call admission control in a broadband network with bursty sources", *Performance Evaluation*, Vol. 38, No. 1, September 1999, pp. 1-19.
- [25] I.Moscholios, M. Logothetis and G. Kokkinakis, "Call-burst blocking of ON-OFF traffic sources with retrials under the complete sharing policy", *Performance Evaluation*, Vol. 59, No.4, March 2005, pp. 279-312.
- [26] N. G. Tarhuni, T. O. Korhonen, E. Mutafungwa, and M. S. Elmusrati, "Multiclass Optical Orthogonal Codes for Multiservice Optical CDMA Codes", *IEEE/OSA Journal of Lightwave Technology*, Vol. 24, No. 2, February 2006, pp. 694-704.
- [27] Simscript II.5, <http://www.simscrip.com/>
- [28] C.-S. Weng, and J. Wu, "Optical Orthogonal Codes With Nonideal Cross Correlation", *IEEE/OSA Journal of Lightwave Technology*, Vol. 19, No. 12, December 2001, pp. 1856-1863.

Analysis of a MAC Layer Covert Channel in 802.11 Networks

Ricardo Gonçalves

Department of Electrical and
Computer Engineering, Naval
Postgraduate School
Monterey, California
santana.goncalves@marinha.pt

Murali Tummala

Department of Electrical and
Computer Engineering, Naval
Postgraduate School
Monterey, California
mtummala@nps.edu

John C. McEachen

Department of Electrical and
Computer Engineering, Naval
Postgraduate School
Monterey, California
mceachen@nps.edu

Abstract—In this work, we present a proof of concept on a new covert channel in IEEE 802.11 networks, making use of the Protocol Version field in the MAC header. This is achieved by forging modified CTS and ACK frames. Forward error correction mechanisms and interleaving were implemented to increase the proposed channel's robustness to error. A laboratory implementation of the proposed channel and the results of tests conducted on the proposed channel, including measurements of channel errors, available data rate for transmission and channel detectability, are presented. The results validate the viability of the proposed covert channel and demonstrate that robustness of the channel to frame errors can be improved by using well known forward error correction and interleaving techniques.

Keywords - IEEE802.11 MAC frame; frame forging; covert channel; protocol version

I. INTRODUCTION

In this paper, it is our intention to analyze and further extend on the proof of concept presented at the Third International Conference on Emerging Network Intelligence (EMERGING 2011) [1]. Additional tests were conducted, in order to evaluate the usability of the proposed covert channel. At EMERGING 2011, we proposed a covert channel that uses the MAC header of control frames to hide the covert information. This is achieved by forging frames that use the Protocol Version (PV) bits in a way that was not intended by the designers of the IEEE 802.11 standard [2]. Specifically, the PV field and selected control bits in the MAC header field are used to accomplish this. Our work also investigates the error robustness and throughput of the channel, supported by experimental results.

As wireless networks become more ubiquitous, so do our dependencies on them. According to an industry report, in 2012 over a billion devices will be shipped with technology based on this standard onboard and the number is projected to be over two billion in 2014 [3]. Mobility and ease of access of wireless networks are very attractive characteristics to the end users, but along with them come additional security concerns [4], [5].

In order to protect wireless networks from being exploited, we need to constantly evaluate their vulnerabilities and devise techniques to mitigate them. Finding possible covert channels presents an ongoing challenge, and the potential uses for such channels range from well-intentioned

authentication mechanisms [6] to malware propagation [7], exfiltration [8] or command and control of botnets [9].

The importance of investigating as many covert channels as possible should be obvious, since each networking standard has its own unique characteristics to exploit. For this reason, it is generally accepted that covert channels cannot be completely eliminated due to numerous variations in their implementation [10], [11].

Many covert channels have been documented over the years and reflect the technological stage of the networks at which they were documented. The idea of network covert channels was documented 25 years ago by Girling [12], although the concept of a system-based covert channel was initially presented by Lampson in 1973 [13]. The vast majority of academic research has focused on documenting covert channels in layer 3 (network layer) or above (transport, session, presentation and application layers) of the OSI model [14]. These types of covert channels based on higher layer protocols span a wider variety of networks, since they are not limited by the physical or medium access mechanisms. The two most explored protocols above layer 2 (data link layer) are IP and TCP [11], [15], [16]. Even higher layer protocols, such as ICMP, HTTP or DNS, have several documented covert channels [17], [18], [19].

Recently, researchers began investigating wireless networks, specifically identifying covert channels in the MAC layer [20], [21], [22], [23]. Frame forging plays a key role in this type of covert channel. Creating fake frames with modified header bits is a recurring theme to implement such channels. MAC header fields such as the sequence number [22], initialization vector [22] or destination address [23], have been used to hide the covert information.

The rest of the paper is organized as follows. Section II presents an overview of the IEEE802.11 MAC frame fields and an analysis of network frame traffic. The proposed covert channel is described in Section III. Section IV presents the results of new experiments. Section V closes this work with a brief conclusion and future work.

II. IEEE802.11 NETWORKS AND FRAME TRAFFIC

IEEE 802.11 based wireless nodes share a common medium for communication. The fundamental building block of the 802.11 architecture is called the Basic Service Set (BSS). One BSS may be connected to other BSSs via a Distribution System (DS). Within this framework, stations

can connect in ad-hoc mode or infrastructure mode. The simpler case is ad-hoc mode, where two stations can connect directly, point to point, without a DS and an Access Point (AP). If we have the stations connecting via an AP and making use of a DS, then we say they are setup in infrastructure mode.

A. 802.11 MAC frame format

A generic MAC format for an 802.11 MAC frame can be seen in Figure 1. The frame consists of the MAC header, the frame body and the Frame Check Sequence (FCS).

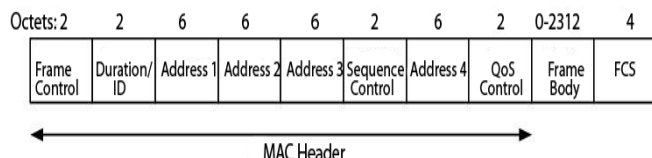


Figure 1. MAC frame format (from [2]).

The first field in the MAC header is the Frame Control (FC), consisting of two octets, and its contents are shown in Figure 2, with the PV field highlighted. This field consists of two bits that represent the version number of the 802.11 protocol being used. As of this writing, PV is expected to be set to zero [2]. This value may change in the future if a newer version of the standard is released.

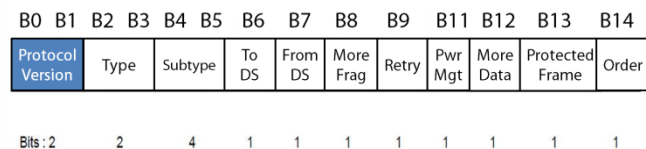


Figure 2. Frame control field (from [2]).

In the proposed covert channel, we utilize the remaining three possible combinations of the PV field to hide the covert information.

B. Frame Types of Interest

Four different types of frames exist in the 802.11 protocol: management, data, reserved and control frames.

Control type frames facilitate the exchange of data frames between stations. Within the existing control subtypes, we are interested in the smaller sized frames, the Acknowledgement (ACK) and the Clear To Send (CTS). These frames also tend to be present in large volume.

The IEEE 802.11 MAC layer makes use of the CSMA/CA scheme, in order to minimize the number of collisions and subsequent frame loss. To address the hidden node problem [24], a RTS/CTS handshake mechanism is used. The CTS is a 14-byte long frame whereas the RTS is 20 bytes long.

The ACK frame is generated when a station correctly receives a packet, and it is intended to signal the source station that the reception was successful. For such reason, this type of frame also tends to be very common in an

operational wireless network. The length of this frame is the same as the CTS, 14 bytes.

Both frames share the same format and they only differ in one bit in the subtype field within the frame control. The ACK frame has the subtype value set to "1101"; the CTS sets it to "1100".

C. Network Analysis

A heavily used 802.11 network on campus is monitored to collect frame traffic on multiple channels. From the MAC frame traffic collected, channel 1 is found to be the one with most traffic volume and number of users. We collected over 22 million packets to analyze the following frame basic characteristics.

Ideally, we want a frame that is short in length, common in occurrence, and still valid if some bits are changed. Additionally, its presence in bursts should not be a rare event. These features are desirable for achieving a reasonable throughput while providing covertness.

The results of our analysis are shown in Figure 3 as a pie chart, which represents the frequency of occurrence of different types of frames. The data frames are dominant, followed by CTS, ACK and beacons. The "others" refers to the sum of all other frames that represent less than 1% individually. From this plot we can clearly see that two types of control frames matching our needs stand out, the ACK and the CTS.

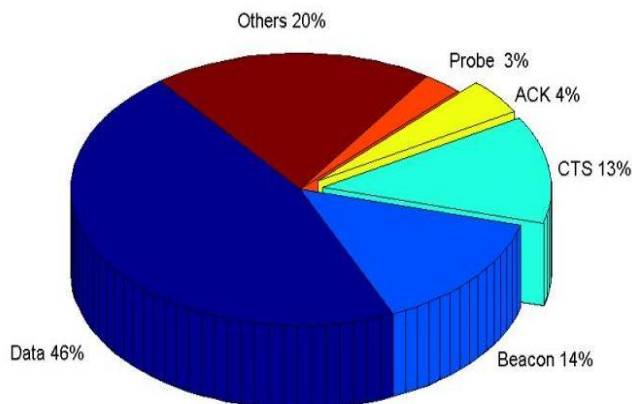


Figure 3. Frequency of occurrence of the monitored frame types.

D. Choosing the Frame Type

In the process of choosing a frame for the covert channel, several frames were considered, such as RTS and ACK. These frames could serve as well as the CTS, but they were found to be less frequent than CTS. In addition, among these three frames, RTS is the longest one with 20 bytes, and the CTS and ACK have only 14 bytes. For this reason, we narrowed the options to ACK and CTS.

From monitoring of frame traffic on the campus wireless network and empirical analysis, we found that the CTSs occur with a frequency two times higher than that of the ACKs. Different traffic scenarios were monitored, ranging from low traffic periods to high levels of utilization of the network. We chose to use CTS for building the proposed covert channel as the CTS traffic volume is large and is of

same frame size as ACK. By choosing CTS, we can minimize the chance of causing a traffic anomaly based on the type and frequency of packets flowing through the network.

Since CTS and ACK have a similar frame structure, it is easier to switch from one to the other, according to our objectives. The main concept of the proposed covert channel applies equally to both frames. It is even possible to have one end of the channel transmitting ACK frames, and the other transmitting CTS frames, without any loss or degradation of performance. Alternating frame types, such as transmitting a forged ACK followed by a forged CTS is also viable. Many other variations are also feasible.

The fact that both CTS and ACK frames do not contain a source address also contributes to a higher level of stealthiness, since it is not possible to immediately identify the source of the transmission.

III. PROPOSED COVERT CHANNEL

This section describes the proposed covert channel and the use of forward error correction and bit interleaving mechanisms to improve its performance.

A. MAC Header Manipulation

In the proposed covert channel we use two bits in the PV field of the MAC header of an 802.11 CTS packet to carry covert information. The proposed covert channel uses the PV bits in a variety of ways to signal the beginning and end of the transmission as well as to carry the information, one bit at a time. A graphical representation of the manipulated bits is shown in Figure 4.

B0	B1	B2	B3	B4	B5	B6	B7	B8	B9	B11	B12	B13	B14
Protocol Version	Type	Subtype	To DS	From DS	More Frag	Retry	Pwr Mgt	More Data	Protected Frame	Order			
Bits: 2	2	4	1	1	1	1	1	1	1	1	1	1	1

Figure 4. Manipulated bits in Frame Control field (blue squares).

In order to facilitate communication in the proposed covert channel, we divide the transmission into three

segments: start message delimiter, message, and end message delimiter. Marking the beginning and end of the covert communication allows us to establish the channel with the covert receiver station, while non-covert receivers will still see the forged frames as non-expected, thus dropping them. The start and end delimiters are realized by transmitting a sequence of five frames with "01" in the PV field. The message bits are transmitted using combinations of "10" as binary "zero" and "11" as binary "one" in the PV field. The message is organized into 8-bit ASCII characters. Figure 5 shows a capture of Wireshark [25] in which we can see the transmission of the ASCII character "A" converted into the binary string "01000001". A total of 18 frames were transmitted. Looking at the first column (Protocol) we see the identification of a valid CTS format, it is only when looking to the second column (Protocol Version) that our frame manipulation becomes noticeable. There we can see the changes in the PV number, from 1 to 3.

B. Forward Error Correction

Since we are operating in a shared media, collisions will eventually occur. This will be interpreted as an error, since a frame carrying covert payload will be lost. To mitigate the effect of frame losses, and thus reduce the number of errors in the covert channel, the use Forward Error Correction (FEC) was considered.

There are several options for implementing FEC: block codes such as Hamming and Reed-Solomon, convolutional codes, turbo codes, or low density parity check codes [26]. In this work, however, a convolutional code was used for error correction.

A convolutional coder takes an m - bit message and encodes it into an n - bit symbol. The ratio $\frac{m}{n}$ is known as the code rate. In our case a code rate of $\frac{2}{3}$ was used, meaning the encoded message will be one and a half times as long as the original message. This will increase the time needed to transmit the same message as before, since a higher number of bits is being sent.

Another important parameter in convolutional coding is the constraint length. This parameter, k , represents the number of bits in the encoder memory that affect the

Protocol	Prot Version	Dest Addr	#	Length	Flags
Clear-to-send, Flags=.....	1	11:0c:f1:0b:7e:1e (RA)	1	1	14 0x00
Clear-to-send, Flags=.....	1	11:0c:f1:0b:7e:1e (RA)	2	2	14 0x00
Clear-to-send, Flags=.....	1	11:0c:f1:0b:7e:1e (RA)	3	3	14 0x00
Clear-to-send, Flags=.....	1	11:0c:f1:0b:7e:1e (RA)	4	4	14 0x00
Clear-to-send, Flags=.....	1	11:0c:f1:0b:7e:1e (RA)	5	5	14 0x00
Clear-to-send, Flags=.....	2	11:0c:f1:0b:7e:1e (RA)	6	6	14 0x00
Clear-to-send, Flags=.....	3	11:0c:f1:0b:7e:1e (RA)	7	7	14 0x00
Clear-to-send, Flags=.....	2	11:0c:f1:0b:7e:1e (RA)	8	8	14 0x00
Clear-to-send, Flags=.....	2	11:0c:f1:0b:7e:1e (RA)	9	9	14 0x00
Clear-to-send, Flags=.....	2	11:0c:f1:0b:7e:1e (RA)	10	10	14 0x00
Clear-to-send, Flags=.....	2	11:0c:f1:0b:7e:1e (RA)	11	11	14 0x00
Clear-to-send, Flags=.....	2	11:0c:f1:0b:7e:1e (RA)	12	12	14 0x00
Clear-to-send, Flags=.....	3	11:0c:f1:0b:7e:1e (RA)	13	13	14 0x00
Clear-to-send, Flags=.....	1	11:0c:f1:0b:7e:1e (RA)	14	14	14 0x00
Clear-to-send, Flags=.....	1	11:0c:f1:0b:7e:1e (RA)	15	15	14 0x00
Clear-to-send, Flags=.....	1	11:0c:f1:0b:7e:1e (RA)	16	16	14 0x00
Clear-to-send, Flags=.....	1	11:0c:f1:0b:7e:1e (RA)	17	17	14 0x00
Clear-to-send, Flags=.....	1	11:0c:f1:0b:7e:1e (RA)	18	18	14 0x00

Figure 5. Wireshark capture of an "A" being transmitted using the proposed covert channel.

generation of the n output bits [26]. A constraint length of 4 is used in our experiments.

Forward error correction is typically applied to the transmission of a stream of bits sent and received sequentially. In our case, however, the bits are embedded into independent frames, which are prone to loss. As a result, when a frame is lost, the receiver has no indication that a bit is missing. Consequently, we now need to know exactly which frames were lost in order to apply the FEC correctly.

One option is to use the eight flag bits in the frame control field of the MAC header to index a longer sequence number, which makes determining the location of lost frames an easier task. These flag bits will not carry any covert information but serve only the error correction function. However, it is important to state that applying this use of the flag bits will increase the probability of detection of the covert channel, since unexpected flag attributions will be present. In this situation, we move from a minimum deviation, from a legitimate CTS, of two bits (as in Figure 4) to a maximum of 10 bits (as in Figure 6). This presents a tradeoff between detectability and error performance, and the user must exercise the option to choose one over the other as dictated by the application. In order not to use the flag bits one could use the type and subtype fields of the MAC header. The IEEE802.11 standard defines some bit combinations of the subtype field as “Reserved” [2]. Exploring these combinations could be an option, although we did not test it.

Figure 6 is a representation of how we accommodated the information and sequence bits within the MAC header.

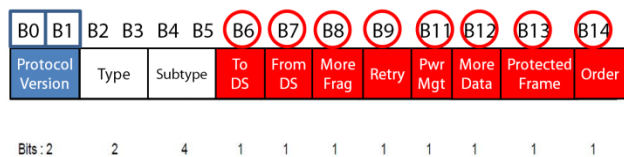


Figure 6. Representation of the frame structure using the flag bits for sequencing (red circles).

The blue squares represent our covert channel bits. These bits are used in the same way as before: the first bit (B0) signals the presence of the channel and the second is payload (B1). The red circles refer to the sequence bits, which are placed in the flag bits of the frame control field.

Given that we have eight flags, this gives us a total of 2^8 possible sequence numbers. This alone provides a reasonable amount of protection against a long burst of frame losses, when compared to the previous approach.

C. Forward Error Correction and Interleaving

We now consider sending more than one bit of information per forged frame.

Since each frame now carries more than one information bit, the loss of one or more frames has a larger impact on the total number of errors in the channel. In order to mitigate this effect, we interleave the bit string resulting from the convolutional coder. This consists of breaking the coded message in blocks of 8 bits, building a matrix with each

block in a different row. By reading the matrix out by column, from top to bottom, we generate a new string of bits, effectively interleaving all the 8 bit blocks [27], [28]. The number of rows depends on the length of the message we are transmitting.

At the output of the convolutional coder we interleave the bits in groups of 8 bits. This results in a new string of zeros and ones, which goes into the covert channel processing block. Here the string is separated in groups of n bits, and each group will become the payload of the forged frames. Figure 7 is a schematic representation of this idea.

Notice that only information bits are encoded and interleaved; in this implementation the convolutional coder is applied after we gather the complete message we want to transmit.

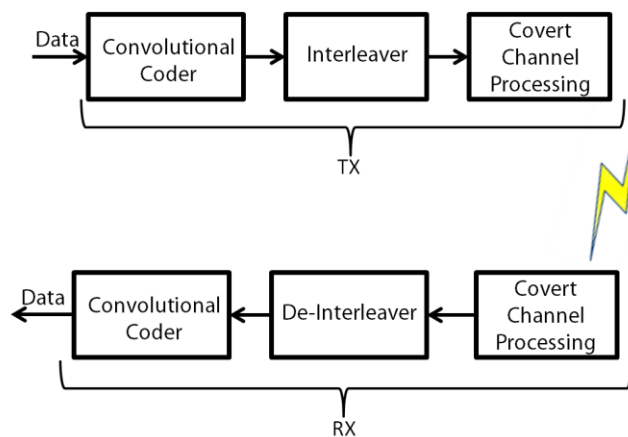


Figure 7. FEC and interleaving block diagram.

One possible implementation is to use six bits for payload. The frame is forged as follows: six information bits are placed in the selected flag bits, three other bits are used for sequence numbers, and the first PV bit is set to one, indicating the use of the covert channel. Figure 8 illustrates the proposed structure. The blue squares indicate payload bits, and the red circles are sequence numbers. The green diamond (B0) indicates the presence of the covert channel. Bits B1, B8 and B9 form the sequence number yielding a sequence length of eight. Bits B10-B15 form the payload, using six bits to carry the message.

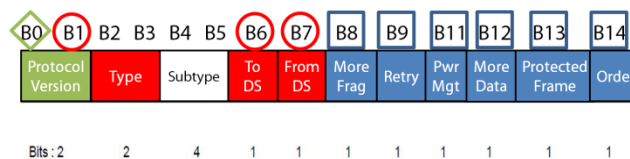


Figure 8. Representation of the frame structure using three bits for sequencing (red squares) and six bits for payload (blue squares).

IV. EXPERIMENTS AND RESULTS

In order to implement the proposed covert channel, we developed the necessary code to forge, transmit, and receive frames. Python [29] was the chosen programming language,

due to its simplicity, available libraries and extension modules that facilitated our task. The elected OS was Linux, for being more flexible, open source and GNU licensed.

The code is divided into three threads running simultaneously, as presented in Figure 9. One thread runs as the receiver, counting the initialing sequence that marks the opening of the covert channel, buffering the received message and identifying the closing sequence. At that point, it starts the recovery part of the process, corresponding to the right half of Figure 7. Thread2 acts as the transmitter, executing all the tasks shown on the left half of Figure 7.

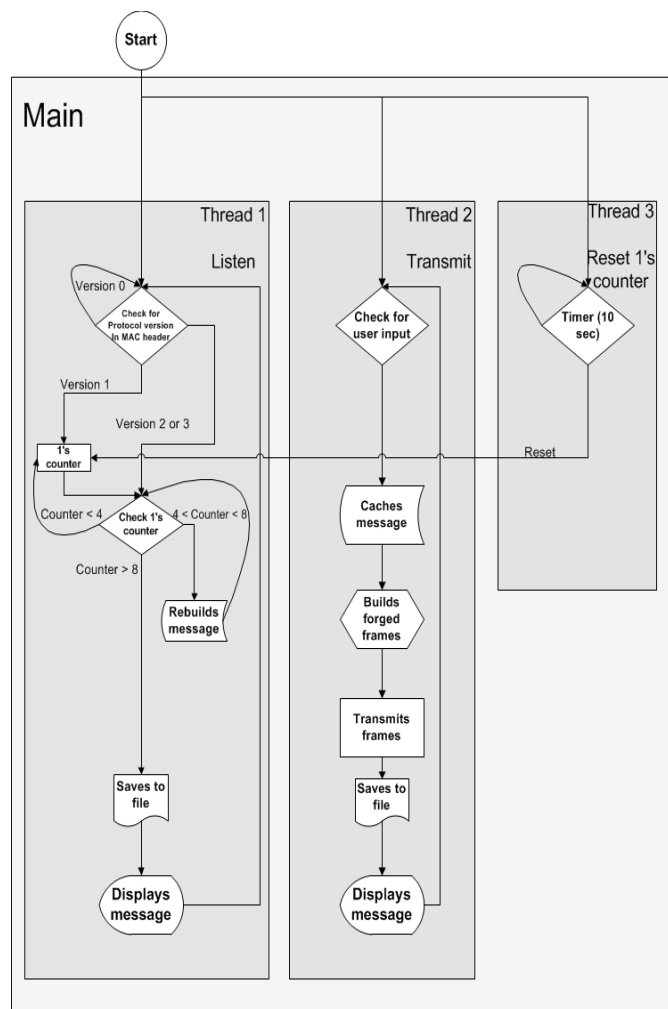


Figure 9. Flow chart of the covert channel code implementation.

Finally, the third thread contains a control mechanism to filter possible discrepancies in the identification of the beginning and end of the covert communication. During our monitoring of real working wireless networks, other version 1 frames (with bad checksums) were found circulating in the network, thus becoming noise to our version 1 frames. Thread3 is responsible for filtering out these unwanted frames.

A. Test bed

Tests were conducted in a laboratorial environment, with controlled levels of interference. All measurements were made using the same stations in the same relative positions inside a closed room. The levels of interference ranged from 0 to 1000 frames per second. ARP frames were used as the interfering frames, at a fixed transmission rate, due to its simplicity to generate with common exploit tools, such as *aireplay-ng* [30]. In order to have a considerable level of interference, all ARP frames were made to be 72 bytes long.

The tested scenario consisted of transmitting the same covert message, while varying the number of payload bits and applying different levels of interfering traffic in each trial. The standard sentence used in our tests has an original length of 1408 bits, which translates to a total of 2112 bits after applying FEC and interleaving, with the intention of improving the error robustness of the channel. In order to collect a statistically relevant sample, each sentence was repeatedly transmitted between 500 to 1500 times for each payload size (from 1 to 6 payload bits) and interference level (from 0 to 1000 in steps of 125 ARP frames per second). This brings the number of analyzed bits close to 60 million for each trial. The different number of sentence transmissions is due to the need of balancing the number of transmitted frames in order to make a fair comparison between trials, since different payload sizes impact on the total number of frames to be forged in order to send the entire message.

Three laptops with the same hardware configuration were used, utilizing a PCM 3COM 3CRPAG175 with an Atheros chip AR5212 as the wireless network adapter. One laptop was setup as transmitter (Station A), another as noise source (Station B), and the third one as passive monitor (Station C). Stations A and B were running Backtrack4 as OS, and Station C ran Windows XP SP2. The monitoring program used was Airopeek NX, version 3.0.1 [31].

It is important to notice that stations A (source of messages) and B (source of interference) are operating in ad-hoc mode, outside any infrastructure wireless network. The stations transmit without coordination from access points. Our intention is to cause collisions, and thus frame losses, which are interpreted as errors for analysis purposes.

Experimental data is then collected by station, C, set to collect all frames in promiscuous mode.

All active communications during the tests are unidirectional, being broadcasted from one unique station. This setting rules out any tests to the receiving part of the covert channel code, since station C is collecting all the traffic for later analysis, not decoding the message in real time.

The expected error performance is displayed in Figure 10, showing the number of errors, in a log scale on the Y-axis, versus the interference level on the X-axis. We expect to see an increase in the number of errors as the interference level rises. At some point, the use of FEC will introduce more errors than the ones originally received, becoming disadvantageous. The blue solid line represents the number of errors after the use of FEC, where the red dotted line

represents the number of error at the reception, before going through FEC. We assume this last condition to be equivalent to having the exact same message without FEC, since we do not process that algorithm, and measure errors in raw as they are received.

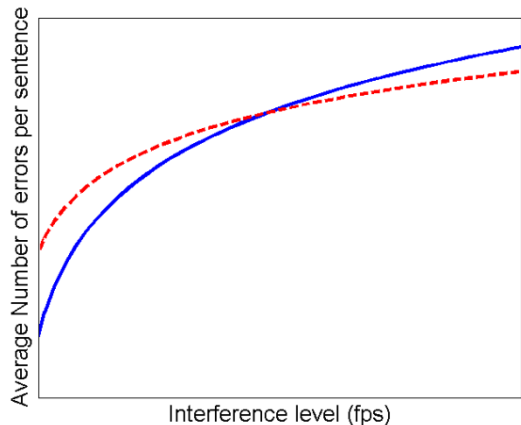


Figure 10. Expected evolution of the number of errors without FEC (red dashed line) and using FEC (blue solid line).

B. Results

1) Fixed payload size of 2 bits

For a payload size of 2 bits and 7 bits for sequencing, the collected data is displayed in Figure 11. In this case we are able to resist some bursts of errors, since the addressing space is still fairly large (2^7), enabling us to pinpoint the missing bits. We can see all the errors being corrected for an interference level up to 125 frames per second.

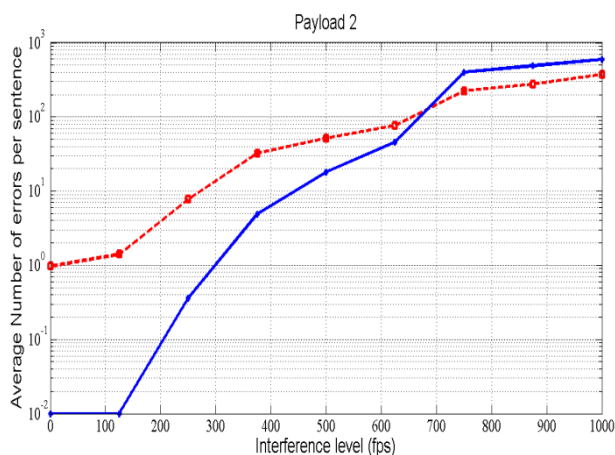


Figure 11. Number of errors for a fixed payload size of 2 bits at different interference levels. Blue solid line is the result after FEC, red dashed line before FEC.

Above that interference level, the number of errors after FEC tends to increase and at approximately 675 frames per second of interference it crosses over and surpasses the number of errors when no FEC is in place. With such payload per frame, it was necessary to generate 1056 frames for the complete message, plus the 10 marking frames. This adds to a total of 119392 bits for each sequence. In this trial the sequence was transmitted 500 times, so the total number of transmitted bits approaches the 60×10^6 .

The benefits of this configuration are present in low to medium levels of interference. This result is consistent with our expectations.

2) Fixed payload size 4 bits

For a payload size of 4 bits and 5 bits for sequencing, the collected data is displayed in Figure 12. Here we can see how the number of errors increases at low interference levels, when compared to the previous results, confirming an expected degradation in the channel quality. The crossover point happens at around 475 frames per second.

By increasing the payload we reduced the number of forged frames to send the covert message. In this case, the number of repetitions of each sentence was 1000, as opposed to the 500 of the previous setting.

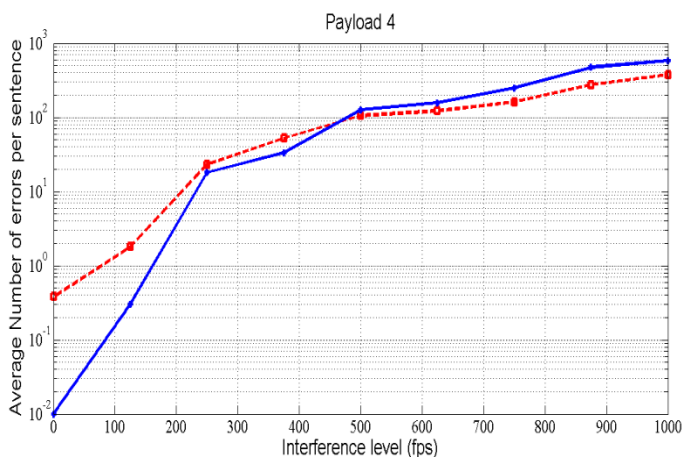


Figure 12. Number of errors for a fixed payload size of 4 bits at different interference levels. Blue solid line is the result after FEC, red dashed line before FEC.

3) Fixed payload size 6 bits

For a payload size of 6 bits and only 3 bits for sequencing, the collected data is displayed in Figure 13.

With these settings, the level of interference needed to induce a large number of errors does not have to be very high. The crossover point happens at a lower level of interference, around 200 frames per second.

For this payload size we had to increase the number of repetitions up to 1500 for each trial.

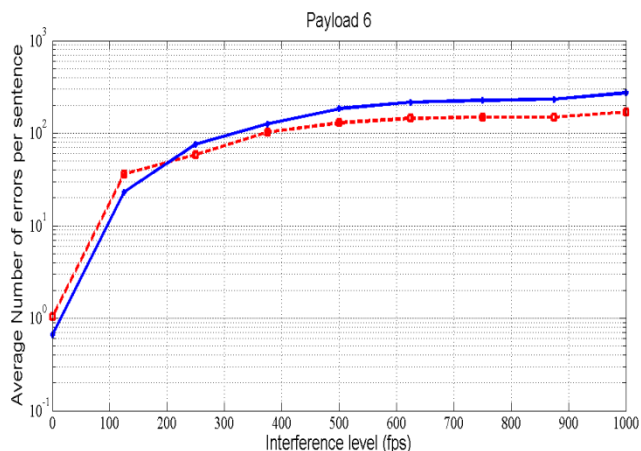


Figure 13. Number of errors for a fixed payload size of 6 bits at different interference levels. Blue solid line is the result after FEC, red dashed line before FEC.

4) Fixed interference rate

Taking a different approach to the collected data, we analyzed the effect of a fixed interference level (500 frames per second) given different payload sizes, ranging from 1 to 6 payload bits. Here we can observe how the crossover point sits between a 3 and 4 payload size. Before that point FEC is an important technique to enhance the channel resilience. From that point on, we can clearly see the effect FEC has in generating more errors than the ones received.

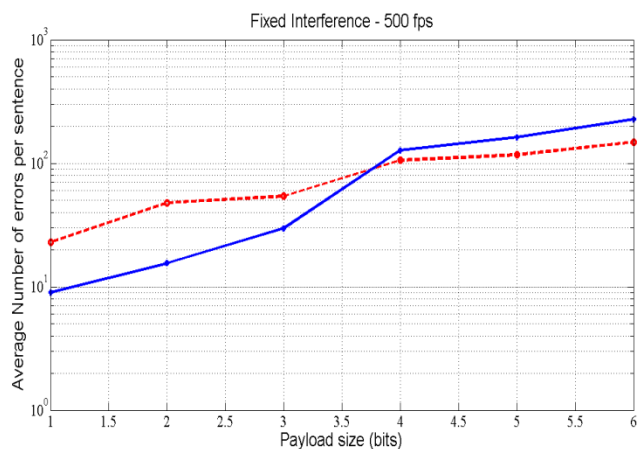


Figure 14. Percentage of errors for a fixed interference rate and payloads between 1 and 6. Blue solidline is the result after FEC, red dashed line before FEC.

A relevant aspect taken from these experiments is the motion of the cross over point, as we change the interference level. This can be used as a reference for changing the payload size as the level of interference changes. To find the level of interference, and since we intend to operate inside a structured network, we can use the data rate information embedded in each packet. This would allow an adaptive covert channel to be created, responding to different levels of interference with different payload sizes.

C. Throughput Analysis

In order to evaluate the throughput offered by the proposed channel, the rate at which the frames are transmitted is measured. Being a proof of concept, code efficiency was not a major concern, and the results are presented for analysis purpose only, meaning significant improvements may be easily achieved. This was done using AiropEEK [31] and by averaging the rate of the forged frames on a per second basis. Depending on the network usage at the time, the frame rate varies significantly. Another factor responsible for this variation is the continuous adjustment of the maximum data rate of the network as dictated by the channel conditions. For IEEE 802.11b networks the maximum network data rate possible values are 1, 2, 5.5, and 11 Mbps [2].

To obtain a benchmark for performance comparison, we first determine the maximum data rate possible for the covert channel under optimal conditions. The following conditions are assumed:

- (i) The channel is ideal with no errors;
- (ii) there is only one station with frames to transmit;
- (iii) we use a data rate of 2 Mbps, the highest possible for 802.11b control frames (basic rate set) [2].

The medium access scheme has to obey some predetermined timing constraints, set by the standard. Figure 15 is a graphical representation of the timing requirements for transmitting a frame.

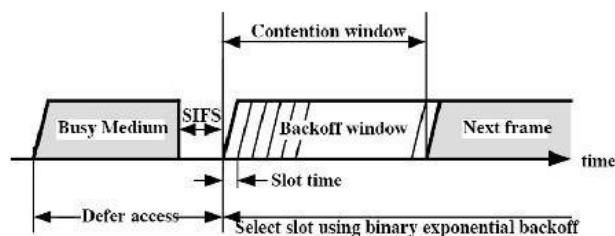


Figure 15. Timing constraints in an 802.11 frame transmission [After 32].

Applying the work of Xiao and Rosdhal [33] and Jun et al. [34] to the proposed covert channel, the minimum amount of time necessary to transmit a forged CTS is $t_{min} = 376 \mu s$, corresponding to a maximum of 2659 forged frames per second. At one bit per frame the maximum bit rate is 2659 bps; at six bits per frame we get 15.954 kbps. The measured throughput values, however, will be significantly smaller.

When we transmit one bit of information in each forged frame, we have an overhead of the start and end delimiters for a total of 10 signaling frames. The measured average frame rate is 61 frames per second. Since each frame represents a bit, and considering our message payload of 1408 bits, we transmit a total of 1418 bits. At 61 frames per second this corresponds to a total transmission time of 23.25 sec, and a useful bit rate or throughput of 60.5 bps.

On the other hand, when we transmit 6 bits per forged frame and introduce the use of interleaving, the measured average transmission rate is 32 frames per second. By transmitting a total of 2122 bits, we obtain a transmission

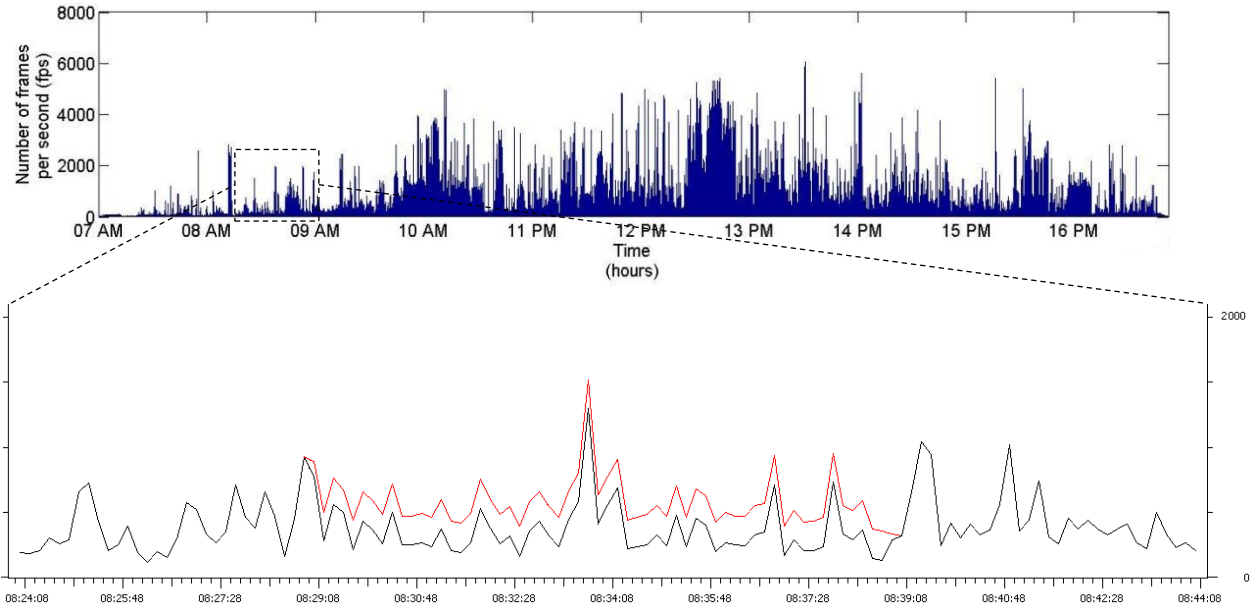


Figure 16. Traffic profile of a low usage WiFi channel on campus

time of 11 seconds. The resulting throughput value is 127.4 bps, considerable improvement over the previous case.

D. Covertness Analysis

By evaluating the impact our proposed channel has in an operating wireless network, we can work to reduce its detectability by making use of traffic profile analysis. Figure 16 is a partial magnification of the traffic profile of a busy channel during a normal working day at campus, where the black (lower) line represents the normal network traffic, and the red (upper) line shows the normal traffic plus the traffic due to covert (forged) frames. As we can see in Figure 16, the difference between the red line and the black line corresponds to the amount of traffic added by the use of the covert channel. Since the network traffic is fairly heavy, the presence of the covert channel is not obvious; our traffic just blends in with the overall traffic.

Selected portion of network traffic profile showing the additional traffic generated by the use of the proposed covert channel (red top line).

Applying the same reasoning to a low traffic channel, in the same campus area, during a normal working day, we can notice a substantial difference. Figure 17 shows the traffic profile of an available but modestly used channel, and without any covert traffic.

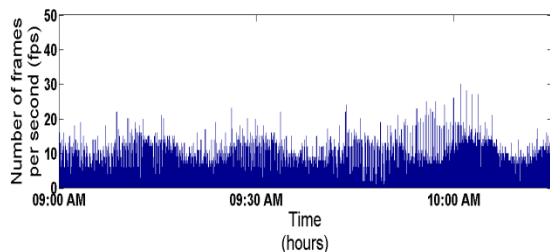


Figure 17. Traffic profile of a low usage WiFi channel on campus.

Figure 18 clearly shows the impact our covert transmissions have in the traffic profile of such channel. The traffic peaks are the result of injecting forged frames. In this case, our covert message being transmitted was a random sequence of 3500 bits. Zooming in and splitting the two types of traffic, as seen in Figure 18, reveals the presence of an abnormal amount of traffic. In this case, there is a significant difference between the two types of traffic, with or without covert transmissions.

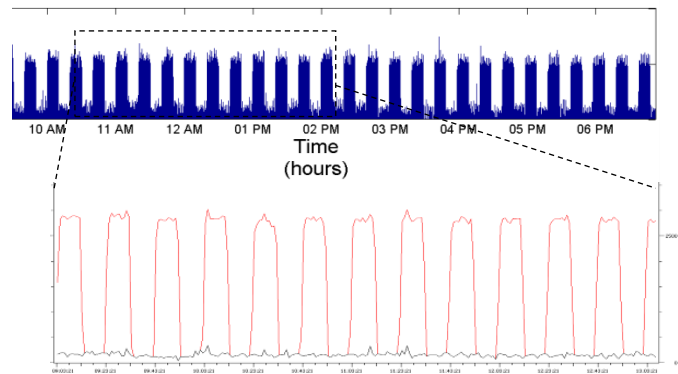


Figure 18. Selected portion of network traffic profile showing the additional traffic generated by the use of the proposed covert channel (red top line).

Figure 19 displays the traffic profile when using different rates of transmission and their impact. The stealthiness of the channel can be improved by spacing the transmission of forged frames. How the covert traffic can be made less visible by introducing spacing between frames is illustrated below. One of the down sides of this manipulation is the obvious reduction of throughput. Segment (a) in Figure 19 corresponds to normal frame transmission with no additional

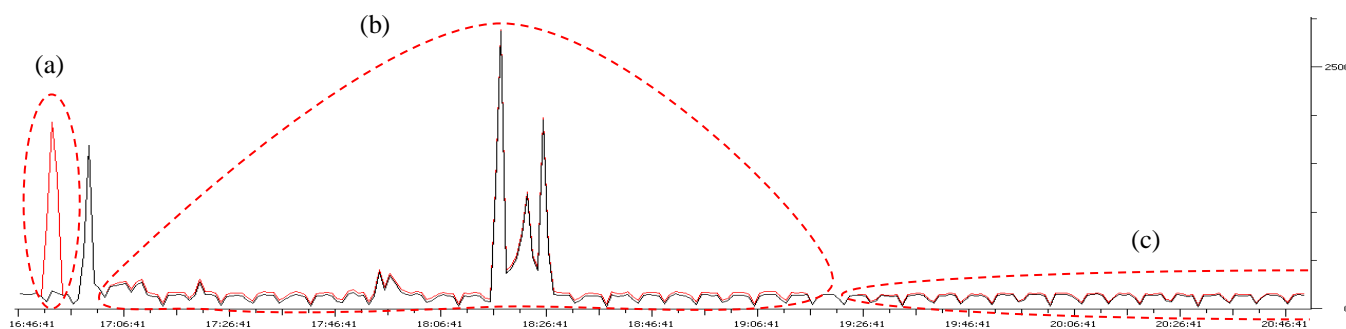


Figure 19. Selected portion of network traffic profile showing the effect of different transmission rates.

spacing between the frames, i.e., no delay was introduced between transmitted frames. For this segment, the total transmission time is approximately two minutes at a measured average of 30 frames per second.

In segment (b), frames are sent once every two seconds, resulting in a total transmission time of 2 hours and 12 minutes. Finally, segment (c) is shown only partially; we sent one frame every four seconds for a total transmission time of 4.5 hours.

The important aspect is that the difference between the legitimate and covert traffic becomes smaller and smaller as the spacing increases; at some point, it is possible to make it almost invisible as we extend the spacing. On the other hand, the throughput is degrading proportionally.

Another technique to camouflage our use of the covert channel is to space the forged frames transmission in a non-uniform way instead of sending the frames at regular time intervals. Although considered, this variation was not tested.

V. CONCLUSIONS

This work presented, implemented, and tested a MAC layer 802.11 covert channel. We used the PV field in the MAC header to hide and transfer the covert information. Within the MAC header we used the PV field, as well as the flag bits, to hide our message.

The proposed covert channel was implemented by developing the necessary code in Python. A GUI chat console is used for message transmission. In our approach, users only have to run a single Python script in order to access the chat console. The test bed used for experiments operated in a Linux environment.

Robustness to errors in the covert channel is improved by the use of forward error correction and bit interleaving. Results indicate significant improvement in the error performance of the channel for low interference rates.

Detectability of the use of the proposed covert channel was also investigated, demonstrating a method of minimizing our exposure to such type of analysis. Throughput is severely affected once we try to reduce our traffic profile footprint.

The achieved throughput of the covert channel was measured under two different scenarios, in which we changed the size of the payload. The maximum channel data rate was also determined. The case of 6-bit payload along with convolutional coding and interleaving yielded the highest measured throughput.

This proof of concept can benefit considerably from future work. This may include code optimization in order to increase the frame rate, testing other error correction algorithms, and embedding this covert channel into legitimate traffic, directly at a firmware level, instead of relying on the injection of forged frames.

REFERENCES

- [1] R. Gonçalves, M. Tummala, and J. McEachen, "A MAC Layer Covert Channel in 802.11 Networks", The Third International Conference on Emerging Network Intelligence EMERGING 2011, November 20-25, 2011 - Lisbon, Portugal
- [2] Institute of Electrical and Electronics Engineers, 802.11, Wireless LAN Medium Access Control (MAC) and Physical Layer (PHY) Specifications (accessed January 17, 2011). <http://ieeexplore.ieee.org>
- [3] D. McGrath, "WLAN chip set shipments projected to double," in EE Times, 2/17/2011. (accessed March 17, 2011) <http://www.eetimes.com/electronics-news/4213260/WLAN-chip-set-shipments-projected-to-double>
- [4] H. Yang, F. Ricciato, S. Lu, and L. Zhang, "Securing a wireless world," in Proceedings of the IEEE, vol.94, Issue 2, pp. 442-454, February 2006.
- [5] Y. Xiao, C. Bandela, and Y. Pan, "Vulnerabilities and security enhancements for the IEEE 802.11 WLANs," in Proceedings of the IEEE Global Telecommunications Conference (GLOBECOM) 2005, pp. 1655-1659, 2005.
- [6] T.E. Calhoun, R. Newman, and R. Beyah, "Authentication in 802.11 LANs Using a Covert Side Channel," in Communications, 2009. ICC '09. IEEE International Conference, pp. 1-6, 14-18 June 2009.
- [7] E. Couture, "Covert Channels," SANS Institute InfoSec Reading Room (accessed January 17, 2011). http://www.sans.org/reading_room/whitepapers/detection/covert-channels_33413
- [8] A. Giani, V. H. Berk, and G. V. Cybenko, "Data Exfiltration and Covert Channels," Process Query Systems, Thayer School of Engineering at Dartmouth (accessed February 02, 2011). http://www.pqsnet.net/~vince/papers/SPIE06_exfil.ps.gz
- [9] D.T. Ha, G. Yan, S. Eidenbenz, and H.Q. Ngo, "On the effectiveness of structural detection and defense against P2P-based botnets," in Dependable Systems & Networks, 2009. DSN '09. IEEE/IFIP International Conference, pp. 297-306, June 29 2009-July 2 2009.
- [10] S. Hammouda, L. Maalej, and Z. Trabelsi, "Towards Optimized TCP/IP Covert Channels Detection, IDS and Firewall Integration," in New Technologies, Mobility and Security, 2008. NTMS '08., pp.1-5, 5-7 Nov. 2008.

- [11] C. H. Rowland, "Covert channels in the TCP/IP protocol suite," in Tech. Rep. 5, First Monday, Peer Reviewed Journal on the Internet, July 1997.
- [12] C.G. Girling, "Covert Channels in LAN's," in Software Engineering, IEEE Transactions, vol. SE-13, no. 2, pp. 292-296, Feb. 1987.
- [13] B. Lampson, "A note on the confinement problem," in Communications of the ACM, vol. 16, pp. 613-615, October 1973.
- [14] U.S. Department of Defense, Trusted Computer System Evaluation Criteria, pp. 80, DoD 5200.28-STD, July 1985.
- [15] S. Cabuk, C.E. Brodley, and C. Shields, "IP Covert Timing Channels: Design and Detection," in Proc. 11th ACM Conf. Computer and Communications Security (CCS), pp. 178-87, October 25-29 2004.
- [16] S. J. Murdoch and S. Lewis, "Embedding Covert Channels into TCP/IP," in Proc. 7th Information Hiding Workshop, June 2005.
- [17] M. Bauer, "New Covert Channels in HTTP: Adding Unwitting Web Browsers to Anonymity Sets," in Proceedings of the 2003 ACM Workshop on Privacy in Electronic Society, pp. 72-78, October 2003.
- [18] A. Galatenko, A. Grusho, A. Kniazev, and E. Timonina, "Statistical Covert Channels Through PROXY Server," Proceedings 3rd International Workshop - Mathematical Methods, Models, and Architectures for Computer Network Security, pp. 424-29, September 2005.
- [19] M. Smeets and M. Koot, "Research report: covert channels," Master's thesis, University of Amsterdam, February 2006.
- [20] S. Li and A. Ephremides, "A network layer covert channel in ad-hoc wireless networks," Sensor and Ad Hoc Communications and Networks, 2004. IEEE SECON 2004. 2004 First Annual IEEE Communications Society Conference, pp. 88-96, 4-7 October 2004.
- [21] T. Calhoun, X. Cao, Y. Li, and R. Beyah, "An 802.11 MAC layer covert channel," in Wireless Communications and Mobile Computing, Wiley InterScience (accessed January 2011).
<http://onlinelibrary.wiley.com/doi/10.1002/wcm.969/pdf>
- [22] L. Frikha, Z. Trabelsi, and W. El-Hajj, "Implementation of a Covert Channel in the 802.11 Header," in Wireless Communications and Mobile Computing Conference, 2008. IWCMC '08., pp. 594-599, 6-8 Aug. 2008.
- [23] L. Butti, Raw Covert (accessed September 2010) http://rfakeap.tuxfamily.org/#Raw_Covert
- [24] F.A. Tobagi and L. Kleinrock, "Packet switching in radio channels: the hidden node problem in carrier sense multiple access modes and the busy tone solution," in IEEE Trans. Commun., vol. 23, pp. 1417-1433, 1975.
- [25] Wireshark v.1.4.0 <http://www.wireshark.org> (accessed October 2010).
- [26] S. Lin and D. J. Costello., Error Control Coding: Fundamentals and Applications, Pearson Prentice Hall, New Jersey, 1983.
- [27] J. Proakis and M. Salehi, Digital Communications, Fifth edition, McGraw Hill, New York, 2008.
- [28] L. Chen, T. Sun, M. Y. Sanadidi, and M. Gerla, "Improving wireless link throughput via interleaved FEC," in Computers and Communications, 2004. Proceedings. ISCC 2004. Ninth International Symposium on , vol.1, no., pp. 539- 544 Vol.1, 28 June-1 July 2004.
- [29] Python™ Programming Language (accessed July 2010) <http://www.python.org/>
- [30] Aircrack-ng / Aireplay-ng (accessed March 2012) <http://www.aircrack-ng.org/doku.php?id=aireplay-ng>
- [31] Airopeek NX v.3.0.1 (accessed December 2010) <http://www.wildpackets.com/>
- [32] W. Stallings, Wireless Communications and Networks, Second edition, Pearson Prentice Hall, New Jersey, 2005.
- [33] Y. Xiao and J. Rosdahl, "Throughput and delay limits of IEEE 802.11," in Communications Letters, IEEE , vol.6, no.8, pp. 355- 357, Aug 2002.
- [34] J. Jun, P. Peddabachagari, and M. Sichitiu, "Theoretical maximum throughput of IEEE 802.11 and its applications," in Network Computing and Applications, 2003. NCA 2003. Second IEEE International Symposium on, pp. 249-256, 16-18 April 2003.

A Framework for the Design, Development and Evaluation of Cognitive Wireless Sensor Networks

Alvaro Araujo Pinto, Elena Romero, Javier Blesa and Octavio Nieto-Taladriz

E.T.S.I Telecomunicacion, Electronic Engineering Dep.

Universidad Politécnica de Madrid

Madrid, Spain

{araujo,elena,jblesa,nieto}@die.upm.es

Abstract—Cognitive Wireless Sensor Networks are an emerging technology with a vast potential to avoid traditional wireless problems such as reliability, interferences and spectrum scarcity. Cognitive Wireless Sensor Networks frameworks are a key issue in the future developments of these networks because they allow a lot of protocols, strategies and optimization algorithms to be tested. A framework composed of a network simulator based on Castalia is presented in this paper. This simulator has been improved with cognitive features and feedback from Cognitive Wireless Sensor Networks real devices. This framework allows an easy and intuitive development of complete cognitive networks with spectrum sensing, learning and collaboration features. This is a crucial issue in order to facilitate the design and development of new algorithms, strategies and protocols for Cognitive Wireless Sensor Networks, and evaluate their performance. The benefits of the proposed framework are demonstrated with four different scenarios and simple cognitive communications strategies. Results show how new concepts have been successfully integrated in the framework and how several areas of research could take advantage of it.

Keywords-Cognitive radio; Wireless Sensor Network; framework; simulator.

I. INTRODUCTION

According to the Wireless World Research Forum (WWRF), seven trillion wireless devices will be serving seven billion people by 2020 [2]. In recent years, Wireless Sensor Networks (WSN) have undoubtedly been one of the fastest growing sectors in wireless and mobile communications. As stated in [3], the WSN market will grow rapidly from \$0.45 billion in 2011 to \$2 billion in 2021. WSNs consist of spatially distributed autonomous sensors that monitor a wide range of environmental conditions and cooperate to share data across the network.

WSNs are being increasingly introduced into our daily lives. Potential fields of application of WSNs are automatic monitoring of forest fires, avalanches, hurricanes, failures of country wide utility equipment, traffic, hospitals, home monitoring, military operations, critical infrastructure protection, to name a few. The emergence of wireless technologies such as Zigbee and IEEE 802.15.4 has allowed the development of interoperable commercial products, which is important for ensuring scalability and low cost.

IEEE 802.15.4 based systems constitute 88% of all WSN deployments up to 2011 [4].

The increasing demand for wireless communication presents the challenge of improving the spectrum utilization efficiency. Most WSN solutions operate on unlicensed frequency bands. In general, they use Industrial, Scientific and Medical (ISM) bands, like the worldwide available 2.4 GHz band. This band is also used by a large number of popular wireless technologies, like Wi-Fi or Bluetooth. For this reason, the unlicensed spectrum bands are becoming overcrowded with the increasing use of WSN based systems. As a result, coexistence issues in unlicensed bands have been the subject of extensive research [5] [6]. In particular, it has been shown that IEEE 802.11 networks can significantly degrade the performance of Zigbee/802.15.4 networks when operating on overlapping frequency bands [6].

To address the spectrum saturation challenge, Cognitive Radio (CR), which enables opportunistic access to the spectrum, has emerged as the key technology. A CR is an intelligent wireless communication system that is aware of its surrounding environment, and adapts its internal parameters to achieve reliable and efficient communications. CR has three main technical features: the cognitive capabilities of its devices, collaboration among terminals and the fact that they learn from their history. CR differentiates between two kinds of users; Primary Users (PUs) are the licensed users, and Secondary Users (SUs) are those who try to use the same bands when they detect a spectral hole.

Adding cognition to the existing WSN infrastructure will bring about many benefits. In fact, WSNs are one of the areas with a highest demand for cognitive networking. In WSNs, the node resources are constrained mainly in terms of battery and computation power, but also in terms of spectrum availability. Hence, with cognitive capabilities, WSNs could find a free channel to communicate either in the unlicensed or the licensed band. However, the cognitive technology will not only provide access to new spectrum bands but will also achieve better propagation characteristics. By adaptively changing system parameters like modulation schemes, transmit power, carrier frequency and constellation size, a wide variety of data rates can be

achieved. This will certainly improve power consumption, network life and reliability in WSNs.

The Cognitive Radio Wireless Network (CWSN) field has not been fully explored yet. Real or simulated scenarios rarely exist. The non-existence of a complete simulator for CWSNs contributes to the scarce appearance of results in the area. In order to enable the design and development of new algorithms, strategies or protocols for CWSNs, and evaluate their performance, simulation and emulation environments are necessary.

As for common WSNs, the initial research of CWSNs is usually done with a WSN simulator. Simulators help developers to avoid possible failures in hardware. Cost and time reduction is another advantage of simulators. There are a lot of WSN simulators that will be further explained and referenced in Section II, but a complete CWSN simulator does not exist. Therefore, in this work we propose a new framework for the development of CWSNs. It consists of a complete CWSN simulator based on Castalia, adapted and improved with cognitive modules.

However, the challenge in simulators is to determine if its simulations achieve a good enough correspondence with real deployments. In this work, the simulator is fed with data provided by real CWSN devices to obtain a more realistic approach. Therefore, a complete simulation framework for CWSNs using regular standards is presented.

This framework can be used to simulate different approaches, such as strategies to reduce energy consumption in CWSNs (to increase lifetime), countermeasures for CWSN specific threats (to increase reliability) or various spectrum sensing strategies.

This paper is organized as follows. In Section II, works in the CWSN simulator and emulator frameworks are reviewed. In Section III, the new CWSN framework is described. In Section IV, a proof of concept is shown. Finally, the conclusions are drawn in Section V.

II. RELATED WORK

Because of the novelty of this research field, there are not many specific frameworks for the design of green communications over CWSNs. It is natural that most of the works are based on WSN simulators.

As can be seen in the previous published work [1], CWSN research is still in the first stage, the design. The second stage requires suitable tools for the simulations. Nowadays, these tools do not exist or they do not have the required characteristics to develop a complete CWSN scenario. There are several WSN simulators used by researchers to develop their work. For example, NS-2 [7] is one of the best-known simulators. The majority of the WSN research society uses this simulator, although its latest release took place in 2008. NS-2 is a discrete network simulator built as an Object-Oriented extension of Tool Command Language and C++. This simulator is open source and provides online documentation. NS-2 can support a considerable range of protocols in all layers.

Another WSN simulator is TOSSIM [8], which is an emulator specifically designed for WSNs running on TinyOS, an open source operating system. This is a very simple but powerful emulator. EmStar [9] is a trace-driven simulator running in real time, specifically designed for WSNs and built in C. EmStar has a robustness feature that can mitigate faults among the sensors. It also provides a lot of modes, making debugging and evaluation much easier. OMNET++ [10] [11] is another very well-known framework among researchers. It proposes a modular library which can be used to develop network simulators. Just by arranging different modules, the developer can create his/her own simulator or scenario.

Several other simulators have been developed for WSNs [12], such as COOJA, OPNET, NetSim, J-Sim, ATEMU, Avrora, QualNet, etc.

None of the above simulators have cognitive features. As it was described in the previous section, a cognitive network has two main characteristics:

- Maintaining awareness of its environment, including the spectrum.
- Optimizing its radio parameters according to the requirements.

These two main features could be divided into several derived characteristics. Any CWSN simulator should be implemented taking into account these necessary characteristics. In the past, some attempts to develop a CWSN simulator have been made. The first approach has been to develop cognitive features over an existing WSN simulator. In [13], the authors propose a new routing model for cognitive networks over NS-2. With this goal in mind, changes to the NS-2 architecture are explained, such as support for multiple channels. Multiple channel support is one of the first changes that any simulator should handle. However, the implemented changes in [14] are not enough because only a few radio parameters, such as transmit power and propagation, can be changed. Besides, it is impossible to use more than one radio interface at the same time with this cognitive layer for NS-2. Moreover, other CWSN aspects like power management, collaboration, scalability and learning are not mentioned or implemented in this NS-2 model.

Despite the limitations of the NS-2 simulator in cognitive scenarios, multiple researchers have chosen NS-2 for their investigations because it is the only WSN simulator with some cognitive features. For example, the work in [15] presents an algorithm to optimize the route selection in a disaster situation. The main idea is that the wireless nodes sense the spectrum. According to some parameters such as latency, jitter or packet error rate, the nodes choose the optimal communication interface between them. The decision is made individually and is transmitted by satellite communications. This scenario is simulated in NS-2 using nodes with three wireless interfaces. The interfaces change

during the simulation time. That is, the nodes cannot use more than one interface at the same time. However, the work does not explain how the spectrum sensing works, and collaboration and learning do not exist. Finally, the scenario presented in this work is a cognitive application with different traffic and protocols than the ones from WSNs.

Another work is presented in [16]. It evaluates a solution for coexistence with wireless LANs, based on a new MAC layer. The simulations are implemented over NS-2, but it does not focus on WSNs. The authors describe how the cognitive nodes sense the channels and agree on the active channel. In order to make this decision, they use a control channel. In this work, the simulator architecture was not modified and the cognitive features are poorly explained. For example, they talk about predicting the length of a spectrum hole. However, it is not explained how this data is obtained. Power management is not presented and the scalability is untested. In addition, only a simulation with 10 nodes is provided.

Apart from the NS-2 simulator and its new cognitive features, some cognitive simulators have appeared over the past few years. The following simulators have not been implemented for WSNs but they include some cognitive features. For example, in [17], the platform presented focuses on spectrum sharing. For that reason, the physical layer and the spectrum resource manager are the modules that implement cognitive features to avoid primary-user collisions. Important characteristics of WSNs such as mobility, consumption and protocols are not in the scope of this simulator.

The authors of [18] present some software to simulate cognitive networks scenarios. They divide their architecture into five modules: the scheduling module, the mobile node module, the statistics module, the wireless environment module and the interface. The cognitive features are implemented in the mobile radio module and the statistics module. Among the mentioned implemented characteristics are spectrum sensing and information storage. Collaboration between nodes is not explained. As in the work in [17], WSN key features are not presented.

Another example of a cognitive simulator is presented in [19]. It focuses on the definition of an Autonomic Communication Element (ACE) architecture. The architecture is not for WSNs and the development is done in RuleML language. The authors present an interesting approach to cognitive nodes. They define some modules that represent the cognitive features. Some of them are the spectrum sensing or the experimental database modules. However, the authors do not explain the implementation of the cognitive strategies in detail and no results or evaluations are presented.

The emerging problem of spectrum saturation in WSNs that we explain in the introduction and the current state of cognitive simulators provide the motivation for this work. Only NS-2 supports today's cognitive characteristics in WSN scenarios, but it has a lot of limitations. The other simulators

present more cognitive features but they obviate the WSN ones.

After the simulation stage, researchers generally use a test-bed, before the real implementation. There are multiple test-beds for specific developments. TWIST [20] and VT-CORNET [21] are the most important test-beds nowadays because of their general purpose features and their quality.

The TKN Wireless Indoor Sensor Network Testbed (TWIST) is a multiplatform, hierarchical test-bed architecture developed at the Technische Universität Berlin. The self-configuration capability, the use of hardware with standardized interfaces and the inclusion of open source software make the TWIST architecture scalable, affordable, and easily replicable. The TWIST instance at the TKN office building is one of the largest remotely accessible test-beds with 204 System Under Test (SUT) sockets, currently populated with 102 eyesIFX and 102 Tmote Sky nodes. The nodes are deployed in a 3D grid spanning 3 floors of an office building at the TUB campus, resulting in more than 1500 m² of instrumented office space.

The Virginia Tech COgnitive Radio NEtwork Testbed (VT-CORNET) is a collection of Cognitive Radio nodes deployed throughout a building at the Virginia Tech main campus. The test-bed consists of a total of 48 Software-Defined Radio nodes. It is implemented with a combination of a highly flexible RF front end, and an openly available Cognitive Radio Open Source System framework.

The ORBIT project, launched in 2003 [22] is a large-scale open-access wireless test-bed. It can be used by the research community working in new wireless communications. In some aspects it is similar to the TWIST test-bed, a large deployment of wireless nodes with spectrum sensing capabilities, but it lacks the possibility of different radio interfaces combined into the same node.

Research on CWSN simulators is emerging, but it is still in a primary state. A simulation with a high number of nodes is necessary in WSN scenarios. It is very expensive to build a lot of real devices to test a concrete low-power strategy. The integration of real data devices and a high number of nodes is only possible using a feedback relation. Currently, there is not a CWSN simulator with standard protocols and feedback from real devices that uses cognitive characteristics for an intelligent energy management in order to test new policies, assess collaboration schemes or validate different optimization mechanisms.

SENDORA, the only simulator with cognitive capabilities does not use real device data for the power model.

Other simulators like NS-2 lack cognitive capabilities such as learning, using different radio interfaces or manage collaboration between nodes. Therefore, an implementation of a completely new cognitive module over an existing WSN simulator, specifically the Castalia Simulator (based on the OMNET++ framework), and a new CWSN device with three different radio standard interfaces are proposed.

III. CWSN FRAMEWORK

Most common network simulators have tested energy models, but these are theoretical models covering general cases. So, it is necessary to introduce real data measured by a cognitive radio prototype developed to make these simulations more realistic. Thus, it is also possible to find differences in commercial solutions using the same technology.

Moreover, the deployment of a network of real devices is very difficult and expensive, especially for a network with a large number of devices. This is the great advantage of the introduction of simulators. By adding data taken from functional prototypes to simulation results, the accuracy of the simulations improves.

Thus, the combination of both elements results in a complete and useful framework to validate optimization mechanisms for energy consumption.

As seen in Section I, cognitive characteristics are applicable to intelligent energy management. Thus, it is important to provide a CWSN framework to test new policies, to assess collaboration schemes and to validate different optimization mechanisms.

The CWSN framework is composed of two fundamental elements: a network simulator and low-power cognitive radio real devices.

A. CWSN Simulator

The CWSN simulator described in this section is based on the well know Castalia simulator, which is in turn based on OMNET++. As it can be seen in Section II, the amount of WSN simulators is very large. Those, along with the fact that attempts to create a cognitive simulator have not reached a decent level of development, have led us to create our own simulator based on a WSN simulator. The decision about which simulator was better was made according to [23], focusing on these reasons:

- The Castalia simulator focuses on WSNs. This feature is very important because of the scope of the simulator. Despite Cognitive Radio Networks (CRNs) having multiple applications and scenarios, this work is focused on CWSNs.
- The Castalia simulator is based on OMNET++, which has a modular and simple implementation. If the goal of this work is to develop a cognitive architecture inside the simulator, new modules and interfaces will be included. OMNET++ makes these additions very easy.
- The Castalia and OMNET++ development is very active with releases every few months. The work is based on Castalia and OMNET++ in order to create a usable tool for any cognitive project. The other important simulator for cognitive scenarios, NS-2, has not received a new release since November, 2011 and the one before that was in 2009.

- Castalia includes a resource manager module in order to monitor parameters such as energy or memory consumption in the nodes.
- The Castalia physical layer and radio models are some of the most realistic models that any researcher can find in the simulator field. As cognitive radio is based on spectrum sensing, a realistic physical layer is an important advantage.

Emphasizing the physical and radio layer, Castalia offers multiple characteristics such as path loss, mobility in the nodes, simple interferences, multiple modulations and sleep states. The cognitive simulator can use all these features in order to create more realistic scenarios.

Having chosen the simulator, the next step is to define the requirements needed by the cognitive simulator, so that it can offer enough features for future works.

1) Requirements

The three main characteristics of cognitive radio are environment awareness, learning, and acting capacity. All the requirements imposed on this simulator try to implement or to improve these characteristics.

- Spectrum sensing. If the cognitive nodes have to be aware of the context, they need to extract that information from the spectrum.
- Multiple frequencies, channels and modulations. An essential characteristic needed to reach the flexibility of a cognitive network is to introduce the possibility of changing between multiple frequencies, channels and modulations.
- Virtual Control Channel (VCC). As we will explain later, the VCC allows the nodes to share information.
- Primary and secondary users. The two roles present in cognitive networks have to be implemented in the simulator too.
- Information storage and learning. The cognitive nodes learn from the captured information.
- Results and data representation. They are essential for the analysis of the results.

Although the Castalia simulator's physical layer is one of the best compared with other simulators, the sensing block is critical for cognitive networks. Consequently, some changes need to be made to improve the sensing stage.

The Castalia simulator supports most common modulations but it is also prepared to include new ones. Moreover, some typical radios for WSNs are included, such as CC1010 or CC2430. Interferences are another important aspect of the sensing module. Noise detected in the spectrum can affect the network's behavior. For that reason, the interference model must be very precise.

Section II shows some attempts to implement multiple radios and multiple channels in simulators. There can be no

doubt about the importance of supporting different real wireless radio interfaces in each node, allowing changes in all parameters: modulation, transmission power, consumption, frequency, etc. Cognitive networks differ from other types of networks due to the adaptation of their parameters according to the information gathered from the environment. Although the Castalia simulator presents the possibility of a limited spectrum sensing, it is not enough for a cognitive network. Multiple changes are necessary in Castalia, starting from a complete spectrum sensing, following with the storing of this information and concluding with the spread of the information which is an important feature of cognitive networks. A Virtual Control Channel (VCC) has been implemented for this purpose.

Normally, WSN simulators make differences in the nodes only when a particular technology forces them. For example, coordinators and end nodes on ZigBee protocol. In these cases, the differences are related to the functionality of the network. However, cognitive networks introduce two roles for all the CRNs: Primary Users (PUs) and Secondary Users (SUs).

Finally, when the simulator executes an application or scenario, the developer needs a simple way to extract the results. Moreover, the number of parameters that the developer can monitor needs to be the highest possible. For this requirement, changes in the resource manager block are necessary.

Once the requirements have been explained, the CWSN simulator is going to be described in detail.

2) Cognitive Radio extension for Castalia

In this work, the structure of Castalia has been modified in order to provide the simulator with Cognitive Radio support. Figures 1 and 2 show the new simulator structure. The code has been modified as little as possible in order to introduce the minimum changes to third-party applications and module implementations.

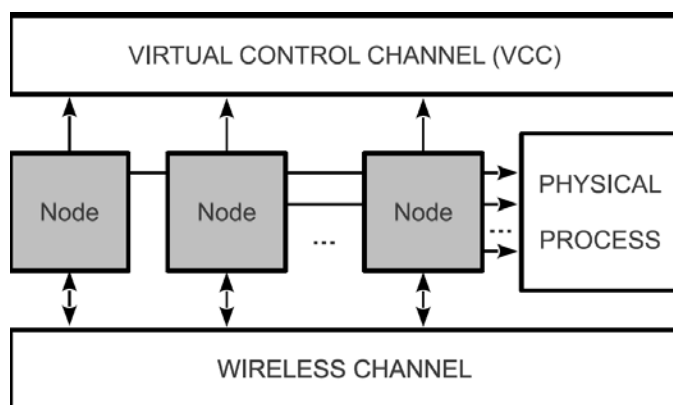


Figure 1. Castalia network architecture adapted to Cognitive Radio

In the new model, the nodes have multiple communication modules which can be configured with

different parameters. They simulate the multiple interfaces of a wireless node. Every interface is connected to the application module and the wireless channel. The new simulator provides the developer with functions to change the default interface used to send data. It provides complete backwards compatibility so previous non-cognitive samples and modules do not have to be modified.

A node with multiple interfaces brings flexibility to the network in a lot of aspects: comparison of performance and consumption between technologies, protocols and modulations, cognitive strategies that imply two or more radios, and freedom to change the parameters of each interface independently.

The existing differences in the scenario configuration file of a multiple interface experiment can be seen in the following code:

```
SN.numIFaces = 2
...
SN.node[*].Communication[0].Radio.RadioParametersFile
= "CC2420.txt"
SN.node[*].Communication[1].Radio.RadioParametersFile
= "ZigBee.txt"
...
```

According to these lines, the nodes would have two interfaces. The first one is a CC2420 node and the second one is a generic ZigBee node. Each one can have a different transmission power, different carrier frequencies or a different modulation.

The parameter *numIFaces* indicates the number of interfaces per node. By default, this parameter is one due to backwards compatibility. Since it is possible to manage more than one communication simultaneously, developers must specify the interface they are referring to.

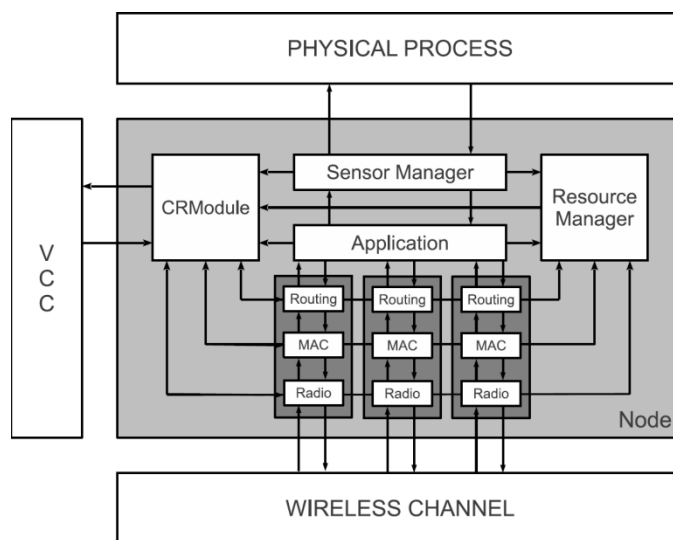


Figure 2. Castalia inner blocks adapted to Cognitive Radio

The Radio module of each communication module provides new API methods for changing the active channel. This change lets developers perform spectrum scans and hops among channels easily. The channel changing feature completes a set of modifications in order to increase the flexibility of the network but also to complete wireless protocols such as Wi-Fi or ZigBee, in which nodes have multiple channels.

Another implemented change in the simulator is the creation of PUs and SUs. Most cognitive applications have both roles, where PUs have preference in the use of the spectrum and SUs try to take advantage of spectrum holes. The application layer is responsible for providing this feature.

The new functionalities have been carried out with the minimum number of modifications to the public API of Castalia, so developers can keep on using the same experiments without changing a large amount of code.

These changes transform Castalia into a simulator capable of running Cognitive Radio experiments, although it still lacks any cognitive capabilities. In order to turn Castalia into a real cognitive simulator it has been equipped with a new module that includes all the cognitive features of the nodes.

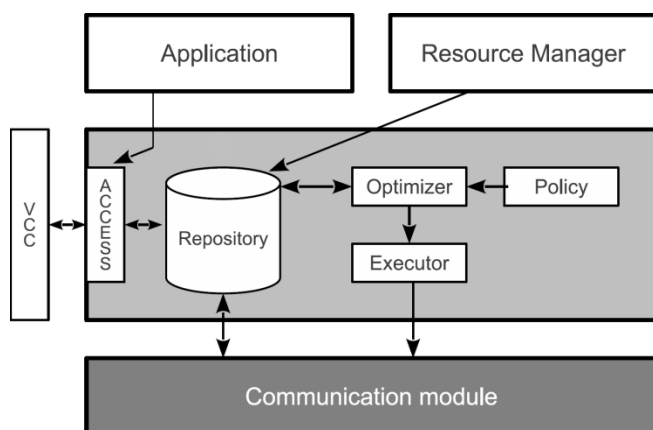


Figure 3. Cognitive Radio Module structure

The CR module structure is shown in Figure 3. Each module is composed of the following elements, extracted from the work in [24]. These modules have been adapted to the existing Castalia structure and provide the developer with a lot of possibilities for the creation of different scenarios. Therefore, multiple interactions between the next modules exist.

a) Repository

An essential requirement for an effective cooperation and collaboration is that the cognitive nodes make the learned information, the decisions made and the current state, available to all interested parties. These neighbors may be secondary users that cooperate in order to make

better decisions or to optimize some policies. This is enabled by means of a distributed repository structure. The nodes store the information they capture in the repository and eventually they also store information from other nodes when they need it. Each node publishes part of its own repository to the network, making it public through the VCC. When a node requires information from another node's repository, it sends a request packet through the VCC. If the information is available and public, the access will be granted.

The kind of information stored depends on the context and the requirements of the system. Some of the modules that feed the repository with information are the communication modules, the application, the resource manager and the optimizer. The repository complements the resource manager module. The resource manager stores information about general characteristics of the nodes and the network such as power and memory consumption. The repository inside the CR module saves information related to cognitive features such as sensing, learning or strategies. The repository is the backbone of the CR module framework and the fundamental component that enables cooperation and dynamic information exchange among cognitive wireless technologies.

An example of the use of the repository could be a collaboration strategy in which nodes learn about the usage of multiple interfaces and frequency bands. When this learning is complete, the nodes can use this information to transmit over empty channels saving energy and improving communications.

b) Access

Information stored in the repository can be an important source for malicious intentions. For this reason, or simply because of the general goal of the network, the access module does not let all nodes access the repositories. The access module controls which part of the repository is public and which nodes are allowed to access it.

As we have said before, security is completely associated with the access module. An example is an application in which nodes store the reputation of the network nodes. If the attacker accesses the repository and increases its own reputation, the attack can affect the behavior of the network.

c) Policy

This module enforces the requirements for the global system depending on several factors: energy consumption, interferences or noise, quality of service, or security. In simple terms, the policy module is a set of weighting parameters that control the priority of the different network goals. The nodes act according to the final composition of services and weights. These policies and weights may vary dynamically and the nodes should be consistent with these variations.

For example, a CWSN can be responsible for monitoring a large forest area. The primary policy could be low energy consumption, but when a fire is detected, the policy changes to offer the best QoS to transmit the alarm.

d) Optimizer

It processes the repository information bearing in mind the requirements imposed by the policy module. Decisions regarding the behavior of the local node are the results of processing. They are stored in the repository and evaluated by the executor module. To summarize, the optimizer makes decisions according to the stored information.

Probably, the optimizer is the most complex submodule of the CR module. To understand how it works, an example is presented: in a scenario where security is the predominant policy, a new node wants to join the network. The optimizer of the coordinator analyzes the information (stored in the repository) about the new node, namely location and transmission power, and it makes the final decision allowing or not the new node to join the network.

e) Executor

The decisions made by the executor need to be distributed to the modules responsible for modifying the parameters. The executor usually sends orders to the communication module, where the radio parameters can be changed or the routing protocol can be modified.

f) Virtual Control Channel

The Virtual Control Channel (VCC), a new method for sharing cognitive information among the CR modules of the nodes, has been included in the architecture. CR modules can access exported information of remote repositories through this channel. It allows the CR modules to be aware of their surroundings and even of the whole network. The VCC gives the nodes a common interface to communicate, ignoring the details of how the data is delivered, and the precise nature and location of the communication partners.

Since all the elements are developed as Castalia modules, they communicate and access each other via the OMNET++ message system. The modularity of OMNET++ and its high level portable language makes this architecture very easy to transfer to a real device. Usually, the standard protocols of WSNs for real devices have resources to create these modules. For example, the repository message can be implemented in the stack of multiple protocols, such as ZigBee. The definition of different interfaces complicates the integration work but it is completely possible.

3) Changes in radio module

Most of the work in this project focuses on developing the cognitive radio module that introduces cognitive behaviors into the simulator. However the Castalia simulator has some characteristics that can be improved.

As we said before, the Castalia simulator only supports one radio interface per node. Nodes can have some of the different MAC layers that Castalia includes: 802.15.4, tunable MAC, etc. However, none of these MACs implement different channels. The goal is that every interface could have a different channel bandwidth, first and last frequencies and number of available channels. By combining multiple channels and multiple interfaces, scenarios are very realistic.

Spectrum sensing is a key factor in cognitive radio. Nodes must analyze the spectrum to detect primary users or to find the best medium to share information with other secondary users. The decision about which channels or interfaces are the best at each time should be based on realistic and plentiful data. For this reason the interference model on the Castalia simulator has been changed. Before these changes, a node only detected a packet if the transmitter operated in the exact same carrier frequency as the receiver. If the frequencies were different, the packet was dropped and it did not create any interferences. Now, the model is more realistic and the packets create interferences if they are within the signal bandwidth. These interferences are proportional to the distance between carriers and are related to the modulation.

Finally, some minimum changes have been made to the resource manager block. As explained before, the resource manager controls the node parameters such as the energy spent or the memory occupied. In accordance with the idea of having the least possible parameters modified in the simulator, changes to control the power consumption of the multiple interfaces have been made.

B. CWSN devices

A test-bed platform to develop cognitive radio communications for WSNs and to obtain its energy consumption model data has been implemented (Figure 4).

The CWSN device tries to optimize communications in real time according to different application needs. Therefore, the device design has to consider power consumption, data rate, reliability, and security in order to be useful for a large number of applications.

For our goal, energy consumption is a very important challenge. It is necessary to control the consumption of each separate component, and to implement shared strategies that try to reduce the overall consumption of the network.

Interference with other wireless devices or noise problems have to be avoided, which implies that nodes have to change their frequency and modulation as fast as possible. For this reason the prototype has three different network interfaces. The reduction of interference can be an important factor to reduce the overall consumption of the network.

CWSNs need to be connected to different kinds of standard commercial devices or internet gateways. Consequently a widely extended wireless solution as an interface has to be implemented.

This prototype has to be capable of collecting data about the state of the network and of sharing the information with other nodes. In addition, each node has to be able to change protocol parameters, the entire protocol and wireless interfaces in real time. Thus, it is mandatory to coordinate all the network devices.



Figure 4. Cognitive Wireless Sensor Network Device prototype

The control function is made by a Microchip PIC32MX795F512H, which is a 32-bit flash microcontroller. It is a high performance processor with low consumption and low cost. The CWSN platform has three radio interfaces:

- A Wi-Fi Microchip device (MRF24WB) which can handle data rates of 2 Mbps and operates in the band between 2.412 and 2.484 GHz. Wi-Fi is based on the IEEE 802.11 standards.
- A MiWi interface, a Microchip protocol which can handle data rates of about 250 kbps and operates in the band between 2.405 and 2.48 GHz. This is a proprietary wireless protocol designed by Microchip Technology that uses small, low-power digital radios based on the IEEE 802.15.4 standard for WPANs. The device used is the MRF24J40MA.
- The last interface is based on the Texas Instruments CC1010. It can handle data rates of 76.8 kbps and operates in a band around 868 Mhz. This interface provides a new communications band in an ISM frequency.

The software has to be able to discover other nodes, sense the radio-electric environment, exchange configuration information, establish communication channels, turn the radio interfaces on or off, and manage the active or asleep state of the node. The network manages data routes optimizing consumption, data rate, reliability and security.

Three wireless interfaces have been used in this device, each with different standards and protocols. The integration of a new interface or device in the consumption model of the simulator is very easy. The only thing necessary is to fill the file with the real device measures.

IV. DEMONSTRATIVE USE OF THE FRAMEWORK

In this section, the results of simulations related to the cognitive framework design are presented. It is not the goal of the simulation to prove the algorithm or mechanism itself. The goal is to check that several new policies, collaboration schemes or optimization mechanisms can be implemented in this framework.

The presented architecture permits the simulation of complete cognitive scenarios with the following characteristics:

- Scalable cognitive networks with a large number of sensors.
- Multiple interfaces and channels in the nodes at the same time.
- Node mobility.
- Resources control such as battery energy.
- Spectrum sensing for multiple channels and interfaces.
- Control communication and collaboration among nodes.
- Knowledge database.
- Learning in execution time.
- Application of multiple policies.

Some different scenarios have been developed in order to test the cognitive framework.

The first scenario demonstrates the new concept of changing the transmission parameters and the energy consumption optimization. The second scenario is similar to the first, but it includes different applications. The third scenario shows how the cognitive feature of spectrum sensing can be useful for some optimizations. Finally, the fourth scenario shows how the spectrum sensing, the repository and the VCC can be used to implement complex cognitive simulations.

The first scenario is related to the capability of changing transmission parameters. It is composed of five nodes, each with 802.11 and 802.15.4 radio interfaces. Four nodes send data to a central node. In this scenario the nodes simulate two different applications. The first one is a multimedia application where both the bit rate and the packet size are high. The transmission rate needs a Wi-Fi interface while a WPAN does not have the capacity for multimedia applications. However, in a WSN, general applications only have monitoring functions (temperature, light, etc.) and the bit rate and the amount of information are very low. In this case, the low-power optimization strategy consists of using the interface with the lowest energy consumption for a specific data rate. When the data rate is high, only 802.11 is possible, but for some specific data rates 802.15.4 is better because of its lower energy consumption. This algorithm could be dynamically changed according to other constraints such as battery life, distance between nodes or quality of service. Real data is used in the power model from a

MRF24J40MA-based device for the 802.15.4 protocol and from a MRF24WB-based device for the Wi-Fi transmissions. In the simulation, power measures from the CWSN device are included (Wi-Fi transmissions consume 74.8 mW while WPAN transmissions reach 3.6 mW). As shown in Figure 5, when the data rate is high, 802.11 is used for the transmission, but when the data rate decreases, 802.15.4 is better because of its lower energy consumption. The second part of this figure (zoomed in Figure 6) shows the consumption with the Wi-Fi and WPAN common sensing application with the same packet size and the same interval between messages.

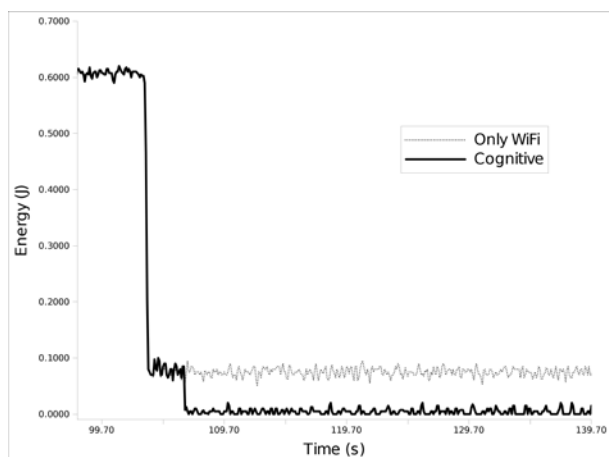


Figure 5. Energy consumption for the Cognitive algorithm and Wi-Fi

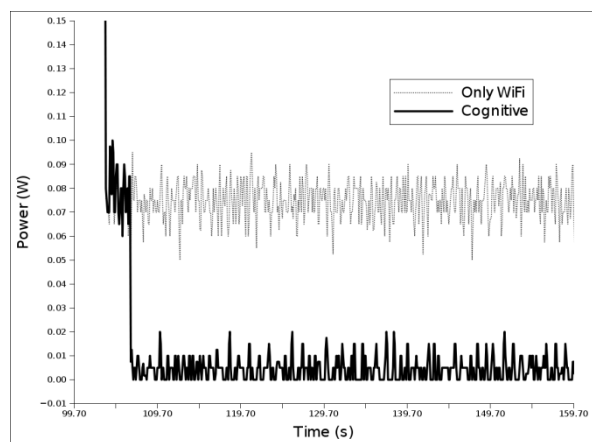


Figure 6. Detail of the energy consumption for the Cognitive algorithm and Wi-Fi

Using a low-power protocol system saves 94% of the energy (Figure 5). Only in the commutation period, where the nodes need to communicate the interface change, the

consumption is similar to Wi-Fi. After that, the energy saving is considerable.

The second scenario simulates an application whose nodes send packets with the maximum payload allowed by the simulator (1000 bytes with 802.11 and 100 bytes with our implementation of the WPAN protocol). The application starts sending a package every 10 ms and this time is increased until the bit rate reached by the 802.11 interface is supported by the WPAN protocol (reached at time 600). Figure 7 shows how the consumption of the WPAN interface in the first period of the simulation time is greater than the one of Wi-Fi. This is because the WPAN protocol needs more transmissions for the same amount of data. This means that using 802.15.4 does not automatically reduce the consumption of every application with a low bit rate, but a cognitive module choosing the right protocol at every moment can achieve that goal.

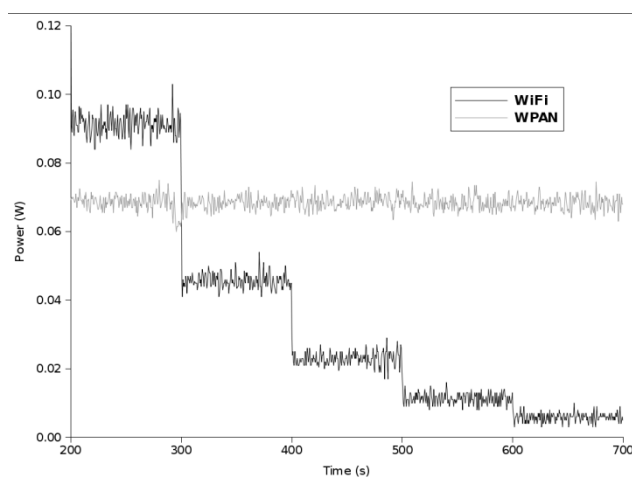


Figure 7. Energy consumption for the Cognitive algorithm and Wi-Fi (Scenario 2)

The third scenario shows the optimization by means of spectrum sensing. It consists of two nodes with 802.15.4 radio interfaces. One of them, the receiver node (B), moves (in a total time of 70 seconds) through space and the other, the transmitter node (A), is fixed (Figure 8). Within the path of movement experienced by the mobile node, sometimes node B will be closer to node A than others. In a common network design, node A will transmit information with a fixed power. That can cause certain packets to be lost (because of the distance between nodes) and others to be transmitted with more power than necessary. Adding cognitive capabilities to this scenario, the network could be aware of the minimum power necessary to ensure the reception of packets while minimizing energy consumption. For this simulation, a power model real data from a MRF24J40MA-based device for the 802.15.4 protocol has been used.

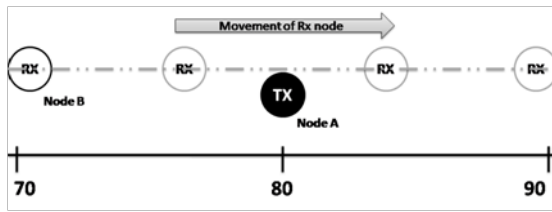


Figure 8. Mobile node scenario

In Figure 9, the instantaneous energy consumption of the transmitter node (node A in Figure 8) is shown. The dotted line represents the consumption of node A in a network without cognitive capabilities and the solid line shows the consumption of the same node when the low-power consumption algorithm is applied. Modifying the transmission power in relation to the distance between nodes can reduce the energy consumption. Using this simple algorithm implies a reduction of up to 60% in some sections.

Increasing the complexity of algorithms or dealing with the problem of consumption in a holistic way (combining several techniques), it will be possible to obtain higher reductions.

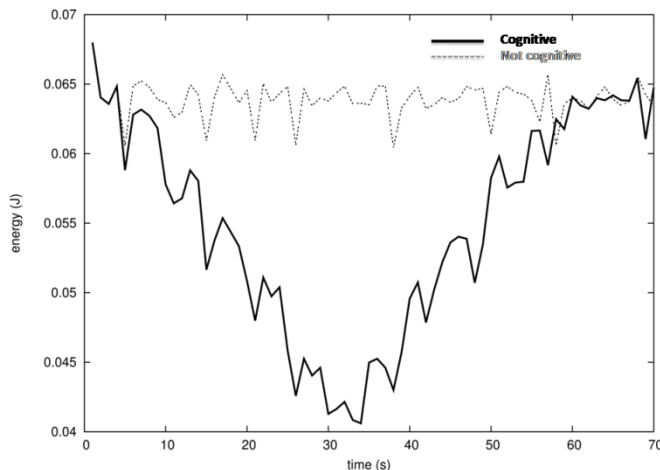


Figure 9. Energy consumption for the Cognitive algorithm and 802.15.4 (Scenario 3)

The fourth scenario is a demonstration of a complex cognitive application where all the cognitive features implemented in the simulator are used to detect anomalies such as broken nodes or intruders.

The simulation consists of 50 nodes with different roles. There is a server that periodically receives information from multiple sensors. The sensors are PUs if they have priority or SUs if they do not. Moreover, SUs collaborate in order to detect anomalies in node behaviors. More specifically, they

detect these anomalies by sensing the spectrum and learning about the transmission power of each node.

During the first seconds of the simulation the nodes learn about the transmission power: number of transmissions, average power transmitted and its standard deviation. This information is stored in the repository inside the cognitive module. After these seconds, the nodes start to detect differences in this learned parameter. The optimizer notifies the application if some anomaly happens, and the application, after multiple warnings, retransmits the alarm to the rest of the nodes. When a fixed number of nodes agree on the anomaly of some node, it is marked as an abnormal node and it cannot further participate in the working of the network.

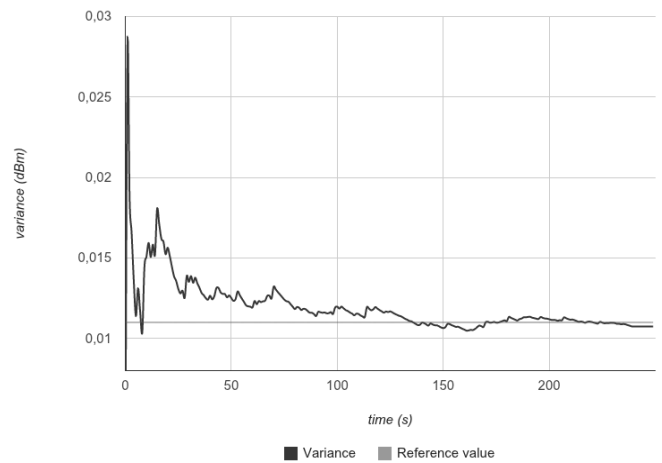


Figure 10. Sensing power and learning average

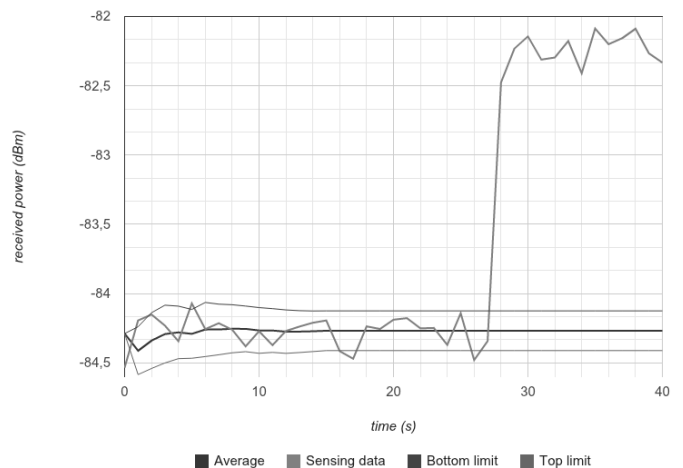


Figure 11. Learning power variance

Therefore, spectrum sensing allows the nodes to detect and analyze the received power; the repository stores all the learned information, the optimizer analyzes the data

according to some policy and finally, the nodes collaborate using the VCC.

The results of a network with 50 nodes are shown in Figure 10 and Figure 11. Figure 10 represents how a SU learns about the transmission power of another node that has an abnormal operation. Sensing power is the power received by the node when it receives a new packet and the learning average is the average of all the packets received by this node. The x axis represents the number of packets that the node has received since the beginning of the simulation.

As we can see, the average is stable with a few samples. The top limit and the bottom limit form a range where the sensing data is considered normal. When the data is out of the limits, the node interprets it as an anomaly.

We can observe how fast the system learns. With a few samples, the variance fluctuates but when the node has more information the variance stabilizes over 1%.

Figure 11 shows the scalability of the solution with 50 nodes in the same network. Moreover, it shows some of the most important features such as spectrum sensing, learning and knowledge storage.

Beside these four scenarios, the simulator has been tested in other works such as in [25], where a security strategy has been implemented over the simulator. Collaboration, security policies, scalability and spectrum sensing are the most important factors in this work. Another example of the use of this simulator is presented in [1]. This work focuses on the use of the cognitive features of the simulator to implement green scenarios with energy saving strategies.

V. CONCLUSION AND FUTURE WORK

The new cognitive paradigm has appeared to cope with very important network problems like spectrum scarcity, interference or reliable connections. Cognitive network features expose new interesting research challenges. The implementation of cognitive features in WSNs is an emerging field with specific characteristics to explore, like new energy saving strategies or new security approaches. CWSNs are still in the first stage of a project, the design. The second stage requires the suitable tools for the simulations and implementations.

At this moment, it is important to have a CWSN framework to test new policies, to assess collaboration schemes and to validate different optimization mechanisms. In this article a CWSN framework is presented. The framework is composed of a network simulator and low-power CWSN real devices. A new cognitive module has been developed over the Castalia simulator and different real interfaces and energy consumption models have been integrated. A CWSN platform has been built using a microcontroller and three different radio interfaces (IEEE 802.11, IEEE 802.15.4, and a CC1010-based interface in the 868 MHz band). This framework uses real devices' implementations to measure different power and

transmission characteristics that are included in the energy consumption model and the communication model. This feedback achieves simulation results that are closer to a real scenario than the ones from regular simulators.

The benefits of the proposed CWSN framework have been demonstrated by implementing four scenarios. Low-power optimization strategies, cognitive applications and security approaches have been implemented using this framework. Results show how cognitive concepts (collaboration, learning, different communication parameters) have been integrated in the simulator with a positive outcome.

In conclusion, this framework represents a good opportunity for the development of new cognitive wireless communication strategies for the new paradigm of CWSNs.

ACKNOWLEDGMENT

This work was funded by the Spanish Ministry of Science and Innovation through the Secretariat of State for Research, under Research Grant AMILCAR TEC2009-14595-C02-01, and through the General Secretariat of Innovation under Research Grant P8/08 within the National Plan for Scientific Research, Development and Technological Innovation 2008-2011.

REFERENCES

- [1] A. Araujo, E. Romero, J. Blesa and O. Nieto-Taladriz, "Cognitive Wireless Sensor Networks Framework for Green Communications Design", II International Conference on Advances in Cognitive Radio. COCORA 2012, pp. 34-40.
- [2] K. David, D. Dixit, and N. Jefferies, "2020 Vision", IEEE Vehicular Technology Magazine, 2010, vol. 5, pp. 22–29.
- [3] Cisco Systems Inc, "Cisco Visual Networking Index: Global Mobile Data Traffic Forecast Update, 2010–2015". White Paper. Feb. 2011.
- [4] S. Methley and C. Forster, "Wireless Sensor Networks Final Report", Technical Report, Plextek Limited, 2008.
- [5] I. Howitt and J. Gutierrez, "IEEE 802.15.4 Low Rate-Wireless Personal Area Network Coexistence Issues". Proc of IEEE Wireless Communications and Networking Conference 2003 (WCNC 2003), vol. 3, pp.1481-1486, doi:10.1109/WCNC.2003.1200605.
- [6] D. Cavalcanti, R. Schmitt and A. Soomro, "Achieving Energy Efficiency and QoS for Low-Rate Applications with 802.11e", IEEE Wireless Communications and Networking Conference, 2007.WCNC 2007, pp. 2143–2148, doi:10.1109/WCNC.2007.401.
- [7] Y. Xue, H.S. Lee, M. Yang, P. Kumarawadu, H. Ghenniwa, and W. Shen, "Performance Evaluation of NS-2 Simulator for Wireless Sensor Networks". Canadian Conference on Electrical and Computer Engineering 2007. CCECE 2007. pp. 1372–1375, doi:10.1109/CCECE.2007.345.
- [8] P. Levis, N. Lee, M. Welsh and D. Culler, "TOSSIM: accurate and scalable simulation of entire TinyOS applications", Proc of the 1st ACM International Conference on Embedded Networked Sensor Systems 2003; SenSys '03. pp. 126–137, doi:10.1145/958491.958506.
- [9] L. Girod, N. Ramanathan, J. Elson, T. Stathopoulos, M. Lukac and D. Estrin, "Emstar A software environment for

- developing and deploying heterogeneous sensor-actuator networks". ACM Transactions on Sensor Networks. Vol 3 Issue 3, August 2007, doi:10.1145/1267060.1267061.
- [10] G. Pongor, "OMNeT: Objective Modular Network Testbed", Proc of the International Workshop on Modeling, Analysis, and Simulation On Computer and Telecommunication Systems 1993; MASCOTS '93. pp. 323–326.
- [11] X. Xian, W. Shi and H. Huang., "Comparison of OMNET++ and other simulator for WSN simulation", 3rd IEEE Conference on Industrial Electronics and Applications, ICIEA 2008. pp. 1439 –1443, doi:10.1109/ICIEA.2008.4582757.
- [12] M. Imran, A. Said and H. Hasbullah, "A survey of simulators, emulators and testbeds for wireless sensor networks", International Symposium in Information Technology 2010 (ITSim 2010), Vol. 2, pp. 897 –902, doi:10.1109/ITSIM.2010.5561571.
- [13] P. Lee, and G. Wei, "NS2 Model for Cognitive Radio Networks Routing", International Symposium on Computer Network and Multimedia Technology 2009. CNMT 2009. pp. 1 –4, doi:10.1109/CNMT.2009.5374689.
- [14] J. Zhong and J. Li, "Cognitive Radio Cognitive Network Simulator", <http://stuweb.ee.mtu.edu/~ljalian/>, Accessed on 2012.
- [15] N. Uchida, G. Sato, K. Takahata and Y. Shibata, "Optimal Route Selection Method with Satellite System for CognitiveWireless Network in Disaster Information Network", IEEE International Conference on Advanced Information Networking and Applications 2011 (AINA 2011), pp. 23 –29, doi:10.1109/AINA.2011.42.
- [16] S.Y. Hung, Y.C. Cheng, E.K. Wu and G.H. Chen, "An Opportunistic Cognitive MAC Protocol for Coexistence with WLAN", IEEE International Conference on Communications, 2008. ICC '08. pp. 4059 – 4063, doi:10.1109/ICC.2008.762.
- [17] X. Tian, T. Tian and S. Li, "A Network Simulation Platform for Hierarchical Spectrum Sharing Based Cognitive Radio Network", International Conference on Computational and Information Sciences 2010 (ICCIS 2010), pp. 613 – 617, doi:10.1109/ICCIS.2010.155.
- [18] M. Zhan, P. Ren and M. Gong, "An Open Software Simulation Platform for Cognitive Radio", 6th International Conference on Wireless Communications Networking and Mobile Computing 2010 (WiCOM 2010), pp. 1 –4, doi:10.1109/WICOM.2010.5600841.
- [19] S. Wang, H. Liu, L. Xie and W. Hu, "Cognitive radio simulation environment realization based on autonomic communication", IEEE 3rd International Conference on Communication Software and Networks 2011 (ICCSN 2011), pp. 402 – 407, doi:10.1109/ICCSN.2011.6013743.
- [20] V. Handziski, A. Kopke, A. Willig and A. Wolisz, "TWIST: A Scalable and Reconfigurable Testbed for Wireless Indoor Experiments with Sensor Networks", 2nd International Workshop on multi-hop Ad Hoc Networks: from Theory to Reality 2006 (RealMAN'06), pp. 63-70, doi:10.1145/1132983.1132995.
- [21] T.R. Newman, A. He, J. Gaeddert, B. Hilburn, T. Bose and J.H. Reed, "Virginia tech cognitive radio network testbed and open source cognitive radio framework", 5th International Conference on Testbeds and Research Infrastructures for the Development of Networks Communities and Workshops 2009, TridentCom 2009, pp. 1-3, doi:10.1109/TRIDENTCOM.2009.4976217.
- [22] D. Raychaudhuri, I. Seskar, M. Ott, S. Ganu, K. Ramachandran, H. Kremo, R. Siracusa, H. Liu and M. Singh, "Overview of the ORBIT Radio Grid Testbed for Evaluation of Next-Generation Wireless Network Protocols", Proc of the IEEE Wireless Communications and Networking Conference (WCNC 2005), Vol 3, pp. 1664-1669, doi:10.1109/WCNC.2005.1424763.
- [23] D. Peditadakis, Y. Tselishchev and A. Boulis, "Performance and scalability evaluation of the Castalia wireless sensor network simulator", Proc of the 3rd International ICST Conference on Simulation Tools and Techniques 2010. SIMUTools '10, pp. 53:1–53:6, doi:10.4108/ICST.SIMUTOOLS2010.8727.
- [24] J. Rabaey, A. Wolisz, A.O. Ercan, A. Araujo, F. Burghardt, S. Mustafa, A. Parsa, S. Pollin, I.H. Wan and P. Malagon, "Connectivity Brokerage - Enabling Seamless Cooperation in Wireless Networks", (A White Paper), October 2010. [Online]. Available: <http://bwrc.eecs.berkeley.edu/php/pubs/pubs.php/1484.html> <retrieved: February, 2012>
- [25] A. Araujo, J. Blesa, E. Romero and O. Nieto, "Cooperative jam Technique to Increase Physical layer Security in CWSN", II International Conference on Advances in Cognitive Radio COCORA 2012, pp. 11–14.

Understanding Internet User Behavior: Towards a Unified Methodology

Christina Lagerstedt, Andreas Aurelius,
Hemamali Pathirana, Claus Popp Larsen
Netlab
Acreeo AB
Kista, Sweden
christina.lagerstedt@acreeo.se
andreas.aurelius@acreeo.se
hemamali.pathirana@acreeo.se
claus.popp.larsen@acreeo.se

Olle Findahl
World Internet Institute
Gävle, Sweden
olle.findahl@wii.se

Abstract—Understanding user behavior and Internet usage patterns is fundamental in developing future access networks and services that meet technical as well as end user needs. User behavior is routinely studied and measured, but with different methods depending on the research discipline of the investigator, and these disciplines rarely cross. We tackle this challenge by combining measurement methods from different research disciplines, with the purpose of finding a complete picture of the user behavior and working towards a unified analysis methodology. In this paper, we provide results, based on measurements performed with three different methods: Internet traffic measurements, web questionnaires and diaries. All measurements were performed in the Acreeo National Testbed, where we have access to both the network infrastructure and the end users. By comparing the different measurement methods we find that it is difficult for the end users to estimate the time they spend on different Internet activities although they are fairly well able to estimate the frequency of usage. We see that it is more difficult for end users to estimate their usage of streaming media applications than their HTTP traffic. We also find that though the diaries are quite accurate, the traffic measurements give us a much more detailed picture of the end user activity. We conclude that having a testbed with real end users is invaluable to this kind of study and we emphasize the importance of having access to Internet traffic to gain detailed knowledge of end user behavior.

Keywords-testbed; traffic measurements; user behavior; FTTH

I. INTRODUCTION

In a previous paper [1], we have described our work on the development of a unified methodology for Internet behavior usage measurements. In this paper we will expand the work concerning the methodology description and include additional results.

As the Internet continues to evolve and offer new services, it takes up a larger part of our lives. We find new ways to communicate, interact and entertain ourselves. This puts new demands on access networks [2] and requires new

insights into the behavior of those who use them. We believe that understanding user behavior and needs is the key to developing future networks and services that are accessible, reliable and that address the needs of real end users.

There are several ways to study user behavior. From the technical side, the data traffic can be measured and analyzed. Other common ways are to use surveys or diaries. Traffic measurements are routinely performed by operators, but results are rarely published because the operators are unwilling to share this information with competitors. On the other hand, published behavior studies are almost always based on surveys with individuals (e.g., telephone interviews with a large population). Such surveys often attract considerable interest in the public debate, and far-reaching conclusions may be drawn.

The question that we deal with in this paper is: To what extent are such surveys reliable? People can forget about their Internet activity, they may not know what they did, they may not know what their children did, they may lie about sensitive subjects, etc. We believe that in order to get a comprehensive picture of the evolution of Internet behavior, a combination of methods from different disciplines is needed. This will lead to a more detailed knowledge of the user behavior, and, by evaluating results from different methods we will obtain a better knowledge of their respective limitations. Furthermore, this way it can be verified whether surveys are correct or whether there perhaps is a systematic bias in survey answers that may lead to misleading results.

The purpose of this study is to develop a unified methodology where different kinds of surveys are combined with actual traffic measurements. We compare three different methods of looking at Internet user behavior;

- 1) Internet protocol (IP) traffic measurements,
- 2) web questionnaire and
- 3) diary.

Combining technical measurements with surveys requires test subjects in order to get statistical data. At Acreo we put a lot of effort into developing the Acreo National Testbed, ANT, which enables us to perform in-depth measurements and test new technology and equipment as well as to interact with end users. We have signed agreements with the end users where they agree to give feedback and participate in surveys and investigations. This means that the network conditions such as network topology, link speeds, service setup, etc as well as user metadata such as the number of people in a household, age, etc are known. This gives us a unique opportunity to perform measurements of user behavior, and to compare the results from different measurement techniques in order to evaluate the validity of the results since we have access to real user traffic measured on a household level.

The rest of the paper is organized in the following way. Section II describes the state of the art. Section III outlines the details and limitations of the specific methods. The test environment and the test population are described in Section IV, while data on the specific measurements is detailed in Section V. The measurement results are compared in a systematic way in Section VI, where we make some general observations and go through the results from the respective methods one-to-one. In this systematic review, we also discuss the limitations of the methods and the currently performed measurements in Section VII. Section VIII is dedicated to conclusions and future work.

II. STATE OF THE ART

There are traffic measurement studies in the literature. Most of these are based on traffic from campus areas [3] [4] or measure highly aggregated traffic [5] [6] [7] [8] [9] [10] [11], which makes it very difficult to draw conclusions about detailed user statistics. IP network traffic studies on a household level can be found in [12] [13] but as far as we know traffic measurements have not been used together with questionnaires and diaries, which are well known and often used methods [14] [15] [16] [17] [18] [19] [20] [21] [22].

Surveys, administered to a sample of the population, are the most common method to get information about Internet behavior [16]. An interviewer can ask questions by phone or at home. The questionnaire can also be sent by post or be available online and be administered by the individuals themselves. Questions can be asked about attitudes, beliefs and past behaviour, i.e., what people generally think and do.

Another way to get to know how people use the Internet is to let them fill in a diary, where they make notes about what they do during the 24 hours of the day. The diary method has a long tradition in social sciences and is normally used in field studies where the data is collected in situ, from real people in real situations [23]. Notes about what the person is doing during the 24 hours of the day are written down.

The method has been used to measure different aspects of Internet behavior such as time displacement [24] or usage patterns [25] although not as frequently as surveys [26].

Both diary studies and surveys are prone to human error in answering questions and filling in diaries. We know that answers gathered from these types of surveys have systematic errors due to the difficulty of estimating time and the unwillingness to answer questions regarding certain areas of Internet usage (e.g, illegal such as file sharing and personal, such as sites with adult content) [27].

A third method, without these limitations, is Internet traffic measurements. This method measures all traffic going in and out from a household or user to the Internet. It can be used to register for example traffic volumes, applications used and web sites visited as well as background traffic such as automatic updates.

III. PROS AND CONS OF THE METHODS

In this section, we will discuss the strengths and weaknesses of the different measurement methods used in this study: web questionnaires, diaries and traffic measurements.

A. Questionnaire

A questionnaire is an efficient way of collecting information from a large number of respondents. Questions are administered to individuals, by phone or at home, by post or online. Questions can be standardized; the sample can be representative of the population, which is a major strength. This method also gives the possibility of covering many areas from attitudes and reflections to general behavior and very detailed information.

A weakness of this method is that the outcome is strongly dependent on the ability of the respondents to answer the questions. This depends partly on the ability of the researcher to formulate relevant and understandable questions and partly on the willingness of the respondents to answer sensitive questions in a truthful way. Also their ability to estimate how often they perform different activities on the Internet and how much time they spend online during an average week is crucial for the outcome of the method. Triangulation with other methods of measuring Internet behavior can help resolve these issues.

B. Diary

If a questionnaire measures past behavior, a diary focuses on the present. It is about real people in their everyday life, at a specific time and in a specific place. This is also the strength of the diary. Diaries also have an exploring quality that surveys lack, which can lead to unexpected discoveries. To keep a diary during a few days requires a high level of commitment from the participants, which is a weakness. There is therefore a need for detailed instructions and frequent administrative contacts [28]. To what extent the behavior noted down in the diaries is exhaustive and reflects

the simultaneous measurements of Internet traffic as well as their regular Internet behavior will become obvious during the triangulation.

C. Traffic Measurements

Traffic measurements record actual network traffic capturing all user activity without bias or human error. Depending on the equipment and methods used, a deep level of detail can be achieved. It is also possible to measure activities that are not induced by active end users such as automatic updates or applications that are left running with no user present such as file sharing applications. This may be both a possibility and a disadvantage, since it may be difficult to distinguish between user induced activities and computer induced activities.

One disadvantage of this method is the enormous amount of data generated. It requires large storage space and efficient analysis tools. The important question is whether the analysis and classification of traffic measurements can make these data comparable with data from the questionnaires and the diaries. There is also the problem of coupling measurements of traffic from an IP-number to a specific end user for example with shared computers or in family households. Having the possibility of addressing a test population with a given profile is also a limiting factor of the method. In general, traffic measurements are collected in geographically specified populations, whereas for a specific test one may require a population which is representative of the country, i.e., defined by parameters such as age, sex, occupation, etc.

IV. TEST ENVIRONMENT AND POPULATION

As mentioned in the introduction, the measurements in this study were performed in the Acreo National Testbed (ANT), which has previously been described in [29] and [30]. The purpose of ANT is to provide an environment for testing new technology and equipment as well as a way to interact with end users. Contrary to lab based testbeds, this is a live network with real end users or test pilots. In return for being test pilots the end user households are given free access to services like Internet and IPTV. Fiber to the home (FTTH) is the main access technology in the testbed, and a schematic picture of the network is shown in Figure 1.

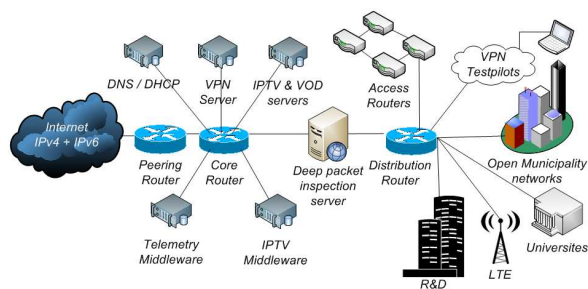


Figure 1: Schematic picture of the Acreo National Testbed, ANT.

The FTTH installation at the test households is active Ethernet providing 100 Mbit/s symmetrical connections to each household. The number of households in the testbed changes over time according to the current tests that are being performed. At the time of this study, there were approximately 40 active households in the testbed. Approximately 20 were apartments in a building centrally located in a town in Sweden. The rest of the households, approximately 20 single dwelling units, were connected to the testbed via a fixed wireless access network, depicted as HSPA (High Speed Packet Access) in Figure 1.

A letter of invitation was sent out to all users in the testbed describing the measurements to be performed and asking for volunteers. A form was attached to the invitation letter, where detailed information about the household was to be filled in, such as the number of people in the household, number of computers, ages, etc. The test pilots were also assured that their answers would be treated anonymously.

Based on the response from the test users, 5 households were selected to take part in this study. The selection criteria for the 5 households were that different kinds of household constellations should be represented. Thus 2 single households and 3 family households were chosen. Of the family households, one had preschool children, one had teenaged children and one had both younger and older children. The household details are summarized in Table 1. Household number 2 had two IP-numbers, one used by the parents that will be denoted 2.1 and one mainly used by the teenagers of the family that will be denoted 2.2.

All the participants, except those twelve years or younger, were later classified into different user groups according to usage patterns revealed by their answers to the web questionnaires. The typology has been accomplished through two separate studies which encompass 2000 telephone interviews, based on a random sample of the Swedish population from 16 years of age and older [31] [32].

Characteristic for the groups of Internet users that turned up in the cluster process is that there were two extremes. One group, the advanced enthusiasts, has access to everything and uses Internets potential fully. The other group, its opposite, the cautious, have limited access to new technology and use it very restrictedly. Between these two extremes there are a number of groups whose usage patterns differ in various ways. But they are essentially variants of two basic patterns: the traditional and the modern. The traditional usage pattern is built around the Internets informative qualities and the modern usage pattern, supported by the young Internet generation, rests on the interactive, communicative characteristics of the Internet.

The participants in the study were sent gratifications in the form of movie tickets when their responses had been received. They were not informed that they would receive any gratifications beforehand and the gratification was thus not an incentive for taking part in the study.

Table 1: Characteristics of the members of the 5 households.

Household	Household members	Age	Education	Usage pattern
1	Man	30	University education	Enthusiastic traditionalist
2	Woman	41	University education	Traditionalist
	Man	46	Higher certificate	Traditionalist
	Boy	15	At school	Advanced enthusiast
	Girl	17	At school	Enthusiastic modernist
3	Woman	34	9-year compulsory University education	Enthusiastic modernist
	Man	32		Traditionalist
	Pre-school child	4		Video and gaming
4	Pre-school child	6		Video and gaming
	Man	58	Higher certificate	Traditionalist
5	Woman	39	Higher certificate	Traditionalist
	Man	35	More than compulsory, no higher certificate	Traditionalist
	Boy	17	At school	Advanced enthusiast
	Boy	12	At school	Moderate use; gaming, file sharing

The measurements in this paper are based on data from 5 testbed households. The reason for using a small population in the study is that we wanted to perform a qualitative analysis of their Internet usage, i.e., the main point is not to gather data for statistical analysis, but rather to study the user behavior in depth, as we have not found any similar studies in the literature. As this is a novel comparative methodology it was also important to develop methods and analysis tools that can be scaled up to considerably larger populations [33] where the amount of data to be handled will be much more extensive. That is, we do not claim to be able to make statistical conclusions in this study, but interesting trends for further study will be pointed out.

We are not able to include all types of users detailed in Table 1 with this small population. We have however made an effort to include households with different profiles to be as inclusive as possible. Nevertheless, before extending our population, we would like to establish a solid foundation for our work on developing a unified methodology that can be used for more substantial conclusions at a later stage.

V. MEASUREMENTS

The combined methodology consists of three parts: traffic measurements, web questionnaires and diaries. The details

of each type of measurement are given below.

A. Traffic Measurements

The traffic measurements have been performed using PacketLogic (PL) [34], a commercial traffic management device used in many commercial broadband access networks all over the world. Traffic is identified based on packet content (deep packet inspection and deep flow inspection) instead of port definitions. The device can identify more than 1000 Internet application protocols, and the signature database is continuously updated. The identification process is connection-oriented, which means that each established connection between two hosts is matched to a certain application protocol. When a new connection is established, the identification of this connection begins. The identification algorithm searches for specific patterns, signatures, in the connection. The patterns are found in the IP header and application payload. The PL uses the traffic in both directions in the identification process. The measurement point is depicted as deep packet inspection in Figure 1.

The PL can track and identify several hundred thousand simultaneous connections, storing statistics in large databases. The statistics database records the short-time average amount of traffic in inbound and outbound directions as well as the total traffic for all nodes in the network. Data may be stored aggregated over 5 minute periods or detailed on a per connection basis.

The measurement setup, although giving detailed measurements, has certain constraints. First, the traffic is measured per household and not per person and the analysis in this paper is therefore done on a per household basis. There is also a 5 minute resolution in the measurements, which may have an impact on measurements of applications that are used in short time periods such as instant messaging. The data cut-off is 1 kbps, which may influence the measurements of certain applications such as gaming where the amount of data is generally very low. The signature database in this study was not up-to-date due to old hardware, which may result in a larger amount of unknown traffic. An upgrade will be performed before follow-up studies are performed. The Internet traffic of each household was measured both during the days when the household recorded their diaries (17-18 May 2009) and for a complete month (May 2009) to get enough statistics to compare with the web questionnaire. Statistics on what web sites were visited by the different households were monitored for two weeks.

B. Web Questionnaires

Each household member was asked to answer a web questionnaire regarding their long-term media and Internet activity/behavior in general during the last weeks and months. In the case of preschool children, the parents were asked to answer for them. The questionnaire used was basically the same as the one used by the World Internet

Institute in their yearly study of the Internet behavior of 2000 Swedes [35]. It contained basic questions concerning family situation, education and occupation as well as questions about attitudes, computer knowledge and Internet activity. The Internet activity questions included questions about the frequency of use of different Internet applications and how often different types of web sites are visited such as banks or newspapers, etc. Finally, the respondents were asked to estimate the total time they usually spend online at home, at work, at school and in other places.

C. Diaries

The members of each household were asked to complete a 24-hour diary logging their activities during two consecutive days, Sunday and Monday 17-18 May 2009. In the diary the test pilots were asked to fill out four columns:

- Daily activity (sleep, work/school, leisure time activities, meals etc.)
- Media usage (TV, newspaper, radio, book, etc.)
- Internet activity when at home (web browsing, playing games online, visiting community, downloading material from the internet, etc.)
- Web address or service/application used

Each day was divided into 15-minute intervals. In the case of preschool children in the household, the parents were asked to note down their Internet activities.

VI. RESULTS

In this section, the results of the measurements are presented. First, some general results are given and then the results from the different methods are compared.

A. General Results

Comparing data from the questionnaires with the results from a representative study of the Swedish population using the same questionnaire, we can classify the Internet usage patterns of the test persons according to the four typical usage patterns that have earlier been found in [31].

The most striking usage pattern is that of the advanced enthusiasts. Two teenage boys in households 2 and 5 belong to this group. They use the Internet for everything to a much larger extent than most people. They share files, use social networks and read blogs. The Internet is very important to them. Their opposites are the cautious. They do not spend much time on the Internet and when they do, its in order to look for facts or find information. No one in this study belongs to this group.

Between these two extremes we find the majority of Internet users, the traditionalists and the modernists. The modernists are mostly interested in communication and entertainment. But they also use the Internet for information and fact-finding. There are three modernists among the test persons. They are all women and two of them, the teenage

girls (household 2), are so called enthusiastic modernists as they spend a lot of time online.

The traditionalists are the largest group in the population as well as among the test persons. They do not spend as much time on the Internet as the preceding groups and are mostly interested in its traditional role as a source of information, for checking facts and for practical matters. They are generally positive to the Internet but regard other media as more important. Two women (household 2 and 5) and five men (household 1, 2, 3, 4, and 5) can be classified according to this usage pattern. The Internet usage patterns among the test persons are shown in Table 1.

The traffic measurements show that the households participating in the study are active mainly during afternoons and evenings with shorter bursts of traffic during the morning and lunch hours. This corresponds to the traffic patterns established both in the ANT-testbed, see Figure 2, and in municipal networks of similar characteristics [36].

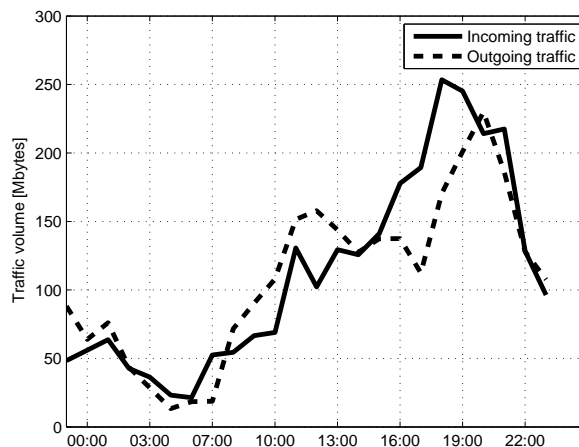


Figure 2: Schematic picture of the Acreo National Testbed, ANT.

We also note that the average time spent online calculated from the traffic measurements is greater during the weekend than the weekdays for the family households while the opposite is true for the households without children, see Table 2. The assumption here is that for the family households, the time of day when household members use Internet applications will be more spread out during the weekend and of course there are more people at home with leisure time. However, this assumption should be confirmed for a larger population.

B. Traffic Measurements (Long Term Behavior) vs. Web Questionnaires (Long Term Behavior)

The over-all estimation in the questionnaires (Q) of the frequency of use of the Internet corresponds to what is shown in the traffic measurements (TM). All households use the Internet daily. However, one older man, a traditionalist in

Table 2: Average time per day spent on Internet applications per household as registered by the traffic measurements performed during May 2009.

Household	All days [min/day]	Weekends [min/day]
1	253	111
2.1 / 2.2	432 / 75	614 / 66
3	588	496
4	196	154
5	1047	1162

Household 4, underestimates his general frequency online. Traffic measurements show that he uses the Internet daily but in his answer to the questionnaire he states that he uses Internet a few times a week. At the same time he says that he visits certain web sites daily, which corresponds with the results from the traffic measurements. So in the main, the questionnaire answers as to how often the test pilots were online, were confirmed by the traffic measurements, see Table 3.

Table 3: Frequency of general Internet usage. A comparison between the results from traffic measurements (TM) and a questionnaire (Q) given to the members of 5 households about their Internet behavior at home. The numbers represent the number of days where activity was registered by the measurement equipment. D=Daily usage, W=Weekly usage, Y=Yes.

Household	Frequency		HTTP (days/month)	
	TM	Q	TM	Q
1	D	D	23	D
2.1	D	D	16	D
2.2	D	D	28	D
3	Y	Y	27	D
4	D	W	28	D
5	D	D	26	D

In the families with teenagers, the questionnaires show that the children are the main users of the Internet. The traffic measurements cannot couple a specific person to a specific Internet activity. However the measurements show a traffic mix corresponding to the expectations from the age group with parents visiting banks and web shops and teenagers using instant messaging, gaming, blogging and visiting social communities [35].

The user penetration of a number of applications seen in the traffic measurements is found in Table 4. This is in good agreement with the answers from the web questionnaires. As is expected, HTTP is used by all households as well as the SSL protocol, which is used by for example Internet shops and banks. All of the households also use HTTP media stream as well as flash video, which means that they look at streaming material on the Internet.

The frequencies of use reported in the questionnaires were seen, on a general level, to correspond well with the measured data. The questionnaire also posed questions about the frequency of use of more specific Internet activities such as using e-mail, visiting banks online, reading newspapers

Table 4: User penetration of specific applications seen in the traffic measurements. Specific use of the Internet. A comparison between traffic measurements (TM) during 28 days and web questionnaires (Q) concerning Internet behaviour at home. Y=Yes, N=No, D=Daily. User penetration of specific applications seen in the traffic measurements.

Household	Application							
	HTTP	HTTP Media Stream	BitTorrent	Spotify	SSL	Flash video	MSN Messenger	Skype
1	x	x	x		x	x	x	
2	x	x	x	x	x	x	x	x
3	x	x		x	x	x		
4	x	x			x	x		
5	x	x	x		x	x	x	

online, visiting social networks, using instant messaging, phoning online, listening to music through Spotify or using file sharing applications to download music or film. The answers from the questionnaires are for the most part confirmed by the traffic measurements, see Table 5. This includes activities such as file sharing and listening to streaming music online through Spotify. The test pilots were able to give estimations of how often they used for example Spotify or file sharing applications and how often they visited certain types of web sites such as newspapers or banks.

Table 5: User penetration of specific applications seen in the traffic measurements. Specific use of the Internet. A comparison between traffic measurements (TM) during 28 days and web questionnaires (Q) concerning Internet behaviour at home. Y=Yes, N=No, D=Daily.

Household	e-mail		Banking		Newspapers	
	TM	Q	TM	Q	TM	Q
1	D	D	Y	Y	Y	D
2.1	D	D	Y	Y	Y	D
2.2	D	D	N	N	Y	D
3	Y	Y	Y	Y	Y	D
4	D	D	Y	Y	Y	D
5	Y	Y	Y	Y	Y	D

One test pilot reported a high online gaming activity in the web questionnaire, which was not recorded by the traffic measurements. A factor influencing the traffic measurements is the cut-off of 1 kbps for the data collection. The transfer rates are usually low for gaming applications and the traffic may thus not register in the statistics. However, the discrepancy between the measurements and the questionnaire is in this case so large that at least a great part of it is deemed to be due to other circumstances for example that he used a computer in some other place for gaming. It has been discussed whether questionnaire answers give a true picture of activities that may be illegal or not socially acceptable.

In this study, the majority of the households answered that they used file sharing applications occasionally, which is in agreement with the measurement results. We thus conclude that the households are comfortable with answering questions about file sharing activities and that eventual errors are not a result of unwillingness to divulge this information. It should be noted here that the test pilots are used to answer questionnaires and may not be representative in the sense that they may be less shy than other users when sharing sensitive information.

Considering streaming media, the estimations of the test pilots were seen to be reliable when answering questions regarding specific streaming media applications, such as Spotify, or specific web sites with streaming media content, such as YouTube. But more general questions concerning how many hours a week they listened to streaming music or watched streaming video, were more problematic for the test pilots to answer and the answers were in some cases incomplete. The result is shown in Table 6. The reason for this difficulty is probably that the question was difficult to understand. The test pilots may not be aware of what using streaming media means although they are familiar with Spotify and Youtube.

Table 6: User penetration of specific applications seen in the traffic measurements. Specific use of the Internet. A comparison between the results from traffic measurements (TM) during 28 days and a questionnaire (Q) given to the members of 5 households about their Internet behavior at home. The category Streaming audio includes applications such as Spotify, SHOUTcast, Flash audio over HTTP, etc. while streaming video includes for example Flash video over HTTP, HTTP media stream and Joost. The numbers represent the number of days where the measurement equipment registered activity. D=Daily, W=Weekly.

Household	Streaming Audio		Streaming Video	
	TM	Q	TM	Q
1	3	W	19	—
2.1	1	Seldom	0	0
2.2	15	D	21	D
3	15	—	6	W
4	18	0	25	W
5	27	—	28	D

We have up to now looked at frequency of use. Now we will compare Internet usage time, in hours and minutes. The question asked in the web questionnaire was: How many hours and minutes per week do you usually use Internet at home? As can be seen in Table 7, the answers correspond well with measurements of http traffic. But the traffic measurement method measures all Internet traffic such as file sharing, streaming media, IP telephony, automatic updates, etc as well as http traffic. As long as the computer is connected to the Internet there will be traffic going to and from the computer. This total Internet time is for every household more than 100 percent longer than their own estimations of their Internet activities. It seems that the Internet users are not able to estimate this total Internet time,

at least not without much more detailed and comprehensible instructions.

Table 7: Time online. A comparison between the results from traffic measurements (TM) and a questionnaire (Q) given to the members of 5 households about their Internet behavior at home.

Household	Hours/week HTTP		Hours/week Total	
	TM	Q	TM	Q
1	16	14	30	—
2.1	9	12	—	—
2.2	50	56	120	132
3	10	8	69	—
4	14	10	23	—
5	49	48	122	—

C. Traffic Measurements (Long Term Behavior) vs. Diaries (Short Term Behavior)

All test persons were asked to fill in a diary and to make notes about what they were doing during two days (48 hours) chosen to be a Sunday and a Monday, 17 and 18 May 2009. During the same time, all Internet traffic going in and out from their IP-number was measured and the web sites visited were logged. On a general level, there was a total correspondence between the diaries and the traffic measurements as to when the test persons were using the Internet, which is shown in Table 8.

Table 8: A comparison between the results from traffic measurements and a two days diary given to the members of 5 households about their Internet behavior at home. D=Daily, day 1=day 1 of the recorded diary.

Household	Frequency		HTTP	
	TM	Q	TM	Q
1	D	D	D	D
2.1	day 1	day 1	day 1	day 1
2.2	D	D	D	D
3	D	D	D	D
4	D	D	D	D
5	D	D	D	D

The activities noted down in the diaries were compared to the traffic measurements and we can see that the same activities were registered in both, see Table 9. Although the diaries generally correspond well with the measured Internet activity, there are also some exceptions. For household 5 the measurements show Internet activity that is not noted down in the diary. The traffic consists of HTTP, HTTP media stream and HTTP download traffic. Also for household 4 one household member has at several times noted down that Spotify (music streaming application) was used in conjunction with either at work or outside. The measurements however show no traffic from this application. Either the usage of this application has taken place away from home or on a device that does not send traffic via the IP monitored by the traffic measurements.

Another noteworthy discrepancy is a number of visits by one of the households to websites containing adult content,

Table 9: Specific Internet activities. A comparison between the results from traffic measurements and a two days diary given to the members of 5 households about their Internet behavior at home. The numbers represent the number of hours during the two days where activity was registered by the measurement equipment. Y=Yes, D=Daily.

Household	E-mail		Banking		Newspapers		Social Network		IM		Spotify [Hours]	
	TM	Diary	TM	Diary	TM	Diary	TM	Diary	TM	Diary	TM	Diary
	1	Y	Y			Y	Y	Y	Y			
2.1	Y	Y	Y	Y								
2.2							D	D	D	D		16
3	Y	Y	Y	Y			Y	Y			15	15
4	Y	Y	Y	Y	Y	Y						
5	Y	Y	Y	Y	Y	Y	Y	Y	Y	Y	Y	

which was registered by the measurement instrument. Compared with what is detailed in the diaries of the household members it is seen that HTTP activity has been written down without any indication of the specific web sites visited. In the case of these types of web sites we would expect both diary and questionnaire material to show less activity or to be less specific than what is actually the case.

One of the households also shows activity from the filesharing application Bit Torrent KRPC which is a protocol keeping track of seeders and content for the Bit Torrent application. In the diaries, no such activity has been noted down. The conclusion here is that there is a computer in the household causing the activity without the presence of an active user. This type of activity that is not user induced is in fact difficult to measure using questionnaires or diaries and adds important details to the results concerning user behavior.

A more general observation is that the Internet usage registered by the traffic measurements seems to be, in several cases, more versatile and complex than what can be found in the diaries. We exemplify this by looking at some of the teenagers participating in the study. They use the Internet in several ways at the same time. They watch TV online while at the same time communicating with friends and visiting a social network site. This combination of activities is not seen in the diary. In the diary they may have noted down only one activity like watching TV online or just surfing. There is a need to define more carefully what is meant by certain concepts and to be aware that several Internet activities can go on at the same time as the main activity.

D. Diaries (Short Term Behavior) vs. Web Questionnaires (Long Term Behavior)

The general usage pattern that can be extracted from the questionnaire also shows up in the diary. The advanced enthusiasts and the enthusiastic modernists are very ac-

tive according to the diaries, and traditionalists with very restricted use of the Internet are the same both in the questionnaire and the diary, see Table 10. Most of the activities the test persons say they perform daily in the questionnaire can also be found in the diary.

Table 10: Time online. A comparison between the results of a web questionnaire and a two days diary given to the members of 5 households about their Internet behavior at home.

Household	Hours/day HTTP	
	Q	Diary
1	2.0	1.25
2.1	1.7	0.75
2.2	3.0	3.25
3	1.2	2.0
4	1.4	1.1
5	7.0	5.5

There are exceptions such as when the test pilot is away from home during one of the two days when the diary was scheduled, or is busy with something completely different from what he/she usually does. But in most cases there is a high correspondence between the daily activities marked in the questionnaire and what is noted in the diary, even if two days are not enough for the whole repertoire of activities to show up. This is especially evident among the frequent users who use the Internet several times a day, as an important part of their everyday life.

VII. DISCUSSION

Three different methods have been used to measure the way people use Internet in their homes: A questionnaire, a diary and traffic measurements. There is a high agreement between the methods. People who are active users of the Internet according to the traffic measurements are also active users according the questionnaire and the diary. Those who say in the questionnaire that they use the Internet rarely also show low Internet activity in the diary and in the traffic measurements.

There is also an agreement on a more specific level. The different activities that the respondents say that they usually do when going online can be found in the technical measurements of the Internet activities, and these activities also show up in the diaries. In most cases there is also a rather good fit between the time of Internet use measured from the traffic measurement and the users own estimate of the hours and minutes online. We found one exception of an underestimation. We also found a boy of 15 years who reported a lot of gaming that was not found in the traffic measurements.

This high level of agreement applies to the use of http websites. There seems to be more problems when it comes to streaming audio and video applications. The reason for this can be that the more passive use of streaming media as a second hand activity is more difficult to estimate, but

also that the questions were not formulated in a comprehensive way. Not everyone knows what streaming audio is. Supporting this conclusion is the very good fit between the traffic measurements and the estimates of those Internet users who listen to the music service Spotify. When the question is specific and tied to a single activity it is also easier to give a good estimate. However, the questionnaire and especially the diary do not give the full picture of the Internet usage. In many cases, a lot of different activities go on at the same time. This is typical of the Internet usage of teenagers and younger people. They visit social websites, communicate with instant messaging, at the same time as they listen to music and watch TV. All these activities do not show up in the diary. Behind the term surfing a lot of activities can be hidden. Only traffic measurements can uncover this more complicated interplay between different activities although the diary form can be further elaborated to cover more complex situations.

At last, there is a more general problem. A direct comparison between traffic measurements and answers from a questionnaire and a diary can be problematic, as they do not measure exactly the same things. There is a lot of network traffic that is not directly induced by the user, such as automatic updates and file sharing activities that happen in the background. For the most part, this is something that the users are unaware of. It is therefore necessary to develop a way to filter out those activities and further develop the traffic measurements, before a fair comparison can be made.

VIII. CONCLUSION AND FUTURE WORK

In this paper, we have proposed and applied a unified methodology using three different methods to study Internet user behavior; traffic measurements, web questionnaires and diaries with the purpose of verifying and comparing the different methods as well as gaining more insight into user behavior.

From the measurements, we conclude that the test pilots are well able to describe some of their short term behavior seen in the diaries, although some activities were not noted in the diaries. The long term behavior seen in the web questionnaires are fairly accurate in describing frequencies of use specific applications and visits to specific web sites. The estimation of the amount of time spent on different activities was seen to differ from that of the traffic measurements, with a slight tendency to underestimate the time spent. An even more powerful conclusion is the complex and rich picture of user behavior, which is obtained via traffic measurements. Here, details and behaviors that are not exposed in diaries or questionnaires are visible. This gives new insights into user behavior as well as valuable feedback for better construction of question based investigations in the future.

The study was conducted in 2009 and since then, the amount of time people spend on the Internet has increased, especially when it comes to the use of smart phones. This

will make it more difficult in the future to estimate the total time of Internet use, as the number of ways you can connect to the Internet increases: computer, mobile phone, TV, game console, etc. It will be more difficult but not impossible.

Another major result is the importance of the testbed to the study. Here, we have the possibility of making measurements in a controlled environment with real end users. From the traffic measurements we gain much more insight into the behavior of the end users than can be obtained from only questionnaires or diaries. However, from the questionnaires and diaries, we also gain a better understanding of how the end user perceives specific services giving valuable information when interpreting the results from the traffic measurements. From the network side, this can be used to improve the quality of service both from the technical and the end user perspective.

We will continue to develop our testbed under the Central Baltic Testbed project. In this project, we will work towards creating a distributed measurement platform. In this way we will have data from a large population spread out across the country. Our future work will continue with a wider study to follow up on the results presented here.

ACKNOWLEDGMENT

The work in this project has been partly financed by the VINNOVA project Broadband Behavior and the European Regional Development Fund project Acreo National Testbed. Also, it has been partly funded by the Celtic IPNQSIS project and Swedish National Strategic Research Area (SRA) within the program TNG (The Next Generation) and the project eWIN.

REFERENCES

- [1] C. Lagerstedt, A. Aurelius, H. Pathirana, C. P. Larsen, and O. Findahl, "Unified methodology for broadband behavior measurements in the acreo national testbed," *The Seventh International Conference on Digital Telecommunications, ICDT*, 2012.
- [2] M. Chesire, A. Wolman, G. M. Voelker, and H. M. Levy, "Measurement and analysis of a streaming-media workload," *Proceedings of the 3rd conference on USENIX Symposium on Internet Technologies and Systems*, vol. 3, 2001.
- [3] M. Alvarez-Campana, A. Azcorra, J. Berrocal, D. Larrabeiti, J. I. Moreno, and J. R. Prez, "Castba: Internet traffic measurements over the spanish r&d atm network," *5th HP Openview University Association Workshop*, 1998.
- [4] Y. Bhole and A. Popescu, "Measurement and analysis of http traffic," *Journal of Network and Systems Management*, vol. 13, no. 4, pp. 357–371, 2005.
- [5] C. Fraleigh, S. Moon, B. Lyles, C. Cotton, M. Khan, D. Moll, R. Rockell, T. Seely, and C. Diot, "Packet-level traffic measurements from the sprint ip backbone," *IEEE Network*, vol. 17, no. 6, pp. 6–16, 2003.

- [6] J. Zhang, J. Yang, C. An, and J. Wang, "Traffic measurement and analysis of tunet," *2005 International Conference on Cyberworlds (CW'05)*, 2005.
- [7] K. Fukuda, K. Cho, and H. Esaki, "The impact of residential broadband traffic on japanese isp backbones," *SIGCOMM Comput. Commun. Rev., ACM*, vol. 35, p. 1522, 2005.
- [8] G. Maier, A. Feldmann, V. Paxson, and M. Allman, "On dominant characteristics of residential broadband internet traffic," *Proceedings of the 9th ACM SIGCOMM conference on Internet measurement conference, ACM*, p. 90102, 2009.
- [9] (2012, 12) Akamai. [Online]. Available: <http://www.akamai.com/stateoftheinternet/>
- [10] (2012, 12) Sandvine. [Online]. Available: <http://www.sandvine.com/downloads/documents/Phenomena\1H\2012\Sandvine\Global\Internet\Phenomena\Report\1H\2012.pdf>
- [11] (2012, 12) Cisco. [Online]. Available: http://www.cisco.com/en/US/netsol/ns827/networking__solutions__sub__solution.html#\~/overview
- [12] M. Kihl, P. Odling, C. Lagerstedt, and A. Aurelius, "Traffic analysis and characterization of internet user behavior," *International Congress on Ultra Modern Telecommunications and Control Systems and Workshops (ICUMT)*, 2010.
- [13] A. Aurelius, C. Lagerstedt, I. Sedano, S. Molnar, M. Kihl, and F. Mata, "Tramms: Monitoring the evolution of residential broadband internet traffic," *Future Network & Mobile Summit 2010 Conference Proceedings*, 2010.
- [14] J. George, "Researching life in e-society with diary studies," in *Proceedings of the 2006 European Conference on Information Systems*, no. 67, June 2006.
- [15] K. Vermaas and L. van de Wijngaert, "Measuring internet behavior: Total time diary and activity diary as research methods," *Journal of Information Technology Theory and Application*, vol. 7, no. 11, 2005.
- [16] O. Findahl, "Vad säger internetstatistiken? (what does internet statistics tell us)," Stiftelsen för internetinfrastruktur .SE, Tech. Rep., 2008.
- [17] (2012, 12) Nordiskt informationscenter fr medie- och kommunikationsforskning, nordicom. [Online]. Available: <http://www.nordicom.gu.se>
- [18] (2012, 12) Nielsen. [Online]. Available: <http://se.nielsen.com/site/index.shtml>
- [19] (2012, 12) Post och telestyrelsen, pts. [Online]. Available: <http://www.pts.se/sv/>
- [20] (2012, 12) Gallup. [Online]. Available: <http://www.gallup.com/home.aspx>
- [21] (2012, 12) Mediamatning i skandinavien, mms. [Online]. Available: <http://www.mms.se/>
- [22] (2012, 12) Statistiska centralbyrån, scb. [Online]. Available: <http://www.scb.se>
- [23] N. Bolger, A. Davis, and E. Rafaeli, "Diary methods: capturing life as it is lived," *Annual Review of Psychology*, vol. 54, p. 579616, 2003.
- [24] J. P. Robinson, "Introduction to issue 2: It, mass media and other daily activity," *IT & Society*, vol. 1, no. 2, pp. 1–8, 2002.
- [25] K. Ishii, "Internet use in japan a time diary method," *Paper presented at the APIRA conference in HongKong and Macao*, 8 2004.
- [26] S. Sieber, "The integration of field work and survey methods," *American Journal of Sociology*, vol. 6, no. 78, pp. 1335–1359, 1973.
- [27] H. Selg and O. Findahl, "Nya anvarndarmonster. jmforande analys av tva anvarndarstudier." Uppsala universitet. Nationellt IT-anvarndarcentrum NITA., Tech. Rep., 10 2008.
- [28] T. Crosbie, "Using activity diaries: Some methodological lessons," *Journal of Research Practice*, vol. 2, no. D1, 2006.
- [29] C. P. Larsen, C. Lindqvist, H. Pathirana, R. Lindström, E. Modin, and A. Aurelius, "Ant: The acreo national testbed status and plans," in *Proc. NOC 2007*, 6 2007.
- [30] (2012, 12) Acreo national testbed, ant. [Online]. Available: <http://www.acreo.se/en/Technology-Areas/Broadband-Technology/Projects/Current-Projects/Acreo-National-Testbed>
- [31] O. Findahl, "The swedes and the internet 2007," World Internet Institute, Gävle, Tech. Rep., 2007.
- [32] —, "The swedes and the internet 2011," World Internet Institute, Gävle, Tech. Rep., 2011.
- [33] W. Cleveland and D. X. Sun, "Internet traffic data," *Journal of the American Statistical Association*, pp. 79–985, 1995.
- [34] (2012, 12) Procera networks. [Online]. Available: <http://proceranetworks.com>
- [35] O. Findahl, "The swedes and the internet 2009," World Internet Institute, Gävle, Tech. Rep., 2009.
- [36] M. Kihl, C. Lagerstedt, A. Aurelius, and P. Odling, "Traffic analysis and characterization of internet user behavior," in *Proceedings of the International Congress on Ultra Modern Telecommunications and Control Systems*, 10 2010, pp. 224–231.

Using Network Proximity for Context-aware Browsing

SpotEx approach for delivering data to mobile subscribers

Dmitry Namiot

Lomonosov Moscow State University
Faculty of Computational Math and Cybernetics
Moscow, Russia
dnamiot@gmail.com

Manfred Sneys-Snepe

Ventspils University College
Ventspils International Radio Astronomy Centre
Ventspils, Latvia
manfreds.sneys@gmail.com

Abstract - This paper describes our SpotEx model for accessing to local data for mobile subscribers. This model is based on ideas of network proximity. In our concept, any existing or even especially created Wi-Fi hot spot or Bluetooth node could be used as presence sensor that can play a role of trigger for opening access for some content (or discovering some content). In our approach we can discover hyper local data as info snippets that are valid (relevant) for mobile subscribers being at this moment nearby some Wi-Fi access point. Info snippets could be either user-generated or collected from the social networks. As the prospect use-cases we can mention for example news and deals delivery in malls, news feeds for office centers and campuses, Smart City projects, personal classifieds and real world games.

Keywords-Wi-Fi; Bluetooth; network proximity; collaborative location; indoor positioning; context-aware computing.

I. INTRODUCTION

This paper describes how the measurements collected from the wireless sensors on the mobile phone could be used for presenting an appropriate content (context-aware information) to mobile subscriber. It is an extended version of our paper from ICDT-2012 conference [1].

In the work that first time introduces the term 'context-aware', Schilit and Theimer [2] refer to context as location, identities of nearby people and objects, and changes to those objects. Other authors define context awareness as complementary element to location awareness. Whereas location may serve as a determinant for resident processes, context may be applied more flexibly with mobile computing with any moving entities, especially with bearers of smart communicators. Context awareness originated as a term from ubiquitous computing, or as so-called pervasive computing, which sought to deal with linking changes in the environment with computer systems, which are otherwise static.

Modern applications adopt a context-aware perspective to manage:

- a) communication among users and among systems, or between the system and the user,
- b) situation-awareness, like modeling location and environment aspects (physical situation) or the current user activity (personal situation)

c) knowledge chunks: determining the set of situation-relevant information, services or behaviors [3].

In our article, we are dealing with context-aware knowledge chunks. Let us start with the base element – location. It is the basic element for all the above mentioned definitions for context-aware. In general, getting location info for mobile subscribers could be pretty standard nowadays (GPS, cell-ID, assisted GPS [4]). The picture is much more complicated for indoor positioning. The Global Positioning System (GPS) loses accuracy indoor [5]. The system design for indoor positioning system (IPS) may vary. On practice, IPS systems can use various optical, radio, or even acoustic technologies. However, all of them require the utilization of their own protocols with their own API. The heterogeneous scenarios are typical for IPS.

One of the most used approaches to indoor location is Wi-Fi based positioning. A standard Wi-Fi based positioning system, such as the one offered by Ekahau [4] is completely software-based and utilizes existing Wi-Fi access points installed in a facility and radio cards already present in the user devices. Companies could deploy also Wi-Fi based radio tags that use industry standard components that adhere to the 802.11 standards. This approach allows for the use of commercial off-the-shelf hardware and drivers to produce a standards-based radio tag that can communicate bi-directionally over the 802.11 networks. For embedded solutions, there is no need for the client to include a specialized tag, transmitter, or receiver.

Because of the entire use of standards-based hardware, such as 802.11b, 802.11g, and 802.11a, a standard Wi-Fi based solution rides the installed base and economies of scale of the networks and end user devices that are proliferating today. Based on the standard and already existing hardware, a company can install the system much faster and significantly reduce initial and long-term support costs. A common infrastructure supports both the data network and the positioning system, something companies strive for. The positioning system works wherever there is Wi-Fi coverage.

Actually, Figure 1 describes the main idea behind the Wi-Fi positioning: signal strength vs. distance. In addition to cost savings in hardware, a standards Wi-Fi based positioning system significantly reduces the potential for RF interference.

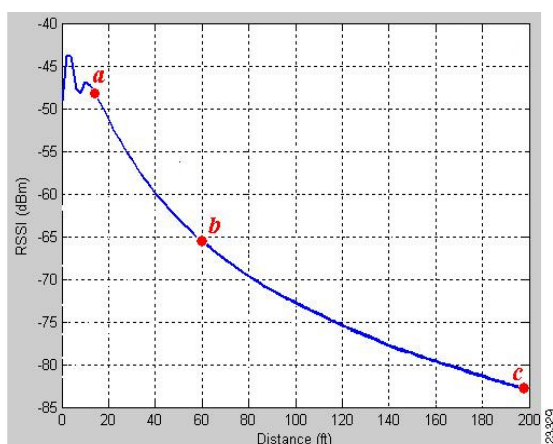


Figure 1. RSSI vs. distance [6]

The total Wi-Fi positioning system shares the same network along with other network clients, so there is no additional installation of a separate wireless networks (as RFID requires) that may cause RF interference with the existing wireless network [7]. The cited article shows that any commodity 802.11's equipment is surprisingly vulnerable to certain patterns of weak or narrow-band interference. This enables to disrupt a link with an interfering signal whose power is 1000 times weaker than the victim's 802.11 signals, or to shut down multiple access points, multiple channel managed network at a location with a single radio interferer.

Wi-Fi location positioning is based on a grid of Wi-Fi hotspots providing, in general, 20–30 meters location accuracy. For more accuracy, there needs to be more access points. There are many articles devoted to Wi-Fi positioning. For example, we can combine a reference point-based approach with a trilateration-based one etc. Several layers of refinement are offered based on the knowledge of the topology and devices deployed. The more data are known, the better adapted to its area the positioning system can be [8].

Figure 1 is very transparent, but it highlights also one of the main weaknesses for this approach. Yes, we can calculate distance to node, but for getting location data we need to know node's location. In other words, for all such systems we need a priori scene preparation. This process could be expensive and it is also almost closes the door for the dynamical systems. What if our basic nodes are moving?

But in the same time Figure 1 shows the way we can use for estimating the relative distance to our wireless node. Let us take at least two mobile devices and replace the distances with the relative values to our basic node. And as the next step we can replace digital values with some literal values that describe proximity (ranges for the relative distances). For example: High (e.g., same room), Medium (e.g., same floor) and Low (e.g., same building). For example, proximity classification for mobile devices using Wi-Fi environment similarity [9] describes an algorithm to compute lists of people and devices that are physically nearby to a

mobile user based on the analysis of signals from existing wireless networks. The system evaluates proximity by classifying the degree of similarity of the Wi-Fi scan data through a statistical Gaussian Mixture Model [10].

Lets us mention also one more interesting approach: collaborative location (CL). And the most interesting approach for our future development is Cooperative Location-sensing. Cooperative Location-sensing system (CLS) is an adaptive location-sensing system that enables devices to estimate their position in a self-organizing manner without the need for an extensive infrastructure or training. A node tries to position itself on its local grid through a voting process in which devices participate by sending position information and casting votes on specific cells.

Simply saying, hosts cooperate and share positioning information. CLS uses a grid representation that allows an easy incorporation of external information to improve the accuracy of the position estimation [11].

The motivation for CL and CLS is very transparent. In many situations, due to environmental, cost, maintenance, and other obstacles, the deployment of a dense infrastructure for location sensing is not feasible. It is exactly what we wrote about infrastructure-less system. In CLS, hosts estimate their distance from their neighboring peers. This can take place with any distance estimation method available (e.g., using signal strength). They can refine their estimations iteratively as they incorporate new positioning information.

Another area that is interesting for our approach is dynamic location based services. Some authors [12] classify them as application oriented LBS vs. classical content oriented. Content-oriented LBS aim to deliver relevant information depending on users' locations. For example, maps, points of interest, etc. Such LBSs are usually part of applications specialized in content delivery, such as a web browser or a front end for SMS messages. Applications oriented LBSs tailored to the user and delivered services dynamically on the basis of current location and execution context. In contrast to content-oriented LBSs, application-oriented LBSs provide a more powerful and richer interaction model, with autonomic installation and removal of dynamically needed components.

At this point, we are ready to make the last proposition before switching to the SpotEx model. Of course, the acronym LBS (Location Based Systems) contains the word "location". But, do we really need the location for the most of the services? As seems to us, the final goal (at least for the majority of services) is to get data related to the location, rather than location itself. Location in the classical form (latitude, longitude) here is just an intermediate result we can use as key for some requests for obtaining data (our final goal). This conclusion opens an opportunity to request data directly using our estimation for the location.

II. SPOTEX

On SpotEx model. What if we stop our traditional indoor positioning schema on the first stage: detection of Wi-Fi networks? This detection actually already provides some information about the location – just due to local nature of Wi-Fi network. And as the second step we add the ability to

describe some rules (if-then operators, or productions) related to the Wi-Fi access points. Our rules will simply use the fact that the particularly Wi-Fi network is detected. And based on this conclusion we will open (read – make them visible) some user-defined messages to mobile terminals. Actually it is a typical example for the context aware computing. The visibility for user-defined text (content) depends on the network context.

The first time this service SpotEx (Spot Expert [13] developed by Dmitry Namiot) was described by the authors in article published in NGMAST-2011 proceedings [14].

Technical details for SpotEx. SpotEx model does not require calibration phase and based on the ideas of proximity. Proximity based rules replace location information, where Wi-Fi host spots work as presence sensors. SpotEx approach does not require from mobile users to be connected to the detected networks. SpotEx uses only broadcasted SSID for networks and any other public information.

Technically, SpotEx contains the following components:

- Server side infrastructure. It includes a database (store) with productions (rules), rules engine and rules editor. Rule editor is a web application (it supports mobile web too) that lets work with rules database. Rules engine is responsible for runtime calculations. Note, that database is located outside of mobile device (at least, in the current implementation). But it could be positioned on the device too (e.g., for Wi-Fi Direct).

- Mobile application. Application is responsible for getting context info, matching it against database with productions and visualizing the output

SpotEx could be deployed on any existing Wi-Fi network (or networks especially created for this service – the most interesting case, see below) without any changes in the infrastructure. Rule editor lets easily define some rules (data chunks) to that network. Data chunk (message in our early papers) here is just some text that should be opened (delivered) to the end-user's mobile terminal as soon as the appropriate rule is fired. For example, as soon as one of the above-mentioned networks is getting detected via our mobile application. The word “delivered” here is a synonym for “being available for reading/downloading”. For end-users the whole process looks like automatic (and anonymous) check-in.

Let us see the proximity marketing use cases. The whole process looks like an “automatic check-in” (by analogue with Foursquare, etc.) Some shop can deliver proximity marketing materials right to mobile terminals as soon as the user is near some selected access point. Rather than directly (manually or via some API) check-in at the particular place (e.g., similar to Foursquare, Facebook Places, etc.) and get back deals info, with SpotEx mobile subscriber can collect deals info automatically. The prospect areas, by our opinion, are information systems for campuses and hyper local news

delivery in Smart City projects. Rules could be easily linked to the public available networks.

Especially, we would like to point attention to the most interesting (by our opinion, of course) use case: Wi-Fi hot spot being opened right on the mobile phone. Most of the modern smart phones let you open Wi-Fi hot spots. We can associate our rules to such hot spot (hot spots) and so our messages (data snippets) become linked to the phones. It is a dynamic LBS – services follows to the moved phone.



Figure 2. Wi-Fi hot spot on Android (Samsung Galaxy)

Figure 2 illustrates Wi-Fi hot spot setup on Android phone. Note, that SpotEx does not require open hot spot. All we need is SSID info.

This use case is probably the most transparent demonstration of SpotEx model. We can open “base” network right on the mobile phone and attach rules for the content to that network. It is all we need for creating a new information channel. There is no infrastructure except the smart phone itself.

Note again that this approach does not touch security and connectivity issues. You do not need to connect mobile subscribers to your hot spot. SpotEx is all about using hot spot attributes for triggers that can discover the content. The term Wi-Fi proximity is used sometimes in connection with Wi-Fi marketing and mean on practice just setting a special splash screen for hot spot that can show some advertising/branded messages for users during the connection to that hot-spot. Unlike this SpotEx treats Wi-Fi hot spots just as sensors.

How our productions data store (base of rules) looks like? Each rule looks like a production (if-then operator). The conditional part includes the following objects:

Wi-Fi network SSID,
signal strength (optionally),
time of the day (optionally),
client ID (see below).

In other words it is a set of operators like:

*IF network_SSID IS 'mycafe' AND time is 1pm – 2pm
THEN { present the coupon for lunch }*

A complete rule-set should be passed to the rule engine for further processing. The rule engine matches each rule (its left part - condition) in the rule set with given facts to decide whether to execute the right part or not. This is called pattern matching process and this process takes place repeatedly. In each cycle the list of facts may be modified: new Wi-Fi network may be detected or access point info may be removed from the list. These changes may cause previously unsatisfied conditions (or clauses) to be satisfied. So, during each cycle the set of rules satisfied must be maintained and updated. In most of the cases, actions of the rules change only a few clauses in the conditions. It is so called temporal redundancy. If a rule engine checks each rule to direct the search for all the facts even if most of them are not modified then it will slow down the process. We can avoid this unnecessary calculation by remembering what has already matched from cycle to cycle and then computing only the changes necessary for the newly added, modified or removed networks data.

Because our rules form the standard production rule based system, we can use old and well know algorithm like Rete [15] for the processing. A Rete-based expert system builds a network of nodes, where each node (except the root) corresponds to a pattern occurring in the left-hand-side (the condition part) of a rule. The path from the root node to a leaf node defines a complete rule's left-hand-side. Each node has a memory of facts, which satisfy that pattern. This structure presents essentially a generalized tree. As new facts are asserted or modified, they propagate along the network, causing nodes to be annotated when that fact matches that pattern. When a fact or combination of facts causes all of the patterns for a given rule to be satisfied, a leaf node is reached, and the corresponding rule is triggered [16].

The main advantage of Rete algorithm is the speed of calculation. Many rules often contain similar clauses or group of clauses. Rete algorithm caches the common components so that they need not be calculated again.

The main drawback of Rete pattern matching is obvious. It is memory intensive. Saving the state of the system using pattern matches and partial matches requires more memory.

The current implementation for mobile client based on Android OS. This application uses *WiFiManager* from Android SDK - the primary API for managing all aspects of Wi-Fi connectivity. This API let us pickup the following information about nearby networks:

SSID - the network name.
BSSID - the address of the access point.

capabilities - describes the authentication, key management, and encryption schemes supported by the access point.

frequency - the frequency in MHz of the channel over which the client is communicating with the access point.

level - the detected signal level in dBm.

So, actually all the above-mentioned elements could be used in our productions. And now we can prepare rules like this:

*IF network_SSID IS 'mycafe' AND level > -60dBm
AND time is 1pm – 2pm AND network_SSID 'myStore' is
not visible THEN {present the deals for dinner }*

Block {present the deals for dinner} is some data (information) snippet presented in the rule. Each snippet has got a title (text) and some HTML content (it could be simply a link to external site for example). Snippets are presenting coupons/discounts info for malls, news data for campuses, etc. Here is a typical example of user's snapshot:

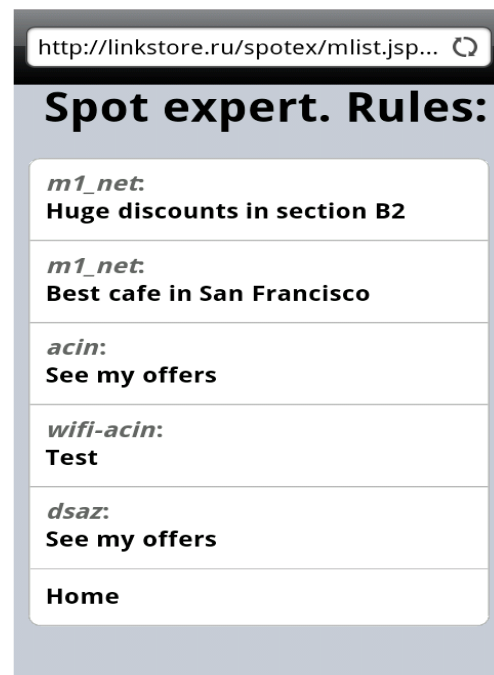


Figure 3. Rules from SpotEx

For Bluetooth mode we can use *BluetoothDevice* class. At least the following data could be used in our productions:

hardware address of Bluetooth device
friendly Bluetooth name of the remote device

Technically any snippet could be presented as a link to some external web site/mobile portal or as a mobile web page created automatically by the rule editor included into SpotEx. Rule editor works in both desktop and mobile web. So, once again, just having an ordinary smart phone is

enough for creating (opening) information channel for delivering hyper-local news data. The following snapshot illustrates how our rule editor looks like:

1. Create a rule for context

IF

SSID (WIFI network) ?

Signal levels in dBm min : max (opt.) ?
 - : -

THEN

Title ?

Message ?
 URL ? Custom text ?

Create rule

Figure 4. SpotEx rule editor

SpotEx as context-aware retrieval tool. In case of presenting our data as links to some existing mobile sites (portals) SpotEx works as some universal discovery tool. De facto, it lets mobile subscribers to be aware about context-relevant web resources. Owners for the web resources can describe own sites via rules rather than present for them individual QR-codes or NFC-tags for example.

In case of describing some content right in the SpotEx the whole system works in this part as a content management system. SpotEx rule editor creates mobile web page for the each provided data snippet and hosts that page on the own server. It means by the way, that for presenting our data we can use any resources that could be presented on HTML pages. In particular, any multimedia content is also supported.

SpotEx mobile application, being executed, creates dynamic HTML page from titles (according to rules that are relevant in the given context) and presents that mobile web page to the user. It works just as a classical rule based expert system: matches existing rules against the existing context and makes the conclusions. Existing content here is a description for "Wi-Fi environment": list of hot spots with attributes. And conclusion here is a list of titles that can be presented as a dynamically created mobile web page. On that page each discovered title could be presented as a hyperlink that points to the appropriate data snippet. Any click on the interested title opens the snippet (shows or discovers data to mobile user).

So, for the mobile users, the whole process looks like browsing, where their browser becomes aware about hyper-local content. It is a typical example of context-aware retrieval. Context-aware retrieval can be described as an extension of classical information retrieval that incorporates the contextual information into the retrieval process, with the aim of delivering information relevant to the users within their current context [17].

Because SpotEx presents data chunks (read – content) as mobile web pages we can follow to the standard security model for web applications. Any content could be public or private (e.g., password protected).

The context-aware retrieval model includes the following elements:

- a collection of discrete documents;
- a set of user's retrieval needs, captured in a query;
- a retrieval task, to deliver the documents that best match the current query, rated on the basis of a relevance measure;
- the user's context, used both in the query formulation and associated with the documents that are candidates for retrieval.

It is obviously, that all the above-mentioned tasks are components of SpotEx. The basic components of Context-Aware Retrieval are: a document collection, which contains the documents that may be retrieved annotated with details of their associated contexts, and the user's current context. In our case the collection of documents is defined by the right parts of our rules. And user's current context is a vector describes visible wireless networks. It is very important also that we can operate not only with snapshots of wireless environments (currently visible networks). Technically the past history is also available. Let us see for example the modern LBS applications based on check-ins. There is at least one important problem – we have not history for any particular check-in. All we can do is just to rely on the history of all previous check-ins. Think, for example, about some check-in in the big mall location. How the person in question reached the check-in point? What was done before?

History can be maintained automatically by the application. For example, a new record of the current context may be added to the history:

- by the time (e.g., every N seconds),
- whenever any retrieval request occurs,
- whenever the current context changes by more than a certain threshold amount,
- whenever user feedback indicates that a particular current context was important.

For example, the route within the building before check-in could provide valuable information for marketing. So we could add some like convoy discovery module to our rule engine. It is really very interesting topic that worth a special investigation.

A crucial property of many context fields is that they are continuous: as the user's context changes new information may need to be retrieved. Such continuous applications normally require fast retrieval, so that the user has the

illusion that new information arrives immediately there is any change in their context [18].

Additional features. As per other functionality of our context-aware browser we can highlight the following notes. At the first hand, we can note that it is the “pull model”, versus the “push model” that proposed by Bluetooth marketing for example. And it could be more convenient (more safe) for the users – there are no automatically downloaded files/messages etc. But in the same time nothing prevents us from updating that dynamic web page automatically (e.g., by the timer) and simulating “pull model” in the user-safety mode.

At the second hand, we can note that because it is browsing, the whole process is anonymous. Indeed, there is no sign-in in the SpotEx. Of course, any data snippet may lead to some business web site/portal, where that site may ask about login, etc., but the SpotEx itself is anonymous. Unlike social networks like Foursquare you do not need to disclose your identity just for looking mall’s deals for example.

But in the same time we still can collect some meaningful statistics in SpotEx. Because the model requires Wi-Fi to be switched on, we have automatically unique ID for the each client. It is MAC-address. It is actually global UUID. So, where we have not login info for our clients, we still can distinguish them. It let us detect for example, the same person, who did that already twice during the last week, opens that the particular data snippet. It means also (and it could be a part of our future research and development) that SpotEx model could be used for creating some sort of indoor analytics (like web analytics but for real places). The following figure illustrates a plot for clicks (opened data snippets per month – y axis) versus visits per month (x axis):

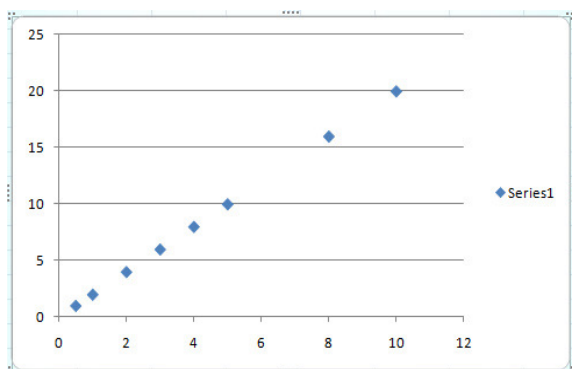


Figure 5. Clicks vs. frequency

Because mobile users in SpotEx model actually work with web pages, we can use pretty standard methods for web server log analysis for discovering user’s activities.

A statistical analysis of the server log may be used to examine traffic patterns by time of day, day of week etc. So, we can detect frequent visitors, usage patterns, etc. And even more – we can use that information in our rules. E.g., some mall may offer special things for frequent visitors, etc. Data

from real time analytics for our info snippets could be used in conditional parts of our rules.

Note also, that for security reasons it is enough to keep hash-codes instead of the real MAC-addresses.

The next stage of development targets the simplicity of preparing data for SpotEx model. What if instead of the separate database with rules (as it is described above) we add the ability to provide a special markup for existing HTML files?

So, rather than writing separate if-then rules we can describe our rules right in HTML code. Technically, we can add for example HTML div blocks with attributes that describe our rules (their conditions). Now, using some JavaScript code we can loop over such div blocks and simply hide non-relevant from them. Custom HTML5 attributes are the best useful candidates here.

In HTML5, we can define custom attributes using the “data” attribute. The exact format is “data-XXXX”, where “XXXX” is replaced with the desired custom attribute name, then set to the desired string value. For example:

```
<div id="my_coupon" data-ssid="myNetwork" data-rssi="-60">
  Get discount for purchasing 2+ items.
</div>
```

Our attribute name must be prefixed with “data-” in order to validate in HTML 5. So in other words, while HTML 5 supports custom attributes, it does not allow for arbitrary attribute names. But that is enough for our development. For example, the above mentioned example could describe the visibility of div block (HTML text) for those mobile users who can detect the presence of

The appeal of custom attributes is that it lets you easily associate tidbits of information with an element, to be parsed later using JavaScript for example. There are two ways to retrieve the value of “data” attributes using JavaScript: the first is via `getAttribute()` method of JavaScript, and the second, by accessing the “dataset” property of the element:

```
var mydiv=document.getElementById('my_coupon')

//Using DOM's getAttribute() property
var ssid=mydiv.getAttribute("data-ssid") //returns "myNetwork"
mydiv.removeAttribute("data-ssid") //removes "data-ssid" attribute entirely

//Using JavaScript's dataset property
var ssid=mydiv.dataset.ssid //returns "myNetwork";
mydiv.dataset.ssid=null; //removes "data-ssid" attribute
```

For doing that we need to make sure that our JavaScript code is aware about the current context. We can achieve that via a special light implementation of local web server. This web server, being hosted right on the mobile phone (on the Android in our case) responds actually only to one type of requests. It returns the current context (Wi-Fi networks) in JSON (JSONP) format.

Why do we need a web server? It lets us stay in the web domain only. There is a simple and clear instruction for web masters:

```
- add SpotEx script to your page
<script type = "text/javascript" src =
http://localhost:8080/spotex.js> </script>
- describe your info snippets as div blocks:
<div rel="spotex" net="WiFi_SSID" levelMin=""
levelMax="">
Your HTML code
</div>
```

Our "old" rules could be presented via collection of attributes.

In this case, JavaScript code loaded from local server will be able to proceed all the div blocks related to SpotEx, and set visibility attributes depending on the context.

Such simple trick let us make any existing HTML page "Wi-Fi context aware". Note that if our script is not available, the page will work as a "standard" HTML page.

This development is placed in line with the modern trends for moving the entirely development into web area. The final goal is to enable rapid development. This embedded web-server could play an important role in the data gathering too.

WiFi Chat. There is also a "side" effect for SpotEx application – WiFiChat service [19]. This mobile application uses the principles described in this article and offers communication tools (web chat and discussions groups) for mobile users nearby the same Wi-Fi access point.

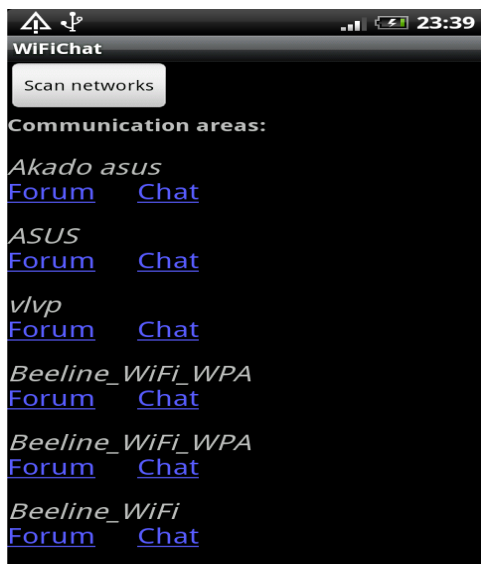


Figure 6. Wi-Fi chat

Think about it as "SpotEx with predefined content". The typical use case – we have Wi-Fi network in the train and this application automatically provides the discussions forum for the passengers. Or, keeping in mind that the "base" Wi-Fi network for this service could be opened right on the phone,

this application can present personal forum (classified for example) as well as web chat for phone owner. This Android application is actually a wrapper for web mashup that combines HTML5 web chat engine and cloud based forums from Disqus.

It is the typical tool for the ad-hoc communications on the go. Think for example for chat in the train where Wi-Fi hot spot is provided, etc.

III. THE FUTURE DEVELOPMENT

Here, we see several almost obvious steps. At the first hand, it is open API. In the current implementation SpotEx front-end actually obtains data in JSON (JSONP) format from our server-side database.

As soon as API is going live, the next step is almost mandatory. It should be something that will simplify the development. The good candidates here are web intents [20] Web Intents is a framework for client-side service discovery and inter-application communication. Services register their intention to be able to handle an action on the user's behalf. Applications request to start an action of a certain verb (for example share, edit, view, pick, etc.) and the system will find the appropriate services for the user to use based on the user's preference. It is the basic.

Intents play the very important role in Android Architecture. Three of the four basic OS component types - activities, services, and broadcast receivers - are activated by an asynchronous message called as intent.

Intents bind individual components to each other at runtime (you can think of them as the messengers that request an action from other components), whether the component belongs to your application or another.

Created intent defines a message to activate either a specific component or a specific type of component - an intent can be either explicit or implicit, respectively.

For activities and services, an intent defines the action to perform (for example, to "view" or "send" something) and may specify the URI of the data to act on (among other things that the component being started might need to know). For example, our intent might convey a request for an activity to show an image or to open a web page. In some cases, you can start an activity to receive a result, in which case, the activity also returns the result in an Intent (for example, we can issue an intent to let the user pick a list of nearby images and have it returned to us - the return intent includes data in some format)

Going to our context aware browsing it means that our mobile devices will be able to present local data without low-level programming.

Web Intents puts the user in control of service integrations and makes the developers life simple.

Here is the modified example for web intents integration for the hypothetical web intents example:

```
1. Register some intent upon loading our HTML
document
document.addEventListener("DOMContentLoaded",
function() {
var regBtn = document.getElementById("register");
```

```
regBtn.addEventListener("click", function() {
  window.navigator.register("http://webintents.org/spotex"
, undefined);
}, false);
```

2. Start intent's activity and pass it extra data (context info)

```
var startButton =
document.getElementById("startActivity");
startButton.addEventListener("click", function() {
  var intent = new Intent();
  intent.action = "http://webintents.org/spotex";

  intent.putExtra("WiFi_List", List_Of_Networks);
  window.navigator.startActivity(intent);
}, false);
```

3. Get local info snippets (note – in JSON rather than XML) and display them in our application

```
window.navigator.onActivity = function(data) {
  var output = document.getElementById("output");
  output.textContent = JSON.stringify(data);
};
}, false);
```

The key point here is *onActivity* callback that returns JSON formatted data. Additionally, web intents based approach is asynchronous by its nature, so, we do not need to organize asynchronous calls by our own.

Also, we are planning to add Bluetooth measurements too. But, by our vision, we should avoid the typical Bluetooth usage cases and does not use push proxy as per classical Bluetooth marketing. We think that the end users do at least not welcome push approach and it is the source of problems with Bluetooth proximity. Vice versa, in SpotEx Bluetooth nodes will be used the same manner we are using Wi-Fi access points – as presence triggers. In other words, we will add the ability to describe rules for Bluetooth nodes too. One of the biggest disadvantages for Bluetooth comparing to Wi-Fi is discovery times. Wi-Fi nodes could be discovered much more quickly than Bluetooth. As it is mentioned in [21], Bluetooth frame can disseminate much more information at once than WiFi (248 bytes vs. 32 bytes), but Bluetooth's discovery process is much more time-consuming than WiFi's (10.24 s versus 1.2 s).

SpotEx approach could be extended also towards accumulating some ideas from the collaborative locations. We can add trilateration terms (conditions) to our rules, but present them in terms of fuzzy logic (close than, relatively close, etc.). It helps us incorporate grid data in case of many devices without any infrastructure preparation.

The next prospect area we are going to bring network proximity in is social data streams. It worth a separate article, so let us briefly describe an idea. For pairing sensors data and social streams (e.g., Twitter's stream), we can describe

thematic stream as data (topics) discovered from the tweets and data recorded from our sensors. Of course, data from sensors depends on the nature of sensors (e.g., proximity sensors, sounds streams, etc.) but in our case, as it was stated above, the set of sensors is limited to wireless networks sensors.

Our idea of integration network proximity and social networks looks like a special check-in service for social networks. What is a typical check-in record in social networks? It is some message (post, status) linked to some location (place). What are the reasons for members in social networks use such special kind of messages? Sometimes it could be stimulated by the business. Practically, user posts advertising for the business in exchange for some benefits. Sometimes it could be used for social connection: let other know where I am and see where my friends are.

But the key point is the special kind of record in the social network – check-in. It could be customized of course. Business can create own forms for check-in records [22], but they are still some posts in the social networks. In other words, they are always part of the social stream.

What if we create a new type of check-in records and separate them from rest of stream? It means that we will provide a separate database that just contains a list of accounts from the social network being concentrated (at this moment!) nearby some place. It is a temporal database, check-in records could be changed constantly and it does not contain the social stream itself – just ID's (e.g., nick names) for accounts.

And how can use this external check-ins database? At the first hand we can list other people at any particular location. Actually, it is always a list of people at "this" location only. Because in our proximity based system there are no lists of location in the traditional form. Each our "location" described via Wi-Fi sensors via visible access points and RSSI. Obviously, all the attributes are dynamical. So, after own check-in, user can see only nearby check-ins. In this approach user is simply unaware about other "places" unless the movement and new check-in.

At the second – we can show (search) social streams nearby. Via public API we can read data feeds for users (if it is possible, of course, and an appropriate stream is not protected).

As it is already mentioned above, the historical data collected by the SpotEx application could provide a meaningful statistics. History in SpotEx is anonymous set of network environment records (snapshots), collected by the mobile users. It lets is threat SpotEx as a tool for social dynamics research too. The classical example of reality mining [23] collected a lot of information from the mobile phones, includes call logs, Bluetooth devices in proximity, cell tower IDs, application usage, and phone status (such as charging and idle). SpotEx is much more accurate in this tight privacy connected topic and can collect only wireless info data. But it means, on practice, that we can collect some like trajectories where instead of location we can use info about wireless nodes. And this idea technically lets us apply some existing studies to our movement log.

At the first hand adding history movement we can introduce context for user's check-ins. We will be able to analyze for example, the movement patterns for reaching the destination (check-in) point. Such information simply does not exist for the traditional LBS applications. And patterns extracted from the log could be used potentially for creating new business rules. Let us see for example convoy discovery. Given a collection of trajectories, it is of interest to discover groups of objects that travel together for more than some minimum duration of time. A number of applications may be envisioned. The typical applications, mentioned in the scientific papers are: the identification of delivery trucks with coherent trajectory patterns may be used for throughput planning, the discovery of common routes among commuters may be used for the scheduling of collective transport, the identification of cars that follow the same routes at the same time may be used for the organization of carpooling, etc. But one specific task could be interesting in the context of proximity marketing (what is one of the main applied areas for SpotEx): provide some special offers for those reached the final point in the group (group buying, group discount, etc.).

The next area we are going to pay attention to is Wi-Fi Direct specification. Wi-Fi Direct devices can connect directly to one another without access to a traditional network, so mobile phones, cameras, printers, PCs, and gaming devices can connect to each other directly to transfer content and share applications anytime and anywhere. Devices can make a one-to-one connection, or a group of several devices can connect simultaneously. They can connect for a single exchange, or they can retain the memory of the connection and link together each time they are in proximity [24].

As per Wi-Fi Direct spec, a single Wi-Fi Direct device could be in charge of the Group, including controlling which devices are allowed to join and when the Group is started. All Wi-Fi Direct devices must be capable of being in charge of a Group, and must be able to negotiate which device adopts this role when forming a Group with another Wi-Fi Direct device. The device that forms the Group will provide the above described dynamically assembled web page with discovered services. It is how SpotEx could be extended to Wi-Fi Direct. Currently SpotEx requires internet connection in order to match network context against rules served as web based database. In Wi-Fi Direct environment we can keep this database on the one of Wi-Fi enabled devices (read – simply on another mobile phone) and perform matching without internet connection. The drawback here is the need for pairing during the connection setup.

IV. CONCLUSION

This paper describes a new context-aware browsing model for mobile users developed on the ideas of Wi-Fi proximity. Service can use existing as well as the especially created (described) Wi-Fi networks as presence triggers for discovering user-defined content right to mobile subscribers.

The proposed approach is completely software based. It is probably its biggest advantage. For using SpotEx you need

nothing except the smart phone. So, there are no prior investments in the hardware. Also this approach supports ad-hoc solutions and does not require the upfront space preparations.

This service could be used for delivering commercial information (deals, discounts, coupons) in malls, hyper-local news data, data discovery in Smart City projects, personal news, etc.

We highlights also our plans for the future research and development that include such prospect directions as analyzing social behavior via network proximity data, integration with social feeds, creating local web server for serving context data, Wi-Fi direct and network proximity, using web intents for context-aware data.

ACKNOWLEDGMENT

Many thanks to the anonymous ICDT-2012 reviewers for the reading and suggested improvements to the paper.

REFERENCES

- [1] D. Namiot and M. Sneps-Sneppe "Wi-Fi Proximity and Context-aware Browsing" ICDT 2012, The Seventh International Conference on Digital Telecommunications ISBN: 978-1-61208-193-9, Chamonix, France April 29 - May 4, 2012 pp. 1-7
- [2] G. Schilit and B. Theimer Disseminating Active Map Information to Mobile Hosts. IEEE Network, 8(5) (1994) pp. 22-32
- [3] C. Bolchini, G. Orsi, E. Quintarelli, F. A. Schreiber, and L. Tanca Context modeling and context awareness: steps forward in the context-addict project. IEEE Data Eng. Bull., 34(2): pp. 47-54
- [4] R. Ahas, S. Silm, O. Järv, E. Saluveer, and M Tiru Using Mobile Positioning Data to Model Locations Meaningful to Users of Mobile Phones; Journal of Urban Technology Volume 17, Issue 1, 2010 pp. 3-27
- [5] Comparison of Wireless Indoor Positioning Technologies http://www.productivet.com/docs-2/Wireless_Comparison.pdf, Retrieved: Nov, 2012
- [6] Y. Daradkeh, D.Namiot, and M Schneps-Schneppe: Context-Aware Browsing for Hyper-Local News Data (CABHLND). International Journal of Interactive Mobile Technologies (iJIM) vol. 6 N.3, 2012 pp. 13-17
- [7] R. Gummadi, D. Wetherall, B. Greenstein, and S. Seshan Understanding and mitigating the impact of RF interference on 802.11 networks. SIGCOMM '07 Proceedings of the 2007 conference on Applications, technologies, architectures, and protocols for computer communications ACM New York, NY, USA ©2007 ISBN: 978-1-59593-713-1 DOI=10.1145/1282380.1282424, pp. 385-396
- [8] F. Lassabe, P. Canalda, P. Chatonnay, and F. Spies "Indoor Wi-Fi positioning: techniques and systems" Annals of Telecommunications Volume 64, Numbers 9-10, pp. 651-664
- [9] A.Carlotto, M. Parodi, C. Bonamico, F.Lavagetto, and M. Valla "Proximity classification for mobile devices using wi-fi environment similarity" MELT '08 Proceedings of the first ACM international workshop on Mobile entity localization and tracking in GPS-less environments 2008 pp. 43-48
- [10] M. A. T. Figueiredo and A. K. Jain, "Unsupervised Learning of Finite Mixture Models", IEEE Transactions on Pattern Analysis and Machine Intelligence 24, 2002 pp. 381-396
- [11] C. Fretzagias and M. Papadopouli Cooperative Location-Sensing for Wireless Networks, Proceedings of the Second

- IEEE International Conference on Pervasive Computing and Communications (PerCom'04), p.121, March 14-17, 2004.
- [12] P.Bellavista, A.Kupper , and S.Helal Location-Based Services: Back to the Future, Pervasive Computing, IEEE, Vol.7, issue 2, 2008, pp. 85-89
- [13] Y. Daradkeh, D. Namiot, amd M. Sneps-Sneppe Spot Expert as Context-Aware Browsing. Journal of Wireless Networking and Communications 2012, vol. 2, N.3 pp. 23-28 DOI: 10.5923/j.jwnc.20120203.03
- [14] D. Namiot and M. Schneps-Schneppe About location-aware mobile messages International Conference and Exhibition on. Next Generation Mobile Applications, Services and Technologies (NGMAST), 2011 14-16 Sept. 2011 pp. 48-53 doi: 10.1109/NGMAST.2011.19
- [15] E. Friedman-Hill Jess in action: rule-based systems in Java. Manning Publications Co. Greenwich, CT, USA 2003 ISBN: 9781930110892
- [16] C. L. Forgy "RETE: A fast algorithm for the many pattern/many object pattern match problem", Artificial Intelligence 19(1): pp. 17-37, September 1982
- [17] P. J. Brown and G. J. F. Jones. Context-aware retrieval: Exploring a new environment for information retrieval and information filtering. Personal Ubiquitous Computing, 5(4): pp. 253–263, 2001.
- [18] P. J. Brown and G. J. F. Jones. Exploiting contextual change in context-aware retrieval SAC '02 Proceedings of the 2002 ACM symposium on Applied computing pp. 650 – 656, ISBN:1-58113-445-2 doi:10.1145/508791.508917
- [19] D.Namiot Context-Aware Browsing -- A Practical Approach. Next Generation Mobile Applications, Services and Technologies (NGMAST), 2012 6th International Conference on, pp.18-23 DOI: 10.1109/NGMAST.2012.13
- [20] Web Intents: <http://webintents.org/>, Retrieved: Nov, 2012
- [21] A. C. Champion, X. Li, Q. Zhai, J. Teng, and D. XuanEnclave: Promoting Unobtrusive and Secure Mobile Communications with a Ubiquitous Electronic World Department of Computer Science and Engineering, The Ohio State University 2012
- [22] D. Namiot and M. Sneps-Sneppe Customized check-in Procedures Smart Spaces and Next Generation Wired/Wireless Networking Lecture Notes in Computer Science, 2011, Volume 6869/2011, pp. 160-164, DOI: 10.1007/978-3-642-22875-9_14
- [23] N. Eagle and A. Pentland "Reality mining: sensing complex social systems" Personal and Ubiquitous Computing archive, Vol. 10 Issue 4, March 2006 pp. 255 - 268 doi:10.1007/s00779-005-0046-3
- [24] Wi-Fi CERTIFIED Wi-Fi Direct http://www.cnetworksolution.com/uploads/wp_Wi-Fi_Direct_20101025_Industry.pdf, Retrieved: Nov, 2012

Inter-domain Peering and Overlay Topologies Support for Content-Aware Networks Dedicated to Multimedia Applications

Eugen Borcoci
Telecommunication Dept.
University POLITEHNICA of
Bucharest
Bucharest, Romania
eugen.borcoci@elcom.pub.ro

Radu Dinel Miruta
Telecommunication Dept.
University POLITEHNICA of
Bucharest
Bucharest, Romania
radu.miruta@elcom.pub.ro

Serban Georgica Obreja
Telecommunication Dept.
University POLITEHNICA of
Bucharest
Bucharest, Romania
serban.obreja@elcom.pub.ro

Abstract — The Content Aware Networking (CAN) is an emerging architectural solution, responding to the significant increase in Internet content orientation. In particular media flows distribution can be well supported by virtual CAN oriented networks, aiming to control and assure the quality of services desired for such real-time services. In case of multi-domain spanning VCAN an inter-domain peering problem has to be solved, to create the VCAN overlay. This paper is a continuation of a previous work and refines a management framework for inter-domain peering in overlay VCAN, QoS enabled, built over multi-domain and multi-provider IP networks. An overlay inter-domain topology service and negotiation protocols are defined in this paper, based on cooperation of the CAN Managers belonging to network domains. Alternative solutions are proposed for VCAN topology creation and their usage is outlined. The scalability and efficiency is preliminary analyzed.

Keywords — *Content-Aware Networking, Network Aware Applications, Multi-domain, Inter-domain peering, Management, Multimedia distribution, Future Internet.*

I. INTRODUCTION

The current Internet limitations are recently recognized, related to the increasing needs of today world and the global spread of this technology. Intensive research efforts are spent in order to find some enhanced architectural solutions or “clean slate” ones, to solve the limitations thus leading to the Future Internet (FI) architectures. Sample of works are presented in [2]-[8][14]. The work [14] emphasizes the strong orientation of the FI towards content and services and shows the importance of management. Network virtualization is seen as an important “tool” to overcome the ossification of the current Internet [2]-[5]. The overview paper [6], identifies the inefficiency of the current Internet for content delivery and analyses new solutions based on *Content Oriented Networking* (CON) with decoupling of content and location identification at networking level. A major idea in recent proposals is the shift from the traditional TCP/IP stack concepts, based on traditional IP network layer to more sophisticated solutions that insert

more intelligence in the network nodes. The new network nodes will process the data packets/content_chunks, based on *content type* recognition or, even more, treating the data objects based on their *names* and not as in traditional TCP/IP stack, i.e., based on *location address*, [6][7]. The TCP/IP stack is changed, in the sense that IP is no longer the thin waist, of the stack [7]. Thus the routing and forwarding paradigms are significantly changed being based on *content names* rather than on destination *IP address*. Also caching content will be available in network nodes, thus giving the possibility to have the content replicas closer to the requester and so, shorter routes between content sources and consumers.

The revolutionary approaches are often referred to as *Information-Centric Networking* (ICN), which is used as an umbrella term for related concepts such as *Content-Oriented Networking* (CON) and *Content-Centric Networking* (CCN), [5][6][7][8]. Apart from novel routing and forwarding functions, the ICN routers have caching capabilities, [7][9], thus shortening the paths between content sources and consumers. These and other reasons (not detailed here), lead to the conclusion that ICN/CCN/CON approach has some strong open issues related to scalability, security, etc. and also needs significant changes of the current Internet deployments and protocols. Last but not least, the complexity of this approach makes necessary to apply autonomic management principles as described in [10].

Therefore, still evolutionary (or incremental) other approaches have been developed in parallel, such as *Content-Aware Networking* (CAN), which aim to create a *content - awareness* by building upon existing Internet network layers. The new concept actually has two aspects: the *Content-Awareness at Network* layer (CAN) and *Network-Awareness at Applications* layers (NAA). These evolutionary solutions are hopefully offering a better support to the development of the networked media systems and also to the market orientation towards content, while being open to future migration to full ICN/CCN. The CAN/NAA approach is claimed by many studies to bring

new benefits for both, Service and Application Layer and Network layer, thus creating a powerful *cross-layer optimization loop* between the transport and applications and services layers, while still allowing a seamless deployment. The network service can better adapt itself to the content which is transported, while the applications and services may take benefit from (limited) information about the network service.

A CAN/NAA architecture has been proposed in the European FP7 ICT running research project, "Media Ecosystem Deployment Through Ubiquitous Content-Aware Network Environments", ALICANTE, [11][12][13]. It defined an architecture, and then specified designed and now is currently implementing a Media Ecosystem, on top of multi-domain IP networks, aiming to offer a large variety of services for different business actors playing roles of consumers and/or providers. Architecturally, this is a "middle-way" solution: it adopted content-type recognition at network level and light virtualization (separation in the Data Plane of the virtual VCANs but has defined a single management and control plane). This solution offers seamless deployment perspectives and tries to avoid the scalability problems of the full ICN/CCN/CON approach.

Several cooperating environments are defined, including several business entities/actors: *User Environment (UE)*, containing the End-Users; *Service Environment (SE)*, containing High Level Service Providers (SP) and Content Providers (CP); *Network Environment (NE)*, where a new CAN Provider exists (CANP - managing and offering Virtual Content Aware Networks- VCANs); traditional Network Providers (NP/ISP) - managing the network elements at IP level. By "environment", it is understood a generic grouping of functions working for a common goal and which possibly vertically span one or more several architectural (sub-) layers.

A Virtual Content Aware Network - VCAN as assumed in this study is *media oriented* in the sense that the network services offered by this *logical data plane* to the upper layers are optimized for media flows requirements expressed by the Service Provider. However regular IP traffic can be as well accepted. A VCAN can span several network domains, where each one is managed independently (a realistic business constraint), while offering different levels of QoS guarantees for media flows needs. Therefore decision regarding the architecture has to be taken, on how to manage the peering, first at the level of the *Data Plane* (including inter-domain routing) and second, in the *Management and Control Plane* (M&C signaling) in order that they cooperate to the realization of a shared VCAN. This is the subject of this paper. Several solutions are analyzed for Management&Control Plane (*cascade, hub, mixed*) and finally the so called "hub model" has been selected. A M&C negotiation protocol is proposed to run between domain managers. The scalability aspects are preliminary discussed.

The Content Aware Network Provider offers to the upper layers enhanced VCAN-based connectivity services, unicast and multicast (QoS enabled) over multi-domain, multi-provider IP networks. The VCAN resources are

managed quasi-statically by provisioning and also dynamically by using adaptation procedures for media flows. The management is based on vertical and horizontal Service Level Agreements (SLAs) negotiated and concluded between providers (e.g., Service Provider-Content Aware Network Provider). In the Data Plane, *content/service description information (metadata)* can also be inserted in the media flow packets by the Content Servers and treated appropriately by the intelligent routers of the VCAN.

The multimedia high level services for which such a system can be used as platform are mainly related to content distribution in real and non-real time (Video on Demand streaming, IPTV, etc.) with several level of QoS guarantees at Service Provider requests. The VCANs are customized for a given content type.

In [1] an overlay inter-domain topology service and negotiation protocols are defined to serve the multi-domain VCAN mapping. It was based on cooperation of the CAN Managers belonging to network domains. The paper [15] studied the mapping the overlay VCANs onto real network resources in a multi-domain context, while satisfying QoS constraints. In that approach the VCAN resources are first logically reserved; later when installation is requested by the SP, they are really allocated in routers. A basic mapping algorithm has been developed.

This paper integrates the results of the previous work [1][15], and brings additional contributions. It refines further the management framework for inter-domain peering in overlay VCAN, QoS enabled, built over multi-domain and multi-provider IP networks. A new variant with global optimization is proposed as different from the basic mapping algorithm presented in [15]. The one-step solution and two step solution for VCAN mapping algorithm are compared and experimental results are presented. Implementation results of the combined algorithm (constrained routing, admission control, QoS reservation and final VCAN mapping) are presented. Scalability is also discussed.

The paper is organized as follows. Section II presents additional samples of related work. Section III recalls the overall architecture. Section IV shortly presents the content awareness features of the system and QoS assurance solutions. Section V is dedicated to the peering solution selected and associated negotiations aiming to extend a VCAN over several domains. Section VI discusses variants of solutions in terms of complexity, scalability and other considerations. Section VII shows how the overlay topology is used in VCAN mapping, and experimental results are presented and discussed. Section VIII contains conclusions and future work outline.

II. OTHER RELATED WORK

The objective of the paper is to develop management solutions to govern the construction of Virtual Content Aware Networks, QoS spanning several independent network domains which should be peered aiming to assure guaranteed QoS enabled transport of real-time and media traffic.

For inter-domain QoS enabled domain peering, there exist basically two kinds of approaches. The first one

[16][17], proposes QoS enhancements for the Border Gateway Protocol (BGP). The BGP advertises QoS related information between network domains – seen at limit as autonomous systems (ASes), and then a QoS aware routing table is built. However, the notion of content awareness at domains level is absent there.

The work [18] discusses creation and routing of/in Content Addressable Network Virtual Topology which is a partially similar with our idea to extend the inter-domain network matrix in a new one with few intra-domain details. They pick a uniform hash function that maps an object to a point in $[0,1]^d$. They divide the d-cube into zones and assign a node to a zone and store (object, location) pair in the zone that owns the zone for the hashed value of the object. The neighbors of a zone are defined as those nodes whose zones overlap over $d-1$ dimensions. If a node i wants to find out where object j is stored, it computes $h(i)$ and then sends a lookup message to its neighbor that is closest to $h(j)$; this continues until the message reaches the node that owns $h(j)$; it then returns the location for object j .

Boosted by the increasing demand for multimedia applications over Internet, the problem of finding routing paths satisfying QoS constraints has been extensively studied by the research community. Representative examples of such QoS constraints are related to bandwidth, delay, jitter and packet loss [19]. Even if the e-2-e delay is often a metric of interest for multimedia content distribution the authors from [19] prefer to minimize delay, maintaining only optimal rate. They proposed an overlay model that represents the real network topology; essentially, it is a regular overlay graph, except the links are not weighted by numbers; instead, the link capacities are variables, and a set of linear capacity constraints express the constraints placed on overlay links by shared bottlenecks. In their model, every node selects d neighbors to which it has links with the highest bandwidth. In a similar mode of establishing the bandwidth capacity uploaded Intra-NRM (Intra-Network Resource Manager) to its associated CAN Manager (CANMgr) for each asked domain, in [19] is used a term of predicted bandwidth. In their work, the highest-bandwidth multicast tree is obtained by a greedy algorithm modified to take linear capacity constraints into consideration.

We have to note that the acronym CAN might create confusion, given that it is used in different texts with several semantics. As an example, the paper [20], introduces the concept of a *Content-Addressable Network (CAN)* as a distributed infrastructure that provides hash table-like functionality on Internet-like scales. It is shown that the CAN is scalable, fault-tolerant and completely self-organizing. However the *Content-Aware Networks* concept considered here has not as fundamental property the addressability based on content names but the adaptation of the transport characteristics to the type of content, mainly in order to assure the required quality of services.

Other solutions for inter-domain QoS peering and routing are based on the overlay network idea [21][22][23][24]. An overlay network can be defined, which first, abstracts each domain with a node, represented by the

domain resource manager, or more detailed with several nodes represented by the ingress-egress pair routers from that domain. There exist protocols to transport QoS and other information between nodes and, based on this information, QoS routing algorithms are used to choose the QoS capable path. In [21] a *Virtual Topology (VT)* is defined by a set of virtual links that map the current link state of the domain without showing internal details of the physical network topology. Then *Push* and *Pull* models for building the VT at each node are considered and analyzed. In the *Push* model each AS advertises its VT to their neighbor ASes. This model is suited for small topologies. In the *Pull* model the Virtual Topology is requested when needed, and only from the ASes situated along the path between given source and destinations; the path itself is determined using BGP.

After routes are found, a negotiation protocol should be run [1][15][23], to establish inter-domains Service Level Specification (SLS) agreements (note that the SLS is the SLA technical part) containing the reciprocal commitments of the parties and in particular clauses for QoS guarantees.

The inter-domain peering in the management and control plane is related on what topology the domain managers discuss with each other. Several solutions are examined and compared (cascade, hub, mixed-mode) [21][22][23]. However, neither solution considers the content awareness capabilities of the multiple domain infrastructure, nor the virtualization aspects. This paper takes these into account. The architecture proposed here realizes parallel Internet planes as in [25], but additionally associates to each plane a VCAN (Virtual Content Aware Network). Over the overlay topology determined, VCANs will be mapped and then finally the VCANs are mapped onto real network links. This achieves cooperation between the network layer and applications and services layers, thus realizing a powerful optimization loop (OL), similar to [26].

III. ALICANTE SYSTEM ARCHITECTURE AND VCAN MANAGEMENT

A. General Architecture

The general ALICANTE architecture is already defined in [11][12][13]. A set of business actors is defined, composed of traditional Service Providers (SP), Content Providers (CP), Network Providers (NP) and End-Users (EU). New business actors are introduced: CAN Provider (CANP) offering virtual layer connectivity services and the Home-Box (HB) - partially managed by the SP, NP, and the end-user. It is located at end-user's premises and gathering content/context-aware and network-aware information. The HB can also act as a CP/SP for other HBs, on behalf of the EUs. Correspondingly, two novel virtual layers exist: the *Content Aware Network layer* and the *Home Box layer*. The novel CAN routers are called *Media-Aware Network Elements (MANE)* to emphasize their additional capabilities: content and context - awareness, controlled QoS/QoE, security and monitoring features, etc.

The CAN layer Management & Control Plane is partially distributed; it supports CAN customization to respond to the Service Environment needs, including: topology, different communication modes like unicast, multicast, broadcast, or even peer-to-peer (P2P), traffic control and QoS constraints, etc. and also allows efficient network resource exploitation. The interface between CAN and the upper layer supports *cross-layer optimizations* interactions in several ways: dynamically provisioning and modification of VCANs as to serve several SPs requirements (only this is the subject of this paper); individual or aggregated media flow adaptation to the current network conditions and terminal context based on Scalable Video Codec technologies; may offer network distance information to Home Boxes to improve their collaboration in P2P style, [26]. A hierarchical monitoring subsystem supervises several points of the service distribution chain and feeds the adaptation subsystems with appropriate information, at the Home Box and Content Aware Network Layers. Fig. 1 presents a partial view of the ALICANTE architecture, with emphasis on the CAN layer and management interaction. The network contains several Network Domains (ND), belonging to NPs (they can be also seen as Autonomous Systems - AS) and access networks (AN).

Note that the Access Networks (AN) are out of scope of VCANs. This decision has two reasons: the access technologies are numerous, with more or less well defined resource management; the scope of the ALICANTE project has been initially and intentionally limited to core network only.

One *CAN Manager* (CANMgr) exists for each IP domain to assure the consistency of VCAN planning, provisioning, (based on negotiation), offering, installation, exploitation termination and advertisement. Each domain has an *Intra-domain Network Resource Manager* (IntraNRM), as the ultimate authority configuring the network nodes. The Content Aware Network layer cooperates with Home Box and Service Environment by offering them CAN services. This solution associates a Content Aware Network Provider component to each Intra-Network Resource Manager component and gives the possibility to an Intra-NRM to upgrade its functionality and become CANP.

B. VCAN Management

The Virtual Content Aware Network Management framework has been already defined in [11][12][13]. Here only a short summary is recalled for the sake of clarity.

Several design decisions among several solutions, have been taken as a trade-off between complexity, optimality and scalability. Some details on the selection are given in the corresponding sections.

- M&C plane and virtualisation degree: light virtualisation (separate virtual Data Planes only); Full virtualisation (all virtual Planes, i.e., Data, Management and Control are separate).

Decision: the light virtualisation model based on a single management and control plane has been adopted in ALICANTE, given less complexity, seamless development

capabilities in real networks and still possibility to offer good transport services for media flows.

- Relationships between Content Aware Network Provider (CANP) and Service Provider (SP) concerning the VCAN services : Static SLA between CANP and SP; Dynamic SLA between CANP and SP:

Decision: Dynamic SLA, aiming at higher flexibility and dynamicity

- Multiple domain capable VCANs – establishment procedure : each CAN Manager manages only one VCAN spanning a single domain; any CAN Manager can initiate and coordinate multi-domain capable VCAN construction

Decision: second choice, given the flexibility

- Support of Content-awareness provided by SP to the CAN layer : CAN layer does not get any support information on content provided by SP; CANP gets content related information from SP via the control plane; SP provides content related information via the control plane and data plane

Decision: all three are adopted to get flexibility. If no information on Content Awareness (CA) from SP, then CAN layer is free to choose its own degree and behavior – related to CA, and therefore selects the methods to enforce CA in the VCANs.

- Inter-domain negotiation style between CAN Managers for multi-domain VCANs establishment: hub Model; cascade/mesh model;

Decision: Hub model, given more control on the VCAN for the initiating CAN Manager

At the Service Manager SM@SP, the CAN Network Resources Manager (CAN_RMGr) performs all actions needed for VCAN support on behalf of SP. It performs, at SP level, VCAN planning, provisioning (negotiation with CANP on behalf of the SP) and then VCAN operation supervision. The *CANMgr@CANP* performs, at the CAN layer, VCAN planning, provisioning and operation. The two entities interact based on the SLA/SLS contract initiated by the SP. The interface implementation for management is based on Simple Object Access Protocol (SOAP)/Web Services.

The contracts/interactions of SLA/SLS types performed in the M&C Plane are shown in Fig. 1. The management interactions are described as follows:

(1) *SP-CANP*: the Service Provider (SP) requests to CAN Provider (CANP) to provision/ modify/ terminate VCANs to which the CANP will finally say yes/no; also CANP might advertise existent VCANs to SP; Actually the CANP is represented by a single CAN Manger which is the initiator of the VCAN construction. The role of an initiator can be played by any CAN Manager.

(2) *CANP-NP*: CANP negotiates resources with NP;

(3) *CANP-CANP*– negotiations are needed between CAN Mangers if the VCAN spans several NP domains;

(4) *Network Interconnection Agreements (NIA)*: between the Network Providers or between NPs and CANPs; these are not new ALICANTE functionalities but are necessary for NP cooperation.

After the SP negotiates a desired VCAN with CANP, it will issue the installation commands to CANP, which in turn configures, via Intra-NRM (action 5), the MANE (Media Aware Network Element) functional blocks (input and output).

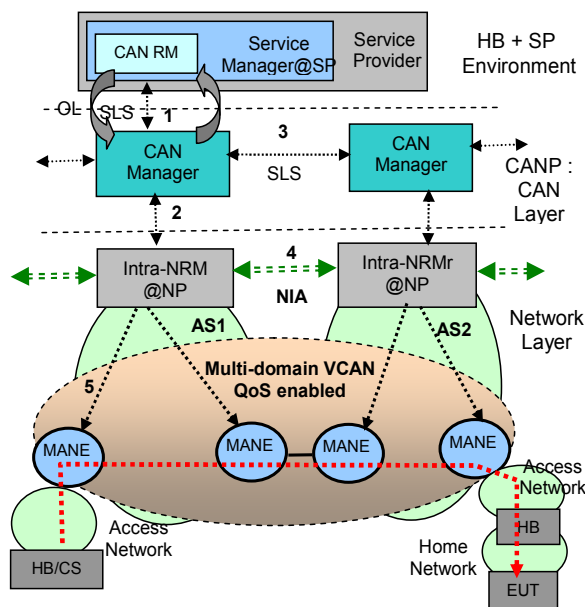


Figure 1 High level ALICANTE architecture: multi-domain VCANs and main management and control interactions

Notations: OL - Optimization Loop; SLS – Service Level Specification; NIA - Network Interconnection Agreement; RM – Resource Management; SP – Service Provider; CANP Content Aware Network provider; NP - Network Provider CS- Content Server; Intra-NRM – Intra domain Network Resource Manager; HB-Home Box; EUT- End User Terminal; MANE – Media Aware Network Element ; AS – Autonomous System

IV. CONTENT AWARENESS AND QoS AT CAN LAYER

The Content Awareness (CA) is realized in three ways:

(i) by concluding a SLA between the Service Provider and CAN provider (SP –CANP) concerning different VCAN construction. The Content Servers (CS) are then instructed by the Service Provider to insert (if they are able to do it) some special *Content Aware Transport Information (CATI)* fields in the headers (e.g in the Real Time Protocol header) of the data packets. How to optimize this insertion is not in the scope of this paper. This CATI simplifies the media flow classification and treatment by the MANE;

(ii) SP-CANP SLA is concluded, but no CATI can be inserted in the data packets (this is the case of legacy Content Servers). The MANE applies *deep packet inspection* for data flow classification and assignment to VCANs. The flows treatment is still based on VCANs characteristics defined in the SLA;

(iii) no SP-CANP SLA exists and no CATI. However, the flows treatment can still be processed in content aware style, but conforming to the local policy at CANP and IntraNRM.

The networking technologies to support QoS enabled VCANs are DiffServ and/or MPLS. The sets of flows are splitted in QoS classes (QC), with a mapping between the VCANs and the QCs. Several levels of QoS granularity can be established when defining VCANs. The QoS behavior of each VCAN (seen as one of the parallel Internet planes) is established in the SP-CANP SLA contract.

Generally a 1-to-1 mapping between a VCAN and a network plane will exist. Customization of VCANs is possible in terms of QoS level of guarantees (weak or strong), QoS granularity, content adaptation procedures, degree of security, etc. A given VCAN can be realized by the CAN Provider, by combining several processes, while being possible to choose different solutions concerning routing and forwarding, packet processing, and resource management.

The definitions of local QoS classes (QC) and extended QCs and meta-QoS classes were adopted in ALICANTE, [16][17][23][25] to allow capturing the notion of QoS capabilities across several domains. Each domain may have its local QoS classes and several local QCs can be combined to form an extended QC. The types of VCANs defined for different QoS granularities based on QoS Classes are VCANs based on meta-QCs [16], VCANs based on local QC composition and hierarchical VCANs based on local QC composition. The last case is the most efficient but also the most complex. Inside each VCAN, several QCs are defined corresponding to platinum, gold, silver, etc. In such a case, the mapping between service flows at SP level and CANs can be done per type of the service: VoD, VoIP, Video-conference, etc.

The definition of QoS classes makes the system robust to traffic overload with protection of desired flows against such overloads. Actually the QoS support for the real-time traffic in the VCANs are assured by :

- QoS constrained routing and logical reservation of traffic trunk pipes (provisioned at SP request);
- installation of them in the network (unicast or multicast mode);
- traffic enforcing rules in the Data Plane.

For unicast VCAN the supporting QoS technology is MPLS cooperating with Differentiated Services (E-LSP solution). For multicast case QoS constrained trees are computed, resource reservation is done and then in the Data plane Diffserv is enforced.

V. CAN MULTI-DOMAIN PEERING

A. Horizontal M&C VCAN Negotiation

A given VCAN may span one or several IP domains. In a multi-domain context, one should distinguish between two topologies (in terms of how the domains are linked with each others): *Data plane topology* and *Management&Control plane (M&C) topology*. The first can be of any kind (depending on SP needs and including the domains spanned by a given VCAN). In a general case, one may have a mesh/graph of domains. The *M&C topology* defines how the CAN Managers associated to different domains inter-communicate for multi-domain VCANs construction. The VCAN initiating CANMgr has to negotiate with other CAN Managers. There exist two main models to organise this communication at management level: *hub model* and *cascade model*, see [16][17][23][25].

The *hub model* was selected for this study; it has the advantage that initiating CAN Manager(CANMgr) can know, each VCAN component (network) and its status. A

drawback is that each CAN Manager should know the inter-domain topology (complete graph) of network domains. They could be of lower tier grade or be Autonomous Systems (AS), involved in a VCAN. Given the tiered hierarchy of the Internet, the number of Network Domains (ND) involved in an E2E chain is not too high (actually is lower than 10, [8]), scalability problem is not so stringent. Two functional components are needed: (1) inter-domain topology discovery protocol; (2) overlay negotiation protocol for SLA/SLS negotiations between CAN Managers.

The *cascade model*, [17][23] is more advantageous for initiating CAN Manager if a chain of domains is to form the VCAN. However, for an arbitrary mesh topology of the NDs composing the VCAN, and for multicast enabled VCAN, this model offers less efficient management capabilities.

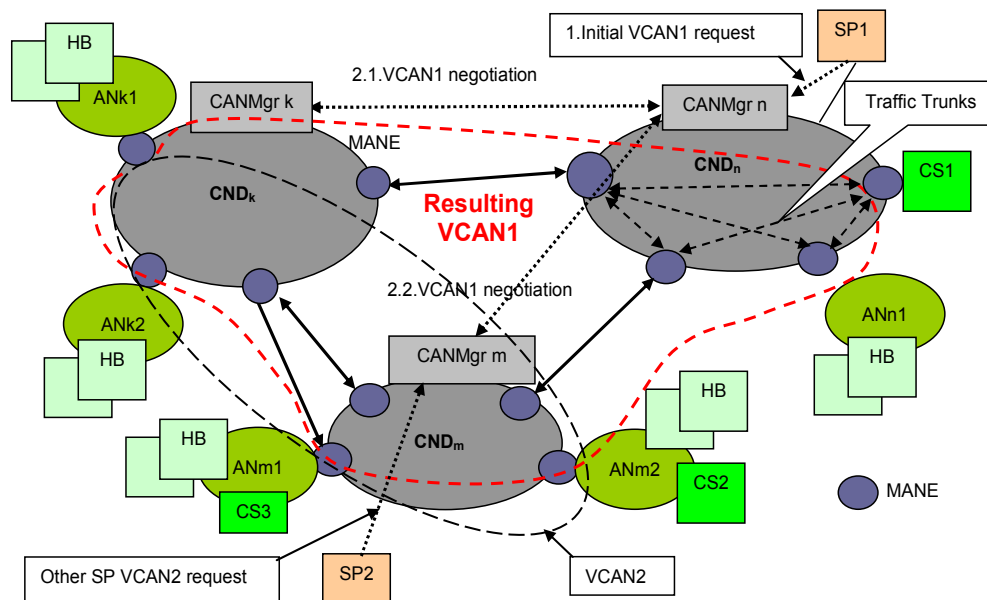


Figure 2 Example of multi-domain VCANs and negotiation signalling for VCAN1(hub model for management plane)

SP – Service Provider; HB - Home Box; CS - Content Server; CND – Core Network Domain; CANMgr – CAN Manager VCAN – Virtual Content Aware Network – logical virtual plane; AN – Access Network; MANE – Media Aware Network Element ;

Fig. 2 shows an example of a multi-domain infrastructure and two VCANs, i.e., VCAN1 and VCAN2. It is supposed that the inter-domain discover protocol has already produced its results, so each CAN Manager knows about the inter-domain graph and have inter-domain routing information, including link capacities and QoS related capabilities. The SP1 asks for a VCAN1 to a CANMgr (Initiator) – see action

1. It was supposed that the SP knew the edge points of this VCAN1, i.e., the Media Aware Network Elements IDs where different sets of HB currently are, or they will be connected. The initiator *CANMgr_n* determines all network domains (ND) involved (from the SP information and its inter-domain knowledge). The initiator CANMgr splits the overall SLS parameters (the VCAN1 is multi-domain), e.g.,

determining ingress-egress points, bandwidth, delay, etc. needed for each domain. Then the initiator CAN Manager negotiates in parallel with all other CAN Managers (actions 2.1, 2.2) to establish the $VCAN1 = \{VCAN1n \cup VCAN1m \cup VCAN1k\}$, where the three components are mapped onto the networks $CNDn, CNDm, CNDk$. In a successful scenario, the multi-domain $VCAN1$ is agreed and then it is later instantiated in the network.

The system allows several Service Providers, each one may ask one or several $VCANs$. In Fig. 2 it is given an example of $SP2$ wanting a $VCAN2$ spanned over $CNDk, CNDm$.

B. Overlay Virtual Topology

Constructing $VCAN$ over one or multiple domains is one of the main tasks of the CAN Manager. Each Core Network Domain (CND) has complete autonomy w.r.t. its network resources including network dimensioning, off-line traffic engineering (TE), and dynamic routing. The Content Aware Network Manager (CANMgr) cooperating with Intra-Network Resource Manager (Intra-NRM) is supposed to know about its network resources.

Given that in ALICANTE each CND has associated the Intra-NRM and CANMgr, one could abstract both under the name of Network Domain Manager (NDMgr). This entity should have an abstract view of its network domain and output links towards neighbors in a form of a set of virtual pipes (called *Traffic Trunks*). A set of such pipes can belong to a given QoS class. As already stated, a multiple domain $VCAN$ should also belong to some QoS class and therefore inter-domain QoS aware routing information is necessary in order to increase the chances of successful SLS establishment, when negotiating the multi-domain $VCAN$. The multi-domain $VCANs$ deployment needs knowledge on a virtual multi-domain topology.

Each Core Network Domain (CND) can assure QoS enabled paths towards some destination network prefixes while implementing its own network technology: DiffServ, MPLS, etc. Also, each CND can be seen in an abstract way as an *Overlay Network Topology (ONT)* expressed in terms of *TTs (traffic trunks)* characterized by of bandwidth, latency, jitter, etc. One TT is belonging to a given QoS class QC_i .

We define an *Overlay Network Service (ONS)* responsible for getting the ONTs related to CNDs belonging to a multi-domain $VCAN$. The CANM Managers will then inter-negotiate the SLS contracts in order to reserve $VCAN$ resources and finally ask installation of them. The overlay topology can be hierarchised on several levels.

Fig. 3.a presents a first level (inter-domain) Overlay Network Topology, in which, each domain CND is seen as a node. The overlay graph of the CNDs belonging to the $VCAN$ is composed of the nodes $CNDk, CNDn, CNDm$. Then, a second order ONT can be defined for one CND. Fig. 3.b shows the ONT for the domain $CNDk$, composed of Traffic Trunks, each one characterized by a bandwidth and a delay. If the initiating CAN Manager knows the ONT graph of the CNDs involved, then provisioning of QoS enabled $VCANs$ can be done.

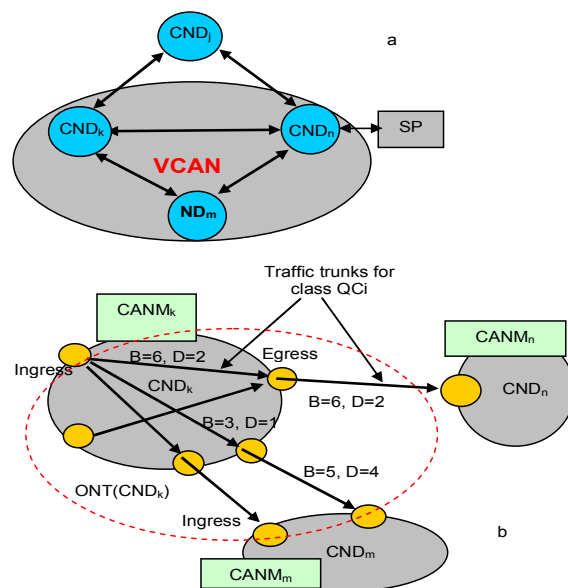


Figure 3 a. Inter-domain overlay network topology (ONT); b. ONT of the domain $CNDk$ (B = bandwidth, D = max delay- generic figures)

The Overlay Network Service can collect the topology information in two ways (see also [21]): a *proactive (push)* mode and a *reactive* (also called *pull* or *on demand*) mode in order to obtain the overlay (virtual) topologies of other NDs.

In the *proactive case*, every CND advertises its Overlay Network Topology (ONT) to other CNDs without being requested for. The advantage is the same as in IP proactive routing protocols: the ONTs of other CNDs are already available at a given ND because they are periodically or event-triggered advertised among CND managers. The advertisement can be executed at an initiative of each CND manager, so this model allows promotion of some routes to other domains. This can be subject of policies. The dynamicity is high (event driven advertisements), but the complexity is also high. Scalability problems exist, because of high control traffic volume and also flooding the neighbor CNDs with (maybe) not needed information.

In the *reactive (on-demand)* mode the ONTs are obtained on demand by an Core Network Domain (CND) interested to reach a given destination prefix. The CND will query each domain of a given path to get the ONTs. No advertising mechanism is necessary. The scalability is higher because only the ONTs of the chosen routes will be obtained. Studies [8] show that the mean End to End (E2E) communication in the Internet usually involves few domains (less than 8). Therefore, the number of domains to be queried to obtain the ONTs is small. The pull model latency is higher (need time for queries and calculations). The updates of ONT knowledge is not event driven w.r.t. other CNDs, because lack of advertisements. For our purposes we have chosen the reactive model.

If a CAN Manager wants to build an ONT it will query its directly linked (at data plane level) neighbor domains (i.e.,

the corresponding CAN Managers). It is supposed that it has the knowledge of such neighbors. There are two possibilities of a query: *a. non-selective query/demand-* i.e., the asking CANMgr wants to know all neighborhood of the asked neighbors; *b. selective demand-* the asking CANMgr wants to know answers only from those neighbor domains which have paths to a given set of destinations.

1) *Non-selective query*

The interrogating CAN Manager receives from SP the IDs of the ingress-egress points of a future VCAN. So, it can determine to which domains it belongs (mapping details between Ingress-egress IP addresses and network domains are out of scope of this paper). Therefore the initiator CAN Manager can know which domains *must* participate to the VCAN. It should also determine what other transit domains also must participate. The process of topology discovery can end when a contiguous graph containing the “must” domain is obtained. Note that non-optimal solution can be obtained if the process is limited to a minimal graph containing the desired ingress-egress-points. The information on reachability of a given point from a domain can be obtained in two ways: by consulting a BGP data base, or based on interrogating the neighbors and so on, until information is obtained.

Example:

1. The SP issues a requests for VCAN (I1, O1, O2, O3) to CANMgr2, assume that this is the VCAN initiator (where $I_k, k= 1,2, \dots, O_n, n= 1, 2, \dots$ are the ingress and egress points of traffic flows (actually these are IP addresses of edge MANE routers).

2. CANMgr2 determines that CND1, CND4, CND5, CND6 *must* participate to the VCAN, because the ingress and egress points {I1, O1, O2, O3} belong to them.

Each queried CANMgr can return – in a first most simple approach only its list of neighbors. At receipt of such information, the interrogating CANMgr updates its topology data base.

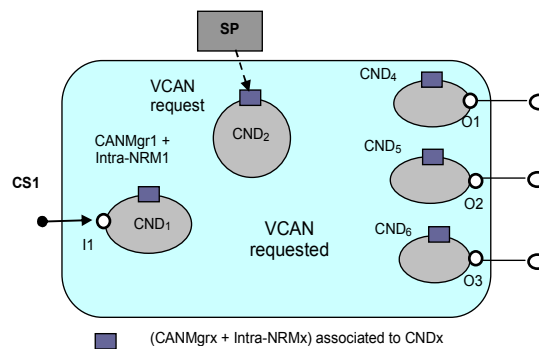


Figure 4 Example of a requested VCAN (I1, O1, O2, O3)

Then it queries the new nodes learned and so on. The process continues until the interrogating node CANMgr learns the whole graph of “international” topology of interest for it. How large is this network zone? The scope of such a zone can be limited by and determined in two ways: by local policies and by considering the request from SP for a given multi-domain VCAN.

Because the events that change the topology structure are not very frequent (hours, days, weeks, months), the topology construction process could be run at large time intervals (once per hour, for example). Consequently the amount of messages used to build the Overlay Network Topology will not overload significantly the network.

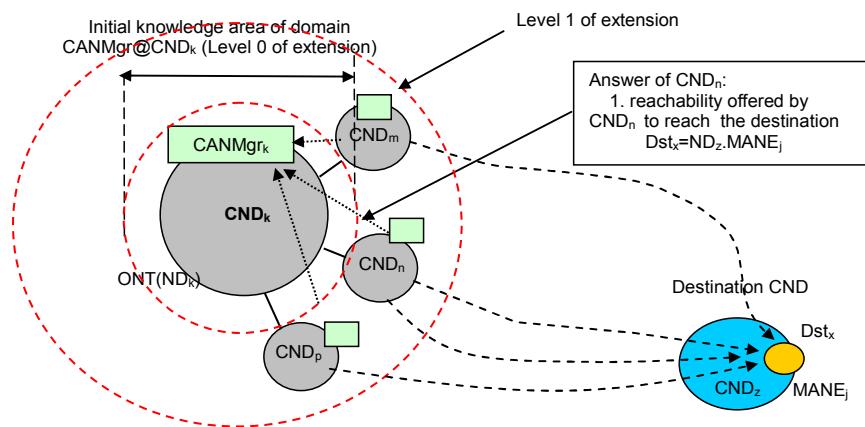


Figure 5 Different areas of ONT knowledge for NDk (Level 0, Level 1, ...) in selective –query mode

2) *Selective query*

The query process is similar, but the answers will be selective, i.e., filtered conforming the required set of destinations. The area of knowledge desired by a given CANMgr can be also determined by the SP request

(proposed VCAN span) and by local policies; it can be enlarged if needed. Fig. 5 shows such an area for two levels of extension.

We summarize the selected design decision- most appropriate to our objectives: *on-demand model based on overlay network topology service; based on non-selective*

and selective queries and simple answers (i.e., reduced ONT topologies obtained from the domains). Advantages of this solution consist in less complexity, less overhead, and preserving privacy and autonomy of intra-domain routing information.

VI. VARIANTS OF SOLUTIONS AND SCALABILITY ISSUES

The complexity, scalability and signaling overhead of the inter-domain peering and ONT information collection depends also on the variants of the VCAN mapping. Even if the detailed discussion of the algorithm of VCAN mapping is not the objective of this paper, we present below some considerations on possible solutions. We consider the general case of multi-domain VCAN.

The VCANs should serve Fully Managed (FM), Partially Managed (PM) and Unmanaged Services (UM)- seen from the QoS level of guarantees, [11][12] point of view. The most demanding in terms of QoS are the FM services. Therefore QoS enabled routing is needed both intra and inter-domain. Given that QoS assurance is required the metrics used for network distances should reflect these requirements. Also constrained routing will be used in order to maximize the chances to successfully conclude the SLSEs associated to VCANs.

A. One step VCAN Mapping

In this case the initiator CAN Manager completely maps a mono/multi-domain VCAN (requested by SP) onto the network infrastructure, by using the complete ONT represented as *Resource Availability Matrices* (RAM) (containing topologies + available capacities) for both inter-domain and intra-domain. The RAM is delivered to the CAN Manager by its associated *Intra-Network Resource Manager* (i.e., RAM is uploaded by the associated Intra-NRM, for its network domain) and other *CAN Managers* concerning the summary of available connectivity resources of the respective domains (Overlay Network Topology - ONT for each domain). The pros and cons in this case are:

Pros:

- Intra-NRM (Intra Network Resource Manager) is not requested to run mapping algorithms but only to dimension its network conforming local policies (more simple functioning);
- It is a more simple solution for unicast VCANs based on MPLS paths - e.g., Intra-NRM establishes a matrix of MPLS pre-provisioned paths, conforming its own policy and offers them to a CAN Manager in abstracted form as intra-domain ONT;
- The CAN (Content Aware Network) Manager has stronger control on VCANs. It can also run a global optimization algorithm when doing VCAN mapping.

- Optimal global solutions can be obtained in terms of resource reservation.

Cons:

- More complexity for the CAN Manager, given that it should collect the complete ONT and also run at inter-domain level the combined algorithm for QoS routing, Admission Control (AC), Resource reservation and VCAN mapping
- Higher signaling overhead;
- Periodic or event triggered or on-demand updates are necessary to refresh the CAN Manager knowledge on the network resources matrix for the network domain to which it is associated;
- Less dynamicity at network level: MPLS paths are pre-provisioned, before knowing the actual SPs requests;
- Not applicable solution for multicast enabled VCANs (i.e VCANs when one has a tree of traffic trunks); the *intra-domain tree* should be constructed - *on demand* of the CAN Manager addressed to its associated Intra-NRM (the tree cannot be pre-provisioned) and mapped onto real network paths.

B. Two steps VCAN Mapping

The Initiator CAN Manager only collects the first level ONT, i.e., obtains a graph containing only the domains abstracted as nodes (see Fig. 3.a). So, the Intra-NRMs and consequently the other CAN Managers (apart from initiator) do not have to deliver to the initiator CAN manager any ONT. The initiator CAN Manager runs the VCAN mapping algorithm on a graph where each core network domain is represented as a node and the edges of the graph are inter-domain links. Then each Intra-NRM performs actually the mapping of VCAN requested resources on its network resource matrix (i.e., intra-domain ONT) for the part of VCAN spanning that domain, by running a similar algorithm.

Pros:

- Intra-NRM does not disclose to the CANP (Content Aware Network Provider) any intra-domain topology (neither detailed nor ONT) except the ingress and egress points; this is a good solution from business point of view;
- More scalable solution for both ONT topology determination and VCAN mapping algorithm based on two hierarchical levels: CAN Manager runs the combined VCAN mapping algorithm at inter-domain level for the first time. Secondly, the CAN Manager of each selected domain as being

part of the path will run again the algorithm for the intra-domain topology;

- Each Intra-NRM having total knowledge on its network resource matrix, runs the combined VCAN mapping algorithm at intra-domain level;
- Suitable solution for multicast capable VCANs (the mapping of the tree onto networks paths is done by the Intra-NRM on demand from CAN Manager and not provisioned in advance;
- More simple solution for CAN Manager in terms of algorithm complexity;
- Less amount of signaling between CAN Managers.

Cons:

- No global optimisation of the multi-domain multicast tree is assured, given that selection process of the inter-domain path does not consider any information about some possible intra-domain bottlenecks;
- Overload of the Intra-NRM with VCAN mapping algorithm;
- Need to establish dynamically MPLS paths - so more complexity (Label distribution protocol is needed).

Considering the *pros* and *cons* of the above solutions, we adopted both of them have been: the first solution for unicast VCANs (one level mapping algorithm running at CAN Manager level) and the second solution for multicast VCANs (two levels - combined algorithm).

C. Summary of VCAN Mapping Solutions Selection

For *inter-domain routing*, a combined algorithm and protocol is proposed to perform jointly *QoS routing*, *admission control*, *VCAN mapping* and *logical resource reservation*, while using the multi-domain graph of the network, available resources (per QoS class) containing the following information: topology, where a domain will be represented as: a node – for unicast/MPLS VCANs; - summary of ONT (Overlay Network Topology) for multicast VCANs; - link capacities for each edge of the graph. For *intra-domain routing* the same combined algorithm and protocol is proposed but only for multicast VCANs, while using the intra-domain graph of the network (per QoS class), containing the following information: intra-domain topology; link capacities for each edge of the graph.

Specifically we have:

Unicast VCANs (mono or multi-domain), supported by MPLS provisioned paths at each network domain level: one level planning and VCAN mapping performed at CAN Manager based on applying the combined algorithm on an inter-domain graph composed of inter-domain links and summary of the domain topologies of the network domains (delivered as RAM – Resource Availability Matrix by Intra-NRMs) to the CAN Manager.

Multicast VCANs (mono or multi-domain), supported by hybrid multicast trees: a hierarchical two-levels approach for VCAN mapping onto multi-domain network infrastructures. The two levels are: inter-domain VCAN mapping, intra-domain VCAN mapping.

D. Routing Metric

A QoS constrained routing is performed over the ONT. A combined metric was proposed [15] for a link, considering the bandwidth request, the bandwidth available, targeting to choose the widest path. The cost of an inter-domain link (i,j) in the ONT can be $C(i,j) = Breq/Bij$, where Bij is the available bandwidth on this link. Note that this cost is not a static one: it depends on the amount of requests and on the capacity available on the link for that class of service.

The simplest cost of the full path will be: *Sum (link costs)*. Additionally one can use: *Sum (link costs) * NHF (path)* where Number of Hops Factor NHF (path) is a weight factor approximately proportional to the number of CNs crossed by this path. This solution will try to reduce the number of transited domains.

The ratio also can be interpreted as link utilization factor; that is why an alternative notation can be used: $C(i,j) = U_{link_ij}$. The constraint is: $(Breq/Bij < 1)$. Therefore in each action of path search the branches not satisfying this constraint should be not considered.

VII. COMPUTATION AND USAGE OF THE OVERLAY TOPOLOGY TO MAP VCANs

A. Operational Phases

This section describes how the overlay topology information is used to map the multi-domain VCANs. The VCAN mapping algorithm is actually a combined one, making jointly a *QoS routing*, *admission control* (considering the bandwidth requests of the SP), *resource reservation* for virtual paths and *VCAN mapping* on these paths. For details of this algorithm one can consult [15]. In order to be more specific the example presented in Fig. 4 is considered.

Supposing that the VCAN initiator CAN Manager learned the inter-domain overlay network topologies (ONT) and inter-link capacities, it can negotiate with SP an SLS contract and to conclude this contract it has to try to map VCANs onto network resources. The VCAN mapping can be done on a single level (jointly inter and intra-domain) or separately on two hierarchical levels: inter-domain and intra-domain. We present here the first solution, i.e., single level VCAN mapping.

We suppose the initiator CAN Manager has knowledge on ONT as presented in Fig. 3.a, i.e., it knows the graph of inter-domain topologies but it does not know anything about intra-domain traffic trunks.

The VCAN mapping problem is the following: given an inter-domain graph and a Traffic Matrix (TM is contained in the SLS produced by SP), how to map the TM onto real network graph as to respect some minimum bandwidth constraints and also optimize the resource usage. The simplest form for TM is expressed as a matrix having entries

{(input, output, bandwidth) ...} for different traffic trunks belonging to the desired QoS class. Note that in a more complex approach several QoS parameters can be considered, e.g., delay, but here we treat the simplified case of only capacity (bandwidth).

We continue the example given in Fig. 4. It is supposed that the desired VCAN has a tree topology. We assume that steps 1 and 2 have been already performed. The following steps follow, ending with a complete VCAN mapping onto real network topology.

3. CANMgr2 (knowing the inter-domain graph) determines that Core Network Ddomain1 (CND1), ..CND6 should participate to VCAN. In particular it adds CND3 to the list in order to reach CND6

As a result, CANMgr2 knows an abstracted graph as in Fig. 6.

4. CANMgr2 determines possible input points and output points (border routers I/Fs IDs) for each domain by using the inter-domain graph. Note that it does not know yet the inter-domain paths. Several solutions might exist. Fig. 7 shows this graph.

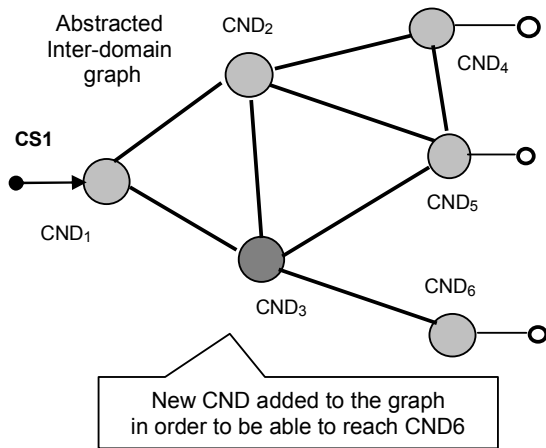


Figure 6. First abstraction of an inter-domain graph determined by CANMgr2 able to realise VCAN spanning

5. CANMgr2 asks the ONT information from each domain in the form of Resource Availability Matrix (RAM). The parameters of the requests have entries like (input, output, bandwidth) for all ingress-egress pairs of points of that domain. This RAM returned is actually the summary overlay topology and capacities of each domain. In this way each domain has not to disclose its actual topology and capacities to a third party.

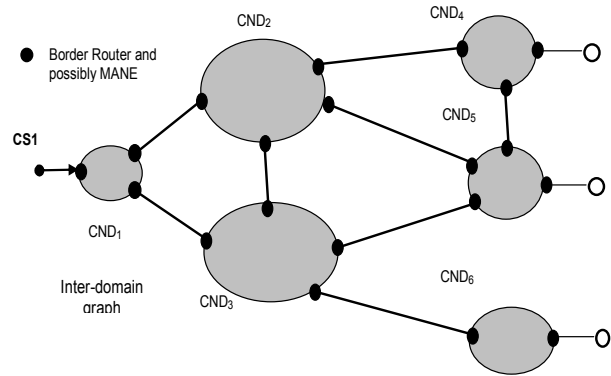


Figure 7 Inter-domain graph known by CANMgr2 with ingress-egress points specification

6. CANMgr2 receives the ONTs and capacities, i.e., the RAMs from all CANMgrs and its Intra-NRM and constructs a detailed graph of available links.

Note 1: that each domain is free to return whatever RAM is wants depending on its own policy. This process is depicted in Fig. 8.

Note2: the CANMgrx does not know yet the capacities needed by VCAN initiator, simply because CANMgr2 does not know yet what to request from CANMgrx. CANMgr 2 only asks for RAM.

7. CANMgr2 computes (modified and combined algorithm based on Dijkstra one) and determines VCAN mapping and the allocation of resources (Fig. 9).

8. CANMgr2 communicates back to each CANMgr and also to its Intra-NRM what resources have been used on intra-and inter-domain links.

9. Each CAN Manager communicates to its Intra-NRM what resources have been booked as reserved, on behalf of this domain.

10. Each CAN Manager and Intra-NRM map internally the portion of the VCAN on some real network paths (e.g., MPLS label switched paths. Note that the solution already exists because at step 5 the RAMs expressing the internal ONT of the domain) have been communicated to the initiator VCAN manager.

11. The RAMs are adjusted accordingly at each domain.

12. The new VCAN is registered in all Data Bases of different CAN Managers.

13. Confirmations are returned to the CANMgr2.

14. CANMgr2 registers this VCAN in its Data Base.

15. CANMgr2 returns response to the Service Provider.

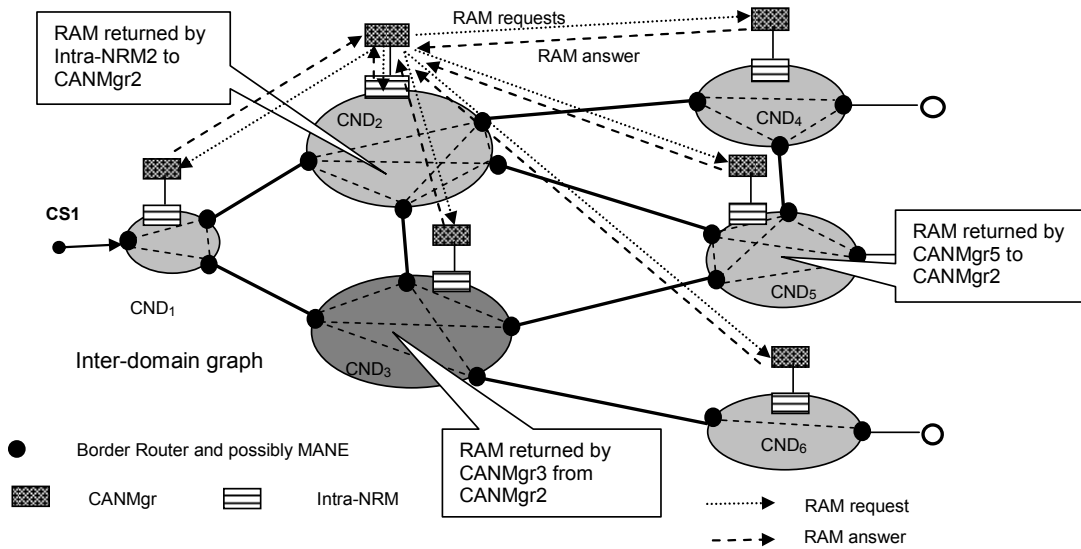


Figure 8 CANMgr2 collects the internal ONT from other CAN Managers by issues RAM requests and getting answers

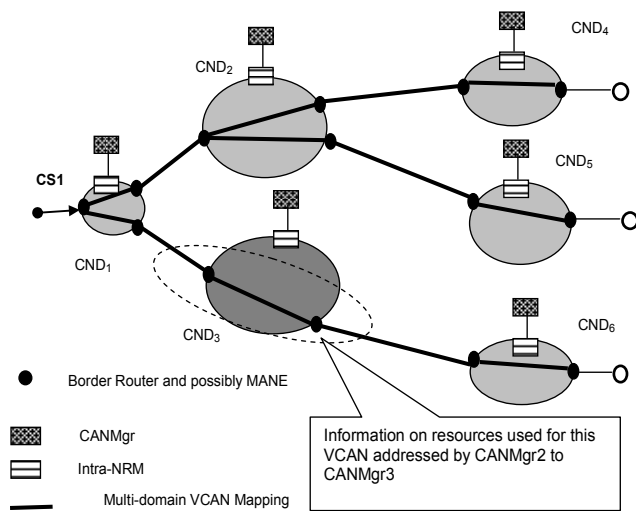


Figure 9 Computed VCAN (tree in this example)

B. VCAN Mapping Algorithm Implementation and Experiments

This section presents an implementation variant and then some numerical examples and experimental results for the procedure proposed in the above sub-Section A.

The VCAN mapping algorithm has been implemented in C, using Visual Studio C++ Express Edition as development environment. The hardware platform used, relevant for the obtained results (especially the average processing time), is a device equipped with Intel(R) Core(TM)2 CPU

T5600@1.83GHz processor and 2,00 GB installed memory (RAM) on a 32-bit OS.

A complete implementation of the CAN Manager and Intra-domain Network Resource Manager and Service Provider software are currently in progress and detailed results will be reported soon.

The multi-domain network is supposed to contain several Core Network Domains CND A, CND B, .. CND F.

The Initiator CAN Manager is supposed to collect the overall ONT composed from inter-domain and intra-domain parts (steps 2-6). Note that in this example to keep it simple, we did not specify exactly who the initiator CAN Manager is. Actually it can be any of them.

Initially the first level inter-domain abstracted ONT (Overlay Network Topology) is collected – expressed in a graph containing only the domains (abstracted as nodes) and inter-domain link capacities (similar to Fig. 6). Then after finishing step 6 of the procedure the inter-domain graph plus each domain ONT is obtained (Fig. 9).

In this example, the first level ONT (image of the network graph) is presented in the Fig. 10 as a matrix M1 where A,B,C, ..F correspond to indexes 0, 1, 2, ..5 of rows and columns. To simplify the presentation, the numbers (entries) stand for generic bandwidth units (capacities) on the inter-domain links (a zero entry value means no link between the corresponding nodes). Here each domain is abstracted as node numbered with an index belonging to the set {0, 1, ..., 5}.

$$M1 = \begin{matrix} & & 0 & 15 & 21 & 0 & 0 & 0 \\ & 15 & 0 & 16 & 18 & 43 & 0 & \\ 21 & 16 & 0 & 0 & 23 & 30 & & \\ 0 & 18 & 0 & 0 & 12 & 0 & & \\ 0 & 43 & 23 & 12 & 0 & 0 & & \\ 0 & 0 & 30 & 0 & 0 & 0 & & \end{matrix}$$

Figure 10 Inter-domain first level non-oriented graph (ONT) example represented as a matrix

After having the first image of the inter-domain ONT, the Initiator CAN Manger performs the steps 3-4-5-6 of the procedure. The result is getting a completed ONT collected from the CND A, ..., F. The complete inter-domain graph is presented in Fig. 11, where the ONTs for the domains A, B, ..., F are also represented (see step 6 in the procedure described in sub-section A).

In Fig. 11, the values attached to the middle of each link represent the segment capacity and the 1 to 6 numbers are the exit point's indexes from a CND (Core Network Domain). For example between CND B and CND D there is a link with 18 bandwidth units' capacity and the exit point from CND B is the one with no 4. The dotted lines inside each CND represent the ONT of each domain, i.e., Resource Availability Matrix - RAMs returned by each Content Aware Network Manger of the domains A, B, ... to the initiator CANMgr. The continuous lines together with dotted lines form the complete inter-domain network graph where each domain is summarized by its ONT.

The graph of Fig. 11 can be represented as a matrix (Fig. 12) and this will be the input to the VCAN mapping algorithm. In the matrix the value 0 means no link between adjacent nodes and other value different from 0 signify that there is a link with the correspondent capacity.

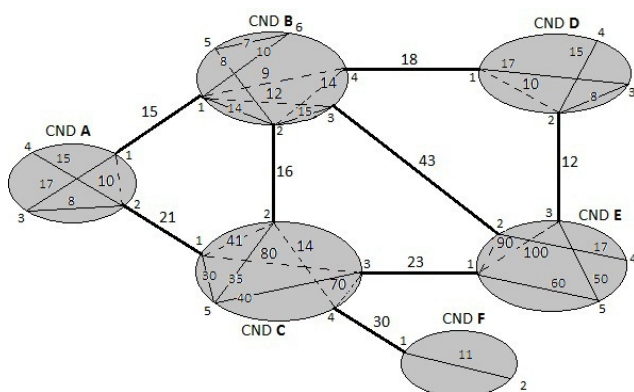


Figure 11 Inter-domain network graph (non-oriented) and summary of domains' ONT collected by the Initiator CABN Manger after finishing the step 6

M2		A		B				C				D		E			F	
		A1	A2	B1	B2	B3	B4	C1	C2	C3	C4	D1	D2	E1	E2	E3	F1	
A	A1	0	10	21	0	0	0	0	0	0	0	0	0	0	0	0	0	0
	A2	10	0	0	0	0	0	19	0	0	0	0	0	0	0	0	0	0
B	B1	21	0	0	0	12	9	0	0	0	0	0	0	0	0	0	0	0
	B2	0	0	0	0	0	14	0	16	0	0	0	0	0	0	0	0	0
	B3	0	0	12	0	0	0	0	0	0	0	0	0	0	43	0	0	0
	B4	0	0	9	14	0	0	0	0	0	0	18	0	0	0	0	0	0
C	C1	0	19	0	0	0	0	0	41	80	0	0	0	0	0	0	0	0
	C2	0	0	0	16	0	0	41	0	0	14	0	0	0	0	0	0	0
	C3	0	0	0	0	0	0	80	0	0	70	0	0	23	0	0	0	0
	C4	0	0	0	0	0	0	0	14	70	0	0	0	0	0	0	0	30
D	D1	0	0	0	0	0	18	0	0	0	0	18	0	0	0	0	0	0
	D2	0	0	0	0	0	0	0	0	0	18	0	0	0	0	12	0	0
E	E1	0	0	0	0	0	0	0	0	23	0	0	0	90	100	0	0	0
	E2	0	0	0	0	43	0	0	0	0	0	0	0	90	0	0	0	0
	E3	0	0	0	0	0	0	0	0	0	0	12	100	0	0	0	0	
F	F1	0	0	0	0	0	0	0	0	0	30	0	0	0	0	0	0	0

Figure 12 The inter-domain graph (ONT) –used as input for VCAN mapping algorithm.

The detailed description of the VCAN mapping algorithm (combined QoS routing and reservation - proposed by the same authors) is not in the scope of this paper. For details one can see [15]. However, for completeness of the example presentation, a short description is given below.

The Service Provider request for a VCAN (Virtual Content Aware Network) can be expressed in the simplest form as a Traffic Demand Matrix (TDM) having entries (input_Id, output_id, bandwidth_requested), i.e., source of request, the destination and the capacity requested.

The primary objective of the algorithm is to select paths based on the criterion of largest capacity (bandwidth) possible and then make resource reservation on those paths.

AS an example, Fig. 13 represents the Traffic Demand Matrix

$$Re\ q = \begin{matrix} & 1 & 12 & 5 \\ 4 & 15 & 7 & \\ & 8 & 11 & 9 \end{matrix}$$

Figure 13 Traffic Demand Matrix example

The indexes of the representation (A1, A2,...) correspond to the extended matrix (where the numbers 0, 1, 2, ..., 15 represents A1, A2, ..., respectively F1).

The results obtained after running the algorithm for M2 matrix are shown in Fig. 14, where the computation time, a total cost of the solution and the degree of request satisfaction is also presented.

```

Request 1->12, carry 5: 1 6 8 12
Request 4->15, carry 7: 4 13 12 8 9 15
Request 8->11, carry 9: 8 12 14 11

Cost: 3.138959 of wich blind: 0.000000 Satisfied requests: 3 / 3

-----
Best cost: 3.138959
Satisfied Requests: 3 / 3
Total time: 0.003000

```

Figure 14 VCAN Mapping algorithm results – simple example

The VCAN system has been implemented as part of ALICANTE work and installed on a pilot testbed. It consists in three fully meshed core network domains, with all nodes as Linux routers (MANE routers and Core Routers in each domain). Each domain has a CAN Manager and an Intra-domain Network Resource Manager. The implementation is made in C under Linux. Unicast VCANs and multicast VCANs have been experimented and validated on this testbed. Results are already submitted to be published in additional papers.

The main blocks of the VCAN Manager implemented have been: CAN Planning, CAN Provisioning, CAN SLS negotiation Protocols, CANMgr interfaces – vertical and horizontal ones.

VIII. CONCLUSIONS AND FUTURE WORK

The paper proposed a management solution for inter-domain peering, to support Content Aware Networks for a multi-domain and multi-provider environment. The management is based on horizontal SLAs negotiated and concluded between CAN providers (represented by CAN Managers) the result being a set of parallel VCANs offering different classes of services to multimedia flows, based on CAN/NAA (Content Aware Network/Network Aware Application) concepts. The inter-domain approach is to develop an overlay topology service to support VCAN construction, thus obtaining several parallel QoS planes. A CAN Manager is initiating the multi-domain VCAN realization by using the overlay topology service. Two solutions are proposed for topology collection in multi-domain environment: one and two steps. The optimization solution in one step is a new contribution of this paper. Pros and cons are discussed related to complexity, scalability, signaling overhead and business point of view and it is concluded that each solution can be better in some scenario: one-step solution for unicast VCDANs and two-step solution for multicast VCANs.

A numerical example and samples of implementation results are given for the one-step algorithm.

Algorithm experimentation for large topologies is in progress and results are already submitted for publication.

The system is currently under complete design and implementation in the framework of the FP7 research project ALICANTE. Further validation and extensive performance evaluation results will be shown in a future work.

Acknowledgments

This work was supported partially by the ALICANTE project (FP7-ICT-248652) and partially by the projects POSDRU/88/1.5/S/61178 together with POSDRU/89/1.5/S/62557.

REFERENCES

- [1] E.Borcoci, R.Miruta, S.Obreja, "Inter-domain Peering in Content-Aware Networks for Multimedia Applications" Proc. of. CTRQ 2012, France, April 2012, <http://www.iaria.org/conferences2012/CTRQ12.htm>
- [2] Baladrón, C., "User-Centric Future Internet and Telecommunication Services", in: G. Tselentis, et. al. (eds.), Towards the Future Internet, IOS Press, 2009, pp. 217-226.
- [3] Turner, J. and Taylor, D., "Diversifying the Internet," Proc. GLOBECOM '05, vol. 2, St. Louis, USA, Nov./Dec. 2005, pp. 760-765.
- [4] Anderson, T., Peterson, L., Shenker, S., and Turner, J., "Overcoming the Internet Impasse through Virtualization", Computer, vol. 38, no. 4, Apr. 2005, pp. 34-41.
- [5] 4WARD, "A clean-slate approach for Future Internet", <http://www.4ward-project.eu/>.
- [6] J.Choi, J.Han, E.Cho, T. Kwon, and Y.Choi, A Survey on Content-Oriented Networking for Efficient Content Delivery, IEEE Communications Magazine, March 2011.
- [7] V. Jacobson et al., "Networking Named Content," CoNEXT '09, New York, NY, 2009, pp. 1-12.
- [8] W.K. Chai, et.al., CURLING: Content-Ubiquitous Resolution and Delivery Infrastructure for Next-Generation Services, IEEE Communications Magazine, March 2011.
- [9] I. Psaras, W. K. Chai, G. Pavlou, "Probabilistic in-network caching for information-centric networks", Proceedings of the second edition of the ICN workshop on Information-centric networking, 2012, pp.55-60, <http://dl.acm.org/citation.cfm?id=2342501>
- [10] M. Femminella, R.o Francescangeli, G. Reali, J. W. Lee, H. Schulzrinne, "An enabling platform for autonomic management of the future internet" IEEE Network, Volume:25, November/December Issue: 6, pp. 24-32.
- [11] FP7 ICT project, "Media Ecosystem Deployment Through Ubiquitous Content-Aware Network Environments", ALICANTE, No248652, <http://www.ict-alicante.eu/> (last accessed: Dec. 2010).
- [12] Borcoci, E., Negru, D. and Timmerer, C., "A Novel Architecture for Multimedia Distribution based on Content-Aware Networking" Proc. of. CTRQ 2010, Athens, June 2010, pp. 162-168.
- [13] ALICANTE, Deliverable D2.1, ALICANTE Overall System and Components Definition and Specifications, <http://www.ict-alicante.eu>, Sept. 2011.
- [14] Schönwälder, J., Fouquet, M., Dreo Rodosek, G., and Hochstatter, I.C., "Future Internet = Content + Services + Management", IEEE Communications Magazine, vol. 47, no. 7, Jul. 2009, pp. 27-33.
- [15] E.Borcoci, R.Miruta, S.Obreja, "Multi-domain Virtual Content-Aware Networks Mapping on Network Resources" – EUSIPCO2012, <http://www.eurasip.org/Proceedings/Eusipco/Eusipco2012/Conference/papers/1569588939.pdf>
- [16] Levis, P., Boucadair, M., Morrand, P., and Trimitzios, P., "The Meta-QoS-Class Concept: a Step Towards Global QoS Interdomain Services", Proc. of IEEE SoftCOM, Oct. 2004.
- [17] Howarth, M.P. et al., "Provisioning for Interdomain Quality of Service: the MESCAL Approach", IEEE Communications Magazine, June 2005, pp. 129-137.

- [18] Abhay Perekth, "Routing on Overlay Networks", University of Berkeley, October 2002, <http://robotics.eecs.berkeley.edu/~wlr/228a02/Lecture%20Slides/routing4.pdf> (last accessed December 19th, 2012)
- [19] Y. Zhu, B. Li, "Overlay Networks with Linear Capacity Constraints", University of Ontario, <http://faculty.uoit.ca/zhu/papers/tpds06.pdf> (last accessed December 19th, 2012)
- [20] Sylvia Ratnasamy, Paul Francis, Mark Handley, Richard Karp, and Scott Shenker. 2001. A scalable content-addressable network. SIGCOMM Comput. Commun. Rev. 31, 4 (August 2001), 161-172. DOI=10.1145/964723.383072 <http://doi.acm.org/10.1145/964723.383072>
- [21] Fabio L. Verdi, Mauricio F. Magalhaes "Using Virtualization to Provide Interdomain QoS-enabled Routing", Journal of Networks, April 2007, pp. 23-32.
- [22] Z. Li, P. Mohapatra, and C. Chuah, Virtual Multi-Homing: On the Feasibility of Combining Overlay Routing with BGP Routing, University of California at Davis Technical Report: CSE-2005-2, 2005. <http://www.cs.ucdavis.edu/research/tech-reports/2005/CSE-2005-2.pdf>
- [23] ENTHRONED, End-to-End QoS through Integrated Management of Content, Networks and Terminals, FP6 project, URL: <http://www.ist-enthrone.org/>.
- [24] Zhi Li, P. Mohapatra, "QRON: QoS-Aware Routing in Overlay Networks", IEEE Journal on Selected Areas in Communications, Vol. 22, No. 1, January 2004, pp.29-39.
- [25] Boucadair, M. et al., "A Framework for End-to-End Service Differentiation: Network Planes and Parallel Internets", IEEE Communications Magazine, Sept. 2007, pp. 134-143.
- [26] Aggarwal, V., Feldmann, A., "Can ISPs and P2P Users Cooperate for Improved Performance?", ACM SIGCOMM Computer Communication Review, vol. 37, no. 3, Jul. 2007, pp. 29-40.

PAPR Reduction of OFDM Signals using Gradual Projection Active Constellation Extension and Sequential Block Grouping Tone Reservation Hybrid Scheme

Eugen-Victor Cuteanu

Communication Department
Politehnica University, Faculty of Electronics and
Telecommunications
Timisoara, Romania
victor.cuteanu@gmail.com

Alexandru Isar

Communication Department
Politehnica University, Faculty of Electronics and
Telecommunications
Timisoara, Romania
alexandru.isar@etc.upt.ro

Abstract—The Orthogonal Frequency Division Multiplexing is one of the widely used modulation techniques in the present broadband wireless technology. The opportunities and challenges of this modulation technique are derived from its native advantages and disadvantages. One of the main problems is the high peak-to-average power ratio of transmission signal due to the superposition of many subcarriers. In previous works, various hybrid peak-to-average power ratio reduction techniques were presented. One of these techniques was the combination of the standard active constellation extension with the sequential tone reservation scheme. This paper presents a new hybrid peak-to-average power ratio reduction technique, which combines other active constellation extension and tone reservation schemes. This is the case of already known smart gradient projection and new proposed signal compression gradual projection active constellation extension and sequential block ordered tone reservation scheme respectively. The simulations shown that the proposed technique realizes an increased peak-to-average power ratio reduction compared to component methods with similar parameters.

Keywords-OFDM; PAPR; Gradual Projection; Active Constellation Extension; Sequential Block Grouping; Tone Reservation

I. INTRODUCTION

The Orthogonal Frequency Division Multiplexing (OFDM) is one of the most efficient and popular modulation techniques used in broadband wireless communication systems like Worldwide Interoperability for Microwave Access (WiMAX), Terrestrial Digital Video Broadcast (DVB-T), or wireline systems like Asymmetric Digital Subscriber Line (ADSL). One of the main practical issues of the OFDM is the Peak-to-Average Power Ratio (PAPR) of the transmitted signal. This high PAPR occurs because of the time-domain superposition of the many data subcarriers which compose the OFDM signal. Due to the large number of subcarriers, the resulting time-domain signal exhibits Rayleigh-like characteristics and large time-domain amplitude variations. These large signal peaks require the high power amplifiers (HPA) to support wide linear dynamic range.

Higher signal level causes non-linear distortions leading to an inefficient operation of HPA, causing intermodulation products resulting unwanted out-of-band power. In order to reduce the PAPR of OFDM signals, many solutions have been proposed and analyzed. For an enhanced PAPR reduction, hybrid techniques were proposed [1]-[6] as well. The efficiency of these methods can be evaluated considering their characteristics of non-linearity, amount of processing and size of side information needed to be sent to receiver.

The class of linear methods is represented by approaches like selective mapping (SLM) [7], Partial Transmit Sequence (PTS) [8], and Tone Reservation (TR) [9].

The SLM method generates several signal replicas based on a set of predefined phase patterns. The algorithm performs vector rotations of each subcarrier from the original frequency domain OFDM signal. For each obtained signal variant, the corresponding PAPR is evaluated. The variant with the lowest PAPR is chosen for the transmission. A similar approach is applied in case of PTS method, where the same rotating phase is applied to a group of subcarriers.

Both methods provide a variable efficiency of PAPR reduction, being dependent by the considered number of angles and phase patterns. An important disadvantage of these methods is that an extended set of different phase patterns leads to an increased computation complexity. To overcome this problem, additional information can be sent to the receiver, in order to reduce its required search space. This approach presents another disadvantage due to reduced payload of each OFDM frame.

Optimizations of these methods have been proposed in several works [10][11].

Another PAPR reduction method is TR, which uses a set of reserved set of subcarriers (tones) to generate signals with lower PAPR level. Besides the advantage of no additional distortion, this method also does not need to transmit additional information to the receiver. Because not all subcarriers are used to transmit useful information, this method is considered to lower the data rate of the OFDM-based systems.

Since the development of the original TR method, in order to reduce the computation complexity and to improve

the performance, several derivate techniques have been proposed: selective mapping of partial tones (SMOPT) [12], One-Tone One-Peak (OTOP) [13] and one-by-one iteration [14].

Another optimized variant of this method proposes to generate tones for the K largest peaks of the signal. The phases of these tones are chosen to be opposite to $\varphi_j + n\pi/2$, where φ_j is the phase of the identified peaks, $j=1, 2, \dots, K$ and $n=0, 1, 2, 3$. The procedure is iterated until convergence reaches the expected threshold [9].

The class of non-linear methods is represented by approaches like active constellation extension (ACE), clipping, partial clipping, and signal compression.

The ACE method change the original OFDM signal by modifying amplitude and phase of tones whose base band modulation symbol is an outer point of the constellation. Those outer signaling points of the conventional constellation are dynamically moved toward outside of the original constellation in order to obtain signal derivatives with reduced PAPR level for the transmitter. The domain for allowed alternative points is chosen so that the signal processing does not reduce the constellation's minimum-distance but lowers the PAPR level [15][16].

For additional PAPR reduction, some proposed derivate methods consider outers points projection onto squares or circles around all the QAM constellation points and intentional distortion within the allowed bounds. The tradeoff between level of the constellation distortion and PAPR level is analyzed and optimized as well [17].

The clipping method is another well known non-linear PAPR reduction technique, where the amplitude of the signal is limited to a given threshold. Because interpolation may generate peak regrowth, different filtering techniques have been proposed. Filtering can also cause peak regrowth, but less than the clipping before interpolation [18].

Another clipping technique supposes that only subcarriers having the highest phase difference between the original signal and its clipped variant will be changed. This is the case of the partial clipping (PC) method [19].

Other group of nonlinear methods is represented by signal companding, originally developed for audio signal compression. These methods are implemented as a digital nonlinear attenuator, which operates at the transmitter before the HPA device.

Some works proposed μ -law or A-law companding functions [20] or exponential companding function [21]. In order to reduce the computation complexity, other companding method uses transfer functions split in linear sub-domains with different coefficients. This is the case of the piecewise-scales method [22]. In order to decrease the computation complexity without using sub-domains, other methods consider polynomial ratio functions [23].

At the receiver, the inverse function for signal expanding is applied. This is implemented as a nonlinear amplifier which performs the reverse operation over the time-domain signal. Therefore the nonlinearity does not alter the signal reconstruction process, but has an important impact over the received noise from the communication channel. Therefore the BER performance is strongly impacted by the obtained noise after the signal expanding block.

For an optimized balance between PAPR reduction level and BER degradation, other methods consider adaptive quasi-nonlinear sigmoid transfer functions [6].

For additional PAPR reduction, different hybrid techniques were proposed as well. Their efficiency depends by the characteristics and types of the component methods.

Combinations of a linear method with a non-linear method present better PAPR reduction with moderate increase of computation complexity, and average BER degradation [2][3]. Also, combination of two linear methods, one operating on the data subcarriers and the other one operating on the non-data subcarriers, presents improved efficiency of PAPR reduction [4].

An important characteristic of these combinations is that their computation complexity depends by the cumulative set of parameters describing the total amount of operations required by the component methods.

Additional to previous work [1], the present paper considers as ACE derivatives, the well known smart gradient projection (SGP) method and proposes the signal compression based gradual projection (CGP) method. Also the present paper, proposes a new TR derivate based on the sequential block grouping (SBG) method.

The rest of the paper is organized as follows. The second section describes the proposed hybrid PAPR reduction scheme, when various ACE and TR derivatives are applied. In the third section is described the clipping method as PAPR reduction method of reference. Next, in the forth section, the simulation results for various ACE-TR combinations, highlighted by the computer simulation, are presented and discussed. The PAPR reduction efficiency is evaluated when the new gradual projection ACE and the new sequential block grouping TR schemes are applied. Based on the obtained results, some conclusions are presented in the fifth section.

II. THE HYBRID METHOD

The proposed hybrid PAPR reduction technique is obtained by serialization of a gradual projection active constellation extension method and sequential tone reservation method.

The main idea for combining the two methods is relying on the observation that the cumulative signal processing for PAPR reduction will increase the overall performance. Furthermore, the idea is based on the fact that each of the considered methods is based on a different principle. One performs a controlled signal distortion and the other realizes different changes of the non-data subcarriers [1].

The block diagram of the proposed method is presented in Figure 1. The performance of the proposed PAPR reduction technique is analyzed with a MATLAB simulator as presented in Figure 2. For this purpose, within this simulator, the samples from the uniformly distributed random generated signal are mapped from binary representation to the M-QAM or M-PSK constellation points. The obtained complex values are grouped in blocks of N elements each, forming the OFDM symbols.

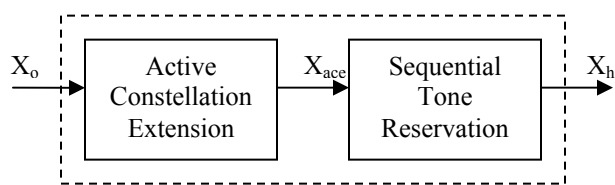


Figure 1. The Hybrid ACE-TR scheme for PAPR reduction.

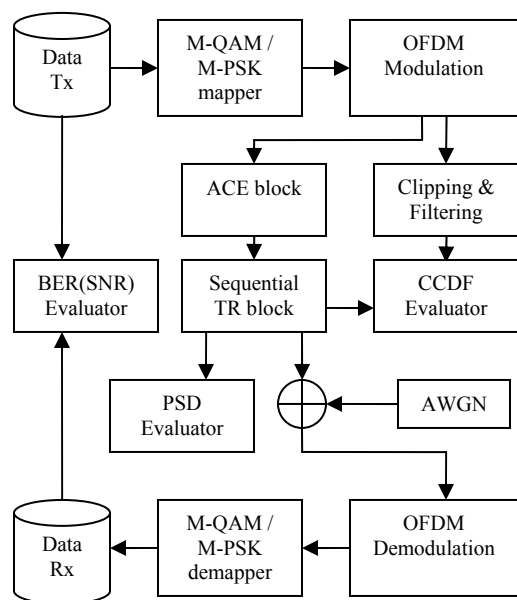


Figure 2. MATLAB model for the analysis of the hybrid PAPR reduction technique.

The obtained OFDM frames are applied to the PAPR reduction blocks. This signal is applied to the Complementary Cumulative Distribution Function (CCDF) block for the evaluation of the PAPR reduction. Next, the resulted signal is applied to the communication channel represented by the complex additive white Gaussian noise. This channel is composed by two independent random Gaussian generated sequences, representing the real and imaginary components of the complex additive noise.

Next, the samples of the noised signal are applied to the demodulator block and M-QAM or M-PSK demapper. Based on the comparison of the obtained received data samples with the initial generated samples, the bit error rate (BER) performance is evaluated.

For a better performance comparison, besides the proposed ACE-TR method, additionally the clipping method [18] is taken into consideration. The PAPR reduction blocks alter the original signal. Due to this fact, for evaluation of communication's performance and efficiency, besides the CCDF and BER characteristics, the simulator estimates the power spectral density (PSD) for the signal obtained after processing for PAPR reduction.

The expression of the PAPR for a given OFDM signal block is given by:

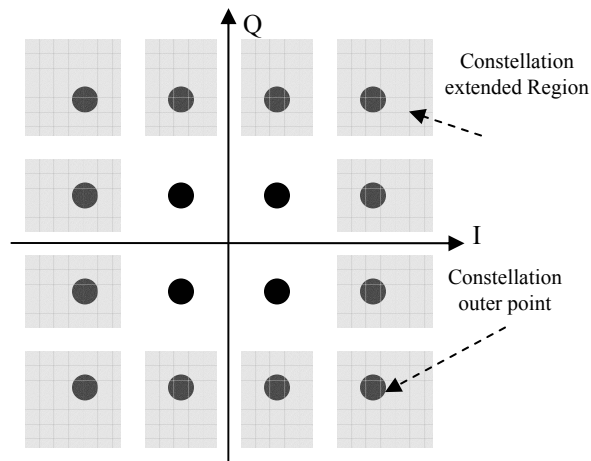


Figure 3. Example of an extended constellation. The original points and allowed extended domain for outer points for 16-QAM are indicated.

$$PAPR(x) = \frac{\max\{x(t)^2\}}{E[x(t)^2]}, \quad (1)$$

where $E[.]$ denotes the expectation operator. This is usually evaluated using the complementary cumulative distribution function (CCDF) of the PAPR:

$$CCDF(Y) = \Pr(PAPR > Y) = 1 - \Pr(PAPR < Y) \quad (2)$$

where Y is a PAPR threshold.

Within the next paragraphs, the considered ACE and TR methods are described.

A. The ACE method

The ACE method requires both time-domain and frequency-domain signal processing. As already mentioned, the main idea of this method is to shift the outer constellation points toward exterior of original constellation generating an alternative representation of the same symbol. The allowed domains for these outer points are presented in Figure 3, when 16-QAM is used as digital modulation.

The boundaries of these domains are constrained by the constellation's minimum-distance. The reason for this limitation is to prevent a decrease of BER performance at the receiver.

In the previous work [1], the considered ACE method was implemented with the projection onto convex sets (POCS) scheme, where ACE constraints are applied after clipping, according with the algorithm presented in [15].

In the preset work, two more ACE derivate methods are considered: one is the SGP-ACE and the other one is the new CGP-ACE proposed method. These methods perform gradual projection, as described in the next paragraphs.

The SGP-ACE method uses a gradient-projection approach, where only a part of the clipping difference is applied to the original time-domain signal. At each iteration,

the ACE constraints are applied in order to ensure that only allowable extension vectors are changed [15].

The implementation of this ACE method requires the following steps:

- 1) Get an OFDM frame with N subcarriers, represented by the frequency-domain signal X_o .
- 2) Compute the corresponding time-domain signal $x[n]$, by use of IFFT function.
- 3) Search the sample with the maximal amplitude x_{max} and its index n_{max} :

$$x_{max} = x[n_{max}]. \quad (3)$$

- 4) Evaluate the average signal amplitude x_{mean} .
- 5) Define the clipping threshold x_{thr} , according with the given clipping rate CR :

$$x_{thr} = x_{max} / CR. \quad (4)$$

- 6) Perform the clipping on the original signal, using the similar relations as in previous algorithm presented. Therefore the new obtained signal satisfies the following condition:

$$\tilde{x}[n] \leq x_{thr} \quad \forall n \in [1, N]. \quad (5)$$

- 7) Compute its corresponding frequency-domain representation:

$$\tilde{X} = FFT(\tilde{x}). \quad (6)$$

- 8) Enforce the ACE constraints, using the same approach as in case of previously presented POCS-ACE method. Some details will be presented at the end of this subsection.

- 9) Apply the IFFT to obtain the time-domain representation of the previously computed signal:

$$\hat{x} = IFFT(\tilde{X}). \quad (7)$$

- 10) Compute the time-domain clipping difference signal, and its corresponding frequency-domain representation:

$$x_{clip}[n] = \hat{x}[n] - x[n], \quad (8)$$

$$X_{clip} = FFT(x_{clip}). \quad (9)$$

- 11) For each sample, compute the projection value according with the following relation:

$$k_{proj}[n] = \Re(x[n] \cdot x_{clip}^*[n]) / |x[n]|, \quad (10)$$

where \Re denotes the real part of the given complex number and x_{clip}^* represents the complex conjugate replica of the previously computed clipping delta signal x_{clip} .

- 12) Compute the approximate balancing for all samples which indicates an amplitude growth, ($k_{proj} > 0$). This can be calculated using one of the following equations:

$$u[n] = \frac{x_{max} - |x[n]|}{k_{proj}[n] - k_{proj}[n_{max}]}, \quad (11)$$

$$u[n] = \frac{x_{max} - |x[n]|}{|x_{clip}[n]| + |x_{clip}[n_{max}]}. \quad (12)$$

Optionally, when a minimum average signal level x_{lim} is desired, the approximate balancing parameter can be calculated with:

$$u[n] = \frac{x_{max} - x_{lim}}{|x_{clip}[n_{max}]}. \quad (13)$$

This adaptation can be done, when the given minimum threshold fulfills the following condition:

$$x_{max} - u[n] \cdot x_{clip}[n_{max}] < x_{lim}. \quad (14)$$

Details about some these aspects and related practical exemplification are available in the original work [15].

- 13) Normalize the obtained approximate balancing vector, to the unitary range:

$$w[n] = u[n] / u_{max}, \quad (15)$$

where:

$$u_{max} = \max(u[n]). \quad (16)$$

This step was additionally introduced in the algorithm, used in this work, in order to reduce the dynamics of this parameter.

- 14) Compute the new limited time-domain signal, based on the clipped signal and the minimum approximate balancing values, according with the following relation:

$$\tilde{x}_{sgp}[n] = x[n] + w_{min} \cdot x_{clip}[n], \quad (17)$$

where:

$$w_{min} = \min(w[n]). \quad (18)$$

- 15) Repeat the procedure according with the given number of cycles, considering the previously obtained time-domain signal as input data for the presented algorithm.

After some iterations, the PAPR reduction per cycles decreases considerably, therefore, optionally, the practical implementation of this algorithm can be optimized in order to reduce the number of iterations. The break condition is given by the value of the approximate balancing parameter. This criteria and relate practical aspects are also detailed in the original work [15].

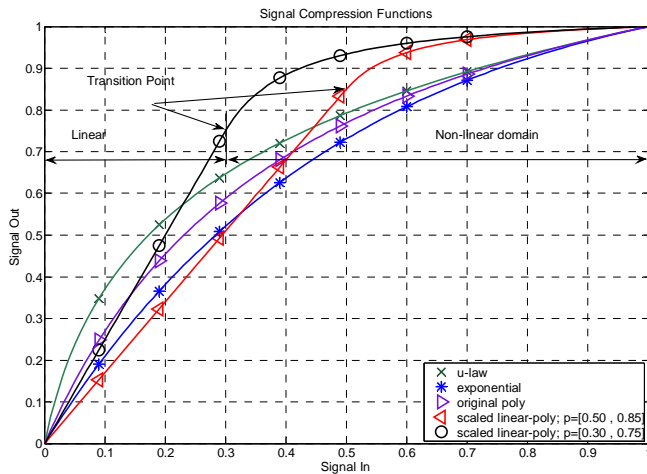


Figure 4. Examples of quasi-nonlinear companding functions.

The presented algorithm performs a gradual projection using a part of the clipping difference at each ACE iteration. The clipping delta signal is obtained by imposing each time the desired threshold to the time-domain signal.

The new proposed CGP-ACE method, instead of using a part of the clipping difference according with a computed ratio at each iteration, applies a progressive signal limitation using a given function. Therefore, in this approach, instead of fixed clipping to the predefined threshold, a progressive signal companding is performed.

The method may present different derivatives according with the chosen compression function. However, since no additional signal distortion or processing at the receiver is desired, the applied compression function must contain a linear part for the sub-domain corresponding to the signal level under the clipping threshold.

In order to realize such transfer function, a quasi-nonlinear compression function of the form proposed in [6] must be used. That type of functions contains a transition point which defines the border between the linear sub-domain and the non-linear sub-domain. Some examples are represented in Figure 5.

Based on these aspects, the implementation of this ACE method requires the following steps:

- 1) Get an OFDM frame with N subcarriers, represented by the frequency-domain signal X_o .
- 2) Compute the corresponding time-domain signal $x[n]$, by use of IFFT function.
- 3) Compute the signal's maxima, mean and threshold values x_{max} , x_{mean} , x_{thr} , same as in the previous algorithm, but only in the first iteration.
- 4) Define the adjustable signal threshold as an increasing value within the range of (x_{max}, x_{thr}) . The present work considers a linear increasing value of the form:

$$x_{adj} = \frac{R-m}{R+2} \cdot x_{max} + \frac{m}{R+2} \cdot x_{thr}, \quad (19)$$

where m is the index of the current iteration, and R is the total number of iterations.

- 5) Establish the transition point for the quasi-nonlinear compression function based on the method proposed in [6]. Considering the previously calculated signal parameters, the threshold point is obtained with the following formulas:

$$\begin{cases} p_x = x_{thr} / x_{max} \\ p_y = x_{thr} / x_{adj} \end{cases} \quad (20)$$

- 6) Compute the companded signal and scale it to the adjustable threshold value, according with the following expression:

$$x_{cmp}[n] = f(x[n]) \cdot \frac{x_{adj}}{x_{max}}, \quad (21)$$

where $f()$ is the quasi-nonlinear companding function, expressed as a ratio of polynomials [6].

- 7) Apply the FFT to compute the frequency-domain representation X_{cmp} of the previously obtained signal.
- 8) Enforce the ACE constraints, same as in the case of previous algorithms.
- 9) Apply the IFFT in order to obtain the time-domain representation \hat{x} of the previously computed signal.
- 10) Compute the ACE difference signal, to obtain the increasing amplitudes compared to the original signal:

$$x_{delta}[n] = \hat{x}[n] - x[n], \quad (22)$$

- 11) Compute the new limited time-domain signal, based on the ACE clipped signal and a factor, according with the following expression:

$$\tilde{x}_{cgp}[n] = x[n] + w \cdot x_{delta}[n], \quad (23)$$

where w is an approximation balance factor, which in case of this algorithm can be constant. When this factor is equal with unity, then the current and previous step are optional.

- 12) Repeat the procedure according with the given number of iterations. The number of cycles can be reduced when the maxim value of the ACE delta signal is smaller than a given value.

This new algorithm performs a gradual projection using as variable characteristic the signal companding function. This function may have different nonlinear characteristics, the main condition being to have a transition point where the linearity of the function changes.

The main common operation of all ACE algorithms is the application of the ACE constraints on the vectors according with the considered extended constellation.

In order to apply the ACE constraints for the outer points of the constellation, their corresponding vectors must be changed. Depending on their relative location versus the location of the original point and on the allowed extended

domain, the algorithm may change vector's amplitude or phase or both.

A solution would be to rotate the vector until the outer point enters back into corresponding extended domain. When this operation is not enough, the vector's amplitude can be increased accordingly.

In the present work, in order to reduce the computation complexity, the ACE constraints are applied by checking and changing the Cartesian coordinates separately. The present algorithm considers: the constellation's minimum-distance d_{min} , the distance between two adjacent extended domains d_{spa} , the coordinate of the original outer point and the coordinate of the actual point obtained after clipping. When the in-phase or quadrature value is under the threshold indicated by the corresponding domain border, the difference d_{ext} is added to shift the point back into its domain. This approach is presented in Figure 5.

Another variant is represented by the particular case where the distance between two adjacent extended domains is set to be equal with the constellation's minimum-distance. In this situation, the only allowed shift of the points is toward constellation's outer region, no lateral offset being permitted. This approach is presented in Figure 6.

For the case of the M-PSK modulation, the ACE constraint is applied using a similar approach. The difference is that for the M-PSK case, all constellation points can be used to lower the PAPR, and their corresponding extended domains are represented by radial sectors with the angular size of $2\pi/M$ radians.

With a similar approach, in case of M-PSK modulation, a particular variant for ACE constraints can be defined. In this model, for all points within constellation, the only allowed shift is in the direction given by the original vector, any lateral offsets being restricted.

An important aspect to mention is that the BER performance is strongly impacted by the chosen ACE constraint model. Therefore, a more restrictive constraints set imply a better BER performance.

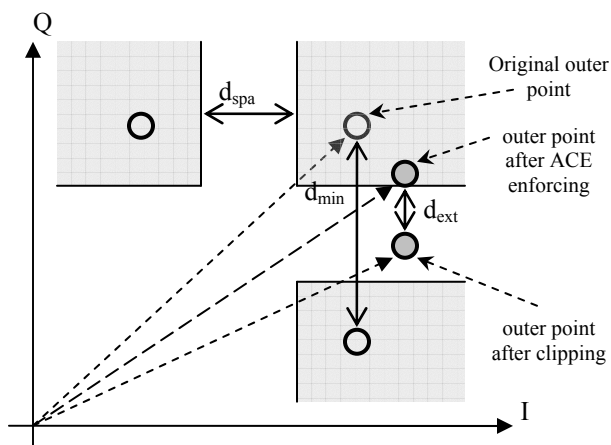


Figure 5. ACE outer point enforcing. Exemplification for 16-QAM.

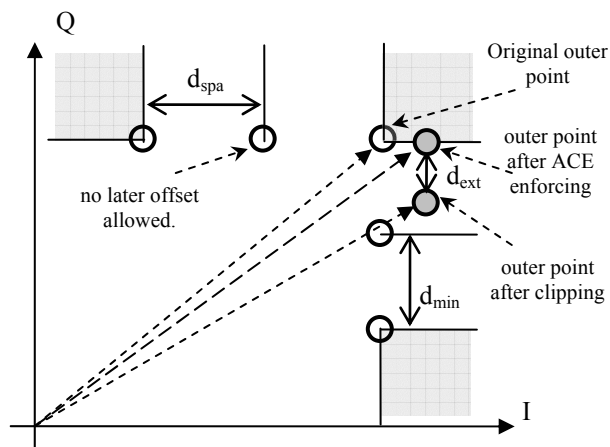


Figure 6. Particular case of ACE outer point enforcing.

B. The TR method

The TR method performs a frequency-domain adaptation of a given OFDM frame, in order to achieve a lower PAPR level for the corresponding time-domain representation. The changes are applied on the set of non-data carriers. The method performs an iterative search using different combination of complex values from a given set, for the considered subcarriers.

A search for the combination which gives the minimum PAPR level would require an exhaustive amount of operations, due to checking of whole search space of all possible values on all non-data subcarriers. Therefore in most of the cases the algorithm is implemented to search for a suboptimal solution, within a given subspace.

In the previous work [1], the considered TR method, performs a sequential search according with an one-by-one scheme as proposed by [9][14]. The block diagram for this method is presented in Figure 7.

It selects T pilot tones positions from a complete set of Q no-data carrier positions and a set of M complex values, forming a set of M^T possible combinations.

This search space may lead to an increased amount of computation. The chosen tone reservation algorithm decreases the computation complexity by attempting a reduced search space by trying all M values on the first pilot $P[0]$, while the other pilots, $P[1], \dots, P[T-1]$, have a "randomized" or zero initial state. Once an optimal value is found, a similar procedure is repeated on the other pilot positions. For further computation complexity reduction, the time-domain signals equivalent for all pilot tones can be computed and stored initially into memory. In this case, more operations are done in time-domain, fact which determines a decreased number of FFT operations [9].

Because the TR method operates on some subcarriers from the frequency-domain signal, the displacement of these non-data subcarriers may impact the method's performance. Depending by position, the allocation of the reserved subcarriers may be symmetrical or lateral occupying the lower or higher part of the signal's spectrum. The

considered variants are presented in Figure 8, Figure 9, and Figure 10, respectively.

The TR method already presented, may provide a small PAPR reduction, due to the use of a limited search subspace. In order to improve the PAPR reduction, the search subspace can be extended by increasing the set of possible values for each subcarrier. Such approach may provide some PAPR reduction with the cost of considerable increased number of operations. Another extension of the search subspace consists in the increasing of the number of combinations of the considered values.

In the present work, some new sequential TR derivate methods are considered. Within the new proposed SBG-TR derivate method, the considered search subspace is extended with more combinations of the given set of carriers values. For this purpose, the SBG-TR method split the set of non-data subcarriers in groups according with a given pattern. An example of such TR grouping is presented in Figure 11. Each of these groups is considered to be a full search subspace.

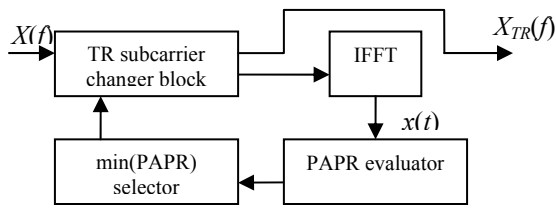


Figure 7. Sequential Tone Reservation method.

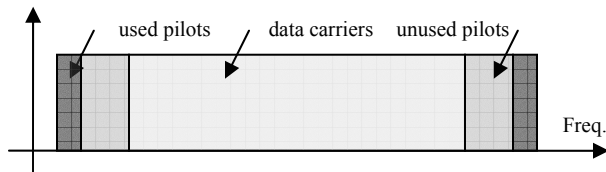


Figure 8. Allocation of reserved tones within an OFDM symbol (symmetrical, outer) Type I

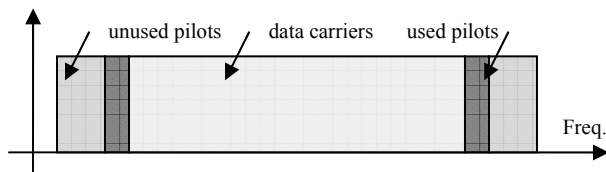


Figure 9. Allocation of reserved tones within an OFDM symbol (symmetrical, inner) - Type II

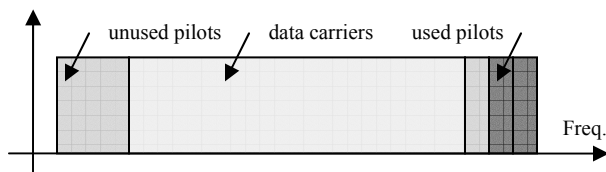


Figure 10. Allocation of reserved tones within an OFDM symbol (lateral, outer) - Type III

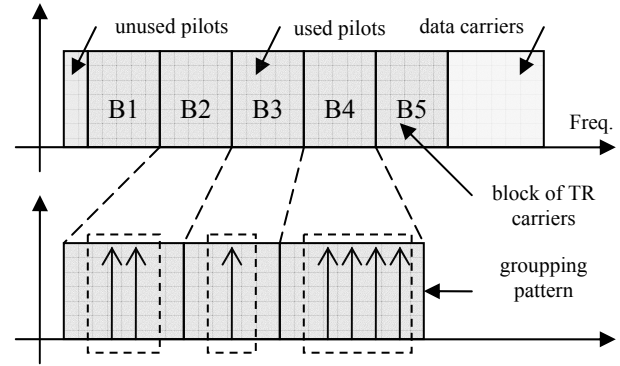


Figure 11. Grouping of TR subcarriers in blocks.

The proposed SBG-TR method, performs search of the optimal combination of vectors values which presents the lowest PAPR within each block, one-by-one. Once the vector values for a block are established, they remain fixed, the search being continued on the next block of non-data subcarriers.

Based on these aspects, the SBG-TR algorithm can be described by the following steps:

- 1) Get an OFDM frame with N data subcarriers, Q non-data subcarriers, T of them being used within the search algorithm.
- 2) Consider a set of M possible complex values for each vector within the selected T non-data subcarriers. In a generalized case, this set may be different for each subcarrier. However, for simplicity, in present work it is considered to be identical for each of these subcarriers.
- 3) Based on a given pattern, group the selected TR subcarriers in B blocks, the number of elements within each block being $K[j]$, where $j=1...B$.
- 4) Reset all non-data subcarriers to an initial state, composed by zero values.
- 5) For each of the B blocks, try all $M^{K[j]}$ combinations, the one presenting the smallest PAPR level for the equivalent time-domain signal representation being stored.
- 6) Optionally, the algorithm may be repeated for another grouping pattern.

The algorithm can be generalized, by considering different order for the TR blocks. The sequence of the block may be ascending, descending, or according with other patterns. Another possible extension of the presented algorithm may consider non-contiguous blocks. These approaches may be used to mix the TR subcarriers from the low frequency domain with those from the high frequency domain.

According with the approach used in this method, the extension of the search subspace is distributed along different parts from the set of TR subcarriers. The size of the search subspace extends with the increase of the number of subcarriers per block. A grouping pattern with fewer subcarriers per block reduces the search subspace accordingly. The particular case of one TR subcarrier per block reduces this algorithm to the original sequential TR method.

Another approach for applying a distributed extension of the search sub-space is to consider a conditioned backtracking algorithm. In this case the total number of backward steps is limited to a given threshold. The forward steps are done when the local gain for PAPR reduction is higher than a given threshold, too. The algorithm may be applied to entire set of TR subcarriers at once, or can be performed on subsets, as in case of the presented algorithm.

When the TR block follows after the ACE block, as Figure 1 indicates, the interfacing of these blocks has to be properly adapted.

Both PAPR reduction blocks have to operate on the same signal, in order to have same frequency spectrum, the non-data subcarriers used within TR block has to be available at the ACE block's input.

The ACE block performs a nonlinear signal processing, which will affect the non-data subcarriers as well. Because these subcarriers are not carrying any information, they have no ACE constraints as method requires for the constellation points of the data subcarriers. From the ACE perspective these non-data subcarriers have the optimal value for lowering PAPR.

Contrary, the TR block will change the values of these non-data subcarriers in order to search an OFDM alternative signal with a decreased PAPR. Because some of these subcarriers will provide no improvement from the PAPR reduction point of view, the initial value set of the ACE block has to be considered.

In order to make the proper adaptation, the TR constellation point set of each non-data subcarrier has to include the initial value obtained after previous signal processing performed by the ACE block.

III. THE CLIPPING METHOD

For analysis of the efficiency of the proposed hybrid technique, also a pure nonlinear method has been considered. This is the clipping method with frequency-domain filtering as presented in [18]. The block diagram of this method is presented in Figure 12. It consists in a zero padding block, an IFFT block, an effective clipping block, and a frequency domain block. For a frequency-domain input signal represented by a vector A_{in} with N elements $[a_0, \dots, a_{N-1}]$ and an oversampling factor p , the zero padding inserts $N(p-1)$ zeros in the middle of this vector, forming the new vector A_{zp} . The clipping block limits the amplitude of the time-domain signal to a given threshold. The resulted signal a_{clip} is then applied to the frequency domain filter where the output signal a_{out} is obtained.

The clipping ratio (CR) applied in this method is defined as ratio of the clipping level A to the root-mean-square power σ of the unclipped baseband signal, being described by the following expression:

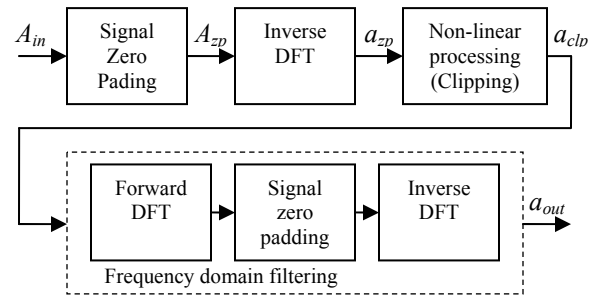


Figure 12. Clipping with filtering PAPR reduction method.

$$CR = 20 \cdot \log_{10} \left(\frac{A}{\sigma} \right). \quad (24)$$

The filtering block is composed by an FFT block, another zero padding block and an IFFT block. It is designated to reduce the out-of-band noise without distorting the in-band discrete signal.

IV. SIMULATION RESULTS

The MATLAB simulations have been performed for base-band signals with $N=128$ subcarriers using M-QAM and M-PSK modulations. The frequency-domain signal is extended with additional $Q=24$ no-data subcarriers. From this set, $T=12$ subcarriers are used for PAPR reduction by the TR method. The corresponding constellation consists in sets of $M=16$ points. For the reference clipping method, the simulation considers the clipping rate CR having some values in the range of 6-14 and the oversampling factor p set to 2.

For the OFDM signal spectrum computation, it was considered that the distance between two adjacent subcarriers is 0.2 MHz.

The results presented in this paper are obtained for OFDM frames with the repartition of non-data subcarriers as previously indicated in Figure 8, Figure 9, and Figure 10, with constellations of the pilot search space points identically with the constellations of the constellation used for data carriers.

These results consider various combinations of the POCS, SGP and CGP ACE methods with the sequential and SBG TR method.

The simulation results show that the proposed scheme improves the PAPR reduction in comparison with the use of only one of the component methods. The improvement for the case of POCS-ACE with sequential TR methods is highlighted in this section with three cases.

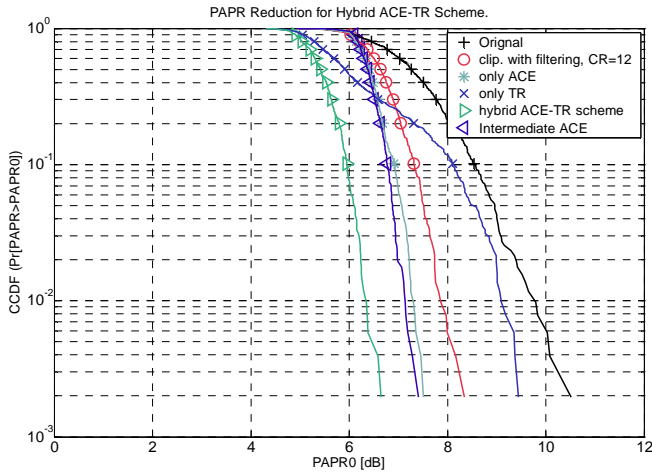


Figure 13. PAPR reduction using hybrid POCS ACE-TR method. Type I

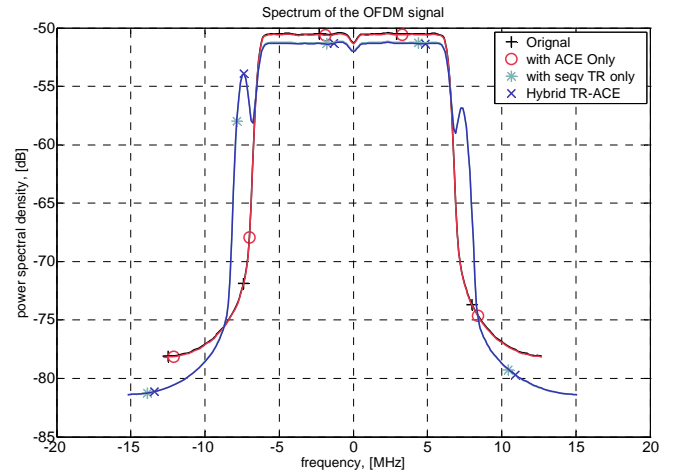


Figure 16. PSD of OFDM signal before/after PAPR reduction. Type I

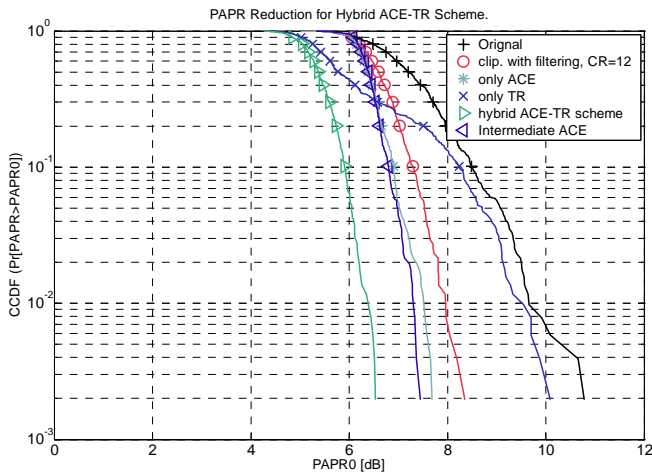


Figure 14. PAPR reduction using hybrid POCS ACE-TR method. Type II

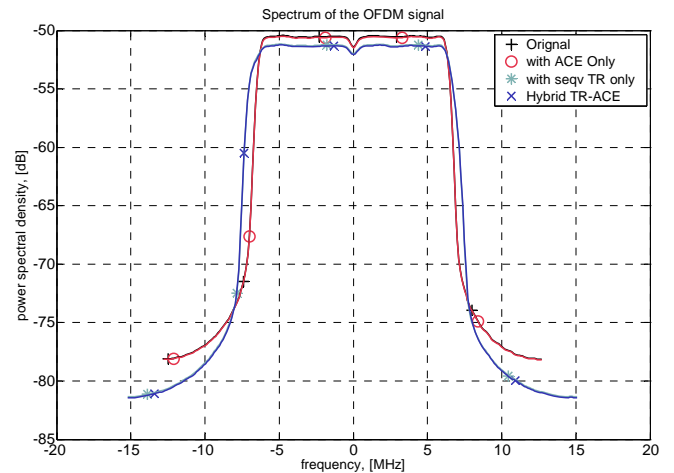


Figure 17. PSD of OFDM signal before/after PAPR reduction. Type II

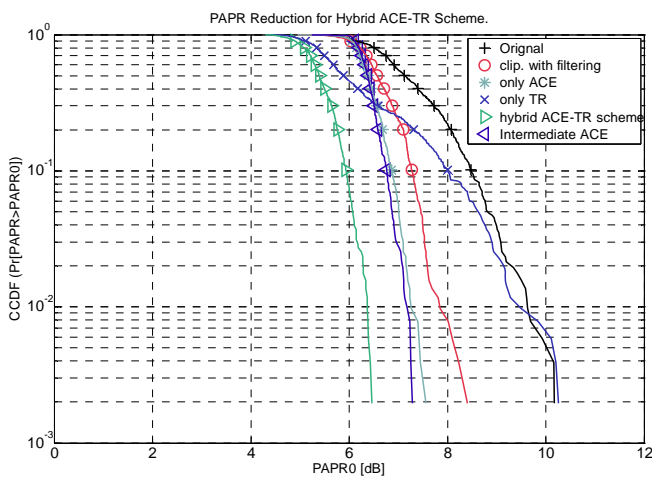


Figure 15. PAPR reduction using hybrid POCS ACE-TR method. Type III

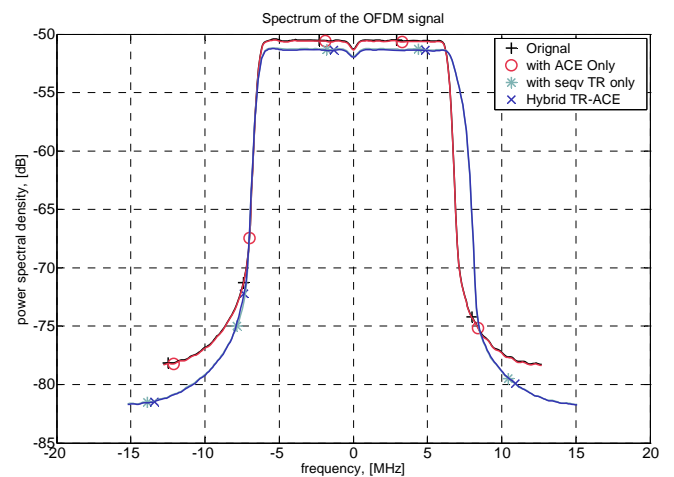


Figure 18. PSD of OFDM signal before/after PAPR reduction. Type III

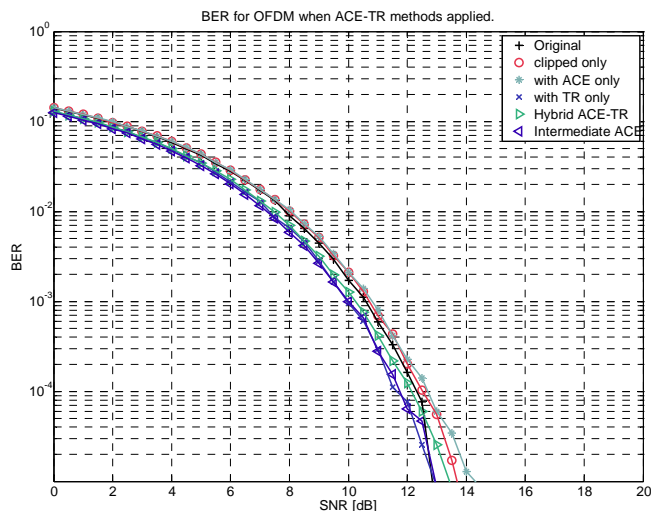


Figure 19. BER of OFDM signal before and after PAPR reduction.

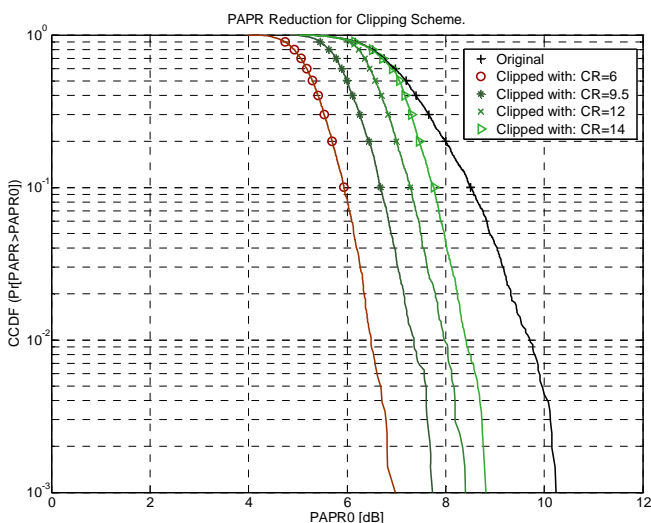


Figure 20. PAPR reduction using clipping method.

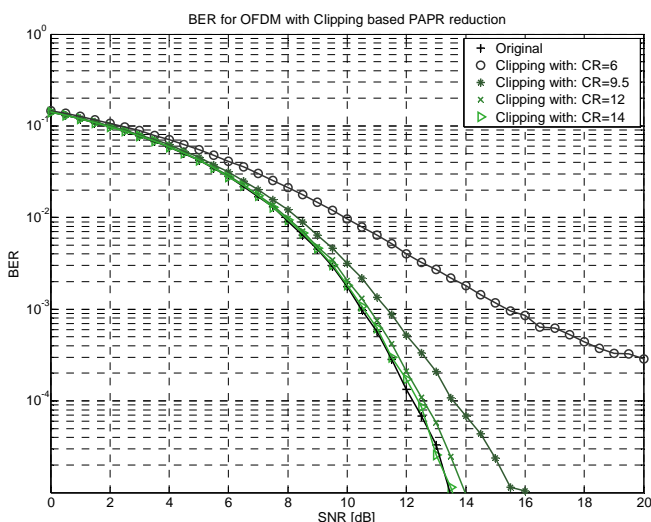


Figure 21. BER of OFDM signal before/after clipping.

In the first case, Figure 13 and Figure 16 indicate the PAPR reduction and signal's frequency spectrum when the OFDM frame has the non-data subcarriers configuration as presented in Figure 8.

In Figure 13, it can be observed that the ACE method performs a better PAPR reduction while the applied TR method obtains a lower PAPR reduction than the clipping at a ratio of $CR=12$. A slight difference can be observed between the ACE applied on the initial OFDM frame and the extended OFDM frame containing the reserved non-data subcarriers. The hybrid ACE-TR provides better PAPR reduction since it accumulates the effects from the two methods.

Due to the insertion of the additional non-data subcarriers on the both sides of the original spectrum, the obtained signal presents an increased bandwidth as indicated in Figure 16.

In the second case, Figure 14 and Figure 17 indicate the PAPR reduction and signal's frequency spectrum for the configuration shown in Figure 9.

Due to a different displacement of the non-data subcarriers, the TR method has a different efficiency for the PAPR reduction. Even if this method has smaller PAPR reduction, with the hybrid method still higher PAPR reduction is obtained. Also, this case presents a smaller increase of the bandwidth for the resulted OFDM signal than the one from the previous one.

In the third case, similarly, Figure 15 and Figure 18 indicate the same signal parameters when the non-data subcarriers are located as is shown in Figure 10.

For the PAPR reduction, this case is quite similar with the first one. The difference consists on the spectrum of the resulted signal, which has a slightly asymmetrical shape.

Figure 19 shows that the BER performance is slightly influenced by the proposed PAPR reduction technique, being better than in case of simple clipping.

For a better evaluation of the performance of the proposed method, the PAPR reduction and corresponding BER characteristic of the clipping method are presented in Figure 20 and Figure 21, respectively.

The simulations shown that, if smaller values for the clipping ratio are considered, the clipping method obtains comparable PAPR reduction as the hybrid method do. The drawback of this case is that the smaller CR values imply an increased signal distortion, and so a worst BER performance.

Therefore the presented simulation results shown that, in all these cases, the hybrid ACE-TR method provides better PAPR reduction than in case of use of only one component method. Additionally, compared with clipping, the combined technique presents no degradation of the BER performance.

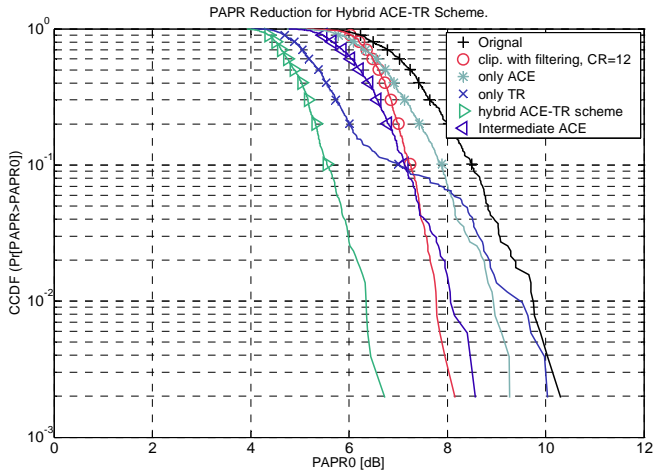


Figure 22. PAPR reduction using hybrid SGP ACE-TR method. Type I

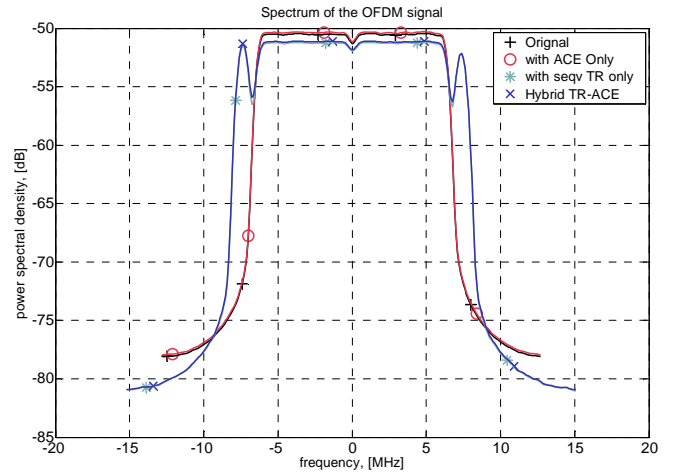


Figure 25. PSD of OFDM signal before/after PAPR reduction. Type I

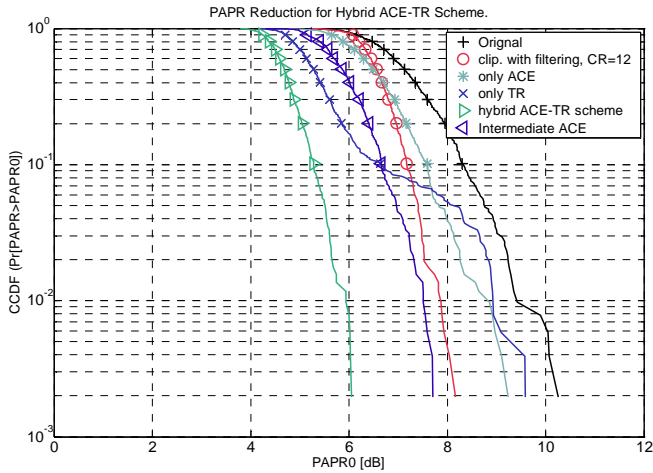


Figure 23. PAPR reduction using hybrid SGP ACE-TR method. Type II

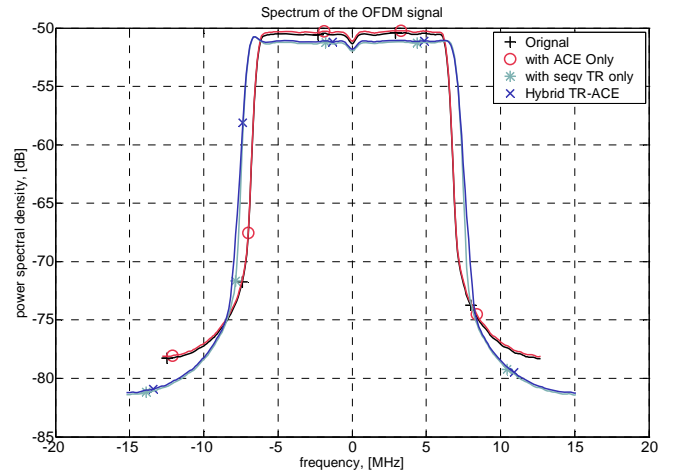


Figure 26. PSD of OFDM signal before/after PAPR reduction. Type II

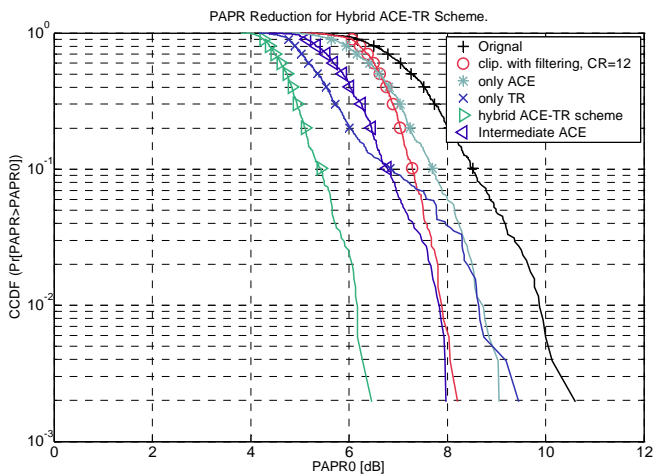


Figure 24. PAPR reduction using hybrid SGP ACE-TR method. Type III

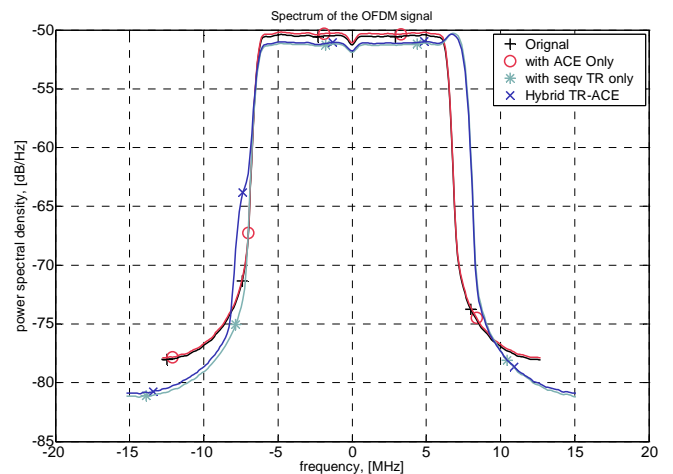


Figure 27. PSD of OFDM signal before/after PAPR reduction. Type III

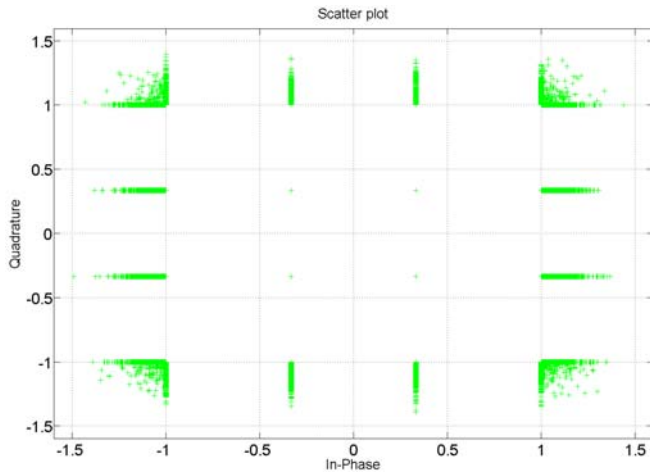


Figure 28. Constellation points dispersion plot in case of hybrid SGP ACE-SBG TR method.

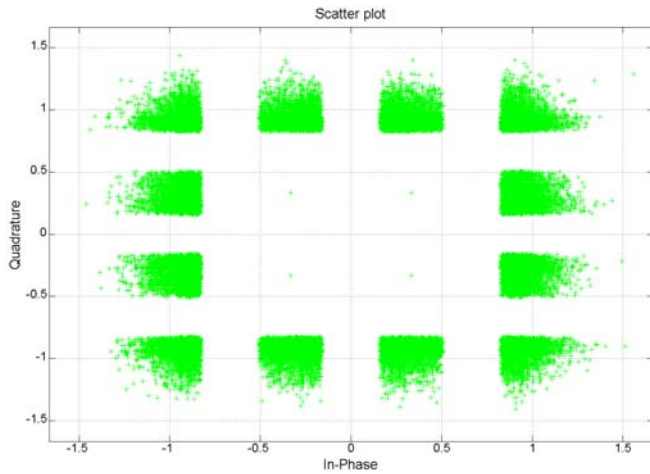


Figure 29. Constellation points dispersion plot in case of hybrid SGP ACE-SBG TR method.

Similar results are obtained when the hybrid scheme uses the SGP ACE and sequential block grouped TR methods. The simulation results are presented for the same non-data subcarrier displacements as presented before.

The used SGP ACE method is based on the approaching balancing according to relation (11) and is set to use 4 iterations per OFDM frame. The sequential block grouping TR method is configured to use 3 subcarriers per block.

The PAPR reduction and signal's frequency spectrum for the first case are presented in Figure 22 and Figure 25 respectively.

Compared with the previous situation, the ACE presents a similar performance like the clipping method. The difference is due to a stronger ACE constraint for constellation points, as presented in Figure 28. The TR schemes also provide a slight different result due simultaneous check of more TR subcarriers.

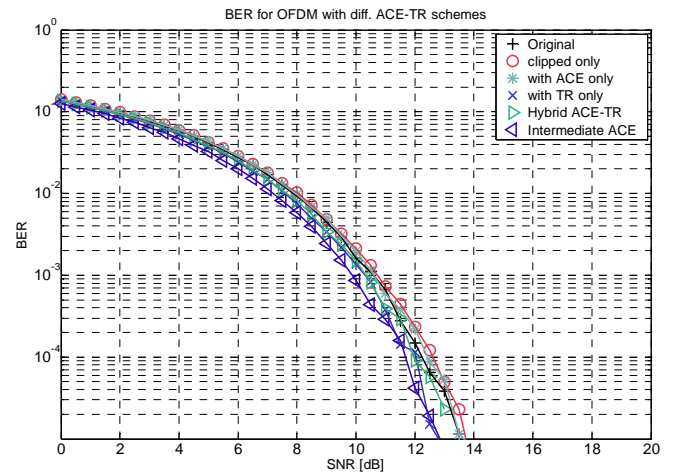


Figure 30. BER of OFDM signal before and after PAPR reduction in case of strength constellation condition.

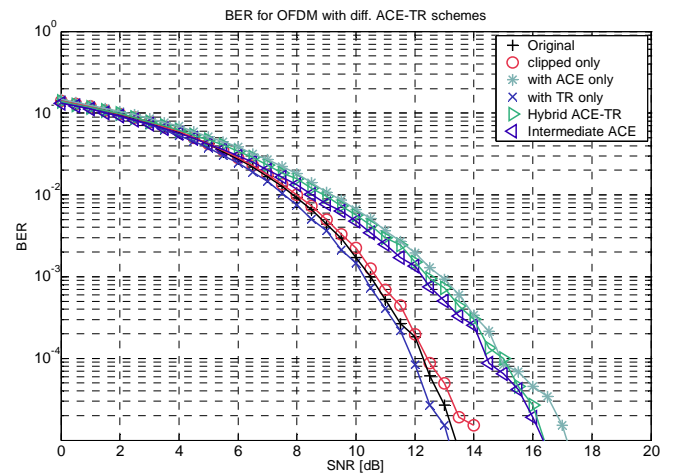


Figure 31. BER of OFDM signal before and after PAPR reduction in case of relaxed constellation condition.

The results for the second case, presented in Figure 23 and Figure 26 respectively, have the same characteristics. Compared with the previous hybrid scheme, in this case the ACE and TR performances are different, the PAPR reduction efficiency of a method being compensated by the other one.

The results for the third case are presented in Figure 24 and Figure 27 respectively. The good efficiency of the SBG TR method is reflected also in the spectral characteristic, where appearance of some non-data subcarriers is observable by the wider bandwidth.

The BER performance corresponding to these cases is shown in Figure 30.

When the ACE constraints become less restrictive, as presented in Figure 29, the PAPR reduction efficiency increases. The disadvantage in this situation is the higher BER degradation as presented in Figure 31.

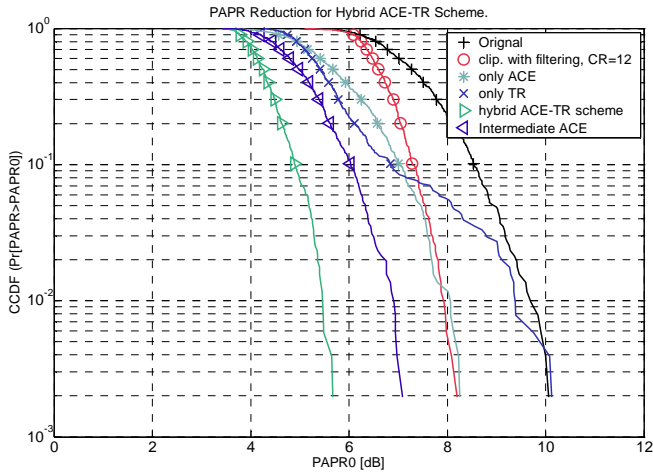


Figure 32. PAPR reduction using hybrid SGP ACE-TR method. Type I

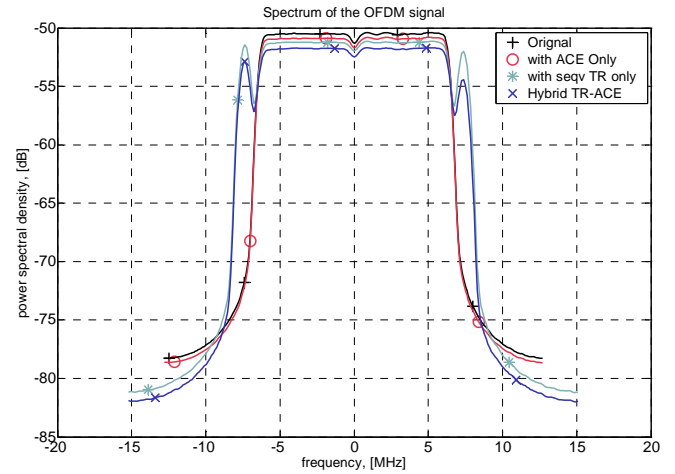


Figure 35. PSD of OFDM signal before/after PAPR reduction. Type I

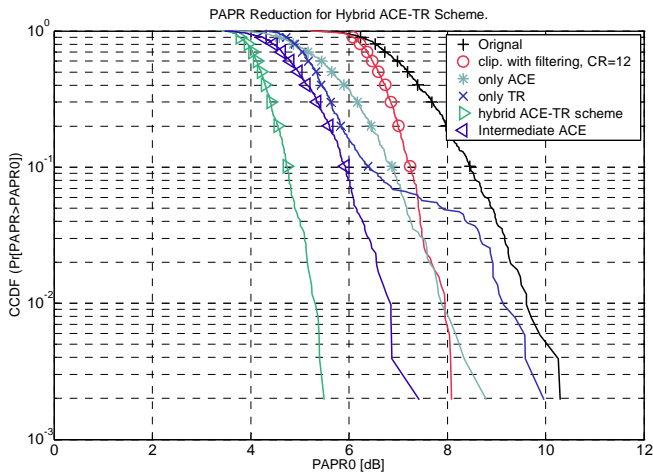


Figure 33. PAPR reduction using hybrid SGP ACE-TR method. Type II

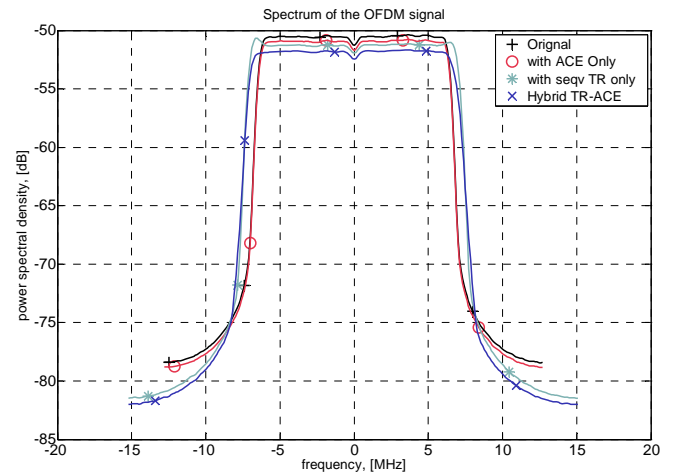


Figure 36. Spectr. of OFDM signal before/after PAPR reduction. Type II

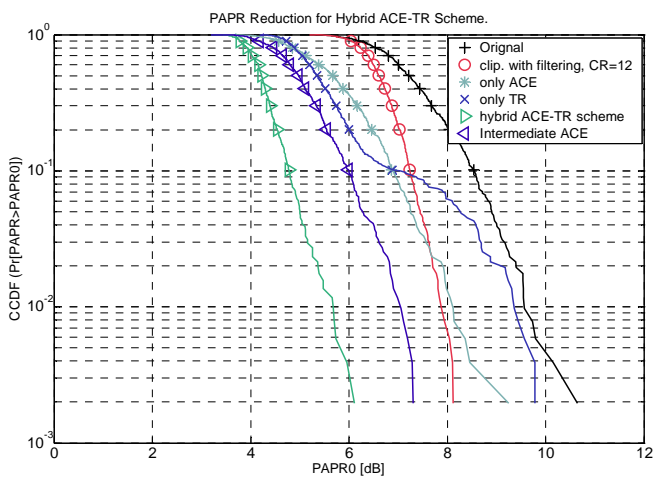


Figure 34. PAPR reduction using hybrid SGP ACE-TR method. Type III

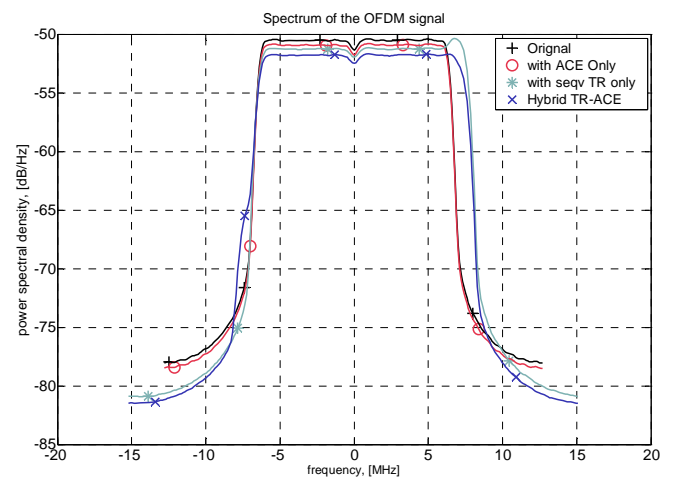


Figure 37. PSD of OFDM signal before/after PAPR reduction. Type III

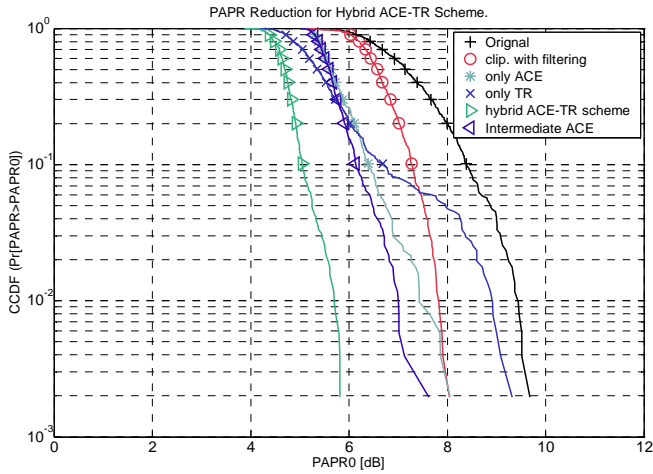


Figure 38. PAPR reduction using hybrid CGP ACE-TR method. Type I

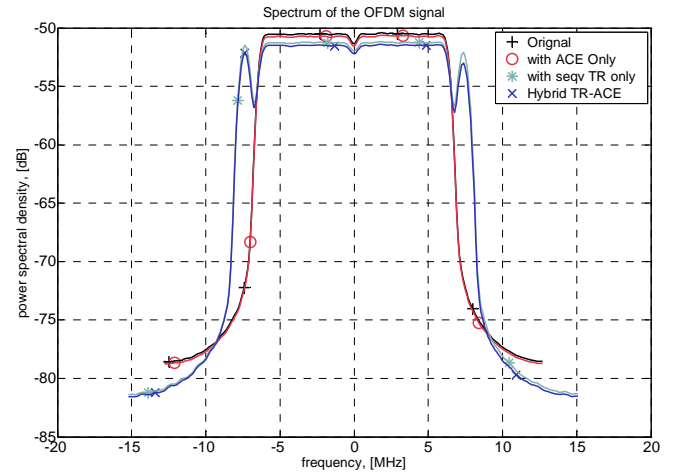


Figure 41. PSD of OFDM signal before/after PAPR reduction. Type I

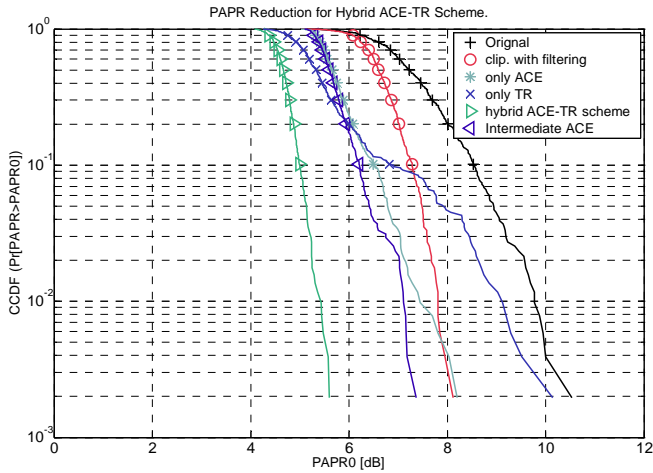


Figure 39. PAPR reduction using hybrid CGP ACE-TR method. Type II

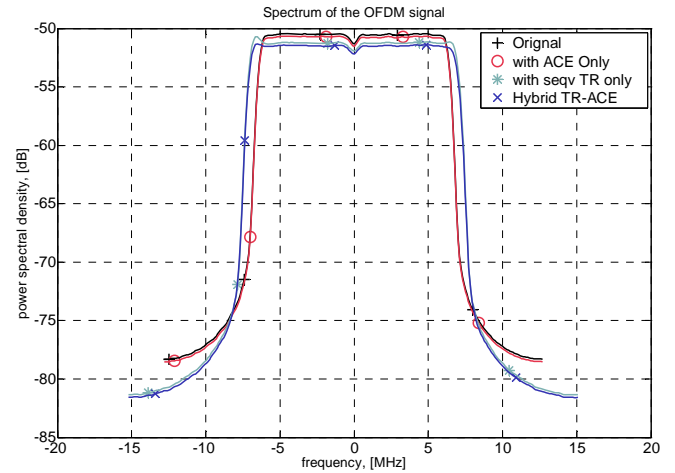


Figure 42. PSD of OFDM signal before/after PAPR reduction. Type II

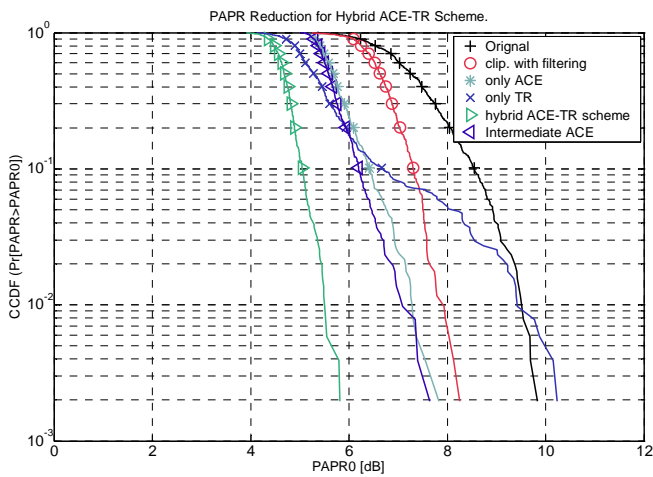


Figure 40. PAPR reduction using hybrid CGP ACE-TR method. Type III

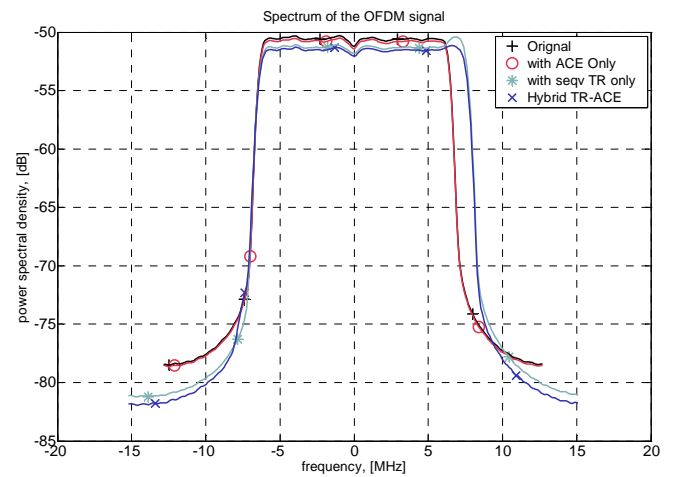


Figure 43. PSD of OFDM signal before/after PAPR reduction. Type III

The simulation results shown that for this relaxed constellation constraints, ACE component method provides better PAPR reduction efficiency.

The simulation results for PAPR reduction and spectral characteristic for the case with the non-data subcarriers displacement of type I, using the SBG ACE method are presented in Figure 32 and Figure 35, respectively. In this case the ACE method presents a better PAPR reduction efficiency compared with the referenced clipping, having a slight BER performance degradation.

Similar simulation results for PAPR reduction and spectral characteristic for the case with non-data subcarriers displacement of type II are presented in Figure 33 and Figure 36, respectively.

The next case, when the non-data subcarriers displacement of type III is used, is presented in Figure 34 and Figure 37, respectively.

A specific aspect of these cases is the slightly different maximal spectral amplitude. This is caused by the different results of the TR method due to the relaxed ACE constraints.

The simulations results consider the new CGP-ACE derivate method as well. For this scheme, the simulations consider 4 iterations, with a fixed step size of 0.7 for the clipping delta signal.

The corresponding PAPR reduction and signal's frequency spectrum for the considered repartition for the non-data subcarrier are presented in the next diagrams as followings: Figure 38 and Figure 41 for the type I, Figure 39 and Figure 42 for the type II and Figure 40 and Figure 43 for type III, respectively.

The simulation results show that the CGP-ACE method presents similar PAPR reduction performance as the SGP-ACE method. Due to its different approach, the time-domain samples have another statistical distribution. The corresponding frequency-domain signal changes accordingly, therefore a slightly different PAPR reduction of the TR method will be obtained.

Therefore, the presented simulation results show that the hybrid method presents a better PAPR reduction also when the SGP ACE and CGP ACE are considered. The new SBG TR method presents a different performance, which is strongly dependent by the used block grouping pattern.

The BER performance depends by the ACE constraints applied on each iteration.

The computational complexity of the algorithm of the hybrid technique is given by the sum of the computational complexity of the component methods. The total amount of operations depends by the used ACE and TR derivate methods.

In case of POCS method, the ACE block performs one IFFT, one clipping, one FFT and one vector shift per iteration. For the presented simulations, we have limited the number of iterations in the ACE block to one, therefore the amount of operations for this block is $O(2 + 2 \cdot N \cdot \log_2(N))$.

In case of the SGP ACE and CGP-ACE, the number of operations increases due to the computing of the approximate balancing factor and signal companding. Therefore the amount of operations for these ACE blocks is of $O(C \cdot (B + 2 \cdot N \cdot \log_2(N)))$, where C is the number of cycles, and B is the number of operations needed to compute approximate balancing factor or companded signal. For the considered SGP and CGP ACE methods, the additional amount of operations B can be approximated to $4 \cdot N$.

In case of the sequential TR method, the PAPR reduction block performs one change for a pilot subcarrier and one IFFT per iteration. Considering the applied algorithm and the size of the search space, a complete operation requires $O(M \cdot T \cdot (1 + N \cdot \log_2(N)))$ computations.

In practice, the amount of operations can be reduced if the time-domain signal corresponding to each single non-data subcarrier is pre-computed and stored in a nonvolatile memory. In this case the amount of operations is reduced to $O(M \cdot T + N \cdot \log_2(N))$.

In case of the sequential block grouping TR method, where for each block, all possible combinations are evaluated, and the total amount of operations increases. When the method uses B blocks, the number of carriers per block is $K = T / B$, therefore the total amount of operations is: $O(B \cdot M^K \cdot (1 + N \cdot \log_2(N)))$.

Based on these expressions, it can be observed that the amount of operations required by the hybrid method is bigger than the number of operations required by other PAPR reduction techniques and depends by number of data subcarriers and the size of the search space used by the TR block.

V. CONCLUSION AND FUTURE WORK

In this paper, which represents a development of [1], we proposed a new PAPR reduction technique based on the combination of different active constellation extension methods with different tone reservation methods.

The paper presents the ACE and TR algorithms used within the hybrid technique. The interfacing of the two PAPR reduction blocks is also explained. Besides the well known POCS and SGP ACE derivatives, the new CGP ACE was proposed. Also for the TR technique, the new SBG-TR derivate method was proposed. These new PAPR reduction methods permit the development of the analysis presented in the original work.

The simulation results, which enhance the results reported in original work, show that the hybrid scheme realizes higher PAPR reduction for various OFDM frame formats. Similar results for PAPR reduction have been obtained for the case when TR block precedes the ACE block.

The ACE and TR methods have various derivatives, bringing different efficiency and performance. The ACE method may be implemented using different constellation restrictions, obtaining different PAPR reduction levels and BER performances. The TR method may use different set of values for the non-data subcarriers. Depending on this set, its computation complexity and PAPR reduction strength may

significantly vary. In case of the proposed SBG TR method, the performance depends by the used block grouping pattern and pilot subcarrier displacement, too.

Compared with other PAPR reduction methods like SLM and PTS, the ACE and TR methods presents a variable PAPR reduction efficiency depending by selected parameters. In many cases their PAPR reduction gain decreases after several iterations.

Therefore the SLM and PTS methods may present increased PAPR reduction, but have the disadvantage of an increased amount of computation complexity due to expended search space.

In future work, we will consider different ACE constraints and TR schemes with different numbers and various sets of values for the non-data carriers.

REFERENCES

- [1] V. Cuteanu and A. Isar, "PAPR Reduction of OFDM Signals using Active Constellation Extension and Tone Reservation Hybrid Scheme", The Eight Advanced International Conference on Telecommunications, pp. 156-163, June 2012.
- [2] V. Cuteanu and A. Isar, "PAPR Reduction of OFDM Signals using Partial Transmit Sequence and Clipping Hybrid Scheme", The Eight Advanced International Conference on Telecommunications, pp. 164-171, June 2012.
- [3] V. Cuteanu and A. Isar, "PAPR Reduction of OFDM Signals Using Selective Mapping and Clipping Hybrid Scheme", The 20th European Signal Processing Conference, pp. 2551-2555, August 2012.
- [4] V. Cuteanu and A. Isar, "Hybrid PAPR Reduction Scheme with Selective Mapping and Tone Reservation", International Conference on Applied Electronics, pp. 55-58, September 2012.
- [5] V. Cuteanu and A. Isar, "PAPR reduction of OFDM signals using hybrid clipping-companding scheme with sigmoid functions", International Conference on Applied Electronics, pp. 75-78, September 2011.
- [6] V. Cuteanu and A. Isar, "PAPR Reduction Scheme with Clipping and Quasilinear Sigmoid Compression Functions", International Conference on Applied Electronics, pp. 59-64, September 2012.
- [7] S. Muller, R. Bauml, R. Fischer, and J. Huber, "OFDM with reduced peak-to-average power ratio by multiple signal representation", Annals of Telecommunications, vol. 53, pp. 58-67, February 1997.
- [8] L. J. Cimini Jr. and N. R. Sollenberger, "Peak-to-average power ratio reduction of an OFDM signal using partial transmit sequences", IEEE Commun. Lett., vol. 4, no. 3, pp. 86-88, March 2000.
- [9] Y.Z. Jiao, X.J. Liu, and X.A. Wang, "A Novel Tone Reservation Scheme with Fast Convergence for PAPR Reduction in OFDM Systems", Consumer Communications and Networking Conference, pp. 398-402, January 2008.
- [10] L. Wang and Y. Cao, "Improved SLM for PAPR Reduction in OFDM Systems", International Workshop on Intelligent Systems and Applications, pp. 1-4, May 2009.
- [11] L. Wang and J. Liu, "PAPR Reduction of OFDM Signals by PTS With Grouping and Recursive Phase Weighting Methods", IEEE Transactions on Broadcasting, vol. 57, no. 2, pp. 299-306, June 2011.
- [12] S. Yoo, S. Yoon, S.Y. Kim, and L. Song, "A novel PAPR reduction scheme for OFDM systems: selective mapping of partial tones (SMOPT)", IEEE Transaction on Consumer Electronics, vol. 52, no. 1, pp. 40-43, February 2006.
- [13] E. Bouquet, S. Haese, M. Drissi, C. Moullec, and K. Sayegrih, "An innovative and low complexity PAPR reduction technique for multicarrier systems," Proc. 9th European Conference on Wireless Technology, pp. 162-165, September 2006.
- [14] C. L. Wang, Y. Ouyang, and H. C. Chen, "A low-complexity peak-to-average power ratio reduction technique for OFDM-based systems", Proc. 60th IEEE Vehicular Technology Conference, vol. 6, pp. 4380-4384, September 2004.
- [15] B.S. Krongold and D. L. Jones, "PAPR Reduction in OFDM via Active Constellation Extension", IEEE Transactions on Broadcasting, Vol. 49, No. 3, pp. 258-268, September 2003.
- [16] A. Kliks and H. Bogucka, "Improving Effectiveness of the Active Constellation Extension Method for PAPR Reduction in Generalized Multicarrier Signals", SpringerLink, Wireless Personal Communication, vol. 61, no. 2, pp. 323-334, May 2010.
- [17] M. Malkin, B. Krongold, and J. M. Cioffi, "Optimal constellation distortion for PAPR reduction in OFDM systems", IEEE 19th Int. Symposium on Personal, Indoor and Mobile Radio Communications, pp. 1-5, September 2008.
- [18] J. Armstrong, "New OFDM Peak-to-Average Power Reduction Scheme", Proc. of IEEE Vehicular Technology, pp. 756-760, May 2001.
- [19] M. Deumal, C. Vilella, J. L. Pijoan, and P. Bergada, "Partially Clipping (PC) Method for the Peak-to-Average Power Ratio (PAPR) Reduction in OFDM", IEEE Int. Symposium on Personal, Indoor and Mobile Radio Communications, vol. 1, pp. 464-468, September 2004.
- [20] X. Wang, T. T. Tjhung, C. S. Ng, and A. A. Kassim, "On the SER Analysis of A-Law Companded OFDM System", in Proc. Global Telecommunication Conference, vol. 2, pp. 756-760, December 2000.
- [21] T. Moazzeni, H. Selvaraj, and Y. Jiang, "A Novel Multi-Exponential Function-based Companding Technique for Uniform Signal Compression over Channels with Limited Dynamic Range", Intl. Journal of Electronics and Telecommunications, Vol. 56, No. 2, pp. 125-128, June 2010.
- [22] X. Huang, J. Lu, J. Zheng, and J. Gu, "Piecewise-scales transform for the reduction of PAPR of OFDM signals", IEEE Global Telecommunications Conference, vol. 1, pp. 564-568, November 2002.

Application of Control Theory to a Commercial Mobile Service Support System

Payam Amani^{a,1}, Bertil Aspernäs^c, Karl Johan Åström^b, Manfred Dellkrantz^b, Maria Kihl^a, Gabriela Radu^a,

Anders Robertsson^b, and Andreas Torstensson^c

^aDept. of Electrical and Information Technology, Lund University, Sweden

^bDept. of Automatic Control, Lund University, Sweden

^cEricsson AB, Karlskrona, Sweden

{payam.amani, maria.kihl}@eit.lth.se, {manfred.dellkrantz, andersro, kja}@control.lth.se,
luminita.radu@gmail.com, bertil.aspernas@telia.com, andreas.torstensson@ericsson.com

Abstract—The Mobile Service Support system (MSS), which Ericsson AB develops, handles the setup of new subscribers and services into a mobile network. Experience from deployed systems show that traffic monitoring and control of the system will be crucial for handling overload situations that may occur at sudden traffic surges. In this paper we identify and explore some important control challenges for this type of systems. Further, we present analysis and experiments showing some advantages of proposed solutions. First, we develop a load-dependent server model for the system, which is validated in testbed experiments. Further, we propose a control design based on the model, and a method for estimation of response times and arrival rates. The main contribution of this paper is that we show how control theory methods and analysis can be used for commercial telecom systems. Parts of our results have been implemented in commercial products, validating the strength of our work.

Keywords— Performance management; telecommunication systems; queuing theory; control theory; database servers; admission control; Kalman filters

I. INTRODUCTION

Resource management of computer systems, which has gained increased attention during recent years, was explored already in the late 60's [1][2]. It is an essential mechanism to handle load disturbances such as traffic surges and changes in user behavior. Poorly managed resources can severely degrade the performance of a system with potentially large financial consequences.

The work presented in this paper is motivated by a commercial Mobile Service Support System (MSS), developed and produced by Ericsson AB. Mobile Service Support Systems are used by the network operators for all processing regarding new subscribers and services in the network. Each new subscriber or service requires processing and data storage in several network nodes. The systems are in general multi-tier systems, implemented as distributed server clusters, where web and application servers process the incoming requests and database servers are used for data

storage. The resource management of these systems, based on measurements of the system states such as actual utilization and response times, is crucial for the optimization of operation cost and the guarantee of service level agreements during load surges, for example during marketing campaigns or various events.

Therefore, the challenge is how to control system performance while providing guarantees on convergence and disturbance rejection. The solution is based on *dynamic control schemes*, which monitors the systems and provides actions when needed. Several types of resource-management mechanisms have been proposed and evaluated in the literature. In larger computer systems, *load balancing* is performed in order to distribute the demand for resources uniformly over a number of resource units (computers, CPUs, memory, etc.), thus avoiding the case that among the nodes with similar functionalities some are under-utilized while others are overloaded [3][4]. During overload periods, when more resources are requested than are available, *admission control* mechanisms reduce the load to the system by blocking or delaying some of the requests [5][6][7][8]. For Internet applications, virtualized server systems can be used to divide physical resources into a number of separated platforms where different web applications are allowed to operate without affecting one another. *Dynamic resource allocation* between the virtualized platforms serves as a new and easy way to perform resource optimization on web server systems [9][10][11]. In the last years, the field of *power and energy management* has become important. Large software systems have high energy consumption, which means that dynamic resource optimization of these systems may considerably lower the operating costs for the network operators [12][13][14][15].

However, all optimization techniques require accurate performance models of the involved computing systems. The operation region is mainly high traffic load scenarios, which means that the computing systems show non-linear dynamics that needs to be characterized accurately [16]. A software system is basically a network of queues, as examples, the CPU ready queue, semaphore queues, socket queues, and I/O device queues, which store requests in waiting of service in the processors. Therefore, queuing models can be used when

¹ This work represents the outcome of a long-term collaboration between Lund University and Ericsson AB and the contributors are listed in alphabetic order.

describing the dynamic behavior of server systems [1][17][18][19].

The concept of Load-Dependent Server (LDS) models, in which the response time of the jobs in the system is a function of the service time of the jobs and current number of jobs waiting to be served has, to the best of our knowledge, firstly been introduced in [20]. In [20][21][22], standard benchmarks were used for workload generation and also regression models to capture the system dynamics. In [23], a queuing network model which represents the load dependent behavior of the LDS was presented and validated with simulations. In [24], a theoretical analysis of the D/G/1 and M/G/1 models with load dependency assumptions was presented.

In this paper, we investigate solutions to some important control challenges identified for the commercial MSS developed by Ericsson AB. We present a load-dependent server model, which is validated in experiments. The model has been previously published in [25]. Further, we extend [25] by proposing and validating an admission control mechanism based on a load-adaptive controller. A modified version of the controller has been implemented in the Ericsson product. Finally, we show how extended Kalman filters can be used for estimating the response times and arrival rates in the system.

The paper is organized as follows. In Section II, the Ericsson product is described and the control challenges identified for the system are presented. In Section III, the testbed used for some of the experiments is described. In Section IV, the load-dependent server model is presented and validated. In Section V, the load-adaptive controller is presented and experiments validating its performance are described. In Section VI, our work on response time estimation based on extended Kalman filters is presented. Finally, in Section VII, some conclusions are presented.

II. SYSTEM AND PROBLEM DESCRIPTION

The Mobile Service Support system (MSS), which Ericsson AB develops, handles the setup of new subscribers and services into a mobile network. It presents to the operator and its business support systems a unified middleware where complex functions, such as setting up a new subscriber or modifying services for an existing subscriber, can be easily invoked. The software architecture is complex with several layers and distributed infrastructures, which means that specific parts of the system will not have complete knowledge of the interactions among other parts of the system.

A. System architecture

The system architecture is illustrated in Figure 1. One request to the MSS from an upstream system normally results in a number of requests downstream out on the mobile network to several different network elements (NEs). A network element is usually a database storing subscriber and service data, for example, the Home Location Register (HLR). A user id, which needs to be fetched from one database, needs to be supplied in a query to another database to get the system consistent.

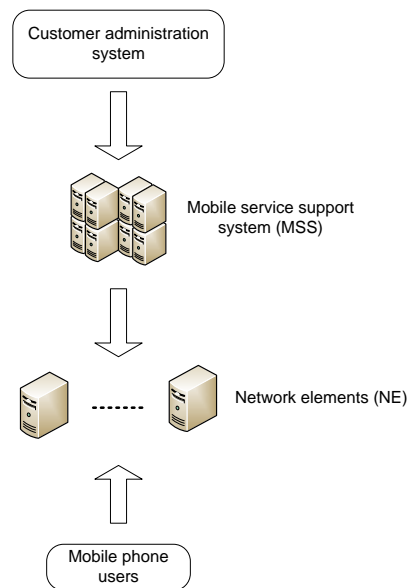


Figure 1. Mobile service support system (MSS)

In parallel to the changes and setups that the MSS performs, the network is also used by the end users. Services being set up by the MSS are queried by base stations and other systems requiring that information. In respect to the MSS, this traffic can be considered as unknown background traffic, in contrast to the known traffic flowing through the MSS.

B. Control challenges

The experience from deployed Ericsson systems shows that there can be problems with overload in the NEs. The measurable load arriving from the MSS and the unknown (not directly measurable) load arriving from mobile users may interfere with each other, creating a race for resources that may lead to overload in a NE. When one NE becomes overloaded and unresponsive, this may result in the entire transaction requiring rollback to avoid in-consistencies in the network. Such a rollback may require manual work which is of course costly for the operator.

To protect against such situations, traffic monitoring and control are crucial. In cooperation with Ericsson AB, some important control challenges have been identified for this type of system. These challenges are described below. In the following sections our collaborative work on these challenges will be presented. The models and control designs are based on response times, as this metric is rather easily measurable in the real system and because the response times can be mapped to the load status of the controlled system using the proposed model.

1) Performance models

The first challenge is to design a performance model for the NEs, since good control designs are based on sufficiently accurate system models. The model should capture the dominant load dynamics of the NEs. Most service performance metrics such as response times and service rates depend on queue state dynamics, which means that queue models are suitable for these systems.

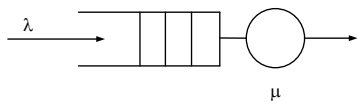


Figure 2. M/M/1 model

For the objective of performance control, simple models, such as single server queues, are often preferred. The model should only capture the dominating load dynamics of the system, since a well-designed control system can handle many model uncertainties [26].

The classical M/M/1 model, where a single-server queue processes requests that arrive according to a Poisson process with exponential distributed service times, see Figure 2, has been shown to accurately capture the response time dynamics of a web server system [27]. However, experience from deployed systems and lab measurements have shown that databases may not have M/M/1 dynamics [28]. Therefore, other models are required that more accurately captures the dynamics of database servers.

2) Admission control in MSS

The NEs are loaded by two traffic sources, the measurable traffic coming to the MSS and the unknown (unmeasurable) traffic coming from the mobile users, as illustrated in Figure 3. The average arrival rates can be denoted as λ for the measurable traffic and λ_u for the unknown traffic. Overload in the NEs can be detected by monitoring the response time of requests sent to each node. When the average requests' response times exceed some threshold, the MSS can classify the involved NE as overloaded and thereby start actions to lower the arrival rate to that particular NE, in order to achieve an acceptable arrival rate, denoted as λ_c . Therefore, the second control challenge is to design an admission control scheme that can handle the unknown traffic at the NEs and further can handle the time varying mean measured traffic rates experienced in the systems.

3) Monitoring and estimation

One of the problems when designing control mechanisms in these types of systems is the lack of performance information. The designed protocols basically provide no means of control communication between the MSS and the NEs that can be used by a control system. Therefore, the third control challenge that has been identified is the design of monitoring and estimation mechanisms that could help in the design of, for example, an admission control scheme. The estimation scheme can be used as feed-forward control in the control system, and thereby improving the performance of the control system compared to when only using feedback control. In collaboration with Ericsson AB, some preliminary work on the application of extended Kalman filters for load estimation have been started for systems as in Figure 3.

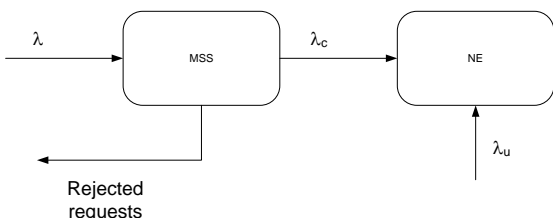


Figure 3. Load at the NEs

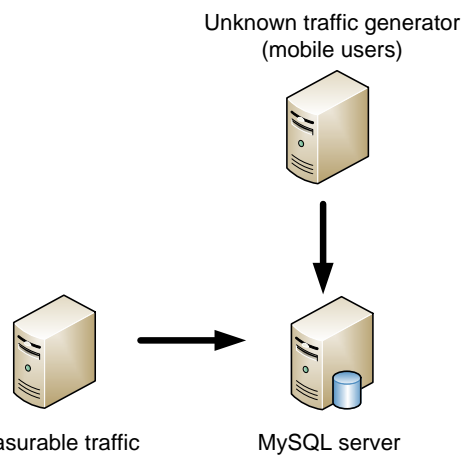


Figure 4. Testbed for the experiment.

III. TESTBED

To validate some of the proposed solutions, we have performed a series of experiments in our server lab. We developed a MSS testbed with two traffic generators, one for the measurable traffic and one for the unknown traffic, and a MySQL 5.1.41 database server as depicted in Figure 4. The computers were connected to a local 100 Mbit/s Ethernet network.

The traffic generators were implemented in Java, using the JDBC MySQL connector, and they were executed on computers with an AMD Phenom II X6 1055T Processor at 2.8 GHz and 4 GB main memory. The operating system was Ubuntu 10.04.2 LTS. The traffic generators use 200 working threads and generate MySQL queries according to a Poisson process with average rate λ and λ_u queries per second. Both traffic generators were validated in order to guarantee that they were not a bottleneck in the experiments.

The database server has several relations with the same structure but with different number of tuples. The maximum number of allowed concurrent connections is set to 100. The structure of the relations comes from the Scalable Wisconsin Benchmark [29] with 10 million tuples. Two basic types of queries are used, SELECT (read) and UPDATE (write).

The queries look like this:

```
SELECT * FROM <relation> WHERE unique1=?;
UPDATE <relation> SET unique2=? WHERE unique1=?;
```

The question marks are replaced with uniformly distributed random numbers from zero to ten million.

IV. PERFORMANCE MODELS

In this section, we focus on the modeling aspects of database servers. The objective is to develop a performance model for the database server that captures the dynamics during high loads. The performance model can be used in resource optimization schemes, as admission control systems, in order to maximize the throughput of the database server, while keeping some latency constraints. One of the challenges for these database servers is that they have a write-heavy workload, which means that the CPU is not the bottleneck during high loads. This means that previous work on

performance modeling of server systems may not be applicable since they assume CPU-intensive workload.

A. M/M/m model with load dependency (M/M/m-LDS)

We propose to add load-dependency to an M/M/m system. In all load-dependent server models, the service time for a request will be dependent on the number of concurrent requests in the system. This load-dependency will model effects of the operating system, memory use, etc., which may cause service degradation when there are many concurrent jobs in a computing system [22]. In the experiment section, we will show that the M/M/m-LDS model accurately captures the behavior of various database workload.

The properties of the load dependent M/M/m model (M/M/m-LDS) are set by an exponential distributed base processing time, $x_{base} = 1/\mu$, and a dependency factor, f . When a request enters the system, it gets the base processing time x_{base} assigned to it. A single request in the system will always have a processing time of x_{base} . Each additional request inside the system increases the residual work for all requests inside the system (including itself) by a percentage equal to the dependency factor f . When a request leaves the system all other requests have their residual work decreased by f percent again. This means that if n concurrent requests enter the system at the same point, they will all have a processing time of

$$x_s(n) = x_{base} \cdot (1+f)^{n-1} \tag{1}$$

A special case is when $f = 0$. It means that there is no load dependency, and all requests will have processing time x_{base} .

The system can process a maximum of m concurrent requests at each time instance. Any additional request will have to wait in the queue. New requests arrive according to a Poisson process with average rate λ .

Therefore, the system can be modeled as a Markov chain as illustrated in Figure 5.

The average service rate of the system depends on the number of concurrent requests in the system, k , derived as follows:

$$\mu_k = \begin{cases} \frac{k\mu}{(1+f)^{k-1}} & \text{if } 0 < k < m \\ \frac{m\mu}{(1+f)^{m-1}} & \text{if } k \geq m \end{cases} \tag{2}$$

By solving the balance equations, stationary probability distribution of existence of k concurrent requests in the system is calculated as below:

$$\pi_k = \begin{cases} \frac{\left(\frac{\lambda}{\mu}\right)^k}{k!} (1+f)^{\frac{k(k-1)}{2}} \pi_0 & \text{if } 0 < k < m \\ \frac{\left(\frac{\lambda}{\mu}\right)^k}{m^{k-m} \cdot m!} (1+f)^{\frac{(m-1)(k-m)}{2}} \pi_0 & \text{if } k \geq m \end{cases} \tag{3}$$

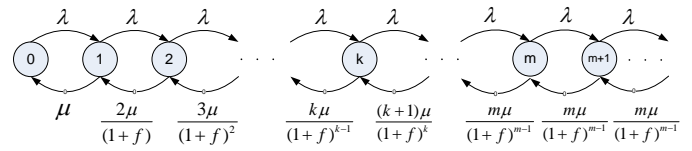


Figure 5. Illustration of M/M/m-LDS model as a Markov chain.

As the sum of the probabilities of all possible states equals to one, π_0 can be derived as follows:

$$\sum_{k=0}^{\infty} \pi_k = 1 \rightarrow \pi_0 = \frac{1}{1 + \sum_{k=1}^{m-1} \frac{\left(\frac{\lambda}{\mu}\right)^k}{k!} (1+f)^{\frac{k(k-1)}{2}} + \frac{\mu \left(\frac{\lambda}{\mu}\right)^m (1+f)^{\frac{m(m-1)}{2}}}{(m-1)! (\mu m - \lambda (1+f)^{m-1})}} \tag{4}$$

The stability condition in this case is

$$\frac{\lambda}{\mu m} (1+f)^{m-1} < 1 \tag{5}$$

The average number of requests in the system, N , can be calculated as below:

$$N = \sum_{k=1}^{\infty} k \cdot \pi_k = N_1 + N_2$$

$$N_1 = \sum_{k=0}^{m-1} \frac{\left(\frac{\lambda}{\mu}\right)^k}{(k-1)!} (1+f)^{\frac{k(k-1)}{2}} \pi_0$$

$$N_2 = \frac{\left(\frac{\lambda}{\mu}\right)^m (1+f)^{\frac{m(m-1)}{2}} (\mu m^2 - \lambda (m-1)(1+f)^{m-1}) \mu}{(m-1)! (\mu m - \lambda (1+f)^{m-1})^2} \pi_0 \tag{6}$$

Finally by means of Little's theorem [30], the average time each request spends in the system, T , can be derived as follows.

$$T = \frac{N}{\lambda} \tag{7}$$

B. M/M/m/n model with load dependency (M/M/m/n-LDS)

In case that the queue is limited to n positions, the probability for an empty system, π_0 , can be determined as follows. This queuing system is named as M/M/m/n-LDS.

$$\pi_0 = \frac{1}{I + II + III}$$

$$I = 1 + \sum_{k=1}^{m-1} \frac{\left(\frac{\lambda}{\mu}\right)^k (1+f)^{\frac{1}{2}k(k-1)}}{k!}$$

$$II = \frac{(1+f)^{\frac{1}{2}m^2 + \frac{1}{2}m + mn - n - 1} \lambda^{n+m+1}}{m^n \mu^{n+m} m! (\lambda (1+f)^{m-1} - \mu m)}$$

$$III = - \frac{(1+f)^{\frac{1}{2}m(m-1)} \lambda^m}{\mu^{m-1} (m-1)! (\lambda (1+f)^{m-1} - \mu m)}$$

$$\tag{8}$$

Further, the average number of requests in the system is as follows:

$$\begin{aligned}
 N &= N_1 - N_2 \\
 N_1 &= \sum_{k=0}^{m-1} \frac{k \left(\frac{\lambda}{\mu}\right)^k (1+f)^{\frac{1}{2}k(k-1)} \cdot \pi_0}{k!} \\
 N_2 &= \frac{\mu(1+f)^{\frac{1}{2}m^2 - \frac{1}{2}m - 1}}{m^{m-1}(-\lambda(1+f)^{m-1} + \mu m)} \cdot \frac{N_{2_{d1}} + N_{2_{d2}} - N_{2_{d3}}}{N_{2_{d1}} + N_{2_{d2}} + N_{2_{d3}}} \\
 N_{2_{d1}} &= -\lambda(n+m)(1+f)^{\left(\frac{1}{2}m^2 + \frac{3}{2}m + mn - n - 1\right)} \left(\frac{\lambda}{\mu}\right)^{n+m+1} \left(\frac{1}{m}\right)^{n+1} \\
 N_{2_{d2}} &= \left(m(1+f)^m \mu(n+m+1)(1+f)^{\left(\frac{1}{2}m^2 + \frac{1}{2}m + mn - n\right)}\right) \left(\frac{\lambda}{\mu}\right)^{n+m+1} \left(\frac{1}{m}\right)^{n+1} \\
 N_{2_{d3}} &= \left(-\lambda(1+f)^m \mu(m-1) + (1+f)\mu m^2\right) \left(\frac{\lambda}{\mu}\right)^m (1+f)^{\frac{1}{2}m(m-1)} \\
 N_{2_{d1}} &= \left(\frac{1}{m}\right)^m (1+f)^{\frac{1}{2}m(m-1)} m! \left(-\lambda(1+f)^{m-1} + \mu m\right) \left(\sum_{k=1}^{m-1} \frac{\left(\frac{\lambda}{\mu}\right)^k (1+f)^{\frac{1}{2}k(k-1)}}{k!}\right) \quad (9) \\
 N_{2_{d2}} &= \left(\frac{-\lambda(1+f)^{\frac{m^2 + mn - n - 1}{2}}}{(\mu m)^{n+m}}\right) + \left(\frac{1}{m}\right)^m (1+f)^{\frac{1}{2}m(m-1)} m! \left(-\lambda(1+f)^{m-1} + \mu m\right) \\
 N_{2_{d3}} &= \mu m \left(\frac{\lambda(1+f)^{m-1}}{\mu m}\right)^m
 \end{aligned}$$

Finally, the average response time for a request can be derived using Little's theorem.

C. Parameter tuning

In a telecom system with latency constraints, the dominant dynamic of the system is often characterized by the average response time, T , when varying the average arrival rate, λ . Tuning of the parameters of the LDS model in a way that it fits the measured data from the actual server system is a necessary step in modeling of such systems. Assuming that λ and T are measurable, there are three main parameters for the M/M/m-LDS model, m , f and μ , to tune in order to fit the model on the measured data. Further, for the M/M/m/n-LDS there is an extra parameter, n , to tune.

Therefore, in Figures 6-10, the effects of changing model parameters on dynamics of average response time versus mean arrival rate of queries are illustrated. In the rest of the paper, this graph will be called the λ/T graph. In each figure, it is assumed that two (three) of the parameters are fixed and the one that is mentioned is the variable. As the equations for calculating the mean response times are rather complex and the parameters are interdependent, more than one set of parameters can be fit on the measured data. Thus using these figures, a heuristic rule for tuning the parameters of the LDS model can be achieved.

In the cases where the M/M/m-LDS model is used, the first parameter to be tuned is the number of servers, m . As it can be seen in Figure 6, by increasing the maximum number of concurrent requests that can be processed in the system, the linear part of the λ/T graph will be shorter and the exponential rising rate of the graph is increased. In this case it is assumed that $(f, \mu) = (0.6, 22)$.

The second parameter to be tuned is the dependency factor, f . As shown in Figure 7, by decreasing the dependency factor, the linear part of the λ/T graph is increased, however, the

change is slower than in the case where m is decreased. On the other hand the exponential rising rate of the graph is increased in comparison with the case where m is decreased. Here, it is assumed that $(m, \mu) = (3, 22)$.

The effects of changing μ on the λ/T graph while fixing the two other parameters is illustrated in Figure 8. As shown in the figure, by increasing μ in equal steps, the λ/T graph will be shifted to the right in equal steps. In this case, where $(m, f) = (3, 0.6)$, the rate of rising of the graph is decreased.

In cases where the M/M/m/n-LDS model is used, there will be a saturation of the response times when the load is high enough to overload the queue. Here, it is assumed that the default values are $(m, n, f, \mu) = (4, 15, 0.6, 22)$. Figure 9 and Figure 10 show the effects when varying m and f respectively. In each case, the values of the other three parameters are constant. The general effect of changing the parameters is similar as for the case with the infinite queue, with the difference that the response times saturate when the load is high.

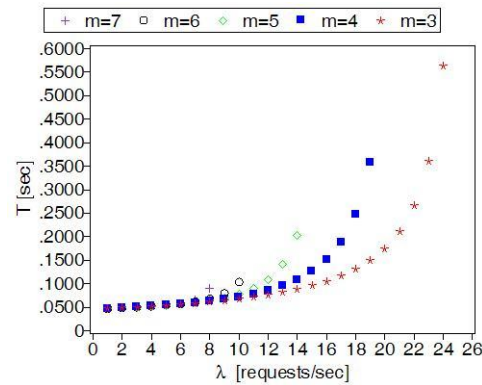


Figure 6. Variations of the λ/T graph for a special scenario with m as variable when $(f, \mu) = (0.7, 22)$.

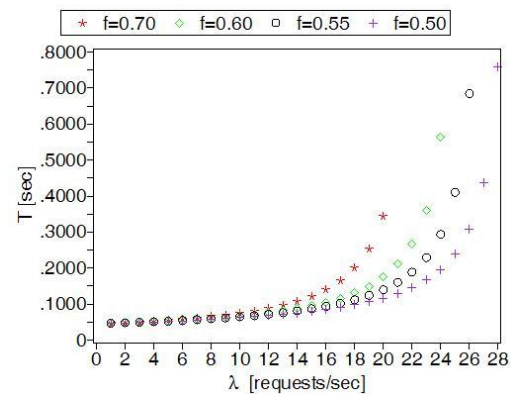


Figure 7. Variations of λ/T graph for a special scenario with f as variable when $(m, \mu) = (3, 22)$.

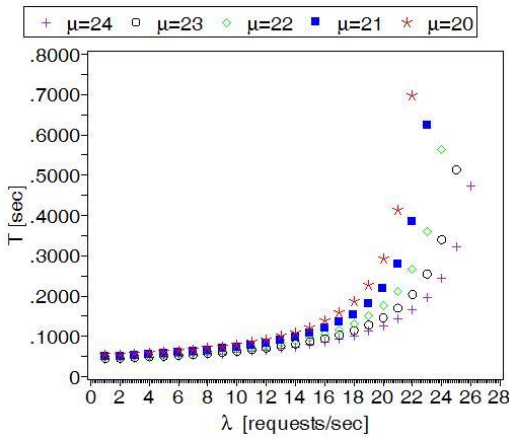


Figure 8. Variations of λ/T graph for a special scenario with μ as variable when $(m, f) = (3, 0.6)$.

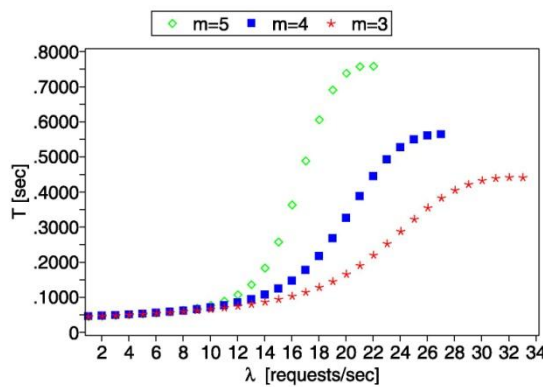


Figure 9. Variations of λ/T graph for a special scenario with m as variable when $(n, f, \mu) = (15, 0.6, 22)$.

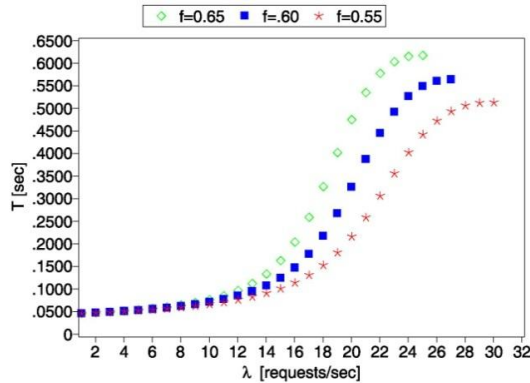


Figure 10. Variations of λ/T graph for a special scenario with f as variable when $(m, n, \mu) = (4, 15, 22)$.

D. Experiments

In order to validate the model, we have performed a series of experiments in our testbed, as described in Section III. In this case, the arrival rate of the unknown traffic was set to zero. The dynamics of the database server highly depends on the mix of requests, since SELECT and UPDATE queries require different amount of server capacity. Therefore, experiments with varying workload mix have been performed.

Figure 11, Figure 12, and Figure 13 show the results from experiments where the arrival rate is varied from low load to

high load. The graphs show the average response times of queries as a function of the arrival rate. We have fitted M/M/m/n-LDS models for the data using the tuning steps described in the previous section. In both scenarios, the CPU utilization was very low, also for high loads. The maximum CPU load was about 5%.

In order to model the network delays, we have added a bias of 0.023 seconds in the average response times of the proposed models.

In Figure 11, the workload is based on 100% UPDATE queries. The fitted model in this case has the following parameters $(m, n, f, \mu) = (3, 81, 0.75, 37.1)$. Figure 12 depicts the same experiment setup when using a mix of 25% SELECT queries and 75% UPDATE queries. The fitted M/M/m/n-LDS model in this case has the following parameters $(m, n, f, \mu) = (6, 73, 0.44, 35.2)$. In Figure 13 only SELECT queries are used. In this case the model parameters are $(m, n, f, \mu) = (6, 240, 1.39, 38)$.

The results verify that the proposed model can represent the average dynamics of a database server with various workloads very well

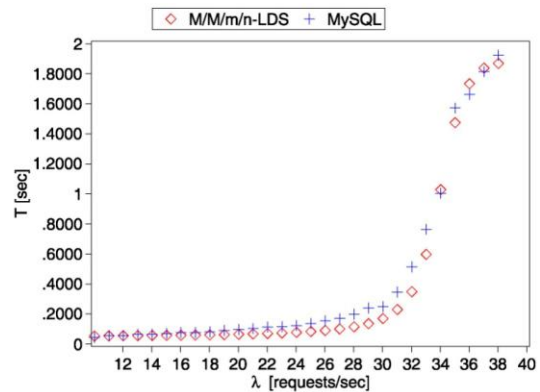


Figure 11. Performance of the M/M/m/n-LDS queuing model in modeling steady state dynamics of a MySQL database server using UPDATE queries.

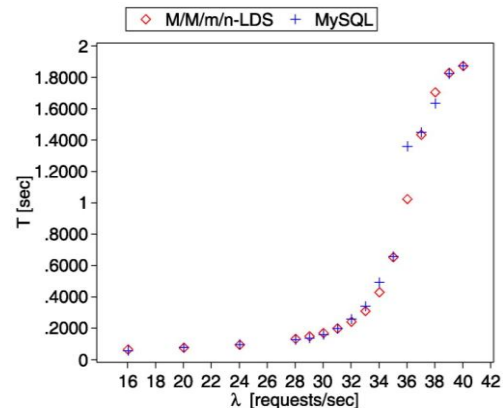


Figure 12. Performance of the M/M/m/n-LDS queuing model in modeling steady state dynamics of a MySQL database server using mixed queries.

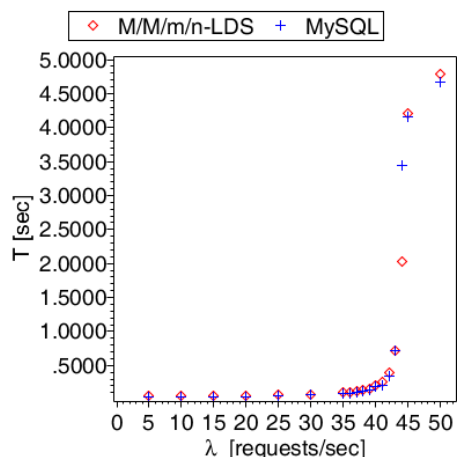


Figure 13. Performance of the M/M/m/n-LDS queuing model in modeling steady state dynamics of a MySQL database server using SELECT queries.

V. ADMISSION CONTROL

As part of the collaboration with Ericsson AB, we have designed an admission control mechanism for the measurable traffic to the NEs, as illustrated previously in Figure 3. As a direct effect of this work, a modified version of the control mechanism has been implemented in the Ericsson product. In this section, the controller design and its validation are described.

A. Control structure

The MSS includes a control system, as illustrated in Figure 14, which should ensure that the load on a specific NE is kept at an acceptable level. The control objective is to keep the mean response times of the NE queries below a desired value while maximizing the throughput. The control actions must be based on a limited amount of control information, due to the standardized protocols and the layered software architecture. The control system includes a controller and a gate.

The controller uses a response time reference value, T_{ref} , and measurements to determine an acceptable workload to the database server. The acceptable workload is defined by the normalized rate of admitted queries, λ_A , which corresponds to the ratio of the average arrival rate of the admitted requests over the higher bound of the average arrival rate of the requests. It is desired that the control system performs robustly in presence of fluctuations in the average arrival rate of the queries sent to the database. Therefore, the controller design is crucial for guaranteeing the control objectives.

The gate ensures the ratio λ_A of arriving queries is admitted to the database. In the experiments, the gate rejects requests that cannot be admitted. However, in the real product, this is not feasible. Instead, the real product has a traffic shaping mechanism that adds delays to the responses to the customer administration system. Since the communication with the customer administration system is synchronous, adding delays to the responses will lower the arrival rate of requests.

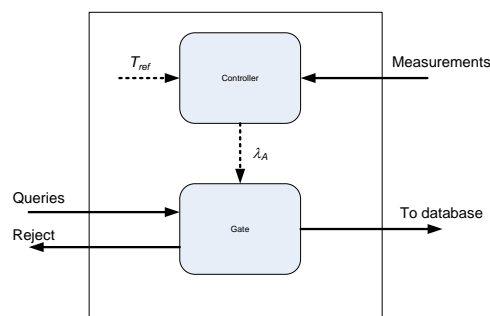


Figure 14. Control system

In this paper, we focus on the controller performance. Therefore, the implementation of the gate is not the main focus as long as it can be assumed that the gate actuates the control signal accurately.

B. Controller design

We have designed a controller that can guarantee the control objectives for the system. The controller, called the Load-Adaptive Controller (LAC), only uses measurements of the query response times. A classical PID controller [26] includes one Proportional part (P), one Integral part (I), and one Derivative part (D) that determines the control signal based on the deviation of the input signal from the reference value. For stochastic systems, the derivative part will amplify the effect of high frequency noise in the response time error and thus deteriorate the overall performance of the system.

Therefore, the LAC is based on a modified PI controller with anti-windup. The LAC adapts its proportional gain with the variations in the mean arrival rates of queries sent to the database. The structure of the modified PI controller is illustrated in Figure 15.

The total load of the NE is determined by the aggregated arrival rates of the measurable and the unknown traffic streams. However, assuming that the unknown traffic is stationary during a limited time period and that the database server behaves as a conservative queuing system [30], a specific admitted ratio of the traffic will correspond to a specific mean response time, as illustrated in Figure 16.

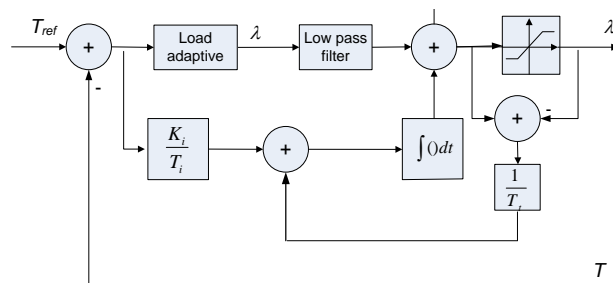


Figure 15. Load-adaptive controller (LAC)

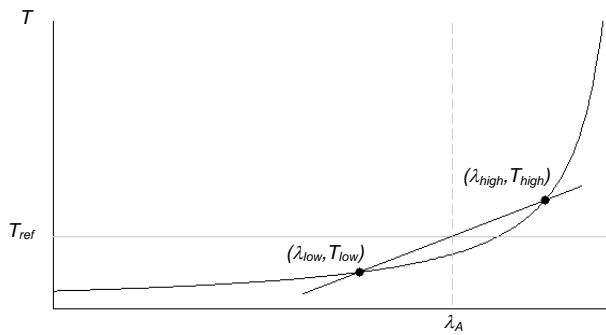


Figure 16. An illustration of the LAC calculations.

The controller continuously keeps track of two points in this graph, one low point, (λ_{low}, T_{low}) , which is situated below the reference response time, T_{ref} , and one high point, $(\lambda_{high}, T_{high})$, which is situated above T_{ref} . As the control system operates only based on measured response times of NE queries, λ_{low} guarantees that those measurements exist for all sampling intervals. The upper limit for mean arrival rates of the queries processed by the NE while not overloading the database is represented by λ_{high} . The starting values for λ_{low} and λ_{high} are set to 5% and 100% respectively.

The admittance rate of the incoming queries is iteratively updated so that its corresponding response time meets the desired value. Every sampling time, the controller calculates the average response time, T , over the last period. If the average response time during sampling period k , T_k , is too high, $(T_k > T_{ref})$, the high point is updated as $(\lambda_{high}, T_{high}) = (\lambda_k, T_k)$ where λ_k is the normalized admitted arrival rate during interval k . If the average response time during interval k is too low, $(T_k < T_{ref})$, the low point is updated as $(\lambda_{low}, T_{low}) = (\lambda_k, T_k)$. It is now assumed that the optimal normalized arrival rate, λ_o , which gives a response time of exactly T_{ref} is in the interval $[\lambda_{low}, \lambda_{high}]$. Therefore, the next normalized admitted arrival rate, λ_{k+1} , can be interpolated from these points using classic geometry:

$$\lambda_{k+1} = \lambda_k + \frac{\lambda_{high} - \lambda_{low}}{T_{high} - T_{low}} (T_{ref} - T_k) \quad (10)$$

Therefore, the quotient $(\lambda_{high} - \lambda_{low}) / (T_{high} - T_{low})$ is used as proportional gain in the P-part of the controller. The algorithm will converge to the desired response time value assuming that the arrival process is stationary or slowly changing. It is obvious that the control gate cannot admit more queries than the incoming ones. This upper limit will be noted in the calculations and treated as a saturation limit of the control signal.

The integral I-part of the controller is used when the P-part is not enough for keeping the steady state error to zero. The integral part uses a controller parameter, K_i , which in conventional PI controllers are equal to the proportional gain. However, in this case, as the proportional gain changes drastically due to the load-adaptive algorithm, using the conventional PI structure will lead to a reduced phase margin which will drive the system to unstable region. Therefore, K_i is

chosen as a static gain and its suitable value is determined in tuning phase of the controller.

Further, the parameter T_i is the integration time constant and T_t is the integrator's reset time constant in the anti-windup mechanism. Anti-windup is added to avoid building up of the integration part when the control gate is saturated or completely open. It is desired to choose small values for T_t so that the integrator resets quickly. Generally, T_t is chosen to be less than T_i .

A low pass filter is added after the proportional gain to smoothen the response time error signal as it is very noisy. The bandwidth of this filter should be suitably chosen so that its effect on the in-band characteristics of the response time errors is minor while attenuating high frequency components of that signal.

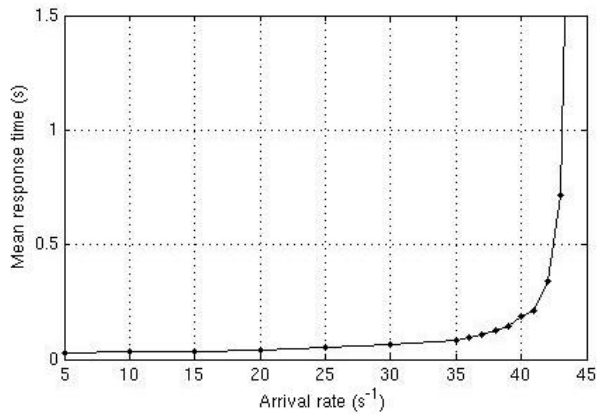
C. Experiments

To investigate the controller performance, a Java implementation of the controller was deployed as a web application to a Glassfish application server, placed on the server acting as traffic generator in Figure 4. The web application also included the traffic generator that generated requests for the web application. For each request, the admission control decides whether to allow the request to be sent to the database or rejected. The traffic generator for unknown traffic did not have an admission control, and was set to a specific average arrival rate that could be altered during run time. All requests sent to the database server were SELECT queries (according to the query structure described earlier). The λ/T graph for this particular scenario setting is shown in Figure 17. The saturation of the system is not shown in the graph for clarity reasons, since the operation region is around the "knee".

To test the performance of the controller, a scenario was chosen where the load changed from slight overload to high overload. The reference response time, T_{ref} , was set to 0.2 seconds. According to the λ/T graph in Figure 17, this corresponds to a total arrival rate of approximately 40 queries per second.

In this paper, two experiments are shown, one with a step in the unknown traffic and one with a step in the measurable traffic. The controller parameters were set to $T_i=4$, $K_i=0.5$, $T_r=1$, and the sampling time $h=0.5$ seconds. T_i was determined as a multiple of the sampling time, chosen so that the controller was able to maximize the throughput while keeping the mean response times below T_{ref} . K_i was set equal to the sampling time. To give the controller time to settle this state was kept for 100 seconds after which a step in the traffic was performed. The resulting graphs are shown in Figure 18 and Figure 19. The graphs show the average dynamics from 100 runs.

In the first experiment, shown in Figure 18, the starting arrival rate was set to 23 requests per second for the measured traffic and 22 requests per second for the unknown traffic. The step increased the arrival rate of the unknown traffic by 10 (to 32) requests per second, resulting in a more severe overload situation.

Figure 17. λ/T graph for the admission control experiments.

The second experiment, shown in Figure 19, was similar to the first experiment. However, the arrival rate step was in the measurable traffic instead. To obtain a similar control signal response as in the first experiment, the step in the controllable traffic had to be larger. Therefore, the observable arrival rate was increased from 23 requests per second to 51 requests per second.

Both experiments show a well-behaved controller, with a reasonable settling time and smooth dynamics after the step.

VI. MONITORING AND ESTIMATION

The system in Figure 1 is complicated with many different queues, caches and databases. Attempting to capture all details gives models that are too complex for on-line control. Extensive experience in the field of control has clearly demonstrated that simple models that capture essential behavior can be very beneficial [31]. One aspect of the collaboration with Ericsson has been to explore if benefits can also be obtained for monitoring and control of the MSS. A crucial issue is what complexity of the models is required for estimation and control of the MSS.

Response time and arrival rates are variables of prime concern. The variables have strong variations, which can be reduced by averaging. A more effective way is to construct estimators that exploit the dynamic behavior of the system. Exploration of such estimators has been one of the goals of the project.

A key feature of the system shown in Figure 1 is that there are two traffic streams. The measured traffic, generated by the customer administration system has a known arrival rate λ_c , can be controlled. The unknown stream, which is created by the mobile phone users, has an arrival rate λ_u that cannot be controlled. Monitoring and control of the system can be improved if good estimates of the average service time are available.

An abstraction of the system in Figure 1 is shown in Figure 20, where an estimator and the controller have been included. In this section, we will focus on the estimator, which only has access to measurements of the measured arrival stream λ and the response time T . All actions by the NEs and the MSS have been represented by one queue that represents the aggregated behaviors.

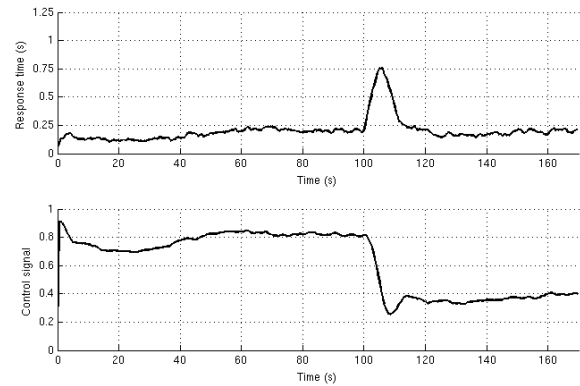


Figure 18. Performance of the LAC with step in unknown traffic.

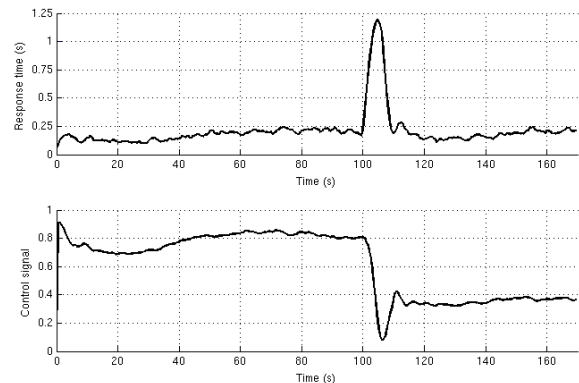


Figure 19. Performance of the LAC with step in observable traffic.

The queue length is represented by the variable x , which captures the aggregated behavior of many different queues in the real system. The variable x can be interpreted as a virtual queue length. The queue length cannot be measured. The actual response time T and the actual arrival times can, however, be measured. Variations in x reflect changes in the system's load.

A. Flow Model

To model the system, we will make an additional abstraction by assuming that the variables x and T are continuous and that they vary continuously in time. The behavior of the system can then be captured by the simple flow model:

$$\frac{dx}{dt} = \lambda - \mu_{\max} f(x) \quad (11)$$

where x is the virtual queue length, λ_c is the known arrival rate, λ_u is the unknown arrival rate, μ_{\max} is the maximum service rate and f is a monotone function with the range $[0, 1]$. The response time is given by

$$T = t_0(1 + x) = t_0(1 + f^{-1}(\rho)) \quad (12)$$

where $t_0 = 1/\mu_{\max}$ is the average time to serve one job when the queue is empty and ρ is the normalized service rate or the utility $\rho = \lambda/\mu_{\max}$.

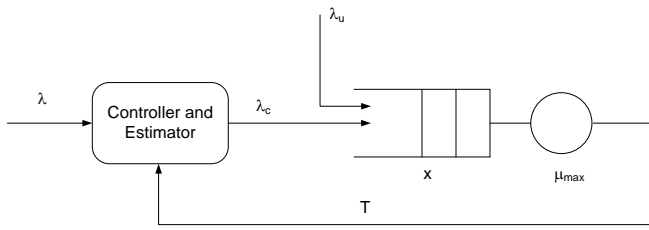


Figure 20. Schematic diagram of an abstraction of the MSS in Figure 1 with a controller and estimator.

The response time goes to infinity as λ approaches μ_{max} if the range of the function f is $[0, 1]$. The function f gives significant freedom in adjusting the behavior to real queue behavior.

The model (11), (12) has been used extensively to model queuing systems [33]. The simple M/M/1 queue can be represented by (12) with $f = x/(x + 1)$ [32].

Even if the model (11), (12) is simple it captures some important features of real queuing systems, for example the fact that response time increases with queue length. The model also captures the behavior that the rate of change of the response time increases with increasing arrival rate. The behavior of the system can be shaped by the function f .

In the project, we have investigated simulated models with servers and we have demonstrated that it is possible to find functions f which matches the steady state behavior of simulated systems. An illustration is given in Figure 21.

B. Estimation algorithm

There are significant variations in the arrival and response times due to their discrete nature. To monitor and control the system it is necessary to smooth these variations. For example, the average arrival rate of the controlled stream can be estimated the simple exponential smoother

$$\begin{aligned} \hat{t}_i^+ &= \hat{t}_i + k_3(h_a - \hat{t}_i) \\ \hat{\lambda}_c^+ &= 1/\hat{t}_i^+ \end{aligned} \tag{13}$$

where t_i is the arrival time and h_a is the time since the last arrival update.

One advantage with the model (11), (12) is that it is possible to use Kalman filtering [31] to combine the model, which captures the gross behavior of the queuing system, with measured data.

If continuous data was available, an extended Kalman filter for the service time is given by

$$\begin{aligned} \frac{d\hat{x}}{dt} &= \lambda_c + \lambda_u - \mu_{max}f(\hat{x}) + k_1(T - t_0(1 + \hat{x})) \\ \frac{d\hat{\lambda}_u}{dt} &= k_2(T - t_0(1 + \hat{x})) \end{aligned} \tag{14}$$

This filter will capture the behavior that response time increases with increasing queue length and arrival rate. The detailed behavior can be shaped by the function f .

It must be considered that the real measurements are events that represent arrival of a request or a completed response. To deal with this, we have developed an event-based Kalman filter.

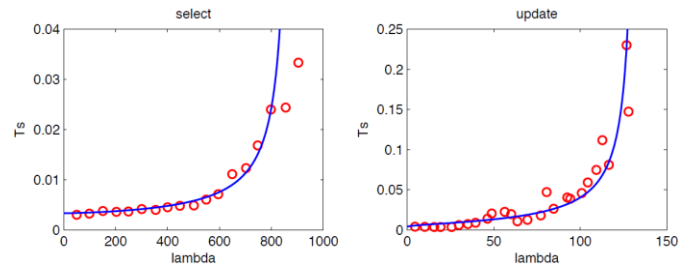


Figure 21. Service times for the operations SELECT (left) and UPDATE on an SQL server and predictions based on the model (12) with $f(x)=(1/(1+x))^n$, $n = 1.5$ and $\mu_{max} = 880$ for SELECT and $n = 0.15$ and $\mu_{max} = 132$ for UPDATE.

At arrivals, the queue length is updated according to the flow model:

$$\hat{x}^+ = \hat{x} + h_d(\hat{\lambda}_c + \hat{\lambda}_u - \mu_{max}f(\hat{x})) \tag{15}$$

This difference equation is simply a forward Euler approximation of (11). Equation (15) is simply a prediction of x based on the model (11). Information about x is obtained when a service is completed. The queue length and the unknown arrival rate are then updated as

$$\begin{aligned} \hat{x}^+ &= \hat{x} + h_d(\lambda_c + \lambda_u - \mu_{max}f(\hat{x}) + k_1(T - \hat{T})) \\ \hat{\lambda}_u^+ &= \hat{\lambda}_u + h_d k_2(T - \hat{T}) \end{aligned} \tag{16}$$

where h_d is the time since the last departure update. The arrival rate can be estimated because it results from the model (11) and (12) that the arrival rate is observable from a measurement of service time [31].

C. Experiment

The Kalman filter estimator was evaluated using a discrete-event simulation program written in Java. The program simulates a single server queue with exponentially distributed service times with mean $\mu_{max}=100$ requests per second. The queue has two arrival processes, representing the measurable and unknown traffic. The Kalman filter has been evaluated for a number of scenarios validating its performance. However, in this paper we show the results of one specific scenario.

In this scenario, the unknown arrival process was a stationary Poisson process with mean 42.5 requests per second. The measurable arrival process was basically a Poisson process with changing average rate. The arrival rate, λ , was the sum of one constant part and one part represented by a sine function as given by

$$\lambda(t) = C + a \cdot \sin(kt) \tag{18}$$

The parameters were chosen so that the system can handle the workload over long time but with periodic overloads, hence

$$\mu_{max} - a < C < \mu_{max} \tag{19}$$

Therefore, the numerical values used in the simulations are $C=42.5$ and $a = 20$ requests per second.

The differential equations describing the behavior of the estimates between events were approximated using first order forward Euler discretization.

Figure 22 shows the response times and the arrival rate, both real values and estimates for a time period of 20 seconds

during the simulation. The estimate error is shown in Figure 23. It can be seen how the Kalman filter manages to follow the real system during the quick rises in response time around time 424 and 427. Here the mean square error is $\sigma = 7.4 \cdot 10^{-4}$ for the period $415 < t < 420$ and $\sigma = 1.1 \cdot 10^{-2}$ for the period $425 < t < 430$. The mean square error for the entire experiment is $\sigma = 1.9 \cdot 10^{-2}$.

VII. CONCLUSIONS

Accurate control designs using control theory are essential for resource management in computer systems. In this paper we have presented work performed in collaboration with Ericsson AB, investigating how control theory can improve the performance of a commercial mobile service support system. Together with Ericsson AB, we have identified three major control challenges, and investigated solutions. The first challenge is to find accurate performance models for the system, with the objective to capture the system dynamics. The second challenge is to develop an admission control scheme that can handle unknown traffic and load surges. The final challenge is to develop estimation methods for accurate prediction of response times and arrival rates in systems with unknown traffic.

In this paper, the challenges have been treated rather independent of each other. However, the future goal is to be able to use all solutions together, in order to improve the system performance and speed up the development process. The performance model could be tuned using real data and then used for validating control designs, which is much easier than implementing the designs in testbeds or the real system. Also, in the future, the estimation algorithms should be incorporated in the control system, improving the control decisions.

ACKNOWLEDGMENT

The authors at Lund University are members of the Lund Center for Control of Complex Engineering Systems (LCCC). Maria Kihl and Anders Robertsson are members of the Excellence Center at Linköping-Lund in Information Technology (eLLIIT). The work is partly funded by the Swedish Research Council, grant VR 2010-5864.

REFERENCES

- [1] B. Brawn and F. Gustavson. "Program behavior in a paging environment", AFIPS Fall Joint Computer Conference, pages 1019-1032, 1968.
- [2] Crocus, "Systemes d'Exploitation des Ordinateurs", Dunod, Paris, 1975.
- [3] Y. Diao, C. Wu, J. Hellerstein, A. Storm, M. Surendra, S. Lightstone, S. Parekh, C. Garcia-Arellano, M. Carroll, L. Chu, and J. Colaco, "Comparative studies of load balancing with control and optimization techniques," American Control Conference, 2005.

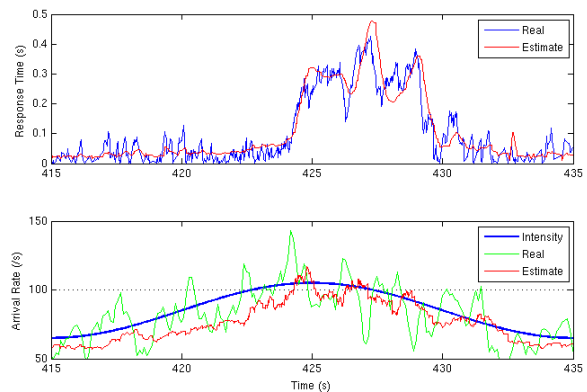


Figure 22. Kalman filter estimates of response times and estimation of arrival rate.

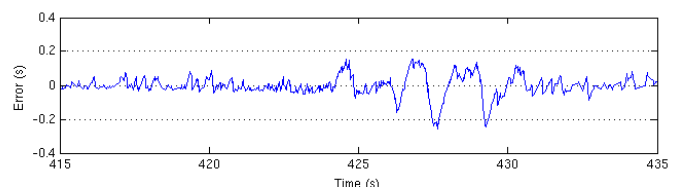


Figure 23. Proposed Kalman filter's response time prediction error.

- [4] Y. Fu, H. Wang, C. Lu, and R. Chandra, "Distributed utilization control for real-time clusters with load balancing," IEEE International Real-Time Systems Symposium, 2006.
- [5] M. Kihl, A. Robertsson, M. Andersson, and B. Wittenmark, "Control theoretic analysis of admission control mechanisms for web server systems," *The World Wide Web Journal*, Springer, vol. 11, no. 1, 2008.
- [6] X. Chen, H. Chen, and P. Mohapatra, "Aces: an efficient admission control scheme for QoS-aware web servers," *Computer Communication*, vol. 26, no. 14, 2003.
- [7] X. Liu, J. Heo, L. Sha, and X. Zhu, "Adaptive control of multi-tiered web applications using queuing predictor," 10th IEEE/IFIP Network Operation Management Symposium, 2006.
- [8] T. Voigt and P. Gunningberg, "Adaptive resource based web server admission control", 7th International Symposium on Computers and Communications, 2002.
- [9] M. Kjaer, M. Kihl, and A. Robertsson, "Resource Allocation and Disturbance Rejection in Web Servers using SLAs and Virtualized Servers", *IEEE Transaction on Network and Service Management*, Vol. 6, No. 4, 2009.
- [10] W. Xu, X. Zhu, S. Singhal, and Z. Wang, "Predictive control for dynamic resource allocation in enterprise data centers," 10th IEEE/IFIP Network Operation Management Symposium, 2006.
- [11] Z. Wang, X. Liu, A. Zhang, C. Stewart, X. Zhu, T. Kelly, and S. Singhal, "AutoParam: automated control of application-level performance in virtualized server environments", 2nd IEEE International Workshop on Feedback Control Implementation and Design in Computing Systems and Networks, 2007.
- [12] R. Bianchini and R. Rajamony, "Power and energy management for server systems," *IEEE Computer*, vol. 37, no. 11, 2004.
- [13] H. Claussen, L.T.W Ho, and F. Pivit, "Leveraging advances in mobile broadband technology to improve environmental sustainability", *Telecommunications Journal of Australia*, Vol. 59, No. 1, 2009.
- [14] T. Horvath, T. Abdelzaher, K. Skadron, and X. Liu, "Dynamic voltage scaling in multitier web servers with end-to-end delay control," *IEEE Transactions on Computers*, vol. 56, no. 4, 2007.

- [15] E. Elnozahy, M. Kistler, and R. Rajamony, "Energy-efficient server clusters," *Lecture Notes in Computer Science 2325*. Springer-Verlag Berlin Heidelberg, 2003.
- [16] M. Kihl, A. Robertsson, and B. Wittenmark, "Performance Modelling and Control of Server Systems using Non-linear Control Theory", 18th International Teletraffic Congress, 2003.
- [17] J. Dilley, R. Friedrich, T. Jin, and J. Rolia, "Web server performance measurement and modeling techniques", *Performance Evaluation*, Vol. 33, No. 1, 1998.
- [18] D. A. Menascé and V. A. F. Almeida. *Capacity Planning for Web Services*, Prentice Hall, 2002.
- [19] R. D. van der Mei, R. Hariharan, and P. K. Reeser, "Web server performance modeling", *Telecommunication Systems*, Vol. 16, No. 3, 2001.
- [20] H. Perros, Y. Dallery, and G. Pujolle, "Analysis of a queueing network model with class dependent window flow control," 11th Annual Joint Conference of the IEEE Computer and Communications Societies, IEEE, pp. 968–977 vol.2, May 1992.
- [21] A. Rak, and A. Sgueglia, "Instantaneous Load Dependent Servers (iLDS) Model for Web Services," International Conference on Complex, Intelligent and Software Intensive Systems, 2010.
- [22] Curiel, M. and Puigjaner, R., "Using load dependent servers to reduce the complexity of large client-server simulation models", *Performance Engineering, LNCS 2047*, Springer-Verlag Berlin Heidelberg, 2001.
- [23] V. Mathur and V. Apte, "A computational complexity-aware model for performance analysis of software servers", IEEE International Symposium on Modelling, Analysis and Simulation of Computer and Telecommunication Systems (MASCOTS), 2004.
- [24] K. K. Leung, Load-dependent service queues with application to congestion control in broadband networks, *Performance Evaluation*, Vol. 50, Issue 1, October 2002, pp 27-40.
- [25] M. Kihl, P. Amani, A. Robertsson, G. Radu, M. Dellkrantz, and B. Aspernäs, "Performance modeling of databases in Telecommunication service management systems", IARIA 7th International Conference on Digital Communications (ICDT), 2012.
- [26] K.J. Åström and B. Wittenmark, *Computer-Controlled Systems*. Upper Saddle River, NJ: Prentice Hall, 1997. Dover reprint 2011.
- [27] J. Cao, M. Andersson, C. Nyberg and M. Kihl, "Web Server Performance Modeling using an M/G/1/K*PS Queue", International Conference on Telecommunication, 2003.
- [28] M. Kihl, G. Cedersjö, A. Robertsson, B. Aspernäs, "Performance measurements and modeling of database servers", Sixth International Workshop on Feedback Control Implementation and Design in Computing Systems and Networks, 2011.
- [29] D.J. DeWitt. The Wisconsin benchmark: Past, present, and future, *The Benchmark Handbook for Database and Transaction Processing Systems*, 1, 1991.
- [30] L. Kleinrock, *Queueing Systems, Volume I: Theory*, Wiley Interscience, New York, 1975.
- [31] K. J. Åström and R. Murray. *Feedback Systems - An Introduction for Scientists and Engineers*. Princeton University Press, 2008.
- [32] D. Tipper and M.K. Sundareshan, "Numerical methods for modeling computer networks under nonstationary conditions", *IEEE Journal on Selected Areas in Communications*, 8(9), pp 1682-1695, Dec 1990.
- [33] Carson E. Agnew, "Dynamic modeling and control of congestion-prone systems", *Operations Research*, 24(3), pp. 400-419, 1976.

The MoSaKa QoS System: Architecture and Evaluation

Philipp Drieß, Florian Evers, and Markus Brückner

Integrated Communication Systems Group

Ilmenau University of Technology, Ilmenau, Germany

Email: {philipp.driess, florian.evers, markus.brueckner}@tu-ilmenau.de

Abstract—The provision of Quality-of-Service (QoS) in packet-switched transmissions over highly mobile satellite terminals presents challenges not solved by existing schemes like *Integrated Services* and *Differentiated Services*. Such schemes rely on stable link conditions, a requirement that cannot be guaranteed in a mobile environment. To support robust audio and video conferencing, an end-to-end reservation-based approach is inevitable. This led to the development of the *MoSaKa QoS System*, which combines a reservation-based QoS scheme with the ability to deal with changing link conditions. The main idea was to enable applications to degrade gracefully if an unstable link deteriorates. Each router implements a cross-layer QoS agent, which tracks the network-layer-based QoS and takes the current status of the lower layers into account. Certain flows can be suspended without canceling them if the capacity of a link deteriorates. To select which flow has to be suspended, an *optimizer* was implemented which examines the flows for their priority and respective QoS requirements. To depict how this optimizer works and how the system performs, a testbed with an emulated satellite link was set up. The obtained results show, that the presented system is able to provide appropriate QoS over unstable links.

Keywords—quality of service; satellite communication; mobile communication; IntServ; signaling

I. INTRODUCTION

This paper is an invited paper that is based on a previous work published at the AICT 2012 conference [1]. At that time, no evaluation results were available. These measurement results are the additional contribution of this paper.

First of all, wire-based transmission systems such as Ethernet provide *stable* links. In other words, the transmission conditions such as the link capacity and error rate do not change over time. In contrast, the transmission conditions of wireless systems are considered *unstable*. For example, if a laptop is carried around, it experiences different kinds of fading effects. Similarly, mobile satellite terminals are constantly affected by trees, clouds and other obstacles that impair the line-of-sight transmission to the satellite.

Such links with changing conditions can not be avoided, which leads to problems regarding support for Quality-of-Service (QoS). Reservation-based schemes like *Integrated Services* (IntServ [2]) depend on networks with *stable* links for their capacity management, which fails if the available capacity is a dynamic parameter. In contrast, *Differentiated*

Services (DiffServ [3]), an architecture that is based on the differentiation of traffic into classes with specific properties, does not offer reservations at all and thus is not able to offer guarantees to the applications.

Having guarantees might be a requirement, depending on the intended use case. In the research project *Mobile Satellite Communications in Ka-Band* (MoSaKa, see [4] for an introduction), a satellite-based communication system was developed to support rescue teams in disaster scenarios. In such a system, voice communication is one very important application, ideally in combination with video. As satellite resources are scarce, not all communication attempts can be admitted. However, continuous communication streams like voice conversations are not the only kind of traffic in disaster communication systems. A multitude of data has to be exchanged, such as digital maps, status reports, and position information. Therefore, a packet-switched approach that is based on the TCP/IP protocol suite is the most flexible approach to build such a network. To serve important applications like voice reliably, a reservation-based scheme that assures QoS has to be implemented, causing the aforementioned problem regarding the unstable characteristics of the link to the satellite. The availability of a QoS system coping with those limitations will be a key factor for being able to use packet-based satellite communication systems as backbones, especially in disaster scenarios.

In this paper, the MoSaKa QoS system, a novel reservation-based QoS architecture that is able to cope with unstable links, is presented. The focus is on satellite-based networks. MoSaKa empowers rescue teams to communicate in environments without communication infrastructure, which is the research area the MoSaKa project is looking at. However, the algorithms shown in this paper could also be applied to other QoS-enabled wireless transmission systems, such as IEEE 802.11e. The whole QoS system was implemented and is available for the GNU/Linux platform. A testbed was set up, that allowed to perform extensive functional tests and performance evaluations. The results of these tests are presented in this paper.

The remainder of this paper is organized as follows: Section II describes the scenario for which the proposed architecture was designed. The requirements for this architec-

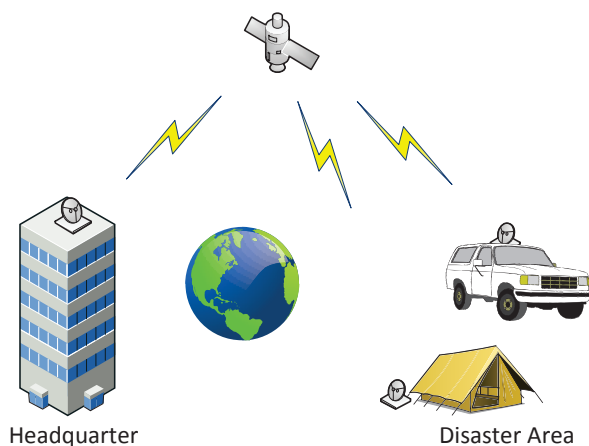


Figure 1. Typical use cases for MoSaKa entities: fixed, nomadic and mobile terminals

ture are derived in Section III. Section IV gives an overview over the related work and highlights the shortcomings of previous approaches. Section V depicts the final architecture of the MoSaKa QoS system by presenting all its functional components. The test environment is presented in Section VI. There the results of multiple functional tests and performance comparisons are provided. The paper is concluded in Section VII with an overview about future work.

II. THE MOSAKA RESEARCH PROJECT

The MoSaKa project aims at developing a complete satellite communication stack from the antennas up to the QoS management, including antenna tracking systems and a decentralized resource allocation scheme. In this paper, the main focus is on the QoS system as it is seen by the higher layers. Layer 2 and below are only mentioned insofar as they are required to explain design decisions regarding the higher layers.

Figure 1 shows a typical usage scenario: some nomadic and mobile terminals deployed in a remote area use the satellite link to communicate with their headquarter. Each terminal uses a dynamic set of services resulting in individual traffic demands. The communication link from each terminal to the satellite is considered unstable: the link quality fluctuates with the movement of the terminal and changing conditions of the environment. Most of these fluctuations are short, but some may persist for a longer span of time.

Large-scale disaster relief operations cause a significant demand for communication. Satellite links are a – comparatively – scarce resource with only a small capacity and long delays.¹ These two effects have to be considered while implementing a system-wide QoS infrastructure.

¹For geostationary orbits at a height of $\approx 36\,000$ km the time-of-flight is already longer than 100 ms for one direction.

III. REQUIREMENTS

Based on the scenario presented in Section II, a set of requirements, that a QoS infrastructure has to fulfill, were derived.

Hard QoS guarantees

Targeted applications, such as for audio and video conferencing, assume a transmission behavior as provided by circuit-switched communication systems. This includes a guaranteed data rate, a deterministic delay, and reasonable low error rate. Providing hard guarantees in IP-based networks can be achieved by end-to-end path reservation schemes. Supporting dynamic reservations requires a signaling scheme, e.g., to setup and cancel paths.

Decentralized resource allocation

A centralized resource management entity is a single point of failure, causes additional signaling traffic towards this entity, and may provide an outdated view of the resources of the whole network especially if the signaling messages are affected by considerable delays. To avoid these effects, a decentralized resource management scheme is preferred.

Efficient handshakes

The main issue in designing an efficient signaling scheme the long transmission delay introduced by the satellite link. With a round trip time of ≈ 400 ms, complex handshakes with multiple messages traveling back and forth are imposing an unacceptable overall delay.

Efficient handling of link instability

Today's QoS systems assume stable links with static resources that can be utilized for reservations. This assumption is no longer valid in mobile, satellite-based communication systems or even in mobile communication systems in general. Over the time, the propagation conditions are subject to change. The QoS infrastructure presented in this paper must be able to cope with such unstable link conditions.

Cross-layer link usage optimization

Satellite-based communication with multiple terminals takes place on a shared broadcast medium. To enable parallel transmissions via one single satellite, the MoSaKa physical and MAC layers have to assign the available link spectrum to all terminals that compete for resources. This happens with respect to the individual resource demands of each terminal. These resource demands are derived from higher-layer QoS requirements that originate from the applications.

Due to the long delay of the broadcast medium, the resource assignment procedure takes place in a distributed manner without central coordination and without any point-to-point negotiation. If the link share of a terminal decreases, the higher layer reservations may not fit into the remaining capacity anymore. In that case, the QoS system has to evaluate

all admitted reservations based on their properties to keep as many of them active as possible.

A resource management system suitable for mobile satellite communication has to address these requirements. Existing solutions fall short in one or the other aspect prompting the development of a new architecture for the MoSaKa project.

IV. RELATED WORK

QoS architectures such as IntServ [2], [5], [6] or DiffServ [3], [7] are well known and have a wide range of acceptance. Nevertheless, they have a variety of issues regarding unstable link conditions.

IntServ

IntServ is an architecture that offers hard guarantees regarding QoS parameters. Applications request reservations via a signaling protocol such as the *Resource Reservation Protocol (RSVP)* [8] or *Next Steps in Signaling (NSIS)* [9], [10], [11] to announce their individual traffic requirements. On each node along the transmission path, an IntServ entity manages and monitors the traffic, taking the amount of permitted resources into account.

Applying IntServ upon an unstable link leads to problems if the link capacity decreases. This results in a situation where the sum of all accepted reservations does not fit into the link budget anymore and reservations are violated. As no feedback mechanism is available, the system has to withdraw reservations. Affected applications can only deal with this situation by reserving a new path with different parameters or ceasing communication altogether. Signaling new paths causes additional message load on the already limited link, contributing further to the congestion.

DiffServ

One of the problems of IntServ in large-scale networks is its bad scalability. Due to the state kept in each intermediate node, IntServ installations do not scale to Internet-sized networks. This prompted the development of DiffServ, a system based on differentiation of traffic into classes, which are treated differently by the network. This allows the assignment of transmission priorities to distinguish different types of traffic.

As DiffServ does not support the reservation of a communication path, it does not offer guarantees. Excessive traffic in a single class is able to exceed the link capacity, causing packet loss for all affected applications.

Specialized QoS systems

In addition to the IntServ and DiffServ models, a whole body of research for networks with non-standard conditions exists. Some of these approaches served as an inspiration for a solution to the problem at hand.

INSIGNIA: The INSIGNIA QoS system [12] is designed to work in highly dynamic, mobile ad-hoc networks. The in-band signaling approach provides guaranteed data rates by reserving paths, and is able to adapt fastly to changing conditions of the network. The receiver-based adaption mechanism performs well in highly meshed networks, but is not suited for networks with a single bottleneck in the backbone, such as a satellite link. Furthermore, the reservation model lacks expressiveness, as it does not incorporate QoS parameters like delay and error rate, which are parameters that offer room for optimization in satellite transmission systems.

DARWIN: DARWIN [13] is an approach implementing an IntServ-like model based on a global resource broker. This enables the system to optimize resource utilization among the whole network. Regarding satellite-based communication systems, QoS requests as well as network status notifications towards the broker are affected by high transmission delays, potentially causing instability.

DVB-RCS2: Digital Video Broadcasting; Second Generation DVB Interactive Satellite System (DVB-RCS2) [14] is an ETSI standard to implement an interactive return channel using the standard DVB-S satellite transmission system. The system implements DiffServ as its QoS approach on the layers 2 and 3. Due to the lack of a reservation system, it does not offer hard transmission guarantees.

Inmarsat BGAN: The BGAN service provided by Inmarsat [15] is one of a few high data rate, bidirectional satellite services offering QoS with hard guarantees. Here, access terminals are able to request predefined channels with a fixed bandwidth from the system. Flexible signalization or end-to-end reservations are not possible.

For use in mobile satellite environments, all aforementioned approaches lack certain desirable features. This prompted the development of a new reservation-based approach similar to IntServ. Whereas the scalability of IntServ in large networks is a problem, it is not an issue in the system at hand. The typical satellite communication system for the disaster scenario will contain only a limited number of users. This makes stateful systems in the backbone feasible. Even more, the guaranteed reservation of communication paths as offered by a reservation-based system is crucial for rescue teams in disaster scenarios. MoSaKa aims to create such a reservation-based QoS system and to tackle the challenges arising from unstable links.

V. THE QOS ARCHITECTURE OF MOSAKA

An IntServ-like architecture such as MoSaKa introduces management entities on each intermediate node as well as on each end system. These entities are aware of all reservations that pass the respective node. In the depicted scenario, static routing in the backhaul is assumed, which ensures that each packet of a flow always takes the same route through the network.

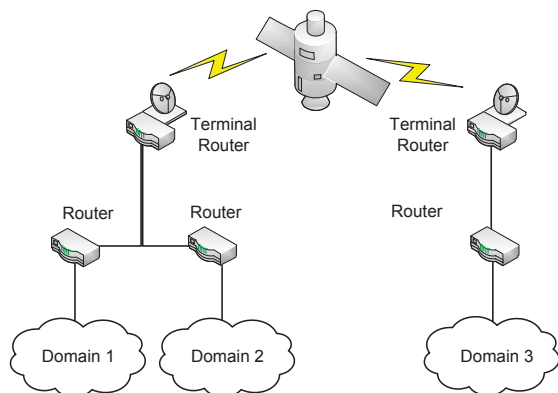


Figure 2. The network of a scenario where the MoSaKa QoS architecture is deployed.

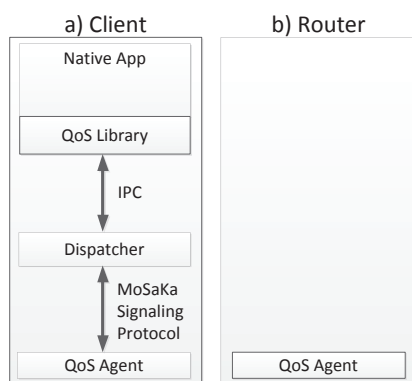


Figure 3. Two kinds of nodes exist in the MoSaKa network: clients and routers. At least, each node requires a QoS Agent running on it. Additional software components are required for clients.

The resulting topology is shown in Figure 2. The central component is the satellite-based communication system with a geostationary satellite and multiple terminals as ground stations. The satellite link is considered to be a bottleneck with a high transmission delay. The terminals act as IP routers and connect local networks to the satellite network. The architecture of the MoSaKa QoS system has no central coordinator.

This approach inherits two issues of IntServ: it has scalability problems and *might* fail if the links are unstable. The former can be neglected with the depicted use case in mind, and the latter is solved by the architecture presented in this paper.

A. Software components

The software components introduced by the MoSaKa QoS architecture are depicted in Figure 3. There are two main components: the QoS Agent and the Dispatcher.

1) *The QoS Agent*: The QoS Agent is a management entity that exists on each node of the network including routers

and clients. This entity is aware of all ongoing reservations that pass the node and has an overview of the transmission resources of each interface that the node possesses. This allows the QoS Agent to decide whether a subsequent reservation can be admitted or has to be rejected. For the purpose of transmitting reservation requests, a signaling protocol such as RSVP or NSIS is required. The QoS Agent intercepts protocol messages and interprets them as necessary. On the satellite terminal, it also communicates with the lower layers to obtain status information regarding the link. This way, it detects link deteriorations.

Furthermore, QoS components like traffic metering and shaping depend highly on the underlying operating system of each node. It is the task of the QoS Agent to adapt the high-level reservations to the QoS primitives available on the node to allow a deployment of the architecture in heterogeneous networks. Each agent consists of a generic part handling the signaling and admission control, and a system-specific part configuring the underlying operating system services.

2) *The Dispatcher*: The Dispatcher is a component that is only required if a given node has applications running on it, making it a client. A Dispatcher acts as a broker between the applications running on the client and the QoS system in the network. The applications talk to the Dispatcher using *interprocess communication* (IPC). The Dispatcher handles all QoS-related interaction with the network relieving the applications from doing so. Additionally, it serves as an entry point for requests and notifications from the network, decoupling the local application structure and the state saved along the communication path. From the network point of view, the Dispatcher is the entity that holds a reservation and renews it as necessary.

Reservations are always triggered by applications. The Dispatcher merely acts as a proxy. Therefore, applications are part of the MoSaKa QoS architecture and need to be modified to take full advantage of the system. One has to distinguish QoS-enabled applications, legacy applications and translator applications.

QoS-enabled applications: As shown in Figure 4 a, a QoS-enabled architecture includes the MoSaKa QoS library. This library offers an high-level API to interact with the QoS architecture and allows the programmer to request transmission resources or to be notified if an active reservation fails or is suspended due to link deterioration. Such an application is aware of its traffic demands and is able to request the appropriate amount of resources before it starts transmitting. Additionally, it is prepared for incoming feedback messages that indicate that the reservation is currently affected.

Legacy applications: All IP-based applications that exist today are considered as legacy applications. They are not aware of an API to request transmission resources, resulting in traffic that is not known to the QoS infrastructure. Two approaches are possible: this traffic can be considered as *best*

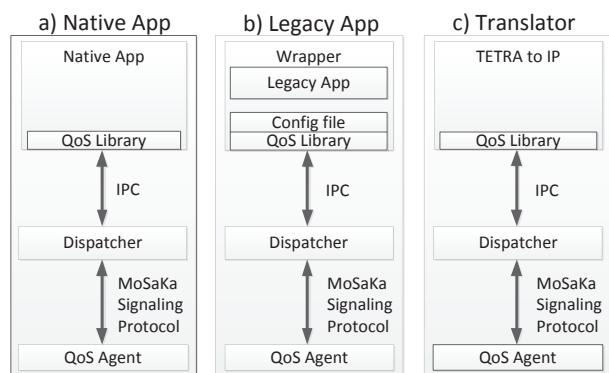


Figure 4. Three kinds of applications are distinguished in the MoSaKa QoS system: Native, legacy and translator applications.

effort traffic, which may or may not pass a bottleneck in the network, or it can be reserved with the help of a *wrapper application* (Figure 4b).

Such a wrapper application loads a predefined set of QoS requirements from a configuration file, initiates the reservation process and then, if successful, executes the legacy application. In that case, the application does not need to know anything about the QoS system, but benefits from it nevertheless, as the required resources are reserved.

The reservation is held all the time even if the legacy application does not emit any traffic. Even worse, to initiate a reservation, the endpoint must be named, which limits the application to a given set of predefined peers. However, such a wrapper can be seen as an intermediate solution until the affected applications implement the QoS scheme.

Translator applications: Translator applications act as a gateway to other kinds of reservation schemes or networks, e.g. circuit-switched telephony systems. Such an entity is a special case of a QoS-enabled application (Figure 4c).

In disaster scenarios, connections with other network types such as *Terrestrial Trunked Radio* (TETRA [16]) may be required. A dedicated gateway node with a TETRA base station and a translator application installed on it can interconnect both networks, allowing TETRA terminals to make telephone calls to the headquarter via the satellite. The translator application is aware of the required resources of a TETRA channel, as the traffic requirements of the codecs are known. This allows the translator application to create suitable reservation requests for the MoSaKa network.

B. The QoS-enabled MoSaKa network

The MoSaKa network consists of two kinds of nodes: intermediate nodes are referred to as routers, and end systems are referred to as clients.

As routers have no applications running on them, the only entity required here is the QoS Agent. The routers that are connected to the satellite system are referred to as terminals.

On such a terminal the QoS Agent is equipped with additional capabilities to manage the link to the satellite.

Clients, as they are considered as user equipment, have applications running on them. Here, the Dispatcher software is required, to logically connect the QoS-enabled applications with the MoSaKa network.

On each network node the QoS Agent has to configure the local packet forwarding entity of the operating system to stop misbehaving applications from congesting the outgoing interfaces. Above all, it must be impossible that traffic, that exceeds the capacity of the outgoing link, causes packet loss for flows that have been negotiated before. This is achieved by relying on platform specific mechanisms to control traffic flows like *Traffic Control* (tc) and *Netfilter* on Linux. On terminals, this includes parameterizing the MoSaKa MAC scheduler on the data link layer of the satellite link.

C. The signaling scheme

On each client, the QoS-enabled applications communicate with the local Dispatcher via an API offered by the MoSaKa QoS library. By accessing this API, an application informs the QoS System about the amount of resources it requires for a transmission to a well-defined peer. The Dispatcher creates a reservation request signaling message that it sends to its peer entity, the Dispatcher residing on the destination node. All signaling messages are intercepted by each QoS Agent along the path, allowing them to decide whether to accept or to deny this reservation request. If such a reservation has to be denied because of insufficient remaining link resources, a negative acknowledgment is sent back to the initiating Dispatcher. This results in a deletion of the pending reservation on all intermediate nodes and leads to a negative acknowledgment to the application via the API of the QoS Library.

If no node fails along the path, the signaling message reaches the Dispatcher at the destination node. This Dispatcher may be aware of local applications, as they are allowed to register to it beforehand. It offers the opportunity for the applications to modify the incoming request (e.g., to change a data rate of a request to better match the expected traffic). After the local handling is done, the Dispatcher sends back an acknowledgment to the originator. Again, this message is intercepted by all QoS Agents and results in an orderly created reservation along the whole path.

D. Feedback mechanism

To tackle changing link conditions, the signaling protocol was equipped with a feedback mechanism. Feedback messages originate from a QoS Agent in the network, after it detected that one of its observed links deteriorates. This QoS Agent sends a feedback message to all applications that hold reservations affected by this degradation.

On each node, the network interface is monitored by the local QoS Agent. Additionally, it is aware of all active reservations that involve this link. Moreover, it allows to

decide whether the remaining capacity is still high enough to serve all reservations. If the capacity falls below the amount of resources assigned to reservations, the QoS Agent starts to optimize. Optimization is done by building a set of allowed reservations starting from the one with the highest priority. Reservations are incrementally added to this set if there is still capacity available. This simple optimization algorithm is suited well for highly hierarchical communication environments, such as those present during disaster relief operations.

After optimization, the QoS Agent has a list of reservations that still have enough link resources. In addition, it has a list of reservations that do not fit into the link anymore. Instead of canceling these reservations, as architectures such as IntServ would have to do, the QoS Agent of MoSaKa is able to set affected reservations *on hold*. Such a suspended reservation is still known to the whole path, but without any active transmission guarantees. Later, if the link recovers, the reservation is resumed by another feedback message.

In the MoSaKa scenario, it is assumed that link degradations are short in nature. Hence, this approach allows a reservation scheme with a low amount of signaling messages. Applications do not need to actively poll the network for free resources, which otherwise would cause an additional signaling load. Furthermore, the data transmission is resumed faster if the network sends resume messages. Such a message can be sent immediately after the link recovered, instead of relying on the applications that would have to poll the network for a new reservation. Needless to say, even if such a subsequent reservation request would be granted, it would be necessary to complete the full handshaking sequence.

Nevertheless, if the link stays degraded for a longer span of time, the QoS Agent may cancel reservations to prevent congesting the network with reservations that cannot be served anyway.

In the MoSaKa QoS architecture, signaling messages are usually exchanged between Dispatchers on two peer nodes, and are intercepted by all QoS Agents on each intermediate node including the end nodes that run the Dispatchers. If a given reservation has to be suspended, the QoS Agent creates signaling messages and sends them to both Dispatchers, allowing all QoS Agents on the path to notice that this reservation is currently *on hold*.

If a signaling message arrives at a Dispatcher, it passes it to the respective application. Here, it triggers a trap in the QoS library informing the application about an accepted, suspended, resumed or canceled reservation.

This feedback scheme is new and allows a graceful degradation of communication. To underline this, one of the most important applications of the MoSaKa scenario is analyzed: Video chat.

E. Impact on Video chat

If a user starts a video chat session with the headquarter, the video chat application tries to reserve resources for the video data and for the audio data separately. As a video chat session is bidirectional, the reservation message contains resource requests for both directions at the same time. For this reason, the signaling handshake completes fully after just one round trip. If the reservation handshake is completed without a rejection from intermediate systems, the path is considered active and can be utilized by both peers.

If the satellite link deteriorates, this is noticed by the QoS Agents on the satellite terminals. Without sufficient transmission resources, they start the optimization process that results in the less important video streams to be set *on hold* to keep the audio streams active. A feedback message is sent to the Dispatchers at both ends of the path, resulting in the deactivation of the video stream in the application. If the link recovers, another feedback allows the video stream to be resumed. This allows applications to provide an indication based on the network state, increasing user satisfaction by making the process transparent. Otherwise, if the link fails to recover, the reservation is canceled by the network.

The *on hold* state enables the system to bridge short link degradations. Degradations are common in mobile satellite communication systems, and dealing with such situations without canceling paths avoids significant signaling effort. More important, the feedback mechanism allows applications to intelligently react to those changes in the network. Especially for satellite links with long delays and a low capacity, such a scheme is essential.

F. MoSaKa Satellite Terminals

To check whether all active reservations fit into the current link capacity, the QoS Agent has to obtain information regarding the link. For that purpose, technology-dependent functionality is required to interact with Ethernet, IEEE 802.11e or the MAC and PHY layers of the MoSaKa satellite terminals.

The MoSaKa satellite link offers QoS-enabled lower layers. From the point of view of the physical layer the satellite link is a shared medium. Each terminal can be received by every other terminal via the satellite. Therefore, it is necessary to allocate and assign parts of the link spectrum to specific sender terminals to prevent collisions. To accommodate changing link conditions, this allocation is not static but takes place every 250 ms. Each active terminal is assigned a short time slot on the lower layer (L2) signaling channel. In this time slot, it broadcasts its resource request to all other terminals. Based on this information, each terminal applies the same resource assignment procedure and comes up with the same resource allocation vector for the next 250 ms data transmission frame. A reservation on the lower layers is valid for only one slot, and has to be renewed continuously by using the L2 signaling channel.

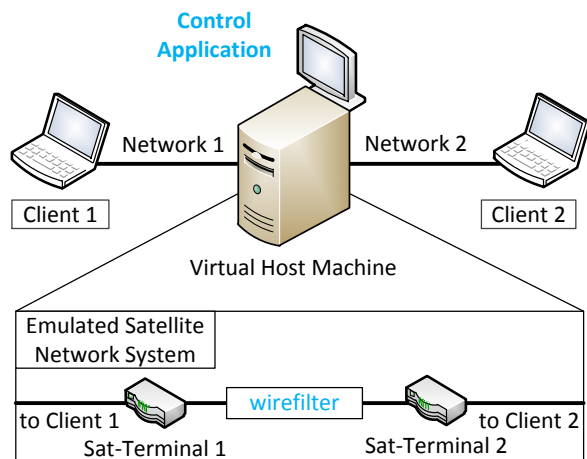


Figure 5. The MoSaKa evaluation testbed comprises two client machines and two virtual satellite terminals connected by an emulated satellite link.

If the link between one terminal and the satellite deteriorates, the QoS Agent on this terminal gets informed about a lower amount of transmission resources that this terminal got assigned for the next data transmission frame. This allows the QoS Agent to check whether all active high-level reservations still fit into the link share, and to take appropriate actions if they do not.

VI. EVALUATION

For the purpose of evaluation, the MoSaKa QoS system was implemented and the testbed depicted in Figure 5 was set up. It incorporates two laptops that act as clients with traffic sources and sinks. A central server is hosting the emulated satellite network components, consisting of two virtualized satellite terminals and an emulated satellite link. For the virtualization, *Kernel-based Virtual Machine* based on Qemu (Qemu/KVM [17]) was chosen as a hypervisor, as it supports hardware virtualization promising performance gains. The host system as well as all guests run a Linux-based operating system with a 3.2.21 kernel. The two guest systems implement the MoSaKa terminal functionality. In addition to the Qemu/KVM hypervisor, Virtual Square *wirefilter* and the *VDE-Switch* [18] are used to connect the guest systems. These components emulate the latency and capacity of a geostationary satellite link. The link parameters are controlled with predefined profiles to emulate arbitrary scenarios in reproducible way.

The measurements were taken using traffic generators adapted to the specific needs of the project. The traffic sources interact with the MoSaKa system to reserve paths. The traffic sinks are able to report received data rate, packet loss rate and transmission delay.

MoSaKa implements a cross-layer approach which tightly

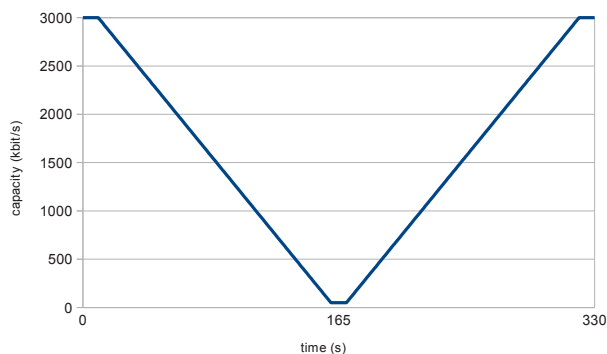


Figure 6. The capacity of the emulated satellite link over time

integrates the functionalities provided by the layers 1 to 3, whereas the lower layers had to be emulated to some extent. Each satellite terminal runs a MAC layer emulation which controls the forwarding of packets on the VDE-Switch link. This way, a real system behavior is emulated as closely as possible.

A. Emulation of changing link conditions

The testbed runs predefined profiles to make reproducible tests possible. The emulated channel adds a fixed delay of 250 ms, but has a variable capacity between 50 kbit/s and 3000 kbit/s.

Figure 6 shows the capacity curve that was used throughout all tests. It starts with a maximum link capacity of 3000 kbit/s. After 10 s the link starts deteriorating linearly and reaches a minimum capacity of 50 kbit/s at 160 s. At 170 s the link starts to recover linearly and reaches its maximum again at after another 150 s. This basic scenario is sufficient to test the behavior of QoS systems. It could be enhanced to model the behavior of satellite links in a more realistic way, e.g., by incorporating weather conditions. However, this would make it harder to highlight the functionality of the MoSaKa QoS system. Thus, we postponed this for future tests, which will also incorporate transmissions over a real satellite system.

B. Functional tests

Two functional tests were performed to show that the basic QoS functions of the MoSaKa QoS system were working correctly. They reflect the goals of the MoSaKa QoS system, especially:

- The QoS system is dealing with changing link conditions.
- Best effort traffic and reserved traffic are isolated.
- Different priorities are distinguished.
- The performance of UDP and TCP is usable.

1) *UDP-only test*: In the first test, three independent UDP flows were sent over the emulated satellite link. All were directed in the same direction, to render the satellite link

Table I
QoS REQUIREMENTS FOR ALL PATHS OF THE UDP-ONLY TEST

flow	reservation@source		emission@source	
	priority	data rate	data rate	packet rate
UDP 1	low	849.6 kBit/s	100 kbyte/s	100 p/s
UDP 2	high	1,699.2 kBit/s	200 kbyte/s	200 p/s
Best Effort	(none)	(2,124 kBit/s)	250 kbyte/s	250 p/s

a bottleneck. All UDP packets carried a payload of 1,000 bytes, whereas each packet was extended by an overhead of 62 bytes. This overhead consisted of 8 bytes for the UDPv6 header, 40 bytes for the IPv6 header and 14 bytes for the header and trailer of the Ethernet frame. For an exemplary flow of 100 UDP packets per second with 1000 bytes payload each, the expected data rate on the medium was 849600 bit/s (see Equation 1).

$$100 \text{ p/s} * 1062 \text{ byte/p} * 8 \text{ bit/byte} = 849600 \text{ bit/s} \quad (1)$$

For each flow, table I lists the expected data rate on the medium. This is exactly the data rate that was also reserved for the path, if a reservation for that particular flow was required. Here, the “Best Effort” flow had no reservations, but the flows “UDP 1” and “UDP 2” had requirements regarding their data rate. Furthermore, flow “UDP 2” had a higher data rate and a higher priority than flow “UDP 1”.

The MoSaKa QoS system was configured to respect priorities and to use feedback messages to indicate that reservations were suspended or resumed. However, the UDP sources ignored these messages and kept on transmitting UDP packets. As a consequence, if a reservation was suspended, the affected UDP packets were transmitted nevertheless, but as best effort traffic. They then shared the remaining link capacity with all other best effort traffic.

The UDP sources emitted UDP packets of a fixed size. Each packet contained a time stamp and a sequence number, allowing the UDP sinks to calculate the received data rate, the transmission delay and the amount of lost packets.

Measurement results: Figure 7 depicts the sum of the data rates of all three UDP flows at the receiver. It is shown very clear that the added data rate at the receiver matched the capacity of the emulated satellite link (Figure 6). The maximum data rate was at about 350 kbyte/s, which equals – all overhead included – the maximum link capacity of 3000 kbit/s. Furthermore, the figure shows that the reservation for flow “UDP 2” (200 kbyte/s, high priority) was active as long as it fitted into the capacity of satellite link. It was suspended after 75 s, resulting in its UDP packets being transmitted as best effort traffic. This resulted in a decreasing data rate at the receiver, as the traffic was no longer isolated. After 253 s, the satellite link recovered and had enough capacity to resume the reservation for flow “UDP 2”. The protection schemes regarding this flow were reactivated, and the reserved data rate was claimed until the test ended.

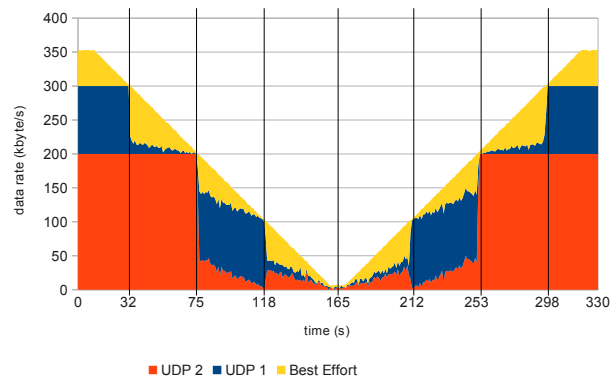


Figure 7. Overall receive data rate during the UDP-only functional test

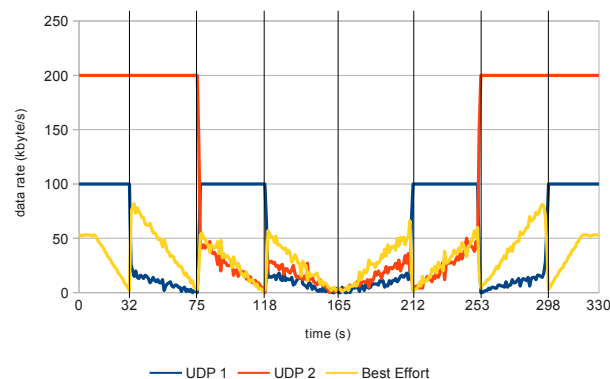


Figure 8. Receive data rate per flow during the UDP-only functional test

Figure 8 visualizes the same set of data, but shows the received data rate of each flow individually. Here, it is very interesting to have a look at flow “UDP 1”. This flow was reserved as well, with a lower data rate than flow “UDP 2”, but also with a lower priority. As a consequence, when the capacity of the link decreased, flow “UDP 1” was suspended in favor of “UDP 2”. This happened the first time at 32 s. Interestingly, after “UDP 2” was suspended at time 75 s, the link had enough capacity to schedule “UDP 1” again, which was resumed immediately. Flow “UDP 1” had protection schemes applied until 118 s, as the capacity became so low that no reservation fitted anymore and only best effort traffic was possible.

During the following phase of link recovery, the same behavior was visible again, with the reservation of “UDP 1” being resumed, suspended, and resumed again. Even if this behavior looks odd, it reflects the expected behavior of a priority-enabled reservation-based QoS system that deals with changing capacities.

As the UDP sinks tracked the sequence number of the

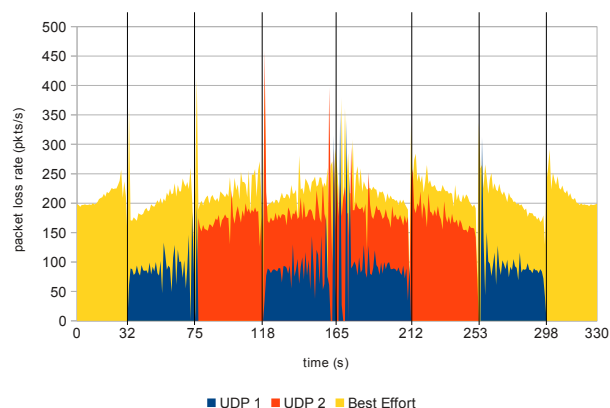


Figure 9. Packet loss rate per UDP flow

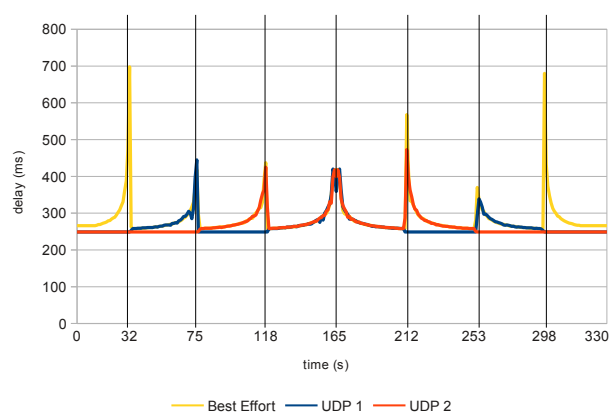


Figure 10. Transmission delay per UDP flow

received packets, they were able to count lost packets. Figure 9 depicts the packet loss rates of all three flows. Flow “UDP 2”, which had the highest priority, showed not a single packet loss before 75 s, but underwent a considerable and increasing packet loss afterwards. Flow “UDP 1”, that was suspended but resumed later as the link capacity decreased, underwent no packet loss while its reservation was active, but suffered from packet loss while it was suspended. The “Best Effort” flow showed packet loss during the whole test. However, the only purpose of this flow was to create enough traffic to stress the link, in order to check if the isolation schemes regarding reserved flows were working correctly.

For each received UDP packet, the UDP sink calculated the respective transmission delay. All clocks were synchronized and each UDP packet contained a time stamp created by the UDP source. Figure 10 shows the transmission delay of each of the three UDP flows, over the time. UDP packets of flows with an active reservation underwent a transmission delay of ≈ 250 ms, which was equal to the delay emulated by wirefilter. Interestingly, this delay was constant, showing that

Table II
QOS REQUIREMENTS FOR ALL PATHS OF THE TCP/UDP-MIXED TEST

flow	reservation@source		emission@source	
	priority	data rate	data rate	packet rate
TCP 1	low	849.6 kBit/s	not applicable	
TCP 2	high	1,699.2 kBit/s	not applicable	
Best Effort	(none)	(2,124 kBit/s)	250 kbyte/s	250 p/s

the Hierarchical Fair Service Curve (HFSC) packet scheduler of the Linux Kernel did not run out of link capacity. Best Effort traffic, which included traffic of flows that have a suspended reservation, experienced an increasing delay. The increasing delay was caused by buffering, as the packet scheduler had to process a UDP packet rate that did not fit into the capacity of the outgoing link anymore. In addition to that, this effect was also caused by the decreased link capacity itself: decreasing the data rate resulted in an increasing amount of time required to send an Ethernet frame.

2) *TCP and UDP coexistence test*: In the second functional test, the behavior of TCP (CUBIC) was investigated. A consideration of TCP is very interesting, as the slow start and congestion control functions of TCP are prone to misbehavior if running over high delay links. Furthermore, if TCP and UDP coexist on the same link, UDP is able to block TCP as TCP has intrinsic congestion control functions that UDP does not have.

This test was similar to the first functional test: three flows were sent in the same direction via the satellite link. One flow was a best effort UDP flow carrying 250 kbyte/s, while the other two flows had QoS requirements that were reserved. In terms of data rate and priority, both reservations were similar to the reservations of the UDP-only test. However, the traffic originated from two TCP connections (see table II). Unfortunately, it is challenging to calculate the data rate for the process of reservation, if only the desired data rate regarding the payload of a TCP connection is given. The slow start algorithm of TCP, a variable segment size, and retransmissions due to packet loss are only three examples why TCP might increase the amount of traffic silently.

Instead of calculating the data rate regarding Ethernet, the reservations of the UDP-only test were applied again. As in the first test, the data rates were measured at the socket level, reflecting the *effective* data rate an application can achieve if TCP is used. From the point of view of the applications, the reserved paths should behave like two exclusively assigned long delay paths with a fixed capacity, until the respective reservation is suspended.

Like in the first functional test, the TCP traffic sources ignored feedback messages. Instead, they kept on feeding their socket with user data, even if the respective reservation was suspended. Due to the flow- and congestion control functions of TCP and the limited size of the send buffers in the TCP stack, the applications were throttled if the data could not be transmitted across the network.

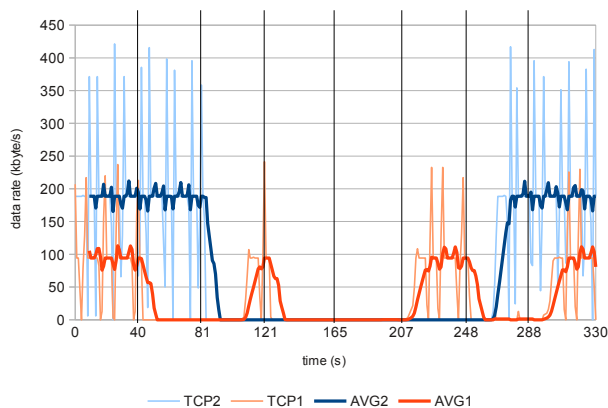


Figure 11. Received data rate per TCP connection

Measurement results: Figure 11 shows the data rates of both TCP connections, which reflect the amount of user data read from the TCP sockets at the sink, over time. The best effort UDP traffic is not depicted anymore, as its only purpose was to saturate the emulated satellite link. Each TCP connection is represented by two lines. Lighter colored lines show the received amount of data on a per-second basis, while the darker lines show an averaged versions of the same data, with a sliding window of 10 seconds applied. Filtering was required, as the effective data rates of payload were fluctuating heavily. This was caused by TCP, which guarantees ordered delivery. Received data has to be delayed if gaps exist, which leads to burst of delivered data if these gaps are closed later.

Both TCP connections were able to saturate their paths, as long as their respective reservation were active. At 40 s, the overall link capacity dropped below the sum of both reserved paths, and “TCP 2” was suspended due to its lower priority. The data rate of “TCP 2” dropped to zero, as it had to compete with the traffic of the best effort UDP flow. At 81 s, the link capacity fell below the limit of holding the reservation of “TCP 1”, and its path was suspended too. Thus, the reservation of “TCP 2” fitted again, and its path was resumed. Interestingly, “TCP 2” was not able to immediately reclaim this capacity, but required nearly 30 seconds to start delivering data to the sink application again. This may be due to the intrinsic retransmission timers and the slow start mechanisms of TCP. Future work will have to look deeper into this topic.

At 121 s, the reservation of “TCP 2” was suspended again due to lacking resources, and both TCP connections were blocked by the best effort UDP flow. As the reservation of “TCP 2” was resumed at 207 s, the delivery of data started within a short amount of time. If compared to 81 s, different recovery behaviors of “TCP 2” were observed. The authors suspect, that these differences were caused by synchronization

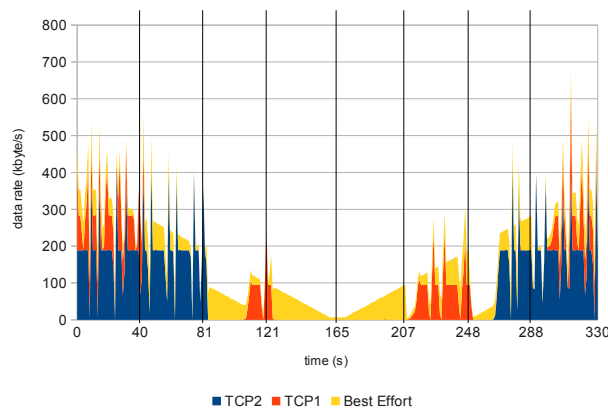


Figure 12. Overall receive data rate of both TCP connections and the best effort UDP flow

issues regarding the retransmission timers of TCP. Different TCP implementations for satellite systems or unstable links may show an improved performance.

Figure 12 depicts an interesting artifact of the testbed that was caused by the emulated satellite link. Here, the overall data rate of all three flows is shown over time. At 81 s, the reservation of “TCP 1” was suspended and the reservation of “TCP 2” was resumed. As discussed, the data rate of the first connection dropped to zero, while the data rate of the second connection did not recover. Thus, the reservation of “TCP 2” was active, but its resources laid idle. The expected behavior of a QoS system would be that idle resources are assigned to best effort traffic, but Figure 12 shows a different behavior. Here, best effort traffic did not claim idle resources of active reservations, resulting in a fall-off between 81 s and 95 s. Future research will have to look into the behavior of the real MoSaKa layer 2 system.

3) *Concluding the functional tests:* Both functional tests showed that the MoSaKa QoS system provided end-to-end guarantees. The UDP-only test revealed a perfect match of the reserved and the delivered data rate. Reserved paths did not influence each other and were protected against best effort traffic. When the link capacity decreased, paths were suspended in the order of their priority. As the affected UDP sources did not react to the feedback messages, their respective traffic was treated as best effort traffic.

Due to the perfect isolation of paths, reserved TCP connections were able to utilize the capacity offered by their respective reservation. However, the tests indicated that the path suspension mechanism may collide with TCP’s intrinsic slow start and retransmission timers. TCP connections were not able to take advantage of short intervals of activated reservations. As TCP is the most important transport protocol in IP-based networks, future work should look into possibilities to fully understand and possibly mitigate this issue by either evaluating feedback messages directly inside

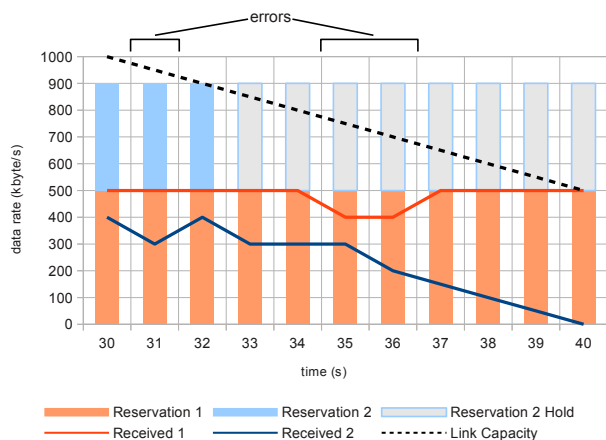


Figure 13. Example of the error analysis according to the MoSaKa QoS system

the TCP protocol entity or by taking network-layer path stability requirements into account.

C. Performance evaluation

In order to evaluate the improvement provided by using the MoSaKa QoS system, it was compared to other methods.

Measurement setup: All comparisons were performed using random sets of 32 reserved UDP-based flows with a total reserved data rate of 3000 kbit/s. Each UDP source emitted a stream of packets with 1000 bytes payload and a constant data rate. The data rate matched the reserved capacity. While the sources involved the MoSaKa QoS system to reserve paths, they did not evaluate any feedback messages. Thus, they did not adapt their output rate in case of a suspended reservation. On the peer node, the UDP sinks reported the received data rate, the packet loss rate and the delay. The link conditions were emulated as described in Section VI-A.

Each test series was evaluated against an independent implementation, checking three rules for each time slot:

- 1) Paths must be prioritized correctly. A path with a higher priority must never be blocked by one with a lower priority.
- 2) If a path still fits into the remaining capacity, it must be enabled.
- 3) Enabled paths must not lose any packets.

Figure 13 illustrates a synthetic example of the analysis process. It comprises two reserved paths, with “Reservation 1” having a high priority and “Reservation 2” having a low priority. Each path has a specific part of the capacity reserved. When the available link capacity falls below the sum of the two reservations at 33 s, “Reservation 2” is suspended. The respective traffic loses its guarantees, and the data rate at the sink falls below its reservation. This is not counted as an error, as this is the specified system behavior in case of a degrading link.

On the other hand, the time slots at 35 s and 36 s are counted as errors regarding “Reservation 1”, and the time slot at 31 s shows an error regarding “Reservation 2”. For each time slot, one can calculate which reservations should be activated and which reservations should be suspended. While flows with a suspended reservation are allowed to undergo packet loss, flows with active reservations must not. If one sink reports packet loss nevertheless, this is counted as an erroneous time slot.

Besides this, the independent implementation of the analysis software does not reason about the source of the errors, but merely implements a black box test with regard to the network. This opens up the opportunity to test against network configurations which support less extensive QoS models than MoSaKa does, or no QoS at all.

Four different QoS models are compared in this paper:

Without QoS: This QoS model served as the baseline representing the current Internet without any QoS guarantees. While individual flows still had an assumed priority and an expected data rate, the network did not obey this information.

This scenario was expected to perform the worst. Usually, routers try to assign available resources fairly, leading to a dropping of packets distributed over all flows.

Without priorities, cancel only: This simple QoS model assumed end-to-end guarantees for reserved flows. The network was able to cancel paths if link conditions deteriorated. However, canceled paths were never resumed. Having different priorities was not supported. This model corresponds to a simple IntServ system that does not offer having priorities.

Even without having priorities and without allowing suspended paths to recover, this model was expected to perform significantly better than the first model. At least for paths that still have an active reservation, the error level should decrease significantly.

With priorities, cancel only: This advanced QoS model allowed having priorities, but it still lacked the ability to re-enable a canceled path after the condition of a link recovered.

Having the ability to obey priorities, such a system should show an even lower error level. The reservations of high priority flows should be kept active longer, leading to less erroneous time slots.

MoSaKa QoS: The MoSaKa QoS model supported both path suspension and obeys priorities. It represents the contribution of the authors.

With both mechanisms in place, MoSaKa should be able to perfectly match the expected behavior, resulting in an error level of zero.

Measurement results: For each of the four QoS models, 20 test series were performed and evaluated, using the same setup as described earlier. The number of erroneous time slots of all 32 flows were averaged, and these averaged error levels were averaged again among all 20 test series. The resulting

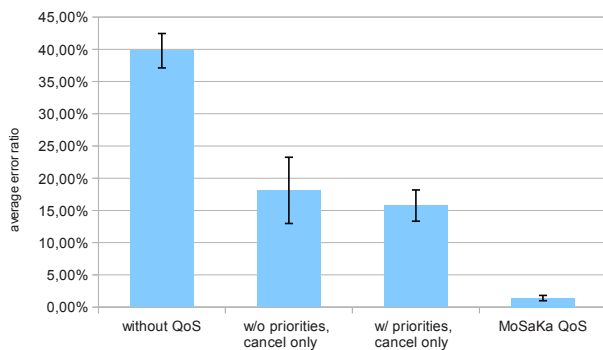


Figure 14. Average error levels of different QoS models

four error levels and their respective standard deviation are shown in Figure 14.

As expected, the first model without any QoS performed worst. If the link capacity dropped below the sum of all flows, the network started dropping packets of all flows. This affected all paths in the same way with no regard to priorities.

Only flows with a low priority showed low error levels, as the analyzer expected these flows to be suspended early. For flows with higher priorities, the error levels increased. On average, in approximately 40% of the time slots of a path's lifetime, the system was not able to provide the *desired* QoS.

Introducing a QoS model, at first a simple one, improved the situation. Even without obeying priorities or providing path suspension, the error levels dropped to 18% on average. If a path was canceled, its resources were freed. These free resources helped keeping the remaining reservations active for a longer time.

Interestingly, testing an advanced QoS model that respects priorities showed only a slight improvement. The average error levels dropped to approximately 16%. With the given link capacity curve as depicted in Figure 6, the most erroneous time slots happened in the second half of each test series. Once a path was canceled, it never recovered. Therefore, its traffic had to compete in the best effort class. This led to a similar situation as in the first model (without QoS), where packet loss affected all paths uniformly.

Having the full feature set of the MoSaKa QoS system, error level dropped to 1.4%. This was not a perfect result, but most of the errors can be attributed to imperfections in the measurement setup. Having time slots of a given duration leads to false negatives when paths switch state within a slot. Decreasing slot durations would help, but that would lead to other problems: introducing shorter slot times complicates the assessment of flows, especially if they have a low packet rate. Then, many of the slots are empty, and the system starts to detect scheduling effects which might move packets between slots, wrongly leading to errors again.

As expected, MoSaKa performed nearly perfect under the

given scenario. Paths were suspended in the correct order and returned to service once the conditions improved.

VII. CONCLUSION AND FUTURE WORK

In this paper, a novel QoS architecture called "MoSaKa QoS" was presented. It was designed for networks that involve mobile satellite-based communication links. Previous reservation-based approaches like IntServ are not suited, as the link to the satellite is considered unstable, i.e., provides a varying data rate. In MoSaKa QoS, this problem was circumvented by the introduction of a novel feedback mechanism, that suspends reservations without canceling them. The applications are informed that their reservation was suspended, allowing them to degrade gracefully. To provide an example, a video conferencing software was equipped with these features.

Furthermore, a testbed was set up, containing all components of the MoSaKa QoS system, besides "real" MoSaKa terminals that communicate via a satellite. Instead of a transmission via a satellite, the respective link was emulated with respect to delay and a capacity that changes over time. Extensive measurements were obtained, showing that the reservation-based QoS system of MoSaKa is working correctly. Additionally, it was shown that TCP is able to saturate the path despite the high delay of the link. Apart from that, the performance of TCP went down if no respective reservation was active, and the TCP connection had to share transmission resources with other best effort traffic. Hence, the MoSaKa QoS system enables TCP to be used over congested bottlenecks, even if the end-to-end connection has a high delay.

Besides that, the MoSaKa QoS system was compared to similar approaches. It was shown that the combination of a feedback mechanism and different priorities for reservations offer the best compliance regarding individual QoS requirements. Without feedback, applications have to poll for resources or stop communication altogether. Without distinguishing priorities, the network may suspend flows that are important to the user.

In brief, the MoSaKa QoS system combines the versatility of packet-switched networks with QoS parameters offered by circuit-switched systems. Thus, it allows the coexistence of high-priority voice communication and other low-priority traffic, which is an essential feature of a communication network designed for rescue teams in disaster relief missions.

The components of the MoSaKa QoS system were implemented and are available for GNU/Linux-based systems. Moreover, a testbed for system-wide tests was set up. However, the "real" MoSaKa satellite terminals with their own L2 and L1 components were not operational yet. Thus, as a first step, the satellite link was emulated by using the Qemu/KVM and VDE-tool packages. The results were as expected. Furthermore, it is interesting to check whether the same tests, applied on a testbed involving a

real satellite link, lead to similar results. Besides that, future tests will incorporate sophisticated models regarding terminal movement and weather conditions, providing a more realistic model of the capacity of the emulated satellite link.

From the point of view of the architecture, further research might look into alternative QoS models based on probability distributions instead of hard thresholds. This includes novel reservation models, which provide sophisticated ways of expressing requirements. This enables the system to adapt better to changing link conditions without consulting the applications.

Regarding the network topology, the current MoSaKa system was designed to have a static IPv6-based routing setup. In the future, the system should adapt to various routing protocols, to enable mobility at the network level. In addition, it is beneficial to add support for QoS-enabled multicast traffic, which is currently not supported by our signaling protocol.

Future research should also investigate the possibilities opened up by the MoSaKa feedback mechanism. Currently available audio and video codecs offer various output profiles with different data rates and quality settings. An integration with the MoSaKa QoS system, with the possibility to specify multiple possible data rates per reservation, promises an advanced scheme for graceful degradation.

Moreover, it is not clear yet how the MoSaKa QoS system should interact with non-MoSaka end systems, such as web servers in the Internet. Currently, as there is no Dispatcher on the peer node, the signaling handshake does not complete. Thus, there is no reservation on the satellite link, rendering TCP unusable if most of the resources are occupied. Possibly, these issues can be solved by introducing translator applications such as proxies, or DiffServ-like classification approaches.

REFERENCES

- [1] P. Drieß, F. Evers, and M. Brückner, "A Resource Management Architecture for Mobile Satellite-based Communication Systems," in *The Eighth Advanced International Conference on Telecommunications, AICT 2012*, Stuttgart, 05 2012.
- [2] J. Wroclawski, "The Use of RSVP with IETF Integrated Services," *RFC 2210*, September 1997.
- [3] S. Blake, D. Black, M. Carlson, E. Davies, Z. Wang, and W. Weiss, "An Architecture for Differentiated Services," *RFC 2475*, December 1998.
- [4] M. Hein, A. Kraus, R. Stephan, C. Volmer, A. Heuberger, E. Eberlein, C. Keip, M. Mehnert, A. Mitschele-Thiel, P. Driess, and T. Volkert, "Perspectives for Mobile Satellite Communications in Ka-Band (MoSaKa)," in *EuCAP 2010: The 4th European Conference on Antennas and Propagation*, Barcelona, Spain, 04 2010.
- [5] J. Wroclawski, "Specification of the Controlled-Load Network Element Service," *RFC 2211*, September 1997.
- [6] S. Shenker, C. Partridge, and R. Guerin, "Specification of Guaranteed Quality of Services," *RFC 2212*, September 1997.
- [7] K. Nichols, S. Blake, F. Baker, and D. Black, "Definition of the Differentiated Services Field (DS Field) in the IPv4 and IPv6 Headers," *RFC 2474*, December 1998.
- [8] A. Mankin, Ed., F. Baker, B. Braden, S. Bradner, M. O'Dell, A. Romanow, A. Weinrib, and L. Zhang, "Resource ReSer-Vation Protocol (RSVP) – Version 1 Applicability Statement Some Guidelines on Deployment," *RFC 2208*, September 1997.
- [9] R. Hancock, G. Karagiannis, J. Loughney, and S. V. den Bosch, "Next Steps in Signaling (NSIS): Framework," *RFC 4080*, June 2005.
- [10] J. Manner, G. Karagiannis, and A. McDonald, "NSIS Signaling Layer Protocol (NSLP) for Quality-of-Service Signaling," *RFC 5974*, October 2010.
- [11] E. G. Ash, E. A. Bader, E. C. Kappler, and E. D. Oran, "QSPEC Template for the Quality-of-Service NSIS Signaling Layer Protocol (NSLP)," *RFC 5975*, October 2005.
- [12] S.-B. Lee, G.-S. Ahn, X. Zhang, and A. T. Campbell, "INSIGNIA: An IP-Based Quality of Service Framework for Mobile ad Hoc Networks," *Journal of Parallel and Distributed Computing*, no. 60, pp. 374–406, 2000.
- [13] P. Chandra, Y.-H. Chu, A. Fisher, G. Jun, C. KosaK, T. E. Ng, P. Steenkiste, E. Takahashi, and H. Zhang, "Darwin: Customizable Resource Management for Value-Added Network Services," *IEEE Network*, vol. 15, no. 1, 2001.
- [14] *Digital Video Broadcasting (DVB); Second Generation DVB Interactive Satellite System (DVB-RCS2); Part 3: Higher Layers Satellite Specification*, ETSI, 5 2012, ETSI TS 101 545-3 V1.1.1 (2012-05).
- [15] "Inmarsat – BGAN," 12 2012. [Online]. Available: <http://www.inmarsat.com/services/BGAN>
- [16] E. Re, M. Ruggieri, and G. Guidotti, "Integration of TETRA with Satellite Networks: A Contribution to the IMT-A Vision," *Wirel. Pers. Commun.*, vol. 45, pp. 559–568, June 2008. [Online]. Available: <http://dl.acm.org/citation.cfm?id=1363306.1363328>
- [17] F. Bellard, "QEMU, a fast and portable dynamic translator," in *Proceedings of the annual conference on USENIX Annual Technical Conference*, ser. ATEC '05. Berkeley, CA, USA: USENIX Association, 2005, pp. 41–41. [Online]. Available: <http://dl.acm.org/citation.cfm?id=1247360.1247401>
- [18] R. Davoli, "VDE: Virtual Distributed Ethernet," in *Proceedings of the First International Conference on Testbeds and Research Infrastructures for the DEvelopment of NeTworks and COMMunities*. Washington, DC, USA: IEEE Computer Society, 2005, pp. 213–220. [Online]. Available: <http://dl.acm.org/citation.cfm?id=1042447.1043718>

Throughput, Stability and Fairness of RFID Anti-Collision Algorithms with Tag Cooperation

Ramiro Sámano-Robles and Atilio Gameiro

Instituto de Telecomunicações, Campus Universitário, Aveiro, 3810-193, Portugal.

emails:ramiro@av.it.pt, amg@ua.pt

Abstract—This paper addresses the design of a class of anti-collision algorithms for passive RFID (radio frequency identification) systems, where tags are allowed to cooperate by relaying (if necessary) the signals of other tags towards the destination. All the relayed signals are combined at the reader side so as to improve tag detection probabilities. The work is focused on asymmetrical scenarios where tags and readers experience different channel statistics. The objective is to include tag cooperation in RFID anti-collision algorithms. To achieve this goal, a framework for medium-access-control and physical (MAC/PHY) cross-layer design of cooperative RFID anti-collision algorithms is here presented. A tag activity model is also proposed where different tag states are initially selected according to the tag activation SINR (signal-to-interference-plus-noise ratio). Tags activated by high SINR values enter into states with relaying capabilities, whereas those with low SINR values act as simple sources of information (non-relaying state). Tags can change state depending on the number of (re)transmissions performed. A Markov model is used to calculate the system steady-state probabilities. Instability is evaluated by the number of tags in the backlog state, while fairness is evaluated by means of the Gini index. Results show that tag cooperation is useful in networks where tags with good channel states and low traffic requests cooperate with tags with bad channel states and low traffic requests.

Index Terms—RFID anti-collision algorithms; cross-layer design; random access theory; cooperative diversity.

I. INTRODUCTION

A. RFID technology and previous works

RFID (Radio Frequency Identification) has been identified as a good candidate for enabling the concept of the Internet-of-Things (IoT). The main idea behind the concept of the IoT is to finally bridge the gap between the virtual world of computers and the physical world of objects. In RFID, a reader or interrogator requests information (via radio frequency signals) to low-cost tags or transponders [1]. These tags, which are in charge of responding to reader's requests, can be attached to objects, animals or humans, and in some cases they can sense environmental parameters such as temperature, position and speed [2]. In passive RFID, where tags reuse the energy radiated by readers, the limited coordination capabilities between the network elements leads to the problem of signal collisions. Therefore, an efficient medium access control (MAC) layer is crucial to the correct operation of RFID [3].

Two types of collision can be identified at the MAC layer of RFID: *tag* and *reader* collision. A tag collision occurs when two or more tags simultaneously respond to the same request.

Anti-collision schemes such as ALOHA and binary tree algorithms are commonly employed to resolve tag collisions [3]. Tag estimation methodologies [4], and modified frame structures [3] have been proposed to improve the performance of these anti-collision algorithms. Two types of reader collision can be also identified: *multiple-reader-to-tag* and *reader-to-reader* [5]. Two types of reader anti-collision algorithms can be distinguished: those based on scheduling and those based on coverage control. Typical scheduling schemes have been subject to standardization: e.g., frequency division multiple access (FDMA) in [6], and listen-before-talk (LBT) in [7]. More advanced schemes such as Colorwave [8] and Pulse [9] implement inter-reader control mechanisms to assist in collision avoidance. These schemes have paved the way for self-organizing RFID anti-collision algorithms. Other solutions such as HiQ [10] employ an analysis of collision patterns to improve reader scheduling and thus reduce collision events in subsequent time slots. In coverage-based algorithms, we can find schemes that reduce the overlapping coverage area between readers (e.g., [11]), and those that monitor interference to adapt power levels accordingly (e.g., [12]).

B. Open issues and objectives

Despite these recent advances in RFID MAC layer design, several issues remain open today. In particular, the last few years have seen the proliferation of advanced signal processing tools for conventional wireless networks (see [13] and [14]) that have not been fully explored in RFID. It is expected that these algorithms will improve the performance of RFID just as they improve conventional systems [15]. However, in order to support a new physical (PHY) layer, an appropriate MAC layer design is also required. This opens a wide range of MAC/PHY cross-layer design issues for RFID.

One of the potential new PHY layer schemes for RFID is known as cooperative diversity (CD). CD has been shown to improve capacity, coverage, fairness and power consumption of conventional wireless networks [20]. In networks with CD, terminals are allowed to relay the packets of other terminals. The network of relays mimics a macroscopic multiple antenna system with high diversity gains. CD in RFID has been explored only at the reader level in [17]. However, tag cooperation, to the best of our knowledge, has not been addressed yet. The main reason for this is the limited processing capabilities of passive tags, which would avoid, in principle, the use of tag-to-tag communication. However, recent developments in

[16] have shown that such tag-to-tag communication can also be achieved in passive RFID.

The objective of this paper is to include tag cooperation in the design of RFID anti-collision algorithms. In this paper it is assumed that passive tag-to-tag communication is feasible. Therefore, our focus is on the study of the consequences of cooperation at the MAC layer rather than on the demonstration of the feasibility of such tag cooperation. Recent results in [16], however, suggest that the tag PHY cooperative layer modeled in this work is feasible or is closed to be enabled by technology developments. To achieve an appropriate analysis of tag cooperative schemes, a new design paradigm, commonly known as MAC/PHY cross-layer design, is also required. MAC/PHY cross-layer design plays a crucial role in the design of conventional systems with CD. For example, the work in [18] uses CD not only to improve PHY layer performance, but also to resolve collisions at the MAC layer. Throughput and stability analysis of ALOHA with CD has been presented in [19]. A unified framework for cross-layer design in CD networks has been described in [20], and a two-transmitter two-receiver cooperative cross-layer algorithm has been proposed in [21], among several other solutions in the literature.

C. Paper contributions

This paper proposes an extension of the framework for MAC/PHY cross-layer design of RFID systems previously presented in [1] to cope with tag cooperation capabilities. The framework includes a tag reception model suitable for MAC/PHY cooperative cross-layer design, where relaying re-transmissions are requested only when the tag is not correctly detected by the destination. Reception probabilities calculated in closed-form in [22] for the particular case of Rayleigh channels are also used in this work. In addition, tag activity is modeled with different tag states that initially depend on the tag activation SINR: tags activated by a relatively high SINR are driven into a state where they are able to relay the signals of other tags in the network. By contrast, tags activated by the minimum SINR are considered to enter a state where they have no relaying capabilities, thereby acting as simple sources of information. The states of the all network, i.e. the collection of tags in their different states, are mapped into a one-dimensional Markov model that can be solved by conventional eigenvalue analysis. The solution provides the steady-state probabilities of the network, which are then used to calculate different metrics of the system, such as throughput, average number of activated tags in the backlog state, backlog delay, and fairness (by means of the Gini index). Numerical results show interesting properties of cooperative diversity in RFID networks. The modeling tools proposed in this paper, which assume an asymmetrical network deployment, and which include in the same design both reader and tag anti-collision cooperative components, also represent a novel contribution and a more realistic modeling approach of complex RFID networks. Therefore, the analytical framework developed here is envisioned for future RFID systems with large numbers of tags and readers where interference becomes a relevant issue in MAC layer design.

TABLE I
NOTATION AND SYMBOLS

Symbols	Meaning
$ \cdot $	Absolute value and set cardinality operator
$\bar{(\cdot)} = 1 - (\cdot)$	Complement to one
\mathcal{R}	Set of available readers
K	Number of available readers
\mathcal{R}_t	Subset of contending readers
$P_{r,k}$	Transmit power of reader k
$p_{r,k}$	Transmission probability of reader k
\mathcal{T}	Set of available tags
J	Number of available tags
\mathcal{T}_t	Subset of contending tags
\mathcal{T}_P	Subset of activated tags
$\mathcal{T}_P^{(d)}$	Subset of tags in state d
D	Maximum number of tag states
$\mathcal{T}_{c,j}$	Subset of tags cooperating with tag j
$\mathcal{T}_{D,k}$	Subset of tags detected by reader k
$P_{t,j}$	Transmit power of tag j
$p_{t,j}$	Transmission probability of tag j
$p_{ret,j}$	Cooperative re-transmission probability of tag j
$h_{k,j}$	Channel between reader k and tag j
$g_{k,m}$	Channel between reader k and tag m
$u_{i,j}$	Channel between tag i and tag j
$\gamma_{k,j}$	SINR of tag j due to a transmissions of reader k
$I_{r_{k,j}}$	Reader interference to the signal of reader k at tag j
I_{t_j}	Interference created by active tags on tag j
$\sigma_{v,j}^2$	Noise variance at tag j
$\tilde{\gamma}_j^{(d)}$	Tag activation threshold for state d
β_j	Backscattering factor of tags j
$\hat{\gamma}_{j,k}$	SINR of the signals of tag j at reader k
\hat{I}_{r_k}	Reader interference on reader k
$\hat{I}_{t_{j,k}}$	Tag interference to the signal of tag j at reader k
$\sigma_{v,k}^2$	Noise variance at reader k
η_k	Leakage ratio for reader k
$\tilde{\gamma}_k$	Detection threshold of reader k
R	Maximum number of transmissions per resolution period
$\xi_{j,i}$	SINR of tag j at tag i
$I_{r,i}$	Reader interference on tag i
$\tilde{\gamma}_i$	Tag detection threshold of tag i
$\hat{\gamma}_{j,k}^{(c)}(n)$	Cooperative SINR of tag j at reader k in time slot n
$\hat{\gamma}_{j,k}^{(tot)}(n)$	MRC SINR of tag j at reader k in time slot n
$\mathcal{N}(n)$, Network state information in time slot n
$Q_{j \mathcal{N}(n)}^{(d)}$	Tag activation probability for state d
$G_{j \mathcal{N}(n)}^{(d)}$	Tag transition probability for state d
\mathbf{s}	Steady-state probability vector
\mathbf{M}	Matrix transition probability
$q_{j \mathcal{N}(n)}$	Tag detection probability
$q_{j \mathcal{N}(n)}^{(c)}$	Cooperative tag detection probability
$q_{j \mathcal{N}(n)}^{(tot)}$	Total cooperative tag detection probability
l_{ep}	Length of resolution period
T_j	Tag j throughput or reading rate
D_b	Delay
F_G	Gini index

D. Paper organization

Section II describes the proposed framework for RFID cross-layer optimization with the signal models for down-link, up-link and cooperative reception. Section III describes the proposed metrics, the tag reception and activation probabilities, and the Markov model for dynamic analysis. Section IV presents the optimization of the throughput and the results obtained in different scenarios. Finally, Section V presents the conclusions of the paper.

II. SYSTEM MODEL AND CROSS-LAYER FRAMEWORK

A. Scenario description and protocol operation

Consider the slotted RFID network depicted in Fig. 1 with a set of K readers denoted by $\mathcal{R} = \{1, \dots, K\}$, and a set of J tags denoted by $\mathcal{T} = \{1, \dots, J\}$. Tags are allowed to relay, if requested, the signals of other tags towards the readers of the network. At the reader side, all the copies of the relayed signal of a given tag are combined (using a maximum ratio combiner -MRC-) so as to achieve high diversity gains. In this paper it is assumed that readers have enough complexity for MRC processing. However, all expressions also apply for systems without MRC. The relaying protocol used in the tags will be decode-and-forward (DF). Four main processes can be identified in the cooperative RFID network in Fig. 1:

- *Tag activation* by the transmission of readers, also called the *down-link transmission*,
- *Backscattering response* by previously activated tags, also called *up-link transmission*,
- Tag detection by neighbor tags or *tag-to-tag communication*, and
- *Relaying* of signals by cooperative tags and the signal combining at the reader side.

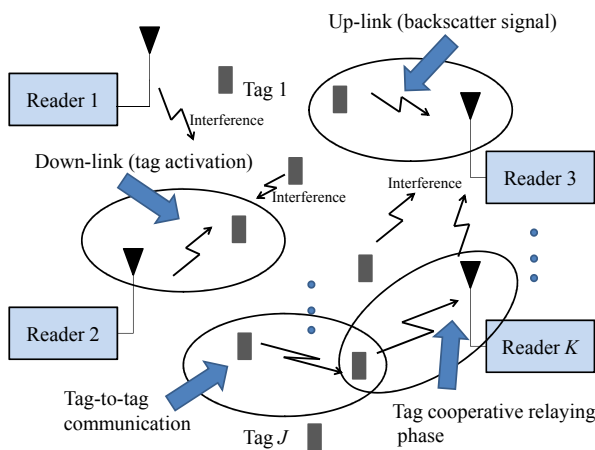


Fig. 1. Multi-tag and Multi-reader deployment scenario with cooperation between tags.

In the down-link, the transmit power of reader k will be denoted by $P_{r,k}$, while its probability of transmission will be denoted by $p_{r,k}$. The subset of active readers at any given time will be denoted by \mathcal{R}_t . Tags are activated whenever the SINR

received from a reader is above an activation threshold $\tilde{\gamma}_j^{(0)}$. A tag will be assumed to be in D possible different states according to the SINR level that was used to activate it. For example, if the SINR is above the minimum SINR threshold for activation $\tilde{\gamma}_j^{(0)}$ and below a second SINR threshold $\tilde{\gamma}_j^{(1)}$, where $\tilde{\gamma}_j^{(1)} > \tilde{\gamma}_j^{(0)}$, then the tag will only act as a source of information. On the contrary, if the SINR that activates a tag is above $\tilde{\gamma}_j^{(d)}$ and below $\tilde{\gamma}_j^{(d+1)}$, with $d > 1$, then the tag is allowed to retransmit either its own signal or that of another tag up to d times. The set of active tags in state d will be denoted here by $\mathcal{T}_P^{(d)}$, where $\mathcal{T}_P^{(d)} \subseteq \mathcal{T}$ and $d \in \{1, \dots, D\}$. These active tags proceed to transmit a backscatter signal to the readers using a randomized transmission scheme. The set of tags that have been activated, regardless of their available energy status, is simply denoted by \mathcal{T}_P , where $\mathcal{T}_P = \bigcup_{d=1}^D \mathcal{T}_P^{(d)}$. The subset of tags that transmit a backscatter signal once they have been activated will be given by \mathcal{T}_t , where $\mathcal{T}_t \subseteq \mathcal{T}_P \subseteq \mathcal{T}$ and where each tag $j \in \mathcal{T}_t$ will transmit with a power level denoted by $P_{t,j}$. Whenever a tag is not correctly detected, the system proceeds to request the immediate retransmission either from the original tag or from another tag that has correctly decoded the original transmission and that has enough energy to relay a copy towards the reader(s). The cooperative retransmission probability of tag j is denoted by $p_{ret,j}$, while the set of tags that have relayed a signal of tag j in time slot n is denoted by $\mathcal{T}_{c,j}(n)$. The maximum number of requested retransmissions is denoted by R . Since in cooperative protocols with half duplex constraints a packet transmission can take a random number of time-slots, the length of a cooperative phase or *epoch-slot* will denoted here by the random variable l_{ep} , where $0 \leq l_{ep} \leq R$. Finally, the set of tags correctly detected by reader k will be denoted by $\mathcal{T}_{D,k}$.

B. Tag activation: Down-link model

Let us consider that the channel between reader k and tag j is given by $h_{k,j}$, while the channel between reader k and reader m is given by $g_{k,m}$, and the channel between tag i and tag j is given by $u_{i,j}$. Therefore, the signal-to-interference-plus-noise ratio (SINR) experienced by tag j due to a transmission of reader k , which is denoted here by $\gamma_{k,j}$, can be expressed as follows:

$$\gamma_{k,j} = \frac{P_{r,k}|h_{k,j}|^2}{I_{r_{k,j}} + I_{t_j} + \sigma_{v,j}^2}, \quad k \in \mathcal{R}_t \quad (1)$$

where $I_{r_{k,j}} = \sum_{m \in \mathcal{R}_t, m \neq k} P_{r,m}|h_{m,j}|^2$ is the interference created by other active readers, $I_{t_j} = \sum_{i \in \mathcal{T}_t, i \neq j} P_{t,i}(|u_{i,j}|^2)$ is the interference created by other contending tags, and $\sigma_{v,j}^2$ is the noise component. If the SINR experienced by a given tag j , which was initially inactive, is above the threshold $\tilde{\gamma}_j^{(d-1)}$ and below the threshold $\tilde{\gamma}_j^{(d)}$, then the tag is assumed to enter into state d . The probability of an initially inactive tag j being activated to state d in epoch-slot n can thus be written as follows:

$$\Pr\{j \in \mathcal{T}_P^{(d)}(n) | j \in \mathcal{T}_P^{(0)}(n-1)\} = \Pr\{\tilde{\gamma}_j^{(d-1)} < \max_k \gamma_{k,j}(n) > \tilde{\gamma}_j^{(d)}\}, \quad (2)$$

which means that the probability of tag j being activated to state d is equal to the probability of the activation SINR being below $\tilde{\gamma}_j^{(d)}$ and above $\tilde{\gamma}_j^{(d-1)}$.

C. Backscattering transmission: up-link model (non-cooperative)

Once a given tag j has been activated, it starts a random transmission process to prevent collisions with other active tags. This random transmission control will be characterized by a Bernoulli process with parameter $p_{t,j}$, which is also the transmission probability. We consider the backscattering factor β_j as the fraction of the received power reused by the tag to reply to the reader. Therefore, the transmit power of tag j can be calculated as $P_{t,j} = \beta_j P_{r,k} |h_{k_{opt},j}|^2$, where $k_{opt} = \arg \max_k \gamma_{k,j}$ denotes the reader that has previously activated the tag. The SINR of the signal of tag j received by reader k can then be written as:

$$\hat{\gamma}_{j,k} = \frac{P_{t,j} |h_{j,k}|^2}{\hat{I}_{r,k} + \hat{I}_{t,j,k} + P_{r,k} \eta_k + \hat{\sigma}_{v,k}^2}, \quad j \in \mathcal{T}_t \quad (3)$$

where $\hat{I}_{r,k} = \sum_{m \neq k} P_{r,m} |g_{m,k}|^2$ is the interference created by active readers, $\hat{I}_{t,j,k} = \sum_{i \neq j} P_{t,i} |h_{i,k}|^2$ is the interference created by other active tags, η_k is the power ratio leaked from the down-link transmission chain, and $\hat{\sigma}_{v,k}^2$ is the noise at the reader side. Tag j can be detected by reader k if the received SINR is above a threshold denoted by $\tilde{\gamma}_k$. The probability of tag j being detected by reader k in the non-cooperative phase will be thus given by

$$\Pr\{j \in \mathcal{T}_{D,k}\} = \Pr\{\hat{\gamma}_{j,k} > \tilde{\gamma}_k\}, \quad (4)$$

which means that the probability of tag j being inside the set of detected tags of reader k is equal to the probability of the SINR of tag j at reader k being above the detection threshold of reader k . Whenever a tag is not correctly detected by the reader(s), the system enters into a cooperative phase with a maximum of R transmissions (one direct transmission and $R - 1$ possible cooperative retransmissions). The cooperative retransmissions are continuously requested until the tag is correctly decoded or until the maximum number of retransmissions $R - 1$ has been reached.

D. Tag-to-tag transmission model

The SINR of the signal of tag j received by tag i can be written as:

$$\xi_{j,i} = \frac{P_{t,j} |u_{j,i}|^2}{I_{r,i} + I_{t_i} + \sigma_{v,i}^2}, \quad j \in \mathcal{T}_t, \quad (5)$$

where $I_{r,i} = \sum_{m \in \mathcal{R}_t} P_{r,m} |h_{m,i}|^2$ is the interference created by active readers. Tag j can be detected by tag i if the received SINR is above a threshold denoted by $\tilde{\gamma}_{i,r}$. The probability of tag j being correctly detected by tag i will be thus given by

$$\Pr\{\xi_{j,i} > \tilde{\gamma}_{i,r}\}, \quad (6)$$

which indicates that the probability of tag j being detected by tag i is simply the probability that its SINR is above the tag detection threshold of tag i .

E. Cooperative relaying phase model

Whenever a given tag is incorrectly detected by the reader, the system will request retransmission by means of an ideal feed-back channel. Tags in a relaying-able state, which have correctly decoded the original transmission and which are allowed to retransmit, proceed to do so in the following time slot. The SINR experienced by the transmission of tag j received by reader k in the cooperative phase is denoted by $\hat{\gamma}_{j,k}^{(c)}$, and it is given by:

$$\hat{\gamma}_{j,k}^{(c)} = \frac{\sum_{i \in \mathcal{T}_{c,j}} P_{t,i} |h_{k,i}|^2}{\hat{I}_{r,k} + \hat{I}_{t,j,k} + P_{r,k} \eta_k + \hat{\sigma}_{v,k}^2}, \quad j \in \mathcal{T}_t \quad (7)$$

Since the reader proceeds to the combining of current and previous received copies of the transmission via the MRC receiver, the total SINR at the p -th time slot of an epoch slot is the summation of all SINRs of the transmissions in previous time slots of the epoch slot:

$$\hat{\gamma}_{j,k}^{(tot)}(p) = \hat{\gamma}_{j,k} + \sum_{w=2}^p \hat{\gamma}_{j,k}^{(c)}(w). \quad (8)$$

The total probability of tag j being detected by reader k in the cooperative phase at the p -th time slot will be thus given by

$$\Pr\{j \in \mathcal{T}_{D,k}\} = \Pr\{\hat{\gamma}_{j,k}^{(tot)}(p) > \tilde{\gamma}_k\}, \quad (9)$$

which simply indicates the probability that the cooperative SINR is above the tag detection threshold of reader k . Since the relaying phases will be activated only when the previous transmissions were not correctly detected, it is convenient to rewrite the previous probability in eq.(9) indicating the statistical dependency on the incorrect reception during the previous time-slots as follows:

$$\Pr\{j \in \mathcal{T}_{D,k}\} = \Pr\{\hat{\gamma}_{j,k}^{(tot)}(p) > \tilde{\gamma}_k | \hat{\gamma}_{j,k}^{(tot)}(p-1) < \tilde{\gamma}_k\}. \quad (10)$$

Closed-form expressions for these conditional reception probabilities in the case of single-user transmission have been derived in [22] for Rayleigh fading channels and will be reused here to calculate performance metrics in subsequent sections.

III. PERFORMANCE METRICS AND MARKOV MODEL

The main performance metric to be used in this paper is the average tag throughput or tag reading rate, which can be defined as the long term ratio of correct tag readings to the total number of time slots used in the measurement. Before providing an expression for this metric, it is first necessary to define the following concepts and tools: the network state information, both the tag activation and tag reception probability models, and the Markov model that will be used for the dynamic performance analysis of the RFID network.

A. Network state information and tag activation model

The network state information can be defined as the collection of all the parameters that completely describe the network at any given epoch slot. In our particular case, the network state information at epoch slot n , denoted by $\mathcal{N}(n)$, is defined

here as the collection of the sets of active readers $\mathcal{R}_t(n)$ and contending tags $\mathcal{T}_t(n)$ during epoch slot n :

$$\mathcal{N}(n) = \{\mathcal{R}_t(n), \mathcal{T}_t(n)\}. \quad (11)$$

Once the network state information has been defined, we can then define the probability of tag j being activated and driven into state d in epoch slot n , given that it was inactive in the previous epoch slot and conditional on a given realization of the network state information $\mathcal{N}(n)$. This can be written, with the help of eq. (1) and (2), as follows:

$$Q_{j|\mathcal{N}(n)}^{(d)} = \Pr\{j \in \mathcal{T}_P^{(d)}(n+1) | \mathcal{N}(n), j \in \mathcal{T}_P^{(0)}(n)\} = \Pr\{\tilde{\gamma}_j^{(d-1)} < \max_k \gamma_{k,j}(n) > \tilde{\gamma}_j^{(d)}\}. \quad (12)$$

Let us now define the probability that tag j downgrades its state from being in state $d+x$ in epoch slot n to being in state d in the following epoch slot, conditional on a given realization of the network state information $\mathcal{N}(n)$. In this paper a tag transmission either in cooperative or non-cooperative mode is the only way for a tag to downgrade its state. In the cooperative phase, the number of retransmissions depends on the length of the epoch slot. These conditions can be mathematically written, with the help of eq.(6), as follows:

$$G_{j|\mathcal{N}(n)}^{(d)} = \Pr\{j \in \mathcal{T}_P^{(d)}(n+1) | \mathcal{N}(n), j \in \mathcal{T}_P^{(d+x)}(n)\} = \begin{cases} \Pr\{l_{ep}(n) > x\} (p_{t,j} + \bar{p}_{t,j} p_{ret,j} \sum_{i \in \mathcal{T}_P^{(d+1)}(n)} \Pr\{\max_k \xi_{i,j}(n) > \tilde{\gamma}_j\}), & d = 0 \\ \Pr\{l_{ep}(n) = x\} (p_{t,j} + \bar{p}_{t,j} p_{ret,j} \sum_{i \in \mathcal{T}_P^{(d+1)}(n)} \Pr\{\max_k \xi_{i,j}(n) > \tilde{\gamma}_j\}), & d > 0 \end{cases}, \quad (13)$$

which contains all the possible transitions between the states of the network whenever a non-cooperative or cooperative transmission have been used. The common term in eq.(13) given by $p_{t,j} + \bar{p}_{t,j} p_{ret,j} \sum_{i \in \mathcal{T}_P^{(d+1)}(n)} \Pr\{\max_k \xi_{i,j}(n) > \tilde{\gamma}_j\}$ indicates the probability that a tag transmits with probability $p_{t,j}$ plus the probability that it cooperates with any of the other tags with probability $\bar{p}_{t,j} p_{ret,j}$ given that it has correctly detected any of the tags that requires cooperation with probability $\sum_{i \in \mathcal{T}_P^{(d+1)}(n)} \Pr\{\max_k \xi_{i,j}(n) > \tilde{\gamma}_j\}$. In the case that $d = 0$ we assume that the length of the cooperative epoch $\Pr\{l_{ep}(n) > x\}$ has exceeded the available number of transmissions of tag j and thus the tag boils down to state zero or to the inactive state. In the case that $d > 0$ we assume that the length of the epoch is exactly equal to the difference between the two tag states $\Pr\{l_{ep}(n) = x\}$. Therefore, this expression contains the behavior of the tags that have overheard the transmission of the other tags and that proceed to act as cooperative relays with a randomized transmission process. For convenience in the analysis, let us rewrite these probabilities in terms of the set of active tags $\mathcal{T}_P(n)$ by averaging over all values of $\mathcal{N}(n)$ where $\mathcal{T}_t(n) \in \mathcal{T}_P(n)$:

$$Q_{j|\mathcal{T}_P(n)}^{(d)} = \sum_{\mathcal{N}(n); \mathcal{T}_t(n) \in \mathcal{T}_P(n)} \Pr\{\mathcal{N}(n)\} Q_{j|\mathcal{N}(n)}^{(d)}, \quad (14)$$

and

$$G_{j|\mathcal{T}_P(n)}^{(d)} = \sum_{\mathcal{N}(n); \mathcal{T}_t(n) \in \mathcal{T}_P(n)} \Pr\{\mathcal{N}(n)\} G_{j|\mathcal{N}(n)}^{(d)}, \quad (15)$$

where $\Pr\{\mathcal{N}(n)\}$ is the probability of occurrence of a given realization of the network state information $\mathcal{N}(n)$. This term can be calculated by considering all the combinations of active tags and readers as follows:

$$\Pr\{\mathcal{N}(n)\} = \prod_{k \in \mathcal{R}_t} p_{r,k} \prod_{m \notin \mathcal{R}_t} \bar{p}_{r,m} \prod_{j \in \mathcal{T}_t} p_{t,j} \prod_{i \notin \mathcal{T}_t} \bar{p}_{t,i} \quad (16)$$

where $\bar{(\cdot)} = 1 - (\cdot)$. This concludes our definitions of the tag activation probability and network state information.

B. Markov model

In order to define the Markov model for dynamic performance analysis, let us now calculate the probability of having a set of active tags $\mathcal{T}_P(n+1)$ in epoch slot $n+1$ conditional on having the set of active tags $\mathcal{T}_P(n)$ during the previous epoch slot. This transition probability must consider all the combinations of tags that either enter (i.e., they are activated in epoch slot n) with probability $Q_{j|\mathcal{T}_P(n)}^{(d)}$ or leave the different sets of active tags in their possible different states (i.e., they transmit once or more in epoch slot n) with probability $G_{j|\mathcal{T}_P(n)}^{(d)}$. This can be expressed as follows:

$$\Pr\{\mathcal{T}_P(n+1) | \mathcal{T}_P(n)\} = \prod_{j \in \mathcal{T}_P^{(0)}(n), j \notin \mathcal{T}_P^{(0)}(n+1)} p_{t,j} \times \prod_{d=1}^D \prod_{i \in \mathcal{T}_P^{(0)}(n), i \in \mathcal{T}_P^{(d)}(n+1)} Q_{i|\mathcal{T}_P(n)}^{(d)} \prod_{l \in \mathcal{T}_P^{(0)}(n), l \in \mathcal{T}_P^{(0)}(n+1)} \bar{Q}_{l|\mathcal{T}_P(n)}^{(d)} \prod_{d=1}^{D-1} \prod_{i \in \mathcal{T}_P^{(d+1)}(n), i \in \mathcal{T}_P^{(d)}(n+1)} G_{i|\mathcal{T}_P(n)}^{(d)} \times \prod_{l \in \mathcal{T}_P^{(d+1)}(n), l \in \mathcal{T}_P^{(d+1)}(n+1)} \bar{G}_{l|\mathcal{T}_P(n)}^{(d)} \quad (17)$$

Let us now arrange the probability of occurrence of all the possible sets of activated tags $\Pr\{\mathcal{T}_P\}$ into a one-dimensional vector given by $\mathbf{s} = [s_0, \dots, s_{JJ}]^T$, where $(\cdot)^T$ is the transpose operator (see Fig. 2). This means that we are mapping the asymmetrical states into a linear state vector where each element represents the probability of occurrence of one different state $\Pr\{\mathcal{T}_P\}$. In the example given in Fig. 2, we have only two tags, where the first system state is given by both tags being active and in a relaying state, while in the second state only tag 1 is active in a relaying state and tag 2 is also active but in a non-relaying state. The remaining states constitute all possible combinations of the states of the two tags in the system. Once these states are mapped into the state vector \mathbf{s} , the transition probabilities between such states ($\Pr\{\mathcal{T}_P(n+1) | \mathcal{T}_P(n)\}$) can also be mapped into a matrix \mathbf{M} , which defines the Markov model for state transition probabilities (see Fig. 2). The i, j entry of the matrix \mathbf{M} denotes the transition probability between state i and state j . The vector of state probabilities

can thus be obtained by solving the following characteristic equation:

$$\mathbf{s} = \mathbf{M}\mathbf{s}, \quad (18)$$

using standard eigenvalue analysis or iterative schemes. Each one of the calculated terms of the vector \mathbf{s} can be mapped back to the original probability space $\Pr\{\mathcal{T}_P\}$, which can then be used to calculate relevant performance metrics as shown in the following subsection.

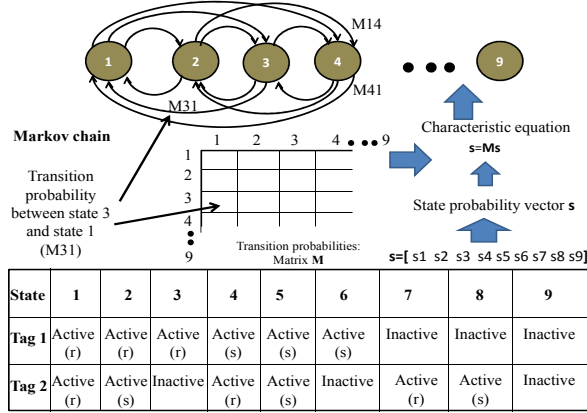


Fig. 2. Example of the Markov model for a two-tag system.

C. Tag detection model

Before calculating the tag throughput, first we must define the correct reception probability of tag j without cooperation, conditional on the network state information $\mathcal{N}(n)$. This reception probability is given, considering eq.(4), by:

$$q_{j|\mathcal{N}(n)} = \Pr\{j \in \mathcal{T}_D(n+1)\} = \sum_{k \in \mathcal{R}} \Pr\{\hat{\gamma}_{j,k} > \tilde{\gamma}_k\}, \quad (19)$$

which indicates the probability that the SINR of tag j is above the detection threshold of one of the existing readers in \mathcal{R} . Similarly, the reception probability of tag j during the cooperative phase in the p -th time slot of an epoch slot can be written, considering eq.(10), as:

$$q_{j|\mathcal{N}(n)}^c(p) = \Pr\{j \in \mathcal{T}_D(n+1)\} = \sum_{k \in \mathcal{R}} \Pr\{\hat{\gamma}_{j,k}^{(tot)}(p) > \tilde{\gamma}_k | \hat{\gamma}_{j,k}^{(tot)}(p-1) < \tilde{\gamma}_k\} \quad (20)$$

Now, the total reception probability in epoch slot n , considering the adaptive activation of the cooperative phase when detection in the previous transmissions have failed, can be calculated, with the help of eq.(20) and eq.(19), as follows:

$$q_{j|\mathcal{N}(n)}^{(tot)} = q_{j|\mathcal{N}(n)} + \bar{q}_{j|\mathcal{N}(n)} \sum_{m=1}^R \prod_{p=1}^{m-1} \bar{q}_{j|\mathcal{N}(n)}^c(p) q_{j|\mathcal{N}(n)}^c(m), \quad (21)$$

which is simply the summation of all cooperative cases with a maximum of R (re)transmissions. Similarly, the average length of an epoch-slot given the transmission of tag j can be calculated as:

$$l_{ep,j|\mathcal{N}(n)} = q_{j|\mathcal{N}(n)} +$$

$$\bar{q}_{j|\mathcal{N}(n)} \sum_{m=1}^R m \prod_{p=1}^{m-1} \bar{q}_{j|\mathcal{N}(n)}^c(p) q_{j|\mathcal{N}(n)}^c(m) \quad (22)$$

It is also convenient to re-write these two previous expressions (eq.(21) and eq.(22)) in terms of the set of active tags $\mathcal{T}_P(n)$ by averaging over all values of $\mathcal{N}(n)$ where $\mathcal{T}_t(n) \in \mathcal{T}_P(n)$, which leads to:

$$q_{j|\mathcal{T}_P(n)}^{(tot)} = \sum_{\mathcal{N}(n); \mathcal{T}_t(n) \in \mathcal{T}_P(n)} \Pr\{\mathcal{N}(n)\} q_{j|\mathcal{N}(n)}^{(tot)}(n) \quad (23)$$

and

$$l_{ep,j|\mathcal{T}_P(n)} = \sum_{\mathcal{N}(n); \mathcal{T}_t(n) \in \mathcal{T}_P(n)} \Pr\{\mathcal{N}(n)\} l_{ep,j|\mathcal{N}(n)}(n) \quad (24)$$

D. Tag throughput, stability and backlog delay

The correct tag detection probability per epoch slot can be obtained by adding all the contributions over the probability space $\Pr\{\mathcal{T}_P\}$ previously calculated with the help of the Markov model in eq.(18). This calculation can be mathematically expressed, using eq.(23), as follows:

$$S_j = \sum_{\mathcal{T}_P, j \in \mathcal{T}_P} \Pr\{\mathcal{T}_P\} p_{t,j} q_{j|\mathcal{T}_P}^{(tot)}. \quad (25)$$

The average length of an epoch slot in the steady state can then be calculated over the probability space as:

$$L = \sum_{\mathcal{T}_P} \Pr\{\mathcal{T}_P\} \left(\sum_{j \in \mathcal{T}_P} l_{ep,j|\mathcal{T}_P(n)} + \prod_{i \in \mathcal{T}_P} \bar{p}_i \right), \quad (26)$$

where the term $\prod_{i \in \mathcal{T}_P} \bar{p}_i$ accounts for the contribution of one time slot when non of the tags has transmitted. Finally, the throughput of tag j can be obtained as the ratio of the correct tag detection probability per epoch-slot from eq.(25) to the average length of an epoch in the steady state from eq.(26):

$$T_j = \frac{S_j}{L} \quad (27)$$

As a measure of stability we will use the average number of activated tags or tags in the backlog state, which can be simply calculated as follows:

$$E[|\mathcal{T}_P|] = \sum_{\mathcal{T}_P} \Pr\{\mathcal{T}_P\} |\mathcal{T}_P|. \quad (28)$$

A high number of active tags means that stability is compromised, while a relatively low number indicates that the algorithm is more stable. The average backlog delay can also be calculated, using an extension of Little's theorem as in [23], as the ratio of the average number of backlogged tags from eq.(28) to the outgoing traffic in eq.(25) [23]:

$$D_b = \frac{E[|\mathcal{T}_P|]}{\sum_j S_j}. \quad (29)$$

E. Fairness

In this paper we will evaluate fairness by means of the Gini index, which is a metric commonly used in the area of economics. The index can be mathematically written as [24]:

$$F_G = \frac{\sum_j \sum_{k \neq j} |T_j - T_k|}{2J \sum_j T_j} \quad (30)$$

A value of the Gini index close to zero means the highest degree of fairness, while a value close to one is related to a worsening of fairness conditions.

IV. RESULTS

Let us now present some graphical results that will demonstrate the benefits of the proposed approach. We consider a scenario with $K = 5$ readers and two groups of tags. The first group has $J_1 = 4$ tags and the second $J_2 = 3$ tags. Tags inside the same group have the same channel statistics, while tags across different groups have different channel statistics. For convenience in the analysis we consider that the maximum number of cooperative retransmissions is 1 or $R = 2$. This also means that only two active states for tags ($D = 2$) will be considered: A relaying state and a non-relaying state. To illustrate the benefits of the proposed approach we will consider ALOHA operation rules both at the reader and tag sides. This means that only transmissions without collision will be considered as useful. In addition, all readers and tags will use the same transmission and retransmission parameters. The idea behind these assumptions is to simplify calculation while preserving some asymmetrical aspects that are addressed by the proposed approach. Tags in the first group are activated with a probability of $Q^{(1)} = 0.1$ to state 1, and with probability $Q^{(2)} = 0.5$ to state 2. Tags in the second group will be assumed to have activation probabilities $Q^{(1)} = 0.2$ and $Q^{(2)} = 0.3$. Non-cooperative reception probabilities for the first group will be given by $q = 0.6$, while for the second one a value of $q = 0.92$ will be used. Cooperative reception between tags will be given by a probability of $q_{coop} = 0.94$. Finally, tags in the relaying able state that have correctly detected the transmission of another tag and that have received the indication from the set of readers to relay a copy, will do it with a probability of $p_{rep} = 0.9$.

Figure 3 illustrates the 3-dimensional perspective of the tag throughput in the case of the cooperative ALOHA protocol versus the probabilities of transmission of tags (p_t) and readers (p_r). The non-cooperative case is illustrated in Fig. 4. The gain of the cooperative case over the non-cooperative case is displayed in Figure 5, where we can observe that the cooperative scheme provides gains for almost all values of transmission probabilities. This confirms that tag cooperative schemes provide some useful gains for the operation of the system. In terms of the number of backlogged users, Figure 6 and Figure 7 display the results for the cooperative and non-cooperative case, respectively, for users in state 1. For users in state 2, the results are displayed in Figure 8 and Figure 9, while the combined state 1 and state 2 is displayed in Figure 10 and Figure 11. It can be observed only a slight improvement in the case of the cooperative cases at low values of tag and reader

transmission probabilities. This effect on the improvement of stability features is more evident in Figure 12 and Figure 13 for the backlog delay of the cooperative and non-cooperative schemes, respectively. The gain in delay reduction in Figure 14 confirms that cooperative schemes experience a reduction of the backlog delay which is useful for improving the stability of the system. Finally, in terms of the fairness indicator, Figure 15 and Figure 16 display the results of the Gini index for the cooperative and non-cooperative case, respectively. It can be observed, particularly in Figure 17, that the relative gain in fairness is slightly improved for the cooperative case, particularly for values with high load or high transmission probability.

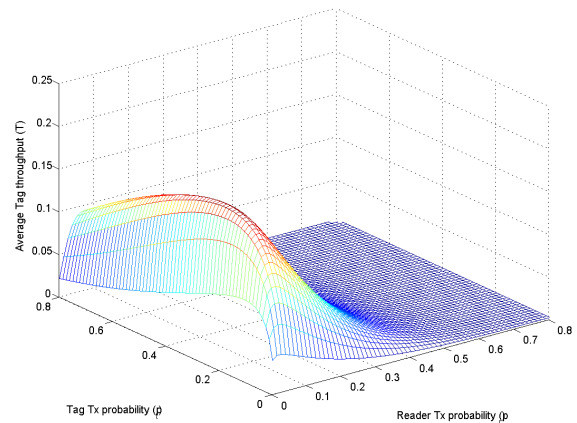


Fig. 3. Throughput (T) vs. reader and tag transmissions probabilities (p_r and p_t) cooperative ALOHA.

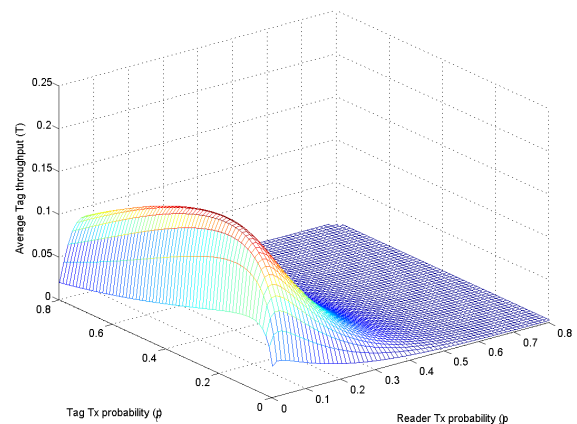


Fig. 4. Throughput (T) vs. reader and tag transmissions probabilities (p_r and p_t) non-cooperative ALOHA.

V. CONCLUSIONS

This paper has provided a framework for the MAC-PHY cross-layer design and optimization of RFID systems with tag cooperation. In addition, the modeling of the tag activity allows for the characterization of different energy harvesting capabilities. This energy harvesting feature allows some of

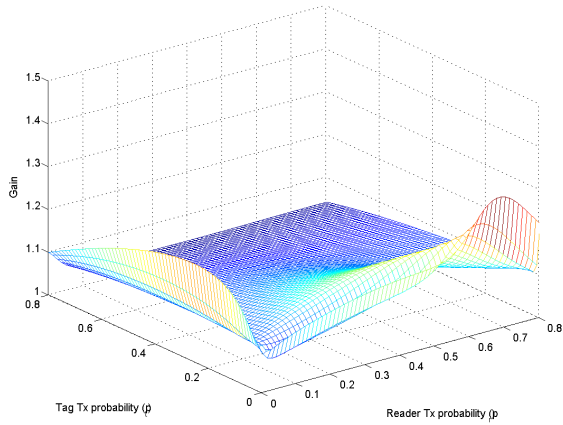


Fig. 5. Throughput Gain.

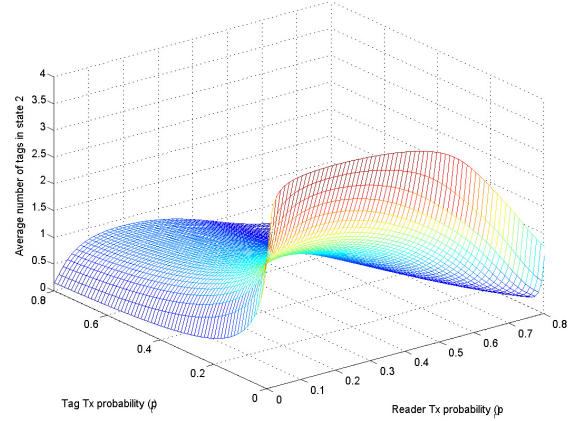


Fig. 8. Average number of active tags ($E[|\mathcal{T}_P^{(2)}|]$) in state 2 vs. reader and tag transmissions probabilities (p_r and p_t) cooperative ALOHA.

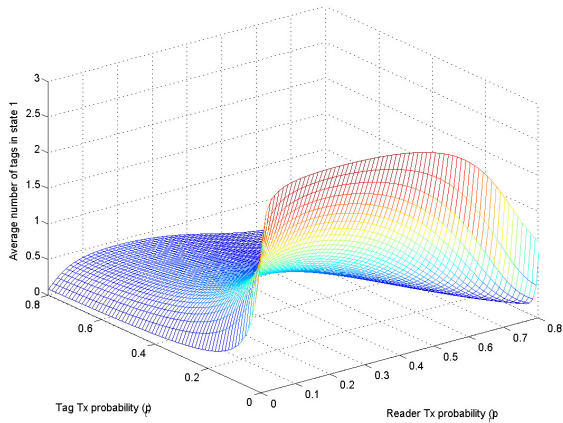


Fig. 6. Average number of active tags ($E[|\mathcal{T}_P^{(1)}|]$) in state 1 vs. reader and tag transmissions probabilities (p_r and p_t) cooperative ALOHA.

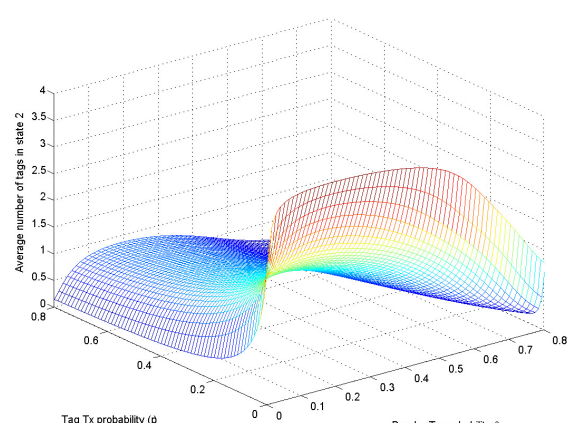


Fig. 9. Average number of active tags ($E[|\mathcal{T}_P^{(2)}|]$) in state 2 vs. reader and tag transmissions probabilities (p_r and p_t) non-cooperative ALOHA.

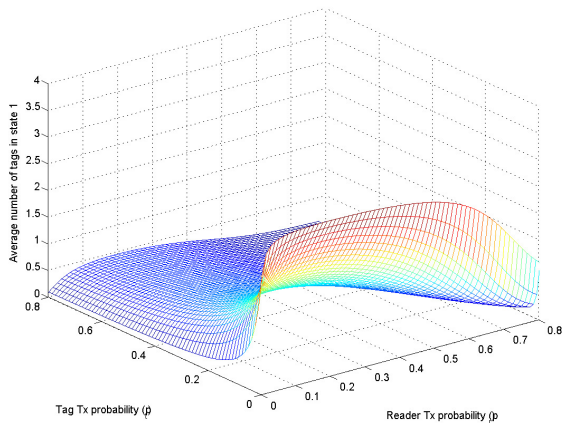


Fig. 7. Average number of active tags ($E[|\mathcal{T}_P^{(1)}|]$) in state 1 vs. reader and tag transmissions probabilities (p_r and p_t) non-cooperative ALOHA.

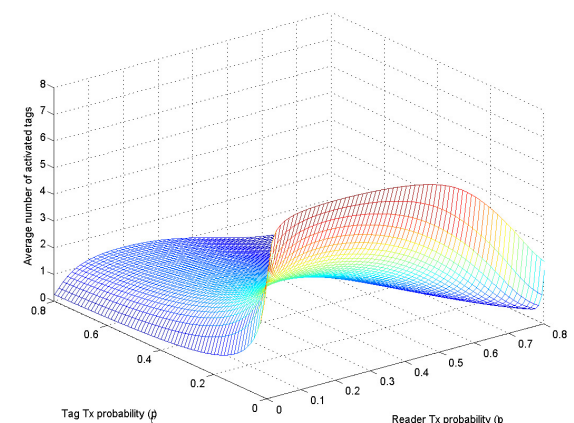


Fig. 10. Average number of active tags ($E[|\mathcal{T}_P|]$) in state 1 and 2 vs. reader and tag transmissions probabilities (p_r and p_t) cooperative ALOHA.

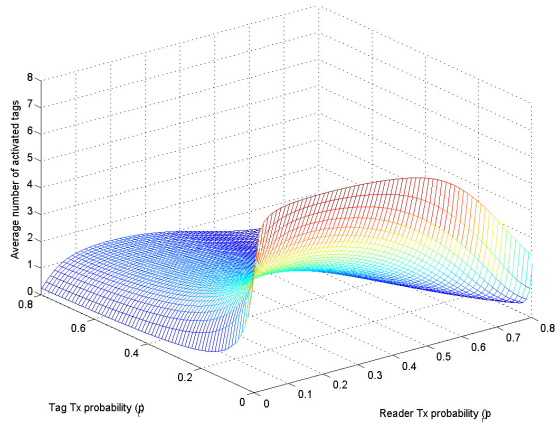


Fig. 11. Average number of active tags ($E[|\mathcal{T}_P|]$) in state 1 and 2 vs. reader and tag transmissions probabilities (p_r and p_t) non-cooperative ALOHA.

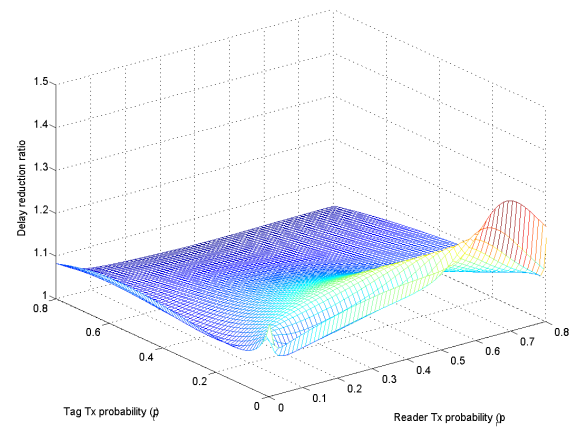


Fig. 14. Average Backlog delay reduction gain.

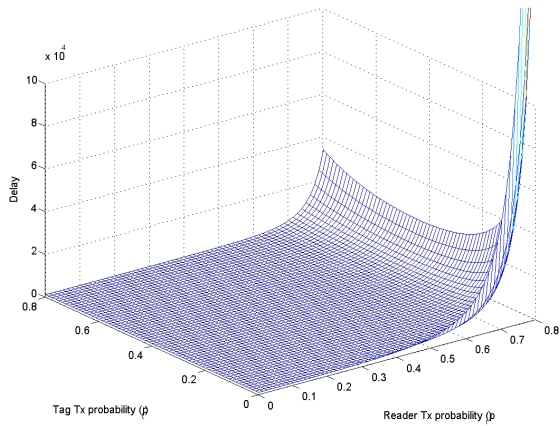


Fig. 12. Average Backlog delay (D_b) vs. reader and tag transmissions probabilities (p_r and p_t) of cooperative ALOHA.

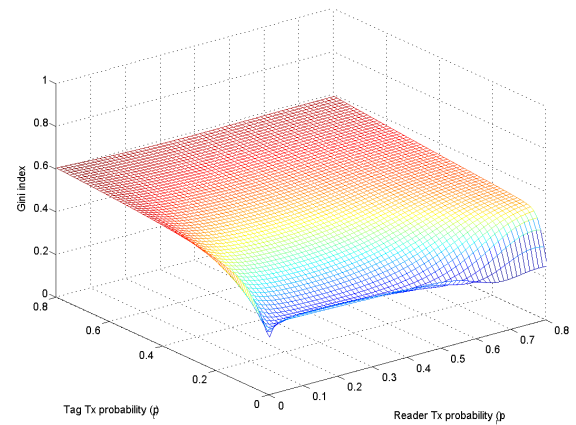


Fig. 15. Gini fairness Indicator (F_G) vs. reader and tag transmissions probabilities (p_r and p_t) of cooperative ALOHA.

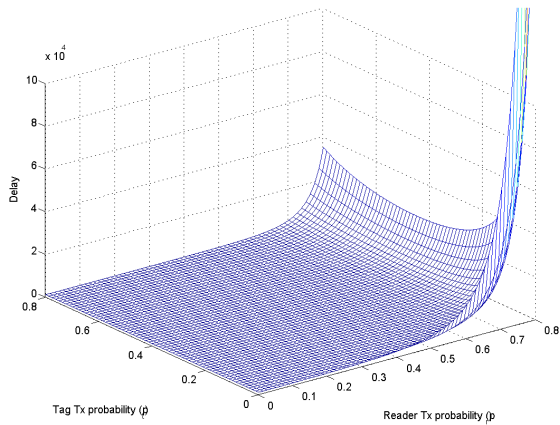


Fig. 13. Average Backlog delay (D_b) vs. reader and tag transmissions probabilities (p_r and p_t) of non-cooperative ALOHA.

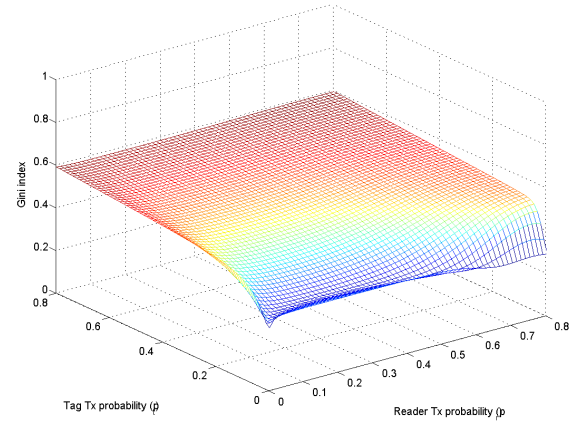


Fig. 16. Gini fairness Indicator (F_G) vs. reader and tag transmissions probabilities (p_r and p_t) of non-cooperative ALOHA.

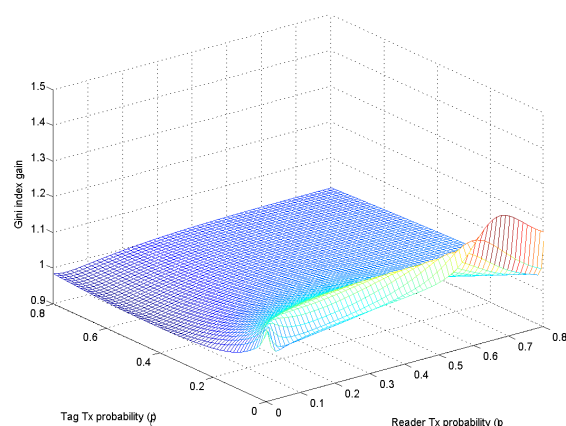


Fig. 17. Gini fairness Indicator gain.

the tags with the larger level of harvested energy to act as relays for other tags with less favored conditions. The model proposed here includes both the contention of the readers to activate the tags and the contention process of the tags to reply to the network of readers. This approach is novel in RFID while being more accurate as we can now shed light on how the processes of activation and detection of tags of RFID occur. The proposed Markov model for asymmetrical systems allows for investigation of stability aspects and dynamic performance assessment. Illustrative results with an ALOHA protocol show that tag cooperation provide general improvements in terms of throughput, stability, backlog delay and fairness over its non-cooperative counterparts. These results pave the way for more advanced cooperation algorithms with improved physical layer processing. The framework developed here can be easily upgraded to cope with new schemes at the physical and medium access layers of RFID and potentially for systems with sensors that will be relevant in the future Internet of Things.

REFERENCES

- [1] R. Samano-Robles and A. Gameiro, "Joint Design of RFID reader and tag anti-collision algorithms: a cross-layer approach," *International Conference on Digital Technologies*, Chamonix, France, 2012.
- [2] R. Weinstein, "RFID: A Technical overview and its application to the enterprise," *IT profesional*, 2005, Vol. 7, No. 3, pp. 27-33.
- [3] L.A. Burdet, "RFID Multiple Access Methods," *ETH Zurich, Summer semester 2004, Seminar "Smart Environments"*.
- [4] D. Liu, Z. Xang, J. Tan, H. Min, and J. Wang, "ALOHA algorithm considering the slot duration difference in RFID system," *2009 IEEE International Conference on RFID*, pp. 56-63.
- [5] S. Birari, "Mitigating the reader collision problem in RFID Networks with mobile readers," Master Thesis.
- [6] "EPC Radio-Frequency Identity Protocols. Class-1 Generation-2 UHF RFID. Protocol for communications at 860 MHz - 960Mhz." Version 1.2.0", EPC Global, 2008., <http://www.epcglobalinc.org/standards/>.
- [7] "ETSI EN 302 208-1,2 v1.1.1, September 2004. CTAN: <http://www.etsi.org>"
- [8] J. Waldrop, D.W. Engels, and S.E. Sarma, "Colorwave: An anticollision algorithm for the reader collision problem," *IEEE Wireless Communications and Networking Conference (WCNC)*, 2003.
- [9] S. Birari, "Mitigating the reader collision problem in RFID Networks with mobile readers," *13th IEEE Int. Conf. on Networks*, 2005, pp. 463-468.
- [10] K.Ho. Junius, "Solving the reader collision problem with a hierarchical q-learning algorithm," *Master's thesis*, MIT, February, 2003.

- [11] S.Y. Kim and J.K. Lee "A study on control method to reduce collisions and interferences between multiple RFID readers and RFID tag," *International Conference on New Trends in Information and Service Science NISS*, 2009, pp.339-343.
- [12] K. Cha, S. Jagannathan, and D. Pommerenke "Adaptive power control with hardware implementation for wireless sensor and RFID networks," *IEEE Systems Journal*, Vol. 1, No. 2, December 2007, pp. 145-159.
- [13] L. Tong, V. Naware and P. Venkatasubramaniam, "Signal Processing in Random Access," *IEEE Signal Processing Magazine, Special issue on Signal processing for networking: An integrated approach*, vol. 21, no. 5, Sep. 2004, pp. 29-39.
- [14] V. Srivastaya and M. Montani "Cross-layer design: a survey and the road ahead," *IEEE Commun. Magazine*, Vol. 43, No. 12, December 2005, pp. 112-119.
- [15] R. Samano-Robles and A. Gameiro "Collision resolution algorithms for RFID applications," *Asia-Pacific Microwave Conference*, 2008, pp. 1-4.
- [16] Nikitin P.V, et al. "Passive tag-to-tag communication," *IEEE International conference on RFID*, 2012, pp. 224-231.
- [17] S. Hong, et al, "ISO/IEC 18000-7 based on RFID multihop relay system," *IEEE 2009*
- [18] L. Dong and A.P. Petropulu, "Multichannel ALLIANCES: A cooperative cross-layer scheme for wireless networks," *IEEE Transactions on Signal Processing*, Vol.56, No. 2, pp. 771-784, 2008.
- [19] R. Samano-Robles and A. Gameiro, "A Slotted-ALOHA protocol with cooperative diversity," *4th annual Wireless Internet Conference WICON 2008*, Maui, Hawaii.
- [20] W.Chen, L. Dai, K.B. Letaief, and Z. Cao "A unified cross-layer framework for resource allocation in cooperative networks," *IEEE Transactions on Wireless Commun.*, vol 7, no.8, pp.3000-3012, 2008.
- [21] Y. Zhou, J. Liu, C. Zhai, and L. Zheng, "Two-transmitter two-receiver Cooperative MAC protocol: cross-layer design and performance analysis," *IEEE Trans. on Vehicular Tech.*, vol. 59, no. 8, pp. 4116-27, 2010.
- [22] R. Samano-Robles and A. Gameiro, "A packet reception model for cooperative diversity in wireless multi-cell networks," *International Conference on Consumer Electronics*, Berlin, Germany, September 2011.
- [23] F. Tobagi and L. Kleinrock "Packet switching in radio channels: part IV-stability considerations and dynamic control in carrier sense multiple access," *IEEE Transactions on Communications*, Vol. 25, No. 10, 1977, pp. 1103-1119.
- [24] "Wolfram Mathworld Gini coefficient definition:" Available at <http://mathworld.wolfram.com/GiniCoefficient.html>

Information Content of Very High Resolution SAR Images: Study of Dependency of SAR Image Structure Descriptors with Incidence Angle

Corneliu Octavian Dumitru

Remote Sensing Technology Institute (IMF)
German Aerospace Center (DLR)
Oberpfaffenhofen – Wessling, Germany
corneliu.dumitru@dlr.de

Mihai Datcu

Remote Sensing Technology Institute (IMF)
German Aerospace Center (DLR)
Oberpfaffenhofen – Wessling, Germany
mihai.datcu@dlr.de

Abstract—This paper provide systematic results of the influence of the Synthetic Aperture Radar image structure descriptors with incidence angle and orbit direction. The evaluation is done on TerraSAR-X data and the interpretation is done semi-automatically. In the first part, we study and assess the behavior of the primitive feature extracted methods for images of the same scene with 2 look angles covering the min-max range of the sensor. After that the influence of the orbit looking is shortly discuss. The tests are done on TerraSAR-X products High Resolution Spotlight mode at 3 m resolution and two sites covering the Berlin and Ottawa area are found to be suitable for this investigation. To identify the best features and appropriate incidence angle for them the Support Vector Machine and as a measure of the classification accuracy the precision–recall were considered. The recall shows that the optimal value of the incidence angle in order to have a higher classification is obtained for a value of the incidence angle closer to upper bound of the sensor range. In the second part of the paper a list of queries that can be asked by Earth Observation users are presented and proposed to be implemented in the next generation of our system. The first contribution of this paper is the evaluation of four primitive features that are very known (gray level co-occurrence matrix, Gabor filter, quadrature mirror filter, and non-linear short time Fourier transform) but not used and compared for SAR images. After the best primitive feature is identified the second contribution of this paper lies in the fact that the parameters of the data namely, incidence angle and orbit direction are systematically investigated in order to find the dependency between these parameters and the accuracy of the retrieved classes.

Keywords-classes; features; incidence angle; orbit direction; query; SAR iamges

I. INTRODUCTION

The specific information in High Resolution (HR) Synthetic Aperture Radar (SAR) images acquired in single polarization is mainly in the "structure", e.g. textures, objects, or scattering signatures. The "spatial context" becomes very important rather than the "pixel based"

descriptors, which are less informational. The adopted solution is to analyze image patches corresponding to ground areas of ca. 200 x 200m. Experiments and tests carried recently confirmed the usefulness of the concept, however further analysis is needed to assess the behavior of the method for the indexing of very large SAR data sets as the case in Image Information Mining (IIM) [1].

There are few publications available [2] ÷ [6] where the images are tiled into patches and generating a large number of classes. In [2], the patch size is 256 x 256m in order to ensure that the extracted information capture the local characteristics within a patch rather the global features across the entire image.

In [3], the TerraSAR-X high resolution Spotlight products (resolution of ~1 m) were tiled into patches of 200 x 200m in order to characterize the large and relatively small structures available in the urban scene. The images covered different region: Las Vegas, Venice, Gizah, and Gauting. From 7,000 extracted patches a set of 30 classes were generated.

In [4], the original images are tiled into patches of 16 x 16 pixels or 128 x 128 pixels. Three classes were extracted (city, forest, and sea) and the results of the classification shows better performances when the image was tiled in patches of 128 x 128 pixels. The same authors propose in [5] a patch contextual approach for high resolution satellite images (resolution of 0.6 m) where the patch size is 200 x 200 pixels. The number of classes was 18.

In our previous work [6], a pyramid with different resolutions (1m, 2m, 2.9m, 4m, and 8m) was considered for TerraSAR-X high resolution Spotlight where each image was tiled into patches at different size in order to have the same area covered on the ground. The patch sizes vary from 400 x 400m (for 1m resolution) to 25 x 25m (for 8m resolution). The two scenes (Venice and Toulouse) were considered for this investigation and 30 classes were identified.

In this paper, we propose to study and experimentally asses the most relevant PF behavior for indexing the content of SAR images as TerraSAR-X. The envisaged algorithms

are very well known but not very used for SAR data. After finding the best primitive feature algorithm considering the optimal size of the patch for high resolution Spotlight mode radiometrically enhanced product equal to 220×220 pixels the second step was to determine the dependency of the SAR imaging with the incidence angle. In the end of the paper a series of queries that can be implemented starting from the TerraSAR-X metadata (available in the XML file attached to the product), TerraSAR-X image, patches, semantic annotation (ontology) of the patches, and primitive features extracted from each patch were presented.

The paper structure is the following. Section II presents the TerraSAR-X products used for tests and based on this a test dataset is built. Section III explains the actual state-of-the-art of the feature extraction methods and shortly describes the applied methods. Section IV describes the methodology used in the next Section. Section V provides the details about the experiments, while Section VI gives some examples of queries that can be implemented in EO systems. Section VII points the conclusion and references given at the end of the paper.

II. TERRASAR-X PRODUCTS

In this section, we discuss the basic TerraSAR-X products that are intended to be used and the *test dataset* that was built for this evaluation.

TerraSAR-X is the German radar satellite and it operates in the X-band with a side-looking SAR based on active phased array antenna technology [7]. It does supply high quality radar data for purposes of scientific observation of the Earth.

The basic products [7] are available in a huge diversity of modes (Stripmap, Spotlight, ScanSAR), types (complex, detected, geocoded), and configurations (Spatially Enhanced

Products or Radiometrically Enhanced Products).

In Figure 1, examples of the basic products are presented in order to understand the diversity of TerraSAR-X satellite and the difference between these products. Note that, in the examples shown in Figure 1, the ScanSAR mode and SSC type are missing because it was not possible to find in the archive these products covering the same area of interest.

The size of the sub-images tiled from the original image and presented in Figure 1 is the same but the coverage on the ground is different because the resolution and/or pixel spacing of this is different.

From this huge diversity of products we selected based on our previous results [6], [34], and [37] the following configuration:

- the high resolution Spotlight (HS) mode as one of the most popular mode used for research,
- the detected product GEC (Geo-coded Ellipsoid Corrected) products because is geo-referenced product and the localisation of the pixels can be realised with a higher accuracy than for other products. In some applications this is very important.
- the radiometrically enhanced (RE) configuration where the range and azimuth resolution are decreased in order to reduce the speckle.

Our *test dataset* is created in order to answer to the following question: “Which is the optimal incidence angle for a better classification?”.

The characteristics of the *test dataset* (configuration of the product presented before) that we identified in the TerraSAR-X archive [34] and selected for this evaluation (Berlin – Germany and Ottawa – Canada) are the following:

- the ground range resolution is about 2.9 meters,
- the single polarisation HH,

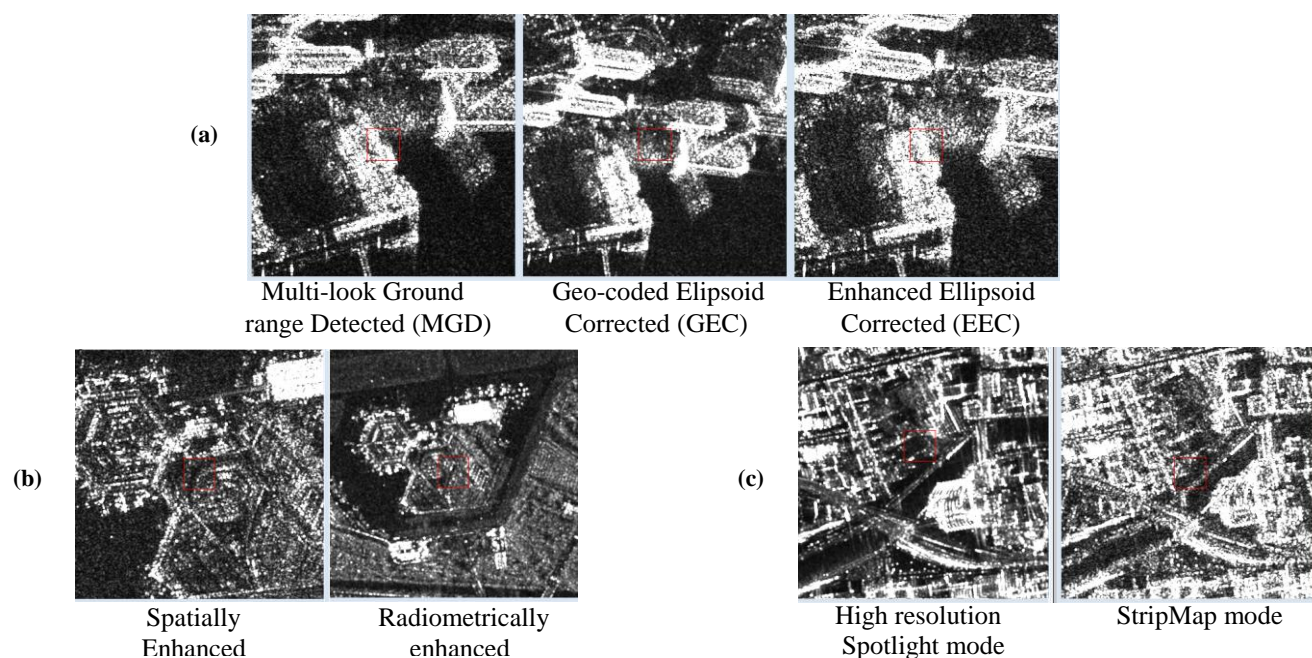


Figure 1. Comparative examples of TerraSAR-X products that covers the diversity of: (a) types, (b) geometric resolution configurations, and (c) modes.

- the orbit looking is ascending for Berlin and descending for Ottawa,
- the incidence angle is 30° and 42° for Berlin and 27° and 41° for Ottawa,
- the number of looks depends by the incidence angle and varies from 5 for an incidence angle of 20° to 9 for an incidence angle of 55° ,
- the size of the images is 5549×3368 pixels in case of Berlin and 4783×3381 pixels in case of Ottawa. From the image a rectangle is selected in order to not have the black letter box effect on the processing of the features (see Figure 10).

In order to understand the difference between different values of the incidence angle in Figure 2-a two examples are presented. The first one corresponds to central station in Berlin and the acquisition of the data was different in order to cover the range of the incidence angle. The second one corresponds to high builds in the financial district of Ottawa and also here the incidence angle was different in order to capture the sensibility of the data with the incidence angle.

Similar examples are presented in Figure 2-b but this time we are interested in the orbit direction and for this reason we selected two area in Berlin having the orbit direction ascending and descending.

For high resolution SAR images the diversity of the classes that can be retrieved from the image is higher than in the case of lower resolution images. In Figure 3 the diversity of the classes identified in our *test dataset* is shown.

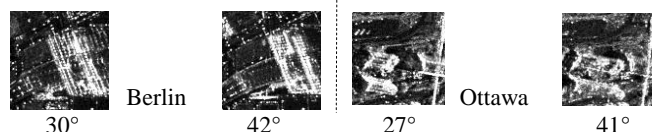


Figure 2-a. Different patches tiled from the images having the incidence angle close to lower and upper bound of the sensor range for Berlin (left side of the image) and Ottawa (right side of the image). The characteristics of the entire image from where the patches were tiled are: TerraSAR-X HS mode with RE configuration at about 2.9 meters resolution with ascending looking for Berlin and descending looking for Ottawa.

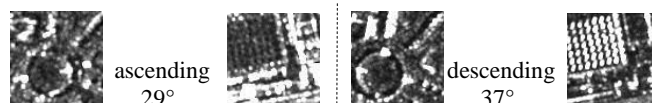


Figure 2-b. Examples of patches covering the same area on ground but with a different orbit direction and incidence angle for the area of Berlin. The characteristics of the image from where the patches were tiled are: TerraSAR-X HS mode with RE configuration at 6.5 meters resolution.

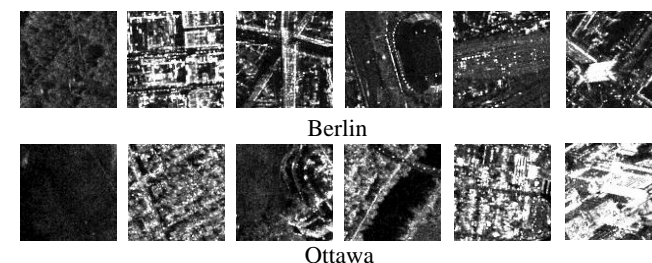


Figure 3. A set of classes that can be extracted from the two investigate sites that are available in our *test dataset*.

III. FEATURES EXTRACTION METHODS

In this section, we select four feature extraction methods that have been proposed in the past several decades by different authors and we compare these for SAR images.

On a conceptual level we decide which features can be extracted in general and on a practical level, we apply the: gray level co-occurrence feature extraction [13] for texture analysis, Gabor filtering [18] to extract any geometrical or neighborhood relationships, quadrature mirror filters [30] for texture analysis, and non-linear short time Fourier transform [32] for spectral characteristics of the image.

We can divide the features in two categories: statistical and spectral [27], [28].

A. Statistical

1) Gray level co-occurrence matrix

a) State of the art

The gray level co-occurrence matrix (GLCM) is a second order statics of how often different combinations of pixel brightness values (gray levels) occur in an image [13].

Haralick et al. [8] compute gray level co-occurrence matrix for a distance of one with four directions (0° , 45° , 90° , and 135°). For a seven-class classification problem, they obtained approximately 80% classification accuracy using texture features in remote sensing images application.

Rignot and Kwok [9] have analyzed SAR images using texture features computed from GLCM. However, they supplement these features with knowledge about the properties of SAR images. For example, image restoration algorithms were used to eliminate the specular noise present in SAR images in order to improve classification results.

Schistad and Jain [10] compare different methods for texture computation in ERS SAR imagery. One of the used and computed methods was GLCM with four directions like in [8]. The *angular second moment, contrast, entropy, cluster shade, inertia, and inverse difference moment* [13] were computed as texture features from the GLCM. A five class classification problem was considered and 29% (an average) classification error using GLCM was obtained.

Randen and Husoy [11] consider GLCM as a reference method and they compared this with other filtering methods (like: QMF, Gabor, discrete cosine transform, etc.) for texture extraction. The size of the gray levels in the image is 8×8 (also chosen by Ohanian and Dubes [12]). On the one hand, if the value is large, the number of pixel pairs contributing to each element in image will be low, and the statistical significance poor. On the other hand, if the gray levels are low, much of the texture information may be lost in the image quantization. The *angular second moment, contrast, correlation, and entropy* were computed as texture features for each orientation. The average of the classification error was 32%.

b) Applied method

The GLCM is created from a gray scale image by selecting either horizontal (0°), vertical (90°), or diagonal (45° or 135°) orientation.

The size of GLCM depends on the number of gray values available in the image. For example, in [29], they obtain for

an input image of 8 bits, i.e., 256 values, a GLCM of 256x256 elements.

In our case, we scale the radiometric range of the input images to 16 steps and obtain a GLCM size of 16x16 elements.

The texture parameters [13] computed from the GLCM are: *mean, variance, entropy, contrast, energy, correlation, homogeneity, autocorrelation, dissimilarity, cluster shade, cluster prominence, and maximum probability.*

B. Spectral

1) Gabor filters

a) State of the art

A Gabor filter is a linear filter used in image processing that is included as a descriptor in MPEG 7 [38].

Randen and Husoy [11] review the major filtering approaches to texture feature extraction and performed a comparative study by comparing with two classical non-filtering approaches (GLCM which is a statistical method and autoregressive which is model based method). The dyadic Gabor filter bank (i.e. Gaussian shaped band-pass filters, with dyadic coverage of the radial spatial frequency range and multiple orientations) proposed by Jain and Farrokhnia [14] was considered for the experiments in [11]. Five radial frequency were used (proposed by [14] for images of size 256 x 256 pixels) and four orientations (0°, 45°, 90°, and 135°). The average error on the classification was 31%.

Du [15] used texture features derived from Gabor filters to segment SAR images. He successfully segmented the SAR images into classes of water, new forming ice, older ice, and multi-year ice. Lee and Philpot [16] also used spectral texture features to segment SAR images.

Shu et al. [17] extract the information at four directions (0°, 45°, 90°, and 135°) by using Gabor filters and then computing the mutual information of each corresponding image pair. The experiments show that the method can work very well even if the SAR image is not filtered; this indicates that the method is robust to speckle noise.

In Manjunath and Ma [18], a Gabor wavelet based texture analysis method is proposed and its application to image databases is demonstrated on Brodatz texture database but also considering the current work related to the idea of browsing large satellite images database. The experiments results demonstrate that these Gabor features are robust. Rotation and scale invariance are important in many applications and the preliminary results obtained by [18] using Gabor features are very promising.

In [19] ÷ [22], the Gabor filters are applied to Brodatz texture database with very good results.

b) Applied method

Frequency and orientation representations of a Gabor filter are similar to those of the human visual system, and it has been found to be particularly appropriate for texture representation and discrimination. In the spatial domain, a 2D Gabor filter is a Gaussian kernel function modulated by a sinusoidal plane wave [18]. The Gabor filters are self-similar

- all filters can be generated from one mother wavelet by dilation and rotation.

We have chosen the Gabor filters designed by Manjunath B.S. and Ma W.Y. at Vision Research Lab, University of California.

The texture parameter results computed from the Gabor filter are *mean* and *variance* for different *scales* and *orientations*.

2) Quadrature mirror filters

a) State of the art

Quadrature Mirror Filter (QMF) banks are multirate (i.e. with variable sampling rate throughout the system) digital filter banks, introduced by Croisier, [23], Esteban and Galand [24]. During the last two decades since the inception of QMF banks, they have been extensively used in speech signal processing, image processing and digital transmultiplexers [25]. QMF banks are used to split a discrete-time signal into a number of bands in the frequency domain to process each sub-band in independent manner.

QMF was used for texture analysis by Randen and Husoy [11] as extended classes of filters which include among others Gabor filters, discrete cosine transform, etc. This is a large class of filters which incorporate both infinite impulse response (IIR) and finite impulse response (FIR) filters. In their experiments the average of the classification error was between 26% and 33%.

b) Applied method

As proposed in [30], statistical features obtained from the filtered images using QMF banks in synergy with some other features can be used for image (satellite image) indexing.

The number of features which can be obtained from the presented algorithm depends upon the level selected for the QMF sub-band decomposition like a wavelet. Features are nothing but the mean and variance of the four filtered and sub-sampled images in the QMF sub-band pyramid.

There are many techniques available to design QMF banks. We have chosen the QMF banks designed by Simoncelli E.P. and Adelson E.H. at the Vision Science Group, The Media Laboratory, Massachusetts Institute of Technology.

The parameters computed from the QMF banks (QMFS) are *mean* and *variance* of the *low pass sub-band, horizontal sub-band, vertical sub-band, and diagonal sub-band*.

3) Non-linear short time Fourier transform

a) State of the art

Much work on extraction of features based on short time Fourier transform is done in speech and audio processing.

The method proposed in [26] was investigated by Li and Ogihara [32] for music information retrieval. They are using short time Fourier transform feature extraction method to extract the timbral texture which is not captured by the popular method in speech and music processing, the Mel-frequency cepstral coefficients. The derived features computed from STFT are: spectral centroid, spectral Rolloff, spectral flux, low energy, and zero crossings.

The goal of Popescu et al. paper [26] is to define an analysis model for High Resolution Spotlight SAR imagery, which is able to integrate the radiometric, as well as

geometric and texture properties of the SAR data, in order to facilitate large data-base queries by informational content indexing of the images. The proposed model use the information contained in the spectra of the SAR signal.

The Short Time Fourier Transform (STFT) was considered in order to extract the features necessary for the Bayesian Support Vector Machine classifier. The features are: spectral centroid, spectral flux, cepstral coefficients, and first and second statistic measures. Using this method a number of 30 classes were recognized from the 9,000 patches of SAR images acquired with TerraSAR-X satellite.

b) Applied method

This method of SAR image feature extraction and complex image information retrieval was first proposed in [31]. This non-parametric analysis is a form of time frequency analysis where the cutting of a spectrum allows the study of the phase responses of scatterers seen from different viewing angles.

The STFT extracts six non-linear features: the first two features are based on statistical properties of the spectrum and the next four features are timbre features used for music genre classification [32].

Non-linear STFT (NLFT) features were initially proposed mainly for feature extraction from complex-valued SAR images, but experiments showed that they give very encouraging results also for real-valued images.

Our proposed algorithm is an implementation of the non-linear STFT feature extraction. The features parameters computed from the STFT are: *mean* of the STFT coefficients, *variance* of the STFT coefficients, *spectral centroid in range*, *spectral centroid in azimuth*, *spectral flux in range*, and *spectral flux in azimuth*.

IV. METHODOLOGY

In this section is presented the methodology used in order to identify the best primitive feature (PF) and the incidence angle /orbit direction that has a good classification accuracy of the TerraSAR-X.

The general approach adopted here is to divide the TerraSAR-X image into a number of sub-images (by tiling the image into patches) [6] and to compute the feature extraction associated to these patches.

For our investigation two sites were considered covering

the area of Berlin (Germany) and Ottawa (Canada).

First step is the evaluation of the best primitive features (GLCM, GAFS, QMFS, and NLFT); features extracted using as a test data the Berlin image. The second step of our evaluation is to try to identify the incidence angle and orbit direction that gives a better accuracy of the classification using the best primitive feature identified during the previous step. The evaluation of the second step is done on both sites available in the *test dataset*, Berlin and Ottawa.

To answer to the two questions regarding the best PF and incidence angle / orbit direction of the TerraSAR-X a tool based on Support Vector Machine with relevance feedback (SVM – RF) was built [6].

The SVM – RF tool supports users to search patches of interest in a large database. The Graphical User Interface of this tool allows Human-Machine Interaction to rank the automatically suggested patches which are expected to be grouped in classes. Visual supported ranking allows enhancing the quality of search results by giving positive and negative examples.

The TerraSAR-X product-image is tiled into patches with the size of 220 x 220 meters, and after that are sub-sampled to 110 x 110 meters for better performances (see reference [39] where comparative results are presented in order to find the optimal patch size).

The feature vector for GLCM has a fix number of parameters for each orientation equal to 12, but in order to capture the information of the object orientation all four orientations (from 1 to 4) of GLCM are taking into account (48 components denoted by GLCM_1_2_3_4). In the case of Gabor filters, 4 scales and 6 orientations (48 features denoted by GAFS 4_6) were considered. For QMFS, the number of levels of wavelet decomposition was set equal to 1 this means a vector of 8 features was obtained (denoted by QMFS 1). The last feature vector is represented by NLFT and the number of features was fixed to 6.

All the features are normalised before being used in the SVM-RF tool. The Z-score normalisation method was selected and used from the methods available in [33].

We define a number of semantic classes and group the patches accordingly, using the SVM-RF tool (see the flowchart in Figure 4) and the human expertise (using as a ground truth the Google Earth). We considered that a patch belong to only one class based on the dominant content of the patch.

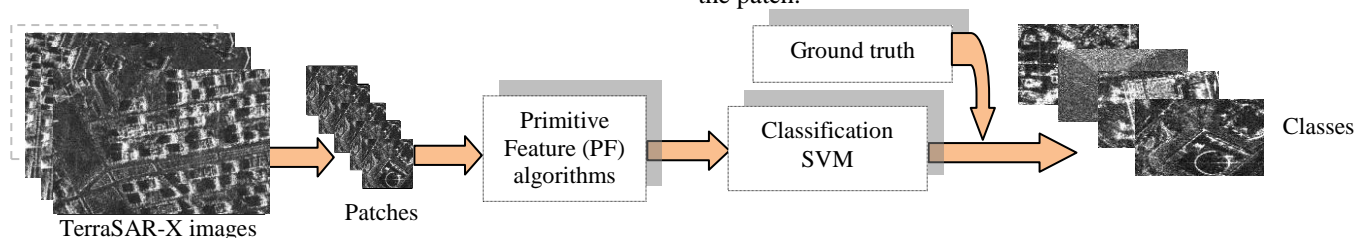


Figure 4. The proposed methodology is the following: (1) the input SAR images are tiled into patches at different size (depending by the resolution and pixel spacing of the image) and the primitive features (GLCM_1_2_3_4, GAFS 4_6, QMFS 1, and NLFT) are computed for each patch; (2) the features are grouped in classes using the Support Vector Machine classifier; (3) the Google Earth is used as a ground truth in order to define the semantic of the generated classes and for visual inspection of these classes. For the evaluation of the best PF the precision-recall metric is computed and after that the PF algorithm having the highest recall is used for the evaluation of the incidence angle and orbit direction following the same procedure.

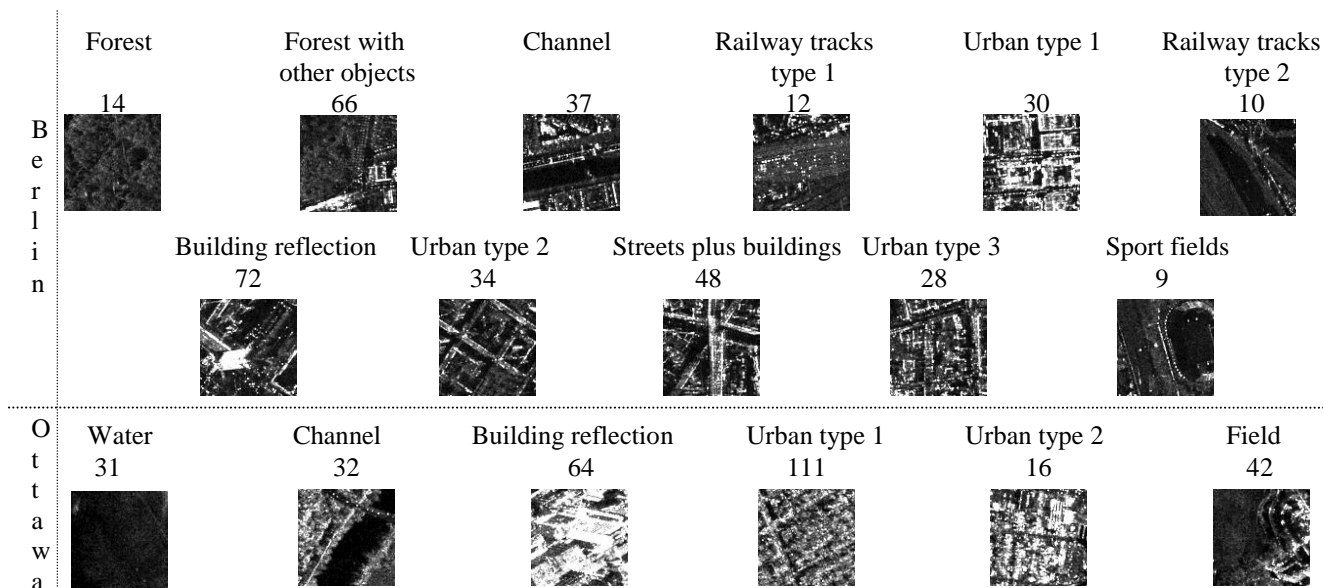


Figure 5. Typical classes that can be extracted from: the Berlin image (the top part of the figure) and the Ottawa image (the bottom part of the figure).

During the evaluation, the number of classes retrieved for Berlin area is equal to 11 and for Ottawa area equal to 6. In Figure 5 the semantic classes are presented with their corresponding number of patches in each class.

For each step (feature extraction method or incidence angle/orbit direction), we tried to detect the classes among the number of identified patches of our *test dataset*. For each class, we give 20% of the patches of each class for the training as positive examples and one patch from the rest of the classes as a negative example and we try to detect the similar patches during 7-10 training iterations. The evaluations stop when the classified patches which are displayed by the Search Engine (SVM - RF tool) remain in a stable result (no new patches are longer found from iteration to another). The procedure is repeated two times for the same class, giving the same positive and negative examples.

For the quantitative assessment, we compared the classification results with the annotated database. We propose as evaluation metric the *precision-recall* that will be computed for each class, feature, and incidence angle.

The *precision* is defined as the fraction of the retrieved images which are relevant, while the *recall* is defined as the fraction of relevant images which have been retrieved.

V. PERFORMANCE EVALUATION

This section is dedicated to the evaluation of the best features that are intended to be used for the evaluation of the incidence angles. In Figure 6 is displayed (for Berlin site with the incidence angle of 30°) the *precision-recall* for each class separately and for all four investigated features.

The average of the *precision-recall* is presented in Table I for these features computed over all the classes.

After the investigation and comparison between the features is finished the following conclusion arise that: the Gabor filters perform better than the other features especially when the *precision* is computed; regarding the *recall*, the

best performance is obtained for quadrature mirror filters. The quadrature mirror filters has the advantage of being faster (in required run time for feature computation) than the Gabor filters.

TABLE I. THE AVERAGE OF THE PRECISION- RECALL

Features	Precision	Recall
GAFS 4_6	90.11%	49.19%
QMFS 1	78.59%	58.77%
GLCM 1_2_3_4	84.26%	50.70%
NLFT	71.86%	55.28%

The discussion reached a point when we have to decide what is need the *precision* that means accuracy of the relevant patches from the total number of retrieved patches or more relevant patches to be retrieved (*recall*). Because our goal is to find similar patches that exist in our *test dataset* the *recall* as a metric is considered and as a consequence of this decision the QMFS is selected from the four features investigated. The *precision* will be presented only informative in the second step where the incidence angle will be evaluate.

From the TerraSAR-X archive [34], we selected two sites that correspond to our requirements in order to have the incidence angle close to lower and upper bound of the TerraSAR-X and different orbit lookings. The range of the satellite for high resolution Spotlight mode is between 20° and 55° . These two sites are Berlin with incidence angle of 30° and 42° with ascending looking and Ottawa with incidence angle of 27° and 41° with descending looking.

In the next figures, Figure 7 and Figure 8, for these two scenes/sites the metric was computed and the results are displayed.

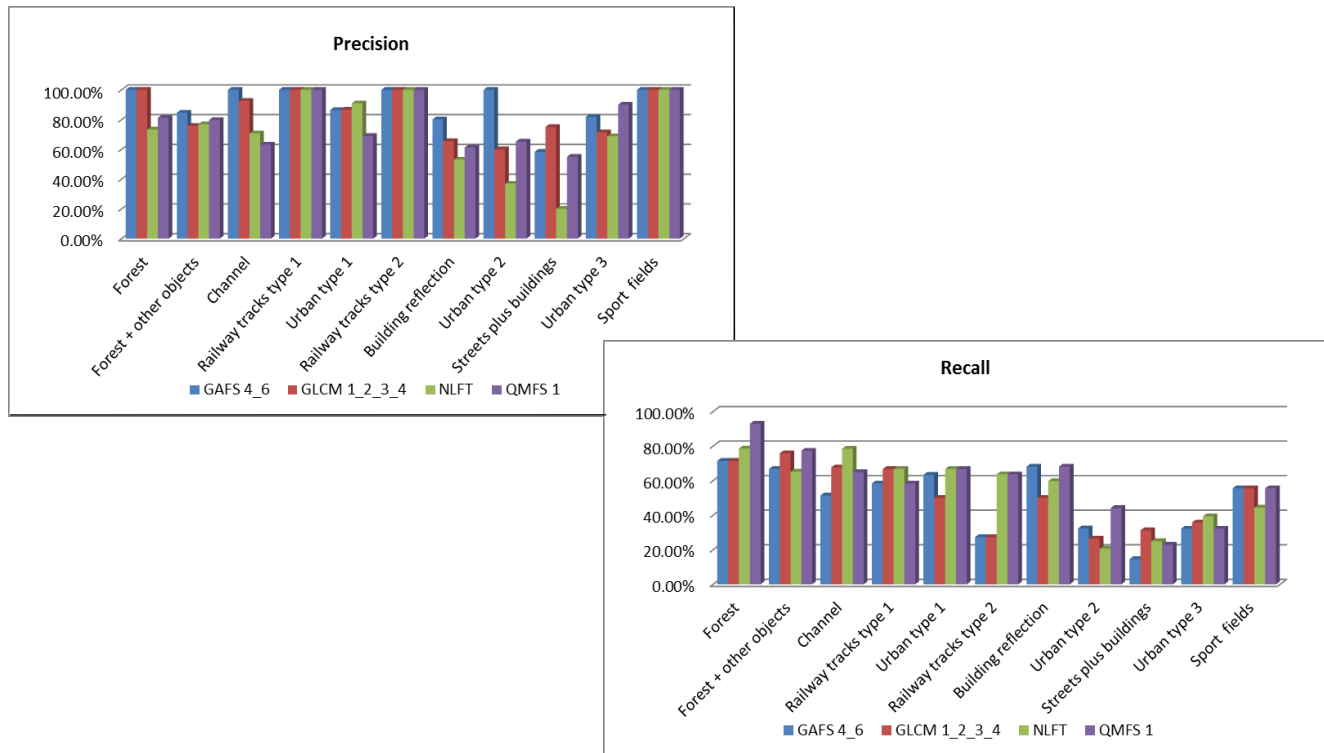


Figure 6. The results of the precision-recall for Berlin. A comparison between all primitive features (GEC-RE product, HS mode, patch size 110x110 pixels).

The best incidence angle in *recall* was obtained for both sites in the case of higher value of the incidence angle; this means a value of the incidence angle close to the upper bound of the sensor range.

This value is 42° for Berlin and 41° for Ottawa where both orbit directions ascending and descending were considered.

Evaluating the accuracy of the classification separately class by class *s* (the *recall* metric higher than 65%) the following observation can be noticed:

- in the case of Berlin better results are obtained for “forest”, “forest plus other objects”, and “building reflection” class.
- in the case of Ottawa better results are obtained for “water”, “building reflection”, “urban”, and “field”.

Another study that is presented in this section regarding the incidence angle is the influence of this parameter when both incidence angles are putted together.

There are two experiments conducted for this study: for the first one, the training was done with examples only from one case (only one incidence angle) in order to have a reference result and second time with examples from both cases (both incidence angles).

For this investigation the Berlin site is taking into account and the results are shown in Figure 9.

The average of the *recall* (marked with green color in Table II) over all the classes in both cases is:

- 32.96% when the training was done using one incidence angle (e.g. 30°),
- 38.30% when the training was done combining examples from both incidence angles.

In Table II, the accuracy of the classification presented as *precision-recall* metric is displayed. In the right side of the table, the *recall* for both cases is presented for each class separately. For eight from eleven classes the *recall* (marked with red color) is better when the training is done with data coming from both incidence angles (incidence angles that are covering the min-max range of the TerraSAR-X sensor). For the rest of the classes higher value in *recall* (marked with pink color) is obtained when the training is done only with data having the incidence angle equal to 30° .

What is interesting here for these three classes (classes: streets with some objects and different types of railway tracks) is that each of these contains objects that have a certain pattern. All these classes can be included in a more general class, namely transportation.

In both cases the class with higher *recall* (metric higher than 65%) is “forest”.

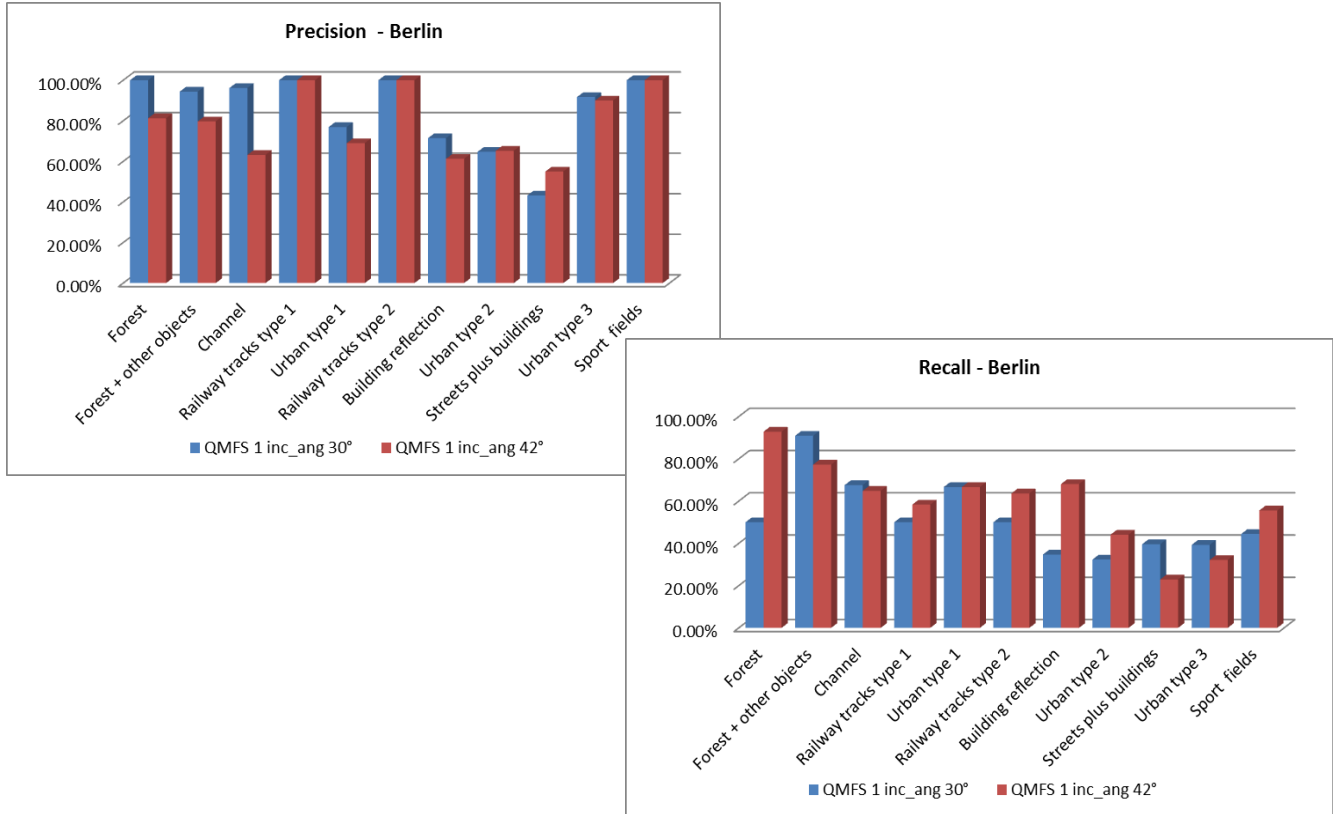


Figure 7. The results of the precision-recall for the center of Berlin. A comparison between the results obtained for both incidence angle 30° and 42°.

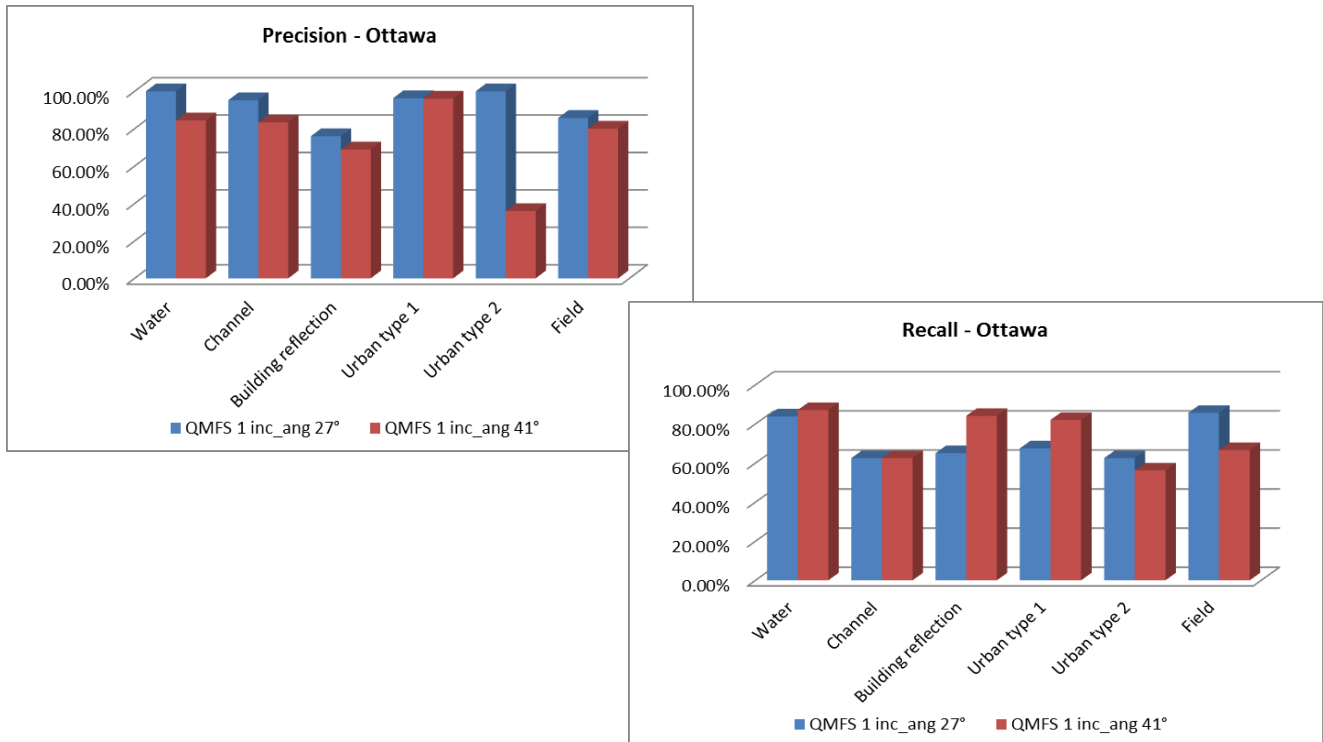


Figure 8. The results of the precision-recall for the center of Ottawa. A comparison between the results obtained for both incidence angle 27° and 41°.

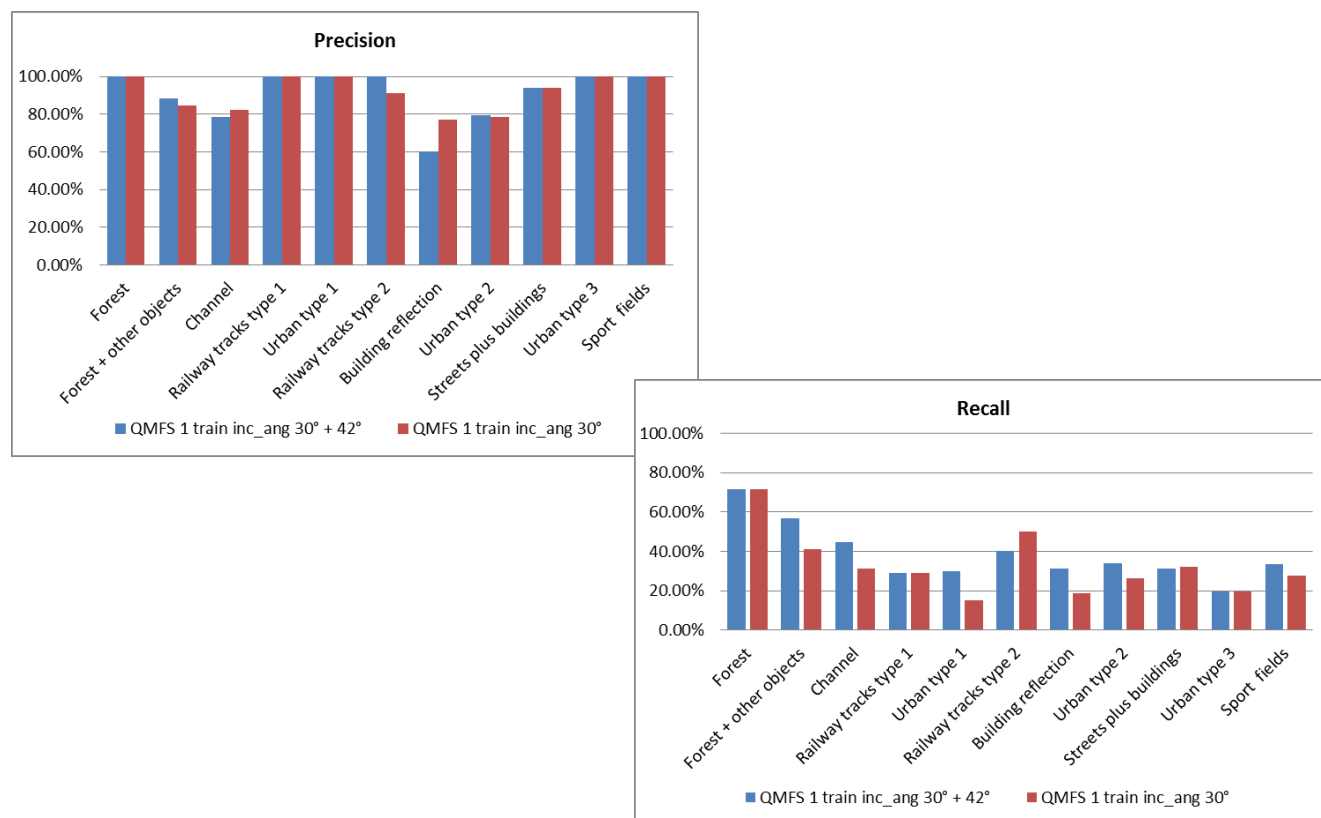


Figure 9. The results of the precision-recall in the case of Berlin. A comparison between the results when the training was done with both incidence angles (30° and 42°) and when the training was done with only one value of the incidence angle (30°).

TABLE II. A COMAPRISON OF THE PRECISION- RECALL REALISED: WHEN THE TRAINING WAS DONE WITH BOTH INCIDENCE ANGLES AND WHEN THE TRAINING WAS DONE WITH ONLY ONE INCIDENCE ANGLE IN THE CASE OF BERLIN AREA. THE FEATURES EXTRACTED ARE QMFS WITH LEVEL OF DECOMPOSITION 1.

Semantic classes	No. of patches	Precision		No. of patches	Recall	
		Incidence angle 30° and 42°	Incidence angle 30°		Incidence angle 30° and 42°	Incidence angle 30°
Forest	28	100.00%	100.00%	14	71.43%	71.13%
Forest + other objects	132	88.24%	84.38%	66	56.82%	40.94%
Channel	74	78.57%	82.14%	37	44.59%	31.08%
Railway tracks type 1	24	100.00%	100.00%	12	29.00%	29.17%
Urban type 1	60	100.00%	100.00%	30	30.00%	15.00%
Railway tracks type 2	20	100.00%	90.91%	10	40.00%	50.00%
Building reflection	144	60.00%	77.14%	72	31.25%	18.75%
Urban type 2	68	79.31%	78.26%	34	33.82%	26.47%
Streets plus buildings	96	93.75%	93.94%	48	31.25%	32.29%
Urban type 3	56	100.00%	100.00%	28	19.64%	19.00%
Sport fields	18	100.00%	100.00%	9	33.34%	27.78%
Total for QMFS and all the classes		90.90%	91.52%		38.30%	32.96%

VI. TYPES OF QUERIES

The purpose of this section is to show how to improve the state of the art of the indexing and querying systems available for Earth Observation [7], [35].

We start this section by presenting a series of queries that can be asked by EO users. These queries are intended to be implemented in the next generation of our system [36]:

- 1) *Query for a product and its metadata:* This type of query is based on the metadata normally stored in the XML file of the TerraSAR-X [6].

“Find all GEC products, high resolution Spotlight mode with HH polarization that has the latitude equal to 52.49826 N and longitude equal to 13.3484534 E”. The results of the query are presented in Table III; these parameters are extracted from the metadata of each TerraSAR-X product.

- 2) *Query for an image and its metadata:* This type of query is based on the image and its attached metadata (e.g., geographic latitude/longitude). This can be useful for a fast query of a location knowing the coordinates of the area [7].

“Find the images with the center of latitude equal to 45.42349 N and longitude equal to -75.69793 E and with an extension of 0.05”. The result of the query gives us a list with 12 images that correspond to specified query (this type of search can be done also on the TerraSAR-X archive [7]).

- 3) *Query for images of products that contain patches that have certain properties.* This type of query can be divided in other sub-categories:

- a) *Query by the land cover/use class of a certain patch:* This type of query is based on the metadata annotated to the patches.

“Find all patches that correspond to sport fields.” The result of this type of query is presented in Figure 10 (all the patches marked with green, red, and magenta color).

- b) *Query by the land cover/use class of a patch and the qualitative or quantitative spatial*

properties of a patch: This type of query allows us to query for patches with some land cover/use class that are spatially related to other patches or to a user defined area.

“Find all patches containing sport fields limited in the west by the channel.” The results of this type of query correspond to only one patch marked with green color in Figure 10.

- c) *Query by correlating the land cover/use class of more than one patch that has various qualitative or quantitative spatial relations between them:* This type of query extends the previous query by allowing the correlation based on land cover/use class of multiple patches with various spatial relations between them.

“Find all patches that correspond to a sport field and within a distance of patches that correspond to urban area (buildings).” There are three such patches (one marked with green color and two with red color in Figure 10) that correspond to the specific query.

Another example is: “Find all patches that correspond to forest (or trees) that have in middle a sport field.” The results are the patches marked with magenta color in Figure 10.

- d) *Query that involves features of a patch but also other properties like the land cover/use class and spatial relations:* This type of query is based on the parameters of the feature extraction algorithms.

“Find the mean and variance of the low pass sub-band filter (the first and second value of the quadrature mirror filters vector) for a patch that corresponds to a railway tracks.” This query can be useful to understand why sometimes some patches may not be grouped together even are containing the same object (e.g. railway tracks). Such example is found for Berlin site (Figure 5) where two classes containing railway tracks are spitted in two different classes.

In Figure 11 is presented an example showing the difference between the quadrature mirror filter (QMF) features extracted from two patches classified as bridge having the incidence angle equal to 27° and 41°.

TABLE III. THE RESULTS OF THE QUERY – TYPE 1.

No.	Product	Time UTC	Incidence angle	Orbit direction
1	GEC, SE., High Resolution Spotlight, HH	2008-10-11 05:25:17	36.08518°	Descending
2	GEC, SE., High Resolution Spotlight, HH	2008-09-30 05:25:17	35.73137°	Descending
3	GEC, SE., High Resolution Spotlight, HH	2008-09-19 05:25:16	35.73308°	Descending
4	GEC, RE, High Resolution Spotlight, HH	2009-03-23 16:43:52	30.01653°	Ascending
5	GEC, RE, High Resolution Spotlight, HH	2009-11-03 16:52:35	41.90324°	Ascending

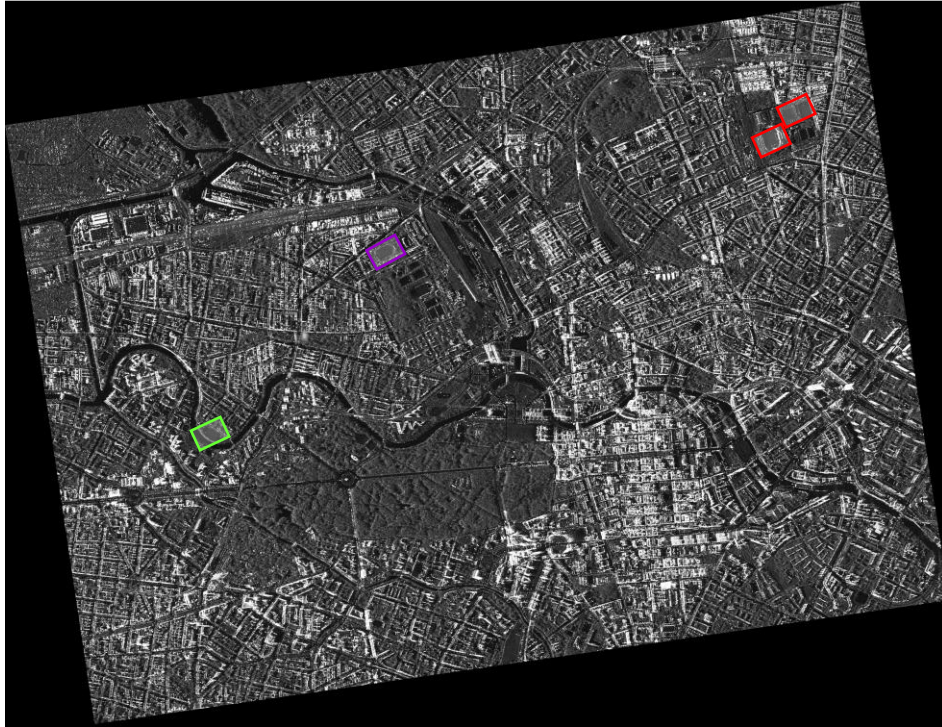


Figure 10. Results of the proposed queries (query type 3 case a), b), and c)) are marked with different color on the quick-look of the image (city of Berlin).

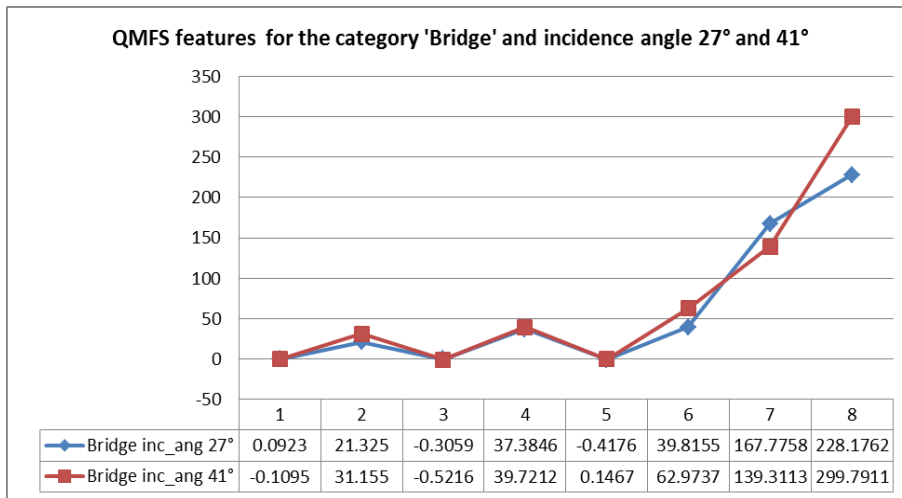


Figure 11. Representation of the QMFS features extracted from the same patch ('bridge') having the incidence angle equal to 27° and 41° in the case of Ottawa area.

VII. CONCLUSION

Based on the results obtained in previous sections a general conclusion regarding the incidence angle can be drawn manely, the value of the incidence angle closer to the lower bound of the sensor range is optimal if the *precision* metric is considered or value of the incidence angle closer to

the upper bound of the sensor range is optimal if the *recall* metric is computed. However, our goal is to retrieve similar patches in a large database and *recall* is the metric that gives as a good measure for this.

Regarding the orbit direction in both cases (Berlin and Ottawa) the classification accuracy obtained for the incidence angle was the same even the orbit looking was

different (ascending looking for Berlin and descending looking for Ottawa). This leads to the idea that the orbit direction can be disregarded because the influence of this is not so major (maybe for some classes can be important). The classification accuracy is given by the incidence angle, the parameters of the data (patch size, pixel spacing, and resolution), and the primitive features used.

As a general remark, the SAR signature depends on the incidence angle of the data and the accuracy of the classification may decrease for different values of the incidence angle.

Examining the types of queries presented in section VI, we noticed that the existing EO portals offer partial or full support for asking queries of type 1 and 2, but cannot be used to answer any of the queries of type 3 and its sub-categories. These queries can only be asked and answered if the knowledge discovery technologies are applied to TerraSAR-X images and the relevant knowledge are extracted and captured by the semantic annotations. In other words the list of queries presented above is intended to be implemented in the next generation of the system [36].

A real use case and/or application that we identified for this type of queries (e.g., type 3) is for example *"finding areas (e.g., sport terrain or field) where refugee camp or hospitals can be placed after an earthquake"* like the one in Haiti in January 12, 2010 that ZKI [37] has faced recently.

ACKNOWLEDGMENT

This work has been partially funded by ESA (European Satellite Agency) under the KLAUS project (contract no. 22823/09/I-AM).

REFERENCES

- [1] C.O. Dumitru and M. Datcu, "Dependency of SAR Image Structure Descriptors with Incidence Angle", in Proc. of SPACOMM, Chamonix, May 2012, pp. 92-97.
- [2] C.-R. Shyu, M. Klaric, G. Scott, A. Barb, C. Davis, and K. Palaniappan, "GeoIRIS: Geospatial Information Retrieval and Indexing System – Content Mining, Semantics Modeling, and Complex Queries", IEEE Trans. Geoscience and Remote Sensing, vol. 45, Issue 4, pp. 839-852, 2007.
- [3] A. Popescu, I. Gavath, and M. Datcu, "Contextual Descriptors for Scene Classes in Very High Resolution SAR Images", IEEE Geoscience and Remote Sensing Letters, 2012, vol. 9, Issue 1, 2012, pp. 80-84.
- [4] P. Birjandi and M., Datcu, "ICA based visual words for describing under meter high resolution satellite images", Proc. of IGARSS 2009, Cape Town, 2009.
- [5] P. Birjandi and M. Datcu, "Topographic independent component analysis model for under meter high resolution satellite images characterization", Proc. of ESA-EUSC-JRC_2009, Torrejon-Spain, 2009.
- [6] C.O. Dumitru, J. Singh, and M. Datcu, "Selection of relevant features and TerraSAR-X products for classification of high resolution SAR images", EUSAR 2012, Nuremberg-Germany, 24-26 April 2012, pp. 243-246.
- [7] TerraSAR-X: "Basic Products Specification Document", Issue: 1.6 (TX-GS-DD-3302), 2009.
- [8] R. M. Haralick, K. Shanmugam, and I. Dinstein, "Textural features for image classification", IEEE Trans. Systems, Man, and Cybernetics, SMC-3, pp. 610-621, 1973.
- [9] E. Rignot and R. Kwok, "Extraction of Textural Features in SAR Images: Statistical Model and Sensitivity", Proc. International Geoscience and Remote Sensing Symposium, Washington, DC, pp. 1979-1982, 1990.
- [10] A.S. Solberg and A. Jain, "Texture Fusion and Feature Selection Applied to SAR Imagery", IEEE Trans. Geoscience and Remote Sensing, vol. 35, no. 2, pp. 475-478, 1990.
- [11] T. Randen and J.H. Husoy, "Filtering for Texture Classification: A Comparative Study", IEEE Trans. Pattern Analysis and Machine Intelligence, vol. 21 no.4, pp. 291-310, 1990.
- [12] P.P. Ohanian and R.C. Dubes, "Performance Evaluation for Four Classes of Textural Features", Pattern Recognition, vol. 25, no. 8, pp. 819-833, 1992.
- [13] GLCM, 2012, Available: http://www.fp.ucalgary.ca/mhallbey/orderliness_group.htm
- [14] A.K. Jain and F. Farrokhnia, "Unsupervised Texture Segmentation Using Gabor Filters", Pattern Recognition, vol. 24, no. 12, pp. 1167-1186, 1991.
- [15] L. J. Du, "Texture Segmentation of SAR Images Using Localized Spatial Filtering", Proc. International Geoscience and Remote Sensing Symposium, Washington, pp.1983-1986, 1990.
- [16] J. H. Lee and W. D. Philpot, "A Spectral-Textural Classifier for Digital Imagery", Proc. International Geoscience and Remote Sensing Symposium, Washington, pp. 2005-2008, 1990.
- [17] L. Shu, T. Tan, M. Tang, and C. Pan, "A Novel Registration Method for SAR and SPOT Images", Proc. IEEE International Conference on Image, pp. II.213-II.216, 2005.
- [18] B. S. Manjunath and W. Y. Ma, "Texture Features for Browsing and Retrieval of Image Data". IEEE Trans. Pattern Analysis and Machine Intelligence, vol.18, pp.837-842, 1996.
- [19] P. Porter and N. Canagarajah, "Robust Rotation-Invariant Texture Classification: Wavelet, Gabor filter and GMRF based Schemes", Proc. Visual Image Processing, vol. 144, no. 3, pp. 180-188, 1997.
- [20] S.E. Grigorescu, N. Petkov, and P. Kruizinga, "Comparison of Texture Features based on Gabor Filters", IEEE Trans. Image Processing, vol. 10, no. 11, pp. 1160-1167, 2002.
- [21] D. Zhang, A. Wong, M. Indrawan, and G. Lu, "Content-based Image Retrieval Using Gabor Texture Features", IEEE Trans. Pattern Analysis and Machine Intelligence, pp. 13-15, 2000.
- [22] M. Torres-Torriti and A. Jouan, "Gabor vs. GMRF Features for SAR Imagery Classification", Proc. Int. Conference on Image Processing, Thessaloniki, vol. 3, pp. 1043 – 1046, 2001.
- [23] A. Croisier, D. Esteban, and C. Galand, "Perfect Channel Splitting by use of Interpolation/Decimation/Tree Decomposition Techniques", Proc. International Conference on Information Science and Systems, Patras Greece, 1976.
- [24] D. Esteban and C. Galand, "Application of quadrature mirror filters to split-band voice coding schemes", Proc. IEEE Int. Conf. ASSP, Hartford, Connecticut, pp. 191-195, 1977.
- [25] P. Vaidyanathan, "Quadrature Mirror Filter Banks, M-band Extensions and Perfect-Reconstruction Techniques", IEEE ASSP Magazine, vol. 4, no. 3, pp. 4-20, 1987.
- [26] A. Popescu, C. Patrascu, I. Gavath, J. Singh, and M. Datcu, "Spotlight TerraSAR-X Data Modeling using Spectral Space-Variant Measures, for scene Targets and Structure Indexing", Proc. The 8th European Conference on Synthetic Aperture Radar, Aachen, Germany, 2010.
- [27] T. Zou, W. Yang, D. Dai, and H. Sun, "Polarimetric SAR Image Classification Using Multifeatures Combination and Extremely Randomized Clustering Forests", EURASIP

- Journal on Advances in Signal Processing vol. 2010, ID 465612, 9 pages, 2010.
- [28] M. Fauvel, J. Chanussot, J.A. Benediktsson, and J.R. Sveinsson, "Spectral and Spatial Classification of Hyperspectral Data using SVMs and Morphological Profiles", IEEE International Geoscience and Remote Sensing Symposium, Barcelona, Spain, pp. 4834-4837, 2002.
 - [29] R. Haralick, K. Shanmugam, and I. Dinstein, "Textural Features for Image Classification", IEEE Trans. Systems, Man, and Cybernetics, vol. 3, no. 6, pp. 610-621, 1973.
 - [30] M. Campedel, E. Moulines, and M. Datcu, "Feature Selection for Satellite Image Indexing", ESA-EUSC: Image Information Mining – Theory and Application to EO, 2005.
 - [31] A. Popescu, I. Gavat, and M. Datcu, M., "Complex SAR image characterization using space variant spectral analysis", Proc. IEEE Radar Conference, pp. 1-4, 2008.
 - [32] Z. Li and M. Ogihara, "Towards Intelligent Music Information Retrieval", IEEE Trans. Multimedia, vol. 8, no. 3, pp. 564-574, 2006.
 - [33] N. Karthikeyani Visalakshi and K. Thangavel, "Impact of Normalization in Distributed K-Means Clustering". Int. Journal of Soft Computing, vol. 4, no. 4, pp. 168-172, 2009.
 - [34] EOWEB portal: <https://centaurus.caf.dlr.de:8443/eoweb-ng/template/default/welcome/entryPage.vm>
 - [35] M. Wolfmueller, D. Dietrich, E. Sireteanu, S. Kiemle, E. Mikusch, M. Boettcher, "Data Flow and Workflow Organization - The Data Management for the TerraSAR-X Payload Ground Segment", IEEE Trans. Geoscience and Remote Sensing, vol. 47, no.1-1, pp. 44-50, 2009.
 - [36] TELEIOS project: Deliverable D6.2.1: Ontologies for the VO for TerraSAR-X data, 2012.
<http://www.earthobservatory.eu/deliverables/FP7-257662-TELEIOS-D6.2.1.pdf>.
 - [37] Center for Satellite Based Crisis Information – ZKI, 2012. Available: <http://www.zki.dlr.de/article/1262>.
 - [38] MPEG 7, 2012. Available:
<http://mpeg.chiariglione.org/standards/mpeg-7/mpeg-7.htm>
 - [39] C.O Dumitru and M. Datcu, "Study and Assessment of Selected Primitive Features Behaviour for SAR Image Description", in Proc. of IGARSS, Munich-Germany, July 2012, pp. 3596-3599, 2012.

Efficient Forwarding Approach on Boundaries of Voids in Wireless Sensor Networks

Mohamed Aissani, Sofiane Bouznad, Salah-Eddine Allia, and Abdelmalek Hariza

Research Unit in Computer Science (UERI), Ecole Militaire Polytechnique (EMP)

P.O. Box 17, Bordj-El-Bahri 16111, Algiers, Algeria

{maissani, bouznad.sofiane}@gmail.com

{s.allia, malik-abd}@hotmail.com

Abstract—Geographical routing protocols are scalable, but they must handle voids appearing in wireless sensor networks. Existing void-handling techniques present limits, particularly in real-time applications. Consequently, we propose in this paper an efficient forwarding approach that orients any packet which arrives at a boundary node in the shortest path towards the sink. The handled voids can be either closed within a deployed sensor network or open located on the network boundary. To keep unchanged the size of each created void for a long time, the use of a 2-hop forwarding mode is privileged in our approach to preserve the limited energy of boundary nodes. The information needed for our mechanisms is provided by simple and reactive algorithms that we propose in this paper to discover and maintain the boundaries of voids. Associated with the SPEED real-time routing protocol, and evaluated in several conditions, our proposal performs very well in terms of packet delivery ratio, end-to-end delay, energy consumption, control packet overhead and energy balancing.

Keywords - Wireless sensor networks; geographical routing; void-handling techniques; closed voids; open voids.

I. INTRODUCTION

Wireless sensor networks (WSNs) can be deployed quickly in sensitive and/or difficult to access areas. Their mission is usually to monitor an area, to take regular measurements and to send alarms to the decision center. Many applications using WSNs are then emerging in several areas, such as defense, security, health, agriculture and smart homes. They generally used geographical routing ensuring scalability and allowing positive progression of packets towards the sink. However, geographical routing has two major problems. First, it is not applicable if a sender node has no opportunity to know its geographical locations. This problem can be solved by virtual coordinate systems. Second, there may be voids between a source node and a sink. These voids can be concave, convex, closed or open. Conversely to the closed voids that appear within a deployed WSN, the open voids are frequently formed on the boundary of this sensor network. A geographical routing path towards the destination node (sink) can be failed due to lack of relay nodes because of a void.

As a contribution in resolving the problem of voids in geographical routing in WSNs, we propose in this paper an oriented 2-hop forwarding approach handling effectively all kinds of voids. To do so, we also propose four reactive

algorithms to discover and then maintain each void that appear in a deployed WSN. Then each data packet received by a boundary node is forwarded towards its destination by using the shortest path and the minimum number of boundary nodes. This strategy aims to reduce the packet end-to-end delay, to economize the energy of boundary nodes and then to preserve for a long time the actual form of each discovered void. Since this paper is an extended version of our published conference paper [1], we incorporate pseudo-codes of the proposed algorithms and expanded experiments by evaluating the performance of the proposed void-handling approach when varying the packet data rate at sources, the packet deadline and the number of voids created in the simulation terrain.

Note that to handle the problem of voids in geographical routing, several solutions are proposed in literature [2]-[15], but they present some shortcomings presented in Section III, particularly in case of time-critical applications using WSNs.

The rest of the paper is organized as follows. Section II presents the problem of voids and discusses the existing void-handling techniques. Section III provides two efficient algorithms for discovery and maintenance of voids in WSNs. Section IV proposes an oriented 2-hop forwarding mode to use by boundary nodes. Section V evaluates performance of the proposed approach with several void radiuses, data packet rate at sources, packet deadlines and number of voids. Section VI concludes the paper.

II. VOID PROBLEM IN GEOGRAPHICAL ROUTING

Routing voids are areas where nodes cannot forward data packets or completely unavailable. These voids are formed due to either the random deployment of nodes or the node failure because of various reasons, such as circuit failure, destruction or energy exhaustion. Therefore, packets to forward are often blocked in their positive progression towards their destination.

Suppose the example in Figure 1, where black nodes are boundary nodes and node s has to forward data packets to destination d . Node s is stuck because it has no neighbor so close to d to be selected as a forwarder node; i.e., the FS (Forwarding candidate neighbors Set) of node s is empty. Once received by node s , data packets cannot progress positively towards destination d . Thanks to a recovery

mode, those packets will be forwarded to node j (or to node k) in a negative progression to bypass the void. This scenario, called the local minimum phenomenon, often occurs when a void appears in a WSN. We then say that s is a stuck (or a blocked) node.

Without using an adequate void-handling technique, data packets can be removed in a WSN wasting the nodes resources and communications can be lost between some pairs of nodes. Such behavior is undesirable in a time-critical application because the loss of some captured information can interfere with the network mission. To reduce the negative impact of voids on the effectiveness of geographical routing, void-handling techniques are available in literature. They fall into two classes: those based on the right-hand rule [2]-[7] and those using the backpressure rule [10]-[13].

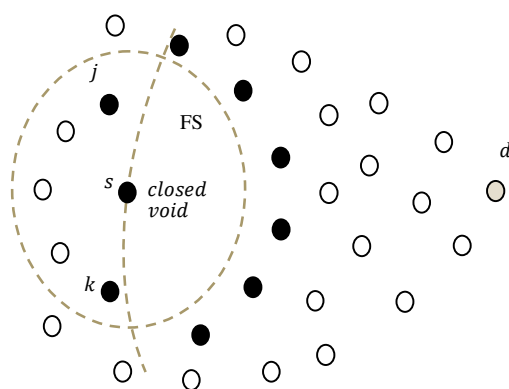


Figure 1. The void problem: the FS of sender s towards destination d is empty.

The techniques belonging to the first class use boundary nodes to route a stuck packet. In most cases, they use long recovery paths, especially in the case of open voids. Proposed in [2], the GPSR (greedy perimeter stateless routing) algorithm uses two forwarding modes: the greedy mode and the perimeter mode. When a sender node is not blocked, it forwards the current packet to the closest neighbor to the destination node (i.e., greedy mode). As a result, the destination is approached hop by hop until reached by the packet. When the greedy mode fails, the packet is routed by using a face routing (i.e., a perimeter forwarding on a planar graph) to bypass the void met. The right-hand rule is thus used on the void boundary until the packet reaches the closest node to the destination. Several other algorithms using the face routing were proposed later [3]-[6]. However, it has been shown in [16] that the use of planarization algorithms, such as Gabriel graphs [2], reduces the number of useful links in a WSN. This influences the exploration of multiple routing paths allowing load balancing, link-failure tolerance and network fluidity. This is not tolerable in WSNs dedicated to time-critical applications.

However, the techniques belonging to the second class uses the backpressure messages, that are broadcasted by stuck nodes near a void, to route the next packets in alternative paths. He et al. [10] describes the QoS routing

protocol SPEED which provides a soft end-to-end real-time to all flows routed in a WSN. In this protocol, each node updates information on its neighbors and uses geographical routing to select paths. In addition, SPEED aims to ensure a certain delivery speed so that each application can estimate the packet end-to-end delay. It deals with a void as it handles a permanent congestion. When a packet is stuck, the sender node drops the packet and broadcasts a backpressure message informing its neighbors about the void met. Then the stuck node will not be considered by the neighbors in their future routing decisions. When neighbors of a node are all stuck, the actual packet is dropped and a backpressure message is broadcasted. This process is repeated until an alternative route is found or the source node is reached by the successive backpressure messages. Extensions to the SPEED protocol have been proposed later in [11]-[13], but the void-avoidance scheme of the protocol was not modified in these extensions.

Indeed, the right-hand rule is not effective in bypassing voids, especially in case of open voids. It requested a lot of boundary nodes and often used long paths on voids boundaries, resulting in excessive energy consumption of boundary nodes and delays packets due to the overload of these bypassing paths. Then the voids tend to expand rapidly due to energy depletion, complicating the sensor network mission. Similarly, the backpressure rule generates many control packets and removes data packets at stuck nodes in concave areas of some voids. Consequently, routing paths become long because of multiple backtrackings which overload links and delay packets. These packets might be removed in the sensor network after expiration of their deadline. This is again not desirable for time-critical applications.

To overcome these weaknesses, we propose in this paper an efficient 2-hop forwarding approach that orients correctly towards the sink each packet received by a boundary node. The proposed approach uses two new mechanisms: the first one, called OVA-vb (Oriented Void Avoidance on a closed void boundary), handles the closed voids within the network whereas the second one, called OVA-nb (Oriented Void Avoidance on the network boundary), handles open voids on the network boundary. The closed voids in a deployed WSN are discovered by the VBD (Void-Boundary Discovery) algorithm and maintained by the VBM (Void-Boundary Maintenance) algorithm that we propose in the next section. Note the present contribution improves our previous works [14][15] by handling both open and closed voids in geographical routing protocols in WSNs.

III. PROPOSED VBD AND VBM ALGORITHMS

Existing algorithms for discovery and maintenance of voids, such as BOUNDHOLE [7] and other algorithms based on the right-hand rule [8][9], insert information on boundary nodes of a void in the VD (Void Discovery) packet, increasing both memory and energy requirements of these nodes and then reducing scalability. These algorithms

also perform a periodical check of a void and rediscover the entire void if one boundary node fails, or it would be economic to discover locally only the changed segment. BOUNDHOLE [7] does not distinguish between an open void and a closed one. Indeed, the outside of a deployed WSN is considered as a great void and data packets that stuck on the network boundary will go on long bypassing paths. Also, the algorithms using the right-hand rule to discover a void do not consider an open void as a particular problem to be handled and they only discover the voids located inside the network. To alleviate these shortcomings, we propose below two effective algorithms (VBD and VBM). The VBD algorithm identifies all nodes forming the boundary of a closed void, calculates and then communicates the void information (i.e., center and radius) to each discovered boundary node. The VBM algorithm detects and updates any changes occurring on the boundary of a closed void that was already discovered in a WSN.

A. Proposed VBD algorithm

To discover the boundary nodes of a closed void, the VBD algorithm uses the right-hand rule on a Gabriel graph (GG) which preserves the network connectivity [2]. This graph is formed by neighbors of a boundary node where all intersections between edges are eliminated to avoid loops problem. The VBD algorithm operates in initial, intermediate and final phases.

1) *Initial phase*: when a blocking situation is detected (i.e., $FS=\emptyset$), node b_i performs the following tasks: (a) broadcasts a 1-hop VP (Void back-Pressure) packet announcing its non-availability for the time VT (Void Time-discovery), (b) drops the data packet to increase the network fluidity and (c) sends a VD (Void-boundary Discovery) packet, marked by its ID, to next boundary-neighbor n_k located at right of vector $\overrightarrow{b_i d}$ (i.e., node n_k having the smallest ω shown in Figure 2-a).

2) *Intermediate phase*: when receiving the VD packet, the boundary node b_{i+1} broadcasts a VP packet and sends the VD packet to the next intermediate boundary neighbor n_k located at right of $\overrightarrow{b_{i+1} b_i}$ as shown in Figure 2-b. This process is repeated by each intermediate neighbor (b_{i+2}, b_{i+3}, \dots) until the VD packet will be received by the initiator boundary node b_0 at the end of its trip around the void (Figure 2-c).

3) *Final phase*: by receiving the VD packet at the end of its trip, node b_0 performs the following tasks: (a) extracts from the VD packet the points Min and Max of the discovered boundary $\{b_0, b_1, \dots, b_n\}$, (b) calculates center v of the void which is the midpoint of the segment \overline{MinMax} , and its radius r given by: $r = Distance(Min, Max)/2$, (c) drops the VD packet and then (d) sends a VU (Void-boundary Update) packet, marked by its ID, through the discovered boundary of a void in the opposite direction of the VD packet (Figure 2-d).

Note that before forwarding the VD packet, node b_i updates its field V1Up by the ID of its successor n_k and checks the field NodeUp in the VD packet. If this field identifies a neighbor then b_i updates its field V2Down (2-hop downstream boundary node) by NodeUp, else V2Down is updated by V1Down. Similarly, each node b_i that receives a VU packet updates its fields about the void and checks the field NodeUp in the VU packet. If this field identifies a neighbor then b_i updates its field V2Up by NodeUp, else V2Up receives V1Up. Note that the fields V2Up (2-hop upstream boundary node) and V2Down are used by the 2-hop forwarding mode of the OVA-vb mechanism which reduces both the node energy consumption and the packet end-to-end delay. The pseudo-code of the proposed VBD algorithm is given in Figure 3.

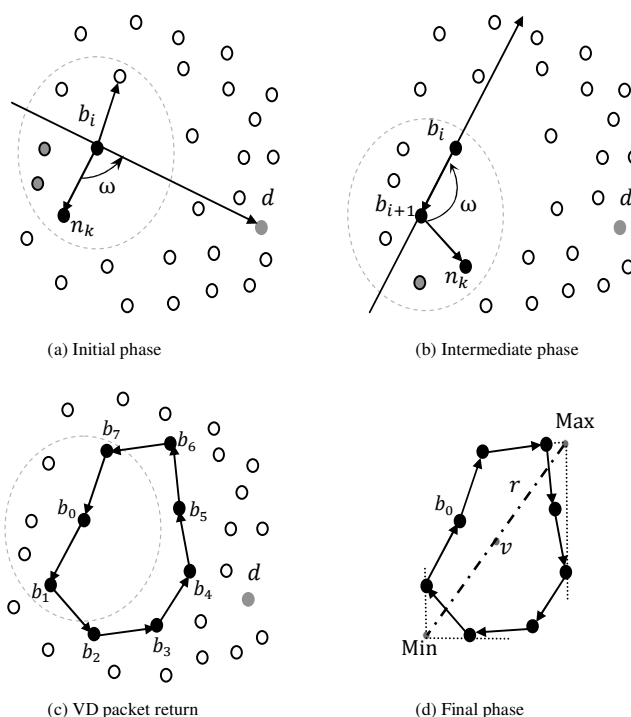


Figure 2. The void discovery process in the VBD algorithm.

B. Proposed VBM algorithm

Some boundary nodes of a closed void in a sensor network may stop working for various reasons. Also, new nodes can be deployed within a closed void to repair it. The proposed VBM algorithm handles these cases as follows.

1) *Boundary-node failure*: each boundary node b_i can detect the absence of its direct ascendant boundary neighbor b_{i-1} thanks to its field V1Up. When b_{i-1} expires in the neighbors table T of node b_i , the later discovers a new segment of nodes and connects it to the old segment of the void by running the VBD algorithm. When node b_5 fails in Figure 5-a, node b_6 discovers the new segment of nodes

$b_6n_1n_2b_4$ that connects to the old segment $b_4b_0b_6$ of the void. When the two segments are connected, the VD packet continues its trip to bring the full information about the new boundary of the closed void. Upon receiving the VD packet at the end, node b_i (i.e., node b_6 in Figure 5-a) runs the final phase of the VBD algorithm updating the void information in fields of the boundary nodes. The pseudo-code of the VBM algorithm handling the case of boundary-node failure is given in Figure 4.

```

Node b treat packet p:
IF (p.type = VD) THEN /* void discovery or maintenance */
    Update the fields of packet p;
    IF (p.VIdent = b.ID) AND (p.NodeUp ≠ b.ID) THEN
        Extract Min and Max from packet p;
        Calculate VCenter and VRadius of the void;
        Use packet VU to update the fields of the void;
        Drop packet ;
    ELSE
        IF (b.V1Up ≠ 0) THEN /* old segment of the void */
            NextHop ← {n, such as: n.ID = b.V1Up};
        ELSE
            Broadcast packet VP to inform all neighbors;
            Build the sets R and L;
            IF (R ≠ ∅) THEN
                NextHop ← {n, such as: cos ω maximal in R};
            ELSE
                NextHop ← {n, such as: cos ω minimal in L};
            ENDF
        ENDF
        Update the fields of boundary node ;
        Forward packet p to successor boundary node in NextHop;
    ENDF
ENDIF

IF (p.type = VU) THEN /* to update the fields of a void */
    Update the fields of packet p;
    Update the fields of boundary node b;
    IF (p.VIdent = b.ID) AND (p.NodeUp ≠ b.ID) THEN
        Drop packet p;
    ELSE
        Forward p to boundary node identified by b.V1Down;
    ENDF
ENDIF
    
```

Figure 3. Pseudo-code of the proposed VBD algorithm.

```

Node n detect absence of a neighbor x:
IF (NT.ExpireTime = 0) THEN /* NT: table of neighbors of n */
    IF (n.VBorder = 1) THEN
        IF (n.V1Up = x.ID) THEN /* x is upstream boundary node */
            Delete neighbor x from NT;
            Execute the VBD algorithm to update the void (Figure 3);
            EXIT;
        ENDF
    ENDF
    Delete neighbor x from NT;
ENDIF
    
```

Figure 4. Pseudo-code of the VBM algorithm when a node fails on boundary of a closed void.

2) *Deployment of nodes within a closed void:* by receiving a location beacon from a new neighbor x , boundary node n checks if x is located inside the void. Based on its updated fields V1Up and V1Down, node n uses its 1-hop boundary neighbors u and r (Figure 5-b) to execute the following verification: if $\widehat{unx} < \widehat{unr}$ then x is located inside the void. If so, node n sends a VS (Void Suppression) packet, marked by its ID, to visit the boundary of the repaired void. Upon receiving the VS packet, each boundary node removes from its list of voids (VList) the repaired void. Note that parts of a void may still exist due to repairing process, but they will be met later by packets and then discovered by the VBD algorithm. The pseudo-code of the VBM algorithm used when nodes are deployed within a closed void is given in Figure 6.

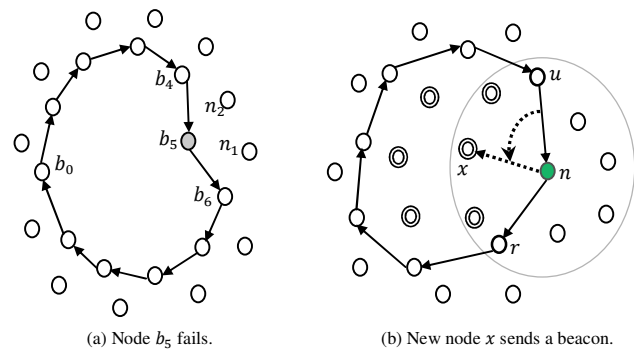


Figure 5. The void-maintenance cases in the VBM algorithm.

```

Node n receives packet p from neighbor x:
IF (p.type = LOC) THEN /* LOC: location packet */
    IF (x ∉ NT) THEN /* NT: table of neighbors of n */
        IF (n.VBorder = 1) THEN /* n is a boundary node */
            Insert neighbor x in NT;
            Calculate the angle formed by nodes u et r (Figure 5-b);
            IF (∠unx < ∠unr) THEN /* x is within a closed void */
                Execute VBD algorithm to update void (Figure 3);
            ENDF
        ENDF
    ELSE
        Update information about neighbor x in NT;
    ENDF
    Drop packet p;
ENDIF
    
```

Figure 6. Pseudo-code of the VBM algorithm used when nodes are deployed within a closed void.

IV. PROPOSED 2-HOP FORWARDING APPROACH

The proposed 2-hop forwarding approach aims to orient towards the sink any packet that arrives at a boundary node by using an optimal path, as shown in Figure 7. When a sender node s has to forward a packet p towards destination d , it forms its FS then distinguishes the three following cases: 1) sender s has no information about voids, 2) sender s is on the network boundary and 3) sender s is on the boundary of closed void.

1) Sender node s has no information about the voids ($s.VList=\emptyset$): if FS is empty then sender s runs the VBD algorithm to discover the void met, else it forwards packet p to its neighbor n in FS (i.e., one of the hatched nodes in Figure 8). The forwarder n is selected according to the protocol routing metric, such as the relay speed used in SPEED [10].

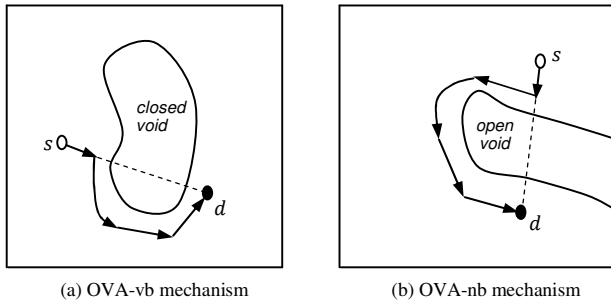


Figure 7. Packet orientation at a boundary node in our approach.

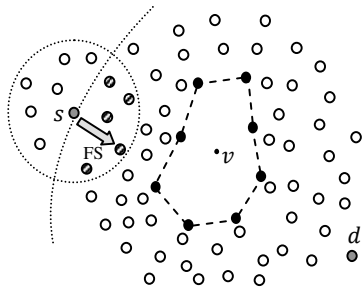


Figure 8. Case 1: sender s has not information about voids.

2) Sender node s is located on the network boundary ($s.NBorder=1$): the sender s uses the OVA-nb mechanism that we proposed in [18] to orient p towards its destination node d by using a 2-hop forwarding mode on the network boundary. Thus, sender s uses the angles $\varphi = \widehat{dvs}$ and $\omega = \widehat{svd}$ (Figure 9) to select the next forwarder n . If $\varphi < \omega$ (Figure 9-a) then sender s selects n from its neighbors located at the right of line (sd) , else (Figure 9-b) n is selected from the neighbors of s that are located at the left of line (sd) . More details about OVA-nb are given in [18].

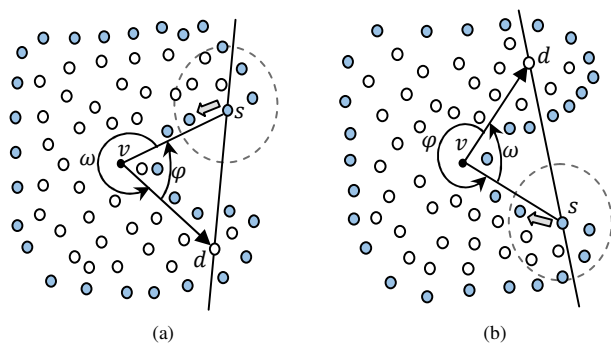


Figure 9. Case 2: sender s is on the network boundary [18]. The next forwarder is located right (a) or left (b) of line (sd) .

3) Sender node s is on boundary of a closed void ($s.VBorder=1$): the sender s uses the OVA-vb mechanism based on a 2-hop forwarding mode on the void boundary. Thus, packet p is oriented in the correct direction around the void by using a non-boundary node as next forwarder as soon as possible, to preserve the actual form of the void for a long time. If sender s have to route on the void boundary (Figure 10-a), it forwards p to its 2-hop upstream node identified by V2Up (or 2-hop downstream node identified by V2Down) depending on the packet orientation (i.e., right or left of \overrightarrow{sv}). If not (i.e., there is at least one non-boundary node in FS as shown in Figure 10-b), sender s forwards p to a neighbor n selected from its RFS (reduced FS) which is formed by the hatched nodes in Figure 10-b. The selection of n is made according to the implemented protocol metric, such as the relay speed used in SPEED [10]. Note that to orient p around a closed void, sender s uses the angle ω shown in Figure 11. If $\sin(\omega) > 0$ (Figure 11-a) then the packet orientation must be at right of \overrightarrow{sv} (i.e., $p.Orient=1$). If not (Figure 11-b) then packet orientation must be at left of \overrightarrow{sv} (i.e., $p.Orient=0$). By using field Orient in p , sender s forms its RFS by neighbors in FS located either at right of \overrightarrow{sd} when $p.Orient=1$ or at left of \overrightarrow{sd} when $p.Orient=0$.

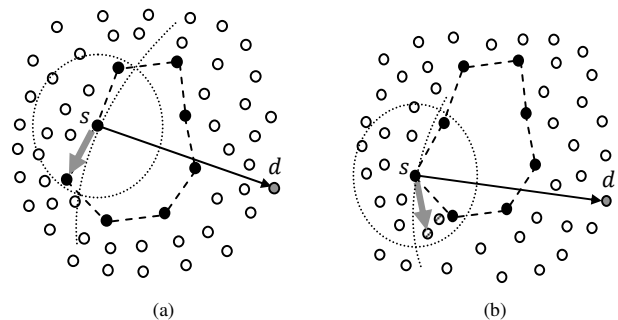


Figure 10. Case 3: sender s is on the boundary of a closed void.

Note that any changes that occur on the boundary (or inside) of a closed void will be immediately detected by a boundary node and then updated by this later after running the VBM algorithm. The reactive maintenance of the open voids on the network boundary is guaranteed by the NBM algorithm that we proposed in [18]. The pseudo-code of the proposed void-handling approach is given in Figure 12.

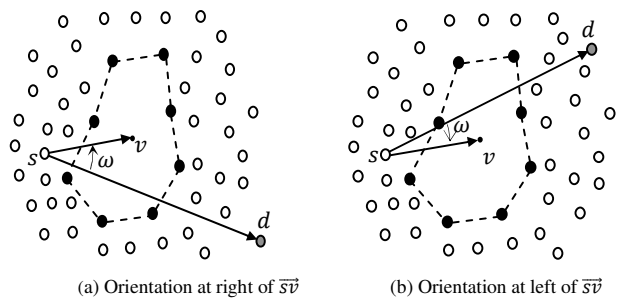


Figure 11. Packet orientation updating in the OVA-vb mechanism.

```

Node  $s$  has to forward  $p$  toward destination  $d$ :
IF ( $s.NBorder = 1$ ) THEN                               /*  $s$  is boundary node */
    Execute the OVA-nb mechanism that we proposed in [18];
ELSE                                                     /* use of OVA-vb mechanism */
    Build FS (Forwarding candidate neighbors Set);
    IF ( $s.VList = \emptyset$ ) THEN                       /*  $s$  not informed about voids */
        IF ( $FS = \emptyset$ ) THEN
            Execute the VBD algorithm to discover the void (Figure 3);
        ELSE
            NextHop  $\leftarrow$  {  $n$ , such as:  $n \in FS$  };
            Forward packet  $p$  to the neighbor in NextHop;
        ENDIF
    ELSE /*  $s$  has information about void(s) */
        Select from  $s.VList$  the nearest void (NearestVoid);
        Build the sets L and R from FS;
        IF (CurrentVoid = NearestVoid) THEN /* same orientation */
            (1): IF ( $p.Orient = 0$ ) THEN
                IF ( $L = \emptyset$ ) THEN
                    NextHop  $\leftarrow$  {  $n$ , such as:  $n.ID = s.V2Down$  };
                ELSE
                    NextHop  $\leftarrow$  {  $n$ , such as:  $n \in L$  };
                ENDIF
            ELSE
                IF ( $R = \emptyset$ ) THEN
                    NextHop  $\leftarrow$  {  $n$ , such as:  $n.ID = s.V2Up$  };
                ELSE
                    NextHop  $\leftarrow$  {  $n$ , such as:  $n \in R$  };
                ENDIF
            ENDIF
        ELSE /* different orientation */
            IF ( $\sin \omega \leq 0$ ) THEN /*  $d$  is left of CurrentVoid */
                 $p.Orient \leftarrow 0$ ;
            ELSE
                 $p.Orient \leftarrow 1$ ;
            ENDIF
            GOTO (1);
        ENDIF
        Forward packet  $p$  to the neighbor in NextHop;
    ENDIF
ENDIF
    
```

Figure 12. Pseudo-code of the proposed 2-hop forwarding approach detailing the OVA-vb mechanism.

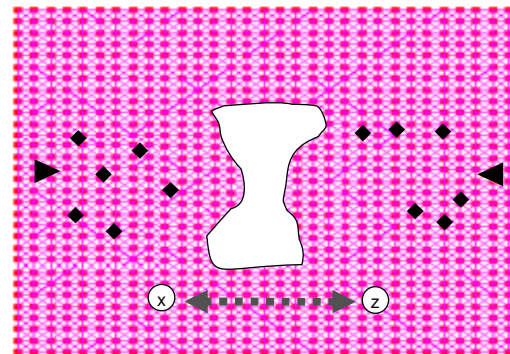
V. PERFORMANCE EVALUATION

In order to evaluate performance of the proposed 2-hop forwarding approach, we associate the proposed OVA-vb and OVA-nb mechanisms with the well-known SPEED real-time routing protocol by using the ns-2 simulator [17]. We compare performance of the resulting protocol, called SPEED-vb, with the performance of the GPSR and SPEED traditional protocols. Note that to handle voids SPEED uses the backpressure rule and GPSR the right-hand rule. We use the two terrains shown in Figure 13 and we vary the void radius (Section V.1), the data packet rate at sources (Section V.2), the packet deadline (Section V.3) and the number of voids created in terrain (Section V.4). The deployed nodes are organized in a grid and the distance between two successive sensor nodes in each terrain is set to 25 meters. For each simulation, we measure packet delivery ratio, control packet overhead, network energy consumption per

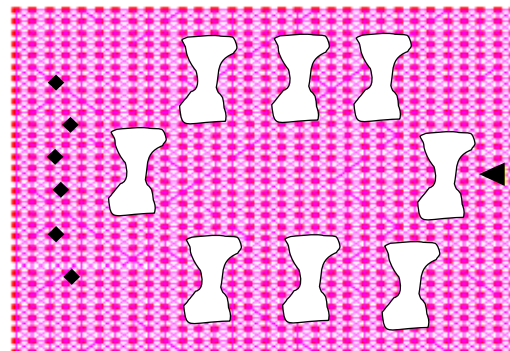
delivered packet, node energy balancing and boundaries energy consumption per delivered packet. Each point in our graphs, presented in this section, is the average results of 15 simulations performed under the same conditions, except that source nodes are chosen randomly for each simulation. Simulation parameters are given in TABLE I.

TABLE I. SIMULATION PARAMETERS.

MAC Layer	IEEE 802.11
Radio Layer	RADIO-NONNOISE
Propagation Model	TwoRayGround
Antenna Model	OmniAntenna
Queue Model	Queue/DropTail/PriQueue
Queue Size	50 packets
Transmission channel	WirelessChannel
Wireless Interface	WirelessPhy
Bandwidth	200 Kbps
CBR Packet Size	32 bytes
Energy Model	energyModel de ns-2
Communication Range	40 meters
Transmission Power	0.666 w
Reception Power	0.395 w



(a) Terrain 1



(b) Terrain 2

◀ : destination node ◆ : source node ○ : other node

Figure 13. The used simulation terrains.

Terrain 1 shown in Figure 13-a, with a size 800×800 meters and 961 nodes, is used principally to measure the impact of the void radius on the routing performance. We create at the center of this terrain one void with a radius

varying between 60 and 200m (meters). Six sources selected randomly from the left side of the void generate periodic CBR (Constant Bit Rate) packets to the first destination placed at right side of this void. Meanwhile, six other sources selected randomly from the right side of the void generate periodic CBR packets to the second destination placed at the left side of the same void. The source rate is set to 1 pps (packet per second) and the desired delivery speed (the $S_{setpoint}$ defined in [10]) is set to 600 mps (meter per second) which leads to an end-to-end packet deadline of 100 ms (milliseconds). To measure the routing performance with the presence of congestion, two nodes x and z, placed under the void in Figure 13-a, exchanged packets with a rate of 10 pps during the simulation time which is set to 224 seconds. The two nodes are enough for congestion and there is no additional traffic excepting the traffic generated by sources.

But Terrain 2 (Figure 13-b), with a size 1240x800 meters and 1296 deployed nodes, is used to measure the impact of the number of voids created in the network on the routing performance. A void with a radius 100 meters is duplicated gradually between the sources and the destination node up to 8 voids in the network. Six sources, selected randomly from the left side of the terrain, periodically send packets to a destination node located on the right side of this terrain. The duration of each simulation using Terrain 2 is fixed to 264 seconds.

1) *Performance when varying void radius:* we use Terrain 1 (Figure 13-a) in which the source rate is set to 1 pps and the packet deadline to 100ms. We vary the void radius from 60m to 200m and we obtain the results shown in the figures 14-17 where the protocols' performance decreases each time the void radius grows because they use long paths around the void. Therefore, deadline of many packets expires before reaching their destination and then they are dropped in the network because we suppose a critical application. We also note that the proposed SPEED-vb protocol is the most efficient with the presence of both small and large voids in a WSN. This is due to the performance of the proposed mechanisms used by the boundary nodes. Figure 14 shows that SPEED is the worst protocol in delivering packets, especially when a void radius is greater than 120m. This protocol overloads its upstream nodes by the backpressure messages generation near the voids. Following the spread of these messages, some sources are blocked and many packets are removed when their deadline expires in congested links. For an acceptable packet deadline (100ms), GPSR performs better than SPEED tanks to its face routing scheme used by boundary nodes. GPSR generates less control packets (Figure 16) that reduces the network congestion. With the adequate orientation of packets ensured by the proposed mechanisms, the SPEED-vb protocol uses the shortest and smoother routing paths compared to the SPEED and GPSR protocols. Therefore, the packet delivery ratio achieved by SPEED-vb

is the highest (Figure 14). For some delivered packets, SPEED consumes much energy of both network (Figure 15) and boundary nodes (Figure 17). This is due to excessive control packets generated by SPEED and its useless routing of delayed packets in the network.

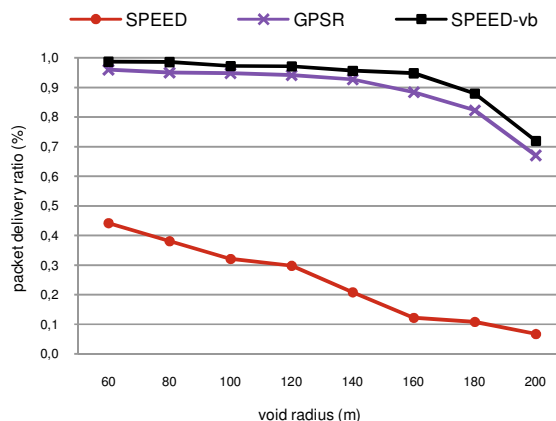


Figure 14. Packet delivery ratio vs. Void radius.

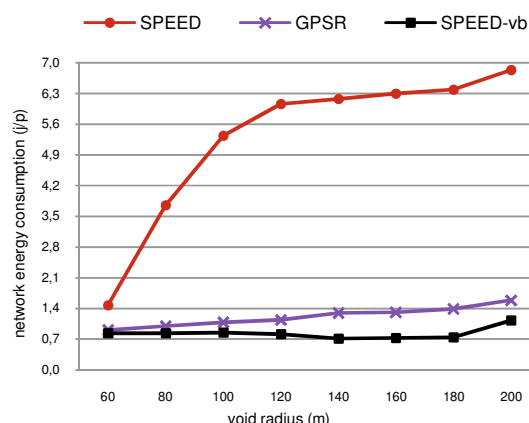


Figure 15. Network energy consumption vs. Void radius.

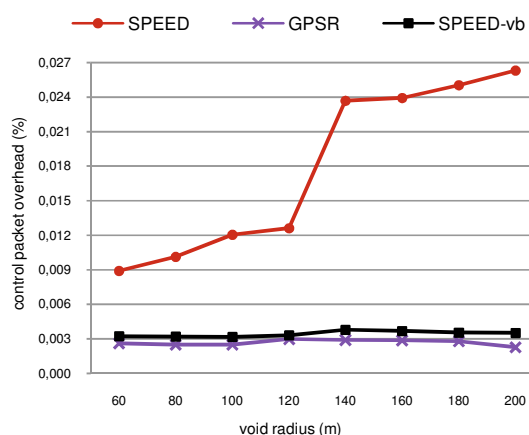


Figure 16. Control packet overhead vs. Void radius.

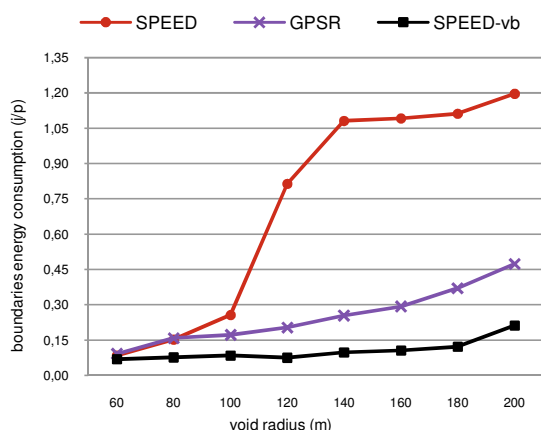


Figure 17. Boundaries energy consumption vs. Void radius.

GPSR is more efficient than SPEED in term of network energy consumption, but it consumes more energy of boundary nodes, especially when the void radius exceeds 100m (Figure 17). For these large voids, GPSR routes most packets on the long parts of the boundary. On the other hand, our SPEED-vb protocol achieves the best tradeoff between the packet delivery ratio and the energy consumption (Figure 15). Since GPSR always uses a unique path connecting a source to the sink, it does not achieve a good node energy balancing.

2) *Performance when varying the source rate:* we use Terrain 1 (Figure 13-a) with 120m as radius of the void created at the center of the terrain and 100ms as deadline of the generated packets. Each source node generates one CBR flow with a rate increased step by step from 2 to 12 pps. For each source rate, we obtained the results shown in the figures 18-21. Thanks to the proposed void-handling mechanisms, SPEED-vb performs better than both GPSR and SPEED for all measured metrics. Indeed, Figure 18 shows that SPEED removes many data packets either by stuck nodes on the void boundary or by other nodes when the packet deadline expires. The deadline expiration is due to network congestion caused by both the backpressure messages broadcasted by sensor nodes near the void (Figure 20) and the use of alternative paths too long around this void. In SPEED, some source nodes located in concave areas of the void are permanently blocked toward the sink after receiving a backpressure message from each forwarding candidate neighbor. This further weakens the performance of SPEED in delivering packets. For few packets delivered and many backpressure messages generated, SPEED has a high energy cost (Figure 19) and consumes unnecessarily the energy of boundary nodes (Figure 21) maximizing the chances of expanding the void rapidly. As the flow generated by a source to a destination in GPSR uses the same routing path, the later will be overloaded mainly when the rate is greater than 3 pps, as shown in Figure 18. Therefore, most of these packets are

delayed and then they are dropped after expiration of their deadlines. Since GPSR uses the face routing to bypass the void, it consumes more energy of boundary nodes than the proposed SPEED-vb protocol as shown in Figure 21.

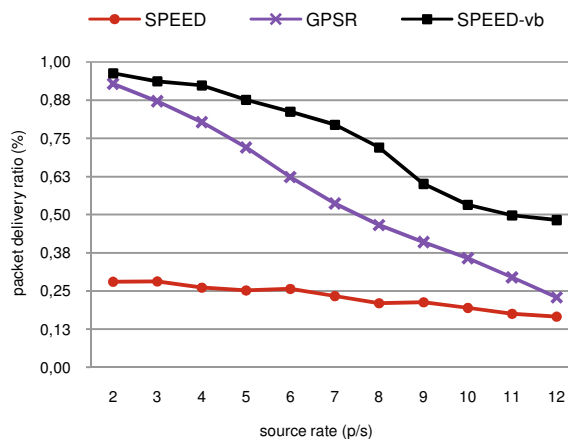


Figure 18. Packet delivery ratio vs. Source rate.

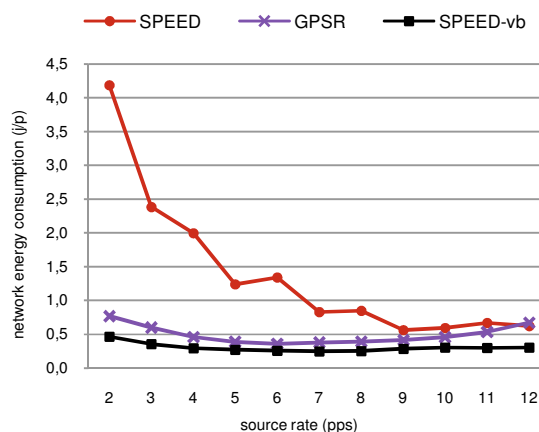


Figure 19. Network energy consumption vs. Source rate.

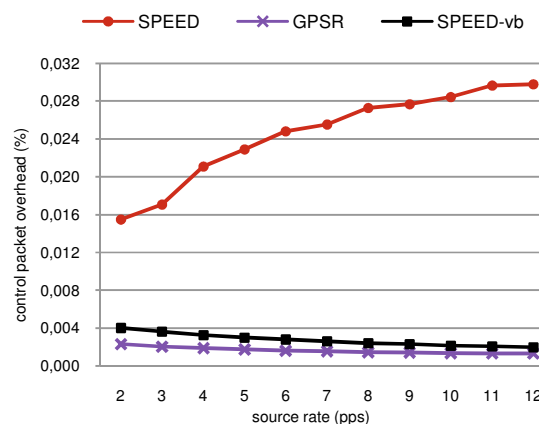


Figure 20. Control packet overhead vs. Source rate.

On the other hand, Figure 20 shows that the GPSR protocol generates less control packets compared to the two other evaluated protocols.

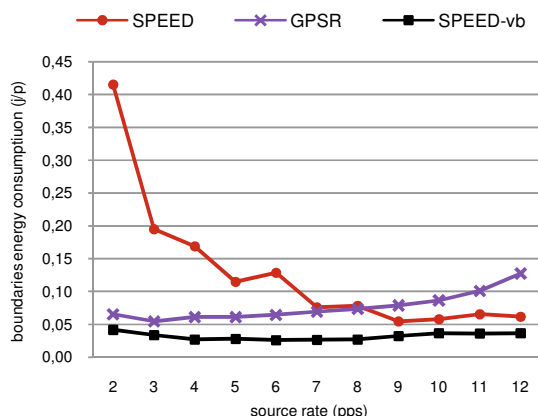


Figure 21. Boundaries energy consumption vs. Source rate.

3) *Performance when varying packet deadline:* we use Terrain 1 (Figure 13-a) with 120m as radius of the void created at the center of the terrain and 1 pps as rate of the generated packets. The packet deadline is increased step by step from 50 to 150ms and the obtained results are shown in the figures 22-25. These results show that SPEED-vb achieved the best performance compared to both GPSR and SPEED, especially for important packet deadlines. The proposed mechanisms effectively oriented many data packets around the open and closed voids and increased the links fluidity in these regions of the network. Figure 24 shows that GPSR is less efficient than other protocols in term of average gain in packet deadline, particularly when the later is less than 110ms. This is because GPSR do not balance the load between the nodes since it uses the same routing path connecting a source to a destination. For all deadlines greater than 100ms, GPSR outperforms SPEED, which generates many backpressure messages overloading nodes and unnecessarily consuming energy of boundary nodes as shown in Figure 25. But the figure proves that SPEED-vb delivers many packets in a shorter average end-to-end delay. Since it balances the load around voids and then increases the network fluidity in these areas, SPEED-vb delivers many packets (Figure 22) and saves more energy of nodes (Figure 23) compared to the protocols GPSR and SPEED. For packet deadlines less than 90ms, GPSR unnecessarily consumes the energy of the nodes because many packets are dropped in the network. These drops are due to frequent delays of packets in unique paths relating a source to a destination. Figure 22 shows that GPSR is equivalent to SPEED-vb in delivering packets when the packet deadline is greater than 100ms. This is due to the face routing applied on the void boundary which justifies the excessive energy consumption of boundary nodes in GPSR (Figure 25).

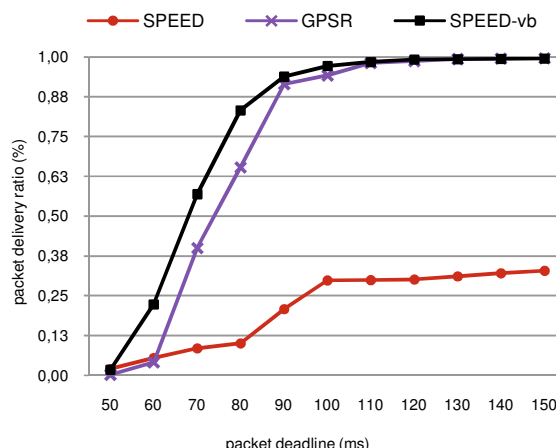


Figure 22. Packet delivery ratio vs. Packet deadline.

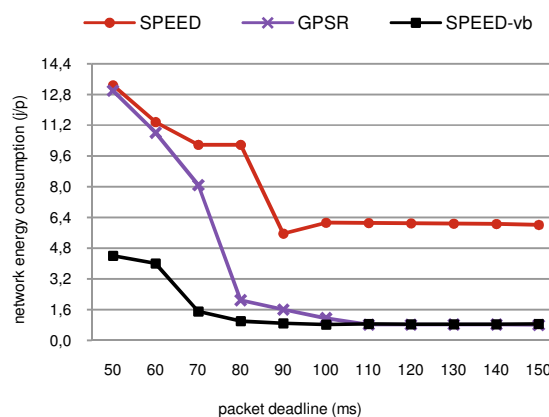


Figure 23. Network energy consumption vs. Packet deadline.

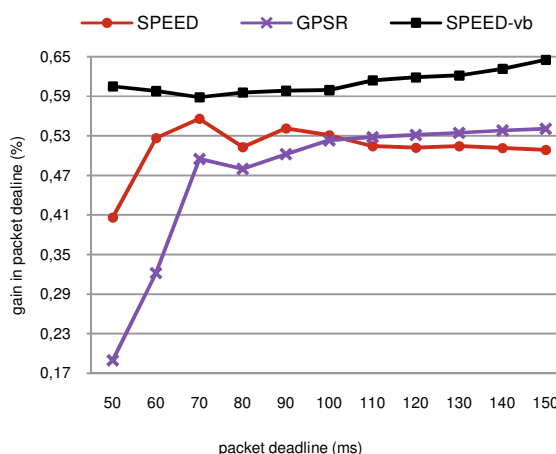


Figure 24. Gain in packet deadline vs. Packet deadline.

In the same time, as shown in Figure 25, the proposed void-handling mechanisms preserve more energy of boundary nodes by both using a 2-hop forwarding mode on the void boundary and orienting packets in the shortest

paths around the void. Moreover, the results shown in Figure 22 show that SPEED delivers few packets and excessively consumes energy of nodes forming the network, especially when the packet deadline is less than 90ms. Indeed, many data packets are dropped in SPEED because their deadline expires in long routing paths that are also overloaded with the backpressure messages broadcasted around the voids.

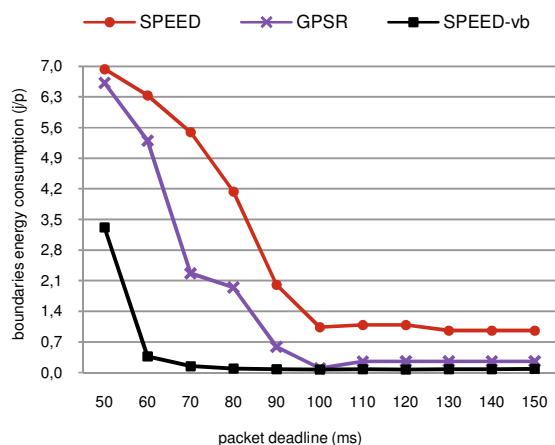


Figure 25. Boundaries energy consumption vs. Packet deadline.

4) *Performance when varying number of voids:* we use Terrain 2 (Figure 13-b) by fixing the source rate to 10 pps and the packet deadline to 100ms. We vary the number of created voids in the network from 1 to 8 and the obtained results are shown in the figures 26-29. These results show that SPEED-vb achieved the best performance compared to the GPSR and SPEED protocols. This is due to the efficiency of the proposed void-handling mechanisms. Since it uses the same routing path to deliver all packets of each flow generated by a source to a destination, the GPSR protocol delays the urgent packets because it overloads some nodes forming the used routing paths. Then many of these packets are dropped because of deadline expires (Figure 26) and energy depletion of nodes forming the routing path is then accelerated. Moreover, Figure 28 shows that the GPSR protocol have the worst node energy balancing. But the proposed SPEED-vb protocol provides the best node energy balancing thanks to its void-handling mechanism and its packet forwarding strategy inherited from the SPEED protocol. Moreover, SPEED is classed second after GPSR in term of node energy balancing as shown in Figure 28. By achieving the best node energy balancing, SPEED-vb certainly helps in extending the network lifetime. We note in Figure 26 that the number of packets delivered by SPEED is too low, especially when the number of created voids is important in the network. With several closed voids in the network, SPEED generates many backpressure packets and then accelerates the number of overloaded nodes.

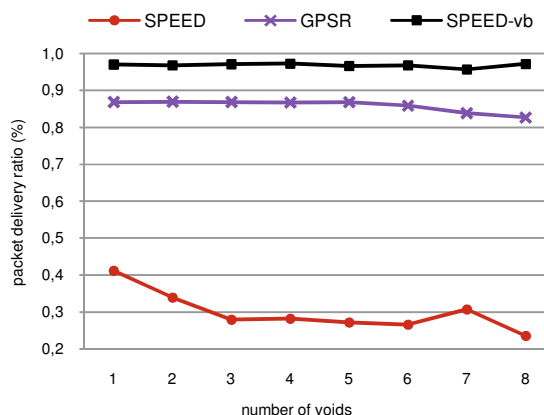


Figure 26. Packet delivery ratio vs. Number of voids.

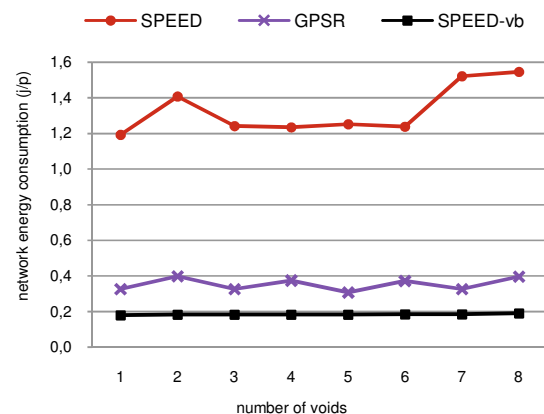


Figure 27. Network energy consumption vs. Number of voids.

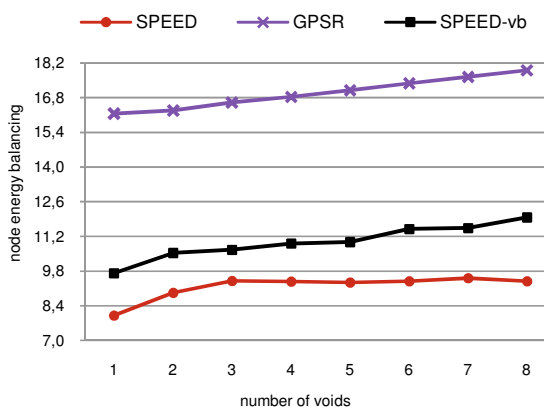


Figure 28. Node energy balancing vs. Number of voids.

We also notice the excessive and wasteful consumption of the network energy in SPEED as shown in Figure 27. But the same figure shows the obtained SPEED-vb protocol consumes less energy according to its packet delivery ratio. Compared to both GPSR and SPEED in Figure 29, the simulation results show that SPEED-vb has a low use of the

boundary nodes when forwarding packets towards the destination node and it orients many of these packets in optimal paths near the voids in the network. Note that when preserving the energy of the boundary nodes, the voids expand slowly and thus contribute to the best operation of the deployed application.

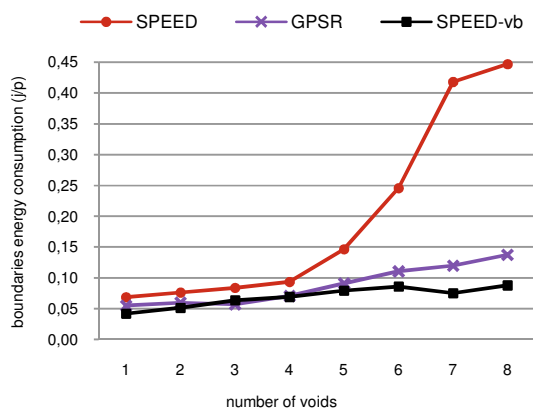


Figure 29. Boundaries energy consumption vs. Number of voids.

VI. CONCLUSION

We have proposed an oriented 2-hop forwarding approach that provides to each data packet received by a boundary node the shortest path towards the destination node. Our void-tolerant approach uses two complementary mechanisms: the first one handles the open voids located on the network boundary and the second one handles the closed voids located within the sensor network. These mechanisms use simple and reactive algorithms that we have proposed to discover and then to maintain each void that appears in a deployed wireless sensor network. We have associated them with the well-known SPEED routing protocol, designed for real-time applications, and the resulting protocol, called SPEED-vb, achieved the best performance compared to the traditional GPSR and SPEED protocols. This comparison was done with several radius of created voids, flow rate at sources, packet deadlines and number of voids created in a same sensor network. The proposed approach, associated to the SPEED-vb protocol, was able to respond to the shortcomings of the existing void-handling techniques in terms of packet delivery ratio, control packet overhead, end-to-end delay, energy consumption and node energy balancing. Note that these techniques are based either on the right-hand rule used in the GPSR protocol or on the backpressure rule used in the SPEED protocol.

Since we are interested by sensor networks dedicated to real-time applications, our future work will focus on the sequencing of data packets at a node based on the time remaining to reach the destination node. The objective is to reduce the number of removed critical data packets due to deadline expiration. We plan to improve the proposed void-handling mechanisms by realizing a trade-off between packet delivery deadlines on short routing paths versus load

balancing. We also plan to check how the propose approach can be applied to congested regions in a sensor network or to the voids created due other problems, like intermittent connectivity.

REFERENCES

- [1] M. Aissani, S. Bouznad, A. Hariza, and S. E. Allia, "Oriented 2-hop Forwarding Approach on Voids Boundaries in Wireless Sensor Networks," Proc. Eighth Advanced International Conference on Telecom. (AICT 2012), IARIA Press, May 2012, pp. 46-51.
- [2] B. Karp and H. Kung, "GPSR: Greedy perimeter stateless routing for wireless networks," Proc. IEEE/ACM Conference on Mobile Computing and Networking, ACM Press, August 2000, pp. 243-254, doi: 10.1145/345910.345953.
- [3] L. Moraru, P. Leone, S. Nikolettseas, and J.D.P Rolim, "Near optimal geographical routing with obstacle avoidance in wireless sensor networks by fast-converging trust-based algorithms," Proc. 3rd ACM Workshop on QoS and Security for Wireless and Mobile Networks, ACM Press, Oct. 2007, pp. 31-38, doi:10.1145/1298239.1298246.
- [4] L. Moraru, P. Leone, S. Nikolettseas, and J. Rolim, "Geographical routing with Early Obstacles Detection and Avoidance in Dense Wireless Sensor Networks," Proc. 7th international conference on Ad-hoc, Mobile and Wireless Networks, Springer-Verlag, Sept. 2008, pp. 148-161, doi: 10.1007/978-3-540-85209-4_12.
- [5] F. Kuhn, R. Wattenhofer, and A. Zollinger, "An Algorithmic Approach to Geographical routing in Ad Hoc and Sensor Networks," IEEE/ACM Transactions on Networking, vol. 16(1), March 2008, pp. 51-62, doi:10.1109/TNET.2007.900372.
- [6] F. Huc, A. Jarry, P. Leone, L. Moraru, S. Nikolettseas, and J. Rolim, "Early Obstacle Detection and Avoidance for All to All Traffic Pattern in Wireless Sensor Networks," Lecture Notes in Computer Science, vol. 5304, Dec. 2009, pp. 102-115, 10.1007/978-3-642-05434-1_11.
- [7] Q. Fang, J. Gao, and L.J. Guibas, "Locating and bypassing routing holes in sensor networks," Journal of Mobile Networks and Applications, vol. 11(2), October 2006, pp. 187-200, doi: 10.1007/s11036-006-4471-y.
- [8] F. Yu, Y. Choi, S. Park, E. Lee, Y. Tian, M. Jin, and S.H. Kim, "Anchor node based virtual modeling of holes in wireless sensor networks," Proc. International Conference on Communications, IEEE Press, June 2008, pp. 3120-3124, doi:10.1109/ICC.2008.587.
- [9] F. Yu, S. Park, E. Lee, and S. H. Kim, "Hole Modeling and Detour Scheme for Geographical routing in Wireless Sensor Networks," Journal of Communications and Networks, vol. 11(4), August 2009, pp. 327-336, doi: 10.1145/1298239.1298246.
- [10] T. He, J.A. Stankovic, C. Lu, and T. Abdelzaher, "A Spatiotemporal Communication Protocol for Wireless Sensor Networks," IEEE Transactions on Parallel and Distributed Systems, vol. 16(10), October 2005, pp. 995-1006, doi: 10.1109/TPDS.2005.116.
- [11] E. Felemban, C. G. Lee, and E. Ekici, "MMSPEED: Multipath Multi-SPEED Protocol for QoS Guarantee of Reliability and Timeliness in Wireless Sensor Networks," IEEE Transactions on Mobile Computing, vol. 5(6), June 2006, pp. 738-754, doi: 10.1109/TMC.2006.79.
- [12] W. Cheng, L. Yuan, Z. Yang, and X. Du, "A real-time Routing Protocol with Constrained Equivalent Delay in Sensor Networks," Proc. 11th IEEE Symposium on Computers and Communications, IEEE Press, June 2006, pp. 597-602, doi: 10.1109/ISCC.2006.16.
- [13] L. Zhao, B. Kan, Y. Xu, and X. Li, "FT-SPEED: A Fault-Tolerant Real-Time Routing Protocol for Wireless Sensor Networks," Proc. International Conference on Wireless Communications, Networking and Mobile Computing, IEEE Press, October 2007, pp. 2531-2534, doi: 10.1109/WICOM.2007.630.

- [14] M. Aissani, A. Mellouk, N. Badache, and B. Saidani, "Oriented Void Avoidance Scheme for Real-Time Routing Protocols in Wireless Sensor Networks," Proc. IEEE Global Communications Conference, IEEE Press, December 2008, doi: 10.1109/GLOCOM.2008.ECP.24.
- [15] M. Aissani, A. Mellouk, N. Badache, and M. Boumaza, "A Novel Approach for Void Avoidance in Wireless Sensor Networks," International Journal of Communication Systems (IJCS), vol. 23(8), August 2010, pp. 945–962, doi: 10.1002/dac.1079.
- [16] K. Seada, A. Helmy, and R. Govindan, "Modeling and analyzing the correctness of geographic face routing under realistic conditions," Ad-Hoc Networks, vol. 5(6), August 2007, pp. 855–871, doi: 10.1016/j.adhoc.2007.02.008.
- [17] Collaboration between researchers at UC Berkeley, LBL, USC/ISI, and Xerox PARC, "The ns Manual", <http://www.isi.edu/nsnam/ns/>, accessed 15 June 2011.
- [18] M. Aissani, S. Bouznad, A. Hariza, and S.E. Allia, "An effective mechanism for handling open voids in wireless sensor networks," Proc. Fifth International Conference on Sensor Technologies and Applications, IARIA Press, August 2011, pp. 24-29.

Carrier Phase Discrimination for a Common Correlation Interval GNSS Receiver Architecture

Pedro A. Roncagliolo, Javier G. García, and Carlos H. Muravchik
 Laboratorio de Electrónica Industrial, Control e Instrumentación (LEICI),
 Dto. Electrotecnia, Facultad Ingeniería, UNLP, La Plata, Argentina.
 Emails: {agustinr, jgarcia, carlosm}@ing.unlp.edu.ar

Abstract—Basic measurements of global navigation satellite system receivers are obtained after the correlation of the incoming signal with locally generated replicas. Usually, correlation intervals are chosen synchronously with the data-bits sent with each satellite signal to avoid bit transitions. As a consequence, the ensuing code and carrier phase estimation signal processing operates at its own time and the navigation task must extrapolate loop measurements to a common instant. We have proposed an alternative receiver architecture using a common correlation interval for all satellite signals. Under this scheme, the correlations made for each satellite in-view have a common interval, chosen in synchronism with the navigation process rather than with the data bits. Naturally, now the bit transitions within a correlation interval require special treatment. The advantages of avoiding measurement extrapolation are shown with a scalar phase lock loop structure intended for high dynamics real-time receivers. The operation of this loop in a common correlation interval receiver needs a carrier phase discriminator structure able to produce outputs for the correlation with bit transitions inside the interval. Three possible carrier discriminator schemes are analyzed in this work. It is shown that the loops operating data-bit asynchronously with any of these schemes have similar tracking threshold and phase estimation quality than those working bit-synchronously. The proposed architecture naturally generates a vector of simultaneous measurements and then it is particularly suited for the implementation of real-time vector tracking loops.

Keywords- Phase Discrimination; GNSS; Real-Time Receivers; Digital Phase Locked Loops; Vector Tracking Loops.

I. INTRODUCTION

Measuring the propagation delay of broadcast signals is the key to the position calculations made in every modern global navigation satellite system (GNSS) receiver. For this purpose, the receiver has to be synchronized with the visible satellite signals. Direct sequence spread spectrum (DS-SS) signals are utilized due to their desired properties of high time-resolution and code division multiple access (CDMA) and therefore code and carrier synchronization are required [2]. A correlation stage is also needed at the receiver to de-spread the incoming signals so that the synchronization and navigation algorithms can operate with reasonable signal-to-noise ratios. The required economy of operations in real-time receivers makes impractical the use of complex estimation schemes and usually tracking loop schemes are adopted for synchronization purposes. Phase measurements are considerably less noisy than code delay and so, code loops are usually aided by carrier

loops [3]. However, the signal phase is affected by the wavelength ambiguity and hence the basic measurement used for standard position determination is code delay. On the contrary, the techniques used in high precision positioning applications usually take advantage of the phase measurements. In general, code delay and carrier phase or frequency measurements used by the GNSS receiver for position and velocity determination are referred to as navigation measurements or raw track data.

Typically, the GNSS signal has also a data structure to send useful information to the receivers, such as orbit parameters needed for satellite position calculations, clock corrections, ionospheric corrections, signal quality indexes, etc. The bits carrying this information are modulated usually in phase, and of course the receiver has to be able to demodulate them. The presence of these data-bits imposes restrictions to the receiver operation from the point of view of navigation measurements generation. Indeed, the correlation time is in principle, limited to the bit duration time and the corresponding signal-to-noise ratio increase due to despreading gain is limited too. In some applications this is not a limitation at all, but in others, such as indoor positioning, the use of some long-correlation techniques is unavoidable [4]. Moreover, since different satellite signals experience different propagation delays, the edges of these bits are in general asynchronous. As a consequence, the correlation intervals used for each signal satellite are also asynchronous. In standard real-time receivers, this causes that the tracking loops for each satellite operate synchronously with the bit edges, but asynchronously among them. For the navigation process, this implies that the measurements do not correspond to the same time instant and the receiver has to extrapolate them [2], [3]. These lag differences make it difficult to take advantage of the correlation between the received signals, since each signal is tracked independently.

The convenience of joint tracking the signals by means of the so-called vector tracking loops, has been envisioned since the conception of the GNSS systems [2]. Nowadays, due to their potential advantages together with the growing computation capacity available in a GNSS receiver, many researchers and developers, are considering vector tracking loop schemes. These loops can obtain up to 6 dB of improvement in tracking threshold, in addition to high dynamic capacity, multipath immunity and robustness [5]. Vector tracking loops have been mainly applied in software-based receivers [6], [7]. Recently, a real-time implementation using field-programmable-gate-

arrays (FPGA) with a fast microprocessor has been reported in [8]. This implementation operates with asynchronous correlations of the different signals, either extrapolating the navigation measurements or asynchronously incorporating the measurements to the main processing algorithm. Other off-line implementations use data bit removal in order to get simultaneous navigation measurements [9].

In a previous work, we proposed a different and novel approach, which is based on the use of synchronous correlations for the received satellite signals so that the navigation measurements are naturally simultaneous [1]. As a consequence, the tracking loops operate asynchronously with respect to the bit edges of the signals and their inputs, i.e., the code and carrier phase errors, have to be calculated for signal intervals with a possible bit-transition inside. The suggested approach is to compute partial correlations before and after the bit edge and calculate a discriminated error based on them. In this work we analyze particularly three different carrier phase discriminators based on this partial correlations. In high signal-to-noise ratio the three schemes show similar performance, which is also similar to the bit synchronous tracking loop results. The main difference between them is their non-linear characteristic, which is evidenced in low signal-to-noise and/or high dynamic situations. This aspect of the discriminators is quantified by means of the resulting tracking threshold, i.e., the lowest signal-to-noise ratio the tracking loop can operate at, computed for different dynamic scenarios.

The rest of paper is organized as follows. A digital model for the received GNSS signal is presented in Section 2. Since the emphasis on this work is on phase discriminator, our unambiguous frequency-aided phase-locked loop (UFA-PLL) scheme will be briefly explained [10]. The advantages of avoiding measurements extrapolation are shown with this tracking loop structure intended for high dynamics real-time receivers. The three phase error discriminators schemes under consideration for the correlation periods with possible bit-transition are presented in Section 3. The computational load of each scheme and their extension for code delay discrimination is also shortly discussed. The considered phase discriminators are applied to UFA-PLL structure in Section 4, and their effects in the phase measurements quality and tracking threshold are determined by means of Monte Carlo simulations. One of the schemes show better performance for low dynamics situations but its performance is severely degraded in high dynamics. In the other two cases, the degradation in the tracking threshold is less than 0.5dB compared with a loop that works with known data-bits, for all the dynamic scenarios considered. Curves of pull-out probability of the different schemes are also provided. The small degradation in tracking threshold caused by the data-bits asynchronous operation is completely insignificant compared to the improvement in the quality of phase measurements due to the absence of extrapolation and the common correlation interval architecture. Finally, the obtained conclusions and future work lines are given in Section 5.

II. DIGITAL MEASUREMENTS MODEL

In a GNSS receiver, the incoming signal must be correlated with the locally generated replicas for each visible satellite. The complex correlations of the signal from a given satellite with carrier power to noise power spectral density C/N_0 and for the i -th correlation interval of duration T can be expressed as [2]

$$C_i = D_i \sqrt{T \frac{C}{N_0}} \text{sinc}(\Delta f_i) R(\Delta \tau_i) e^{j(\pi \Delta f_i T + \Delta \theta_i)} + n_i \quad (1)$$

where $\Delta \tau_i = \tau_i - \hat{\tau}_i$ is the code delay estimation error, $\Delta f_i = f_i - \hat{f}_i$ the frequency estimation error, both assumed constant during the integration time, and $\Delta \theta_i = \theta_i - \hat{\theta}_i$ the initial phase estimation error. The term n_i is a complex white Gaussian noise sequence with unit variance, $R(\cdot)$ is the code correlation function and $\text{sinc}(x) = \sin(\pi x)/(\pi x)$. This expression assumes that there are binary data bits $D_i = \pm 1$ and that correlations are computed within the same bit period. This type of modulation, i.e., binary phase shift keying (BPSK), is used in the GPS civil signal and in the data components of composite modernized GNSS signals.

After the acquisition process has been completed, i.e., in tracking conditions [2], code and frequency estimation errors are sufficiently small so that the functions $\text{sinc}(\cdot)$ and $R(\cdot)$ can be approximated by one. Hence, (1) becomes

$$C_i = I_i + jQ_i = D_i \sqrt{T \frac{C}{N_0}} e^{j\Delta \phi_i} + n_i \quad (2)$$

where we have defined $\Delta \phi_i = \phi_i - \hat{\phi}_i$, with $\phi_i = \pi f_i T + \theta_i$ and $\hat{\phi}_i = \pi \hat{f}_i T + \hat{\theta}_i$. With the help of these sequences the carrier tracking loop can be modeled as a digital single-input single-output (SISO) system. It is important to note that Δf_i and $\Delta \phi_i$ can be interpreted as the average frequency error and average phase error during the correlation interval respectively.

The phase estimation error is obtained from the angle of the complex correlation. In the case of BPSK modulation the phase error must be insensitive to the bit changes and a two quadrant discriminator should be utilized. Then,

$$e_i = \tan^{-1} \left(\frac{Q_i}{I_i} \right) = [\Delta \phi_i + n_{\phi_i}]_{\pi} \quad (3)$$

where the notation $[\cdot]_{\pi}$ indicates that its argument is kept within the interval $(-\frac{\pi}{2}, \frac{\pi}{2}]$ by adding or subtracting π as many times as needed. The noise term n_{ϕ_i} has zero mean and a complicated probability distribution in general. However, in high C/N_0 conditions it can be approximated by a Gaussian distribution with zero mean and variance $1/(2TC/N_0)$.

A. Phase Discriminator

The unambiguous frequency-aided (UFA) algorithm uses the frequency error information to correct the non-linearity of a phase-locked loop (PLL), instead of adding a frequency-locked loop (FLL) to cope with high dynamics. Thus, the advantages of a frequency loop are added to the PLL obtaining the same dynamic tolerance of an FLL but also avoiding cycle slips during tracking [11], [10]. The UFA phase discriminator

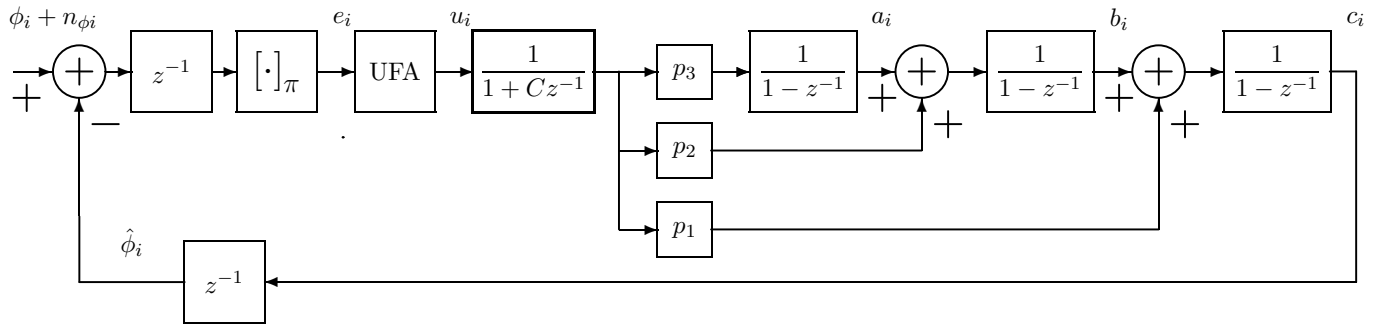


Fig. 1. Block diagram of the UFA-PLL model.

works correcting the ambiguous values of e_i by adding or subtracting an integer number of π . The correction is such that the difference between successive values of the corrected phase error u_i is less than a quarter of a cycle in magnitude. Then, the corrected phase error estimate, with starting value $u_0 = e_0$, is

$$u_i = e_i - I_\pi(e_i - u_{i-1}) \quad (4)$$

where $I_\pi(x) = x - [x]_\pi$ acts similarly to the integer part function, but with steps at the multiples of π . Created in this way, the sequence of phase errors u_i has unambiguous values as long as the loop frequency error is lower than $1/(4T)$ in magnitude, i.e., half of the Nyquist rate from uniform sampling theory. Under this condition, the sequence u_i allows to measure the loop frequency error with a simple difference of successive phase errors, giving to the UFA-PLL the same extra-information that usually has an FLL but not a PLL. In previous works we have also shown that the UFA-PLL has the same noise resistance, and so the same tracking threshold, than an equivalent FLL [12].

B. Carrier Phase Tracking Loop

For the purpose of comparing different correlation intervals approaches, throughout the rest of this work we consider a specific carrier tracking loop. We chose a digital UFA-PLL as shown in Figure 1 whose filter coefficients are $C = 0.5$, $p_1 = C = 0.5$, $p_2 = 0.105$, and $p_3 = 0.0123$. For the selected correlation time, $T = 5\text{ms}$, the resulting PLL has an equivalent noise bandwidth $B_N = 75.6\text{Hz}$. Notice that two delays are included in the loop model. One of them is due to the time spent in computation of the correlation. The other delay appears because the estimated values used to compute the correlations have to be known before the calculations begin. That is, the value $\hat{\phi}_i$ is obtained with the loop filter output of the $(i - 1)$ -th correlation interval, which in turn is calculated with the estimation errors of $\hat{\phi}_{(i-2)}$. The loop filter is optimized for the tracking of acceleration steps, which produces a quadratic ramp of phase at the loop input. These demanding high dynamics scenarios can be found for example in sounding rockets, at engine turn-on and turn-off. This loop design has been implemented in experimental GPS receivers [11]. According to the analysis made in [13] this design is almost optimal for tracking steps of 20g, in the sense that for

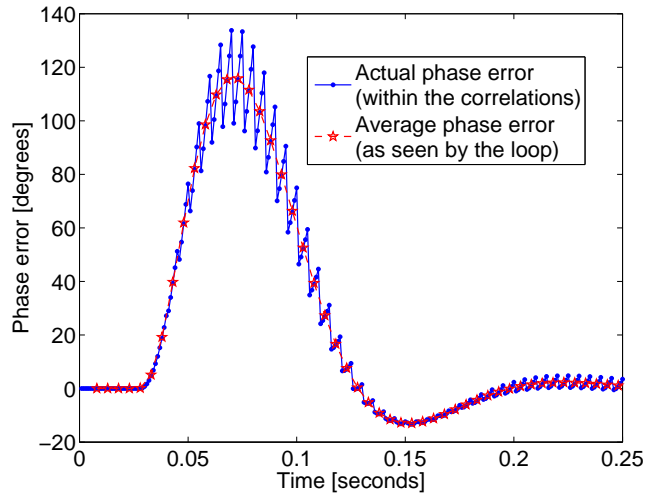


Fig. 2. Phase error during a step of 20g. Loop transient response.

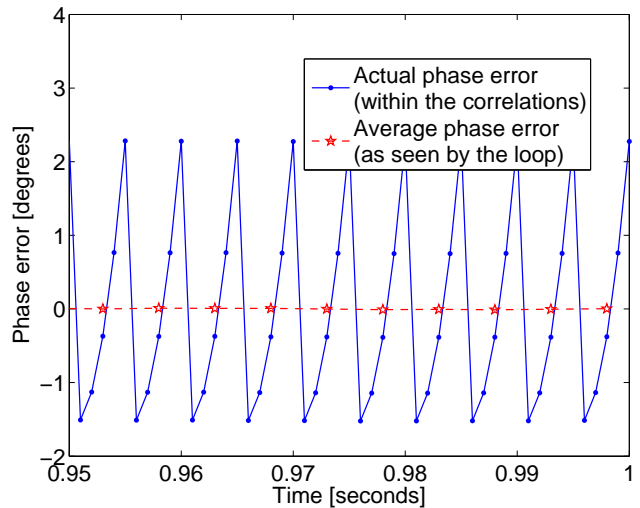


Fig. 3. Phase error during a step of 20g. Loop stationary state response.

a given C/N_0 it approximately produces the smallest pull-out probability. More details and properties of this loop can be found in [10].

This loop is simulated at a higher sampling rate than

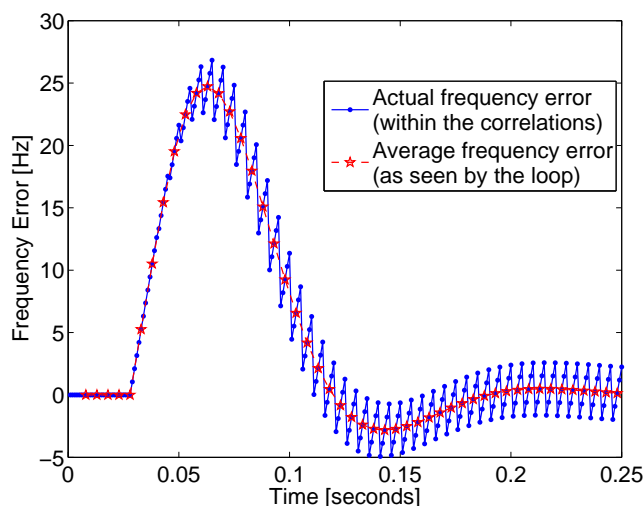


Fig. 4. Frequency estimation error during a step of 20g. Loop transient response.

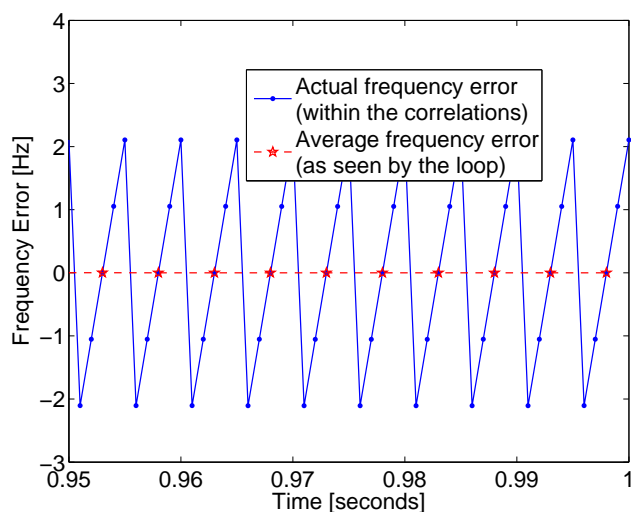


Fig. 5. Frequency estimation error during a step of 20g. Loop stationary state response.

the loop iteration in order to quantify the quality of phase measurements obtained from the tracking loops. If the loop operates synchronously with the data bits, it cannot be synchronous with the navigation process in general. Therefore, the measurement instants can occur at any instant during a correlation interval, not necessarily in the middle. The phase measurement extrapolation made by the navigation process is done based on the same information that the loop has about the phase dynamic. Typically, if the measurement instant is not the middle of the correlation interval, the loop frequency estimate for this interval is used to linearly extrapolate this value. The phase measurement obtained in this way, is the same that the instant phase error inside the correlation interval because the carrier local replica is generated with the same logic. In order to quantify the effects of navigation measurements extrapolation without increasing the simulation time

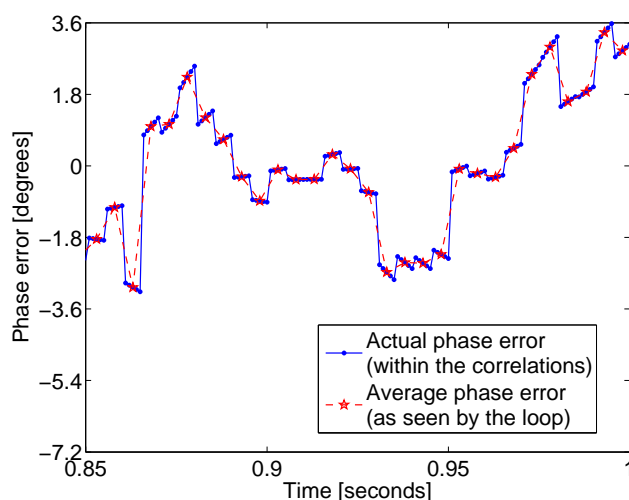


Fig. 6. Phase estimation error with $C/N_0 = 48$ dB/Hz.

excessively, a time step of 1ms was selected. This implies a quantization of the measurement times to 5 possible values within a correlation interval of $T = 5$ ms. The phase estimate used for each middle instant of this period is $\hat{\phi}_i = c_{(i-1)}$, and the frequency estimate for this whole 5 ms period is $\hat{f}_i = b_{(i-1)} + a_{(i-1)}/2$. This frequency estimate was chosen because, as can be seen in the following simulations, it has zero stationary error for acceleration steps.

As an example, consider the phase estimation error produced by the loop for an acceleration step of 20 g without noise. The result is plotted in Figures 2 and 3 to appreciate the estimation error inside the correlation interval. Clearly, the phase error is not constant during each correlation period. In fact, since the estimated carrier has constant frequency for each period, the loop fits the incoming phase with a piecewise linear approximation. Hence, a residual quadratic ramp of phase appears as an estimation error. Notice that the level of error is lower if the relative location within the correlation interval is close to the middle. Even when the digital loop has zero stationary state response to acceleration steps, the error in the middle of the correlation interval is not zero because the loop works with the average phase error of each interval. The same situation is found for the frequency estimation, plotted in Figures 4 and 5. Here, the residual error is a linear ramp inside each interval, and then average error equal to zero produce zero error in the middle of the interval.

As long as pull-out or cycle slips do not occur, the loop response is linear and the noise effects can be analyzed separately. As an example, the loop response to noise only with $C/N_0 = 48$ dB/Hz is plotted in Figure 6. In this case, the resulting phase error seems to be lower if the relative location within the correlation interval is close to the beginning. This effect can be understood if we notice that in fact, the loop calculates a carrier prediction for the following correlation interval based on the available measurements. And as the prediction time grows, so does the noise variance of this

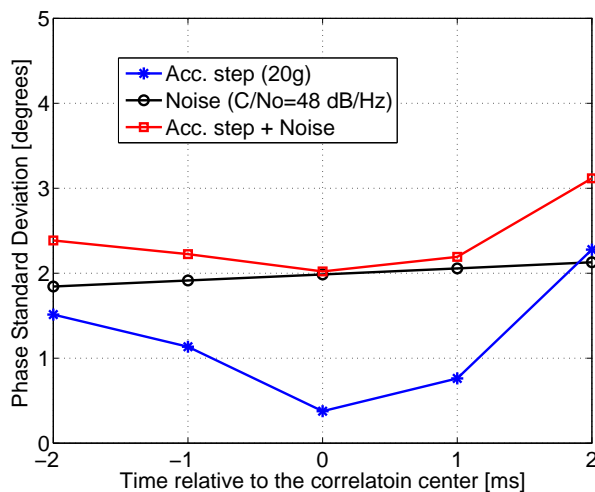


Fig. 7. Phase estimation error within the correlation interval.

prediction. Signal and noise results are summarized in Figure 7 where each contribution to the phase standard deviation is plotted for the different relative location within the correlation period. The signal parts correspond to the time average of a 1-second run like that shown in Figure 2. The noise variance was estimated with an average of 10000 runs of 1 second with only Gaussian noise of variance $\frac{1}{2TC/N_0}$ as input, and discarding the first third of the record to avoid the main part of the loop transient. It is possible to verify that the standard deviation for the loop output, i.e., at the middle point, is the same as that obtained with the equivalent noise bandwidth of the loop and the input noise variance. Indeed,

$$\sigma_{\phi_i}^2 = \frac{1}{2TC/N_0} \times 2B_N T = \frac{B_N}{C/N_0} \quad (5)$$

The expression gives $\sigma_{\phi_i} = 1.98^\circ$ when $C/N_0 = 48\text{dB/Hz}$, as seen in ordinates of Figure 7. In summary, the phase estimation quality changes depending on the time when the navigation measurement is taken during the correlation interval. In the presented example better estimates are obtained if the measurements are taken at the middle, and this can only be done if the loop is synchronous with the navigation process and therefore it is bit-asynchronous. In a bit-synchronous loop, when the measurement instant is taken next to the end of the correlation interval the increase in noise standard deviation is $3.1^\circ/2^\circ \approx 1.55$, i.e., 55%. This analysis clearly shows that even for a GNSS receiver with scalar tracking loops, the common correlation interval scheme can be considerably beneficial, if the effect of bit transitions can be properly handled. This is the aim of the next section.

III. BIT ASYNCHRONOUS PHASE DISCRIMINATION

Assume the receiver is tracking a given satellite and it knows when a data bit edge will occur during a correlation interval. This requires that a bit synchronization stage has been completed previously. This is not a limitation since the required signal strength for tracking at the high dynamics considered

in this work must be high enough to detect bit transitions. For the same reason, multiple data-bits long correlation intervals will not be considered. However, notice that the receiver will not use bit transitions to synchronize the correlation intervals. In our scheme, the receiver uses them to compute the code and phase errors as described in the following and the correlation intervals are dictated by the navigation task. Specifically, assume for the i -th correlation interval of duration T the bit edge will occur T_1 seconds after the beginning and T_2 seconds before its end. Clearly, $T_1 + T_2 = T$. In that case, a coherent correlation of T seconds will not be effective since the possible change of phase will produce a signal cancellation. The worst case when there is a bit reversal is $T_1 = T_2 = T/2$, where a complete signal cancellation occurs. Therefore, the receiver should compute two partial correlations, namely C_1 and C_2 . Then, for a given correlation interval the partial correlation can be expressed as

$$C_1 = I_1 + jQ_1 = D_1 \sqrt{T_1 \frac{C}{N_0}} e^{j\Delta\phi_1} + n_1 \quad (6)$$

$$C_2 = I_2 + jQ_2 = D_2 \sqrt{T_2 \frac{C}{N_0}} e^{j\Delta\phi_2} + n_2 \quad (7)$$

where the subscripts i have been omitted to simplify the notation. Notice that $\Delta\phi_2 = \Delta\phi_1 + 2\pi f_i T$, if f_i is the frequency error, assumed constant during this whole correlation interval, and n_1 and n_2 are independent zero-mean and unit-variance complex gaussian noise. Based on these two partial correlations, different phase discriminators can be computed. In the following subsections we describe three of them. Their comparison in terms of tracking threshold is left for the next section.

A. Partial-Decision Directed (PDD) Discriminator

One possible approach to combine the phase information of both partial correlations is to estimate the corresponding data-bits based on the in-phase value. Then, this data-bit estimates, \hat{d}_1 and \hat{d}_2 , can be used to correct the bit transition and add the partial correlations. Then, the phase of the resulting total correlation will be the sought for phase error value. The expression of this phase discriminator for the i -th correlation interval is

$$\begin{aligned} e_{PDD} &= \tan^{-1} \left(\frac{\hat{d}_1 Q_1 + \hat{d}_2 Q_2}{\hat{d}_1 I_1 + \hat{d}_2 I_2} \right) \\ &= \tan^{-1} \left(\frac{\text{sgn}(I_1) Q_1 + \text{sgn}(I_2) Q_2}{|I_1| + |I_2|} \right) \end{aligned} \quad (8)$$

where the notation $\text{sgn}(\cdot)$ indicate the sign function. Of course, the longer the correlation time, the better is the data-bit estimate. But, if one correlation is long necessarily the other will be short. However, it can be argued that when a short correlation is added, even in error, its effect will not be so harmful because the other partial correlation will dominate in the sum.

B. Partial-Phase Weighted Average (PWA) Discriminator

Another possible discriminator can be obtained from the phase errors of both partial correlations. This is the approach used in [1]. The phase errors, obtained as in (3), corresponding to C_1 and C_2 respectively are

$$e_1 = \tan^{-1} \left(\frac{Q_1}{I_1} \right) = [\Delta\phi_1 + n_{\phi_1}]_{\pi} \quad (9)$$

$$e_2 = \tan^{-1} \left(\frac{Q_2}{I_2} \right) = [\Delta\phi_2 + n_{\phi_2}]_{\pi} \quad (10)$$

where $\Delta\phi_1 = \Delta\theta_i + \pi\Delta f_i T_1$ and $\Delta\phi_2 = \Delta\theta_i + 2\pi\Delta f_i T_1 + \pi\Delta f_i T_2$ according to the assumed linear evolution of the phase error. Leaving aside for a moment the nonlinearity of the $\tan^{-1}(\cdot)$ function, we can think that these two phase errors are partial averages and therefore they should be averaged to obtain the desired phase error for the i -th correlation interval. The weighted average of them, adjusted to the duration of each correlation, should be

$$\begin{aligned} e_{PWA} &= \frac{T_1}{T} e_1 + \frac{T_2}{T} e_2 \\ &\approx \Delta\theta_i + \pi\Delta f_i T + n_{eq} = \Delta\phi_i + n_{eq} \end{aligned} \quad (11)$$

with n_{eq} equal to the weighted average of n_{ϕ_1} and n_{ϕ_2} . Under the Gaussian approximation for both noise terms, n_{eq} has a Gaussian distribution with zero mean and variance $1/(2TC/N_0)$. That is, the same variance as if the bit edge was not present. Of course, if either T_1 or T_2 are not long enough the approximation is not valid, and we still have to deal with the nonlinearity of the $\tan^{-1}(\cdot)$ function.

The issue about the nonlinearity is caused by the ambiguity of the phase, indicated by the function $[\cdot]_{\pi}$. If this operation acts after the weighted average we would obtain a result equivalent to (3) for the correlation interval with a bit transition. However, in (11) the $[\cdot]_{\pi}$ function actually is applied before the average, and then the result is not correct. Fortunately, the same idea used to build the UFA algorithm can be applied here to test the result and correct it when needed. The hypothesis is that the frequency error is kept under $1/(4T)$ in magnitude. Hence, the signal part of a difference between the partial phase errors in (9) must be bounded. Indeed, (9) can be written as

$$e_1 = \tan^{-1} \left(\frac{Q_1}{I_1} \right) = \Delta\phi_1 + n_{\phi_1} + k_1\pi \quad (12)$$

$$e_2 = \tan^{-1} \left(\frac{Q_2}{I_2} \right) = \Delta\phi_2 + n_{\phi_2} + k_2\pi \quad (13)$$

with $k_1, k_2 \in \mathbb{Z}$. Then, different values of k_1 and k_2 will produce a wrong result at the average (11). This situation has to be detected, and a simple hypothesis test can be built. The decision variable is

$$e_1 - e_2 = \Delta\theta_1 - \Delta\theta_2 + n_d + k_d\pi = \pi\Delta f_i T + n_d + k_d\pi \quad (14)$$

where $n_d = n_{\phi_1} - n_{\phi_2}$ and $k_d = k_1 - k_2$. Since $|\Delta f_i T| < 1/4$ and n_d is a zero mean symmetrically distributed noise term, the optimum decision for the k_d value is $\hat{k}_d = I_{\pi}(e_1 - e_2)/\pi$. Notice that the possible values for k_d are only three: -1, 0

TABLE I
Standard deviation for different discrimination schemes.

Scheme	Noise (48dB/Hz)	Acc.(20g)	Acc. + Noise
KD	1.975	0.377	2.015
PDD	1.976	0.377	2.011
PWA	1.975	0.377	2.013
SIP	1.99	0.373	2.027

and 1. Then, if $\hat{k}_d = 0$ no correction is needed and (11) can be applied directly. If $\hat{k}_d \neq 0$, either e_1 or e_2 have to be corrected. Which one is not important since the π ambiguity of the e_i value will be solved later by the UFA algorithm. For simplicity, assume e_2 is corrected when $\hat{k}_d \neq 0$. Then, the final expression for this phase error discriminator is

$$e_{PWA} = \frac{T_1}{T} e_1 + \frac{T_2}{T} \{e_2 + I_{\pi}(e_1 - e_2)\}. \quad (15)$$

C. Squared-Input Phase (SIP) Discriminator

The bit transition caused by a BPSK modulation can be also avoided squaring the signal. This technique, usually called Squaring Loops has been used traditionally in analog BPSK synchronization schemes [14]. This idea was also used to extend the correlation interval non-coherently beyond the data-bit duration [15]. In our case, if the partial correlations are squared, then they can be added without the adverse effect of the data-bit. Clearly, the noise is also present and in low signal-to-noise ratio conditions this causes a squaring loss. The squaring operation also produces a duplication of the correlation phase and therefore a correction factor should be applied. The expression of this phase discriminator for the i -th correlation interval is

$$\begin{aligned} e_{SIP} &= \frac{1}{2} \angle \{ (I_1 + jQ_1)^2 + (I_2 + jQ_2)^2 \} \\ &= \frac{1}{2} \tan_2^{-1} \left\{ \frac{2(I_1 Q_1 + I_2 Q_2)}{I_1^2 - Q_1^2 + I_2^2 - Q_2^2} \right\} \end{aligned} \quad (16)$$

where the subscript 2 indicates that actually a four-quadrant inverse tangent should be used.

The three discrimination schemes were simulated in the same conditions as the bit-synchronous loop. In this case, only the phase error in the middle of the correlation interval matters since under the common correlation interval architecture the receiver can choose this measurement instant and no extrapolations are needed. The results after 10000 runs of the loop with random data-bit transition location in each case are summarized in the Table I. In each case, the statistical significance of the result was checked, i.e., the empirical standard deviation of the estimated value was in the order of a thousandth of the empirical mean. For comparison purposes a loop with known data-bits (KD) was also included. This loop uses the same discriminator as in the bit-synchronous case because it can correct the partial correlations and add them coherently.

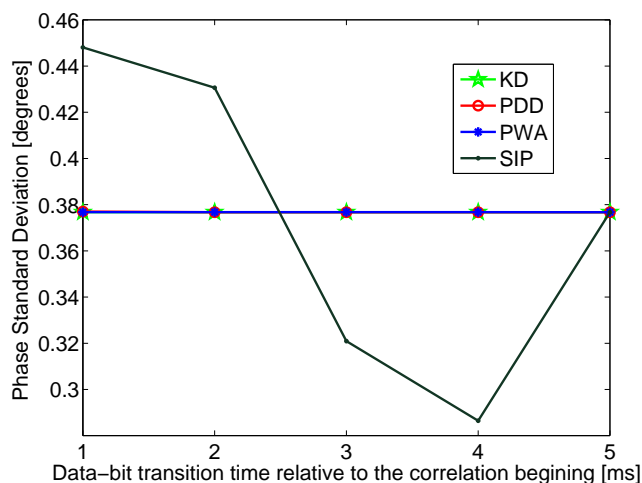


Fig. 8. Phase estimation error with different transition locations.

Except for the squaring scheme, the noise and signal response are the same as in the loop with known data-bits, and also in the data-bit synchronous loop. On the contrary, the last scheme (SIP) has a little more output noise and, in average, a little less noise in the signal estimation. However, this value is highly dependent on the data-bit transition location. The response to an acceleration step without noise is plotted in Fig. 8 for fixed transition location inside the correlation interval. While this value is almost constant for the other schemes, it changes considerably for the squaring one.

From the computational cost point of view, the first scheme is the best. One inverse tangent is used as the case of the usual phase discriminator. Only the sign corrections are needed before the complex sum. In the second case, one more inverse tangent calculation is needed each time a bit transition is present, plus the weighted average. The logic needed for the last π ambiguity correction can be neglected compared with the cost of angle calculations and multiplications. And in the last scheme, two complex square operations are required instead of and additional inverse tangent. Which one is more demanding will depend on the specific implementation of the receiver processor unit.

Naturally, the ideas of the partial data-bit estimation, the weighted average for combining partial discriminated errors, or the squaring operation can be extended to be applied for the case of code delay error estimation in the presence of a bit transition. Significant changes of the code delay are not expected during a correlation interval, and in the case of high dynamics the code loop is aided by the carrier loop and then only the residual and low code dynamics is tracked. Thus, the code delay error will not evolve significantly during the two partial correlations, and the significant effect will be only to reduce the noise to the same level obtained with a correlation time T . In addition, the delay discriminators are not ambiguous and then no further corrections are needed in the case of the weighted average.

IV. TRACKING THRESHOLD ESTIMATION

In this section, the non-linear performance of the three proposed bit-asynchronous schemes for different acceleration and signal levels is determined by means of simulation. Main consequences of this non-linear behavior are cycle slips and pull-out events, i.e., to lose lock with the tracked signal. If a cycle slip occurs, it will produce a loop transient that could end with a pull-out event or not. This temporary loss of phase lock can degrade the data bit demodulation, but as long as the frequency error is low enough, useful navigation measurements can be generated. Actually, since the expression (1) was used for the calculation of 1ms correlations used in the simulations, a frequency error also produces a signal power reduction due to the $\text{sinc}(\cdot)$ function factor. Therefore, the adopted criterion to declare a pull-out was that the frequency error exceeds $1/T = 200$ Hz. In this situation, the signal power is completely attenuated and then it can be considered as a practically irrecoverable state. An error of less than 200 Hz is a critical situation but it could still be recoverable. For each value of acceleration and C/N_0 , 100,000 runs of 1 second (200 samples) were computed. Each run has an acceleration step of the selected value at the beginning.

Four UFA-PLLs were simulated for comparison. One operates with known data-bits and it is equivalent to a data-bit synchronous loop. The other three loops implement the proposed schemes for carrier phase discrimination during a bit transition according to (8), (15) and (16). Pull-out events were detected using the previously mentioned criteria, and the pull-out probability (POP) of each scheme was estimated as the ratio between the number of runs with a pull-out event and the number of total runs simulated. Since the POP is computed for 1 second of tracking it can be also interpreted as the inverse of the mean-time to lose lock (MTLL) in seconds. The results are presented in Figs. 9, 10, 11, and 12, where POP level curves have been plotted for values of 0.1, 0.2 and so on. The tracking threshold of each scheme is defined usually when the POP reaches a level of 0.1. Then, the region of operation to the right of the 0.1 curve in each scheme. The first considered scheme shows practically the same tracking threshold as the loop with known data-bits in the low dynamic situation. However, its performance has an important degradation when the dynamics is increased. This effect can be explained by the fact that during high dynamic situations, the received phase changes appreciably during the correlation interval, and the bit detection based on partial correlations is poor. The other two proposed schemes exhibit only a small degradation in their tracking thresholds with respect to the loop with known data. Actually, comparing Figs. 10 and 11 with Fig. 9 it can be clearly seen that the difference between them is always less than 0.5 dB.

The pull-out probabilities estimated for the scenarios without acceleration, and with acceleration steps of 20g, 40g, and 60g are plotted in Figs. 13, 14, 15, and 16, respectively. These curves show in more detail that the scheme based on partial bit detection has a better performance when there

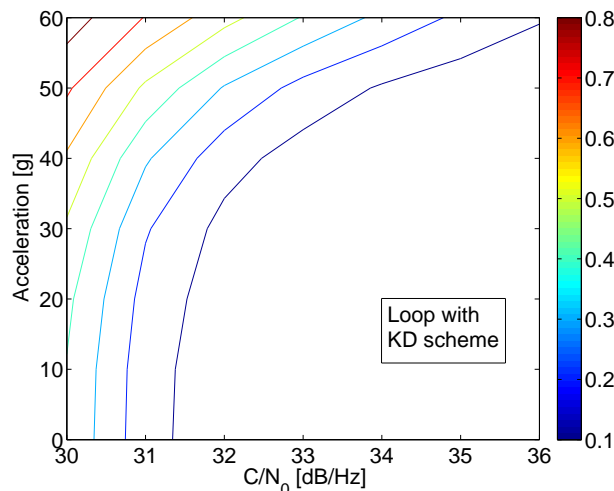


Fig. 9. POP of loop with known data and its tracking threshold.

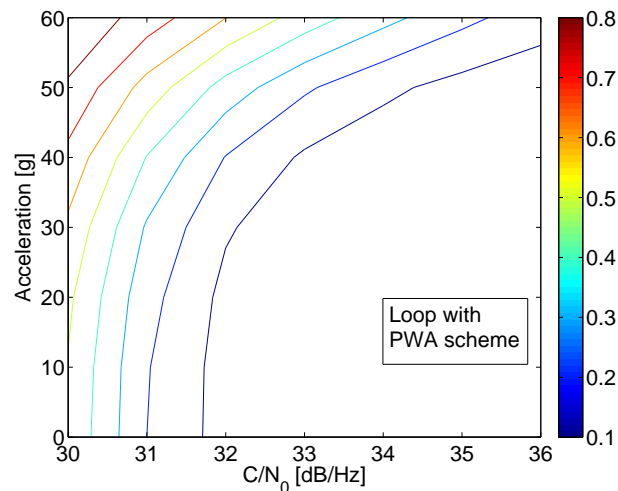


Fig. 11. POP of loop with PWA scheme and its tracking threshold.

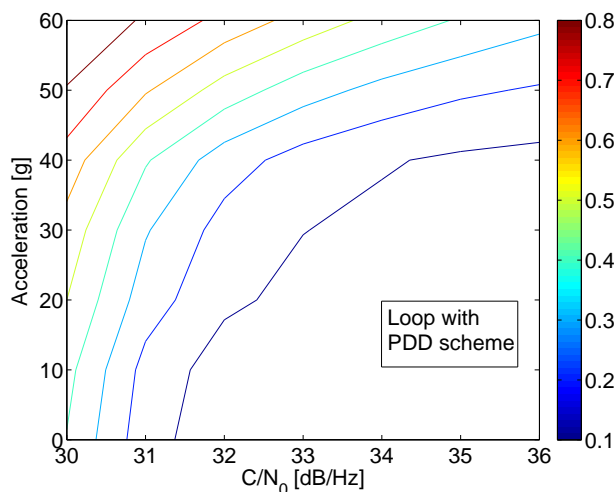


Fig. 10. POP of loop with PDD scheme and its tracking threshold.

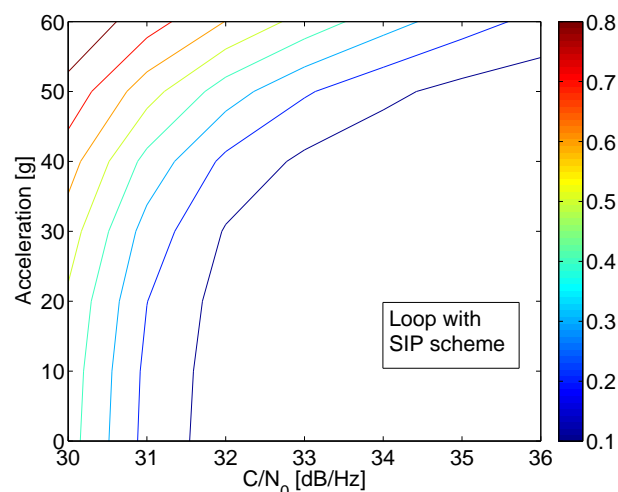


Fig. 12. POP loop with SIP scheme and its tracking threshold.

is no acceleration and how this performance change in the more demanding dynamic scenarios. It can also be seen that the partial-phase weighted average scheme has a worse performance in low and moderate dynamic scenarios than the squared-input one, but the situation changes when very high dynamics is considered. In particular, the weighted average scheme has the best performance for the 60g acceleration condition. Notice that in n Fig. 13 there are no results for $C/N_0 = 36\text{dB/Hz}$ because the number of runs simulated do not allow a dependable estimate of them.

V. CONCLUSIONS AND FUTURE WORK

The proposed GNSS receiver architecture is based on bit-asynchronous tracking loops and is intended for high performance real-time receivers. Under this architecture, the tracking loop operation is synchronous with the navigation measurement generation process, rather than with the data-

bits as it is done traditionally. In this way, the measurement instants of the tracked signals do not need to be extrapolated to a common instant and therefore a significant improvement can be obtained. An example was shown where a phase noise standard deviation increase of up to 55% can be avoided by controlling the measurement instant. Three different carrier discrimination schemes designed for GNSS receivers operating with such a common correlation interval for all the tracked satellite signals have been presented.

The effect of a possible bit-transition inside the correlation interval is managed by the calculation of two partial correlations. The proposed carrier discrimination schemes work based on these partial correlations. The proposed schemes were applied to a UFA-PLL designed for high dynamic GNSS receivers. We found that the data-bit asynchronous operation with either of the proposed schemes produces negligible impact on tracking estimation phase noise for high signal-to-

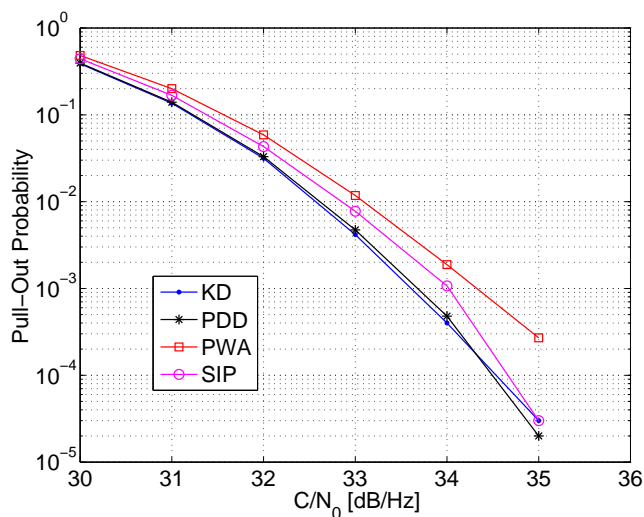


Fig. 13. POP of different schemes without acceleration.

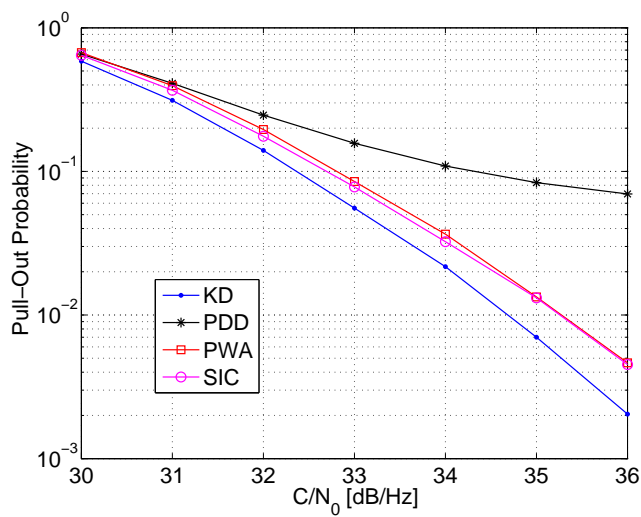


Fig. 15. POP loop of different schemes at 40g of acceleration.

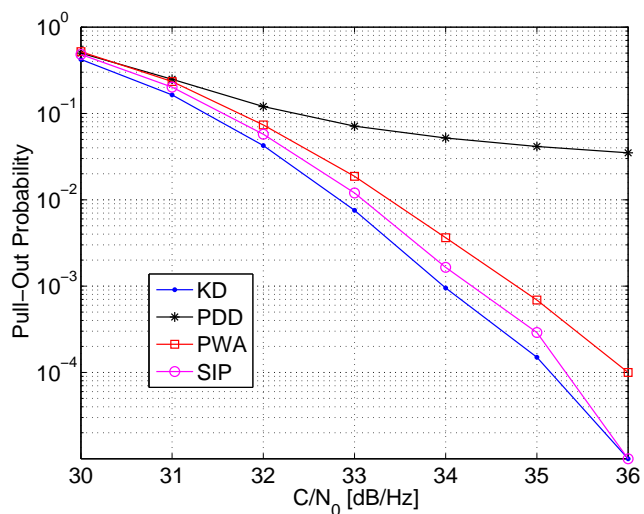


Fig. 14. POP of different schemes at 20g of acceleration.

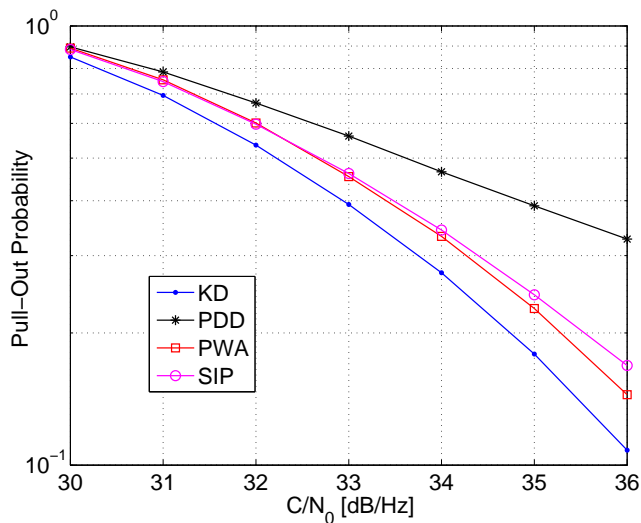


Fig. 16. POP loop of different schemes at 60g of acceleration.

noise ratio conditions. Their non-linear performance, in low signal-to-noise ratio conditions, was quantified through pull-out probabilities estimation based on extensive Monte Carlo simulations. It was found that each of the proposed schemes is more appropriate for different dynamic levels. The scheme based on partial-bit decision works better in low dynamic conditions, the squared-input one is preferable for moderate dynamics, while the partial-phase weighted average is better for very high dynamic situations. The extension of these schemes for code delay error estimation was briefly discussed.

In terms of computational cost, there is some increase due to the calculation of the partial correlations and ensuing error discrimination. However, the operation of the different satellite tracking loops with the same timing can reduce the processor load depending on the adopted hardware/software architecture. Nevertheless, this new GNSS receiver architecture main potential is for the implementation of vector tracking loops in

real time, since it will allow operating with a simultaneous vector of measurements from the received satellite signals obtained from correlations computed at a common time. In this case, a correlation stage capable of computing the two partial results for the same receiver estimates when the possible transition location is fed as an extra parameter could be very beneficial for a real-time implementation. An implementation of such a correlator architecture in an FPGA has already been implemented and reported in [16]. The authors are now working on the vector tracking loop formulation in real-time with this philosophy.

VI. ACKNOWLEDGMENT

This work was funded by ANPCyT PICT 00535 and UNLP 11-I-127 and CIC-PBA.

REFERENCES

- [1] P. A. Roncagliolo, J. García, and C. H. Muravchik, "Data-Bits Asynchronous Tracking Loop Scheme for High Performance Real-Time GNSS Receivers," in *Proceedings of The Fourth International Conference on Advances in Satellite and Space Communications, SPACOMM 2012*, Chamonix, Mont Blanc, France, April 2012, pp. 108 – 113.
- [2] B. W. Parkinson and J. J. Spilker (eds.), *Global Positioning System: Theory and Applications*. Washington: American Institute of Aeronautics and Astronautics (AIAA), 1996.
- [3] E. D. Kaplan, *Understanding GPS: Principles and Applications*. Boston: Artech House, 1996.
- [4] van Diggelen, F., "Indoor GPS theory & implementation," in *Proceedings of The Position Location and Navigation Symposium (PLANS), 2002 IEEE/ION*, Palm Springs, CA, USA, August 2002, pp. 240 – 247.
- [5] M. Lashley, D. M. Bevly, and J. Y. Hung, "A valid comparison of vector and scalar tracking loops," in *Proceedings of The Position Location and Navigation Symposium (PLANS), 2010 IEEE/ION*, Indian Wells, CA, USA, May 2010, pp. 464 – 474.
- [6] M. Lashley, D. M. Bevly, and J. Y. Hung, "Performance analysis of vector tracking algorithms for weak gps signals in high dynamics," *IEEE Journal of Selected Topics in Signal Processing*, vol. 3, no. 4, pp. 661 – 673, August 2009.
- [7] S. Zhao and D. Akos, "An Open Source GPS/GNSS Vector Tracking Loop - Implementation, Filter Tuning, and Results," in *Proceedings of the 2011 International Technical Meeting of The Institute of Navigation, ION ITM 2011*, San Diego, CA, USA, January 2011, pp. 1293 – 1305.
- [8] W. L. Edwards, M. Lashley, and D. M. Bevly, "FPGA Implementation of a Vector Tracking GPS Receiver using Model-Based Tools," in *Proceedings of the 22nd International Technical Meeting of The Satellite Division of the Institute of Navigation, ION GNSS 2009*, Savannah, GA, USA, September 2009, pp. 273 – 280.
- [9] T. Lin, J. T. Curran, C. O'Driscoll, and G. Lachapelle, "Implementation of a Navigation Domain GNSS Signal Tracking Loop," in *Proceedings of the 24th International Technical Meeting of The Satellite Division of the Institute of Navigation, ION GNSS 2011*, Portland, Oregon, USA, September 2011, pp. 3644 – 3652.
- [10] P. A. Roncagliolo, J. G. García, and C. H. Muravchik, "Optimized Carrier Tracking Loop Design for Real-Time High-Dynamics GNSS Receivers," *International Journal of Navigation and Observation*, vol. 2012, p. 18.
- [11] P. A. Roncagliolo and J. G. García, "High Dynamics and False Lock Resistant GNSS Carrier Tracking Loops," in *Proc. of The 20th Int. Technical Meeting of The Satellite Division of The Institute of Navigation, ION GNSS 2007*, Fort Worth, Texas, September 2007, pp. 2364 – 2375.
- [12] P. A. Roncagliolo, J. G. García, and C. H. Muravchik, "Pull-out Probability and Tracking Threshold Analysis for High Dynamics GNSS Carrier Loops," in *Proceedings of The 21st International Technical Meeting of The Satellite Division of The Institute of Navigation, ION GNSS 2008*, Fort Worth, Texas, USA, September 2008, pp. 221 – 228.
- [13] P. A. Roncagliolo, J. G. García, and C.H. Muravchik, "Pull-out Probability Considerations in High Dynamics GNSS Tracking Loops Design," in *Proceedings of The 10th International Symposium on Spread Spectrum Techniques and Applications, ISSSTA 2008*, Bologna, Italy, August 2008, pp. 53 – 57.
- [14] J. G. Proakis, *Digital Communications, 3rd Edition*. New Jersey: McGraw Hill, 1995.
- [15] D. Borio and G. Lachapelle, "A non-coherent architecture for GNSS digital tracking loops," *Annals of Telecommunications*, vol. 64, no. 9, 2009.
- [16] J. G. Diaz, J. G. García, and P. A. Roncagliolo, "An FPGA implementation of a data-bit asynchronous GPS/GLONASS correlator," in *Micro-Nanoelectronics, Technology and Applications (EAMTA), 2012 Argentine School of*, aug. 2012, pp. 27 –33.

Maximal Rate of Mobile Wireless Optical Link in Indoor Environment

Nicolas Barbot, Seyed Sina Torkestani, Stephanie Sahuguede, Anne Julien-Vergonjanne, and Jean-Pierre Cancès
 XLIM DPT-C2S2 UMR CNRS 7252/ ENSIL, 16 rue d'Atlantis, 87068 LIMOGES, FRANCE
 {nicolas.barbot, seyed.torkestani, s_sahuguede, anne, cancès}@ensil.unilim.fr

Abstract—In this paper, we investigate the performance of an indoor wireless optical communication system by taking into account emitter mobility. We consider the two typical optical link configurations, which are Line of Sight (LOS) and diffuse ones. Mobility is described by using Gaussian statistical model of the emitter location. In order to determine the maximal rate, which can be obtained for each configuration, we first determine the outage probability of the link because of emitter mobility. From this, we also estimate the outage capacity, which corresponds to the maximal information rate for a given outage probability value. We analyze the different configuration performance and we point out the trade-off between emitted power and LOS and diffuse schemes constraints (tracking and blocking effect). We finally present the performance of two error control mechanisms, which are Automatic Repeat reQuest (ARQ) and Luby Transform (LT) codes and we compare the obtained rates to the outage capacity. We show that LT codes outperform ARQ mechanism for high outage probability values and provide a robust solution for indoor optical channel when mobility is considered.

Keywords—Indoor Wireless Optical Communications; Line of Sight Links; Diffuse Links; Outage probability; Outage Capacity; Fountain Codes

I. INTRODUCTION

This article constitutes an extended version of [1] and enhances the results about outage capacity of optical links by presenting the performance of Luby Transform (LT) codes and Automatic Repeat reQuest (ARQ). The results permit evaluating the gap between practical error control mechanisms and the bound.

Nowadays, Wireless Optical Communications (WOC) based on Infrared (IR) transmissions are popular indoor technologies, which offer many advantages such as low complexity implementation and high secured transmissions [2]. Besides, WOC are considered as powerful alternative or complementary solutions to radio frequency ones for many indoor and home applications [3], [4]. Actually, IR systems intrinsically offer several benefits over radio frequency systems due to unregulated and quasi-unlimited bandwidth, the absence of multipath fading and the robustness to electromagnetic interferences, which is important in health concerned environments such as hospitals for example [5], [6].

To establish a WOC link, two main transmission configurations are commonly used: Line of Sight (LOS) scheme and diffuse one. Many works have already been published on the LOS and diffuse WOC system design especially considering the wireless optical channel as a stationary one [7]–[12]. The

LOS propagation system has been studied for point-to-point communications. Based on a direct propagation, this is the most basic technology and the most commonly investigated one for IR short-range transmissions [7] because guaranteeing high Signal to Noise Ratio (*SNR*). However, misalignments between emitter and receiver have a strong impact on the path loss and can severely degrade LOS performance. On the contrary, for diffuse configuration, the optical emitter projects wide-beams on reflecting surfaces of the indoor environment and the diffuse reflections are used to establish the link with the receiver. In such a scheme, it is not necessary to ensure a perfect aligned path. This permits obtaining higher coverage area but at the cost of a reduction of the optical received power (lower *SNR*) [8], [9].

By considering emitter mobility in the indoor environment, the received power for both LOS and diffuse schemes can significantly decrease because of random distance variations between emitter and receiver. In this case, the mobile WOC channel is non-stationary and performance is based on link outage analysis. To guarantee a high Quality of Service (QoS) and an efficient link, it is thus important to assess the impact of mobility in the design of the communicating system. For this purpose, from the outage probability evaluation, we determine the outage capacity of the wireless optical link in the two configurations and we establish the maximal rate that can be achieved by ARQ and LT codes.

In this paper, our first contribution is the determination of the WOC performance for a mobile emitter in a rectangular shaped room where the receiver is fixed and located in the middle of the ceiling. We introduce a statistical model of the non stationary optical channel to evaluate the performance in terms of outage probability for the two configurations LOS and diffuse. Moreover, to establish the maximal data rate that can be achieved we then estimate the channel capacity considering outage events in the case of indoor LOS and diffuse transmissions because of emitter mobility.

In addition, over such non-stationary channel, reliable transmissions cannot be achieved by using a fixed rate code and is classically obtained using Hybrid Automatic Repeat-reQuest (H-ARQ) [13] combining error correcting code and error control mechanism. Another interesting and original method introduced by Luby consists in using fountain codes or LT codes [14], [15] instead of ARQ. A second contribution of the study is to provide the performance of two error control mechanisms, which are ARQ and LT codes for the investigated

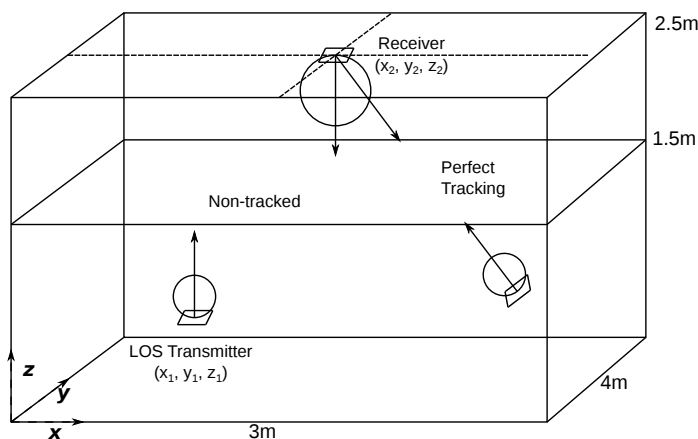


Fig. 1. Room Configuration in LOS case

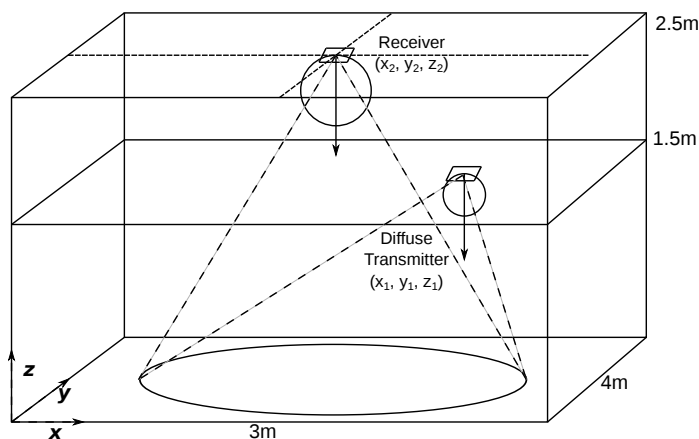


Fig. 2. Room Configuration in diffuse case

mobile WOC. We finally compare the results to the maximal theoretical rate corresponding to outage capacity.

The paper is organized as follows: after presenting related works in Section II, the optical transmission system is described in Section III. We then evaluate the outage probability in Section IV in LOS and diffuse configurations using a statistical approach. In Section V, we determine the outage capacity for both configurations considering the non-stationary channel. We finally present ARQ and LT mechanisms in part VI and analyze the attainable rates before concluding.

II. RELATED WORK

Optical channel capacity has already been studied in the case of Free Space Optical (FSO) transmissions over atmospheric channel subject to scintillation effect [16], [17], respectively with and without Channel Side Information (CSI). Capacities of outdoor optical channel have also been explored in [18] where the authors analyze the effect of pointing errors between emitter and receiver. Besides, in [19] and [20], the capacity considering multiple receivers is established. However, to the best of our knowledge, capacity of indoor mobile optical channel has not been yet investigated. Considering a statistical model of the mobile indoor optical channel, our work can be used to determine outage probability and outage capacity for LOS and diffuse transmissions. Since performance of LOS transmission greatly depends on the alignment between the emitter and the receiver, we provide results for a full-tracked and a non-tracked LOS systems.

To estimate system reliability, we also investigate the use of error control mechanism above the physical layer. Recently, it has been shown that LT codes have many advantages over a large range of applications [21]. LT codes use an encoder to produce an infinite packet stream from a finite length message. The LT decoder simply collects the received packets and can decode the message once enough packets have been received. LT codes provide an efficient way to achieve reliable communication for very difficult channels conditions since they do not require feedback channel. Few researchers have applied fountain codes over wireless optical channel [22]–[24]. In [22],

authors investigate raptor codes obtained by concatenation of an LT code with an high rate error correcting code such as a Low-Density Parity-Check code (LDPC), in order to improve performance on FSO links affected by scintillation effect and tracking errors. The authors in [23] study the performance of fountain codes to maximize data rate on hybrid RF/FSO links. In [24] we have investigated LT codes performance over indoor mobile wireless optical channel for a fixed data rate.

In this paper, we investigate the maximal data rate that can be achieved by using LT codes and we compare the results to ARQ ones and to outage capacity.

III. SYSTEM DESCRIPTION

We consider an indoor environment and a communication link between a mobile emitter in the environment and a base station placed on the ceiling.

A. Studied Scenarios Description

The emitter is at (x_1, y_1, z_1) in a room supposed to be free of any obstacles and represented by a box of dimensions (3m, 4m, 2.5m). The receiver is supposed to be placed in the middle of the ceiling at $(x_2 = 1.5m, y_2 = 2m, z_2 = 2.5m)$ and is pointed toward the floor. We consider here an empty room to provide general results and for simplicity.

We define two scenarios in order to investigate the emitter mobility impact on the performance. The first one considers that the emitter is oriented toward the ceiling such as a direct path can be established with the receiver. This corresponds to LOS transmission. Since LOS performance greatly depends on the alignment of both emitter and receiver, we consider two cases. In full-tracked case, both emitter and receiver are perfectly aligned and in non-tracked case the emitter maintains a fixed vertical orientation (see Figure 1).

In the second scenario, the emitter is pointed toward the floor and the transmission is based on reflected paths. This corresponds to diffuse transmission configuration (see Figure 2).

B. Optical Transmission Model

Data are sent by using an IR communication system based on Intensity Modulation and Direct Detection (IM/DD). The transmitted signal is thus an optical power and at the reception, the photodetector current is proportional to the received optical signal intensity. Consequently, the WOC link can be modeled by a linear system and the photocurrent $Y(t)$ at the receiver can be written as [7]:

$$Y(t) = RX(t) \otimes h(t) + N(t) \tag{1}$$

where $X(t)$ is the instantaneous optical power, R is the photodiode responsivity, and $h(t)$ represents the impulse response of the optical channel. $N(t)$ represents the additive noise present over the wireless link.

In addition, for LOS case, we consider that the directivity of both optical emitter and receiver does not allow multipath propagation. For diffuse case, delay spread D is typically equal to 10 ns [7] and is supposed to be negligible compared to low rate transmission ($D \ll 1/R_b$). For higher rates, intersymbol interference can be compensated by an equalization module. Thus the impulse response is only characterized by its static gain H such as:

$$h(t) = H\delta(t). \tag{2}$$

On Off Keying (OOK) modulation is used to transmit symbols over the optical channel [25]. At the reception, the electrical SNR is proportional to the received optical power squared due to photo-diode detection [7]:

$$SNR = \frac{2R^2 P_t^2 H^2}{N_0 R_b} \tag{3}$$

where P_t is the average transmitted power, N_0 , the noise power-spectral density and R_b the transmission data rate.

In this study, we have chosen $R = 0.55$ A/W. N_0 is determined considering that shot noise is the dominant noise source, which can be considered as Gaussian noise [8]: $N_0 = 2I_b q$ with mean current $I_b = 200 \mu\text{A}$ and $q = 1.6 \times 10^{-19}$ C thus $N_0 = 6.4 \times 10^{-23}$ W/Hz.

For LOS transmission, the path loss H can be expressed as a function of the distance and the orientation of the emitter and receiver (see Figure 3) [7]:

$$H = \begin{cases} \frac{A}{\pi d^2} \cos \phi \cos \theta & 0 \leq \theta \leq \theta_c \\ 0 & \theta > \theta_c \end{cases} \tag{4}$$

where A is the photo-detector physical surface, d is the distance between emitter and receiver, and ϕ and θ are the angles of incidence with respect to the emitter and receiver axis respectively. The angle θ_c is the Field Of View (FOV) of the receiver.

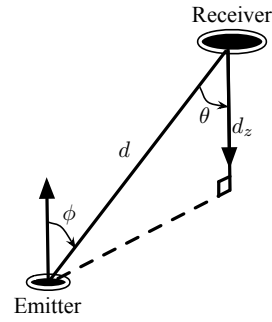


Fig. 3. LOS transmission description

Considering the first LOS scenario, we can thus write the path loss expression corresponding to each case as:

$$H_{ft} = \frac{A}{\pi d^2} \cos \phi \cos \theta = \frac{A}{\pi d^2} \tag{5}$$

$$H_{nt} = \frac{A}{\pi d^2} \cos \phi \cos \theta = \frac{A d_z^2}{\pi d^4} \tag{6}$$

where H_{ft} and H_{nt} correspond to the static gains of respectively full-tracked and non-tracked cases. and d_z is the vertical distance between emitter and receiver (see Figure 3).

In the second scenario, for the diffuse configuration the channel gain expression is obtained using ceiling bounce model [26]. The received power is computed by summing all the contributions of tiny elements of the reflective surface (the floor). The static gain can be thus expressed by:

$$H = \frac{\rho A z_1^2 z_2^2}{\pi^2} \times \iint_{\substack{\text{reflective} \\ \text{plan included} \\ \text{in FOV}}} \frac{dxdy}{(z_1^2 + (x-x_1)^2 + (y-y_1)^2)^2 (z_2^2 + (x-x_2)^2 + (y-y_2)^2)^2} \tag{7}$$

where ρ is the floor reflectivity and is set to 0.8 in this study.

For both LOS and diffuse configurations, we consider in the following that the photodetector has a physical surface $A = 1$ cm² and FOV set to 70°. Considering that the optical sources have Lambertian patterns, the optical emitted power P_t is limited to 300 mW in order to respect eye safety regulations [7]. In this study, for LOS cases, we consider two different P_t values 300 mW and 20 mW. The latter corresponds to the typical indoor transmitted power value [27]. For diffuse case, we have set the optical power to 300 mW [27].

In order to represent the emitter mobility, we model its location within the room by Gaussian distributions for simplicity, in x axis from 0 to 3m, in y axis from 0 to 4m and in z axis from 0 to 1.5m. The mobility volume dimensions are represented in Figure 1 and Figure 2. We suppose that

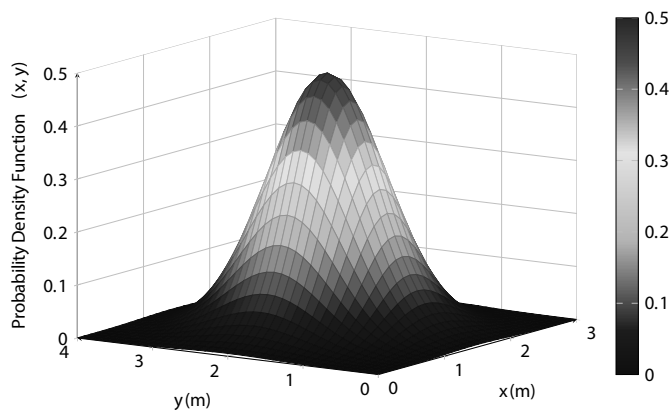


Fig. 4. Probability density function of the emitter location

the emitter presence is more probable in the middle of the room. Thus, the means of the position distributions along x and y axis are chosen equal to respectively 1.5 m and 2 m. In addition, the mean of the distribution along z axis is chosen equal to 1.2 m. This corresponds for example to an emitter placed at the belt level of a person. The variances of the x , y , z distributions are defined so that to include 98% of distribution data inside the room. Consequently, the emitter mobility is described along x y z axis by respectively $\mathcal{N}(1.5, 0.25)$ and $\mathcal{N}(2, 0.36)$ and $\mathcal{N}(1.2, 0.09)$ distributions. In addition, the tails of the distributions have been removed to respect the defined dimensions. Figure 4 shows the probability density function (pdf) of the emitter location in two dimensions.

By considering mobility, H varies due to the distance variations between the emitter and the receiver. Note that, taking into account obstacles or another mobility scenario would modify the emitter position pdf, but the analysis presented in the following remains the same.

IV. OUTAGE PROBABILITY

In the studied context, H variations are slow compared to bit duration even for the lowest considered data rate. Optical channel can be thus considered as a slow fading channel [7]. Consequently, average Bit Error Rate (BER) does not represent a good metric to describe transmission performance since each transmission experiments a different path loss. Instead, the outage probability is used to estimate the performance. The outage probability is defined as the probability that the capacity C of the channel does not support the rate R_0 of the transmission [28]. Since the capacity is a monotonic function of SNR , the outage probability can be expressed as a function of a SNR threshold (SNR_0) and corresponds to the probability that the SNR value at a given time drops below SNR_0 :

$$P_{out} = \Pr[C(SNR) < R_0] = \Pr[SNR < SNR_0] \quad (8)$$

Assuming the mobility scenario we have defined, it is possible to determine the value of the outage probability for a

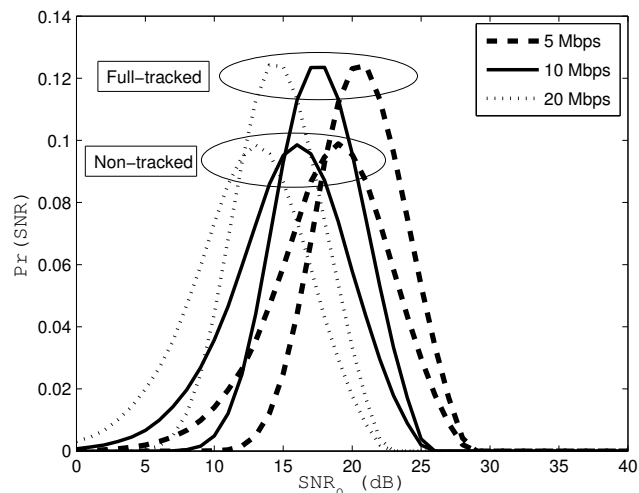


Fig. 5. Distribution of SNR in LOS case for $P_t = 20$ mW

given SNR_0 using Monte Carlo (MC) method. This method is proceeded according to the emitter position Gaussian distribution. For each point, the SNR is computed from (3) and from H expressions (5), (6) or (7) depending on the configuration (LOS or diffuse).

SNR distributions for LOS configuration are presented in Figure 5 for full-tracked and non-tracked cases and for different data rates of 5, 10 and 20 Mbps.

We can note that the SNR distribution in LOS configuration admits a minimum value corresponding to a case where the emitter is placed on the floor, in a corner ($d = d_{max}$). Maximum SNR value is obtained when the emitter is placed beneath the receiver at a maximum height of 1.5m (because of mobility scenario). For example, for full-tracked system and a data rate of 10 Mbps, we can see in Figure 5 that the minimum and maximum SNR values correspond respectively to 5.8 dB and 25.82 dB.

Moreover, if we compare the SNR distributions in full-tracked and non-tracked cases, we observe as expected that, for the same data rates the SNR distributions of non-tracked systems admit lower average values and greater spreading.

Figure 6 presents the SNR distributions for diffuse configuration, with $P_t = 300$ mW and for different data rates.

First, we can see that the SNR distributions of diffuse configuration for the same data rates than previously, admit a greater spreading than in the LOS cases. Moreover, we remark for example that for $R_b = 10$ Mbps, the average SNR value ($\overline{SNR} = 17.4$ dB) is lower than in the full-tracked LOS case ($\overline{SNR} = 19.1$ dB) and is slightly lower than in the non-tracked LOS case ($\overline{SNR} = 17.6$ dB). This shows that diffuse channel is more penalizing than LOS cases in our defined mobility scenario. This is due to the greater distance between emitter and receiver in diffuse configuration than in LOS cases.

These SNR distributions represent the non-stationnarity due to the mobility scenario we study for the indoor optical

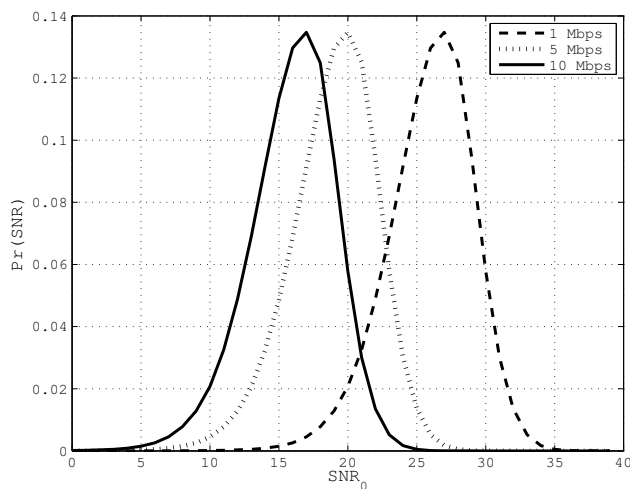


Fig. 6. Distribution of SNR in diffuse case for $P_t = 300$ mW

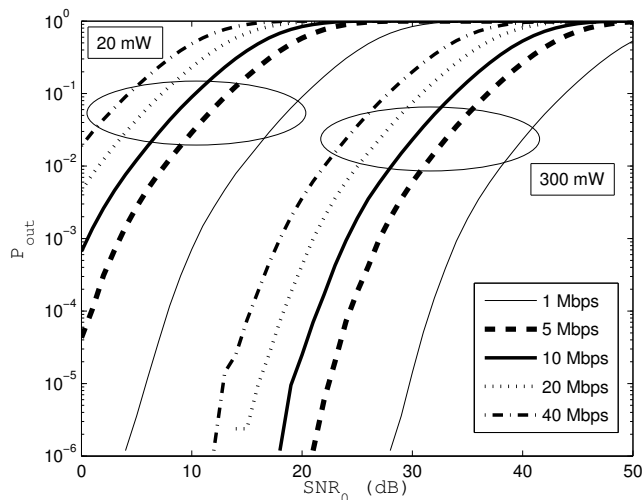


Fig. 8. Outage Probability versus SNR_0 in LOS configuration for non-tracked case

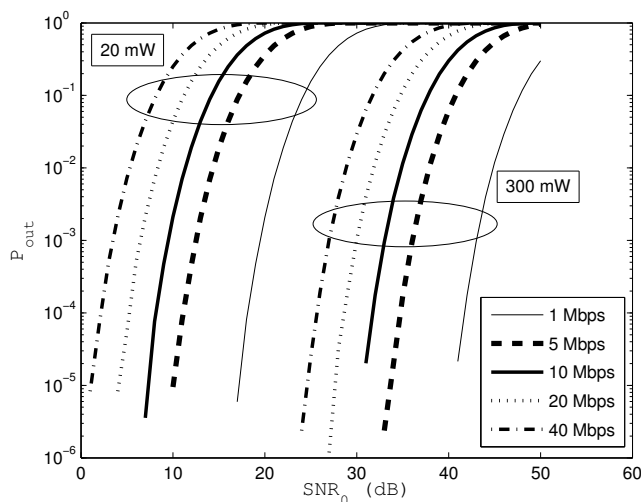


Fig. 7. Outage Probability versus SNR_0 in LOS configuration for full-tracked case

wireless channel in both LOS and diffuse configurations.

From these distributions, we can now estimate the outage probability, which is equal to the fraction of points whose SNR is below the threshold SNR_0 .

Figures 7 and 8 present outage probability P_{out} versus SNR_0 , estimated with MC method for LOS scenario with full-tracked and non-tracked systems and for two different P_t values of 300 mW and 20 mW. The results have been plotted for different data rates R_b .

As expected, we can see that, for both LOS cases, outage probability increases when the SNR_0 threshold value increases. Moreover, for a given Quality of Service (QoS) *i.e.*, for a given SNR_0 , this performance degradation also depends on the data rate of the transmission and becomes

more significant when R_b increases. In addition, we can see that for the same SNR_0 , the outage probability can be reduced at the cost of an increase of the optical transmitted power. For example if a non-tracked system experiments an outage probability of 10^{-3} at 5 Mbps with $P_t = 20$ mW, the results reported in Figure 8 show that the outage probability can drop below 10^{-6} if the optical power is increased up to 300mW.

Also, if a system with $P_t = 20$ mW requires a SNR_0 of 13.6dB (to ensure a BER below 10^{-6} when the system is not in outage), and if the targeted outage probability is 10^{-3} , the results reported in Figures 7 and 8 show that the data rate has to be chosen below 5 Mbps for full-tracked system and below 1 Mbps for non-tracked system.

As expected, the maximal data rate for a given QoS, is obtained for full-tracked LOS system. However it can be noted that maintaining perfect tracking is a hard task. We now investigate diffuse transmission performance, which does not need tracking system and is intrinsically robust to blocking effect. Figure 9 presents the outage probability as a function of the SNR_0 in diffuse configuration.

As a first remark, we can see that the outage probability variations exhibit the same behavior as in LOS cases. Moreover for a given QoS, the rate that can be achieved by diffuse systems is lower than LOS cases. For example if we consider the same outage probability of 10^{-3} and the same SNR_0 of 13.6 dB as previously, we observe in Figure 9 that the rate of diffuse link has to be lower than 600 Kbps whereas it was of 5 Mbps (respectively 1 Mbps) for full-tracked LOS case (respectively non-tracked LOS). However, diffuse system is more robust than non-tracked LOS case against blocking effect. Besides diffuse systems do not require any tracking device as for full-tracked LOS case, and thus simplify the implementation. Thus there is a trade-off between performance and complexity.

In order to estimate the maximum theoretical rate that can

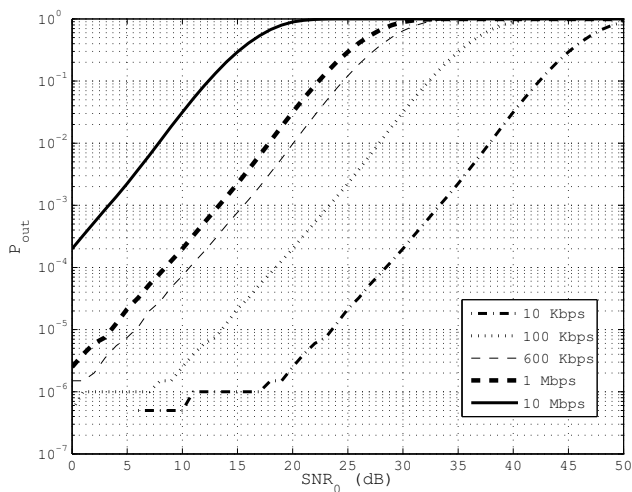


Fig. 9. Outage Probability versus SNR_0 in diffuse configuration

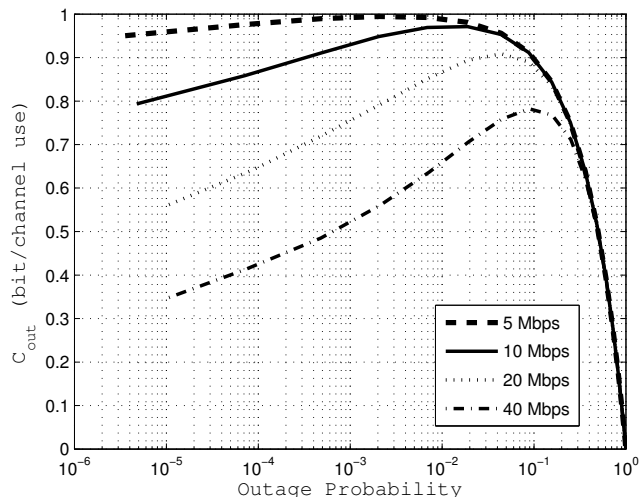


Fig. 10. Capacity of LOS wireless indoor channel for full-tracked system

be achieved in LOS and diffuse configurations when mobility is considered, we now introduce the outage capacity, which provides the maximal information rate for a given outage probability.

V. OUTAGE CAPACITY

We consider a binary input (due to the OOK modulation) and continuous output Additive White Gaussian Noise (AWGN) channel due to the noise present over the optical channel.

For stationary channel, the capacity of binary input continuous output AWGN channel does not admit a close form. Thus, this capacity has to be evaluated by using [29]:

$$C(SNR) = \sup_{p(x)} \int_{-\infty}^{\infty} \sum_{i=0}^1 p(y|x_i)p(x_i) \log \left(\frac{p(y|x_i)}{\sum_{k=0}^1 p(y|x_k)p(x_k)} \right) dy \tag{9}$$

where $p(y|x)$ are the conditional probabilities of the received signal and follow Gaussian distributions $\mathcal{N}(RHX, R_bN_0)$. $p(x)$ corresponds to the probability of the binary symbol x . Since the channel is symmetric, equation (9) is maximized when $p(x=0)$ and $p(x=1)$ are equal to 0.5. Moreover, the capacity is bounded between 0 and 1 due to the binary input.

For non-stationary (flat fading) channel, the capacity depends on the information available at the receiver [28]. In this paper, we assume that the receiver has full and perfect knowledge of the Channel State Information (CSI). This can be obtained by inserting pilot symbols during the transmission. At the receiver, these pilot symbols are used to evaluate instantaneous SNR (or equivalently, instantaneous H).

The outage capacity, which well describes the performance of quasi-static channel, is defined as the average information rate that can be received with a given outage probability. The emitter fixes a rate *a priori* and sends data over the

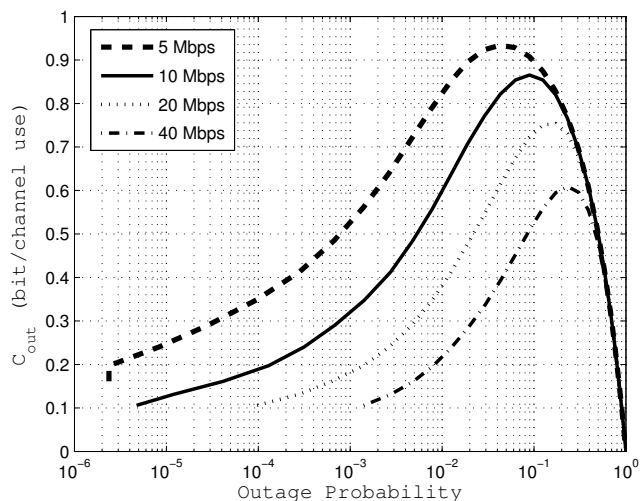


Fig. 11. Capacity of LOS wireless indoor channel for non-tracked system

channel of capacity $C(SNR)$ (see eq. (9)). With a given outage probability, the average information rate correctly received is [28]:

$$C_{out} = (1 - P_{out}(SNR_0)) C(SNR_0) \tag{10}$$

Note that C_{out} is proportional to $(1 - P_{out})$, which corresponds to the absence of transmitted information (*i.e.*, a null capacity) during outage events.

Figures 10 and 11 present outage capacity versus outage probability for LOS system in full-tracked and non-tracked configurations for a typical emitted power value of 20 mW and different data rate R_b . In both cases, outage capacity is computed with (9) and (10). The outage probability has been estimated using previously described MC method.

We can see that when the outage probability decreases, the

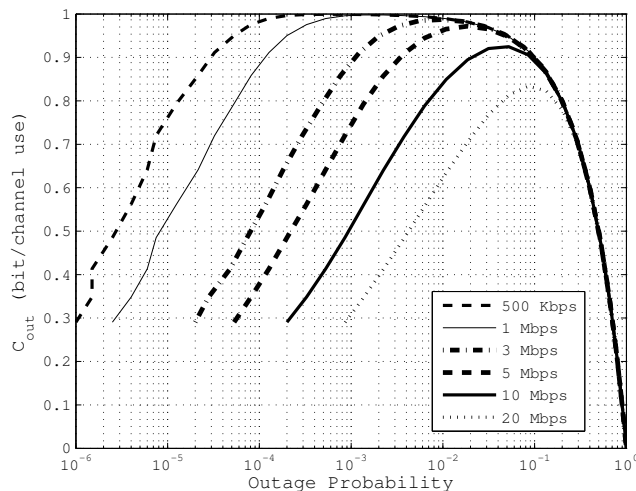


Fig. 12. Capacity of diffuse wireless indoor channel

outage capacity increases and then slowly decreases for very low outage probabilities. Outage capacity below 1 means that, by using Forward Error Correction (FEC) at the physical layer and error control mechanism at the application one, reliable transmission over the channel can be achieved. Capacity equal to 1 means that there is no need to use FEC to achieve the maximal information rate.

When P_{out} tends to 1, the receiver is always in outage and the maximum information rate that can be transmitted between emitter and receiver tends to 0 ($C_{out} = 0$). On the other side, when P_{out} tends to zero, C_{out} attempts a minimal value equal to $C(SNR_{min})$ where SNR_{min} is the lower SNR that can be received in the room.

Between these two values of P_{out} , we can see that there is a given value of the outage probability maximizing the channel capacity. This value depends on the data rate, and increases when data rate decreases. This permits designing an efficient link with maximal achievable rate.

From results reported in Figure 10 and 11 we can see that for LOS configurations, the maximal capacity is obtained for P_{out} belonging in $[5 \times 10^{-2}, 10^{-1}]$ for data rates R_b between 5 and 40 Mbps for both full-tracked and non-tracked cases. Moreover in full-tracked case (respectively in non-tracked case), we can note that the maximal capacity varies from 1 to 0.8 bit/channel use (respectively 0.95 to 0.6 bit/channel use) for data rates between 5Mbps and 40Mbps. Thus, this shows that information rate in full-tracked LOS case is higher than in non-tracked case but at the cost of a complex implementation because of tracking devices.

Figure 12 presents outage capacity versus outage probability for diffuse configuration and with an optical power of $P_t = 300$ mW. The results have been plotted for different data rate values between 500 kbps and 20 Mbps. The outage probability has been estimated using previously described MC method.

In diffuse configuration same remarks than in LOS cases

can be done. The outage probability, which maximizes the capacity is obtained in the interval $[10^{-3}, 10^{-1}]$ for data rates between 500 kbps and 20 Mbps. The corresponding outage capacity is included in the interval $[1, 0.85]$.

To compare the different configurations, we consider a data rate of 20 Mbps. The maximal capacity values and corresponding outage probability ones in full-tracked, non-tracked and diffuse cases are reported in Table I.

As expected we can see that the full-tracked LOS performance outperforms the other ones but at the cost of a more complex implementation. Moreover we can note that non-tracked LOS and diffuse cases permit obtaining quite same information rate even though the optical emitted power in non-tracked case (20 mW) is lower than in the diffuse case (300 mW). This illustrates the trade-off between optical emitted power and robustness to blocking effects that is the main advantage of diffuse systems.

Outage capacity provides the maximal theoretical information rate that we can obtain over the optical channel considering mobility. Unfortunately, real systems operate at a lower rate, which depends among other on the error control mechanism. In the following, we illustrate the performance that can be achieved at the application layer.

VI. PERFORMANCE OF LT CODES

We consider two error control mechanisms: stop-and-wait ARQ [13], which is the simplest technique for short range application, and LT codes [14].

ARQ mechanism uses feedback channel in order to acknowledge each received packet and is penalized by timeouts when packets are lost. Assuming a perfect feedback channel (no loss of acknowledgement), the average information rate that can be achieved by stop-and-wait ARQ can be expressed as a function of the outage probability and the outage capacity:

$$R_{ARQ} = \frac{(1 - P_{out})C(SNR_0)}{(1 - P_{out}) + aP_{out}} \quad (11)$$

where a , the ratio between the ARQ timeout and the transmission time has been set to $a = 5$.

For LT codes, performance is characterized by the code overhead ϵ , which corresponds to the additional information required to decode the received packets. In order to satisfy memory requirements of both emitter and receiver we consider very short length LT codes with $K = 100$. This means that the original message has been divided into $K = 100$ packets.

TABLE I
PERFORMANCE COMPARISON FOR 20 MBPS

Configuration	Power (mW)	P_{out}	$C_{out, max}$
Full-tracked LOS	20	4×10^{-2}	0.9
Non-tracked LOS	20	2×10^{-1}	0.75
Diffuse	300	10^{-1}	0.81

The key parameter for LT codes is the degree distribution ρ , which is a probability distribution defining the number of blocks combined in a packet.

The code overhead value and the computational cost of the decoding process are linked to the degree distribution and it is important to optimize this value. In order to design an efficient degree distribution for short length LT codes, we define the cost function as the average overhead and we optimize the degree distribution ρ in order to minimize the overhead. Since the cost function is noisy (it can produce different results for the same parameters) and not differentiable, classical optimization methods cannot be applied. We have chosen Differential Evolution method [30], which is based on a genetic algorithm, in order to minimize the cost function. The resulting degree distribution we have obtained is presented in Table II. This corresponds to an average overhead $\epsilon = 23\%$.

Finally, the information rate that can be achieved by LT code depends on the overhead and is equal to:

$$R_{LT} = \frac{1}{1 + \epsilon}(1 - P_{out})C(SNR_0). \quad (12)$$

Figure 13 presents the information rate that can be achieved by using ARQ mechanism and LT codes as a function of the outage probability for LOS transmissions considering the different cases (full-tracked and non-tracked cases) and for a data rate R_b of 20 Mbps. Outage capacity we have previously obtained and corresponding to the maximal theoretical information rate is also plotted.

We can see that for low P_{out} values, ARQ mechanism is well suited in all cases. However, for high P_{out} values the information rate obtained with ARQ does not achieve the outage capacity since the transmission is stopped during timeouts. However, LT codes are not an efficient mechanism for low P_{out} values because of code overhead but permit providing an higher rate than ARQ for high P_{out} values. To illustrate the performance, we compare in Table III the information rates obtained by ARQ and LT codes for the optimal outage probability in the two LOS cases *i.e.*, 4×10^{-2} in the full-tracked case and 2×10^{-1} in the non-tracked case.

We can see that for full-tracked case, ARQ mechanism is the best solution since tracking system ensures high QoS. However, for the non-tracked case, it is worth using LT codes due to channel state degradations linked to misalignments.

In addition, from results in Figure 13, we can remark that a non-tracked system designed with LT codes can provide an

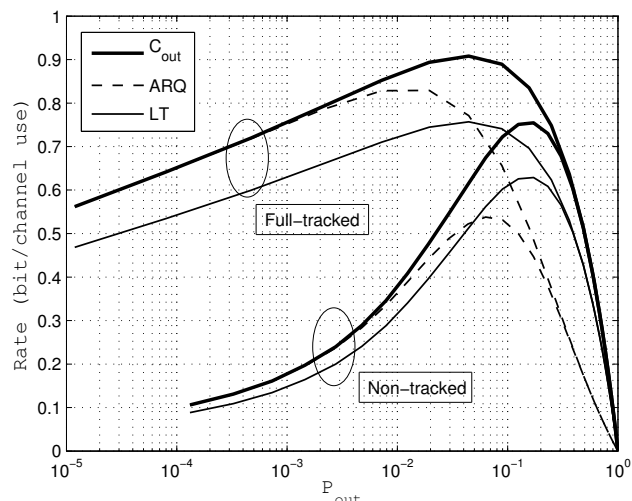


Fig. 13. Information rate of ARQ and LT codes in LOS cases for 20 Mbps

higher rate than full-tracked case. This means that mechanical complexity can be reduced while maintaining identical rate if LT codes are used instead of ARQ. For example, we consider a full-tracked system using ARQ with an outage probability of 0.1 (see Figure13). The effective data rate is equal to $R_{eff} = R \times R_b = 12.2$ Mbps where R is the information rate. This result is the same as for a non-tracked system with the same P_{out} but using LT codes. This means that LT codes can reduce the mechanical complexity of LOS system while maintaining the achievable rate.

Figure 14 presents the available rate that can be obtained with ARQ and LT codes for the diffuse configuration considering an average transmitted power of 300 mW and different data rates of 5 Mbps, 20 Mbps and 50 Mbps.

The curves present the same behavior as for the LOS configurations. ARQ mechanism constitutes an efficient solution for low P_{out} values but is penalized when the outage probability increases. However, LT codes are well suited for high P_{out} values. Moreover, for P_{out} corresponding to the maximal outage probability, we can see that, as the data rate increases, the performance of LT codes become higher than ARQ. For example, with $R_b = 5$ Mbps and for the optimal P_{out} value, ARQ outperforms LT codes with an information rate of 0.9 bit/channel use compared to 0.81 bit/channel use. On the contrary, for 50 Mbps, LT code performance (0.53 bit/channel) overcomes ARQ one (0.35 bit/channel use).

TABLE II
DEGREE DISTRIBUTION OF LT CODE FOR $K = 100$

$\rho_{[1:5]}$	0.0736	0.4340	0.1875	0.0721	0.0394
$\rho_{[6:10]}$	0.0259	0	0	0	0
$\rho_{[11:15]}$	0	0	0.0125	0.0177	0.0250
$\rho_{[16:20]}$	0.0397	0.0145	0.0148	0	0.0432

TABLE III
ARQ AND LT CODE PERFORMANCE COMPARISON FOR 20 MBPS

Configuration	P_{out}	$C_{out} max$	ARQ	LT Codes
Full-tracked LOS	4×10^{-2}	0.97	0.9	0.8
Non-tracked LOS	2×10^{-1}	0.86	0.63	0.71
Diffuse	10^{-1}	0.84	0.59	0.79

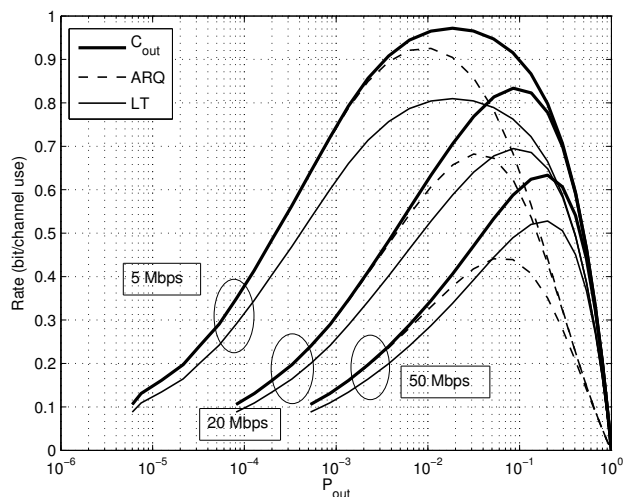


Fig. 14. Information rate of ARQ and LT codes in diffuse configuration for $R_b = 5, 20$ and 50 Mbps

Table III also compares the information rate for the optimal P_{out} of LOS and diffuse configurations for $R_b = 20$ Mbps. We can see that, as in the non-tracked LOS case, LT codes can provide higher rate than ARQ mechanism for diffuse case. Moreover, the gain provided by LT codes for diffuse case is more significant than for non-tracked LOS case. Thus, we have illustrated that LT codes can be a robust error control mechanism especially when channel conditions are degraded.

VII. CONCLUSION

In this paper, we have investigated the performance of indoor wireless optical channel. Our goal was to determine the maximal rate, which can be obtained by taking into account emitter mobility. For this purpose, we have first studied the outage probability considering two kinds of optical transmissions that is Line Of Sight configuration with full-tracked and non-tracked schemes and diffuse one, which is a more robust solution against blocking effect. From outage analysis, we have then estimated the maximal theoretical rate corresponding to the outage capacity. We have seen that outage capacity can be maximized for high outage probability values. As expected, the best performance has been obtained with full-tracked LOS cases. However this solution requires a complex implementation because of tracking devices. On the other side, we have noted that non-tracked schemes and diffuse one had quite the same performance even though the optical emitted power was different. This has shown the trade-off between emitted power, tracking complexity and robustness to blocking effect.

To complete the theoretical results, performance of ARQ and LT codes has also been investigated and compared to the outage capacity. For LOS and diffuse configurations and considering the optimal outage probability values, we have shown that the maximal rate using LT codes was higher than the rate using ARQ. Besides, we have illustrated that by using

LT codes instead of ARQ in LOS configuration, it was possible to achieve the same performance as in full-tracked LOS but without any tracking system. For diffuse configuration, we have shown that the use of LT codes was more efficient than ARQ when channel conditions are degraded because of data rate increase. Thus, LT codes can provide a more robust error control mechanism than ARQ for indoor wireless optical channel especially when mobility and misalignment have a significant impact. Numerous perspectives can be investigated to enhance this work, among which comparison with experimental results and cross-layer design to improve error control mechanism performance.

REFERENCES

- [1] N. Barbot, S. S. Torkestani, S. Sahuguede, A. Julien-Vergonjanne, and J. P. Cances, "Outage capacity of mobile wireless optical link in indoor environment," in *The Eighth Advanced International Conference on Telecommunications (AICT)*. IARIA, 2012, pp. 133–137.
- [2] D. Borah, A. Boucouvalas, C. Davis, S. Hranilovic, and K. Yiannopoulos, "A review of communication-oriented optical wireless systems," *EURASIP Journal on Wireless Communications and Networking*, vol. 2012, no. 1, p. 91, 2012.
- [3] H. Elgala, R. Mesleh, and H. Haas, "Indoor optical wireless communication: potential and state-of-the-art," *Communications Magazine, IEEE*, vol. 49, no. 9, pp. 56–62, 2011.
- [4] H. Le Minh, Z. Ghassemlooy, D. O'Brien, and G. Faulkner, "Indoor gigabit optical wireless communications: challenges and possibilities," in *Transparent Optical Networks (ICTON), 2010 12th International Conference on*. IEEE, 2010, pp. 1–6.
- [5] M. Wallin, T. Marve, and P. Hakansson, "Modern wireless telecommunication technologies and their electromagnetic compatibility with life-supporting equipment," *Anesthesia & Analgesia*, vol. 101, no. 5, pp. 1393–1400, 2005.
- [6] S. S. Torkestani, N. Barbot, S. Sahuguede, A. Julien-Vergonjanne, and J. P. Cances, "Performance and transmission power bound analysis for optical wireless based mobile healthcare applications," in *Personal Indoor and Mobile Radio Communications (PIMRC), 2011 IEEE 22nd International Symposium on*. IEEE, 2011, pp. 2198–2202.
- [7] J. Kahn and J. Barry, "Wireless infrared communications," *Proceedings of the IEEE*, vol. 85, no. 2, pp. 265–298, 1997.
- [8] F. Gfeller and U. Bapst, "Wireless in-house data communication via diffuse infrared radiation," *Proceedings of the IEEE*, vol. 67, no. 11, pp. 1474–1486, 1979.
- [9] F. Khozeimeh and S. Hranilovic, "A dynamic spot diffusing architecture for indoor wireless optical communications," in *Communications, 2006. ICC'06. IEEE International Conference on*, vol. 6. IEEE, 2006, pp. 2829–2834.
- [10] Z. Ghassemlooy and A. Hayes, "Indoor optical wireless communications systems—part i: Review," *School of Engineering, Northumbria University*, 2003.
- [11] O'Brien *et al.*, "Short range optical wireless communications," in *Wireless world research forum*, 2005, pp. 1–22.
- [12] J. Kahn, W. Krause, and J. Carruthers, "Experimental characterization of non-directed indoor infrared channels," *Communications, IEEE Transactions on*, vol. 43, no. 234, pp. 1613–1623, 1995.
- [13] S. Lin, D. Costello, and M. Miller, "Automatic-repeat-request error-control schemes," *Communications Magazine, IEEE*, vol. 22, no. 12, pp. 5–17, 1984.
- [14] M. Luby, "LT codes," in *Foundations of Computer Science, 2002. Proceedings. The 43rd Annual IEEE Symposium on*. IEEE, 2002, pp. 271–280.
- [15] A. Shokrollahi, "Raptor codes," *Information Theory, IEEE Transactions on*, vol. 52, no. 6, pp. 2551–2567, 2006.
- [16] J. Anguita, I. Djordjevic, M. Neifeld, and B. Vasic, "Shannon capacities and error-correction codes for optical atmospheric turbulent channels," *Journal of Optical Networking*, vol. 4, no. 9, pp. 586–601, 2005.
- [17] J. Li and M. Uysal, "Optical wireless communications: system model, capacity and coding," in *Vehicular Technology Conference, 2003. VTC 2003-Fall. 2003 IEEE 58th*, vol. 1. IEEE, 2003, pp. 168–172.

- [18] A. Farid and S. Hranilovic, "Outage capacity optimization for free-space optical links with pointing errors," *Journal of lightwave technology*, vol. 25, no. 7, pp. 1702–1710, 2007.
- [19] A. Belmonte and J. Kahn, "Capacity of coherent free-space optical links using diversity-combining techniques," *Opt. Express*, vol. 17, no. 15, pp. 12 601–12 611, 2009.
- [20] S. Hranilovic, "On the design of bandwidth efficient signalling for indoor wireless optical channels," *International Journal of Communication Systems*, vol. 18, no. 3, pp. 205–228, 2005.
- [21] P. Cataldi, M. Shatarski, M. Grangetto, and E. Magli, "Implementation and performance evaluation of LT and raptor codes for multimedia applications," in *Intelligent Information Hiding and Multimedia Signal Processing, 2006. IHH-MSP'06. International Conference on*. IEEE, 2006, pp. 263–266.
- [22] W. Zhang and S. Hranilovic, "Short-length raptor codes for mobile free-space optical channels," in *Communications, 2009. ICC'09. IEEE International Conference on*. IEEE, 2009, pp. 1–5.
- [23] W. Zhang, S. Hranilovic, and C. Shi, "Soft-switching hybrid fso/rf links using short-length raptor codes: Design and implementation," *Selected Areas in Communications, IEEE Journal on*, vol. 27, no. 9, pp. 1698–1708, 2009.
- [24] N. Barbot, S. S. Torkestani, S. Sahuguede, A. Julien-Vergonjanne, and J. P. Cances, "LT codes performance over indoor mobile wireless optical channel," in *8th IEEE, IET International Symposium on Communication Systems, Networks and Digital Signal Processing (CSNDSP 2012)*, Poznań, Poland, Jul. 2012.
- [25] H. Park and J. Barry, "Modulation analysis for wireless infrared communications," in *Communications, 1995. ICC'95 Seattle, Gateway to Globalization', 1995 IEEE International Conference on*, vol. 2. IEEE, 1995, pp. 1182–1186.
- [26] J. Carruthers and J. Kahn, "Modeling of nondirected wireless infrared channels," *Communications, IEEE Transactions on*, vol. 45, no. 10, pp. 1260–1268, 1997.
- [27] R. Ramirez-Iniguez and R. Green, "Indoor optical wireless communications," in *Optical Wireless Communications (Ref. No. 1999/128), IEE Colloquium on*. IET, 1999, pp. 14–1.
- [28] A. Goldsmith, *Wireless communications*. Cambridge Univ Pr, 2005.
- [29] J. Proakis, *Digital communications*. McGraw-hill, 1987, vol. 1221.
- [30] R. Storn and K. Price, "Differential evolution—a simple and efficient heuristic for global optimization over continuous spaces," *Journal of global optimization*, vol. 11, no. 4, pp. 341–359, 1997.

Reliable JPEG Image Transmission Using Unequal Error Protection with Modified Non-Binary Turbo Codes

Tulsi Pawan Fowdur

Dept of Electrical and Electronic Engineering
University of Mauritius
Reduit, Mauritius
e-mail: p.fowdur@uom.ac.mu

Yashvin Beni

Dept of Electrical and Electronic Engineering
University of Mauritius
Reduit, Mauritius
e-mail: yashvinbeni@gmail.com

Abstract— JPEG is a widely deployed image compression standard used in several applications. However, JPEG image transmission is challenging and sophisticated strategies are required for reliable transmission. This paper proposes a JPEG image transmission using non-binary Turbo codes with Unequal Error Protection (UEP), extrinsic information scaling and iterative detection. UEP is achieved by applying a lower code-rate to protect the DC-layer of the image more efficiently and a higher code-rate for protecting the AC-layer. Additionally, the non-binary Turbo code is modified by scaling its extrinsic information to improve performance and by using a stopping criterion to limit the number of iterations required for decoding. The proposed UEP scheme provides a gain of at least 10 dB in Peak Signal to Noise Ratio (PSNR) over an Equal Error Protection (EEP) scheme when duo-binary Turbo codes are used and a gain of at least 14 dB in PSNR when triple binary codes are used, over a range of E_b/N_0 values. Moreover, the use of triple binary turbo codes provides greater bandwidth efficiency.

Keywords- JPEG; UEP; Non-Binary Turbo Codes.

I. INTRODUCTION

This paper builds upon the scheme proposed in [1] to develop an enhanced JPEG image transmission scheme with non-binary Turbo codes. JPEG is a Discrete Cosine Transform (DCT) based image compression algorithm, which employs Huffman coding to generate a compressed bit-stream [2]. It is a widely adopted standard and forms an integral part of several applications such as web browsing and telemedicine [3]. However, the use of Huffman coding renders the JPEG coded bit-stream very sensitive to error propagation because a single bit in error can cause a complete loss of synchronisation. As such, sophisticated coding solutions are required to ensure reliable transmission. One solution is to use powerful error-correcting codes such as Turbo codes, which are well suited to protect image data as recently demonstrated in [4]. Error resilient and concealment techniques also provide a significant improvement in transmission fidelity [5], [6]. Moreover, a highly efficient strategy for achieving robust JPEG image transmission is UEP. UEP consists of exploiting the fact that the DCT operation in JPEG, segments the image into layers of unequal importance. Hence, by allocating different levels

of protection to these layers, a significant gain in the overall quality of the received image can be obtained.

Several efficient UEP schemes have been developed for JPEG image transmission using Turbo codes. For example, in [7], UEP and joint source channel decoding with a-priori statistics were combined and applied to JPEG image transmission. Both Turbo codes and Turbo and Turbo Trellis Coded Modulation were used and major gains in PSNR were obtained over conventional JPEG image transmission schemes. An error resilient wireless JPEG image transmission scheme, which employed product Turbo or Reed Solomon codes alongside an optimal UEP algorithm was proposed in [8]. In [9], an UEP scheme, which employs s-random odd-even interleaving with odd-even puncturing, as well as a new UEP scheme for the soft output Viterbi algorithm, were proposed. Improved BER and PSNR performances in JPEG image transmission were obtained with these UEP schemes [9]. In [10], a novel Turbo UEP coding scheme was proposed whereby two error protection levels of Turbo codes are achieved by a new rate-compatible puncturing mechanism. With the scheme of [10], the quality of the image transmission is improved without any additional bit rate or coding delay due to UEP. Moreover, in [11], the performance of an adaptive Wiener-Turbo system with JPEG and bit plane compressions was evaluated over Rician and Rayleigh fading channels. The scheme exploited the neighborhood relation of pixels for each color plane by employing a Turbo decoder, JPEG encoder/decoders, and adaptive Wiener filtering. It also adapted the compression ratios according to the importance of the image to be transferred and could recover high quality JPEG and bit plane compressed images [11]. Furthermore, in [12], a dichotomic technique for searching the optimal UEP strategy for the transmission of JPEG 2000 images and video over a wireless channel was proposed. A method of virtual interleaving was also adopted for the transmission of high bit rate streams over packet loss channels, guaranteeing a large PSNR advantage over a plain transmission scheme [12]. Finally, in [13], the performance of three UEP schemes for progressive JPEG image transmission using delay-constrained hybrid ARQ, with iterative bit and symbol combining was proposed. Gains of over 9 dB in PSNR were obtained with the UEP schemes as compared to their corresponding EEP schemes.

In contrast with previous works, which considered binary Turbo codes, this paper extends the work of [1] to investigate the performance an UEP scheme based on non-binary Turbo codes whereby both duo-binary and triple binary Turbo codes are used. These codes provide better convergence of iterative decoding, have reduced latency, lower sensitivity to puncturing, larger minimum distance and lower memory requirement [14]. The non-binary code is modified with a scale factor [15], [16] and stopping criterion [17] to further improve the performance of the UEP scheme. Also, triple binary Turbo codes have the advantage of providing greater bandwidth efficiency. The proposed UEP scheme allocates more protection to the DC layer, which contains the most significant part the image after the DCT operation, and less protection to the AC layer. This is achieved by using the puncturing matrices specified for the duo-binary Turbo code of the DVB-RCS standard [18] and also a puncturing pattern suitable for triple-binary Turbo codes. The UEP scheme with duo-binary Turbo codes outperforms the EEP scheme by at least 10 dB in PSNR and the one with triple binary Turbo codes outperforms its EEP counterpart by at least 15 dB in PSNR over a range of E_b/N_0 values. Moreover, the gain in PSNR increases as the couple or triple length of the non-binary code is increased.

The organization of this paper is as follows. Section II describes the complete system model. Section III presents the simulation results and analysis. Section IV concludes the paper.

II. SYSTEM MODEL

The complete encoding process is shown in Figure 1. The input image is fed to the JPEG encoder, which operates on blocks of 8x8 pixels and performs DCT, quantization and zig-zag ordering [2]. The AC and DC coefficients are then separated into the AC and DC layers. The DC layer regroups the first coefficient from all 8x8 blocks obtained after zig-zag ordering and the AC-layer is the concatenation of the 63 coefficients from all 8x8 blocks. For example in a 256x256 image, there are 1024 blocks of size 8x8 and each block has one DC coefficient and 63 AC coefficients. The DC layer hence contains 1024 coefficients and the AC layer contains 1024x63 coefficients. To prevent error propagation, the AC and DC layers are divided into blocks of 63 and 64 coefficients respectively. The blocks of the DC layer undergo Differential Pulse Code Modulation (DPCM) and DC-Huffman coding. Each block is encoded separately and after Huffman coding a header is inserted to indicate the size in bits of the resulting DC-packet. The blocks of the AC-layer undergo Run-Length Encoding (RLE) followed by AC-Huffman coding and a header is appended to indicate the size of each AC-packet. Each DC and AC packet can be decoded independently and errors within a packet do not propagate throughout the DC or AC layer. The headers are assumed to be transmitted error-free through a side-channel. A code-rate allocation is performed to provide UEP to the DC and AC packets. The DC packets are given the lowest code-rate while the AC-packets are allocated a higher code-rate. The packets are then converted into couples or triplets

of length N before being sent to the Non-binary Turbo encoder.

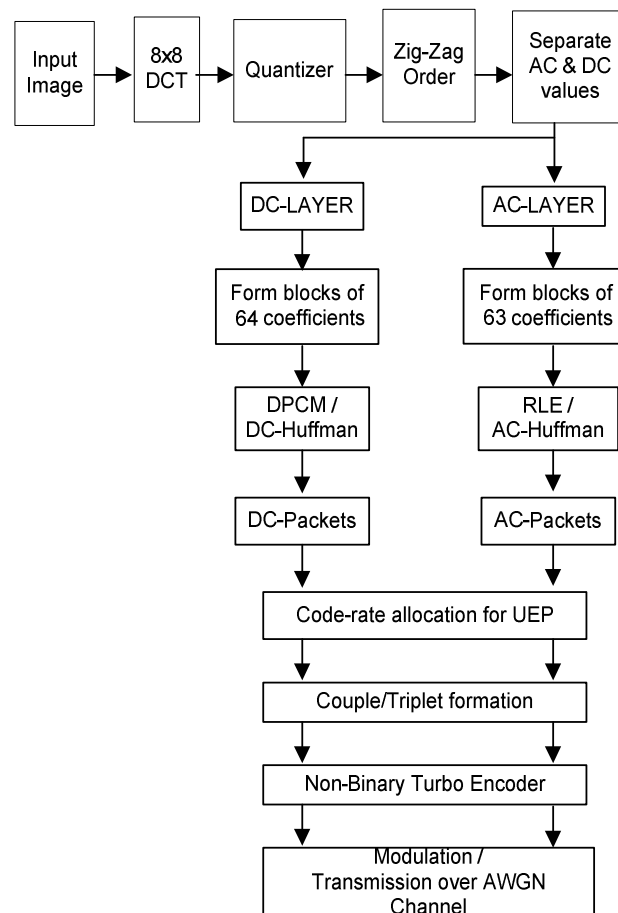


Figure 1. Complete encoding system with UEP.

The block diagram of the duo-binary encoder used is shown in Figure 2. The packets are first partitioned into blocks of length $2N$ bits. N is typically the couple length of the duo-binary encoder. From each block of length $2N$, a couple is formed by dividing it into two streams of length N each. The upper stream is denoted as A and lower stream as B . A and B , together, form a couple of length N , which is the input unit to the encoder. $D1, D2$ and $D3$ are shift registers, A and B are the systematic output, $W1$ and $Y1$ are the parity outputs from the upper encoder and $W2$ and $Y2$ are the parity outputs from the lower encoder. The polynomials defining the connections are described in octal and symbolic notations as follows [18], [19]:

1. For the feedback branch: 15 equivalently $1 + D + D^3$ (in symbolic notation);
2. For $Y1/ Y2$ parity bits: 13, equivalently $1 + D^2 + D^3$;
3. For the $W1/W2$ parity bits: 11, equivalently $1 + D^3$.

The double binary code uses a two-level interleaving denoted by INT on Figure 2.

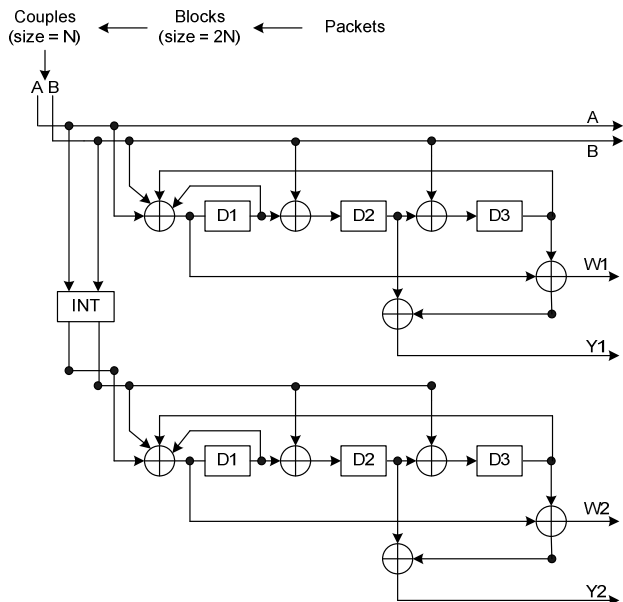


Figure 2. Duo-Binary Turbo encoder.

Let N be the number of bits per couple. The first level interleaving is an inter-symbol permutation performed between the couples and the second one is intra-symbol permutation, which is performed within the couples. The two levels of interleaving are described as follows [18], [19]:

Level 1

```

for j=0,...,N-1
  if (j modulo 2) =0
    Invert the couple i.e., (A,B)=(B,A)
  endif
endfor
    
```

Level 2

```

for j=0,...,N-1
  if (j modulo 4)=0
    P=0
  elseif (j modulo 4)=1
    P=N/2 + P1;
  elseif (j modulo 4) =2
    P=P2
  elseif (j modulo 4) =3
    P=N/2+P3
  endif
  Index = (P0*j + P + 1) modulo N
  Permute symbol at position j to position Index
endfor
    
```

The default permutation parameters used for couple sizes of 64 and 212 are given in Table I [18]:

TABLE I
DUO-BINARY PERMUTATION PARAMETERS

Couple Size (N)	P0	{P1,P2,P3}
64	7	{34,32,2}
212	13	{106,108,2}

There are seven code rates that are defined in the DVB-RCS standard and they are: $R=1/3, 2/5, 1/2, 2/3, 3/4, 4/5, 6/7$. The rates are achieved by selectively deleting parity bits $Y1, W1$ and $Y2, W2$. Table II shows the puncturing patterns for rates $1/3, 2/3$ and $4/5$ [18].

TABLE II
DUO-BINARY PUNCTURING PATTERNS

Rate	Puncturing pattern
$\frac{1}{3}$	$Y \begin{bmatrix} 1 \\ \end{bmatrix}$ $W \begin{bmatrix} 1 \\ \end{bmatrix}$
$\frac{2}{3}$	$Y \begin{bmatrix} 1 & 0 \\ \end{bmatrix}$ $W \begin{bmatrix} 0 & 0 \\ \end{bmatrix}$
$\frac{4}{5}$	$Y \begin{bmatrix} 1 & 0 & 0 & 0 \\ \end{bmatrix}$ $W \begin{bmatrix} 0 & 0 & 0 & 0 \\ \end{bmatrix}$

After puncturing, QPSK modulation is performed as per the mapping given in Table III where $(A, B), (Y1, W1)$ and $(Y2, W2)$ are mapped to the complex symbols x_{0i}, x_{1i} and x_{2i} , respectively. The symbols are multiplexed and transmitted over a complex AWGN channel and the receiver obtains y_{0i}, y_{1i} , and y_{2i} .

TABLE III
QPSK MAPPING PARAMETERS

Couple Bits	Symbol	Mapping
00	0	$1/\sqrt{2}+1/\sqrt{2}i$
01	1	$1/\sqrt{2}-1/\sqrt{2}i$
10	2	$-1/\sqrt{2}+1/\sqrt{2}i$
11	3	$-1/\sqrt{2}-1/\sqrt{2}i$

Figure 3 shows the block diagram for the triple binary encoder. The packets are first partitioned into blocks of length $3N$ bits. N is the triplet length of the triple-binary encoder. From each block of length $3N$, a triplet is formed by dividing it into three streams of length N each. The streams are denoted as A, B and C respectively. A, B and C form a triplet of length N , which is the input unit to the encoder. The systematic outputs are A, B and C while the parity outputs from the upper encoder are $W1, Z1, Y1$ and the parity outputs from the lower encoder are $W2, Z2$ and $Y2$. The connections of the encoder are defined by the polynomials in octal and symbolic notation as follows [18], [20]:

1. For the feedback branch: 23, equivalently $1 + D^3 + D^4$.
2. For the Z parity bits: 35, $1 + D + D^2 + D^3$.
3. For the Y parity bits: 31, equivalently $1 + D + D^4$.
4. For the W parity bits: 21, equivalently $1 + D^4$.

Unlike duo-binary codes, interleaving for triple binary codes occurs only at one level. Thus, only inter-symbol interleaving is used [18], [20], which is described as follows:

```

for j=0,...,N-1
    if (j modulo 4=0)
        P=0
    elseif (j modulo 4=1)
        P=N/2 +P1
    elseif (j modulo 4=2)
        P=P2
    elseif (j modulo 4=3)
        P=N/2 +P3
    endif

    Index = (P0*j + P+1) modulo N
    Permute symbol at position j to position Index
endfor
    
```

endfor

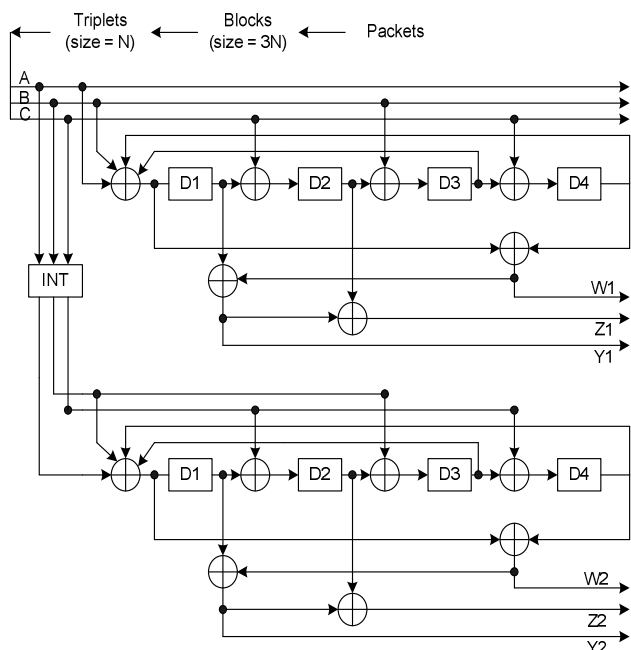


Figure 3. Triple Binary Encoder.

The default permutation parameters used for triplet sizes of 152 and 224 are given in Table IV [18], [20]:

Triplet Size (N)	{P0,P1,P2,P3}
152	{11,34,16,2}
224	{23,114,8,118}

In the DVB-RCS duo-binary code, puncturing is carried out on each individual bit. However for the triple binary code, puncturing is performed symbol-wise. Three code rates have been employed for the triple binary code: 1/3, 2/3 and 4/5. The systematic bits (A, B, C), the parity bits (W1, Z1, Y1) and (W2, Z2, Y2) are first converted to symbols Q0, Q1 and Q2 respectively. Puncturing is then performed on the

parity symbols Q1 and Q2 using the patterns given in Table V.

Rate	Puncturing pattern
1/3	Q1&Q2 [1 1]
2/3	Q1&Q2[1 0 0 0]
4/5	Q1&Q2[1 0 0 0 0 0 0]

After puncturing, 8-PSK modulation is performed as per the mapping given in Table VI where Q0, Q1 and Q2 are mapped to the complex symbols x_{0t} , x_{1t} and x_{2t} respectively.

Couple Bits	Symbol	Mapping
000	0	1+0i
001	1	$1/\sqrt{2}+1/\sqrt{2}i$
010	2	$-1/\sqrt{2}+1/\sqrt{2}i$
011	3	0+1i
100	4	$1/\sqrt{2}-1/\sqrt{2}i$
101	5	0-1i
110	6	-1+0i
111	7	$-1/\sqrt{2}-1/\sqrt{2}i$

The symbols are multiplexed and transmitted over a complex AWGN channel and the receiver obtains y_{0t} , y_{1t} and y_{2t} . The decoding system is shown in Figure 4.

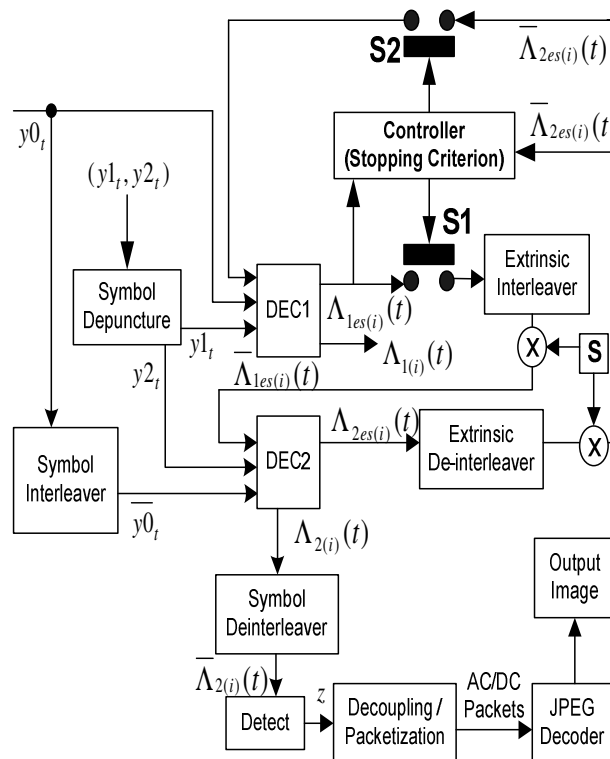


Figure 4. Decoding system with enhanced non-binary Decoder.

The received noisy parity symbols $y1_t$ and $y2_t$ are de-punctured and then sent to the decoders. DEC1 receives $y0_t$ and $y1_t$, while DEC2 receives the interleaved counterpart of $y0_t$, i.e., $\overline{y0}_t$ and $y2_t$. The decoders employ the Max-Log-MAP algorithm to compute the following parameters [18], [19], [20], [21], [22], [23]:

(a) $\overline{\gamma}_t^{q(i)}(l', l)$: The branch transition probability from state l' to l of symbol i at time instant t . For the duo-binary decoder, $i \in (0,1,2,3)$ for decoder q , where $q = 1$ or 2 and for the triple binary decoder, $i \in (0,1,2,3,4,5,6,7)$. It is computed as follows for the first decoder:

$$\overline{\gamma}_t^{1(i)}(l', l) = p(u_t^2 = i) - \frac{[y0_t^I - x0_t^{I(i)}(l)]^2 + [y0_t^Q - x0_t^{Q(i)}(l)]^2 + [y1_t^I - x1_t^{I(i)}(l)]^2 + [y1_t^Q - x1_t^{Q(i)}(l)]^2}{[y0_t^I - x0_t^{I(i)}(l)]^2 + [y0_t^Q - x0_t^{Q(i)}(l)]^2 + [y1_t^I - x1_t^{I(i)}(l)]^2 + [y1_t^Q - x1_t^{Q(i)}(l)]^2} \quad (1)$$

where

$p(u_t^2 = i)$ is the a-priori probability of symbol i obtained from the second decoder,

$x0_t^{I(i)}(l)$ and $x0_t^{Q(i)}(l)$ are the modulated in-phase and quadrature components of the complex systematic symbol $x0_t$ at time t , associated with the transition from state $S_{t-1} = l'$ to $S_t = l$ and input symbol i . $x1_t^{I(i)}(l)$ and $x1_t^{Q(i)}(l)$ represent the same for the symbol $x1_t$,

$y0_t^{I(i)}(l)$ and $y0_t^{Q(i)}(l)$ are the in-phase and quadrature components of $y0_t$, while $y1_t^{I(i)}(l)$ and $y1_t^{Q(i)}(l)$ are the in-phase and quadrature components of $y1_t$.

For the second decoder, the computation of $\overline{\gamma}_t^{2(i)}(l', l)$ is similar to equation (1) except that it uses the modulated in-phase and quadrature components of $y2_t$, $x0_t$, $x2_t$, the interleaved counterpart of $y0_t$, and the a-priori probability of symbol i obtained from the first decoder i.e., $p(u_t^1 = i)$.

(b) $\overline{\alpha}_t^q(l)$: The forward recursive variable at time t and state l . It is computed according to the following equation for a decoder with M_s states:

$$\overline{\alpha}_t^q(l) = \log \sum_{l'=0}^{M_s-1} e^{\overline{\alpha}_{t-1}^q(l') + \overline{\gamma}_t^{q(i)}(l', l)} \quad (2)$$

With the Max-log-map simplification, equation (2) can be expressed as follows:

$$\overline{\alpha}_t^q(l) = \max \left(\overline{\alpha}_{t-1}^q(l') + \overline{\gamma}_t^{q(i)}(l', l) \right) \text{ for } 0 \leq l' \leq M_s - 1 \quad (3)$$

(c) $\overline{\beta}_t^q(l)$ is the backward recursive variable computed at time t as follows:

$$\overline{\beta}_t^q(l) = \log \sum_{l'=0}^{M_s-1} e^{\overline{\beta}_{t+1}^q(l') + \overline{\gamma}_{t+1}^{q(i)}(l', l)} \quad (4)$$

With the Max-log-map simplification, equation (4) can be expressed as follows:

$$\overline{\beta}_t^q(l) = \max \left(\overline{\beta}_{t-1}^q(l') + \overline{\gamma}_t^{q(i)}(l', l) \right) \text{ for } 0 \leq l' \leq M_s - 1 \quad (5)$$

(d) $\Lambda_{q(i)}(t)$, which is the Log Likelihood Ratio (LLR) of symbol i where $i \in (1,2,3)$ for the case of a duo-binary decoder and $i \in (1,2,3,4,5,6,7)$ for the case of a triple binary decoder. The LLRs are normalized to the symbol '0'. This parameter is computed as follows [15], [16], [17], [18], [19], [23]:

$$\Lambda_{q(i)}(t) = \log \left[\frac{\sum_{l'=0}^{M_s-1} e^{\overline{\alpha}_{t-1}^q(l') + \overline{\gamma}_t^{q(i)}(l', l) + \overline{\beta}_t^q(l)}}{\sum_{l'=0}^{M_s-1} e^{\overline{\alpha}_{t-1}^q(l') + \overline{\gamma}_t^{q(0)}(l', l) + \overline{\beta}_t^q(l)}} \right] \quad (6)$$

The LLR of symbol $i = 0$ is zero. With the Max-log-map simplification, Equation (6) can be expressed as follows:

$$\Lambda_{q(i)}(t) = \max \left(\overline{\alpha}_{t-1}^q(l') + \overline{\gamma}_t^{q(i)}(l', l) + \overline{\beta}_t^q(l) \right) - \max \left(\overline{\alpha}_{t-1}^q(l') + \overline{\gamma}_t^{q(0)}(l', l) + \overline{\beta}_t^q(l) \right) \text{ for } 0 \leq l' \leq M_s - 1 \quad (7)$$

(e) $\Lambda_{1es(i)}(t)$ and $\Lambda_{2es(i)}(t)$: The extrinsic information of symbol i where $i \in (1,2,3)$ for the case of duo-binary and $i \in (1,2,3,4,5,6,7)$ for triple binary decoding. They are generated by DEC1 and DEC2 respectively and computed as follows:

$$\Lambda_{1es(i)}(t) = \Lambda_{1(i)}(t) - \overline{\Lambda}_{2es(i)}(t) - \Lambda_{1in(i)}(t) \quad (8)$$

$$\Lambda_{2es(i)}(t) = \Lambda_{2(i)}(t) - \overline{\Lambda}_{1es(i)}(t) - \Lambda_{2in(i)}(t) \quad (9)$$

It is to be noted that $\Lambda_{1es(0)}(t) = 0$ and $\Lambda_{2es(0)}(t) = 0$.

$\Lambda_{1in(i)}(t)$ and $\Lambda_{2in(i)}(t)$ are the intrinsic information of symbol i where $i \in (0,1,2,3)$ or $(0,1,2,3,4,5,6,7)$. They are generated by DEC1 and DEC2 respectively. The generic equation for $\Lambda_{1in(i)}(t)$ is as follows [18], [19], [20], [21], [22]:

$$\Lambda_{1in(i)}(t) = \log \left[\frac{p(y0_t | u_t = i)}{p(y0_t | u_t = 0)} \right] \quad (10)$$

where

u_t is the systematic part of the encoded symbols and corresponds to (A_t, B_t) for the duo-binary encoder where the symbols take values $i \in (0,1,2,3)$ and (A_t, B_t, C_t) for the triple binary encoder where $i \in (0,1,2,3,4,5,6,7)$.

For duo-binary transmission, u_t is modulated to obtain the complex symbol $x0_t$, which takes values as per Table III. The intrinsic information of symbol $i = 1$, from the first decoder is computed as follows:

$$\begin{aligned} \Lambda_{1in(1)}(t) &= \log \left[\frac{p(y0_t | x0_t = 1/\sqrt{2}, -1/\sqrt{2})}{p(y0_t | x0_t = 1/\sqrt{2}, 1/\sqrt{2})} \right] \\ &= -\frac{2}{\sqrt{2}\sigma^2} y0_t^Q \end{aligned} \quad (11)$$

where $y0_t^I$ and $y0_t^Q$ are the in-phase and quadrature components of $y0_t$ and σ^2 is the noise variance. Similarly, the intrinsic information for the symbols $i = (2, 3)$ are obtained as follows:

$$\Lambda_{1in(2)}(t) = -\frac{2}{\sqrt{2}\sigma^2} y0_t^I \quad (12)$$

$$\Lambda_{1in(3)}(t) = -\frac{2}{\sqrt{2}\sigma^2} (y0_t^I + y0_t^Q) \quad (13)$$

For the symbol $i = 0$, the intrinsic information is zero. Regarding the second decoder, the computations are similar except that the interleaved counterpart of $y0_t$ is used.

For triple-binary transmission, u_t is modulated to obtain the complex symbol $x0_t$, which takes values as per Table VI. The intrinsic information of symbol $i = 1$, from the first decoder is computed as follows:

$$\begin{aligned} \Lambda_{1in(1)}(t) &= \log \left[\frac{p(y0_t | x0_t = 1/\sqrt{2}, 1/\sqrt{2})}{p(y0_t | x0_t = 1, 0)} \right] \\ &= \frac{1}{2\sigma^2} (\sqrt{2}y0_t^I + \sqrt{2}y0_t^Q - 2y0_t^I) \end{aligned} \quad (14)$$

The intrinsic information for the symbols $i = (2, 3, 4, 5, 6, 7)$ are obtained in a similar way and the details are given in [18], [19], [20], [21], [22]. Again for the symbol $i = 0$, the intrinsic information is zero and for the second decoder, the interleaved counterpart of $y0_t$ is used.

The a-priori probabilities are computed as follows by the first duo-binary decoder [18], [19], [20], [21], [22]:

$$p(u_t^1 = 0) = -\max(0, \Lambda_{1es(1)}(t), \Lambda_{1es(2)}(t), \Lambda_{1es(3)}(t)) \quad (15)$$

$$p(u_t^1 = i) = \Lambda_{1es(i)}(t) - \max(0, \Lambda_{1es(1)}(t), \Lambda_{1es(2)}(t), \Lambda_{1es(3)}(t)) \quad (16)$$

where $i = (1, 2, 3)$.

Regarding the first triple binary decoder, the a-priori probabilities are computed as follows:

$$p(u_t^1 = 0) = -\max \left(0, \Lambda_{1es(1)}(t), \Lambda_{1es(2)}(t), \Lambda_{1es(3)}(t), \Lambda_{1es(4)}(t), \Lambda_{1es(5)}(t), \Lambda_{1es(6)}(t), \Lambda_{1es(7)}(t) \right) \quad (17)$$

$$p(u_t^1 = i) = \Lambda_{1es(i)}(t) - \max \left(0, \Lambda_{1es(1)}(t), \Lambda_{1es(2)}(t), \Lambda_{1es(3)}(t), \Lambda_{1es(4)}(t), \Lambda_{1es(5)}(t), \Lambda_{1es(6)}(t), \Lambda_{1es(7)}(t) \right) \quad (18)$$

where $i \in (1, 2, 3, 4, 5, 6, 7)$.

For the second decoder, $\Lambda_{2es(i)}(t)$ is used in the above equations instead of $\Lambda_{1es(i)}(t)$.

Further details on the computation of these parameters are given in [18], [19], [20], [21], [22].

In the enhanced non-binary decoder, the extrinsic information produced by both decoders are multiplied by a scale factor S as shown in Figure 4. The application of the scale factor improves performance because the extrinsic information value output by the Turbo decoder is most of the time too optimistic, hence by scaling it, better performance is achieved [15], [16]. The controller unit accepts the extrinsic information from both decoders and

uses a stopping criterion [17] to stop the iterative decoding process. At the start of the iterative decoding process, switches S1 and S2 are ON and when a given condition is met, the controller unit turns OFF both switches to stop the iterative decoding process. In this way, the decoder avoids the use of extra iterations and reduces the decoding complexity. This technique also reduces the power consumption of the decoder.

A detailed algorithm for the decoding process using duobinary Turbo codes is now presented. In this algorithm, steps 4-12 correspond to the operations of DEC1 and steps 13-21 of DEC2. The parameters $M_{11}^r(t), M_{12}^r(t), M_{21}^r(t), M_{22}^r(t)$ are used in the stopping criterion and the function $f(\)$ counts the number of sign changes between the two arguments that are passed to it. The function *detect*() determines the maximum of the LLR values and outputs either symbol 0,1,2, or 3. The variable j increases by 1 because the decoder processes one couple at a time up to a maximum of N_c , which is the total number of couples in the image. The variable r also increases by 1 up to a maximum limit of r_{max} . However, the variable $num_iterations$, which is used to count the number of iterations consumed by the decoder, is incremented by 0.5. This is because the stopping criterion can stop the decoding process after either DEC1 or DEC2 whereby each decoder consumes 0.5 iterations. For example, if for a given couple, the decoding process completes 2 full iterations and then at the third iteration i.e., $r=3$, after passing through DEC1, the stopping criterion is satisfied, then only 0.5 additional iteration is consumed and hence $num_iterations$ will be 2.5 and not 3. The complete decoding algorithm is as follows:

1. $num_iterations = 0$
2. for $j = 1:N_c$
3. for $r = 1:r_{max}$
4. Compute: $\overline{\gamma}_t^{l(i)}(l, l), \overline{\alpha}_t^1(l), \overline{\beta}_t^1(l), \Lambda_{1es(i)}(t), \Lambda_{1(i)}(t)$
5. $num_iterations = num_iterations + 0.5.$
6. $M_{11}^r(t) = \max(\Lambda_{1es(2)}(t), \Lambda_{1es(3)}(t)) - \max(\Lambda_{1es(0)}(t), \Lambda_{1es(1)}(t))$
7. $M_{12}^r(t) = \max(\Lambda_{1es(1)}(t), \Lambda_{1es(3)}(t)) - \max(\Lambda_{1es(0)}(t), \Lambda_{1es(2)}(t))$
8. if ($r>1$)
9. if ($f(M_{11}^r(t), M_{11}^{r-1}(t)) \leq \frac{1}{N}$ or $f(M_{12}^r(t), M_{12}^{r-1}(t)) \leq \frac{1}{N}$)
10. break
11. endif

12. endif
13. Compute: $\overline{\gamma}_t^{2(i)}(l, l), \overline{\alpha}_t^2(l), \overline{\beta}_t^2(l), \Lambda_{2es(i)}(t), \Lambda_{2(i)}(t)$
14. $num_iterations = num_iterations + 0.5.$
15. $M_{21}^r(t) = \max(\Lambda_{2es(2)}(t), \Lambda_{2es(3)}(t)) - \max(\Lambda_{2es(0)}(t), \Lambda_{2es(1)}(t))$
16. $M_{22}^r(t) = \max(\Lambda_{2es(1)}(t), \Lambda_{2es(3)}(t)) - \max(\Lambda_{2es(0)}(t), \Lambda_{2es(2)}(t))$
17. if ($r>1$)
18. if ($f(M_{21}^r(t), M_{21}^{r-1}(t)) \leq \frac{1}{N}$ or $f(M_{22}^r(t), M_{22}^{r-1}(t)) \leq \frac{1}{N}$)
19. break
20. endif
21. endif
22. endfor
23. Decoded couple, $z = detect(\overline{\Lambda}_{2(i)}(t))$
24. endfor
25. Convert the received couples into AC and DC packets.
26. Perform JPEG decoding on the received packets.

The corresponding algorithm for triple binary Turbo codes is as follows:

1. $num_iterations = 0$
2. for $j = 1:N_c$
3. for $r = 1:r_{max}$
4. Compute: $\overline{\gamma}_t^{1(i)}(l, l), \overline{\alpha}_t^1(l), \overline{\beta}_t^1(l), \Lambda_{1es(i)}(t), \Lambda_{1(i)}(t)$
5. $num_iterations = num_iterations + 0.5.$
6. $M_{11}^r(t) = \max\left(\begin{matrix} \Lambda_{1es(4)}(t), \Lambda_{1es(5)}(t) \\ \Lambda_{1es(6)}(t), \Lambda_{1es(7)}(t) \end{matrix}\right) - \max\left(\begin{matrix} \Lambda_{1es(0)}(t), \Lambda_{1es(1)}(t) \\ \Lambda_{1es(2)}(t), \Lambda_{1es(3)}(t) \end{matrix}\right)$
7. $M_{12}^r(t) = \max\left(\begin{matrix} \Lambda_{1es(2)}(t), \Lambda_{1es(3)}(t) \\ \Lambda_{1es(6)}(t), \Lambda_{1es(7)}(t) \end{matrix}\right) - \max\left(\begin{matrix} \Lambda_{1es(0)}(t), \Lambda_{1es(1)}(t) \\ \Lambda_{1es(4)}(t), \Lambda_{1es(5)}(t) \end{matrix}\right)$
8. $M_{13}^r(t) = \max\left(\begin{matrix} \Lambda_{1es(1)}(t), \Lambda_{1es(3)}(t) \\ \Lambda_{1es(5)}(t), \Lambda_{1es(7)}(t) \end{matrix}\right) - \max\left(\begin{matrix} \Lambda_{1es(0)}(t), \Lambda_{1es(2)}(t) \\ \Lambda_{1es(4)}(t), \Lambda_{1es(6)}(t) \end{matrix}\right)$
9. flag = 0

```

10.   if (r>1)
11.       if  $\left( \begin{array}{l} f(M_{11}^r(t), M_{11}^{r-1}(t)) \leq \frac{1}{N} \text{ or} \\ f(M_{12}^r(t), M_{12}^{r-1}(t)) \leq \frac{1}{N} \text{ or} \\ f(M_{13}^r(t), M_{13}^{r-1}(t)) \leq \frac{1}{N} \end{array} \right)$ 
12.           Decoded triplet,  $z = detect \left( \Lambda_{1(i)}(t) \right)$ 
13.           flag = 1
14.           break
15.       endif
16.   endif
17.   Compute:  $\overline{\gamma}_t^{2(i)}(l, l), \overline{\alpha}_t^2(l), \overline{\beta}_t^2(l), \Lambda_{2es(i)}(t), \Lambda_{2(i)}(t)$ 
18.   num_iterations = num_iterations + 0.5.
19.    $M_{21}^r(t) = \max \left( \Lambda_{2es(4)}(t), \Lambda_{2es(5)}(t) \right) - \max \left( \Lambda_{2es(0)}(t), \Lambda_{2es(1)}(t) \right)$ 
20.    $M_{22}^r(t) = \max \left( \Lambda_{2es(2)}(t), \Lambda_{2es(3)}(t) \right) - \max \left( \Lambda_{2es(0)}(t), \Lambda_{2es(1)}(t) \right)$ 
21.    $M_{23}^r(t) = \max \left( \Lambda_{2es(1)}(t), \Lambda_{2es(3)}(t) \right) - \max \left( \Lambda_{2es(0)}(t), \Lambda_{2es(2)}(t) \right)$ 
22.   if (r>1)
23.       if  $\left( \begin{array}{l} f(M_{21}^r(t), M_{21}^{r-1}(t)) \leq \frac{1}{N} \text{ or} \\ f(M_{22}^r(t), M_{22}^{r-1}(t)) \leq \frac{1}{N} \text{ or} \\ f(M_{23}^r(t), M_{23}^{r-1}(t)) \leq \frac{1}{N} \end{array} \right)$ 
24.           Decoded triplet,  $z = detect \left( \overline{\Lambda}_{2(i)}(t) \right)$ 
25.           flag = 1
26.           break
27.       endif
28.   endif
29.   if(flag = 0)
30.       Decoded triplet,  $z = detect \left( \overline{\Lambda}_{2(i)}(t) \right)$ 
31.   endif
32.   endfor

```

33. Convert the received couples into AC and DC packets.
34. Perform JPEG decoding on the received packets.

The algorithm for the triple binary decoder uses six parameters $M_{11}^r(t), M_{12}^r(t), M_{13}^r(t), M_{21}^r(t), M_{22}^r(t), M_{23}^r(t)$ for the stopping criterion whereas the duo-binary decoder uses only four. The computations of these parameters are also different for triple binary as compared to duo-binary. Another minor difference is that in the triple binary system the triplet can be decoded at three points. First at line 12 where the stopping criterion is met at the first decoder, second at line 23 where the criterion is met at the second decoder and third at line 28, where the stopping criterion is not met and the couple is decoded from the LLR obtained after all decoding iterations have been performed.

III. SIMULATION RESULTS AND ANALYSIS

The performances of the following four schemes for JPEG image transmission are compared for both double-binary and triple binary Turbo codes:

Scheme 1- UEP with scale factor: This scheme employs UEP to provide different levels of protection to the AC and DC packets of the image. It also uses a scale factor, S, to enhance the performance of the duo-binary Turbo code by scaling the extrinsic information, as depicted in Figure 4. The value of S is set in the range $0 < S < 1.0$.

Scheme 2 - UEP without scale factor: This scheme is similarly to Scheme 1 but the extrinsic information is not scaled and the value of S is set to 1.0 in Figure 4.

Scheme 3 - EEP with scale factor: It is similar to Scheme 1 but equal protection is given to the AC and DC packets.

Scheme 4 - EEP without scale factor: This scheme is similar to Scheme 3 but the scale factor, S, is set to 1.0.

In all simulations, the 256x256 Lena image is used as input. Moreover, it is assumed that the headers are transmitted error free over a strongly protected side channel. The overall coding rate, O_c , was limited to $O_c < 0.97$ bits/pixel and to ensure a fair comparison, the overall coding rate for UEP was less than or equal to that of EEP. However, with UEP the DC packets are more strongly protected with a code-rate of 1/3 while the AC packets are allocated a code-rate of 4/5. On the other hand the EEP schemes allocate a fixed code-rate of 2/3 to both DC and AC packets. The overall coding rate, O_c , is computed as follows:

$$O_c = \frac{1}{T} \left(\frac{T_{DC}}{R_{DC}} + \frac{T_{AC}}{R_{AC}} \right) \quad (19)$$

where

T is total number of pixels in the image,
 T_{DC} is the total number of bits in the DC packets,
 R_{DC} is the code-rate allocated to the DC packets,
 T_{AC} is the total number of bits in the AC packets,
 R_{AC} is the code-rate allocated to the AC packets.

Parameters and results for duo-binary Turbo codes

In this simulation, the DVB-RCS standard duo-binary Turbo code [15] has been used with a stopping criterion. The encoder structure is given in Figure 2 and the generator polynomials are given in Section II. Puncturing matrices are chosen as per the DVB-RCS standard and are given in Table II. The value of S has been set to 0.75 in this simulation for Schemes 1 and 3. The source coding rate, S_c , and O_c , vary with the couple length because different numbers of padding bits are required to convert the bit stream from the JPEG encoder into couples of length N . Table VII gives the values of O_c and S_c for different couple lengths, N .

TABLE VII
 CODING RATES FOR DIFFERENT VALUES OF N

N	T_{DC}	T_{AC}	S_c	O_c	
				UEP	EEP
64	5760	36096	0.639	0.952	0.958
212	5936	36040	0.641	0.959	0.961

Figure 5 shows the graph of PSNR versus E_b/N_0 for the four schemes with $N = 64$.

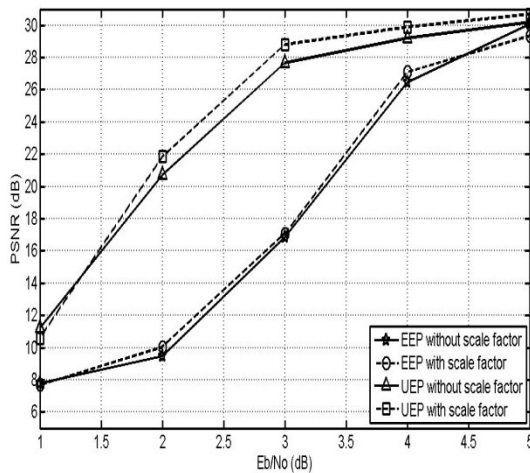


Figure 5. Graph of PSNR against E_b/N_0 for $N = 64$.

The UEP scheme with scale factor provides a gain of 7dB in PSNR over the EEP schemes at $E_b/N_0 = 1.5$ dB and a major gain of 12dB in PSNR in the range $2\text{dB} \leq E_b/N_0 \leq 3\text{dB}$. It also outperforms the UEP scheme without scale factor by 1dB in PSNR in the range $2\text{dB} \leq E_b/N_0 \leq 3\text{dB}$. The UEP scheme outperforms the EEP schemes because with UEP the DC layer is recovered with fewer errors than the AC-layer and hence, the image can be reconstructed with

much less distortions. However, it is observed that at high E_b/N_0 values, the gain obtained with UEP over EEP decreases because the overall number of errors introduced in the image is considerably less, and convergence occurs.

The graph of number of iterations versus E_b/N_0 for $N = 64$ is shown in Figure 6. The stopping criterion allows the number of iterations and hence the decoding complexity to decrease progressively as the E_b/N_0 is increased. Interestingly, the UEP scheme with scale factor requires less iterations than the EEP schemes in the range $1\text{dB} \leq E_b/N_0 \leq 3\text{dB}$ and provides an impressive reduction of 5.5 iterations over the EEP scheme without scale factor at $E_b/N_0 = 1\text{dB}$.

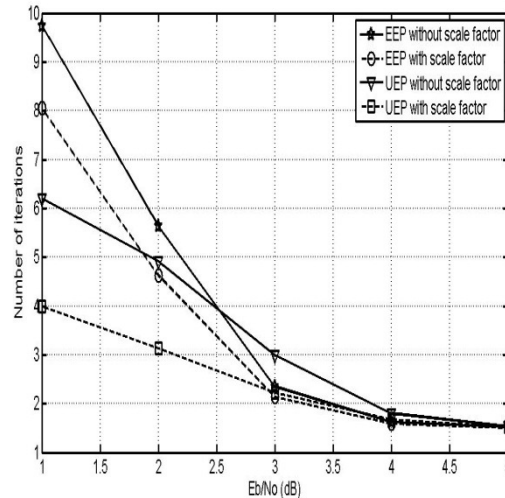


Figure 6. Number of iterations against E_b/N_0 for $N = 64$.

Figure 7 shows the graph of PSNR versus E_b/N_0 for the four schemes with $N = 212$.

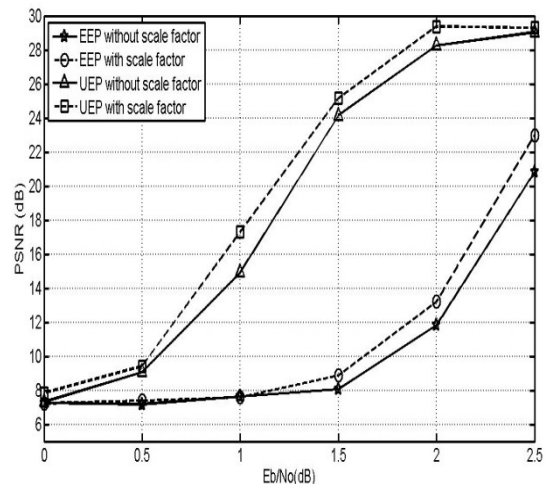


Figure 7. Graph of PSNR against E_b/N_0 for $N = 212$.

The UEP scheme with scale factor provides a gain of 10 dB in PSNR over the EEP schemes at $E_b/N_0 = 1$ dB and a major gain of 15 dB in PSNR in the range

$1.5 \text{ dB} \leq E_b/N_0 \leq 2 \text{ dB}$. It also outperforms the UEP scheme without scale factor by about 1dB in PSNR in the range $1 \text{ dB} \leq E_b/N_0 \leq 2 \text{ dB}$. Moreover, with $N = 212$ the UEP scheme with scale factor outperforms the UEP scheme with scale factor for $N = 64$, by an average of 5 dB in PSNR. The gain is greater with a couple length of $N=212$ because the performance of the duo-binary Turbo code improves with increase in couple length.

The graph of number of iterations versus E_b/N_0 for $N = 212$ is shown in Figure 8. It is observed that when $N=212$, the UEP scheme with scale factor takes less iterations than the EEP schemes only in the range $0 \text{ dB} \leq E_b/N_0 \leq 1 \text{ dB}$. For $E_b/N_0 > 1.5 \text{ dB}$ the EEP scheme with scale factor requires significantly less iterations than the UEP schemes, for example, at $E_b/N_0 = 2.5 \text{ dB}$ it requires 5 iterations less than the UEP scheme without scale factor. A possible explanation for that is that the threshold used in the stopping criterion was not optimized for $N = 212$ and was maintained at $1/N$.

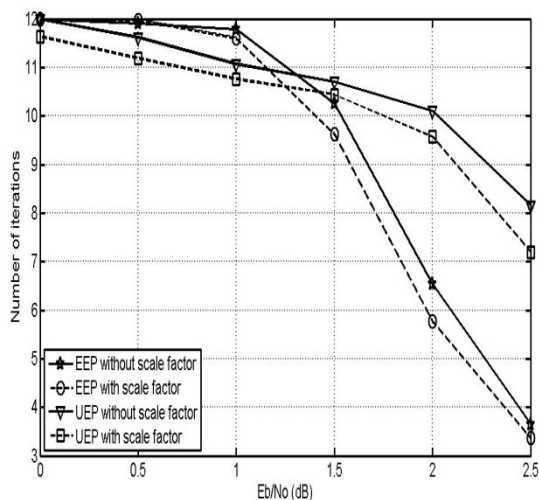


Figure 8. Number of iterations against E_b/N_0 for $N = 212$.

Some decoded images with the UEP scheme with scale factor and the EEP scheme with scale factor at $E_b/N_0 = 2 \text{ dB}$ for $N = 212$ are shown in Figure 9.



(a) PSNR = 13.69dB EEP Scheme 3
(b) PSNR = 29.14dB UEP Scheme 1

Figure 9. Decoded images at $E_b/N_0 = 2 \text{ dB}$ with $N = 212$.

The images again confirm the superiority of the proposed UEP scheme.

Parameters and results for triple-binary Turbo codes

The encoder structure of the triple binary Turbo code used is given in Figure 3 and the generator polynomials are given in Section II. Puncturing matrices are chosen as per Table VI. The scale factor S is set to 0.75 in the range $1 \text{ dB} \leq E_b/N_0 \leq 1.5 \text{ dB}$ and increased to 0.9 in the range $1.7 \text{ dB} \leq E_b/N_0 \leq 2.5 \text{ dB}$ for the UEP Scheme 1. This increase was required because the scale factor of 0.75 was causing a degradation in performance for $E_b/N_0 > 1.5 \text{ dB}$ in the case of the UEP scheme with triple binary codes. However, for the EEP Scheme 3 it is set to $S = 0.75$ for the range $0 \text{ dB} \leq E_b/N_0 \leq 2.5 \text{ dB}$.

The source coding rate, S_c , and O_c , vary with the triplet length because different numbers of padding bits are required to convert the bit stream from the JPEG encoder into triplets of length N . Table VIII gives the values of O_c and S_c for different triplet lengths, N .

TABLE VIII
CODING RATES FOR DIFFERENT VALUES OF N

N	T_{DC}	T_{AC}	S_c	O_c	
				UEP	EEP
152	5928	36024	0.640	0.958	0.960
224	5936	36040	0.641	0.969	0.969

Figure 10 shows the graph of PSNR versus E_b/N_0 for the four schemes with $N = 152$.

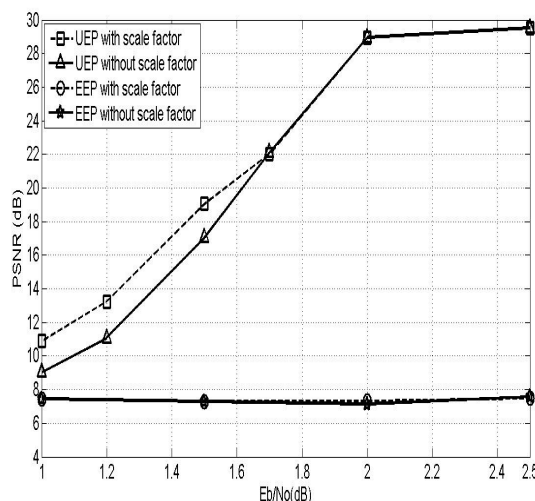


Figure 10. Graph of PSNR against E_b/N_0 for $N = 152$.

The UEP scheme with scale factor provides a gain of 14 dB in PSNR over the EEP schemes at $E_b/N_0 = 1.7 \text{ dB}$ and a major gain of 20dB in PSNR in the range $2 \text{ dB} \leq E_b/N_0 \leq 2.5 \text{ dB}$. In the case of triple-binary codes it is observed that the

EEP scheme shows hardly any improvement in PSNR over the range $1\text{dB} \leq E_b/N_0 \leq 2.5\text{dB}$ because it uses a code-rate of $2/3$ the convergence range for this code-rate is between $3.5\text{dB} \leq E_b/N_0 \leq 5.5\text{dB}$. Hence the UEP schemes provide the additional benefit of converging much faster than the EEP scheme. The UEP scheme with scale factor also outperforms the UEP scheme without scale factor by 1dB in PSNR in the range $1\text{dB} \leq E_b/N_0 \leq 1.5\text{dB}$. However, it is observed that for E_b/N_0 values $\geq 1.7\text{dB}$, the UEP scheme with scale factor has an almost similar performance to the UEP scheme without scale factor due to convergence.

The graph of number of iterations versus E_b/N_0 for $N = 152$ is shown in Figure 11. Again the stopping criterion allows the number of iterations and hence the decoding complexity to decrease progressively as the E_b/N_0 is increased. Interestingly, the UEP scheme with scale factor requires on average 1.5 less iterations than the EEP schemes in the range $1\text{dB} \leq E_b/N_0 \leq 2.5\text{dB}$. At 1.7dB, there is an increase in the number of iterations for the UEP scheme with scale factor because the scale factor was increased to 0.9.

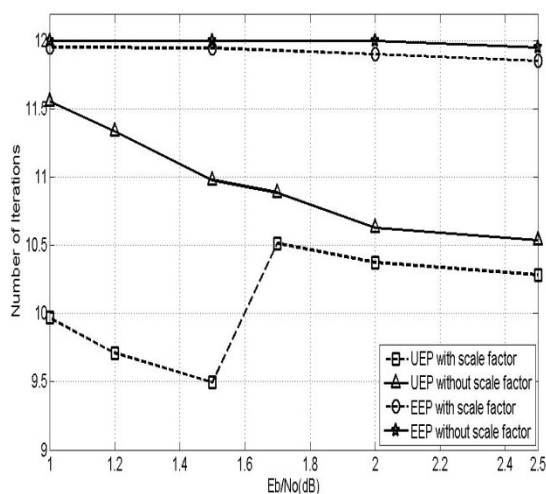


Figure 11. Number of iterations against E_b/N_0 for $N = 152$.

Figure 12 shows the graph of PSNR versus E_b/N_0 for the four schemes with $N = 224$. The UEP scheme with scale factor provides a gain of 14 dB in PSNR over the EEP schemes at $E_b/N_0 = 1.5\text{dB}$ and a major gain of 20dB in PSNR in the range $1.7\text{dB} \leq E_b/N_0 \leq 2.5\text{dB}$. It also outperforms the UEP scheme without scale factor by an average of 1dB in PSNR in the range $1\text{dB} \leq E_b/N_0 \leq 1.7\text{dB}$. Moreover, with $N = 224$ the UEP scheme with scale factor outperforms the UEP scheme with scale factor for $N = 152$, by an average of 5 dB in PSNR at $E_b/N_0 = 1.7\text{dB}$. The gain is greater with a couple length of $N=224$ because the performance of the triple-binary Turbo code also improves with increase in couple length.

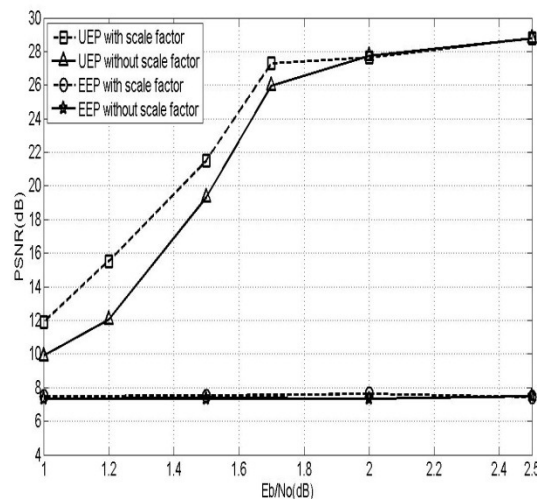


Figure 12. Graph of PSNR against E_b/N_0 for $N = 224$.

The graph of number of iterations versus E_b/N_0 for $N = 224$ is shown in Figure 13. It is observed that when $N=224$, the UEP scheme the UEP scheme with scale factor requires on average 1 iteration less than the EEP schemes in the range $1\text{dB} \leq E_b/N_0 \leq 2.5\text{dB}$. At 1.7dB, there is a slight increase in the number of iterations for the UEP scheme with scale factor because the scale factor was increased to 0.9.

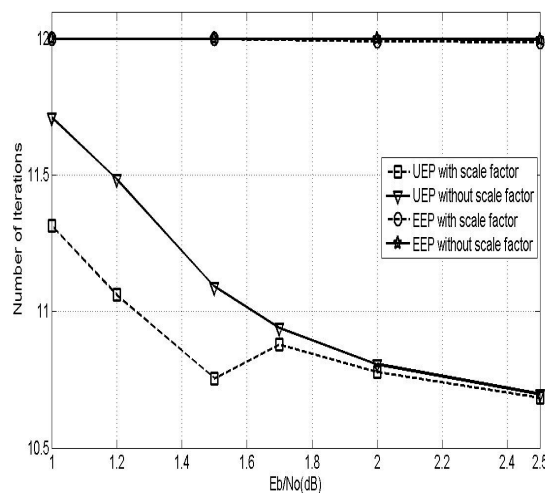


Figure 13. Number of iterations against E_b/N_0 for $N = 224$.

Some decoded images with the UEP scheme with scale factor and the EEP scheme with scale factor at $E_b/N_0 = 2\text{dB}$ for $N = 152$ are shown in Figure 14. The images again confirm the superiority of the proposed UEP scheme.

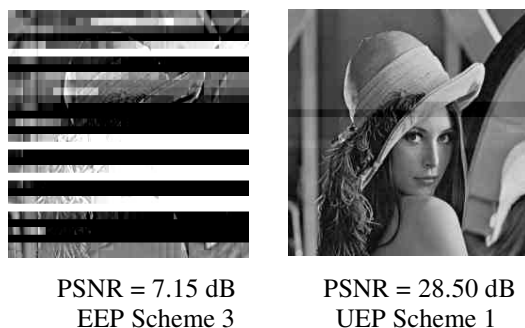


Figure 14. Decoded images at $E_b/N_0 = 2\text{dB}$ with $N = 152$.

An interesting benefit of using triple binary Turbo codes is that it provides greater bandwidth efficient than the duo-binary Turbo codes. However it has a greater encoder and decoder complexity.

There are two ways in which the UEP scheme can lead to an increase in complexity with respect to the EEP scheme. First, in the case of duo-binary Turbo codes, over a certain E_b/N_0 range, as observed in Figure 6, the UEP scheme requires more iterations than the EEP scheme. Second, with the UEP scheme, the non-binary Turbo encoder must treat the AC and DC packets separately and use different code-rates, hence different puncturing patterns are required for each of them. The same applies for the non-binary Turbo decoder, whereby a different de-puncturing process must be used for the AC and DC packets.

IV. CONCLUSION

This paper proposed an efficient UEP scheme for JPEG image transmission with modified non-binary Turbo codes whereby an extrinsic scale factor and a stopping criterion were incorporated. The performances of four schemes were compared with different couple and triplet lengths. The results showed that over a range of E_b/N_0 values, major gains of the order of 10 dB in PSNR are obtained with the UEP scheme with duo-binary Turbo codes and gains of the order of 14 dB in PSNR are obtained with triple-binary Turbo codes, over conventional EEP schemes. Furthermore, the application of the scale factor coupled with the stopping criterion improved the PSNR performance and reduced the number of iterations required, hence the decoding complexity. Except for the UEP scheme with duo-binary Turbo codes with couple length of 212, all the other UEP schemes required less iterations than the EEP schemes. However, for duo-binary Turbo codes with a couple length of 212, at higher E_b/N_0 values, the EEP schemes required less iterations. Another observation was that the performance of the UEP schemes improved with an increase in the couple or triplet length. Finally, the use of triple binary Turbo codes provided the added benefit of greater

bandwidth efficiency. An interesting future work would be to optimize the threshold used in the stopping criterion for couple lengths greater than 64, so as to reduce the number of iterations required by the UEP scheme with duo-binary Turbo codes.

ACKNOWLEDGMENT

The authors would like to thank the University of Mauritius for providing the necessary facilities for conducting this research.

REFERENCES

- [1] Tulsi Pawan Fowdur and Yashvin Beni, "An Unequal Error Protection Scheme for JPEG Image Transmission Using Enhanced Duo-Binary Turbo Codes", Fifth International Conference on Communication Theory, Reliability, and Quality of Service (CTRQ 2012), Chamonix / Mont Blanc, France, April-May 2012, pp.62-67.
- [2] R.C. Gonzalez, R.E Woods, and S.L Eddins, Digital Image Processing in Matlab, 2nd ed., Gatesmark Publishing, (2009).
- [3] L.G. Yamamoto, "Using JPEG image transmission to facilitate telemedicine," The American Journal of Medicine, vol. 13, pp. 55-57, 2009.
- [4] Ersin GOSE, "Adaptive Wiener-turbo systems with JPEG & bit plane compressions in image transmission," Turk J Elec Eng & Comp Sci, vol. 19, no.1, 2011. (doi:10.3906/elk-1003-461).
- [5] L.W. Kang and J.J. Leou, "An error resilient coding scheme for JPEG image transmission based on data embedding and side-match vector quantization," J. Vis. Commun. Image, R.17, pp. 876-891, 2006.
- [6] K.S. Kim, H.Y. Lee, and H.K. Lee, "Supplementary loss concealment technique for image transmission through data hiding," Multimed Tools Appl, vol. 44, pp. 1-16, 2009. (DOI 10.1007/s11042-009-0265-0).
- [7] T.P. Fowdur and K.M.S. Soyjaudah, "Hybrid Joint Source Channel Decoding for Progressive JPEG Image Transmission," Circuits Systems and Signal Processing, vol. 29, pp. 857-879, 2010. (DOI 10.1007/s00034-010-9188-2).
- [8] M. Padmaja, M. Kondaiah and K.S. RamaKrishna, "Error Resilient Image Transmission over Wireless Fading Channels," International Journal of Engineering Science and Technology, vol. 2(5), pp. 1242-1249, 2010.
- [9] A.M. Lakhdar, R.Méliani, and M. Kandouci, "Research on Unequal Error Protection with Punctured Turbo Codes in JPEG Image Transmission System," SJEE, vol.4, no.1, pp. 95-108, June 2007.
- [10] Qian Mao, Boqing Xu and Yanping Qin, "A New Scheme to Improve the Quality of Compressed Image Transmission by Turbo Unequal Error Protection Codes", Seventh International Conference on Intelligent Information Hiding and Multimedia Signal Processing (IIH-MSP), Dalian, China, pp. 226 - 229, 2011.
- [11] Ersin GOSE, "Adaptive Wiener-turbo systems with JPEG & bit plane compressions in image transmission," Turk J Elec Eng & Comp Sci, Vol.19, No.1, pp.141-155, 2011.
- [12] G.Baruffa, P. Micanti, and F.Frescura, "Error Protection and Interleaving for Wireless Transmission of JPEG 2000 Images and Video". IEEE Transactions on Image Processing, Vol .18(2), pp. 346-356, 2009.

- [13] T.P Fowdur and K.M.S Soyjaudah, "Highly Scalable JPEG Image Transmission with Unequal Error Protection and Optimal Feedback," *Telecommunication Systems*, vol.49, Issue 4, pp. 355-377, 2012. (DOI: 10.1007/s11235-010-9379-y). (Published online: 25 June 2010)
- [14] C.Douillard and C.Berrou,"Turbo codes with Rate- $m/(m+1)$ Constituent Convolutional Codes," in *IEEE Trans. Commun*, pp. 1630-1638, October 2005.
- [15] J.Vogt and A.Finger, "Improving the MAX-Log-MAP Turbo decoder," *Electronics letters*, vol. 36, no. 23, November 2000.
- [16] T.Gnanasekaran and K. Duraiswamy, "Performance of Unequal Error Protection Using MAP Algorithm and Modified MAP in AWGN and Fading Channel," *Journal of Computer Science*, vol. 4 (7), pp. 585-590,2008.
- [17] B.S. Shim, D.H. Jeong, and S.J. Lim, "A new stopping criterion for turbo codes," in *Adv Communication Technology*, Ikhkan, pp. 1111-1116, 2006.
- [18] M.R. Soleymani, Y.Gao and U.Vilapornasawai,Turbo coding for satellite and Wireless Communication, Kluwer Academic Publishers, 2002.
- [19] European Telecommunications Standards Institute, Interaction channel for satellite distributions systems, ETSI EN 301 790,V1.3.1 March 2003.
- [20] Yingzi Gao and M R Soleymani, "Spectrally Efficient Non-binary Turbo Codes: Beyond DVB-RCS standard," *Proceedings of 21th Biennial Symposium on Communications*, vol. 3, pp. 951-955, May 2002.
- [21] Y. Ould-Cheikh-Mouhamedou, S. Crozier and P. Kabal, "Distance measurement method for double binary turbo codes and a new interleaver design for DVB-RCS," *Global Telecommunications Conference 2004, (GLOBECOM '04)*, vol. 1, pp. 172 – 178,2004 .
- [22] Youssof Ould Cheikh Mouhamedou, *On Distance Measurement Methods for Turbo Codes*, McGill University, Montreal, PhD Thesis 2005. Available Online: <http://www-mmsp.ece.mcgill.ca/MMSP/Theses/2005/Ould-Cheikh-MouhamedouT2005.pdf> [Accessed: August 2011]
- [23] Branka Vucetic., and Jinhong Yuan, *Turbo Codes : Principles and Applications*, Kluwer Academic Publishers, 2000.



www.iariajournals.org

International Journal On Advances in Intelligent Systems

✦ ICAS, ACHI, ICCGI, UBICOMM, ADVCOMP, CENTRIC, GEOProcessing, SEMAPRO, BIOSYSCOM, BIOINFO, BIOTECHNO, FUTURE COMPUTING, SERVICE COMPUTATION, COGNITIVE, ADAPTIVE, CONTENT, PATTERNS, CLOUD COMPUTING, COMPUTATION TOOLS, ENERGY, COLLA, IMMM, INTELLI, SMART, DATA ANALYTICS

✦ issn: 1942-2679

International Journal On Advances in Internet Technology

✦ ICDS, ICIW, CTRQ, UBICOMM, ICSNC, AFIN, INTERNET, AP2PS, EMERGING, MOBILITY, WEB

✦ issn: 1942-2652

International Journal On Advances in Life Sciences

✦ eTELEMED, eKNOW, eL&mL, BIODIV, BIOENVIRONMENT, BIOGREEN, BIOSYSCOM, BIOINFO, BIOTECHNO, SOTICS, GLOBAL HEALTH

✦ issn: 1942-2660

International Journal On Advances in Networks and Services

✦ ICN, ICNS, ICIW, ICWMC, SENSORCOMM, MESH, CENTRIC, MMEDIA, SERVICE COMPUTATION, VEHICULAR, INNOV

✦ issn: 1942-2644

International Journal On Advances in Security

✦ ICQNM, SECURWARE, MESH, DEPEND, INTERNET, CYBERLAWS

✦ issn: 1942-2636

International Journal On Advances in Software

✦ ICSEA, ICCGI, ADVCOMP, GEOProcessing, DBKDA, INTENSIVE, VALID, SIMUL, FUTURE COMPUTING, SERVICE COMPUTATION, COGNITIVE, ADAPTIVE, CONTENT, PATTERNS, CLOUD COMPUTING, COMPUTATION TOOLS, IMMM, MOBILITY, VEHICULAR, DATA ANALYTICS

✦ issn: 1942-2628

International Journal On Advances in Systems and Measurements

✦ ICQNM, ICONS, ICIMP, SENSORCOMM, CENICS, VALID, SIMUL, INFOCOMP

✦ issn: 1942-261x

International Journal On Advances in Telecommunications

✦ AICT, ICDT, ICWMC, ICSNC, CTRQ, SPACOMM, MMEDIA, COCORA, PESARO, INNOV

✦ issn: 1942-2601